JOURNAL OF MECHANICS OF MATERIALS AND STRUCTURES

msp.org/jomms

Founded by Charles R. Steele and Marie-Louise Steele

msp

HUY DUONG BUI

Jean Salençon and André Zaoui

L'original français se trouve page 212.

Huy Duong Bui, member of the French Academy of Sciences, passed away on May 29, 2013 at the age of 76. He was a founding member of the French Academy of Technologies, a member of the European Academy of Sciences and a Fellow of the Institute of Physics (London). He was also a Knight in the French Ordre national de la Légion d'honneur.

Huy Duong Bui was born in Hanoi on March 16, 1937. As a child in Vietnam, he had been kept away from town and deprived of schooling for a long time because of harsh years of wars, floods and famine: a refugee in the countryside with his family, he learned hunting and fishing from his father; he also learned to gaze at the stars and, above all, he developed the practical turn of mind, manual skill, intellectual curiosity and ingenuity which would mark his personality. His paternal grandfather, an educated man, gave him an appetite for studying and taught him the basics in Vietnamese and arithmetic. But, having been deprived of schooling up to the age of 12, he failed the entrance exam to the French Lycée of Hanoi because his French was not good enough. Thus, Bui (as we used to call him) attended a private school for three years and then spent two more years as a self-educated young man, which resulted in an easy success at the Baccalauréat exam in 1955. Because he was noticed as a student of exceptional intelligence he was awarded one of the few scholarships to study in France in the preparatory classes for the Grandes Écoles. So he entered the "Math Sup" class of Professor Jean Itard (otherwise well-known as a historian of mathematics) in Lycée Henri IV (Paris), almost one quarter late due to administrative delays. After one more quarter, he had made up for this handicap and, after one year of "Math Spe", he entered the École Polytechnique in 1957. He graduated in 1959 and then entered the École Nationale Supérieure des Mines of Paris for a two-year specialised program. Bui's scientific career would then begin.
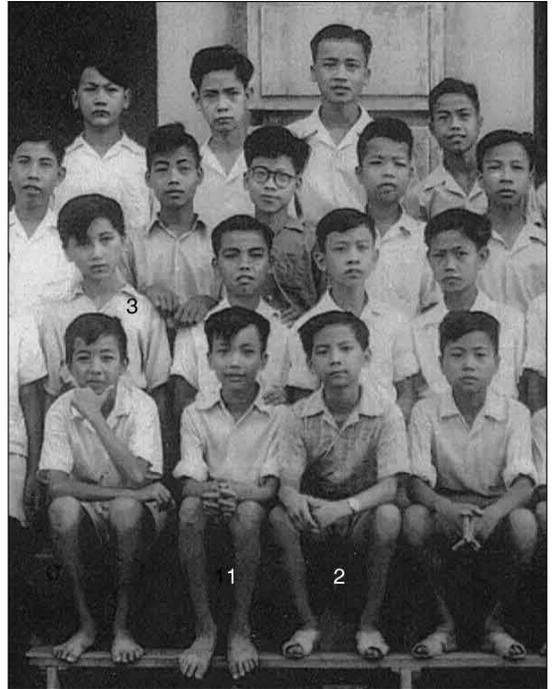
H. D. Bui (1) and two cousins (2, 3) in 1949.

In a biographical text which he regularly updated until a few months before he died, Bui goodhumouredly reveals that it was his failure to pass the "little psychotechnical tests, really just disjointed children's games" that were then much in vogue, during an IBM hiring interview, which led him in

December 1961 to the Solid Mechanics Laboratory at the École Polytechnique, which Professor Jean Mandel had just founded.

Bui's admission to this nascent laboratory was not without practical difficulties, but they were eventually solved with his hiring by the electric utility company Électricité de France (EDF) to perform studies in solid mechanics relevant to nuclear power plants, then still in the planning stages. In fact, Bui's scientific career is intimately tied to this laboratory, where he remained throughout his life in various administrative positions. This unusual situation, maintained thanks to the far-sightedness of successive directors of EDF Direction des Études et Recherches (DER), largely explains the nature of Bui's scientific work, which was motivated, if not guided, by the research needs of the French energy supply programme.

Apart from its extent and consistency, Bui's scientific work has been characterised from the beginning by its elegance and subtlety. It falls squarely within the mechanics of deformable solids, but not without incursions into fluid mechanics when necessary for the analysis of coupled problems. His scientific contributions can be grouped into four main fields: mechanics of materials, fracture mechanics, numerical methods with a special emphasis on boundary integral equations, and inverse and identification problems. This classification will serve as a useful guide in this outline, although it tends to hide the logical and chronological development and interconnected of Bui's interests, which blends results he obtained in all these different fields.

Mechanics of materials. Bui's PhD thesis, defended in 1969, dealt with the elastoplastic behaviour of metals. Motivated by the research programme linked to the Mediterranean gas pipeline, it contains in embryo several topics in which Bui was later to excel. First, it was an experimental study which Bui designed and performed personally: starting from the initial boundary of the elastic domain he established the work-hardening evolution of the yield surface according to the incremental load applied to the specimen. For this, Bui devised and carried out combined tension-compression and torsion tests on aluminium, iron and copper thin tubes; he introduced disruptive metrological advances which allowed him to gain at least one order of magnitude on the permanent strain offset. This point constituted an essential breakthrough; it must be well understood that the boundary of the elastic domain in a given work-hardening state can only be determined from the detection of new permanent strains observed along various loading paths, and that these new permanent strains themselves modify the hardening state at the same time! In particular, the results obtained, which were completely novel and are now referred to as seminal, showed an unexpected behaviour during the early stages of work-hardening which was contrary to the Bauschinger effect. They also allowed the investigation of the influence of the loading path, the occurrence of corners on the yield surface and the relevance of the "normality rule". Moreover Bui developed in his thesis a theoretical analysis in the same spirit as Hill and Mandel: through a pioneer approach of "homogenisation of random media" he made up a physical model which could explain the overall elastoplastic behaviour of the metallic polycrystal he had investigated experimentally, from the single crystal behaviour.

At the end of the 70s, Bui resumed working in mechanics of materials under the pressure of the research programme on the constitutive equations of steels used in the EDF power plants, with a special interest in the critical aspects of damaging and fracture and in the "micro-macro" relationships. Then, during the 90s, he became interested in the micromechanics of solid surfaces, the discontinuity interfaces of materials — such as welds — or load discontinuities — such as thermal shocks. Concerning this latter

topic, he brought to light the (very localised, bounded, discontinuous, with an unbounded gradient) stress singularity he named "the thorn singularity"; this concept made it possible to explain observed superficial damaging phenomena, such as thermal crazing, and constituted an advance, followed by others, towards the control of superficial damaging phenomena of materials.

To finish with this topic, which has essential industrial applications, it is worth mentioning that Bui made important technical contributions by putting his scientific expertise to use in helping to draft the building code for the construction of fast neutron nuclear power plants. He was also involved, as the EDF project manager, in the Brite-Euram contract on fibre-reinforced concrete, a subject motivated by the early damages observed on some cooling towers. Bui also took part in the investigation of mechanical and rheological problems posed by the underground storage of radioactive waste; his skills in combining theory, numerical computations and in situ tests proved very useful in that research.

Fracture mechanics. Bui got interested in fracture mechanics soon after his thesis. Following the main trend of research at that time, he devoted himself to the characterisation of singularities at the crack tip in order to derive the stress intensity factors, a key tool in brittle fracture mechanics:

— He stated a conservation law dual to that established by Eshelby in 1956.
— He constructed the invariant integral I dual to the J integral of Rice and Cherepanov, so as to make it possible to get numerical upper and lower bounds of their common value.
— He constructed two invariant integrals which allowed him to separate fracture modes I and II in the J integral (these results were implemented in CEA and EDF computer code).
— With a view toward applications to thermoelastic fracture mechanics, he established a method for the construction of a "divergence-free" conservation law for problems that naturally exhibit a source term, which makes the accurate computation of singularities easier.

Together with Amestoy and Dang Van, using multiple-scale techniques and matched asymptotic expansions, Bui gave an analytical solution to the problem of a bifurcated crack, which had only been treated numerically before; later he completed this result with Amestoy and Leblond for the case of a curved bifurcated branch. With Ehrlacher and Nguyen, he stated the logarithmic singularity of the temperature field due to the point heat source which appears at the tip of a crack propagating in an elastic solid — a result that conformed with the experimental evidence then available, which he confirmed through his own experiments. The introduction of a decohesion law with a threshold in the constitutive equations of an elastic material allowed Bui and Ehrlacher to derive analytical solutions to the quasistatic and dynamic crack propagation problems in mode III (mathematical problem of a free boundary between the damaged zone and the still elastic zone) and, incidentally, to solve Rice's paradox in the theory of ductile fracture for a perfectly plastic material.

1967
Fresnes

To investigate dynamic fracture, Bui originated what is called the compact compression specimen (also known as the "clothes peg" specimen), which proved itself a remarkably effective tool of experimental analysis, and he used it in the study of the leakage flow rate through cracks. So, he was led to study various aspects of fluid-crack interactions taking surface tension into account, especially for nuclear power plant safety. Let us briefly quote the results he obtained in the field of hydraulic fracturing: a model of two-dimensional flow of a viscous fluid at the tip of a motionless crack, which can remove the pressure singularity induced by classical modelling; a model of the interaction for a propagating crack introducing the capillary tension and assuming void formation between the fluid convex meniscus and the crack tip: the coupled problem was solved numerically and brought the flow two-dimensional structure to light. Bui was recognised as an expert for these problems which now have numerous industrial applications.

Bui was one of the world leaders in the field of brittle fracture mechanics. The book he published in 1978 is still authoritative today.

Boundary integral equation methods. This topic is obviously closely connected to the preceding ones. First, Bui noticed some anomalies in the numerical results obtained in thermo-elastoplasticity; reconsidering the integral equations currently used by researchers and engineers, he showed that the corresponding integral kernel was not complete, and restored the exact equations by adding a point distribution. Later on, he investigated this field again; he tackled dynamic problems and, with Bonnet and Loret, he exhibited a very simple regularisation method for the singular elastodynamics integral equations, which led to higher accuracy in its numerical implementation. This method has been used, among others, by Madariaga (IPG, Institute of Earth Physics of Paris) and Bonnet in a paper published in Wave Motion in 1991. In a later paper, Bui proposed a nonsingular variational method which saves symmetry and yields an a posteriori error indicator.

Inverse problems and identification. On this fourth main topic, Bui published the book *Inverse problems in the mechanics of materials: an introduction* in 1993. It has been translated from French into, among other languages, English, Japanese, Chinese and Russian. Paul Germain, who wrote the preface to the French original, called it a "tour de force": "The ability to fully expound in under 230 pages such a difficult body of knowledge can only be the result of wide and deep learning . . . that feeds a thought process involving the constant reworking of acquired knowledge; it is also founded, crucially, on personal experience of the applications and methods exposed in this book". Indeed, Bui did not lack personal experience in this field, but it is mainly his geometrical mind, rich with the notions of duality, symmetry and reciprocity, that inspired his dazzling intuitions and his singularly elegant treatments; at the same time, his mathematical ability allowed him to find disconcertingly simple analytical solutions to problems where so many others rushed in with numerical approaches. Thus, he was able to solve many problems related to crack, fault or matter lack detection or the reconstruction of load paths. A few examples:

— a direct analytical derivation of the dynamic stress intensity factor from the experimental measurement of forces and velocities applied at the surface, by solving a convolution equation (Bui and Maigre);

— the partition of kinetic, elastic and dissipated energies in a problem of crack propagation when the applied force, associated velocity, and crack length and opening are known experimentally;

— the identification of the elastic moduli tensor field in an inhomogeneous solid body from just measurements of forces and displacements at the boundary. Up to then, the available results only

concerned the isotropic material and Bui showed that the identification was possible up to 6 elastic constants.

It was once more at EDF's instigation that Bui got involved in the study of the inversion of microgravity data which were measured on the Pyramid of Cheops: he diagnosed the presence of hollow internal spirals which, several years later, could be related to the construction theory with spiral internal ramps proposed by the architects Henri and Jean-Pierre Houdin.

Bui trained a great number of young researchers and engineers. He succeeded in passing on not only his scientific knowledge and know-how but also his enthusiasm for research and passion for bringing together science and industry, theory and experiments, and basic and applied research. EDF is in his debt not only for his contribution to the development of the Mechanics and Numerical Models Department and the LaMSiD, a mixed EDF-CNRS research unit, and for his scientific expertise and penetrating analyses of scientific and technological progress, but above all for the exceptional human contingent that he built up through his research on the key problems of nuclear industry. The author of more than 100 papers and 4 books, some of which were translated into 7 languages, he not only helped advance the state of the art on most of the great topics in solid mechanics of the last fifty years, but also made a major contribution to the expansion of nuclear technology and to the success of the French nuclear industry.

His scientific portrait would not be complete if his personality were not evoked too, a personality made of discretion and scientific curiosity, of reserve and human warmth, of enthusiasm and modesty, of understanding and compassion towards others. This is unanimously attested to not only by his co-workers, researchers, students, engineers, technicians and administrative people, but also by a number of doctoral students under the guidance of other advisors who knew that his office door was always open when they needed scientific advice or comfort amid difficulties. This is also true for his fellow doctoral students in the Laboratory of Mechanics, including the undersigned, who, to various degrees, have benefited from his interest and advice, suggestions or recommendations, concerning theory, bibliography, experiments or methodology.

Georges Charpak bestowed nobility on the word "handyman": in this sense, we can qualify Bui as a "handyman of genius" as well as an outstanding theoretician. We all retain Bui's memory as a figure who radiated intelligence and ingenuity as well as kindness and generosity.

Bui had been suffering for a long time from asthma, which gradually made his voice fainter and fainter, but he died of a serious disease which was only diagnosed in November 2012. He accepted this illness not with resignation but with philosophy; shortly before he died, he wrote to his dearest and nearest: "For me, death is the continuation of life in another form." He passed away with serenity and confidence.

In the conclusion of the 2013 edition of his memoirs, which he gathered under the title "Schrödinger's cat in quantum mechanics and its double in solid mechanics", he thanked all his co-workers and the personalities who helped him for the progress of his career and he wrote this especially touching dedication:

> *To the memory of my father and my mother; she was lost with so many other "boat people" in the China Sea.*

Following his wishes, his own ashes were scattered in that same China Sea.

Jean Salençon and André Zaoui
October 2014

HUY DUONG BUI

Huy Duong Bui, membre de l'Académie des sciences est décédé le 29 mai 2013 à l'âge de 76 ans. Il était membre fondateur de l'Académie des technologies, membre de l'Acadḿie européenne des sciences (EURASC) et Fellow de l'Institute of Physics (Londres). Il était aussi Chevalier dans l'Ordre national de la légion d'honneur.

Huy Duong Bui était né à Hanoi le 18 mars 1937. Enfant, au Vietnam, il fut longtemps tenu éloigné de la ville et privé d'école par de dures années de guerre, d'inondations et de famine : réfugié à la campagne avec sa famille, il y avait appris de son père la chasse et la pêche, il avait aussi contemplé les étoiles et, surtout, développé un sens pratique, une habilité manuelle, une curiosité et une inventivité qui allaient marquer sa personnalité. Son grand-père paternel, un « lettré », lui donna le goût d'étudier et lui enseigna les bases du vietnamien et de l'arithmétique. Privé d'école jusqu'à l'âge de 12 ans, son niveau insuffisant en français lui fermait les portes du lycée français de Hanoï et c'est en suivant pendant 3 ans des cours privés, puis en étudiant pendant 2 ans en autodidacte, que Bui (c'est ainsi que nous avions coutume de l'ap-

peler) réussit brillamment au baccalauréat en 1955. Remarqué pour son intelligence exceptionnelle, il obtint alors une des rares bourses d'étude en classes préparatoires et intégra le 25 novembre, soit avec presqu'un trimestre de retard, la classe de mathématiques supérieures du lycée Henri IV du professeur Jean ITARD (bien connu par ailleurs comme historien des mathématiques). En un trimestre ce handicap était rattrapé et, après une année de mathématiques spéciales, Bui était reçu dans la promotion 1957 de l'École polytechnique. Sorti en 1959, il entrait à l'École nationale supérieure des mines de Paris pour une spécialisation de deux ans. La carrière scientifique de Bui allait ensuite commencer.

Dans une notice qu'il a tenue à jour jusque peu de temps avant son décès, Bui révèle avec amusement que c'est le fait d'avoir échoué aux « petits tests psychotechniques, jeux d'enfants mal enchainés » qui étaient alors très en vogue, lors de son entretien d'embauche chez IBM qui l'a
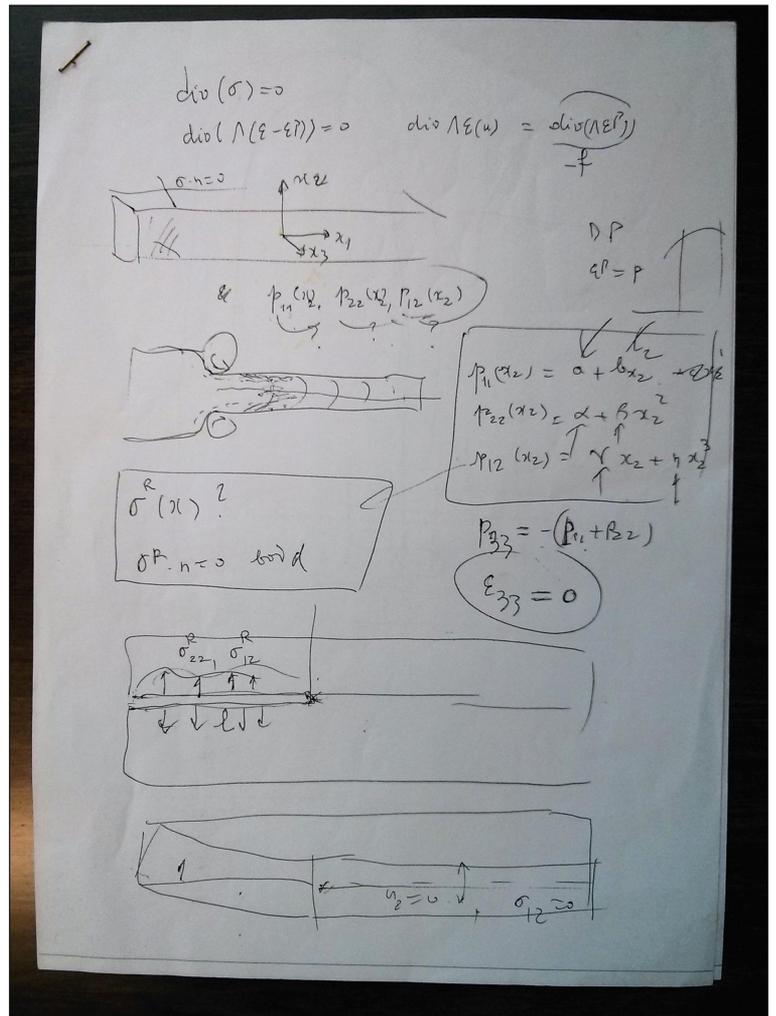
conduit en décembre 1961 au Laboratoire de mécanique de l'École polytechnique que venait de fonder le professeur Jean Mandel.

L'entrée de BUI dans ce laboratoire naissant posait des difficultés matérielles qui furent opportunément résolues par EDF en l'embauchant pour réaliser des études en mécanique des solides destinées aux futures centrales nucléaires. En fait la carrière scientifique de BUI est attachée à ce laboratoire où il a toujours été présent, dans des positions administratives diverses. Cette situation originale, permise par la clairvoyance de directeurs successifs de la Direction des Études et Recherches (DER) d'EDF, explique, pour une bonne part, la nature des travaux scientifiques de BUI : motivés, sinon guidés, par les besoins de recherche du programme énergétique français.

Indépendamment de son ampleur et de sa cohérence, l'œuvre scientifique de BUI se caractérise, dès ses premiers travaux, par l'élégance et la subtilité. Elle se situe sans ambiguïté en mécanique des solides déformables, sans pour autant négliger, lorsque cela se révèle nécessaire, des incursions dans le domaine de la mécanique des fluides pour l'analyse de problèmes couplés. On peut regrouper ces travaux scientifiques en quatre grands domaines : la mécanique des matériaux, la mécanique de la rupture, les méthodes numériques par équations intégrales de frontière, les problèmes inverses et les problèmes d'identification. Une telle classification a certes le mérite de structurer l'exposé mais peut aussi occulter le cheminement logique et chronologique des travaux de BUI qui mêle les résultats obtenus dans ces domaines.

Mécanique des matériaux. La thèse de BUI, soutenue en 1969, portait sur l'élastoplasticité des métaux. Motivée par le programme de recherche lié au gazoduc transméditerranéen, on y trouve en germes plusieurs des sujets sur lesquels BUI allait, par la suite, exceller. C'est d'abord une étude expérimentale, menée par BUI lui-même, pour déterminer l'évolution de la frontière du domaine d'élasticité des métaux par écrouissage à partir du domaine d'élasticité initial, suivant la nature de la sollicitation incrémentale imposée au matériau. BUI avait pour cela conçu et réalisé des expériences en traction-compression et torsion sur des tubes minces d'aluminium, de fer, de cuivre avec une avancée métrologique significative qui lui faisait gagner au moins un ordre de grandeur sur l'accroissement de déformation permanente qu'il pouvait détecter. Il s'agissait là d'une percée essentielle : il faut en effet bien comprendre que la détermination de la frontière du domaine d'élasticité dans un état d'écrouissage donné ne peut se faire qu'en détectant, pour divers trajets de chargement, l'apparition de déformations permanentes nouvelles, mais que ces mêmes déformations permanentes modifient immédiatement l'état d'écrouissage ! Les résultats obtenus, totalement originaux, auxquels il est encore fait référence à ce jour, ont notamment mis en évidence dans les tout premiers pas de l'écrouissage un effet inattendu, contraire à l'effet BAUSCHINGER. Ils ont aussi permis d'examiner l'influence du trajet de charge, l'apparition de point coniques, et la pertinence de la « règle de normalité ». Dans cette même thèse, BUI a développé une analyse théorique, dans la ligne des préoccupations de HILL et MANDEL à l'époque, où il a construit, par une démarche pionnière « d'homogénéisation des milieux aléatoires » un modèle physique expliquant, à partir du comportement du monocristal, le comportement qu'il avait observé pour le polycristal métallique élastoplastique.

BUI est revenu à la mécanique des matériaux vers la fin des années 70 sous la pression du programme de recherche sur les lois de comportement des aciers utilisés dans les centrales EDF, en s'intéressant particulièrement aux aspects cruciaux de l'endommagement et de la rupture et aux relations « micro-macro ». Puis, dans les années 90, il s'est intéressé à la micromécanique près de la surface d'un solide, aux interfaces de discontinuités des matériaux — telles que les soudures — ou du chargement — telles que

le choc thermique. C'est à ce propos qu'il a mis en évidence la singularité de contrainte dite « Épine », (très localisée, bornée, discontinue, à gradient non borné) qui permettait d'expliquer les phénomènes de dégradation superficielle observés, tels que le faïençage thermique, et constituait une avancée, suivie par d'autres, vers la maîtrise des phénomènes d'endommagement superficiels des matériaux.

Pour en terminer avec ce domaine, dont les applications industrielles sont essentielles, on peut signaler que BUI a su mettre ses compétences scientifiques au service de l'application technique en participant à la rédaction du très important code de construction des centrales nucléaires à neutrons rapides. Il a participé, en tant que Chef de projet EDF, au contrat BRITE-EURAM sur le béton renforcé de fibres, sujet motivé par la dégradation trop rapide de certaines tours de réfrigération. BUI est aussi intervenu dans les problèmes mécaniques et rhéologiques liés au stockage souterrain des déchets radioactifs : il a apporté au groupement d'études concerné son habileté à marier théorie, calculs numériques et essais in situ.

Mécanique de la rupture. BUI s'est intéressé à la mécanique de la rupture dès après sa thèse. Suivant la ligne de recherche privilégiée à l'époque, il s'est attaché à la caractérisation des singularités en fond de fissure pour déterminer les facteurs d'intensité de contrainte, essentiels en mécanique de la rupture fragile. Il a ainsi :
— énoncé la loi de conservation duale de celle établie par ESHELBY en 1956 ;
— construit l'intégrale invariante I duale de l'intégrale J de RICE et CHEREPANOV, permettant ainsi l'encadrement numérique de leur valeur commune ;
— construit les deux intégrales invariantes qui permettent de découpler, dans l'intégrale J, les modes de rupture I et II (résultats qui furent implantés dans les codes de calcul CEA, EDF) ;
— établi, pour les applications à la mécanique de la rupture thermoélastique, une méthode de construction d'une loi de conservation de type « divergence nulle » pour les problèmes qui se présentent naturellement avec un terme de source, ce qui facilite le calcul précis des singularités.

En appliquant les techniques des échelles multiples et des développements asymptotiques raccordés, avec AMESTOY et DANG VAN, BUI a résolu analytiquement le problème de la fissure déviée qui n'était jusque-là abordé que par voie numérique ; il a complété ce résultat par la suite avec AMESTOY et LE-BLOND dans le cas où la branche déviée est courbe. Avec EHRLACHER et NGUYEN, il a établi la singularité logarithmique du champ de température due à la source ponctuelle de chaleur qui apparaît à la pointe d'une fissure en propagation dans un solide élastique : résultat conforme aux évidences expérimentales disponibles alors, qu'il a aussi confirmé par ses propres expériences. Par l'introduction d'une loi de décohésion à seuil dans les équations de comportement du matériau élastique, BUI et EHRLACHER ont mis en évidence des solutions analytiques pour les problèmes de propagations quasi-statique et dynamique des fissures en mode III (problème mathématique à frontière libre séparant la zone endommagée de la zone encore élastique) levant, à cette occasion, le paradoxe de RICE en théorie de la rupture ductile pour le matériau parfaitement plastique.

Pour l'étude de la rupture dynamique, BUI a inspiré l'invention de l'éprouvette en « pince à linge » qui s'est révélée un outil remarquable d'analyse expérimentale, permettant aussi l'étude du débit de fuite à travers des fissures. C'est ce qui l'a conduit à étudier divers aspects de l'interaction fluide-fissure en présence de tension superficielle notamment pour la sécurité des centrales nucléaires. Pour être bref on peut retenir les résultats qu'il a obtenus dans le domaine de la fracturation hydraulique : modèle d'écoulement bidimensionnel du fluide visqueux à la pointe d'une fissure immobile qui permet de faire

disparaître la singularité en pression induite par les modèles classiques ; pour la fissure qui se propage, modélisation de l'interaction en introduisant la tension capillaire et en supposant l'existence d'un vide entre le ménisque convexe de fluide et la tête de la fissure : le problème couplé a été résolu numériquement, mettant en évidence la structure bidimensionnelle de l'écoulement. Cette compétence a fait de BUI un expert reconnu pour ces problèmes dont les applications industrielles sont nombreuses comme l'actualité ne manque pas de nous le rappeler.

BUI était un des « très grands » de la Mécanique de la rupture fragile. Son livre, publié en 1978 fait encore autorité de nos jours.

Méthodes des équations intégrales de frontières. Ce domaine est évidemment très lié aux précédents. En thermo-élasto-plasticité BUI, constatant les anomalies des résultats numériques, a réexaminé les équations intégrales jusque là utilisées par les chercheurs et les ingénieurs, montré que le noyau intégral en était incomplet et rétabli les équations exactes en rajoutant une distribution ponctuelle. Il a repris ultérieurement ce domaine de recherche, abordé les problèmes dynamiques et, avec BONNET et LORET, mis en évidence une méthode très simple de régularisation des équations intégrales singulières de l'élastodynamique aboutissant à une grande précision dans la mise en œuvre numérique. Cette méthode a été utilisée notamment par MADARIAGA (IPG) et BONNET dans un article paru en 1991 dans Wave Motion. Dans un article ultérieur BUI a proposé une méthode variationnelle, non singulière, qui préserve la symétrie et fournit un indicateur d'erreur a posteriori.

2003 Washington DC

Problèmes inverses et identification. Sur ce quatrième grand thème, BUI a publié en 1993 un livre intitulé Introduction aux Problèmes Inverses en Mécanique des Matériaux qui a fait l'objet, notamment, de traductions en anglais, japonais, chinois et russe, ouvrage qualifié par Paul GERMAIN dans sa préface de « tour de force » : « exposer en moins de 230 pages et de façon complète un ensemble aussi difficile ne peut être le fruit que d'une culture vaste et approfondie [...] nourrissant une réflexion personnelle qui repense constamment toutes les connaissances acquises et aussi, sans doute ici le point essentiel, d'une expérience personnelle des applications et des méthodes présentées dans l'ouvrage ». Il est de fait que BUI ne manquait pas sur ce sujet d'expérience personnelle mais c'est bien son esprit géométrique, nourri des notions de dualité, de symétrie et de réciprocité qui lui a inspiré ses intuitions fulgurantes et ses traitements d'une rare élégance, en même temps que son habileté mathématique lui a permis de trouver des solutions analytiques d'une simplicité déconcertante là où d'autres s'engouffraient dans les seules approches numériques. Il a ainsi pu résoudre quantité de problèmes de détection de fissures, de

localisation de failles ou de défaut de matière comme de reconstitution de trajets de chargement. À titre d'exemples :

— l'obtention analytique directe du facteur d'intensité dynamique des contraintes à partir des mesures expérimentales des forces et des vitesses appliquées à la surface du solide, par la résolution d'une équation de convolution (BUI et MAIGRE) ;

— la séparation des énergies cinétique, élastique et dissipée dans un problème de propagation de fissure si l'on connaît expérimentalement la force appliquée et la vitesse correspondante et aussi la longueur et l'ouverture de la fissure.

— L'identification du tenseur des modules d'élasticité dans un solide non homogène à partir des seules mesures à la frontière : forces et déplacements connus. Les résultats disponibles se limitaient au cas du matériau isotrope (2 modules) et BUI a montré que l'identification était possible jusqu'à 6 coefficients d'élasticité.

C'est encore à l'instigation d'EDF que BUI s'est intéressé à l'inversion de données de microgravimétrie acquises sur la pyramide de Chéops, diagnostiquant la présence de spirales internes évidées qui, plusieurs années plus tard, put être mise en relation avec la théorie de la construction par rampe spirale interne proposée par les architectes Henri et Jean-Pierre HOUDIN.

BUI a formé de très nombreux jeunes chercheurs et ingénieurs, à qui il a su communiquer non seulement son savoir et son savoir-faire scientifiques mais aussi son enthousiasme pour la recherche et sa passion pour le rapprochement entre science et industrie, entre théorie et expérience, entre recherche de base et recherche appliquée. À EDF il a apporté, au-delà de sa contribution au développement du Département Mécanique et Modèles Numériques ou du LaMSiD, Laboratoire commun EDF/CNRS, son

expertise scientifique, ses analyses visionnaires sur l'évolution des sciences et des techniques et surtout le capital humain exceptionnel qu'il a su former par la recherche sur des problématiques clés de l'industrie nucléaire. Auteur de plus de 100 articles et de 4 livres dont certains traduits en sept langues, il a non seulement fait avancer la plupart des grands thèmes de la mécanique des solides de ces cinquante dernières années mais aussi apporté une contribution de premier plan à l'essor des technologies nucléaires et aux succès de l'industrie nucléaire française.

Son portrait scientifique serait incomplet si n'était aussi évoquée sa personnalité, toute de discrétion et de curiosité scientifique, de réserve et de chaleur humaine, d'enthousiasme et de modestie, de compréhension et de compassion pour autrui. En témoignent unanimement non seulement ses collaborateurs directs, chercheurs, doctorants, ingénieurs, techniciens et administratifs, mais aussi nombre d'étudiants en cours de thèse sous la direction d'autres chercheurs qui savaient trouver sa porte toujours ouverte pour y recevoir conseils scientifiques mais aussi réconfort face aux difficultés, sans oublier ses premiers condisciples en cours de thèse, comme lui, au Laboratoire de Mécanique, qui, à des degrés divers, ont, comme les signataires de cette notice, bénéficié de son intérêt et de ses conseils, suggestions ou recommandations, tant sur le plan théorique et bibliographique qu'expérimental et méthodologique.

Georges CHARPAK a su donner au mot « bricoleur » des lettres de noblesse qui nous permettent de qualifier BUI de « Bricoleur de génie » en même temps que de théoricien hors pair. BUI laisse à tous le souvenir d'une personnalité irradiant l'intelligence et l'ingéniosité en même temps que la bienveillance et la générosité.

Si BUI souffrait depuis de longues années d'un asthme qui avait peu à peu éteint sa voix, c'est une grave maladie, diagnostiquée en novembre 2012, qui l'a emporté. Il a accepté cette maladie, non pas avec résignation mais avec philosophie ; peu avant sa mort il écrivait à ses proches « Pour moi la mort c'est la continuation de la vie sous une autre forme ». Il s'est éteint en sérénité et en confiance.

En conclusion de l'édition 2013 de ses souvenirs rassemblés sous le titre « Le chat de Schrödinger en mécanique quantique et son double en mécanique des solides », après avoir remercié tous ses collaborateurs et collaboratrices ainsi que les personnalités qui lui avaient apporté leur aide dans le déroulement de sa carrière, BUI a inscrit la dédicace suivante, particulièrement émouvante :

> *À la mémoire de mon père et de ma mère, disparue avec tant d'autres « boat people »*
> *en Mer de Chine.*

Selon son vœu, ses propres cendres ont été dispersées dans cette même Mer de Chine.

Jean Salençon et André Zaoui
Octobre 2014

JEAN SALENÇON: jean.salencon@polytechnique.org
Laboratoire des Mécanique des Solides, École Polytechnique, 91128 Palaiseau CEDEX, France

ANDRÉ ZAOUI: andrezaoui@orange.fr
Laboratoire des Mécanique des Solides, École Polytechnique, 91128 Palaiseau CEDEX, France

msp

THE RECIPROCITY LIKELIHOOD MAXIMIZATION:
A VARIATIONAL APPROACH OF THE RECIPROCITY GAP METHOD

STÉPHANE ANDRIEUX

We introduce a new concept allowing the recasting of the reciprocity gap method into a variational method. The reciprocity likelihood functional maximization gives rise to nested approximation properties when performed on minimization spaces with increasing dimensions and leads to direct identification methods grounded on the reciprocity property. Application to the identification of point sources is given for illustration of the solution procedure of identification, and an analysis of the effect of noisy data shows that the proposed methods exhibit very good robustness.

1. Identification problems and results with the reciprocity gap method

The kind of identification or inverse problems addressed here is the following:

given: a solid Ω and a physical phenomenon described by a linear "equilibrium" operator A acting on vector fields u, defined in the solid, and provided a pair of data $u = U^m$ and $Bu \cdot \boldsymbol{n} = F^m$ is known on the whole external boundary of the solid $\partial\Omega$, with external outside unit normal $\boldsymbol{n}$, for a field satisfying $Au = 0$,

determine: the eventual sources or objects buried inside the solids (cracks, flaws, holes, inclusions, etc.).

Examples of such equilibrium operators are the Laplace operator, describing isotropic conduction of heat or electricity, the Lamé operator in the elastostatic framework, the Helmholtz operator in acoustics, the Darcy operator for saturated porous media, etc. Although the reciprocity gap method can be applied to nonsymmetric or non-self-adjoint operators, where the reciprocity property does not directly hold, the reciprocity likelihood concept is developed for symmetric or self-adjoint ones.

B is the natural (or Neumann) boundary condition operator associated with A. The data usually comes from an experiment performed on the solid, for example, by prescribing a flux or an external force on the solid and measuring the response on the boundary. Unlike other kinds of inverse problems, the whole Neumann-to-Dirichlet map or Poincaré–Steklov operator is not supposed to be known, even if one can have access to more than one single experiment (or data pair). On the other hand, data on the whole boundary is supposed to be available. These data form a redundant data pair with respect to the operator A (namely Dirichlet and Neumann boundary data available simultaneously on the boundary).

Practical identification is achieved through identification procedures. Various propositions appeared in the literature; they can be separated into two broad classes that we shall quickly review in the particular case of crack-identification problems with the Laplace equation although similar methods and results have been obtained for other operators, namely acting on vector fields, as in elasticity.

First are direct iterative methods grounded on a variational property of the solution: after designing a functional of the geometrical parameters describing the cracked domain, iterative resolutions of Laplace problems are performed in order to minimize (or get a stationary point of) the functional. To this class belong classical least-squares methods or more sophisticated functional-minimization methods as adaptations of the functional of [Kohn and Vogelius 1984]. This class relies on a lot of resolutions of elliptic problems, which are generally costly and always need the introduction of the point of departure of the algorithm (the initial guess), the choice of which is difficult and can significantly alter the speed of convergence or even the converged solution itself. Moreover, for the identification of geometries, a remeshing of the solid is necessary for each iteration.

The second class of methods uses families of particular fields and avoids any resolution of the PDEs underlying the physical phenomenon used in the identification or uses only a few: auxiliary field methods [Bui 2011]. The reciprocity gap method belongs to this last class of methods sometimes called sampling or probe methods in the inverse scattering community because no resolution of any PDE is needed.

To obtain or to approximate the solution of this kind of identification problem, the reciprocity gap concept has been introduced first for the Laplace operator [Andrieux and Ben Abda 1992; 1993], the concept being suited to symmetric operators as it relies on the reciprocity property. More precisely, the reciprocity gap RG is a linear form acting on auxiliary fields defined on the safe domain (without flaws or source distribution) and satisfying the operator equation. For each auxiliary field picked out of the auxiliary field subspace, the computation of the action of the form RG supplies scalar information on the "difference" between the actual solid and the safe one. The concept has been extended to general operators by using auxiliary fields, which are solutions of the adjoint (or conjugate) operator equation [Andrieux 1995]. A comprehensive introduction to the reciprocity gap concept can be found in [Andrieux and Bui 2011].

Numerous identification results, both theoretical and constructive (identification formulas), have been obtained by using appropriate auxiliary field families. For planar crack identification, results were obtained for the Laplace and Lamé operators [Andrieux and Ben Abda 1992; 1996; Andrieux et al. 1999], for the heat equation [Ben Abda and Bui 2001], for viscoelastic media, in inverse scattering [Bui et al. 1999; Ben Abda et al. 2005; Colton and Haddar 2005], and in elastodynamics with the concept of the instantaneous reciprocity gap [Bui et al. 2004; 2005]. Mention must be made of [Ikehata 1999] using similar concepts but with a different use. For source distribution identification, [El Badia and Ha Duong 1998; El Badia et al. 2000] gave identification algorithms for point sources with the Laplace equation and [Alves and Silvestre 2004] for the Stokes equation.

Recently, Shifrin and Shushpannikov [2010; 2011; 2013b; 2013a] derived results in elasticity for the identification of inclusions in 3D for a single traction experiment, based on approximation of the solution for an infinite medium. This use of the reciprocity gap with an approximate solution is close to the assumption of infinite medium taking advantage of the Eshelby results [1957] proposed for inclusion identification by [Andrieux et al. 2006].

2. Recollection of the reciprocity gap method

Let us recall briefly the reciprocity gap definition and the associated identification method for the simplest case of a scalar isotropic conduction equation. A is the Laplace operator, u is a scalar field, and $\boldsymbol{B}$ is the gradient operator so that on the boundary $\boldsymbol{B}u \cdot \boldsymbol{n} = \nabla u \cdot \boldsymbol{n}$. The bilinear form a associated to the

operator A is

$$a(u, v) = \int_{\Omega} \nabla u \cdot \nabla v \, d\Omega. \tag{1}$$

A collection of cracks $\{\Gamma_i : i = 1, N\}$ can be buried inside the solid, and some source distribution $s(x)$ can also appear so that we have, inside the domain occupied by the solid, the equations

$$\begin{cases} -\Delta u = s & \text{in } \Omega \setminus \Gamma_i, \, i = 1, \ldots, n, \\ \nabla u \cdot \boldsymbol{n}_i = 0 & \text{on } \Gamma_i, \, i = 1, \ldots, n. \end{cases} \tag{2}$$

The problem of identification of the crack geometry and the source distribution is set provided a pair of boundary data is available on the whole external boundary of the domain Ω:

$$\nabla u \cdot n = F^m, \quad u = U^m \text{ on } \partial\Omega. \tag{3}$$

Definition. For any field v belonging to the Sobolev space $H^1(\Omega)$, the reciprocity gap RG is the linear form defined by

$$\text{RG}(v) = \int_{\partial\Omega} (F^m v - \nabla v \cdot \boldsymbol{n} U^m) \, dS. \tag{4}$$

The RG definition uses only the known quantities of the identification problem. The term "reciprocity gap" has been coined after the Betti–Maxwell reciprocity property: for two harmonic fields u and v in the domain Ω, one has

$$\int_{\partial\Omega} (\nabla u \cdot \boldsymbol{n} v - \nabla v \cdot \boldsymbol{n} u) \, dS = 0. \tag{5}$$

The idea here is that the form RG is vanishing on every harmonic field v in Ω if there are neither cracks nor source distributions in the actual solid; it is on the contrary nonzero if some cracks or source distributions exist, measuring then in some sense the "difference" between the safe and the actual solids. More precisely, the following fundamental property of the reciprocity gap holds:

Fundamental property. *For every harmonic field v in Ω, the reciprocity gap has the interpretation*

$$\text{RG}(v) = \int_{\Omega} s v \, d\Omega + \sum_{i=1}^{N} \int_{\Gamma_i} \nabla v \cdot \boldsymbol{n}_i [u] \, d\Gamma_i. \tag{6}$$

In (5), $[u]$ stands for the jump of the field u across the cracks.

The reciprocity gap method consists of selecting appropriate auxiliary harmonic fields v, each of them giving one piece of scalar information about the sources and the cracks or more precisely on the actual field u on the support of the cracks or of the source distribution. For planar cracks lying in a single plane Π with normal N_{Π}, and with $s = 0$, it is easy to see that, using linear fields x^i as auxiliary fields, the normal N_{Π} can be recovered with the explicit formula [Andrieux and Ben Abda 1992]

$$N_{\Pi} = \frac{\text{RG}(x^i) \boldsymbol{e}_i}{\sqrt{\text{RG}(x^1) + \text{RG}(x^2) + \text{RG}(x^3)}}. \tag{7}$$

The formula involves only a straightforward computation of the linear form RG on three fields and does not require any resolution of a partial differential equation. The identification results mentioned in the introduction have been obtained by such ad hoc choices for the auxiliary fields. For example, the complete

identification results for infinite-parameter identification such as geometry of the cracks relies on the choice of a Hilbertian basis of the space of the auxiliary fields fulfilling the operator equation defined by A (here harmonic fields) in the sound domain. The reciprocity gap method is then a constructive method of identification, but a general method for choosing the relevant auxiliary fields is still lacking. That is why we turn to an alternative way of using the reciprocity gap linear form. Before that, a general abstract setting is introduced in the next section.

3. Abstract general form of the reciprocity gap

The abstract form of the reciprocity gap is built from the weak formulation of the physical problem at hand. We suppose thus that we have

- a symmetric bilinear form $a(u, v)$, continuous on a functional (Hilbert) space $W(\Omega \setminus \Gamma)$, where Γ is a collection of (unknown) cracks, and

- two linear and continuous forms, corresponding respectively to natural boundary conditions on the external boundary of Ω and to the interior source distribution,

$$l_f(v) = \int_{\partial \Omega} f v \, dS, \qquad l_s(v) = \int_{\Omega} s v \, d\Omega \qquad (8)$$

so that the weak form of the operator equation is

$$u \in W(\Omega \setminus \Gamma), \qquad a(u, v) = l_f(v) + l_s(v) \quad \text{for all } v \in W(\Omega \setminus \Gamma). \qquad (9)$$

It is assumed here that external solicitation is exerted on neither the crack lips nor the special constitutive equation linking the jumps of the field u to the dual quantity $\boldsymbol{B}u \cdot \boldsymbol{n}$ so that $\boldsymbol{B}u \cdot \boldsymbol{n} = 0$ on the crack lips. The bilinear form a can vanish on a finite-dimensional subspace R of W (rigid body motions in mechanics, constant fields for stationary heat conduction, etc.):

$$r \in R \implies a(r, v) = 0 \quad \text{for all } v \in W(\Omega \setminus \Gamma). \qquad (10)$$

With the bilinear form a coercive on the quotient space of W by R and the operator B on the boundary defined via a Green formula, the solution of (8) is determined up to a field belonging to R and uniqueness is obtained by adding a finite set of linear conditions on the solution. Existence of solutions is ensured provided a compatibility condition on the solicitations f and s is fulfilled:

$$l_f(r) + l_s(r) = 0 \quad \text{for all } r \in R. \qquad (11)$$

For the identification problem, let us assume that the domain $\Omega \setminus \Gamma$, the bilinear form a, and the source distribution s are parametrized by a (possibly infinite) set of parameters p belonging to a parameter space P (we have to assume that when the parameters p are in the space P the coerciveness of a is preserved). The identification problem addressed here is then to determine a set (or several sets) of parameters, provided the value of the field u and its dual counterpart $\boldsymbol{B}u \cdot \boldsymbol{n}$, (U^m, F^m), are given on the whole external boundary $\partial \Omega$ of the solid:

$$\text{determine } p \in P \quad \text{such that} \quad \begin{cases} a(u, v; p) = l_{F^m}(v) + l_{s(p)}(v) & \text{for all } v \in W(p), \\ l_{F^m}(r) + l_{s(p)}(r) = 0 & \text{for all } r \in R, \\ u|_{\partial \Omega} = U^m. \end{cases} \qquad (12)$$

This formulation encompasses the cases of crack identification (the parameters p are describing the geometry of the cracks), source distribution identification (parameters p describe both geometry of the support and intensity), and inclusion identification (the parameters p describe the geometry of the support and value of the contrast of material properties in the bilinear form a).

In this context, a enjoys a reciprocity property

$$\left.\begin{array}{ll} a(u_1, v) = l_1(v) & \text{for all } v, \\ a(u_2, v) = l_2(v) & \text{for all } v \end{array}\right\} \implies l_1(u_2) = l_2(u_1)$$

and the reciprocity gap is defined by the residual of the reciprocity property:

$$\mathrm{RG}(v) = l_{F^m}(v) - \int_{\partial\Omega} \boldsymbol{B}v \cdot \boldsymbol{n} U^m \, dS. \tag{13}$$

The RG form does not depend on the parameters p as it is assumed that all the heterogeneities or sources buried inside the solid are strictly in the interior of the domain (the case of an emerging crack has been addressed in [Andrieux et al. 1998]). The space of auxiliary fields to be used in the reciprocity gap method is simply $W(\Omega)$, and the fundamental property reads:

Fundamental property. *For every v in $W(\Omega)$ fulfilling the equation*

$$a(v, w) = l_{\boldsymbol{B}v\cdot\boldsymbol{n}}(w) \quad \text{for all } w \in W(\Omega), \tag{14}$$

the reciprocity gap has the interpretation

$$\mathrm{RG}(v) = \sum_{i=1}^{N} \int_{\Gamma_i} \boldsymbol{B}v \cdot \boldsymbol{n}_i [u] \, d\Gamma_i - l_{s(p)}(v) - \Delta a(u, v; p), \tag{15}$$

where $\Delta a(u, v; p) = a(u, v; p) - a(u, v; 0)$ with the convention that $p = 0$ corresponds to the sound solid.

This property is grounded on the symmetry of the bilinear form a. The interpretation of the RG linear form makes more precise the nature of the information brought by its calculation for every auxiliary field. The identification procedure is the same as in the preceding section: select an appropriate family of auxiliary fields and exploit the set of scalar equations obtained by computing the RG form for each field of the family in order to gain information on the parameters p. As already said, there is not yet a systematic way to choose the family and to exploit the information gained on p.

4. General definition and properties of the reciprocity likelihood

The general idea is to search for a variational usage of the reciprocity gap linear form in order to derive the minimization process as the "systematic" way for the identification procedure. For that purpose, we revisit the exploitation of the reciprocity property by using the reciprocity gap not between the actual and the safe solids but between the actual solid and a solid where some flaws exist, corresponding here to a given set of parameters p, say q. It is clear that, if the q parameters coincide with the "true" values p_0, then the reciprocity property is recovered between boundary data and the values on boundary of the auxiliary fields because they are acting on the same solid. Then the reciprocity gap is the null linear form on the subspace of auxiliary fields satisfying the operator equation in the solid Ω with parameters q. Conversely, if the reciprocity gap is not the null form, then a parameter set leading to a lower value of

the norm of RG must be preferred to a parameter set leading to higher values of the norm. The opposite of the square of the norm of RG will be called the reciprocity likelihood, and the proposed identification procedure will consist of maximizing the reciprocity likelihood over the parameter space P (that is, minimizing the norm of RG).

Let us define the vector space V_q of auxiliary fields fulfilling the equilibrium equation in the solid $\Omega(q)$ parametrized by the set of parameters q and furthermore canceling the linear form related to the source distribution $s(q)$, W_0, the space of fields with a null trace on the external boundary:

$$V_q = \{v \in W[\Omega(q)] : a(v, w; q) = 0 \text{ for all } w \in W_0[\Omega(q)], \ l_{s(q)}(v) = 0\}, \tag{16a}$$

$$W_0(q) = \{h \in W[\Omega(q)] : h|_{\partial\Omega} = 0\}. \tag{16b}$$

It is now clear that, for any given parameters q, the reciprocity gap does not vanish on V_q, but the following property establishes that the set of parameters q causing the RG form to vanish on the V_q space is exactly the set of parameters that are likely with respect to the data or measurements at hand:

Optimality of the reciprocity gap. *Let p_0 be a set of parameters such that the reciprocity gap vanishes on V_{p_0}.*

If the source distribution is zero or if the source distribution is nonzero but there exists no field of R except zero that vanishes on the external boundary $\partial\Omega$ of the solid,

$$(r \in R \text{ and } r|_{\partial\Omega} = 0) \implies r = 0, \tag{17}$$

then there exists a field v_0 in $W(p_0)$ satisfying

$$\begin{cases} a(v_0, w; p_0) = l_{s(p_0)}(w) & \text{for all } w \in W_0(p), \\ v_0|_{\partial\Omega} = U^m, \ \boldsymbol{B}v_0 \cdot \boldsymbol{n}|_{\partial\Omega} = F^m. \end{cases} \tag{18}$$

This property means that, as soon as the reciprocity gap vanishes on the space V_{p_0}, there exist a collection of cracks, a source distribution, a set of inclusions (described by p_0), and a field v_0 that fulfills the equilibrium equation and meets exactly the values of the given boundary condition pair (U^m, F^m). The proof of this property is given in Appendix A.

The optimality property of RG allows us to propose a new formulation for the identification problem addressed here: search for the space V_{p_0} where the reciprocity gap linear form is zero. To obtain a variational formulation of this problem, i.e., to define a functional or a function on the space P whose minimization or maximization will furnish candidates for the identified parameters, a natural way is to use the norm of the linear form RG on the linear space V_p. The lower the value of this norm, the greater the likelihood of the parameters p with respect to the data at hand so that we shall define the opposite of the square of the RG norm as the *reciprocity likelihood functional* (as a function of p). The solution procedure will be to maximize it over P. In order to give meaning to the norm of RG on the space V_p, it is necessary to establish the following topological properties:

Topological properties of RG and V_p. *Assume the following for every p in P:*

(i) *$W(p)$ is a Hilbert space with scalar product and norm denoted by*

$$\langle u, v \rangle_{W(p)}, \qquad \|u\|_{W(p)} = \sqrt{\langle u, u \rangle_{W(p)}}.$$

(ii) *The trace operator $\gamma : W(p) \to T_{W(p)}$ with $v \mapsto \gamma v = v|_{\partial\Omega}$ is continuous: $\|\gamma v\|_{T_{W(p)}} \leq c\|v\|_{W(p)}$.*

(iii) *The bilinear form a is coercive and continuous on V_p:*

there exist $\alpha(p)$ and $\beta(p)$, $0 < \alpha < \beta < +\infty$,

$$\text{such that,   for all } (u, v) \in V_p^2, \quad \begin{cases} \alpha\|v\|_{W(p)}^2 \le a(v, v; p), \\ a(v, u; p) \le \beta\|v\|_{W(p)}\|u\|_{W(p)}. \end{cases}$$

(iv) *The linear form $l_{s(p)}$ is continuous on V_p:*

$$\text{there exists } \eta(p) > 0 \quad \text{such that,   for all } v \in V_p, \quad |l_{s(p)}(v)| \le \eta\|v\|_{W(p)}.$$

Then the linear subspace V_p of $W(p)$ is closed, and the linear form RG is continuous on V_p.

The proof of this property is given in Appendix B. We can now define the *reciprocity likelihood* using the classical definition of the norm of a linear form.

Definition. For p belonging to P, the reciprocity likelihood $RL(p)$ is the opposite of the square of the norm of the linear form RG on the space V_p:

$$RL(p) = -\|RG\|_{V_p}^2 \tag{19}$$

with

$$V_p = \{v \in W(p) : a(v, w; p) = 0 \text{ for all } w \in W_0(p), \ l_{s(p)}(v) = 0\},$$

$$W_0(p) = \{w \in W(p) : \gamma(p) = 0\},$$

$$RG(v) = \int_{\partial\Omega} (F^m v - \boldsymbol{B}v \cdot \boldsymbol{n}U^m) \, dS,$$

$$\|RG\|_{V_p} = \sup_{v \in V_p - \{0\}} \frac{RG(v)}{\|v\|_{W(p)}}.$$

Thanks to the optimality property of RG, the identification problem (12) is equivalent to the maximization of the reciprocity likelihood, and the optimal value of RL is zero:

$$p = \underset{q \in P}{\text{ArgMax}}\, RL(q) \iff p \in P, \quad \begin{cases} a(u, v; p) = l_{F^m}(v) + l_{s(p)}(v) & \text{for all } v \in W(p), \\ l_{F^m}(r) + l_{s(p)}(r) = 0 & \text{for all } r \in R, \\ u|_{\partial\Omega} = U^m. \end{cases} \tag{20}$$

As it can be seen, the variational formulation of the identification problem is quite general. Some illustrations on the specific identification problems for point source distributions will be given in the sequel. Let us have two preliminary remarks.

Remark 1. The reciprocity likelihood maximization method enables one to determine a solution to the identification problem even if the model used (bilinear form a and linear form $l_{s(p)}$) or the parameter space chosen (geometry of the cracks or inclusions, etc.) are only approximations that are not totally compatible with the experimental data (U^m, F^m). Indeed, the maximization will produce a set of parameters that are the most likely in the actual context even if the maximum will not be zero. Moreover, one can determine nested approximations for the parameters p (with growing reciprocity likelihood) by using nested subsets of the global parameter space:

$$\left.\begin{array}{l} P_1^h \subset P_2^h \subset P, \\ p_i^h = \text{ArgMax}_{q \in P_i^h}\, RL(q) \end{array}\right\} \implies RL(p_1^h) \le RL(p_2^h) \implies p_2^h \text{ is a better identification than } p_1^h.$$

Remark 2. The practical calculation of the RL functional is generally not achievable because the space V_p is generally non-finite-dimensional so that the norm of the reciprocity gap cannot be computed exactly in most cases. Nevertheless, it is possible to compute an approximation of RL by using a finite-dimensional space with dimension $n_d V_p^{n_d}$ approximating V_p:

$$\mathrm{RL}_{n_d}(p) = -\left[\sup_{v \in V_p^{n_d} - \{0\}} \frac{\mathrm{RG}(v)}{\|v\|_{W(p)}}\right]^2. \tag{21}$$

When the space V_p is approximated by the finite-dimensional space $V_p^{n_d}$, the reciprocity property will not be fulfilled (for the optimal parameter set) for all the auxiliary fields but for only on a subspace of the auxiliary fields space. But again the nested approximation spaces for V_p (with increasing dimension) lead to increasing quality of the identification results.

In current applications, two approximations are then made: one on the parameters space and the other on the linear space of the auxiliary fields, approximated by a finite-dimensional space, so that the RL maximization would generally read

$$p_{n_d}^h = \underset{q \in P^h}{\mathrm{ArgMax}}\, \mathrm{RL}_{n_d}(q). \tag{22}$$

The following result can prove useful in the applications when computing the norm of RL_{n_d}:

Norm of a linear form on a finite-dimensional vector space. *Let V^n be a vector space of dimension n with scalar product $\langle \cdot, \cdot \rangle$, $(\phi^\alpha)_{\alpha=1,\ldots,n}$ a linearly independent family of vectors of V^n, and l a linear form on V^n. The norm of l is given by*

$$\|l\|_{V^n} = \sqrt{{}^t l M^{-1} l}, \qquad M^{\alpha\beta} = \langle \phi^\alpha, \phi^\beta \rangle, \qquad l^\alpha = l(\phi^\alpha). \tag{23}$$

The reciprocity likelihood maximization method can then be summarized by:

RLM method. (1) Choose a finite set of independent auxiliary fields $(\phi^\alpha)_{\alpha=1,\ldots,n_d}$ satisfying

$$a(\phi^\alpha, w; p) = 0 \quad \text{for all } w \in W_0(p), \qquad l_{s(p)}(\phi^\alpha) = 0,$$

providing a vector basis for the approximated space of auxiliary fields $V_p^{n_d}$.

(2) Maximize the approximated reciprocity likelihood function defined by

$$p^{\mathrm{opt}} = \underset{q \in P}{\mathrm{ArgMin}}\, M_{\alpha\beta}^{-1}(q)\, \mathrm{RG}(\phi^\alpha(q))\, \mathrm{RG}(\phi^\beta(q)), \qquad M^{\alpha\beta}(q) = \langle \phi^\alpha(q), \phi^\beta(q) \rangle.$$

5. Application to the identification of point source distributions for a conduction equation

This 2D problem has been addressed by [El Badia and Ha Duong 1998; El Badia et al. 2000] with the reciprocity gap functional, by a direct approach, similar to the one described in Section 2. Consider the problem

$$\begin{cases} -\Delta u = \lambda \sum_{i=1}^{i=S} \delta_{X_i} & \text{in } \Omega, \\ \nabla u \cdot \boldsymbol{n} = F^m & \text{on } \partial\Omega, \\ u = U^m & \text{on } \partial\Omega. \end{cases} \tag{24}$$

The inverse problem consists in determining the location X_i of the sources whose intensity λ is known from the redundant boundary data (U^m, F^m). El Badia and Ha-Duong proved that, if an upper bound of the number of sources S is known, then the redundant boundary data pair determines exactly the source locations. They also give an identification algorithm. The reciprocity gap is given here by (4) as in Section 2.

An alternative algorithm based on the reciprocity likelihood method is the following. First, the intensity λ of the point sources being known, the number of sources is determined by computing the reciprocity gap on the constant (harmonic) field $v = 1$:

$$S = -\frac{1}{\lambda} \operatorname{RG}(1). \tag{25}$$

From now on, λ is set at the value $\lambda = 1$. The space V_p is parametrized by the positions of the sources $p = (x_i, y_i)_{i=1,\dots,S}$

$$V_p = \{v \in W[\Omega(p)] : a(v, w; p) = 0 \text{ for all } w \in W_0[\Omega(p)], \ l_{s(p)}(v) = 0\},$$
$$W_0(p) = \{h \in W[\Omega(p)] : h|_{\partial\Omega} = 0\},$$

namely here

$$V_q = \left\{v \in H^1(\Omega) : \int_\Omega \nabla v \nabla w \, d\Omega = 0 \text{ for all } w \in H_0^1(\Omega), \ \sum_{i=1}^S v(x_i, y_i) = 0\right\}. \tag{26}$$

To build a finite-dimensional approximation $V_p^{n_d}$ of this space, we have to choose a linearly independent family of n_d functions $(\phi^\alpha)_{\alpha=1,\dots,n_d}$ in V_p. For that, it suffices to select a family of n_d independent harmonic fields $(\psi^\alpha)_{\alpha=1,\dots,n_d}$ and to take as the $(\phi^\alpha)_{\alpha=1,\dots,n_d}$ family

$$\begin{cases} \phi^\alpha(x, y) = \psi^\alpha(x, y) - \sigma^\alpha(q), \\ \sigma^\alpha(q) = \dfrac{1}{S} \displaystyle\sum_{i=1}^S \psi^\alpha(x_i, y_i). \end{cases} \tag{27}$$

Remark that the family $(\psi^\alpha)_{\alpha=1,\dots,n}$ is independent of the parameters q. To derive the matrix M appearing in the RLM for finite-dimensional V_q spaces (see the RLM method), we just calculate

$$\begin{aligned} M^{\alpha\beta} &= \langle \phi^\alpha, \phi^\beta \rangle \\ &= \int_\Omega \nabla\phi^\alpha \cdot \Delta\phi^\beta + \phi^\alpha \phi^\beta \\ &= \int_\Omega \psi^\alpha \psi^\beta + \frac{1}{2} \int_{\partial\Omega} (\nabla\psi^\alpha \cdot \boldsymbol{n}\psi^\beta + \nabla\psi^\beta \cdot \boldsymbol{n}\psi^\alpha) + \sigma^\alpha \sigma^\beta - \int_\Omega \sigma^\alpha \psi^\beta + \sigma^\beta \psi^\alpha. \end{aligned} \tag{28}$$

Only the last two terms (involving the σ quantities) in the last expression are functions of the parameters p. Once the matrix M is built, the RL function

$$\operatorname{RL}(p) = -M_{\alpha\beta}^{-1}(p) \operatorname{RG}(\phi^\alpha(p)) \operatorname{RG}(\phi^\beta(p)) \tag{29}$$
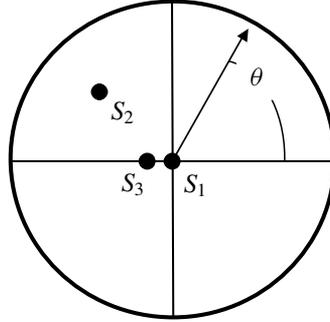
Figure 1. Unit disc with three point sources.

is computed by the following scheme, which requires solving the same linear system (p-dependent) n_d times:

$$X^\alpha(p) = \text{RG}(\phi^\alpha(p)), \qquad M(p)Y(p) = X(p), \qquad \text{RL}(p) = -X(p) \cdot Y(p). \tag{30}$$

The computation of the RL function is then very cost-effective because, as for the reciprocity gap methods, no resolution of any PDE is needed.

As an example, consider the identification of a source distribution in the unit disc as depicted in Figure 1.

Choose the $(\psi^\alpha)_{\alpha=1,\ldots,2n_d}$ family in the polar coordinate system centered at the disc center:

$$\psi^\alpha(r, \theta) = \sqrt{\frac{2\pi(\alpha + 1)}{1 + 2\alpha(\alpha + 1)}} r^\alpha \cos(\alpha\theta), \quad \alpha = 1, \ldots, n_d,$$

$$\psi^\alpha(r, \theta) = \sqrt{\frac{2\pi(\beta + 1)}{1 + 2\beta(\beta + 1)}} r^\beta \sin(\beta\theta), \quad \alpha = n_d + 1, \ldots, 2n_d \quad \text{with } \beta = \alpha - n_d. \tag{31}$$

These functions are obviously harmonic, and because they form a orthonormal family for the $H^1(\Omega)$ scalar product, the M matrix and its inverse turn out to have very simple expressions:

$$M = I_{n_d} + \sigma \otimes \sigma, \qquad M^{-1} = I_{n_d} - \frac{1}{1 + \|\sigma\|^2} \sigma \otimes \sigma. \tag{32}$$

It is thus possible to have a closed-form expression for the RL functional

$$-\text{RL}(p) = \sum_{\alpha=1}^{2n} (\text{RG}(\psi^\alpha) + S\sigma^\alpha)^2 - \sum_{\alpha,\beta} \frac{\sigma^\alpha \sigma^\beta}{1 + \|\sigma\|^2} (\text{RG}(\psi^\alpha) + S\sigma^\alpha)(\text{ER}(\psi^\beta) + S\sigma^\beta), \tag{33}$$

where only the σ terms depend on the parameters p.

To study the overall performance of the reciprocity likelihood maximization method, three cases are examined with one, two, and six sources. The data (U^m, F^m) on the boundary of the unit disc are provided by the closed-form solution to the Laplace equation with point source distribution

$$u(X) = \frac{1}{2\pi} \sum_{i=1}^{S} \log\|X - X_i\|. \tag{34}$$
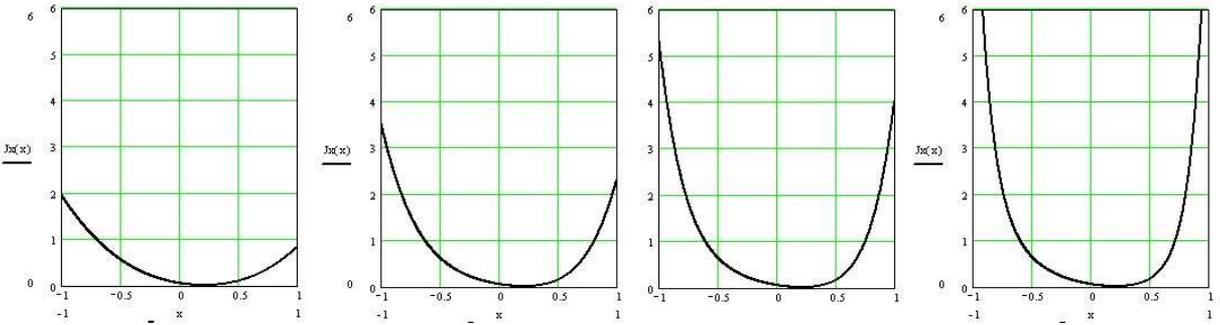
Figure 2. The function $J(x) = -\operatorname{RL}(x)$ for dimensions $n_d = 1, 2, 3, 6$, respectively, of the space $V_p^{n_d}$.

Identification of a single point source. The source is located on the Ox axis with $x = 0.21$. The parameters p reduce to the abscissa x of the source. Figure 2 displays the function $J(x) = -\operatorname{RL}(x)$ when the dimension $2n_d$ of the approximation space of V_p is varied from 2 to 12, that is, when one to six auxiliary functions are used or when the dimension of the matrix M follows the same way (2×2 to 12×12). The symmetry of the solution leads to a symmetry that can be observed on the data on the boundary so that the reciprocity gap vanishes on the half-part of the function set. The effective dimension used for the approximation space for V_p is only n_d and can then take odd values.

The behavior of the $J = -\operatorname{RL}$ function is very good even for a single auxiliary function ($n_d = 1$) where the computation time is negligible, the matrix M being reduced to a single scalar. When the number of functions increases, the computation of the RL function, which remains very quick, leads to sharper minima and a stabilization of the local form of the function around its minimum (maximum of the RL function).

Identification of two point sources. Let us now consider the case of two point sources in the unit disc: $S = 2$, $(x_1, y_1) = (0.21, 0.0)$, and $(x_2, y_2) = (-0.70, 0.0)$, which corresponds to the temperature field plotted in Figure 3. If the ordinates of the sources are known or more simply by exploiting the symmetry of the measurements with respect to the Oy axis, the RL function becomes a function of the abscissae of the sources $\operatorname{RL} = \operatorname{RL}(x_1, x_2)$. Because the identification problems have families of solutions that
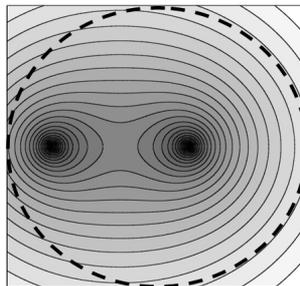
Figure 3. Level lines of the temperature within the unit disc with the two point sources to be identified.
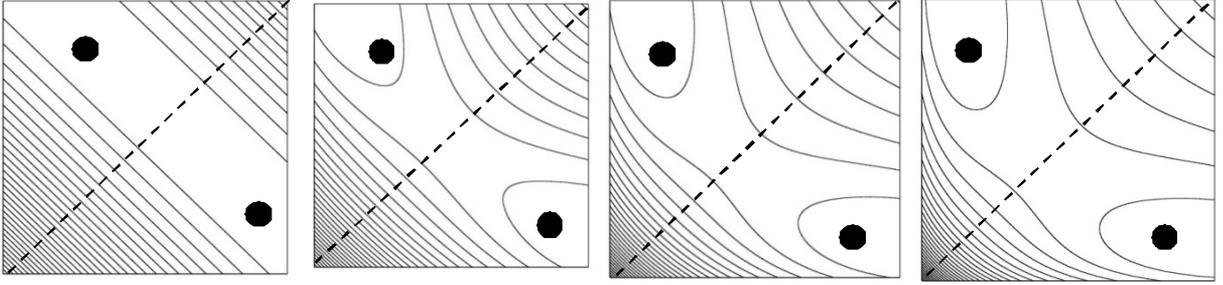
Figure 4. Level lines of the reciprocity likelihood function on the square $(x_1, x_2) = [-0.8, 0.3] \times [-0.8, 0.3]$ for dimensions $n = 2, 4, 8, 12$, respectively, of the space V_p^n (number of ψ functions). The dots correspond to the exact locations of the sources.

are symmetric with respect to the line $x_1 = x_2$ in the parameter space (x_1, x_2), the maximization of the reciprocity likelihood function (or the minimization of its opposite J) has to be conducted in only one half of the square, say $x_1 < x_2$.

One can notice here again an almost convex behavior of the RL function on each triangle except for the first case ($n = 1$), where the use of only one auxiliary field (dim $V_p^n = 1$) is obviously insufficient to capture the details of the temperature field. Here the information given by the boundary data is evidently underexploited.

In the other cases, the identification via an optimization procedure is quite easy and the addition of new auxiliary fields seems to have no significant effect for $n > 4$, showing then the sharpness of the reciprocity likelihood concept.

Identification of point sources by direct maximization of **RL.** The general problem of identification of S sources by direct maximization of the reciprocity likelihood is now addressed, that is, the determination of the locations of the sources $q = [X_k]_{k=1,...,S} = [(x_k, y_k)]_{k=1,...,S}$. As seen in the preceding case, the order of the sources is irrelevant so that there exist several maxima in $[-1, 1]^{2S}$ corresponding to the same family of sources with the same value of the maximum $\text{RL}(p_{\max})$. The selected (converged) family depends on the starting point of the descent algorithm (initial guess). Here the departure locations of the six sources are disposed on a spiral curve in order to have a good initial distribution (Figure 5).
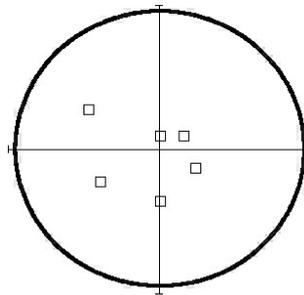
Figure 5. Initial distribution of the six sources to be identified by the RLM.
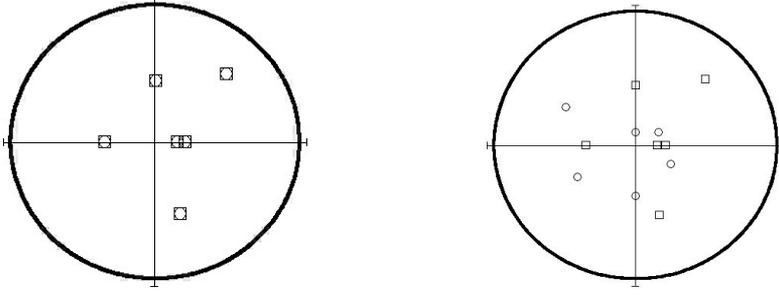
Figure 6. Identified (circles) and real (squares) locations of six sources with $2n_d = 12, 8$ auxiliary functions, respectively.

The gradient of the RL functional with respect to the source locations is straightforward to calculate and is given by

$$\nabla \text{RL}(q) = -2 \sum_{\alpha=1}^{n} (\text{RL}(\psi^\alpha) + S\sigma^\alpha) \nabla \sigma^\alpha$$
$$- 2 \sum_{\alpha,\beta} \frac{\sigma^\alpha}{1 + \|\sigma\|^2} \Big[(\text{RL}(\psi^\alpha) + S\sigma^\alpha)(\text{RL}(\psi^\beta) + S\sigma^\beta) + S\sigma^\beta(\text{RL}(\psi^\alpha) + S\sigma^\alpha) \Big] \nabla \sigma^\beta$$
$$+ 2 \Big[\sum_{\alpha,\beta} \sigma^\alpha \sigma^\beta (\text{RL}(\psi^\alpha) + S\sigma^\alpha)(\text{RL}(\psi^\beta) + S\sigma^\beta) \Big] \frac{\sum_{\alpha=1}^{n} \sigma^\alpha \nabla \sigma^\alpha}{[1 + \|\sigma\|^2]^2} \tag{35}$$

with $\nabla \sigma^\beta = \sum_{i=1}^{m} \nabla \psi^\beta (S_i)$.

The computation of the function RL and its gradients is very cost-effective as it requires only integrals over the boundary of the unit disc of products of the data and the trace of the auxiliary fields. For six sources, the number of parameters to be identified is twelve. Figure 6 (left) displays the converged locations of the sources in the unit disc when the initial guess is the spiral distribution of Figure 5. The dimension of the space $V_p^{n_d}$ is also 12, that is, $n_d = 6$ (results are identical with $n_d = 7$). The locations are perfectly recovered with only one data pair (U^m, F^m). The number of iterations with the line search option of MATLAB [2000] is 123 (194 for $n = 7$) with a tolerance on the gradient of 10^{-6}.

We shall note in particular that the two very close sources situated on the horizontal axis are very well separated. On the other hand, with a lower number of auxiliary functions, eight for example ($n_d = 4$), the maximization stops after 36 iterations because of a too low value of the gradient: the source locations are very badly estimated as seen in Figure 6 (right).

In this case, the RL functional does not contain enough information (or enough probing of the reciprocity property) so that it is too "flat" in a large vicinity of the eventual maxima.

6. Analysis of the effect of noisy data

In this part, the effect of noise on the Cauchy data (u and $\partial_r u$) on the boundary is analyzed for the last example (identification of a six-source distribution). The noise is added to the data with the form

$$f^{\text{noisy}}(\theta) = f(\theta)(1 + \epsilon^{\text{noise}} \text{rand}\,\theta), \tag{36}$$
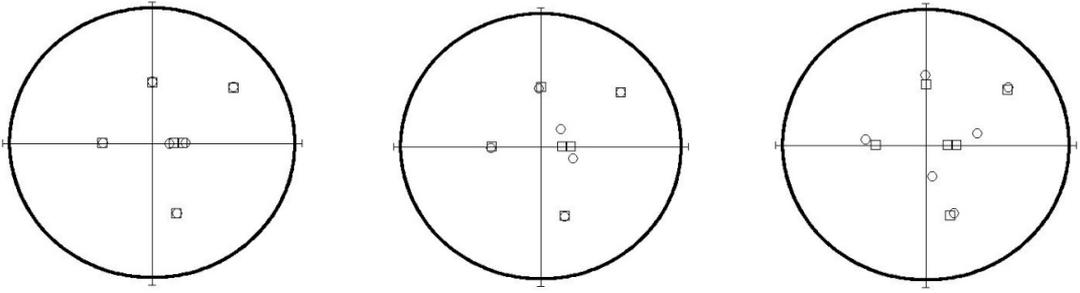
Figure 7. Identified (circles) and real (squares) location of six sources with noisy data (1%, 10%, and 25% noise, respectively).

where rand is the uniform distribution on the segment $[-0.5, 0.5]$ and ϵ^{noise} is the noise level.

One can observe that up to 25% noise the sources are very well recovered except for the two close sources situated on the Ox axis, where the estimation of the location of these sources degrades with the increase of the noise in a symmetric way with regard to the axis Ox. This robustness can be explained by Figure 8. Indeed, the method uses computations of the RG form on auxiliary fields that are very regular and with increasing "space frequency" (with α). It is then clear that the product of the noisy data fields (u and $\partial_r u$) with these auxiliary fields is insensitive to the high-frequency noise for the lowest value of α in (30) and more and more sensitive with growing values of α.

Then the low value of the number of auxiliary fields needed for the identification (as mentioned in Section 5) ensure the good robustness of the identification procedure. For this reason, significantly better
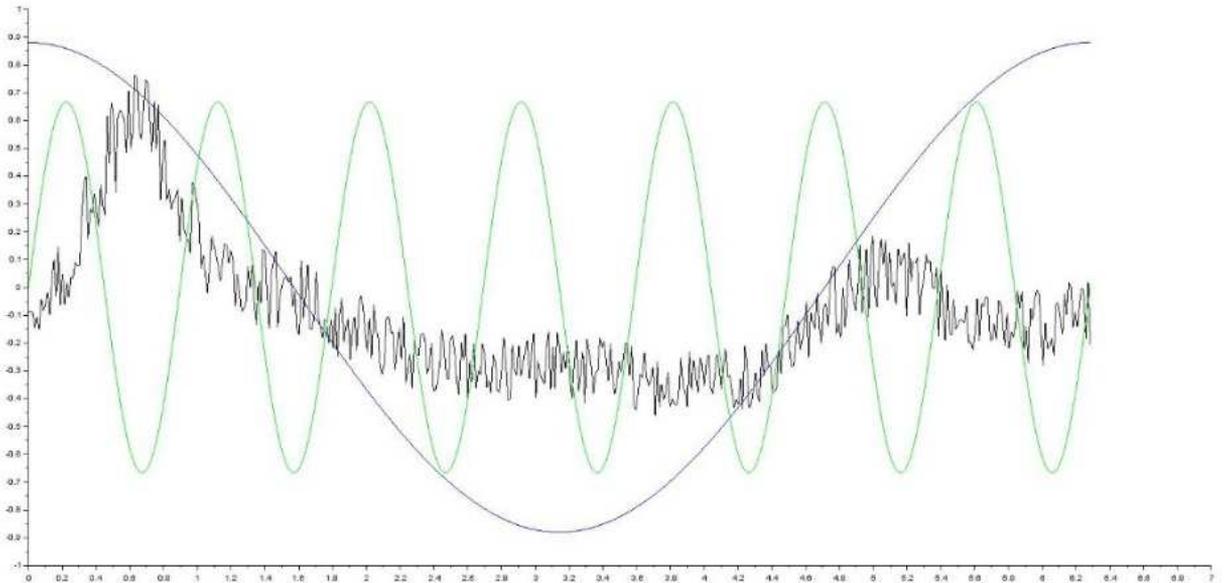
Figure 8. Plot of the noisy data (15% noise) and of two auxiliary fields ($\alpha = 1$ and $\alpha = 5$) on the external boundary.
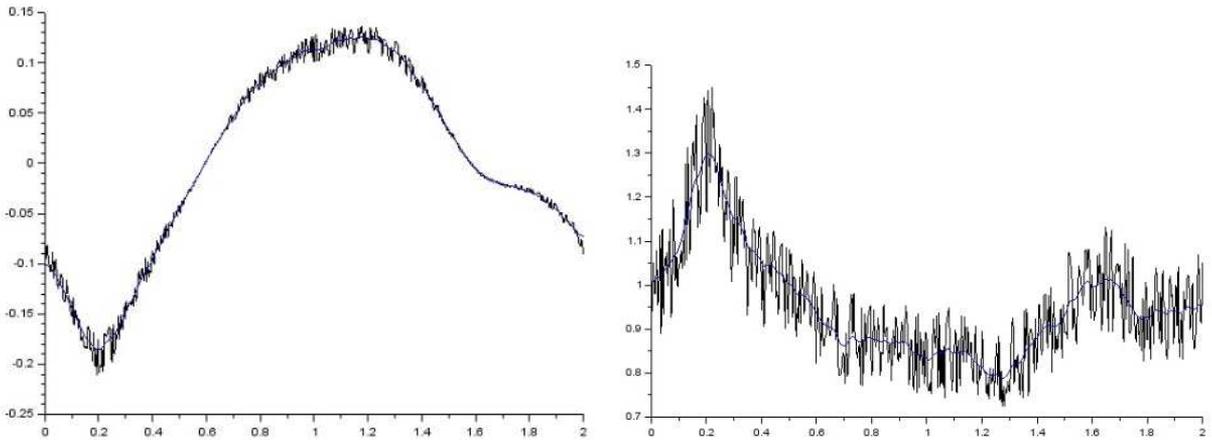
Figure 9. Plots of the noisy data (25% noise) and the regularized data obtained by a Tikhonov regularization. Left: U^m. Right: F^m.

results cannot be expected when using a smoothing of the noisy data with a regularization before processing it with the reciprocity likelihood method. This regularization enables one to compute a smoothed version f^r of a function f over an interval I via the regularized projection

$$f^r = \underset{g}{\text{ArgMin}} \int_I [f(x) - g(x)]^2 \, dx + \eta S(g), \tag{37}$$

where $S(g)$ is a stabilizing functional (Tikhonov [Tikhonov and Arsenin 1977] or total variation [Rudin et al. 1992]) and η the regularization parameter. Here a Tikhonov regularization must be preferred to the total variation regularization because the real data exhibits no discontinuities or strong gradient zones, and only oscillations due to the noise on each measurement points have to be damped out. An example of Tikhonov regularization is displayed in Figure 9 for a noise level of 25%.

The comparison of the results with and without prior regularization shows that they are indeed quite similar.
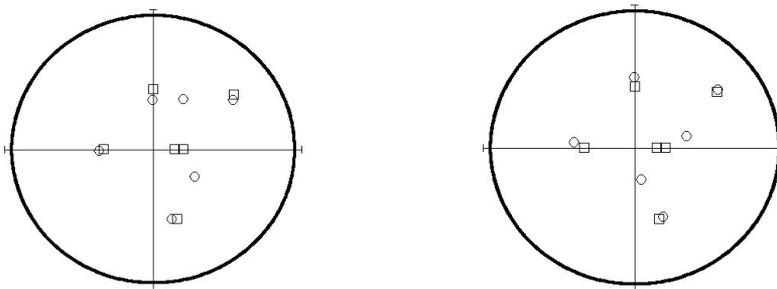
Figure 10. Identified (circles) and real (squares) location of six sources with noisy data. Left: 25% noise with prior Tikhonov regularization. Right: 25% noise without prior regularization.

Nevertheless, the prior regularization would prove useful for the case of more numerous sources because the identification procedure would have to involve more auxiliary fields and then more computations of the RG linear form on fields with higher spatial wave number.

7. Conclusion

We derived a new identification method with the reciprocity gap that produces a systematic way for addressing the identification problem of sources and cracks of inclusion in a solid provided redundant data are available on the whole external boundary. The concept of reciprocity likelihood has been designed and is applicable to any symmetric elliptic operator. The minimization of the reciprocity likelihood function provides a systematic way for using the reciprocity gap concept by avoiding the choice of auxiliary fields and the design of a method for exploiting the information given by the value of the reciprocity gap on it. On the other hand, it is necessary to carefully define the parametrization of objects to be identified. Very good performance and robustness with respect to the noise in the data have been observed for the identification of point source distributions. Applications to crack detection and inclusion identification are in progress.

Appendix A: Proof of the optimality property of the reciprocity gap

Let v_0 be the field in $W(p_0)$ meeting the Dirichlet boundary condition on $\partial\Omega$ and satisfying the equilibrium condition with the source distribution $s(p_0)$. The existence of v_0 is ensured by the Lax–Milgram theorem [Brezis 2011] applied to the linear problem

$$\begin{cases} a(v_0, w; p_0) = l_{s(p_0)}(w) & \text{for all } w \in W_0(p_0), \\ v_0|_{\partial\Omega} = U^m. \end{cases} \tag{A-1}$$

To prove the optimality property of RG, it remains to show that v_0 also meets the Neumann boundary condition: $\boldsymbol{B}v_0 \cdot \boldsymbol{n} = F^m$ on $\partial\Omega$. For that purpose, let us remark that the following reciprocity property holds, thanks to the symmetry of the bilinear form $a(\,\cdot\,,\,\cdot\,; p_0)$ and to the fact that the fields in the space V_{p_0} are canceling the linear form $l_{s(p_0)}$:

$$\int_{\partial\Omega} \boldsymbol{B}v_0 \cdot \boldsymbol{n}v \, dS = \int_{\partial\Omega} \boldsymbol{B}v \cdot \boldsymbol{n}v_0 \, dS \quad \text{for all } v \in V_{p_0}. \tag{A-2}$$

Indeed,

$$\left.\begin{aligned}
a(v_0, w; p) &= l_{s(p_0)}(w) + l_{\boldsymbol{B}v_0\cdot\boldsymbol{n}}(w) && \text{for all } w \in W(p_0), \\
a(v, w; p) &= l_{\boldsymbol{B}v_0\cdot\boldsymbol{n}}(w) && \text{for all } w \in W(p_0) \text{ and } v \in V_{p_0}, \\
l_{s(p_0)}(v) &= 0 && \text{for all } v \in V_{p_0}
\end{aligned}\right\}$$
$$\Longrightarrow \; l_{\boldsymbol{B}v_0\cdot\boldsymbol{n}}(v) = l_{\boldsymbol{B}v\cdot\boldsymbol{n}}(v_0) \quad \text{for all } v \in V_{p_0}. \tag{A-3}$$

Because of the condition (A-1), the reciprocity property involves the data U^m:

$$\int_{\partial\Omega} \boldsymbol{B}v_0 \cdot \boldsymbol{n}v \, dS = \int_{\partial\Omega} \boldsymbol{B}v \cdot \boldsymbol{n}U^m \, dS \quad \text{for all } v \in V_{p_0}. \tag{A-4}$$

Using now the assumption that the reciprocity gap vanishes on the space V_{p_0},

$$\int_{\partial\Omega} F^m v \, dS = \int_{\partial\Omega} \boldsymbol{B} v \cdot \boldsymbol{n} U^m \, dS \quad \text{for all } v \in V_{p_0}, \tag{A-5}$$

one obtains by subtracting the two last equalities

$$\int_{\partial\Omega} (F^m - \boldsymbol{B} v_0 \cdot \boldsymbol{n}) v \, dS = 0 \quad \text{for all } v \in V_{p_0}. \tag{A-6}$$

The result $\boldsymbol{B} v_0 \cdot \boldsymbol{n} = F^m$ would follow, by duality arguments, if equality (A-6) can be extended to all the external traces g of fields in $W(p_0)$, namely if

$$\text{for all } g \in T_{W(p_0)} \text{ there exists } v_g \in W(p_0) \quad \text{such that} \quad \begin{cases} a(v_g, w; p) = 0 & \text{for all } w \in W_0(p_0), \\ l_{s(p_0)}(v_g) = 0, \\ v_g|_{\partial\Omega_{\text{ext}}} = g. \end{cases} \tag{A-7}$$

To prove this last property, and for a given g in $T_{W(p_0)}$, let us define the unique field v^g in $W(p_0)$ to be the solution of the problem

$$\begin{cases} a(v^g, w; p_0) = l_{s(p_0)}(w) & \text{for all } w \in W_0(p_0), \\ v^g|_{\partial\Omega} = g. \end{cases} \tag{A-8}$$

Existence and uniqueness of v^g follow again by the Lax–Milgram theorem. Two cases are now possible:

(i) $l_{s(p_0)}(v^g) = 0$; then v^g is in V_{p_0} and we can take $v_g = v^g$.

(ii) $l_{s(p_0)}(v^g) \neq 0$; then define v_g by $v_g = v^g - (l_{s(p_0)}(v^g)/l_{s(p_0)}(v^0)) v^0$.

For this last case, it is straightforward to verify that v_g belongs to in V_{p_0} and that its trace is g:

$$l_{s(p_0)}(v_g) = l_{s(p_0)}(v^g) - l_{s(p_0)}(v^g) \frac{l_{s(p_0)}(v^0)}{l_{s(p_0)}(v^0)} = 0, \qquad v_g|_{\partial\Omega} = v^g|_{\partial\Omega} - \frac{l_{s(p_0)}(v^g)}{l_{s(p_0)}(v^0)} v^0|_{\partial\Omega} = g - 0 = g. \tag{A-9}$$

Furthermore, $l_{s(p_0)}(v^0)$ cannot vanish because $l_{s(p_0)}(v^0) = a(v^0, v^0; p_0)$ so that the only possibility would be that v^0 belongs to R. With the assumption that only the null field in R can vanish on the boundary, this leads to a contradiction because the source distribution is not zero.

If there is no source, only case one is relevant.

Appendix B: Proof of the topological properties of V_p and RG

The proof of the closure of V_p contains two steps. First, we build a characterization of this space. Let $T_{W(p)}^{*e(p)}$ be the closed subspace of the dual of $T_{W(p)}$, where the compatibility conditions (10) for the equilibrium are met:

$$T_{W(p)}^{*e(p)} = \{ g \in T_{W(p)}^* : l_g(r) + l_{s(p)}(r) = 0 \text{ for all } r \in R \}. \tag{B-1}$$

Define the function L as

$$L : T_{W(p)}^{*e(p)} \to V_p \text{ with } g \mapsto v(g) \quad \text{such that} \quad a(v, w; p) = l_g(w) + l_{s(p)}(w) \quad \text{for all } w \in W(p). \tag{B-2}$$

This function associates with any loading g on $\partial\Omega$ the equilibrium solution in the solid $\Omega(p)$ submitted to the source $s(p)$. L is surjective (just take $g = \boldsymbol{B}v \cdot n$ for v in V_p; g fulfills the compatibility condition because $R \subset W$) and injective by the Lax–Milgram theorem.

The second step is to show that L is continuous, leading then to the conclusion. Indeed, for every convergent sequence v_n in $W(p)$ of vectors of V_p, one can associate to L a convergent sequence g_n in $T_{W(p)}^{*e(p)}$ because strong convergence in $W(p)$ implies the weak convergence and then the convergence of $a(v_n, w)$ for every w. The limit of g_n is necessarily in $T_{W(p)}^{*e(p)}$ as it is a closed space. Finally, the image of this limit of L is in V_p and corresponds to the limit of v_n. So the limits of convergent sequences of V_p are in V_p, which shows that it is closed.

Let us now show that L is continuous. For any g_1 and g_2 in $T_{W(p)}^{*e(p)}$, we have with $v_i = L(g_i)$

$$a(v_1 - v_2, w; p) = l_{g_1-g_2}(w) \quad \text{for all } w \in W(p). \tag{B-3}$$

Thanks to the coerciveness of a and the continuity of the trace operator γ, one can obtain the inequality

$$\alpha\|v_1 - v_2\|_{W(p)}^2 \le a(v_1 - v_2, v_1 - v_2; p) \le \beta\|g_1 - g_2\|_{T*W(p)}\|\gamma v_1 - \gamma v_2\|_{T_{W(p)}} \\ \le \beta c\|g_1 - g_2\|_{W(p)}\|v_1 - v_2\|_{T_{W(p)}}, \tag{B-4}$$

showing that L is continuous. The continuity of RG results from the Schwartz inequality

$$|\mathrm{RG}(v)| \le \|F^m\|_{T*W(p)}\|v\|_{T_{W(p)}} + \|\boldsymbol{B}v \cdot \boldsymbol{n}\|_{T*W(p)}\|U^m\|_{T_{W(p)}} \tag{B-5}$$

as well as the continuity of g, a and $l_{s(p)}$ because we have

$$l_{\boldsymbol{B}v\cdot\boldsymbol{n}}(w) = a(v, w; p) - l_{s(p)}(w) \quad \text{for all } w \in W(p). \tag{B-6}$$

Acknowledgment

References

[Alves and Silvestre 2004] C. J. S. Alves and A. L. Silvestre, "On the determination of point-forces on a Stokes system", *Math. Comput. Simulat.* **66**:4–5 (2004), 385–397.

[Andrieux 1995] S. Andrieux, "Fonctionnelles d'écart à la réciprocité généralisé et identification de fissures par des mesures surabondantes de surface", *C. R. Acad. Sci. I Math.* **320**:12 (1995), 1553–1559.

[Andrieux and Ben Abda 1992] S. Andrieux and A. Ben Abda, "Identification de fissures planes par une donnée de bord unique: un procédé direct de localisation et d'identification", *C. R. Acad. Sci. I Math.* **315**:12 (1992), 1323–1328.

[Andrieux and Ben Abda 1993] S. Andrieux and A. Ben Abda, "The reciprocity gap: a general concept for flaws identification problems", *Mech. Res. Commun.* **20**:5 (1993), 415–420.

[Andrieux and Ben Abda 1996] S. Andrieux and A. Ben Abda, "Identification of planar cracks by complete overdetermined data: inversion formulae", *Inverse Probl.* **12**:5 (1996), 553–563.

[Andrieux and Bui 2011] S. Andrieux and H. D. Bui, "On some nonlinear inverse problems in elasticity", *Theor. Appl. Mech.* **38**:2 (2011), 125–154.

[Andrieux et al. 1998] S. Andrieux, A. Ben Abda, and M. Jaoua, "On the inverse emergent plane crack problem", *Math. Methods Appl. Sci.* **21**:10 (1998), 895–906.

[Andrieux et al. 1999] S. Andrieux, A. Ben Abda, and H. D. Bui, "Reciprocity principle and crack identification", *Inverse Probl.* **15**:1 (1999), 59–65.

[Andrieux et al. 2006] S. Andrieux, H. D. Bui, and K. Hadj-Sassi, "New results with the reciprocity gap functional for the identification of cracks and small inclusions", in *7th World Congress on Computational Mechanics* (Los Angeles, 2006), 2006.

[Ben Abda and Bui 2001] A. Ben Abda and H. D. Bui, "Reciprocity principle and crack identification in transient thermal problems", *J. Inverse Ill-Posed Probl.* **9**:1 (2001), 1–6.

[Ben Abda et al. 2005] A. Ben Abda, F. Delbary, and H. Haddar, "On the use of the reciprocity-gap functional in inverse scattering from planar cracks", *Math. Models Methods Appl. Sci.* **15**:10 (2005), 1553–1574.

[Brezis 2011] H. Brezis, *Functional analysis, Sobolev spaces and partial differential equations*, Springer, New York, 2011.

[Bui 2011] H. D. Bui, *Duality, symmetry and symmetry lost in solid mechanics: selected works of H. D. Bui*, edited by A. Ehrlacher and X. Markenscoff, Presse des Ponts, Paris, 2011.

[Bui et al. 1999] H. D. Bui, A. Constantinescu, and H. Maigre, "Diffraction acoustique inverse de fissure plane: solution explicite pour un solide borné", *C. R. Acad. Sci. II B* **327**:10 (1999), 971–976.

[Bui et al. 2004] H. D. Bui, A. Constantinescu, and H. Maigre, "Numerical identification of linear cracks in 2D elastodynamics using the instantaneous reciprocity gap", *Inverse Probl.* **20**:4 (2004), 993–1001.

[Bui et al. 2005] H. D. Bui, A. Constantinescu, and H. Maigre, "An exact inversion formula from determining a planar fault from boundary measurements", *J. Inverse Ill-Posed Probl.* **13**:6 (2005), 553–565.

[Colton and Haddar 2005] D. Colton and H. Haddar, "An application of the reciprocity gap functional to inverse scattering theory", *Inverse Probl.* **21**:1 (2005), 383–398.

[El Badia and Ha Duong 1998] A. El Badia and T. Ha Duong, "Some remarks on the problem of source identification from boundary measurements", *Inverse Probl.* **14**:4 (1998), 883–891.

[El Badia et al. 2000] A. El Badia, T. Ha Duong, and F. Moutazaim, "Numerical solution for the identification of source terms from boundary measurements", *Inverse Probl. Eng.* **8**:4 (2000), 345–364.

[Eshelby 1957] J. D. Eshelby, "The determination of the elastic field of an ellipsoidal inclusion, and related problems", *Proc. Roy. Soc. London A* **241** (1957), 376–396.

[Ikehata 1999] M. Ikehata, "Enclosing a polygonal cavity in a two-dimensional bounded domain from Cauchy data", *Inverse Probl.* **15**:5 (1999), 1231–1241.

[Kohn and Vogelius 1984] R. Kohn and M. Vogelius, "Determining conductivity by boundary measurements", *Comm. Pure Appl. Math.* **37**:3 (1984), 289–298.

[MATLAB 2000] MATLAB R12, The MathWorks, Inc., Natick, MA, 2000.

[Rudin et al. 1992] L. I. Rudin, S. Osher, and E. Fatemi, "Nonlinear total variation based noise removal algorithms", *Physica D* **60**:1–4 (1992), 259–268.

[Shifrin and Shushpannikov 2010] E. I. Shifrin and P. S. Shushpannikov, "Identification of a spheroidal defect in an elastic solid using a reciprocity gap functional", *Inverse Probl.* **26**:5 (2010), 055001.

[Shifrin and Shushpannikov 2011] E. I. Shifrin and P. S. Shushpannikov, "Identification of an ellipsoidal defect in an elastic solid using boundary measurements", *Int. J. Solids Struct.* **48**:7–8 (2011), 1154–1163.

[Shifrin and Shushpannikov 2013a] E. I. Shifrin and P. S. Shushpannikov, "Identification of small well-separated defects in an isotropic elastic body using boundary measurements", *Int. J. Solids Struct.* **50**:22–23 (2013), 3707–3716.

[Shifrin and Shushpannikov 2013b] E. I. Shifrin and P. S. Shushpannikov, "Reconstruction of an ellipsoidal defect in anisotropic elastic solid, using results of one static test", *Inverse Probl. Sci. Eng.* **21**:5 (2013), 781–800.

[Tikhonov and Arsenin 1977] A. N. Tikhonov and V. A. Arsenin, *Solutions of ill-posed problems*, Winston & Sons, Washington, 1977.

STÉPHANE ANDRIEUX: stephane.andrieux@edf.fr
Laboratoire de Mécanique des Structures Industrielles Durables, UMR EDF-CNRS-CEA 8193, 1 Avenue du Général de Gaulle, 92141 Clamart, France

msp

STABILITY OF DISCRETE TOPOLOGICAL DEFECTS IN GRAPHENE

Maria Pilar Ariza and Juan Pedro Mendez

While improving graphene production techniques seems to be critical for the successful development of practical graphene-based devices, another technological bottleneck stems from the fact that not all mechanisms controlling the coupled thermal-mechanical-electrical behavior of graphene-based materials are fully known at present. In this work, we specifically aim to propose a methodology to investigate the behavior of controlled distributions of point defects in graphene. We present a bondwise force-constant model derived from the adaptive intermolecular reactive empirical bond-order (AIREBO) potential and compare the force-constant values with those obtained from other interatomic potentials. In addition, we present a particular computational scheme that, while preserving the advantages of discrete dislocation theory, allows the assessment of the stability of discrete defects. In particular, we study two dislocation dipole configurations: glide and shuffle.

1. Introduction

Ever since its meteoric rise to prominence, graphene has been touted as a promising novel material, owing to its extraordinary mechanical, electrical, optical and thermal properties. In addition to its high breaking strength and high Young's modulus (42 N/m and 1 TPa [Lee et al. 2008]), graphene exhibits high thermal mobility (> 4000 W/mK [Balandin et al. 2008]), low resistivity ($\approx 30\,\Omega^{-1}$ [Bae et al. 2010]) and high electronic conductivity (> 15000 cm^2/(V $\cdot$ s) [Geim and Novoselov 2007]); i.e., electrons in graphene are allowed to travel long distances without scattering. Other features that have made this material deeply peculiar are its low weight (0.77 mg/m^2), its capability to absorb a fraction of incident white light (around 2.3% [Nair et al. 2008]) and its impermeability to gases [Bunch et al. 2008], among other intriguing properties.

By virtue of these features, today graphene offers a wide range of benefits, and indeed new innovative applications of graphene come to light every day. For instance, graphene has been thought to be an ideal alternative to carbon fibers for structural applications in aeronautics or a substitute of indium tin oxide (ITO) in touchscreens or flexible panel displays [Bae et al. 2010], liquid crystal displays (LCD) [Jung et al. 2014; Blake et al. 2008] and organic light emitting diodes (OLED) [Wu et al. 2010] in optoelectronics. Unfortunately, it was recognized early on [Novoselov et al. 2005; Zhang et al. 2005] that pristine defect-free graphene has no band gap and, therefore, is of limited use for semiconductor-based electronics. Immediately thereafter, many attempts were made to engineer band gaps in graphene, for example by using doped graphene, nanoribbons, electric fields, mechanical strain or engineering defects, among other means [Yazyev and Louie 2010a; Zhang et al. 2012].

Graphene material properties and, in particular, experimentally observed topological defects have been analyzed by using different interatomic potentials and computational approaches ranging from *ab initio* to molecular dynamics. Furthermore, empirical tight-binding models have been applied, allowing for a proper description of the electronic structure of graphene. In particular, Jeong et al. [2008] have studied the stability of dislocation dipoles with 5–7 core structures using *ab initio* calculations whereas Yazyev and Louie [2010b] have focused on the thermodynamics and electronic properties of dislocations and grain boundaries. Molecular dynamics simulations carried out by Liu et al. [2011] investigated the atomic structures and energies of symmetric tilt grain boundaries using the empirical AIREBO potential. The aforementioned potential is an extension of the reactive empirical bond-order REBO potential developed by Brenner [1990], which additionally includes torsion, dispersion and nonbonded repulsion interactions. Thus, the AIREBO potential [Stuart et al. 2000] is suitable for modeling chemical reactions.

We have previously presented [Ariza and Ortiz 2010; Ariza et al. 2010] an analysis of discrete dislocations in graphene based on the discrete dislocation theory in crystals [Ariza and Ortiz 2005]. This said theory combines lattice harmonics, the theory of eigendeformations and the discrete Fourier transform, leading to analytically tractable expressions of the stored energy of defective graphene. In contrast, owing to its reliance on force constants, the theory of discrete dislocations provides harmonic defect structures and their corresponding energies. Therefore, the anharmonic part of the interatomic potentials should be included for the sake of completeness. In this work, we present fully nonlinear solutions obtained by the *method of forces*, i.e., by appending unknown forces to the discrete dislocation energy so as to equilibrate the lattice with respect to the fully nonlinear potential. Specifically, we have first computed the harmonic dislocation core structures and energies predicted by the force constants model obtained from the AIREBO potential and then studied their dynamic stability taking into account the full potential. We have focused on two dislocation dipole configurations: glide and shuffle.

2. The discrete dislocation theory

A general discrete dislocation theory in crystal, and its specialization to graphene, has been presented by Ariza and Ortiz [2005; 2010]. In this section, we present a brief summary of the discrete dislocation (DD) theory extended to graphene. Following this theory, we regard the graphene lattice as a collection of cells $\mathscr{C}$ of different dimensions, endowed with discrete differential operators, discrete codifferential operators and a discrete integral. In particular, the graphene complex is bidimensional and consists of: atoms, or 0-cells; atomic bonds, or 1-cells; and hexagonal cells, or 2-cells (Figure 1). For ease of indexing, we denote by $E_p(\mathscr{C})$ the set of cells of dimension p in the graphene complex and by $e_p(l, \alpha)$ the p-cell of type α and integer coordinates $l \in Z^2$.
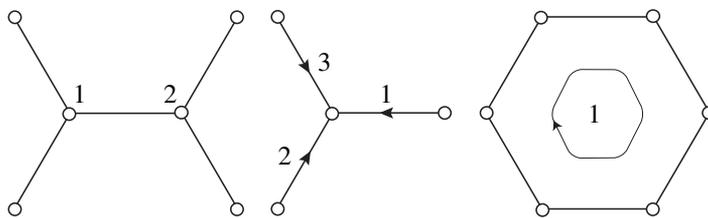
Figure 1. The oriented 0-, 1- and 2-cells of graphene grouped by type.
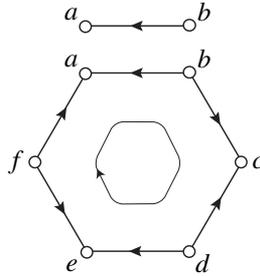
Figure 2. Diagram for the definition of the discrete differential operators of graphene.

These cells provide the support for defining functions, or forms, of different dimensions. Thus, we refer to a function defined over the atoms (or 0-cells), over the atomic bonds (or 1-cells) or over the hexagonal areas (or 2-cells) as a 0-form, 1-form or 2-form, respectively. As we shall see, forms provide the vehicle for describing the behavior of graphene lattice, including displacements, eigendeformations and dislocation densities.

In order to define differential operators, we need to orient all cells; see Figure 2. Suppose that ω is a 0-form defined over the atoms and e_{ab} is an atomic bond defined by atoms a and b and oriented from b to a (Figure 2). Then, the differential $d\omega(e_{ab})$ of ω at e_{ab} is defined as

$$d\omega(e_{ab}) = \omega(e_a) - \omega(e_b). \tag{2-1}$$

Similarly, for 1-forms and 2-forms, we have

$$d\omega(e_{abcdef}) = -\omega(e_{ab}) + \omega(e_{bc}) - \omega(e_{cd}) + \omega(e_{de}) - \omega(e_{ef}) + \omega(e_{fa}) \tag{2-2}$$

and

$$d\omega = \sum_{e_2 \in E_2(\mathscr{C})} \omega(e_2). \tag{2-3}$$

Thus, the differential operator maps: 0-forms, defined over atoms, to 1-forms, defined over atomic bonds; 1-forms, defined over atomic bonds, to 2-forms, defined over hexagonal cells; and 2-forms, defined over hexagonal cells, to vectors. Thus, the defined discrete differential operators may be regarded as the discrete counterparts of the familiar gradient, curl and divergence of vector calculus. It is readily verified from the definition of the discrete differential operators [Munkres 1984] that

$$d^2 = 0, \tag{2-4}$$

which is the discrete counterpart of the identities $\text{rot} \circ \text{grad} = 0$ and $\text{div} \circ \text{rot} = 0$.

Next, by grouping cells of $\mathscr{C}$ by types, one might notice that cells of the same type are translations of each other, and therefore, they are arranged as simple Bravais lattices (Figure 3). Graphene lattice has two different atoms (labeled as 1 and 2), three different atomic bonds (labeled as 1, 2 and 3) and one hexagonal area (labeled as 1). Owing to the translation invariance of the cells, we can take advantage of the definition of the discrete Fourier transform (DFT) and its properties such as the discrete Parseval's identity and the discrete convolution theorem. Thus, the DFT of a p-form ω is

$$\hat{\omega}(\boldsymbol{\theta}, \alpha) = \sum_{l \in \mathbb{Z}^2} \omega(l, \alpha) e^{-i\boldsymbol{\theta} \cdot l}, \tag{2-5}$$
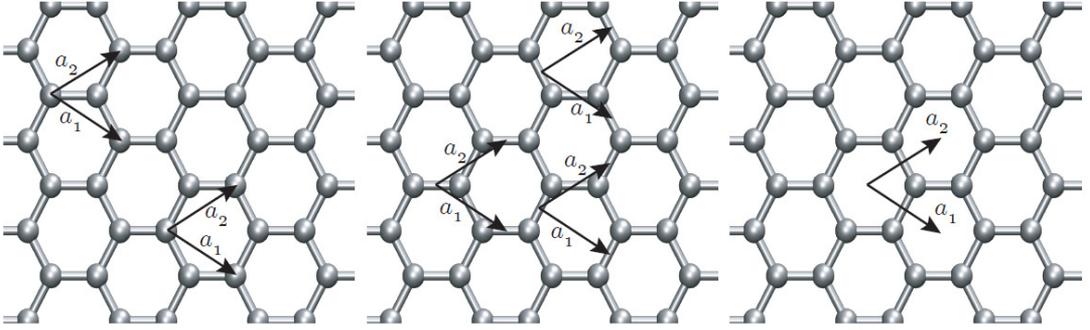
Figure 3. The simple Bravais lattices defined by the atoms, atomic bonds and hexagonal cells of graphene.

where $l \in \mathbb{Z}^2$ are the integer coordinates of the Bravais lattice and α takes the values of 1 or 2 for 0-forms, 1, 2, or 3 for 1-forms and 1 for 2-forms.

Similarly, the DFT of a differential p-form $d\omega$ is

$$\widehat{d\omega}(\boldsymbol{\theta}, \alpha) = \sum_{\beta=1}^{N_p} Q\left(\begin{matrix} \boldsymbol{\theta} \\ \alpha \quad \beta \end{matrix}\right) \hat{\omega}(\boldsymbol{\theta}, \beta), \tag{2-6}$$

where the coefficients $Q\left(\begin{smallmatrix} \boldsymbol{\theta} \\ \alpha \quad \beta \end{smallmatrix}\right)$ represent the differential structure of the lattice. For the graphene differential structure defined in (2-1) and (2-2),

$$Q_1(\boldsymbol{\theta}) = \begin{pmatrix} 1 & -e^{i\theta_2} \\ 1 & -1 \\ 1 & -e^{-i\theta_3} \end{pmatrix}, \tag{2-7a}$$

$$Q_2(\boldsymbol{\theta}) = (e^{i\theta_3} - 1, 1 - e^{i\theta_1}, e^{i\theta_1} - e^{i\theta_3}), \tag{2-7b}$$

where

$$\theta_3 = \theta_2 - \theta_1. \tag{2-8}$$

Equations (2-7) define the differential of 0- and 1-forms in their Fourier representations, respectively. Within this differential operator framework and by the translational invariance of the energy of lattice, we can write the energy of a harmonic crystal as

$$E(\boldsymbol{u}) = \frac{1}{2} \sum_{e_1 \in E_1} \sum_{e_1' \in E_1} B_{ij}(e_1, e_1') \, du_i(e_1) \, du_j(e_1') \equiv \tfrac{1}{2} \langle \boldsymbol{B} \, d\boldsymbol{u}, d\boldsymbol{u} \rangle, \tag{2-9}$$

where $B_{ij}(e_1, e_1')$ are bondwise force constants, giving the interaction energy resulting from a unit differential displacement in the j-th coordinate direction at bond e_1' and a unit differential displacement in the i-th coordinate direction at bond e_1.

Equivalently,

$$E(\boldsymbol{u}) = \frac{1}{2} \sum_{e_0 \in E_0} \sum_{e_0' \in E_0} A_{ij}(e_0, e_0') u_i(e_0) u_j(e_0') \equiv \tfrac{1}{2} \langle \boldsymbol{A} \, \boldsymbol{u}, \boldsymbol{u} \rangle, \tag{2-10}$$
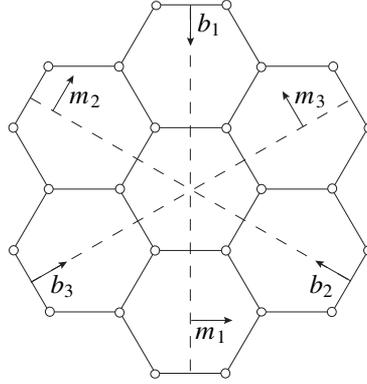
Figure 4. Resulting slip lines and Burger vectors, defining the operative slip systems of graphene.

where $A_{ij}(e_0, e_0')$ are atomic force constants, giving the interaction energy resulting from a unit differential displacement in the j-th coordinate direction at atom e_0' and a unit differential displacement in the i-th coordinate direction at atom e_0.

Moreover, by the translation invariance of lattice, we can express $\boldsymbol{B}\, d\boldsymbol{u}$ and $\boldsymbol{A}\boldsymbol{u}$ in convolution form, and then using the Parseval's identity and the convolution theorem, we express the DFT representation of the harmonic energy as

$$E(\boldsymbol{u}) = \frac{1}{(2\pi)^2} \int_{[-\pi,\pi]^2} \tfrac{1}{2}\langle \widehat{\boldsymbol{\Psi}}(\boldsymbol{\theta})\,\widehat{d\boldsymbol{u}}(\boldsymbol{\theta}), \widehat{d\boldsymbol{u}}^*(\boldsymbol{\theta})\rangle\, d^2\boldsymbol{\theta}, \tag{2-11a}$$

$$E(\boldsymbol{u}) = \frac{1}{(2\pi)^2} \int_{[-\pi,\pi]^2} \tfrac{1}{2}\langle \widehat{\boldsymbol{\Phi}}(\boldsymbol{\theta})\,\hat{\boldsymbol{u}}(\boldsymbol{\theta}), \hat{\boldsymbol{u}}^*(\boldsymbol{\theta})\rangle\, d^2\boldsymbol{\theta}. \tag{2-11b}$$

The preceding representations show that the force-constant fields are related by

$$\widehat{\Phi}_{ij} = \boldsymbol{Q}_1^T \widehat{\Psi}_{ij}\, \boldsymbol{Q}_1^*. \tag{2-12}$$

Moreover, it is possible now to achieve an expression for the energy of a defective crystal including dislocations. To accomplish this, we include in (2-9) the eigendeformations $\boldsymbol{\beta}$ corresponding to crystal slips [Mura 1987]

$$E(\boldsymbol{u}, \beta) = \frac{1}{2} \sum_{e_1 \in E_1} \sum_{e_1' \in E_1} \boldsymbol{B}(e_1, e_1')(d\boldsymbol{u}(e_1) - \boldsymbol{\beta}(e_1))(d\boldsymbol{u}(e_1') - \boldsymbol{\beta}(e_1'))$$

$$\equiv \tfrac{1}{2}\langle \boldsymbol{B}(d\boldsymbol{u} - \boldsymbol{\beta}), (d\boldsymbol{u} - \boldsymbol{\beta})\rangle, \tag{2-13}$$

where the sums take place over the atomic bonds of the crystal lattice, $\boldsymbol{u}(e_0)$ is the atomic displacement of atom e_0, $d\boldsymbol{u}(e_1)$ is the deformation of atomic bond e_1, $\boldsymbol{\beta}(e_1)$ is the eigendeformation at bond e_1 and $\boldsymbol{B}(e_1, e_1')$ are bondwise force constants. The local values $\boldsymbol{\beta}(e_1)$ of the eigendeformation field are constrained to defining lattice-invariant deformations; see Figure 4. And finally, the stored energy of a crystal and the respective displacement field is obtained by minimizing (2-13) with respect to $\boldsymbol{u}$:

$$\inf_{\boldsymbol{u}} E(\boldsymbol{u}, \boldsymbol{\beta}) = E(\boldsymbol{\beta}). \tag{2-14}$$

3. Harmonic graphene model

Bond-order potentials have widely been employed to model complex materials, including C-based materials, e.g., graphite, diamond and graphene. Tersoff potentials [1988] are a clear example of bond-order potentials among others such as Finnis–Sinclair potentials [1984], ReaxFF potential [van Duin et al. 2001] and REBO potentials [Brenner 1990]. The latter one is based on Tersoff potentials with additional terms that correct for an inherent overbinding of radicals and that include nonlocal effects. However, REBO potentials include neither torsion of bonds nor nonbonded interactions; both contributions are crucial to model correctly the behavior of graphene. The AIREBO potential [Stuart et al. 2000], which is derived from the REBO potential, includes these effects through the addition of two new terms: a Lennard-Jones potential, E^{LJ}, accounting for long-range interaction, and a torsion term, E^{tors}.

3.1. *AIREBO potential.* In this section, the AIREBO potential is briefly described and particularized to graphene. This empirical potential consists of a sum of different terms

$$E = \frac{1}{2} \sum_i \sum_{j \neq i} \left[E_{ij}^{\text{REBO}} + E_{ij}^{\text{LJ}} + \sum_{k \neq i,j} \sum_{l \neq i,j,k} E_{kijl}^{\text{tors}} \right], \tag{3-1}$$

where E_{ij}^{REBO} is the REBO interaction, E_{ij}^{LJ} is the Lennard-Jones interaction and E_{kijl}^{tors} is the torsion interaction.

The REBO part combines the repulsive and the attractive terms as

$$E_{ij}^{\text{REBO}} = V_{ij}^R(r_{ij}) + b_{ij} V_{ij}^A(r_{ij}), \tag{3-2}$$

where b_{ij} is the bonding term that specifies the interaction between atoms i and j and their respective neighbors, i.e., b_{ij} depends on the bond angles between the bonding environment surrounding atoms i and j and the bond ij and is a monotonic decreasing function with respect to the coordination number N as $b \sim N^{-1/2}$:

$$b_{ij} = \frac{1}{2}[p_{ij}^{\sigma\pi} + p_{ji}^{\sigma\pi}] + \pi_{ij}^{rc} + \pi_{ij}^{dh}. \tag{3-3}$$

The repulsive term exclusively depends on the atom types i and j through the Q_{ij}, A_{ij} and α_{ij} parameters (Table 1) and the bond length r_{ij}:

$$V_{ij}^R = w_{ij}(r_{ij}) \left[1 + \frac{Q_{ij}}{r_{ij}} \right] A_{ij} e^{-\alpha_{ij} r_{ij}}, \tag{3-4}$$

where w_{ij} is a bond weighting factor. Notice that the repulsive term tends to infinity as the bond length between atoms i and j goes to zero.

Parameter	Q_{ij} (Å)	α_{ij} (Å^{-1})	A_{ij} (eV)	$B_{ij}^{(1)}$ (eV)	$B_{ij}^{(2)}$ (eV)	$B_{ij}^{(3)}$ (eV)
CC	0.313460	4.7465391	10953.544	12388.792	17.567065	30.714932
Parameter	$\beta_{ij}^{(1)}$ (Å^{-1})	$\beta_{ij}^{(2)}$ (Å^{-1})	$\beta_{ij}^{(3)}$ (Å^{-1})	ϵ_{ij} (eV)	$\sigma_{ij}^{(2)}$ (Å)	ϵ_{iccj} (eV)
CC	4.7204523	1.4332132	1.3826913	0.00284	3.40	0.3079

Table 1. AIREBO parameters for the attractive, repulsive, LJ and torsion terms.

Parameter	r_{cc} (Å)	N_c	N	s	r'_{cc} (Å)	r_{cc}^{LJ} (Å)	b_{cc}
Minimum	1.7	3.2	2	0.1	1.7	σ_{cc}	0.77
Maximum	2	3.7	3	0.1	2	$2^{1/6}\sigma_{cc}$	0.81

Table 2. Switching parameters between CC bonds.

Similarly, the attractive term also depends on the atom types i and j ($B_{ij}^{(n)}$ and $\beta_{ij}^{(n)}$) and the bond length as

$$V_{ij}^A = -w_{ij} \sum_{n=1}^{3} B_{ij}^{(n)} e^{-\beta_{ij}^{(n)} r_{ij}}. \tag{3-5}$$

The bond weighting factor $w_{ij}(r_{ij})$ smoothly switches off the REBO interaction when the atom pairs exceed the typical bonding distance between carbon atoms for graphene (Table 2):

$$w_{ij}(r_{ij}) = S'(t_c(r_{ij})), \tag{3-6}$$

where $S'(t)$ is

$$S'(t) = \Theta(-t) + \tfrac{1}{2}\Theta(t)\Theta(1-t)[1 + \cos \pi t] \tag{3-7}$$

and $t_c(r_{ij})$ is given by

$$t_c(r_{ij}) = \frac{r_{ij} - r_{ij}^{\min}}{r_{ij}^{\max} - r_{ij}^{\min}}. \tag{3-8}$$

The $p_{ij}^{\sigma\pi}$ and $p_{ji}^{\sigma\pi}$ terms in (3-3) take into account the covalent bond interaction:

$$p_{ij}^{\sigma\pi} = \frac{1}{\sqrt{1 + \sum_{k \neq i,j} w_k(r_k) g_i(\cos\theta_{jik}) + P_{ij}(N_{ij}^C)}}, \tag{3-9}$$

$$p_{ji}^{\sigma\pi} = \frac{1}{\sqrt{1 + \sum_{l \neq i,j} w_l(r_l) g_i(\cos\theta_{ijl}) + P_{ji}(N_{ij}^C)}}, \tag{3-10}$$

$$g_C(\cos\theta_{jik}) = g_C^{(1)}(\cos\theta_{jik}) + S'(t_N(N_{ij}))\big[g_C^{(2)}(\cos\theta_{jik}) - g_C^{(1)}(\cos\theta_{jik})\big], \tag{3-11}$$

where g_i is a penalty function that penalizes the bonds that are very close to one another and θ_{jik} and θ_{ijl} (Figure 5) are the bond angles between the vectors (r_i, r_{ik}) and (r_i, r_{jl}), respectively:

$$\cos\theta_{jik} = \frac{r_i \cdot r_{ik}}{r_i r_{ik}}, \tag{3-12}$$

$$\cos\theta_{ijl} = \frac{r_i \cdot r_{jl}}{r_i r_{jl}}. \tag{3-13}$$

The scaling function $t_N(N_{ij})$ in (3-11) is a function of the local coordination number, N_{ij}, and the upper and lower bound coordination numbers, $N_{ij}^{\max}$ and $N_{ij}^{\min}$, which are related to the material:

$$t_N(N_{ij}) = \frac{N_{ij} - N_{ij}^{\min}}{N_{ij}^{\max} - N_{ij}^{\min}}. \tag{3-14}$$
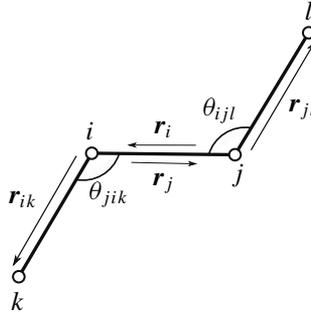
Figure 5. Angle convection.

	$\cos\theta$	g_i	$\partial g_i/\partial\cos\theta$	$\partial^2 g_i/\partial(\cos\theta)^2$
	-1	-0.010000	0.104000	0.000000
	$-\frac{2}{3}$	0.028207	0.131443	0.140229
$g_C^{(1)}$	$-\frac{1}{2}$	0.052804	0.170000	0.370000
	$-\frac{1}{3}$	0.097321	0.400000	1.98000
	1	1.00000	2.83457	10.2647
	-1	-0.010000	0.104000	0.000000
	$-\frac{2}{3}$	0.028207	0.131443	0.140229
$g_C^{(2)}$	$-\frac{1}{2}$	0.052804	0.170000	0.370000
	$-\frac{1}{3}$	0.097321	0.400000	1.98000
	1	8.00000	20.2436	43.9336

Table 3. Interpolation points for the function g_C.

In particular, for graphene,

$$N_{ij} = N_{ij}^C = \left(\sum_{k\neq i}\delta_{kC}w_k(r_k)\right) - \delta_{jC}w_i(r_i). \tag{3-15}$$

The $g_C^{(1)}(\cos\theta_{jik})$ and $g_C^{(2)}(\cos\theta_{jik})$ values and their respective first and second derivatives with respect to the angle in (3-11) are known values and are listed in Table 3.

The third term in (3-3), π_{ij}^{rc}, depends on the coordination numbers. Particularly, π_{ij}^{rc} is zero for graphene lattice with periodic boundary conditions. And the fourth term in (3-3), π_{ij}^{dh}, is based on the torsion angles, w_{kijl}:

$$\pi_{ij}^{dh} = T_{ij}(N_{ij}, N_{ji}, N_{ij}^{\text{conj}}) \sum_{k\neq i,j}\sum_{l\neq i,j}(1-\cos^2\omega_{kijl})$$
$$\times w_{ik}'(r_{ik})w_{jl}'(r_{jl})\Theta(\sin\theta_{jik}-s^{\min})\Theta(\sin\theta_{ijl}-s^{\min}) \tag{3-16}$$

with

$$w_{ij}'(r_{ij}) = S'(t_c'(r_{ij})) \tag{3-17}$$

and

$$t'_c(r_{ij}) = \frac{r_{ij} - r_{ij}^{\min}}{r_{ij}^{\max'} - r_{ij}^{\min}}. \tag{3-18}$$

The torsion angle, w_{kijl}, is defined as the angle between the plane defined by the vectors (r_{ji}, r_{ik}) and (r_{ij}, r_{jl}):

$$\cos \omega_{kijl} = \frac{\boldsymbol{r}_{ji} \wedge \boldsymbol{r}_{ik}}{r_{ji} r_{ik}} \cdot \frac{\boldsymbol{r}_{ij} \wedge \boldsymbol{r}_{jl}}{r_{ij} r_{jl}}. \tag{3-19}$$

The Lennard-Jones term, E_{ij}^{LJ}, in (3-1) includes the long-range interaction between pairs of atoms

$$E_{ij}^{\mathrm{LJ}} = S(t_r(r_{ij})) S(t_b(b_{ij}^*)) + [1 - S(t_r(r_{ij}))] C_{ij}^{\mathrm{LJ}}(r_{ij}) V_{ij}^{\mathrm{LJ}}, \tag{3-20}$$

where V_{ij}^{LJ} is a Lennard-Jones potential, 6-12 type,

$$V_{ij}^{\mathrm{LJ}} = 4\epsilon_{ij} \left[\left(\frac{\sigma_{ij}}{r_{ij}} \right)^{12} - \left(\frac{\sigma_{ij}}{r_{ij}} \right)^{6} \right] \tag{3-21}$$

and $S(t)$ is a switching function

$$S(t) = \Theta(-t) + \Theta(t)\Theta(1-t)[1 - t^2(3 - 2t)]. \tag{3-22}$$

Finally, the torsion term in (3-1), E_{kijl}^{tors}, considers the torsion long-range interaction as a function of the dihedral angle determined by atoms i, j, k and l:

$$E_{ij}^{\mathrm{tors}} = \sum_{k \neq i, j} \sum_{l \neq i, j, k} w_{ij}(r_{ij}) w_{jk}(r_{jk}) w_{kl}(r_{kl}) V_{ijkl}^{\mathrm{tors}}, \tag{3-23}$$

where

$$V_{ijkl}^{\mathrm{tors}} = \epsilon_{ijkl} \left[\tfrac{256}{405} \cos^{10}\left(\frac{\omega_{ijkl}}{2} \right) - \tfrac{1}{10} \right]. \tag{3-24}$$

3.2. Force-constant model. As proved in Section 2, the energy of a defective crystal lattice can be written in terms of either bondwise force constants, $\boldsymbol{\Psi}$, or atomic force constants, $\boldsymbol{\Phi}$. The former can be obtained through the second linearization of a given interatomic potential; thus, the latter ones are derived by means of relation (2-12). In general, given a potential E, the atomic force constants are obtained by

$$\Psi_{ij} \begin{pmatrix} \boldsymbol{l} - \boldsymbol{l}' \\ ab \quad cd \end{pmatrix} = \frac{\partial^2 E}{\partial r(\boldsymbol{l}', cd)_j \, \partial r(\boldsymbol{l}, ab)_i}, \tag{3-25}$$

where $r(\boldsymbol{l}, ab)_i$ is the i-th component of the vector corresponding to the atomic bond between atoms a and b with label $\boldsymbol{l}$ and $r(\boldsymbol{l}', cd)_j$ is the j-th component of the vector between atoms c and d with label $\boldsymbol{l}'$. Once the bondwise force constants are computed by using the above equation, a straightforward calculation using (2-12) provides the corresponding atomic force constants $\boldsymbol{\Phi}$.

In this section, we tackle the definition of a bondwise force-constants model from the AIREBO potential, and thus, first and second linearizations of energy (3-1) are needed. In order to accomplish an accurate description of interatomic forces in graphene, our model encompasses atomic interactions up to second-nearest neighbors for the REBO term and up to fourth-nearest neighbors for the LJ and torsion terms. The analytical expressions of the first and second derivatives of the functions defining the AIREBO

	(a)	(b)	(c)	(d)	(e)
α_1	364.0	497.2	527.7	409.7	399.0
β_1	247.0	173.8	68.1	145.0	135.7
δ_1	100.5	107.0	118.3	98.9	292.8
α_2	−30.8	−41.4	5.8	−40.8	−79.6
β_2	72.3	58.1	32.7	74.2	67.8
γ_2	−17.8	−3.0	26.7	−9.1	39.2
δ_2	−11.5	−15.9	−16.9	−8.2	0.9
α_3		−20.6	0.0	−33.2	0.0
β_3		34.5	0.0	50.1	0.0
δ_3		9.1	3.7	5.8	−34.3
α_4			0.0	10.5	0.0
β_4			0.0	5.0	0.0
γ_4			0.0	2.2	0.0
δ_4			−1.8	−5.2	17.1

Table 4. Comparison of force-constants values obtained from different interatomic potentials and considering interactions (a) up to second neighbors [Ariza and Ortiz 2010], (b) up to third neighbors [Mendez and Ariza 2015] and (c)–(e) up to fourth neighbors [Ariza et al. 2011; Tewary and Yang 2009; Wirtz and Rubio 2004].

potential have been provided in [Ariza et al. 2011]. Table 4 shows a comparison of the force-constants values we have obtained from the linearization of different interatomic potentials, i.e., a harmonic model [Aizawa et al. 1990], a reactive empirical bond-order potential [Stuart et al. 2000] and a tight binding potential [Xu et al. 1992]. These computed force constants have been validated against experimental phonon dispersion curves and previous force-constants models for graphene. Wirtz and Rubio [2004] have obtained their force constants model by fitting to density-functional theory (generalized-gradient approximation) quantum-mechanics calculations of the phonon dispersion curves of graphene whereas Tewary and Yang [2009] employed a potential based on the Tersoff potential and added a term of radial energy.

4. Anharmonic contribution of the AIREBO potential

The discrete dislocation theory in crystals combines lattice harmonics, the theory of eigendeformations [Mura 1987] and the discrete Fourier transform, leading to analytically tractable expressions of the stored energy of defective graphene (see (2-13)). However, despite its robustness and accuracy, a question of interest concerns the formulation of convergent schemes that relax discrete dislocation structures in accordance to a full interatomic potential. A particular scheme that preserves the advantages of the discrete dislocation theory, and in particular the ability to use Green's functions, was proposed by [Gallego and Ortiz 1993]. In this scheme, the fully nonlinear solution is obtained by the *method of forces*, i.e., by appending unknown forces to the *discrete dislocation* energy so as to equilibrate the lattice with respect to the fully nonlinear atomistic potential.

Thus, given an eigendeformation field, $\boldsymbol{\beta}$, constrained to defining lattice-invariant deformations, the discrete dislocation theory provides a harmonic displacement field, $\boldsymbol{u}_H$, that minimizes the harmonic part

of the potential such that

$$DE_H(\boldsymbol{u}_H) = 0, \tag{4-1}$$

where E_H is the harmonic part of the full potential, $Df(\cdot)$ denotes the derivative of f with respect to its argument and $\boldsymbol{u}_H$ represents the harmonic displacement field corresponding to the eigendeformation field, $\boldsymbol{\beta}$. The total harmonic energy including applied forces $\boldsymbol{f}$ is given by

$$E_H(\boldsymbol{u}, \boldsymbol{\beta}) = \tfrac{1}{2}\langle \boldsymbol{B}(d\boldsymbol{u} - \boldsymbol{\beta}), (d\boldsymbol{u} - \boldsymbol{\beta})\rangle - \langle \boldsymbol{f}, \boldsymbol{u}\rangle = \tfrac{1}{2}\langle \boldsymbol{A}\boldsymbol{u}, \boldsymbol{u}\rangle - \langle \delta(\boldsymbol{B}\boldsymbol{\beta}), \boldsymbol{u}\rangle + \tfrac{1}{2}\langle \boldsymbol{B}\boldsymbol{\beta}, \boldsymbol{\beta}\rangle - \langle \boldsymbol{f}, \boldsymbol{u}\rangle. \tag{4-2}$$

Next, minimization of E_H with respect to $\boldsymbol{u}$ at fixed $\boldsymbol{\beta}$ yields the equilibrium equation

$$\boldsymbol{u}_H^* = \boldsymbol{A}^{-1}(\boldsymbol{f}^E + \boldsymbol{f}), \tag{4-3}$$

where

$$\boldsymbol{f}^E = \delta \boldsymbol{B}\boldsymbol{\beta} \tag{4-4}$$

is the distribution of eigenforces corresponding to $\boldsymbol{\beta}$. We thus continue to apply forces $\boldsymbol{f}$ such that the entire lattice can be equilibrated, and therefore, the resulting harmonic field $\boldsymbol{u}_H^*$ minimizes a given anharmonic energy E. The equilibrium equations for the equilibrating forces $\boldsymbol{f}$ are

$$DE(\boldsymbol{A}^{-1}(\boldsymbol{f}^E + \boldsymbol{f})) = 0. \tag{4-5}$$

Because of the good starting accuracy of the discrete dislocation theory, the corrective forces decay very rapidly away from the core of defects and, hence, represent highly localized corrections.

5. Glide and shuffle dislocation dipoles in graphene

Slip in graphene occurs on three different planes defined by their normal vectors, m_i, $i = 1, 2, 3$, (see Figure 4) which correspond to the close-packed atomic planes in graphene. At first glance, for each slip plane, gliding might occur across either a zigzag chain of bonds or across parallel bonds (Figure 6). The first case defines the so-called glide dislocations whereas the latter one refers to shuffle dislocations.

In a previous work, we have investigated two mechanisms of crystallographic slip in graphene, corresponding to glide and shuffle generalized stacking faults [Ariza et al. 2012]. The calculations were
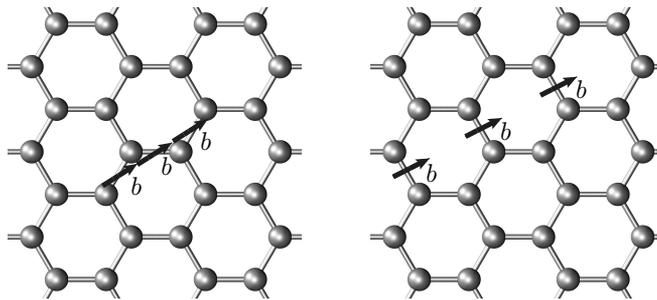
Figure 6. Detail of the distribution of eigendeformation $\boldsymbol{\beta}$, consisting of one Burgers vector over (left) a chain of three zigzag bonds and (right) three consecutive parallel bonds.
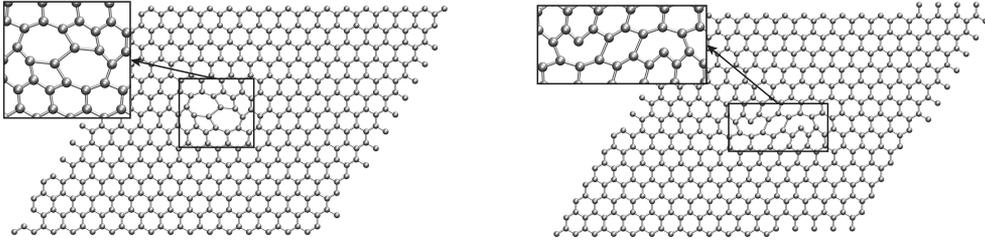
Figure 7. Dislocation core structures predicted by DD theory (left) glide dislocation dipole ($L = 3$) and (right) shuffle dislocation dipole ($L = 3$).
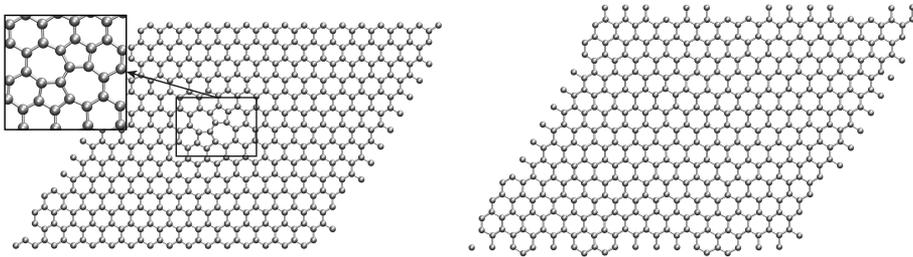
Figure 8. Dislocation core structure after relaxation obtained by means of the anharmonic extension of the DD theory (left) glide dislocation dipole ($L = 3$) and (right) shuffle dislocation dipole ($L = 3$).

performed using the Sandia National Laboratories Large-scale Atomic/Molecular Massively Parallel Simulator (LAMMPS) and two different interatomic reactive potentials: AIREBO and ReaxFF [Stuart et al. 2000; van Duin et al. 2001]. The γ-surfaces of a crystal shed useful light on the structure and stability of extended defects such as dislocation dipoles and dissociated cores. The outcome of the aforementioned study was that glide dislocation dipoles are stable in graphene down to exceedingly small separations of the order of a few lattice spacings and dissociation of perfect dislocations into partial dislocations are unlikely in both configurations. The assessment of the dynamical stability of partial dislocations was carried out by inserting the discrete dislocation configurations predicted by the DD theory into molecular dynamics calculations as initial conditions.

In this section, the stability analysis of discrete dislocation structures is achieved by using the computational scheme outlined above. For ease of indexing, we denote by $L = n$ the length of the dislocation and it represents that the distribution of eigendeformations is applied over n atomic bonds. In this work, we endeavor to assess the stability of glide and shuffle dislocation dipoles. We start by predicting the harmonic core structures and energies of these two dislocations by means of DD theory (see Figure 7). In particular, for configurations corresponding to $L = 3$, we aim to validate our computational scheme by studying whether glide and shuffle dislocation dipoles are metastable or not. Thus, the initial discrete configuration is allowed to relax in accordance to the full interatomic potential AIREBO as was described in Section 4.

Figure 8 shows the computed relaxed configurations and confirms the known metastable character of very short glide dislocations in graphene. Moreover, Table 5 compares the defect energies of the two

Dipole $L = 3$	DD theory (eV)	After relaxation (eV)
Glide	17.07	5.87
Shuffle	20.20	~ 0

Table 5. Computed energies initially predicted by DD theory and obtained after relaxation considering the full interatomic potential for a glide and shuffle dislocation dipole ($L = 3$).
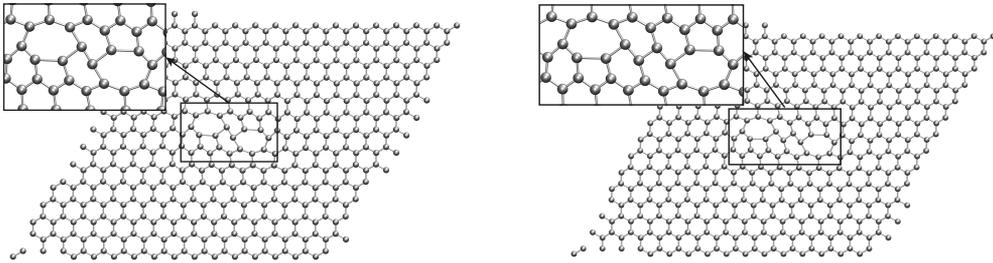
Figure 9. Dislocation core predicted by DD theory (left) glide dislocation dipole ($L = 5$) and (right) glide dislocation dipole ($L = 7$).
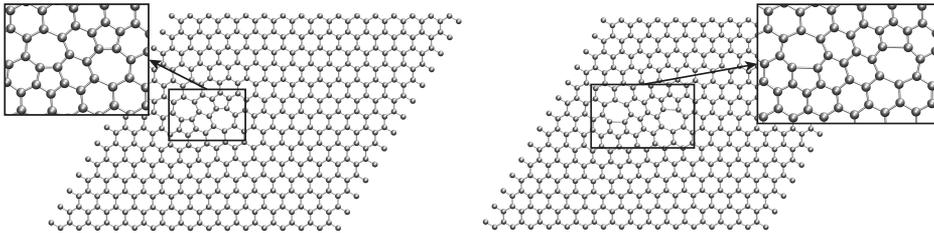
Figure 10. Dislocation core after relaxation (left) glide dislocation dipole ($L = 5$) and (right) glide dislocation dipole ($L = 7$), computed using the extension of the DD theory.

Glide dipole	DD theory (eV)	After relaxation (eV)
$L = 5$	19.87	10.93
$L = 7$	21.74	19.49

Table 6. Stored energies initially predicted by DD theory and those obtained after relaxation considering the full interatomic potential for a glide and shuffle dislocation dipole ($L = 5, 7$).

different dipoles, before and after relaxation. For the shuffle configuration, the stored energy decreases during the relaxation process down to zero.

Next, following the same procedure, we have investigated the relaxed configurations corresponding to two glide dislocation dipoles with $L = 5$ and $L = 7$ (Figures 9 and 10). The stored energies computed before and after relaxation are included in Table 6; these values are in agreement with similar calculations reported in the literature. The relaxed dislocation core structures shown in Figure 10 also agree with those observed in molecular dynamics calculations.

6. Conclusions

We have presented an assessment of the stability of discrete dislocations in graphene. The assessment is based on an extension of the discrete dislocation theory that takes into account the anharmonic part of the interatomic potentials. Thus, we have obtained fully nonlinear solutions by using the *method of forces*, i.e., by appending unknown forces to the discrete dislocation energy so as to equilibrate the lattice with respect to the fully nonlinear potential. Specifically, we have first computed the harmonic dislocation core structures and energies predicted by the force constants model obtained from the AIREBO potential and then studied their dynamic stability.

References

[Aizawa et al. 1990] T. Aizawa, R. Souda, S. Otani, Y. Ishizawa, and C. Oshima, "Bond softening in monolayer graphite formed on transition-metal carbide surfaces", *Phys. Rev. B* **42**:18 (1990), 11469–11478.

[Ariza and Ortiz 2005] M. P. Ariza and M. Ortiz, "Discrete crystal elasticity and discrete dislocations in crystals", *Arch. Ration. Mech. Anal.* **178**:2 (2005), 149–226.

[Ariza and Ortiz 2010] M. P. Ariza and M. Ortiz, "Discrete dislocations in graphene", *J. Mech. Phys. Solids* **58**:5 (2010), 710–734.

[Ariza et al. 2010] M. P. Ariza, M. Ortiz, and R. Serrano, "Long-term dynamic stability of discrete dislocations in graphene at finite temperature", *Int. J. Fracture* **166**:1–2 (2010), 215–223.

[Ariza et al. 2011] M. P. Ariza, C. Ventura, and M. Ortiz, "Modelo de fuerzas interatómicas para el grafeno a partir del potencial AIREBO", *Rev. Int. Métod. Numér.* **27**:2 (2011), 105–116.

[Ariza et al. 2012] M. P. Ariza, R. Serrano, J. P. Mendez, and M. Ortiz, "Stacking faults and partial dislocations in graphene", *Philos. Mag.* **92**:16 (2012), 2004–2021.

[Bae et al. 2010] S. Bae, H. Kim, Y. Lee, X. Xu, J.-S. Park, Y. Zheng, J. Balakrishnan, T. Lei, H. R. Kim, Y. I. Song, Y.-J. Kim, K. S. Kim, B. Özyilmaz, J.-H. Ahn, B. H. Hong, and S. Iijima, "Roll-to-roll production of 30-inch graphene films for transparent electrodes", *Nat. Nanotechnol.* **5**:8 (2010), 574–578.

[Balandin et al. 2008] A. A. Balandin, S. Ghosh, W. Bao, I. Calizo, D. Teweldebrhan, F. Miao, and C. N. Lau, "Superior thermal conductivity of single-layer graphene", *Nano Lett.* **8**:3 (2008), 902–907.

[Blake et al. 2008] P. Blake, P. D. Brimicombe, R. R. Nair, T. J. Booth, D. Jiang, F. Schedin, L. A. Ponomarenko, S. V. Morozov, H. F. Gleeson, E. W. Hill, A. K. Geim, and K. S. Novoselov, "Graphene-based liquid crystal device", *Nano Lett.* **8**:6 (2008), 1704–1708.

[Brenner 1990] D. W. Brenner, "Empirical potential for hydrocarbons for use in simulating the chemical vapor deposition of diamond films", *Phys. Rev. B* **42**:15 (1990), 9458–9471.

[Bunch et al. 2008] J. S. Bunch, S. S. Verbridge, J. S. Alden, A. M. van der Zande, J. M. Parpia, H. G. Craighead, and P. L. McEuen, "Impermeable atomic membranes from graphene sheets", *Nano Lett.* **8**:8 (2008), 2458–2462.

[van Duin et al. 2001] A. C. T. van Duin, S. Dasgupta, F. Lorant, and I. Goddard, W. A., "ReaxFF: a reactive force field for hydrocarbons", *J. Phys. Chem. A* **105**:41 (2001), 9396–9409.

[Finnis and Sinclair 1984] M. W. Finnis and J. E. Sinclair, "A simple empirical *N*-body potential for transition metals", *Philos. Mag. A* **50**:1 (1984), 45–55.

[Gallego and Ortiz 1993] R. Gallego and M. Ortiz, "A harmonic/anharmonic energy partition method for lattice statics computations", *Model. Simul. Mater. Sc.* **1**:4 (1993), 417–436.

[Geim and Novoselov 2007] A. K. Geim and K. S. Novoselov, "The rise of graphene", *Nat. Mater.* **6**:3 (2007), 183–191.

[Jeong et al. 2008] B. W. Jeong, J. Ihm, and G. D. Lee, "Stability of dislocation defect with two pentagon-heptagon pairs in graphene", *Phy. Rev. B* **78**:16 (2008), 165403.

[Jung et al. 2014] Y. U. Jung, K.-W. Park, S.-T. Hur, S.-W. Choi, and S. J. Kang, "High-transmittance liquid-crystal displays using graphene conducting layers", *Liq. Cryst.* **41**:1 (2014), 101–105.

[Lee et al. 2008] C. Lee, X. Wei, J. W. Kysar, and J. Hone, "Measurement of the elastic properties and intrinsic strength of monolayer graphene", *Science* **321**:5887 (2008), 385–388.

[Liu et al. 2011] T.-H. Liu, G. Gajewski, C.-W. Pao, and C. C.-C., "Structure, energy, and structural transformations of graphene grain boundaries from atomistic simulations", *Carbon* **49**:7 (2011), 2306–2317.

[Mendez and Ariza 2015] J. P. Mendez and M. P. Ariza, "Harmonic tight-binding model for graphene", preprint, 2015. To appear in *J. Comput. Phys.*

[Munkres 1984] J. R. Munkres, *Elements of algebraic topology*, Addison-Wesley, Menlo Park, CA, 1984.

[Mura 1987] T. Mura, *Micromechanics of defects in solids*, 2nd ed., Mechanics of Elastic and Inelastic Solids **3**, Kluwer, Dordrecht, Netherlands, 1987.

[Nair et al. 2008] R. R. Nair, P. Blake, A. N. Grigorenko, K. S. Novoselov, T. J. Booth, T. Stauber, N. M. R. Peres, and A. K. Geim, "Fine structure constant defines visual transparency of graphene", *Science* **320**:5881 (2008), 1308.

[Novoselov et al. 2005] K. S. Novoselov, A. K. Geim, S. V. Morozov, D. Jiang, M. I. Katsnelson, I. V. Grigorieva, S. V. Dubonos, and A. A. Firsov, "Two-dimensional gas of massless Dirac fermions in graphene", *Nature* **438**:7065 (2005), 197–200.

[Stuart et al. 2000] S. J. Stuart, A. B. Tutein, and J. A. Harrison, "A reactive potential for hydrocarbons with intermolecular interactions", *Journal of Chemical Physics* **112**:14 (2000), 6472–6486.

[Tersoff 1988] J. Tersoff, "New empirical approach for the structure and energy of covalent systems", *Phys. Rev. B* **37**:12 (1988), 6991–7000.

[Tewary and Yang 2009] V. K. Tewary and B. Yang, "Parametric interatomic potential for graphene", *Phys. Rev. B* **79**:7 (2009), 075442.

[Wirtz and Rubio 2004] L. Wirtz and A. Rubio, "The phonon dispersion of graphite revisited", *Solid State Commun.* **131**:3–4 (2004), 141–152.

[Wu et al. 2010] W. Wu, Z. Liu, L. A. Jauregui, Q. Yu, R. Pillai, H. Cao, J. Bao, Y. P. Chen, and S.-S. Pei, "Wafer-scale synthesis of graphene by chemical vapor deposition and its application in hydrogen sensing", *Sensor. Actuat. B. Chem.* **150**:1 (2010), 296–300.

[Xu et al. 1992] C. H. Xu, C. Z. Wang, C. T. Chan, and K. M. Ho, "A transferable tight-binding potential for carbon", *J. Phys. Condens. Mat.* **4**:28 (1992), 6047–6054.

[Yazyev and Louie 2010a] O. V. Yazyev and S. G. Louie, "Electronic transport in polycrystalline graphene", *Nat. Mater.* **9**:10 (2010), 806–809.

[Yazyev and Louie 2010b] O. V. Yazyev and S. G. Louie, "Topological defects in graphene: dislocations and grain boundaries", *Phy. Rev. B* **81**:19 (2010), 195420.

[Zhang et al. 2005] Y. Zhang, Y.-W. Tan, H. L. Stormer, and P. Kim, "Experimental observation of the quantum Hall effect and Berry's phase in graphene", *Nature* **438**:7065 (2005), 201–204.

[Zhang et al. 2012] J. Zhang, J. Gao, L. Liu, and J. Zhao, "Electronic and transport gaps of graphene opened by grain boundaries", *J. Appl. Phys.* **112**:5 (2012), 053713.

MARIA PILAR ARIZA: mpariza@us.es
Escuela Técnica Superior de Ingeniería, Universidad de Sevilla, Camino de los Descubrimientos, s/n, 41092 Sevilla, Spain

JUAN PEDRO MENDEZ: jmendez@us.es
Escuela Técnica Superior de Ingeniería, Universidad de Sevilla, Camino de los Descubrimientos, s/n, 41092 Sevilla, Spain

msp

A NOTE ON WEAR OF ELASTIC SLIDING PARTS
WITH VARYING CONTACT AREA

MICHELE CIAVARELLA AND NICOLA MENGA

Wear of sliding parts in the transient regime depends on elastic behavior of the bulk of the materials, and in general the contact area cannot be assumed to be constant, so that the problem is nonlinear. Here we look at the simple example of the classical Hertzian geometry, obtaining a simple solution for transient to uniform pressure (which is also the "rigid" limit solution) assuming out-of-plane sliding, and the approximation of the "Winkler foundation" in plane strain. Wear is assumed to vary according to the Reye–Archard law, which applies locally and only to the wearing indenter. As a further improvement, we give a more refined solution using a Winkler constant which adapts to the changing size of the contact.

1. Introduction

Wear, together with fatigue, is one of the major causes of malfunctioning and disservice of engineering components. As such, the literature on wear is huge, particularly on the experimental side. Well known are Ashby's wear maps [Lim and Ashby 1987], which fit a large number of experiments and permit estimation of different regimes of wear, which depend on temperature at the interface and in the bulk, and, correspondingly, the orders of magnitude of variation in the wear coefficient, mainly dependent on pressure and relative speed.

Even for a constant speed, we generally distinguish two different phases: "running-in", in which transient processes occur, and "steady state". It should be remarked that there are different possible definitions of "running-in". Some authors suggest a running-in phase in which essentially the roughness is altered, and there is a departure from the later regime of "linear behavior", described by the Reye–Archard law [Reye 1860; Archard and Hirst 1956]. Another interpretation of "running-in", more relevant to the present paper, describes the phase where the pressure distribution changes in time due to elasticity effects. For a contact which changes pressure and also size in time, both phenomena may in principle be at work, but we shall concentrate in this paper on the second meaning of running-in, assuming the Reye–Archard law to apply throughout the process. It is perhaps interesting to remark that Reye's work, though earlier, remained somehow unnoticed in the English-speaking literature, which tends to cite Archard's work [Archard and Hirst 1956].[1] Both describe the dependence of worn volume V on normal load as linear and on hardness as inverse:

$$V = \frac{kPS}{\text{HB}}, \tag{1-1}$$

[1]As Villaggio [2001] says, "Reye's model became very popular in Europe (in Italy was promulgated by Panetti [1947]), and it is still taught in university courses of applied mechanics. But, strangely enough, this theory has been totally ignored in English and American literature."

where S is sliding distance, P is normal load, and HB is Brinell hardness. In this form, k is a dimensionless constant which, in the original Archard model, expresses the (unknown a priori) probability of an asperity to wear when sliding it by a length equal to twice its contact diameter (see also http://en.wikipedia.org/wiki/Archard_equation). It varies from about 10^{-2} for mild steel on mild steel to 2–3 orders of magnitude less for tool steels on metals, and even lower on plastic. Some values for ceramic on ceramic are as low as 10^{-6}. Notice that this law holds until the nominal pressure is lower than the yield. Above that, k grows with P, and hence we depart from linearity. Naturally, the many orders of magnitude of variation in k hide many possible changes of mechanisms and dependence on other constants, for example, toughness of the materials; and indeed the wear rate in certain ranges can increase, be independent of, or decrease with hardness depending on the particular toughness [Hornbogen 1975].

Often, as said before, running-in is associated to elasticity-dominated effects (see, for example, [Goryacheva 1998]). One class of problem is when the contact area is fixed in time, which permits special linear techniques to be used, like the eigenfunction expansion of the transient pressure distribution. However, another important class of problem does not neglect the change of contact area during the wear process, and hence cannot rely on linearity and the superposition principle.

Most of the present literature is concerned with FEM implementation of Archard's law (see, for example, [Mattei et al. 2011; Põdra and Andersson 1999; Sfantos and Aliabadi 2007]), and therefore the computational cost of a reasonably complex problem is significant. An approximate solution using the Winkler approximation for the contact, namely that the displacement is a local function of the pressure, is possible in closed form. In particular, here we extend the 2D treatment of [Goryacheva 1998] to provide full solutions also for pressure distribution. In common with Goryacheva, we shall assume wear is only acting on the indenter, and not in the half-plane. Finally, as a further extension, a section is added on an "adaptive" Winkler solution, in which the modulus is corrected for the changing contact area. This gives some hint of the degree of approximation of the solution. That the results with Winkler models can be very good compared to the full continuum problem is known in the literature (see, for example, [Põdra and Andersson 1997]).

2. General formulation

The problem we plan to solve is that of an elastic indenter that slides out-of-plane, over a Winkler half-plane. The indenter can also be elastic but, without loss of generality, we shall assume it is rigid. The half-plane is wearing much more slowly than the punch, so that we can neglect its wear process altogether. This is clearly not correct in general, but is a limit approximation when the wear coefficient of the indenter is much larger than that of the half-plane. If the contact repeats itself in some patterns, like in the case of a pin-on-disk situation, or pad-disk assembly, this amounts to assuming that wear of the disk is negligible compared to that of the pin or pad. The geometry and the symbols are described in Figure 1, where $d(t)$ is the indentation depth, $b(t)$ is the contact semiwidth, $u(x, t)$ is the displacement of the Winkler foundation, $w(x, t)$ is the indenter wear, and $g_0(x)$ is the initial gap function.

We shall consider the most interesting case, that of contact area growing in time, which is typical if the contact load is constant or increasing in time, although the more general cases of decreasing or variable loads require similar considerations (see, for example, [Goryacheva 1998] for the more general case).
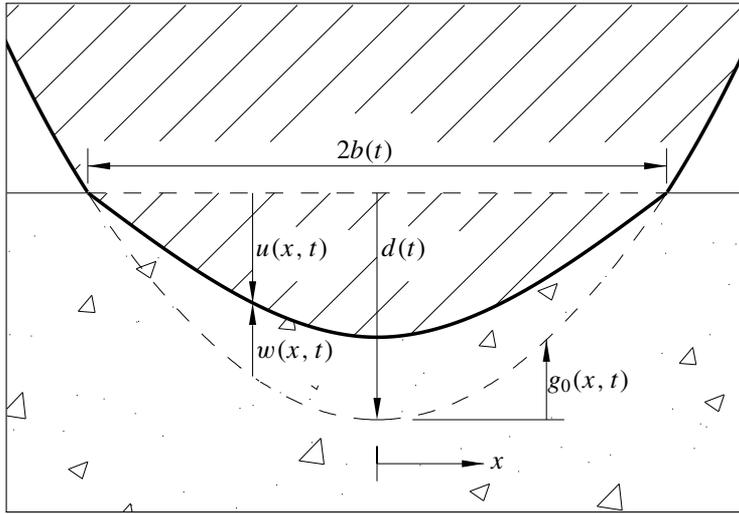
Figure 1. Indenter geometry and symbols. The figure takes into account the Winkler behavior for a contact area $2b(t)$ that is expanding in time. Triangles are used to indicate the elastic material in the half-plane.

2A. *Formulation.* With reference to Figure 1, inside the contact area the displacement field is

$$u(x, t) = d(t) - g_0(x) - w(x, t). \tag{2-1}$$

As in the classical Winkler model, simple proportionality of pressure and displacement is assumed:

$$p(x, t) = k(t)u(x, t), \tag{2-2}$$

where $k(t)$ is the proportionality coefficient, or Winkler constant, having units of pressure per unit displacement — time-dependent in the most general formulation.

The Winkler model permits us to solve the pressure distribution in the contact area. In fact, inside the contact region, using (2-2) in (2-1) we have

$$p(x, t) = k(t)[d(t) - g_0(x) - w(x, t)]. \tag{2-3}$$

By integrating (2-3) over the contact length $[-b(t), b(t)]$, we find the state equation of the problem, which relates the contact evolution (constants b, d), the indenter wear, and the external load per unit length $P(t)$:

$$\frac{P(t)}{k(t)} = 2b(t)d(t) - \int_{-b(t)}^{b(t)} [g_0(x) + w(x, t)] \, dx. \tag{2-4}$$

2B. *Indentation evolution.* The profile wear is modeled by the Reye–Archard law. Hence, if $v(t)$ is the relative slip velocity, f is the friction coefficient, and β is the wear coefficient, we can write

$$\frac{\partial w(x, t)}{\partial t} = \beta f v(t) p(x, t) = \alpha(t) p(x, t), \tag{2-5}$$

where $\alpha(t) = \beta f v(t)$ is a parameter which takes into account the generally time-dependent velocity and $w(t)$ is the profile wear in the normal direction with respect to the contact area.

The indentation evolution $d(t)$ is obtained by differentiating (2-4) with respect to time. Using (2-5) and the condition that the edges of the contact region are progressively entering contact and hence have no wear, i.e., $w(b(t), t) = w(-b(t), t) = 0$, we find that

$$P'(t) = d'(t)2k(t)b(t) - \left[k(t)\alpha(t) - \frac{k'(t)}{k(t)} \right] P(t),$$
(2-6)

which can be easy integrated to give $d(t)$ and then $b(t) = g_0^{-1}[d(t)]$.

2C. *Pressure field evolution.* Let us now look at the pressure behavior at a fixed position $\bar{x}$,

$$p(\bar{x}, t) = p(t).$$

The pressure field evolution is governed by (2-3). Differentiating it with respect to time and using (2-5), we find

$$p'(t) + \left[k(t)\alpha(t) - \frac{k'(t)}{k(t)} \right] p(t) = k(t)d'(t),$$
(2-7)

that is, a first-order ODE which can be solved by the variation of constants method, finding

$$p(t) = q(t)e^{-B(t)},$$
(2-8)

where $B(t)$ is a general primitive of the coefficient,

$$B(t) = \int \left[k(t)\alpha(t) - \frac{k'(t)}{k(t)} \right] dt,$$
(2-9)

and where

$$q(t) = \int k(t)d'(t)e^{B(t)} \, dt + C,$$
(2-10)

with C an arbitrary constant of integration.

The initial condition to find the correct value of C depends on whether the particular value of $\bar{x}$ is inside or outside the original contact area. In particular,

$$\begin{cases} \text{if } \bar{x} \in [-b(0), b(0)], \text{ then } p(\bar{x}, 0) = k[d(0) - g_0(\bar{x})]; \\ \text{else } p(\bar{x}, t) = 0 \text{ for } t < \bar{t}, \end{cases}$$
(2-11)

where $\bar{t}$ is the time at which $|\bar{x}| = b(t)$.

3. Constant P, k, α

In order to develop analytical results, we will now focus on classical Hertzian indenters, although the approach to be described does not need any kind of limitation in terms of indenter geometry. The Hertzian indenter is characterized by its curvature radius R and

$$g_0(x) = \frac{x^2}{2R}.$$
(3-1)
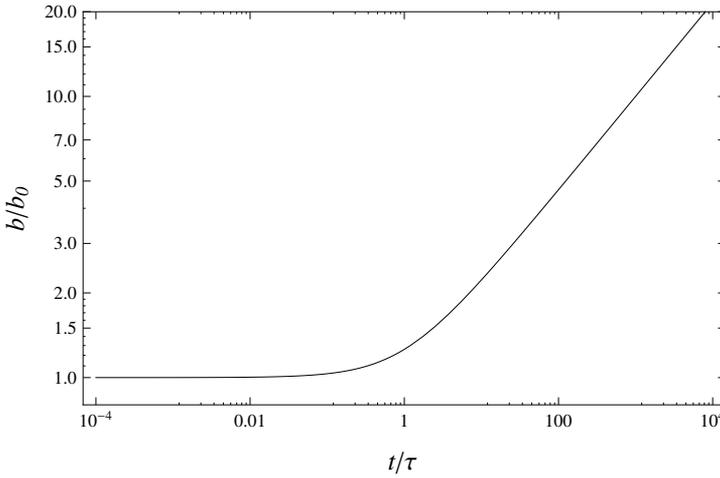
Figure 2. Dimensionless contact area vs. dimensionless time; b_0 is the initial contact area.

Assuming the load, the Winkler constant and the relative sliding speed between the indenter and the half-plane are all constant,

$$P(t) = P, \quad k(t) = k, \quad \alpha(t) = \alpha, \tag{3-2}$$

after some algebra (2-6) can be solved, finding

$$d(t) = \left(\frac{3P}{4k\sqrt{2R}}\right)^{2/3} (1 + \alpha k t)^{2/3}. \tag{3-3}$$

The initial condition depends on the Winkler constant k, but the steady state does not — and this explains the success of rigid models, which predict the steady state from purely kinematic considerations. For example, the design of brakes systems is classically based upon rigid models (see [Sfantos and Aliabadi 2007]). This important simplification is valid for every indenter shape described by $g_0(x)$, not only for the Hertzian case, but it requires the assumptions of constant normal load and constant relative sliding speed.

Further, by (3-1), the contact area evolution is

$$b(t) = \sqrt{2R}\left(\frac{3P}{4k\sqrt{2R}}\right)^{1/3} (1 + \alpha k t)^{1/3}, \tag{3-4}$$

and it is shown in Figure 2. The "cross-over" time is a characteristic time of the process defined as

$$\tau = \frac{1}{k\alpha}. \tag{3-5}$$

3A. *Pressure field.* The pressure field evolution is a little more complex to evaluate. Using the above assumptions, (2-10) can be solved by differentiating (3-3) in time, finding

$$q(t) = \frac{2\alpha k^2}{3}\left(\frac{3P}{4k\sqrt{2R}}\right)^{2/3} \int \frac{e^{\alpha k t}}{(1 + \alpha k t)^{1/3}} \, dt + C,$$
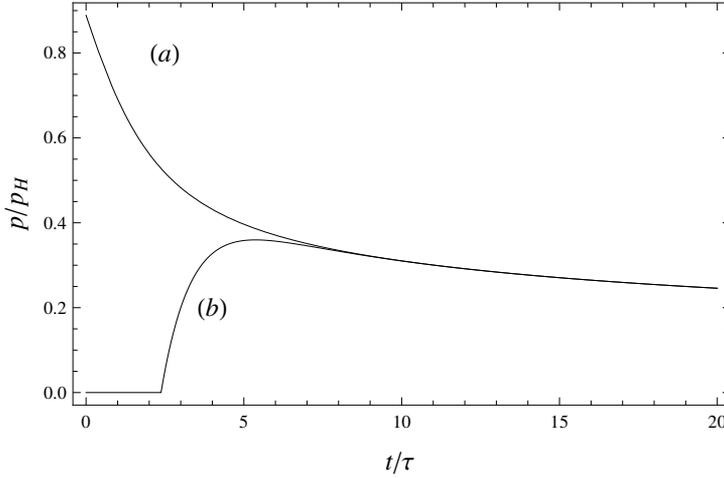
Figure 3. Pressure evolution vs. time. (a) $x = \frac{1}{3}b_0$ and (b) $x = \frac{3}{2}b_0$. Pressure values are nondimensionalized to the Hertzian initial peak pressure.

and the integral can be solved in terms of the exponential integral function:

$$\int \frac{e^{\alpha k t}}{(1 + \alpha k t)^{1/3}} \, dt = -\frac{(1 + \alpha k t)^{2/3} \, \mathrm{Ei}_{1/3}(-1 - \alpha k t)}{\alpha k e}.$$

Therefore, according to (2-8), the pressure trend in time will be

$$p(t) = -\frac{2\alpha k^2}{3} \left(\frac{3P}{4k\sqrt{2R}} \right)^{2/3} \frac{(1 + \alpha k t)^{2/3} \, \mathrm{Ei}_{1/3}(-1 - \alpha k t)}{\alpha k e} e^{-\alpha k t} + C e^{-\alpha k t},$$

where the initial condition C can be found by (2-11).

Figure 3 shows the pressure evolution in time for different fixed $\bar{x}$. As expected, inside the initial contact area (curve (a)) the pressure is monotonically decreasing and the reduction ratio is also monotonically decreasing. This is obviously due to the increase of the contact area in time because of wear. Outside the initial contact area, the pressure is initially zero (curve (b)), because the point is not yet in contact. When, due to wear of the indenter, contact occurs, the contact pressure suddenly increases. The pressure increase ratio is not only influenced by the rate of wear, but also by the local slope of the unworn profile which comes into contact. Both curves converge on the uniform pressure final stage.

4. The Winkler adaptive model

Winkler's model can be applied to Hertzian contact as described in [Johnson 1985], which suggests that in our case a time-varying Winkler modulus can be defined by considering the time variation of the contact area and using the value suggested by Johnson which would give the best fit for the contact area semiwidth in the Hertzian case. Specifically,

$$k(t) = m \frac{E^*}{b_{ad}(t)} \text{ (plane contact)}, \tag{4-1}$$

where $b_{ad}(t)$ is the semiwidth of the contact in our case, and $E^* = E/(1 - \nu^2)$ is the plain strain modulus. The numerical coefficient m can be chosen in order to match the initial Hertzian contact solution in terms of the contact semiwidth

$$b_{ad}(0) = a_H, \tag{4-2}$$

which gives $m = \frac{3\pi}{8}$, or the contact pressure peak

$$d_{ad}(0)k(0) = p_H, \tag{4-3}$$

which gives $m = \frac{8}{3\pi}$.

Hence, (2-6) becomes

$$d'_{ad}(t) = \frac{d_{ad}(t)P'(t) + mEd_{ad}^{1/2}(t)\alpha P(t)}{2\sqrt{2R}mE\left[d(t) - \frac{P(t)}{4mE}\right]}. \tag{4-4}$$

Following the procedure used in the main part of the paper, it is possible to evaluate the trend of penetration and contact area for constant normal load. After some algebra, we find that the implicit expression for penetration is

$$\frac{32R}{9\alpha^2 P^2}d_{ad}^3 - \frac{16R}{3P\alpha^2 mE}d_{ad}^2 + \frac{2R}{\alpha^2 m^2 E^2}d_{ad} = t^2.$$

In Figure 4, the contact semiwidth is plotted as a function of time for both adaptive (solid line) and constant (dashed line) Winkler modulus models. In particular, the results are obtained choosing the coefficient m according to (2-8). As expected, the behavior is different only at small times, while the long time limit does not depend on the Winkler stiffness, and thus the trend is the same.

The adaptive Winkler enhancement clearly affects the contact pressure evolution in time, which can be evaluated numerically by (2-7).
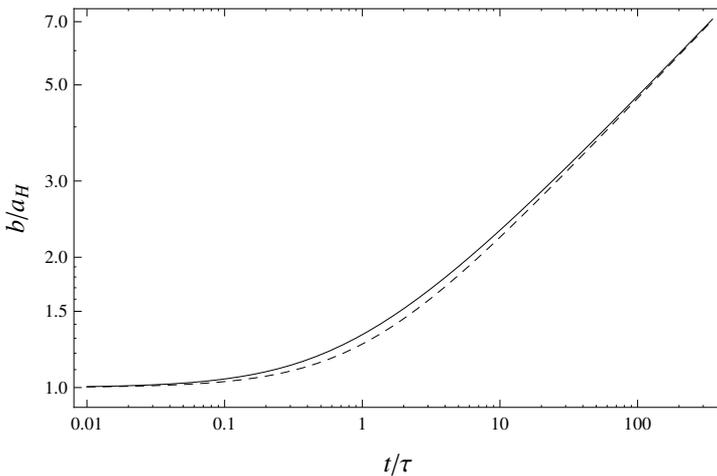
Figure 4. The comparison between contact semiwidths b obtained with constant (solid) and adaptive (dashed) Winkler models; a_H is the Hertzian contact semiwidth.
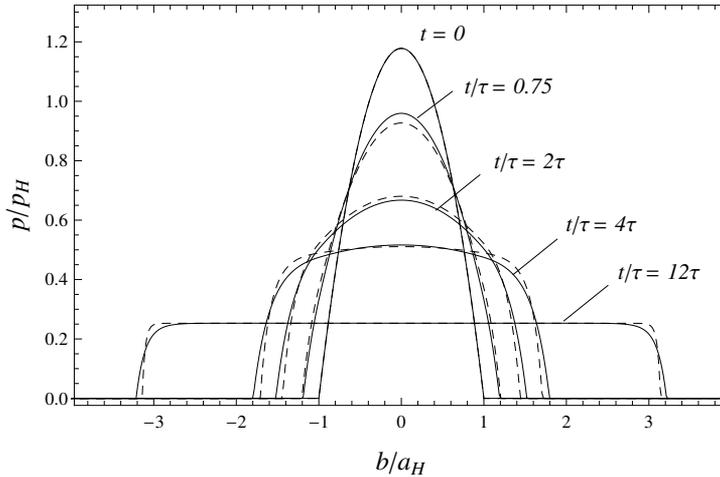
Figure 5. The pressure distribution inside the contact area for different times. Dashed lines give the solution obtained with constant Winkler modulus. Solid lines are obtained by introducing the adaptive Winkler model. The quantities p_H and a_H represent the Hertzian peak pressure and initial contact area.

Figure 5 shows this evolution in the cases of constant Winkler modulus (dashed line) and adaptive Winkler model (solid line). As in the Winkler approximation, the pressure distribution is proportional to the shape of indenter; the initial distribution is obviously parabolic, and as wear proceeds, the pressure distribution tends towards the uniform condition. It is also possible to see that the effect of the adaptive correction is to round the pressure distribution.

5. FEM comparison

A detailed comparison between simple and adaptive Winkler solutions and a FEM model was performed in order to study the accuracy of the Winkler solutions. In particular, we developed an ANSYS Parametric Design Language model of a half-cylinder with about 1000 elements. The contact between the cylinder and the rigid plane surface was modeled using CONTA178 elements, in which the gap of each element in contact is varied during the wear process by adding an artificial length corresponding to the progressive wear, proportional to the local pressure at the given iteration. This process corresponds to an Euler forward integration of the wear equations, and thus it was expected to be stable only for sufficiently small wear coefficient. To the best of the authors' knowledge, this FEM procedure has not been previously suggested. However, it is extremely simple to implement, does not require remeshing of the worn profiles, and in principle could be also used together with substructuring-superelement formulations in which only the degrees of freedom of the nodes in contact are active.

In Figure 6 the solutions of the Winkler models (dashed = simple, solid = adaptive) are compared to the FEM results (circles) for the contact area evolution as a function of time.

The adaptive Winkler model prediction clearly shows an improved fitting of FEM results compared with the simple Winkler model. In particular, after a brief time interval, the adaptive Winkler model
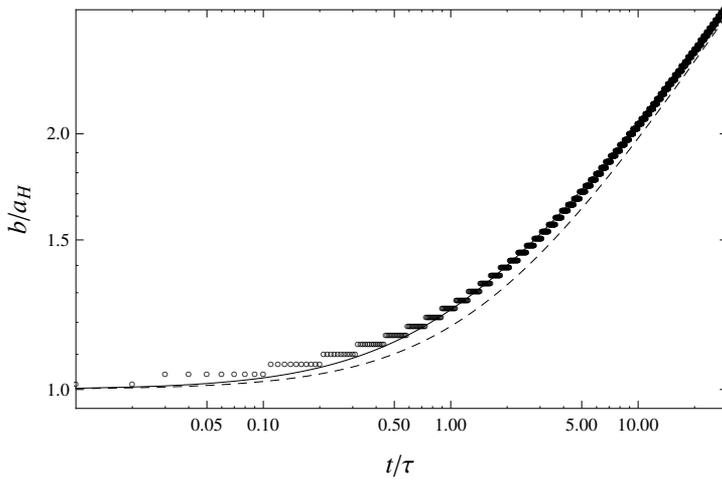
Figure 6. The dimensionless contact area semiwidth vs. the dimensionless time for different models. The circles are the FEM result, the solid line shows the adaptive Winkler result, and the dashed line shows the simple Winkler result.

correctly matches the solution obtained by FEM simulation in terms of contact area evolution, despite that the constants in the adaptive model are, strictly speaking, valid for a Hertzian pressure distribution.

Further, in Figure 7, the pressure distribution within the contact area is shown for the Winkler models and the FEM elastic model, for a particular time $t/\tau = 0.8$. As expected, the adaptive Winkler model, while it improves the prediction of contact area size, is still somewhat far from the "exact" pressure distribution shape obtained by FEM simulations. However, this is intrinsic from the beginning, when the
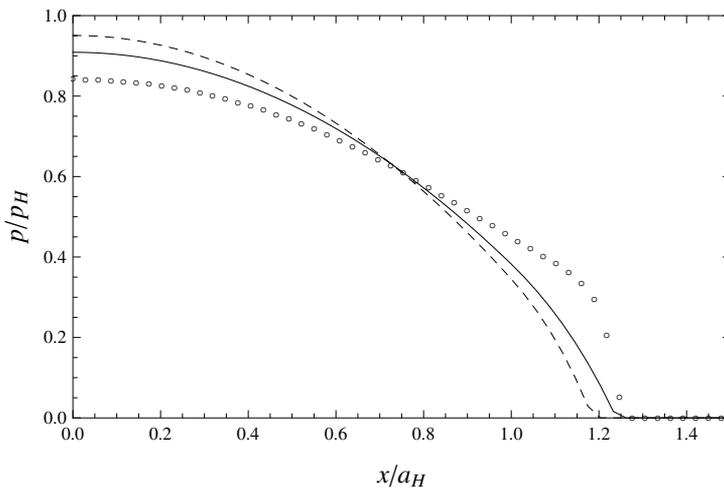
Figure 7. The dimensionless pressure distribution within the contact area at $t/\tau = 0.8$. The circles are the FEM result, the solid line shows the adaptive Winkler result, and the dashed line shows the simple Winkler result.

Hertzian elliptical distribution cannot match the parabolic Winkler distribution. In this respect, the error tends to be reduced from the initial value.

6. Conclusions

We have obtained some simple analytical results for 2D Hertzian rigid indenters sliding on a Winkler half-plane, on the assumption that only one of the bodies (the indenter) wears out. The full solutions for pressure distribution, contact area, and indentation depth have been obtained. The Winkler modulus can be also changed in time in an "adaptive" way, considering the varying dimension of the contact area, so as to improve the solution.

A comparison with a full continuum problem has been performed by means of FEM simulation using a very simple yet effective method to model wear, which adds wear in the "initial gap" of the contact elements. It is found that the introduction of the adaptive Winkler model improves the fixed load contact area prediction in time, and that generally the Winkler model shows a reasonable solution, considering the inevitable error intrinsic in the assumption of the pressure distribution shape.

References

[Archard and Hirst 1956] J. F. Archard and W. Hirst, "The wear of metals under unlubricated conditions", *Proceedings of the Royal Society of London A: Mathematical, Physical and Engineering Sciences* **236**:1206 (1956), 397–410.

[Goryacheva 1998] I. G. Goryacheva, *Contact mechanics in tribology*, Solid Mechanics and its Applications **61**, Kluwer, Dordrecht, 1998.

[Hornbogen 1975] E. Hornbogen, "The role of fracture toughness in the wear of metals", *Wear* **33**:2 (1975), 251–259.

[Johnson 1985] K. L. Johnson, *Contact mechanics*, Cambridge University Press, 1985.

[Lim and Ashby 1987] S. C. Lim and M. F. Ashby, "Overview no. 55: Wear-mechanism maps", *Acta Metallurgica* **35**:1 (1987), 1–24.

[Mattei et al. 2011] L. Mattei, F. Di Puccio, B. Piccigallo, and E. Ciulli, "Lubrication and wear modelling of artificial hip joints: a review", *Tribology International* **44**:5 (2011), 532–549.

[Panetti 1947] M. Panetti, *Meccanica applicata*, Levrotto e Bella, Torino, 1947.

[Põdra and Andersson 1997] P. Põdra and S. Andersson, "Wear simulation with the Winkler surface model", *Wear* **207**:1–2 (1997), 79–85.

[Põdra and Andersson 1999] P. Põdra and S. Andersson, "Simulating sliding wear with finite element method", *Tribology International* **32**:2 (1999), 71–81.

[Reye 1860] T. Reye, "Zur theorie der zapfenreibung", *Der Civilingenieur* **4** (1860), 235–255.

[Sfantos and Aliabadi 2007] G. K. Sfantos and M. H. Aliabadi, "Total hip arthroplasty wear simulation using the boundary element method", *Journal of Biomechanics* **40**:2 (2007), 378–389.

[Villaggio 2001] P. Villaggio, "Wear of an elastic block", *Meccanica* **36**:3 (2001), 243–249.

MICHELE CIAVARELLA: mciava@poliba.it
Dipartimento di Meccanica, Matematica e Management, Politecnico di Bari, Viale Japigia 182, 70126 Bari, Italy

NICOLA MENGA: nicola.menga@poliba.it
Dipartimento di Meccanica, Matematica e Management, Politecnico di Bari, Viale Japigia 182, 70126 Bari, Italy

msp

FRACTURE DEVELOPMENT ON A WEAK INTERFACE NEAR A WEDGE

ALEXANDER N. GALYBIN, ROBERT V. GOLDSTEIN AND KONSTANTIN B. USTINOV

Formation of a fracture consisting in shear-opening delamination and Coulomb's frictional sliding zones along a weak interface in an elastic isotropic homogeneous plane subjected to wedging and external compression is studied. The shear-opening delamination is modelled by a mixed-mode crack; the frictional sliding zones are modelled by pure shear cracks. The interface is assumed to be much weaker than the material of the plane, so that only interface cracks are considered. The wedge is modelled by a pair of edge dislocations. Two particular cases have been considered: far-field and near-field asymptotics, corresponding to the cases of large and small ratios of the distance between the wedge and the interface and the distance between two dislocations modelling the wedge, respectively.

The possibility of formation of finite sliding zones ahead of the delamination on the weak interface is demonstrated. It is shown that, depending on the combination of external parameters (ratio of the dislocation burgers vector and elastic modulus, distance from the dislocation to the interface, magnitude of applied compression, cohesion and friction angle of the interface), two configurations of cracks may be observed: one mixed-mode crack, and three cracks — one central mixed mode crack and two external symmetrical shear cracks. The central part of the sliding zone is also open.

1. Introduction

Delamination occurring on a part of a weak interface ahead of an approaching fracture is explained by the presence of the tensile stress component parallel to the fracture; see [Cook et al. 1964]. This phenomenon is observed in various materials in lab experiments as well as in nature; e.g., dyke-sill transformations; see [Gudmundsson 2011]. It is widely accepted (see the references above) that the delamination can affect the crack propagation throughout the interface or serve as a barrier for crack arrest. Besides crack growth, there are other situations that may also lead to interface destruction, such as, for instance, wedging due to thermal expansion or rockmass fracturing near excavations. It should be understood that, in addition to tensile stresses, the interface is also subjected to shear stresses that can be high enough to affect the fracture processes developing on the interface. Experiments [Goldstein and Osipenko 2012; 2015] have shown that the appearance of sliding zones over the interface is capable of initiating secondary cracks perpendicular to the interface. Somewhat similar mechanisms are reported in [Zhou et al. 2010] for hydrofracture modelling.

There are numerical studies of fracture development on weak interfaces; e.g., [Cooke and Underwood 2001; Akulich and Zvyagin 2008]. These studies model both delamination and slip on the interface without employing any fracture characteristics (e.g., stress intensity factors or energy release rate) that control fracture, which is a serious drawback. Early work by Galybin [1997] takes into account fracture characteristics for the determination of the length of the sliding zones but do not consider delamination.

Keywords: mixed-mode interface crack, edge dislocation, delamination, sliding, singular integral equations.
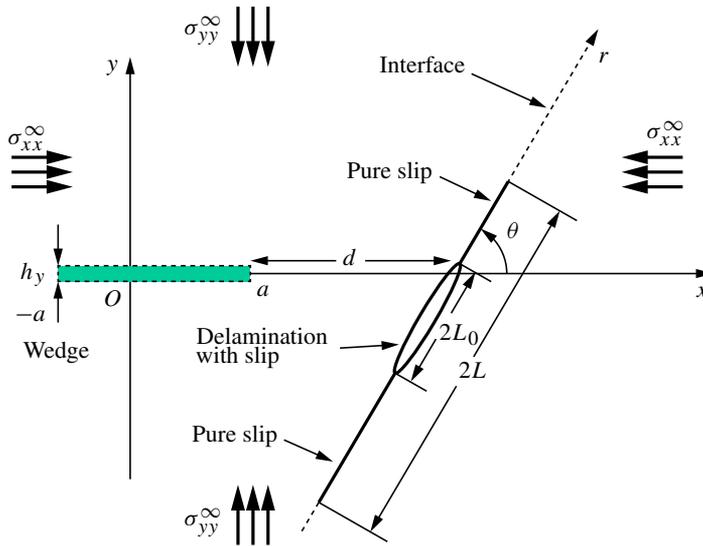
Figure 1. Geometry and loads.

Cracks at the interface of Coulomb's friction type between elastic and rigid bodies were considered in works by Bui and Oueslati [2004; 2005] and Bui [2006] with and without delamination. They obtained analytical solutions, with the emphasis on possible nonuniqueness arising from nonlinearity of the frictional contact crack problem and dependency of the solution on the (unspecified) loading history. The nonuniqueness and path dependence of the solution for problems involving Coulomb's friction contact was also emphasised in works of Dundurs and Comninou [1981; 1983] and Mendelsohn and Whang [1988].

In this study we model both delamination (as combined mode I-mode II cracks) and sliding zones (mode II cracks) caused by a wedge (modelled by edge dislocations) in a compressed elastic plane with a weak interface (which is considered as a plane of reduced strength). The sizes of opening and sliding zones are found from the solution. The back influence of the interface cracks on the dislocations is not taken into account, which allows one to apply the method suggested in [Galybin and Mukhamediev 2012; 2014] for estimation of the size of the delamination and the length of the pure sliding zones. The case with both opening and shear zones along the interface was studied before, for example by Gorbatikh et al. [2001]. Their work deals with the case when a part of the contour is traction-free under compressive normal loads at infinity, and the size of this traction-free zone is prescribed by the geometry of the problem. Such a formulation makes sense when a narrow cavity of certain special form is cut out from the plane.

The configuration shown in Figure 1 is studied. The ends of the delamination zone $(-L_0, L_0)$ are determined from the condition $K_I = 0$, and the ends of the pure sliding zones $(-L, L)$ ("shear crack" in the figure) from the condition $K_{II} = 0$, where K_I and K_{II} are the stress intensity factors for opening and transverse shear modes, respectively. Moreover, a more general case is considered, for which the shear zones appear also on two symmetric intervals outside the interval $(-L, L)$. For this case a system of three nonlinear equations will be examined.

2. Wedge in elastic plane

The complex potentials that characterise the stress field of an isotropic elastic plane with an edge dislocation of magnitude $h = h_x + i h_y$ whose core is placed at a point z_0 have the form [Muskhelishvili 1977]

$$\Phi(z) = \frac{H}{z - z_0}, \quad \Psi(z) = \frac{\bar{H}}{z - z_0} + \frac{\bar{z}_0 H}{(z - z_0)^2}, \tag{1}$$

where, for the condition of plane strain, one has

$$H = -\frac{i G (h_x + i h_y)}{\pi (1 + \kappa)}, \quad \kappa = 3 - 4\nu, \tag{2}$$

where G is the shear modulus of the plane and ν is Poisson's ratio. Note that the minus sign in (2) is due to the assumption that the cut is made to the left from the core, which can be directly checked by using the Kolosov–Muskhelishvili formulas for the displacements.

Let us assume that $z_0 = a$, $h_x = 0$ and $h_y = h > 0$; this also means that $H = \bar{H} > 0$, which results in the following expressions for the complex potentials:

$$\Phi_1(z) = \frac{H}{z - a}, \quad \Psi_1(z) = -z \Phi_1'(z) = \frac{z H}{(z - a)^2}. \tag{3}$$

Let us introduce the second dislocation, with the core at the point $z_0 = -a$ and with magnitude $h_x = 0$ and $h_y = -h > 0$ (thus, H in (3) should be replaced by $-H$); then the previous expressions for the complex potentials yield

$$\Phi_2(z) = \frac{-H}{z + a}, \quad \Psi_2(z) = -z \Phi_2'(z) = \frac{-z H}{(z + a)^2}. \tag{4}$$

The superposition of the stress fields (3) and (4) gives

$$\Phi_{\text{wedge}}(z) = \frac{S}{z^2 - a^2}, \quad \Psi_{\text{wedge}}(z) = -z \Phi_{\text{wedge}}'(z) = \frac{2 z^2 S}{(z^2 - a^2)^2}, \quad S = 2 a H. \tag{5}$$

The complex potentials in (5) give the solution for the wedge of finite length inserted into the elastic plane. Here S is a parameter that has dimension of force, and it is proportional to the area of the wedge penetrated into the plane. We further assume this value to be a constant.

By using the Kolosov–Muskhelishvili formulas one obtains the following expressions for the mean stresses $P = 0.5(\sigma_x + \sigma_y)$ and for the complex stress deviator function $D = 0.5(\sigma_y - \sigma_x) + i \sigma_{xy}$:

$$P(z, \bar{z}) = \Phi + \bar{\Phi} = \frac{S}{z^2 - a^2} + \frac{S}{\bar{z}^2 - a^2}, \quad D(z, \bar{z}) = \bar{z} \Phi' + \Psi = (\bar{z} - z) \Phi' = \frac{2 z (z - \bar{z}) S}{(z^2 - a^2)^2}. \tag{6}$$

The normal (σ_{nn}) and shear (σ_{nt}) stresses acting on an inclined plane (at an angle θ_0 to the x-axis) are given by

$$\sigma_n - i \sigma_t = P(z, \bar{z}) + e^{2 i \theta_0} D(z, \bar{z}) = 2 S \left[\operatorname{Re} \frac{1}{z^2 - a^2} + e^{2 i \theta_0} \frac{z (z - \bar{z})}{(z^2 - a^2)^2} \right]. \tag{7}$$

Let us assume that a weak interface is located on a line (see Figure 1) specified by

$$z = a + w, \quad w = d + r e^{i \theta}, \quad \theta = \text{const}, \tag{8}$$

where the value of $r = 0$ corresponds to the point of intersection of the interface with the continuation of the wedge line, the point $z = a + d$ in Figure 1.

Then the stresses on the interface can be presented in the form

$$\sigma_n - i\sigma_t = \frac{2S}{(a+d)^2}\left[\operatorname{Re}\frac{1}{(1+\rho e^{i\theta})^2 - \delta^2} + \frac{2i\rho \sin\theta e^{2i\theta}(1+\rho e^{i\theta})}{((1+\rho e^{i\theta})^2 - \delta^2)^2}\right], \quad \rho = \frac{r}{a+d}, \quad \delta = \frac{a}{a+d}. \quad (9)$$

Hereafter, σ_n and σ_t are the normal and shear components of stress along the interface.

We consider two configurations:

Configuration 1 (far field asymptotics). Assume that $a \ll |w|$ ($a \ll d$). Then the complex potentials in (5) become

$$\Phi_{\text{wedge}}(z) = \frac{S}{z^2}, \quad \Psi_{\text{wedge}}(z) = -z\Phi'_{\text{wedge}}(z) = \frac{2S}{z^2}, \quad S = \text{const}. \quad (10)$$

This asymptotic behavior coincides with the far field asymptotics for a mode I crack of length $2a$ and average opening S/G.

The stresses on the interface are found from (9) to be

$$\sigma_n - i\sigma_t = \frac{2S}{d^2}\left[\operatorname{Re}\frac{1}{(1+\rho e^{i\theta})^2} + \frac{2i\rho \sin\theta e^{2i\theta}}{(1+\rho e^{i\theta})^3}\right], \quad \rho = \frac{r}{d}. \quad (11)$$

The expression in brackets in (11) represents dimensionless stresses (normalised by $2S/d^2$) acting on the interface far from the wedge. They are shown in Figure 2 as functions of ρ for different interface inclinations.

Configuration 2 (near field asymptotics). Let us assume that $|w| \ll a$ ($d \ll a$). Then the stress functions in (6) take the form

$$P(w, \bar{w}) = \frac{S}{2a}\frac{w + \bar{w}}{w\bar{w}}, \quad D(w, \bar{w}) = \frac{S}{2a}\frac{w - \bar{w}}{w^2}. \quad (12)$$

It should be noted that these functions correspond to the case of a single dislocation with the core at the origin (they can also be found from (3) by assuming that $a = 0$, because $2aH = S$). The stresses on the interface are obtained from (12) in the form

$$\sigma_n - i\sigma_t = \frac{S}{ad}\left[\operatorname{Re}\frac{1}{1+\rho e^{i\theta}} + \frac{i\rho e^{2i\theta} \sin\theta}{(1+\rho e^{i\theta})^2}\right], \quad \rho = \frac{r}{d}. \quad (13)$$

The dimensionless (normalised by $S/(ad)$) stresses on the interface located close to the right end of the wedge are shown in Figure 3 for various interface inclinations as functions of ρ.

Comparing the stress profiles in Figures 2 and 3, one can notice that the stress distributions look qualitatively similar to each other. For the general configuration they differ only quantitatively from those depicted in Figures 2 and 3 for the full range of the parameters a, d and R. It should be noted that the dimensional magnitudes of the stresses near the wedge are much greater than their values far from the wedge. Thus, interface fracturing due to the stresses induced by the wedge is most likely to occur close to the wedge. Therefore, we further restrict our consideration to Configuration 2, which also allows one to reduce the number of parameters controlling the stress field.
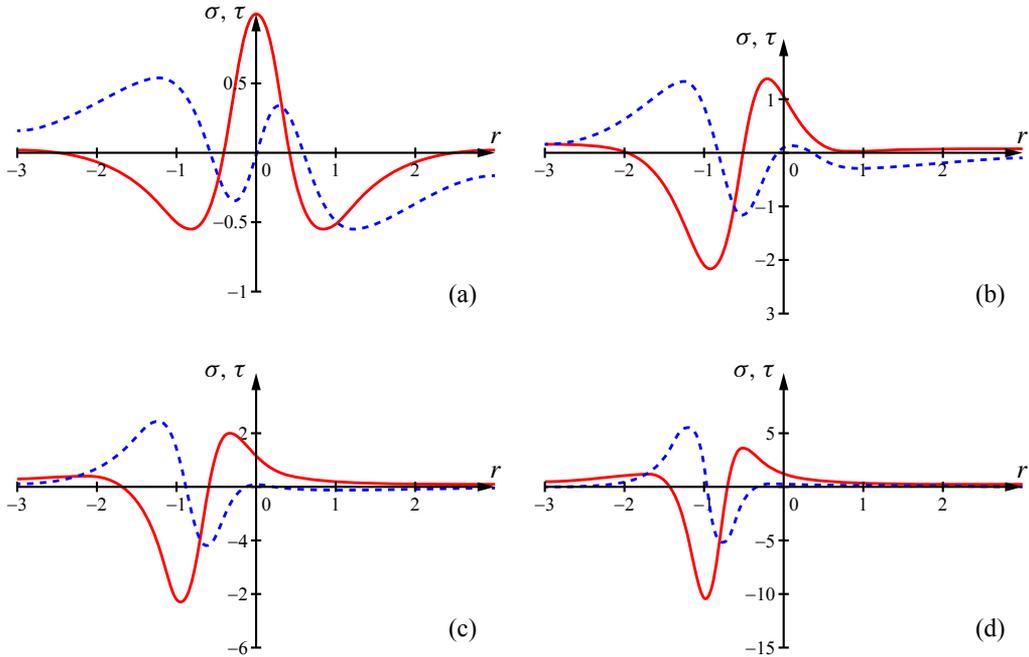
Figure 2. Profiles of dimensionless stresses caused by the wedge on the interface inclined at (a) $\theta = \pi/2$, (b) $\theta = \pi/3$, (c) $\theta = \pi/4$, (d) $\theta = \pi/6$ for Configuration 1 as functions of the parameter ρ; solid lines are normal stresses, dashed lines are shear stresses.

The total stresses should also reflect the remote loads, which create the following stresses on the interface:

$$\sigma_n^0 - i\sigma_t^0 = \frac{\sigma_{yy}^\infty + \sigma_{xx}^\infty}{2} + e^{2i\theta}\frac{\sigma_{yy}^\infty - \sigma_{xx}^\infty}{2} = \sigma_{yy}^\infty \cos^2\theta + \sigma_{xx}^\infty \sin^2\theta + i(\sigma_{yy}^\infty - \sigma_{xx}^\infty)\cos\theta\sin\theta. \quad (14)$$

It is evident from (14) that, for the case of compressive loads at infinity, the shear stresses on the interface can be of any sign depending on the difference of principal stresses at infinity, while the normal stress is always negative. The latter means that the external stress can compensate for the tensile normal stresses on the interface caused by the wedge. However, when the distance d is small, the stress magnitudes are unbounded, which indicates that the remote stresses cannot compensate for the stress concentration near the wedge, and hence a delamination zone should appear on the interface regardless of compression at infinity. The position of this zone depends on the interface inclination angle. As is evident from the profiles of normal stresses in Figure 3, for steep angles the delamination zone has to appear close to the point $z = a + d$, while for shallow angles the middle of this zone should be shifted to the left and down as shown in Figure 1. This delamination zone is also subjected to shear stresses that induce relative slip of the delamination surfaces. The direction of the slip is defined by the sign of the total shear stress, which can alternate. If the shear stresses due to remote loads are negative (vertical compression dominates) then the slip in the leftward direction should dominate (as the peak of the shear stresses caused by the wedge is also negative). In general, the slip zone can be longer than the delamination zone, and includes some
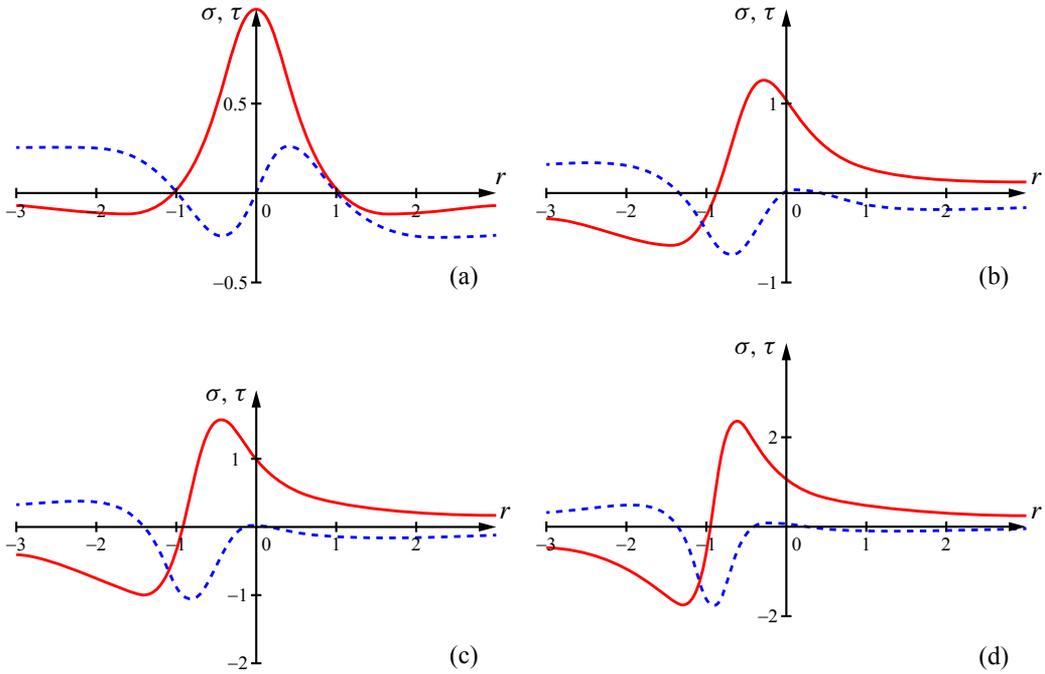
Figure 3. Profiles of dimensionless stresses caused by the wedge on the interface inclined at (a) $\theta = \pi/2$, (b) $\theta = \pi/3$, (c) $\theta = \pi/4$, (d) $\theta = \pi/6$ for Configuration 2 as functions of the parameter ρ; solid lines are normal stresses, dashed lines are shear stresses.

parts with pure slip, as shown in Figure 1. Therefore one arrives at the problem, in which the opening zone is placed within the shear zone.

We further model the delamination zone as a combined mode I–mode II crack (contour Γ_0) and the pure slip zones as mode II cracks (contour Γ_1). In the latter case there is no crack opening, which means that the normal displacement u_n is continuous across the crack contour Γ_1. For simplicity we assume that the slip is subjected to the Mohr–Coulomb criteria. The boundary conditions of the problem can be presented in terms of total stresses as follows:

$$\sigma_n - i\sigma_t = 0 \quad \text{on } \Gamma_0,$$
$$|\sigma_t| = C - \sigma_n \tan\phi, \quad \sigma_n < 0, \quad u_n^+ = u_n^- \quad \text{on } \Gamma_1, \tag{15}$$
$$\sigma_{ij} \to \sigma_{ij}^\infty \quad \text{at infinity.}$$

Here C is cohesion and ϕ is the friction angle along the weak interface; plus and minus stand for the upper and lower surfaces of the crack, respectively.

For simplicity we will further study the symmetric case of the perpendicular interface $\theta = \pi/2$; in this case the centre of the crack is placed at the point $z = d + i0$ and the contours are represented by the symmetric intervals $\Gamma_0 = (-L_0, L_0)$ and $\Gamma_1 = (-L, -L_0) \cup (L_0, L)$ of the range of the dimensionless parameter ρ. The total contour is further denoted as $\Gamma = \Gamma_0 \cup \Gamma_1 = (-L, L)$.

By introducing the dimensionless parameter

$$\tilde{H} = \frac{1}{\pi(1+\kappa)} \frac{G}{|\sigma_{xx}^{\infty}|} \frac{h_y}{d}, \tag{16}$$

one can present the dimensionless stresses (normalised by σ_{xx}^{∞}) on the interface as

$$\tilde{\sigma}_{xx}(\rho) = 2\tilde{H} \frac{1-\rho^2}{(1+\rho^2)^2}, \quad \tilde{\sigma}_{xy}(\rho) = 2\tilde{H} \frac{\rho(1-\rho^2)}{(1+\rho^2)^2}, \quad -\infty < \rho < +\infty. \tag{17}$$

Later on, the tilde sign over the dimensionless stresses and parameters is removed. The remote vertical compression does not play any role in symmetric arrangement, therefore $\sigma_{yy}^{\infty} = 0$.

It follows from (17) that the normal stresses due to the wedge are tensile on the interval $(-1, 1)$, with the maximum at $\rho = 0$, while the shear stresses change sign three times when crossing the points corresponding the values of the parameter $\rho = -1, 0, 1$; they have extrema of the same magnitudes at the points specified by the values $\rho = \pm\sqrt{2} \pm 1$. The profiles of (17) are shown in Figure 3a for $H = 1$. As mentioned, the maximum normal stresses on the interface are unbounded when d tends to zero. In the meantime, the size of the zone with tensile stresses also tends to zero when d tends to zero.

3. Singular integral equations for the cracks on the interface

Since the interface is subjected to tension and shear, it is possible that a combined open-shear crack appears in the central part and pure shear cracks at the periphery. These cracks can be considered separately because the normal opening does not induce shear stresses on the interface and the jump of the tangential displacement does not cause normal stresses.

The boundary conditions for the determination of the dimensionless normal stresses caused by crack opening, $\sigma_{xx}^{\text{crack}}$, on the interval $(-L_0, L_0)$ have the form

$$\sigma_{xx}^{\text{crack}}(y) - 1 + 2H \frac{1-y^2}{(1+y^2)^2} = 0, \quad |y| < L_0. \tag{18}$$

The second boundary condition in (15) for the determination of the dimensionless shear stresses caused by the crack opening, $\sigma_{xy}^{\text{crack}}$, on the interval $(-L, L)$ can be expressed in the piecewise form

$$\sigma_{xy}^{\text{crack}}(y) + 2H \frac{y(1-y^2)}{(1+y^2)^2} = 0, \quad |y| < L_0,$$
$$\left| \sigma_{xy}^{\text{crack}}(y) + 2H \frac{y(1-y^2)}{(1+y^2)^2} \right| = C - k\sigma_{xx}^{\text{total}}(y), \quad \sigma_{xx}^{\text{total}}(y) < 0, \quad |y| > L_0, \quad y \in \Gamma, \tag{19}$$

where $k = \tan\phi$ is the friction coefficient and we have introduced the notation

$$\sigma_{xx}^{\text{total}}(y) = \sigma_{xx}^{\text{crack}}(y) - 1 + 2H \frac{1-y^2}{(1+y^2)^2}, \quad |y| > L_0. \tag{20}$$

A singular integral equation (SIE) for the problem in (18) has the form

$$\frac{1}{\pi} \int_{-L_0}^{L_0} \frac{u(t)}{t-y} dt = 1 - 2H \frac{1-y^2}{(1+y^2)^2}, \quad |y| < L_0. \tag{21}$$

Here $u(t)$ is a sought function proportional to the density of the normal displacement discontinuity on $(-L_0, L_0)$ that satisfies the condition of single-valuedness of the normal displacements

$$\int_{-L_0}^{L_0} u(t)\, dt = 0. \tag{22}$$

When deriving the SIE for the boundary value problem (19), one has to remove the absolute value sign in the left-hand side of the second equation in (19). This can be done by examining the directions of the total shear stresses. The shear stresses caused by the shear crack should have the opposite signs as those caused by the wedge in order to compensate for the excess in the left-hand side of the second formula in (19). Thus, the absolute value sign can be removed by introducing the step-like function

$$\chi(y) = \begin{cases} 0 & |y| < L_0, \\ \operatorname{sgn}[y(1 - y^2)] & |y| > L_0. \end{cases} \tag{23}$$

As the result, the SIE for the problem specified by (19) takes the form

$$\frac{1}{\pi} \int_\Gamma \frac{v(t)}{t - y}\, dt = -2H \frac{y(1 - y^2)}{(1 + y^2)^2} + \chi(y)(C - k\sigma_{xx}^{\text{total}}(y)), \quad y \in \Gamma. \tag{24}$$

Here $v(t)$ is a sought function proportional to the density of the tangential displacement discontinuity on $(-L, L)$ that satisfies the condition of single-valuedness of the tangential displacements. The form of this condition depends on the number of pure slip zones of the entire contour. It is obvious that, due to the lack of friction on the central part, on the interval $(-L_0, L_0)$ the shear crack in the centre always has length greater than the length of the open zone. We further assume that the slip is on $(-L, L)$ and $L_0 < L$.

If the resistance to shear stresses is small, then the slip can also grow outside $(-L, L)$, where the intensity of the shear stresses is the same as in the middle, but they decay slowly (see Figure 3a). Let us further assume that the slip develops on the intervals $A < |y| < B$, such that the inequalities

$$0 < L_0 < L \le A \le B \tag{25}$$

hold and the entire contour Γ is given by

$$\Gamma = (-B, -A) \cup (-L, L) \cup (A, B). \tag{26}$$

Then the conditions of single-valuedness for the SIE (24) take the form

$$\int_{-B}^{-A} v(t)\, dt = 0, \quad \int_{-L}^{L} v(t)\, dt = 0, \quad \int_{A}^{B} v(t)\, dt = 0. \tag{27}$$

Note that if $A = B$ then it is necessary to satisfy the second condition in (27) only.

The mode I–mode II crack length can be estimated from a criterion of crack growth, in particular by knowing fracture toughness of the interface material, which requires calculation of the stress intensity factors $(K_{\text{I}}, K_{\text{II}})$, respectively, at the ends of all cracks. For the estimation of the maximum L_0 one can use the condition $K_{\text{I}} = 0$, otherwise the Mohr–Coulomb friction condition cannot be satisfied in the vicinity of the mode I crack end due to unbounded tensile normal stresses, which violates the inequality $\sigma_{xx}^{\text{total}}(y) < 0$ in the second condition in (19).

For the determination of the ends of the slip zones it is also reasonable to use the condition $K_{\mathrm{II}} = 0$, which allows one to determine the maximum possible lengths of all slip zones. As the stress intensity factors (SIFs) can be determined from the asymptotics of the sought function at the crack ends, one can employ the following conditions that address $K_{\mathrm{I}} = 0$ and $K_{\mathrm{II}} = 0$:

$$U(L_0) = 0, \quad V(L) = 0, \quad V(A) = 0, \quad V(B) = 0, \tag{28}$$

where

$$U(t) = u(t)\sqrt{L_0^2 - t^2}, \quad V(t) = v(t)\sqrt{(L^2 - t^2)(t^2 - B^2)(t^2 - A^2)}. \tag{29}$$

In the next section we find analytical expressions for the SIFs in both problems (21)–(22) and (24), (27).

4. Solution for the delamination zone

The solution of the SIE (21) unbounded at the ends and satisfying (22) is given by the formula (see for example [Muskhelishvili 1977])

$$u(t) = \frac{-1}{\pi\sqrt{L_0^2 - t^2}} \int_{-L_0}^{L_0} \frac{\sqrt{L_0^2 - x^2}}{x - t}\left(1 - 2H\frac{1 - x^2}{(1 + x^2)^2}\right) dx, \quad |t| < L_0. \tag{30}$$

The integral in the right-hand side of (30) can be evaluated analytically; the solution assumes the form

$$u(t) = \frac{t}{\sqrt{L_0^2 - t^2}}\left(1 + \frac{2H}{\sqrt{L_0^2 + 1}}\frac{t^2 - 2L_0^2 - 1}{(t^2 + 1)^2}\right). \tag{31}$$

The mode I SIF obtained from (31) has the form

$$\frac{K_{\mathrm{I}}}{\sigma_{xx}^\infty\sqrt{\pi L_0}} = 1 - 2H(L_0^2 + 1)^{-3/2}. \tag{32}$$

The length of the crack is determined from the condition $K_{\mathrm{I}} = 0$. This leads to the following relationships between the half-length L_0 and the parameter H:

$$2H = (L_0^2 + 1)^{3/2}, \quad L_0 = \sqrt{(2H)^{2/3} - 1}. \tag{33}$$

One of these parameters can be considered as independent; let it be L_0 from now on.

Then the solution bounded at both ends is given by the formula

$$u(t) = -t\frac{t^2 + 2L_0^2 + 3}{(t^2 + 1)^2}\sqrt{L_0^2 - t^2}. \tag{34}$$

Note that this solution exists for $2H > 1$, which holds if

$$\frac{1}{2\pi(1 - \nu)}\frac{G}{|\sigma_x^\infty|} > \frac{d}{h_y}. \tag{35}$$

It is evident from (35) that the solution does not exist only if the distance between the wedge and the interface is essentially greater than the wedge magnitude, i.e., if the shear modulus is greater than the remote compression.
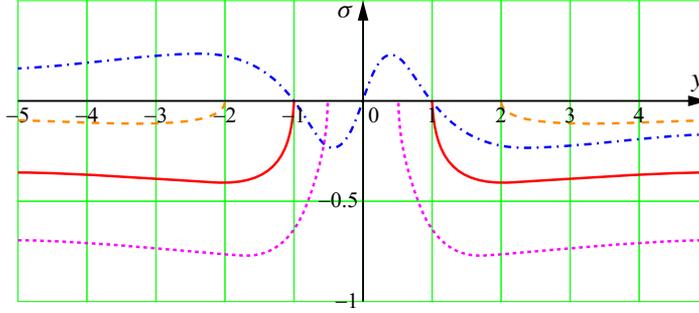
Figure 4. The stresses on the interface after delamination for $L_0 = 0.5, 1, 2$; dots are normal stress for $L_0 = 0.5$, solid line is normal stress for $L_0 = 1$, dashed line is normal stress for $L_0 = 2$, dash-dotted line is shear stress.

The crack growth is stable if $dK_I/dL_0 < 0$ and unstable if $dK_I/dL_0 > 0$. This derivative is always positive, because

$$\frac{dK_I}{dL_0} = \sigma_x^\infty \frac{d}{dL_0}\Big[\big(1 - 2H(L_0^2 + 1)^{-3/2}\big)\sqrt{\pi L_0}\Big] = 3\sigma_x^\infty \sqrt{\frac{\pi}{L_0}} \frac{L_0^2}{L_0^2 + 1} > 0. \tag{36}$$

This indicates that the growth is unstable.

The normal stresses on the interface caused by the mode I crack are found from the solution (34) by means of the integral

$$\sigma_{xx}^{\text{crack}}(y) = \frac{1}{\pi} \int_{-L_0}^{L_0} \frac{u(t)}{t - y}\, dt = \frac{-1}{\pi} \int_{-L_0}^{L_0} \frac{t}{t - y} \frac{t^2 + 2L_0^2 + 3}{(t^2 + 1)^2} \sqrt{L_0^2 - t^2}\, dt. \tag{37}$$

Evaluation of the integral in the right-hand side of (37) yields

$$\sigma_{xx}^{\text{crack}}(y) = \frac{-1}{(1 + y^2)^2}\Big[\big(1 - (2L_0^2 + 1)y^2\big)\big(\sqrt{L_0^2 + 1} - 1\big) + L_0^2\sqrt{L_0^2 + 1}(1 + y^2)$$
$$+ (2L_0^2 + 3 + y^2)\big(\sqrt{1 - L_0^2/y^2} - 1\big)\Big], \quad |y| > L_0. \tag{38}$$

The total stresses on the interfaces are found by substitution of (38) into (20) followed by simplifications:

$$\sigma_{xx}^{\text{total}}(y) = \frac{-y^2(y^2 + 2L_0^2 + 3)}{(1 + y^2)^2}\sqrt{1 - L_0^2/y^2}, \quad |y| > L_0. \tag{39}$$

Figure 4 shows the profiles of the dimensionless (divided by $2H$) shear (dash-dotted curve) and normal stresses after appearance of the delamination zone for $L_0 = 0.5, 1, 2$.

The normal stress attains its minimum at the point

$$y_{\min} = \sqrt{\frac{3L_0^4 + 5L_0^2 + 3 + \sqrt{9L_0^4 + 6L_0^2 + 9}(L_0^2 + 1)}{3L_0^2 + 2}}. \tag{40}$$

The minimal values of the normal stresses, $\sigma_{\min}$, are shown in Figure 5 as a function of the half-length of the delamination zone, L_0. Note that $y_{\min} = \sqrt{3}$ at $L_0 = 0$, hence $\min \sigma_{xx}^{\text{total}} = -\frac{9}{8}$.
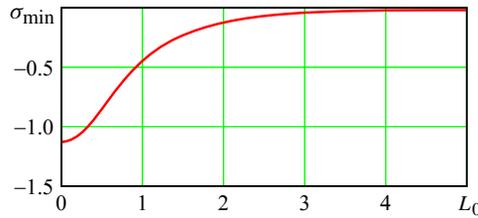
Figure 5. Minimum of normal stresses on the interface as a function of the half-length of the delamination L_0.

5. Solution for the slip zones

Let us introduce the function

$$F(y) = |\sigma_{xy}(y)| + k\sigma_{xx}^{\text{total}}(y) - C, \tag{41}$$

where $\sigma_{xy}(y) = -(L_0^2 + 1)^{3/2} y(1 - y^2)(1 + y^2)^{-2}$ is the dimensionless shear stress on the interface caused by the wedge with the delamination zone of the length determined with the use of (33).

The function $F(y)$ in (41) is actually the right-hand side of the SIE in (24). It should be positive ($F(y) > 0$) at least at one point in order for slip zones to appear over the interface. Three situations are shown in Figure 6 ($L_0 = 0.5, 1, 2$) to illustrate possible profiles of the function $F(y)$ for the strength parameters $k = \tan 15°$ and $C = 0$.

As is evident from Figure 6, up to three sliding zones can be formed. For instance, at $L_0 = 0.5$ (dotted line), $F(y) < 0$ outside the central part, i.e., resistance to slip at the periphery is higher than the shear stress, thus one can expect the appearance of a single shear zone. At $L_0 = 1$ (solid line), two symmetric intervals exist where $F(y) > 0$, which indicates a possibility of three nonconnecting shear zones. When $L_0 = 2$ (dashed line), $F(y) > 0$, which corresponds to the case in which three pure shear cracks may coalesce into one (the slip directions could be different in different parts of this zone).

Let us consider the most typical cases.

It is seen from the figures above that the slip resistance depends on the half-length L_0 essentially. Thus, at $L_0 > 2$ one observes that $\min |\sigma_{xx}^{\text{total}}| < 0.12$, which, taking into account the friction coefficient
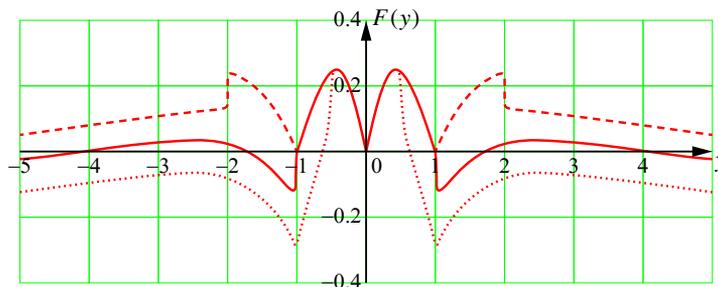
Figure 6. The function in (41) for the cases $L_0 = 0.5, 1, 2$ at $k = \tan 15°$ and $C = 0.1$; dashed line corresponds to $L_0 = 2$, solid line corresponds to $L_0 = 1$, dotted line corresponds to $L_0 = 0.5$.

in the Mohr–Coulomb criterion, makes the term $k\sigma_{xx}^{\text{total}}$ insignificant as compared to the shear stresses, which vary within the range $0.18 < |\sigma_{xy}| < 0.25$ for $2 < y < 5$. If the remote compression is greater than cohesion then the term C in the SIE (24) is also small. Then the slip zones are mostly defined by the magnitudes of the shear stresses caused by the wedge; hence, the second term in (24) can be neglected. This means that the slip occurs over the interval $(-L, L)$, $L > L_0 > 2$, and $L = B$; see (25)–(26).

The mode II SIF at the right end of the slip zone can be found analytically as follows:

$$\frac{K_{\text{II}}}{|\sigma_x^\infty|\sqrt{\pi L}} = 2H \int_{-L}^{L} \sqrt{\frac{L+y}{L-y}} \frac{y(1-y^2)}{(1+y^2)^2} \, dy = -2H\pi \left(1 - \frac{2L^2+1}{(L^2+1)^{3/2}}\right). \tag{42}$$

The right-hand side of (42) is zero at

$$L^* = \sqrt{\tfrac{1}{2}(1+\sqrt{5})} \approx 1.272,$$

which indicates that for the range $L > 2$ one has $K_{\text{II}} < 0$, i.e., the theoretical length of the sliding zone obtained by the condition $K_{\text{II}} = 0$ is infinite. In practice it can essentially exceed the length of the delamination zone provided that the latter is greater than the distance from the wedge to the interface.

One should note that the value $L^* = 1.272$ is the maximum possible half-length of the central mode II crack in the absence of friction and cohesion. In principle, it is possible that $L^* = L_0 = 1.272$ and simultaneously that $K_{\text{I}} = K_{\text{II}} = 0$, which is true if $H = 2.118$.

Let us analyse another limiting case, when the shear resistance on $A < |y| < B$ is greater than the shear stresses. Then the slip can occur only in the middle part $(-L, L)$. Moreover, on the interval $(-L_0, L_0)$, shear resistance is absent due to delamination. The dimensionless mode II SIF at the right end in this case is found by substituting (24) into the integral in (42):

$$\tilde{K}_{\text{II}} = \frac{K_{\text{II}}}{|\sigma_x^\infty|\sqrt{\pi L}} = 2H \int_{-L}^{L} \sqrt{\frac{L+y}{L-y}} \frac{y(1-y^2)}{(1+y^2)^2} \, dy - \int_{-L}^{L} \sqrt{\frac{L+y}{L-y}} \chi(y)(C - k\sigma_{xx}^{\text{total}}(y)) \, dy. \tag{43}$$

Since the function $\chi(y)$ is odd (see (23)) and the term in the brackets is even, one can present the second integral in (43) in the form

$$\int_{-L}^{L} \sqrt{\frac{L+y}{L-y}} \chi(y)(C - k\sigma_{xx}^{\text{total}}(y)) \, dy = 2 \int_{L_0}^{L} \frac{y(C - k\sigma_{xx}^{\text{total}}(y))}{\sqrt{L^2 - y^2}} \, dy. \tag{44}$$

The single shear crack can propagate inside different zones; for example, for $L_0 = 0.5$ in Figure 6 the slip can begin within the interval $(-1, 1)$, where the shear stress changes its direction at the origin. However, it is also possible that the slip could take place over the large zone including the interval $(-1, 1)$, as is shown, for example, for the case $L_0 = 1.5$, $k = \tan 15°$, $C = 0.2$ in Figure 7. In this case the slip directions will be different on opposite sides of the points $y = -1, +1$.

Therefore, the following three scenarios are possible:
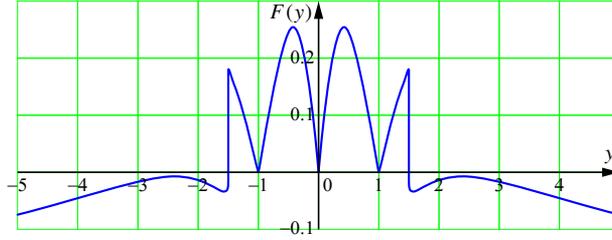
Figure 7. The function (41) for $L_0 = 1.5$ at $k = \tan 15°$ and $C = 0.2$.

(1) If $L_0 > 1$, then $\chi(y) = -1$ and (44) takes the form

$$\int_{-L}^{L} \sqrt{\frac{L+y}{L-y}} \chi(y)(C - k\sigma_{xx}^{\text{total}}(y))\, dy = -\int_{L_0}^{L} \frac{2y(C - k\sigma_{xx}^{\text{total}}(y))}{\sqrt{L^2 - y^2}}\, dy$$

$$= -2C\sqrt{L^2 - L_0^2} + kG_1(L_0, L), \tag{45}$$

where

$$G_1(L_0, L) = \frac{2}{(1 + L_0^2)^{3/2}} \int_{L_0}^{L} \frac{\sqrt{y^2 - L_0^2}}{\sqrt{L^2 - y^2}} \frac{y^2(y^2 + 2L_0^2 + 3)}{(y^2 + 1)^2}\, dy. \tag{46}$$

In this case the final expression for K_{II} can be presented in the form

$$\tilde{K}_{\text{II}} = -\pi(L_0^2 + 1)^{3/2}\left(1 - \frac{2L^2 + 1}{(L^2 + 1)^{3/2}}\right) + 2C\sqrt{L^2 - L_0^2} + kG_1(L_0, L). \tag{47}$$

(2) If $L_0 < L < 1$, then $\chi(y) = 1$ and (44) has a form similar to (45) but with the opposite sign, hence the expression for K_{II} takes the form

$$\tilde{K}_{\text{II}} = -\pi(L_0^2 + 1)^{3/2}\left(1 - \frac{2L^2 + 1}{(L^2 + 1)^{3/2}}\right) - 2C\sqrt{L^2 - L_0^2} - kG_1(L_0, L). \tag{48}$$

(3) If $L_0 < 1$, then $\chi(y)$ can alter its sign, and if $L > 1$, then it is necessary to consider two integrals, hence (44) takes the form

$$\int_{-L}^{L} \sqrt{\frac{L+y}{L-y}} \chi(y)(C - k\sigma_{xx}^{\text{total}}(y))\, dy$$

$$= \int_{L_0}^{1} \frac{2y(C - k\sigma_{xx}^{\text{total}}(y))}{\sqrt{L^2 - y^2}}\, dy - \int_{1}^{L} \frac{2y(C - k\sigma_{xx}^{\text{total}}(y))}{\sqrt{L^2 - y^2}}\, dy$$

$$= \int_{L_0}^{L} \frac{2y(C - k\sigma_{xx}^{\text{total}}(y))}{\sqrt{L^2 - y^2}}\, dy - 2\int_{1}^{L} \frac{2y(C - k\sigma_{xx}^{\text{total}}(y))}{\sqrt{L^2 - y^2}}\, dy$$

$$= 2C\left(\sqrt{L^2 - L_0^2} - 2\sqrt{L^2 - 1}\right) - k(G_1(L_0, L) - 2G_2(L_0, L)), \tag{49}$$
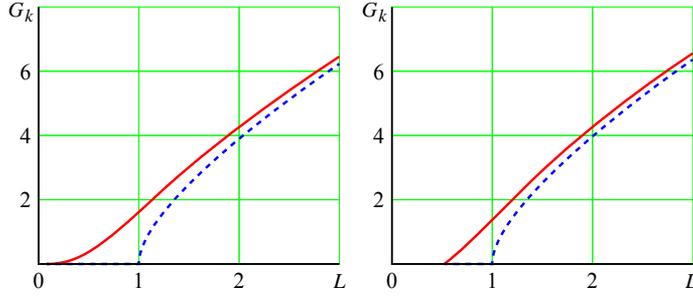
Figure 8. The integrals $G_k(L_0, L)$ as functions of L (solid curve for G_1, dashed curve for G_2). Left: $L_0 = 0.1$. Right: $L_0 = 0.5$.

where

$$G_2(L_0, L) = \frac{2}{(1 + L_0^2)^{3/2}} \int_{L_0}^{1} \frac{\sqrt{y^2 - L_0^2}}{\sqrt{L^2 - y^2}} \frac{y^2(y^2 + 2L_0^2 + 3)}{(y^2 + 1)^2} \, dy. \tag{50}$$

If $L_0 < 1$ and $L > 1$, then the final expression for K_{II} is

$$\tilde{K}_{\mathrm{II}} = -\pi(L_0^2 + 1)^{3/2}\left(1 - \frac{2L^2 + 1}{(L^2 + 1)^{3/2}}\right) - 2C\left(\sqrt{L^2 - L_0^2} - 2\sqrt{L^2 - 1}\right)$$
$$- k(G_1(L_0, L) - 2G_2(L_0, L)). \tag{51}$$

The integrals $G_k(L_0, L)$, $k = 1, 2$, can be expressed as elliptical integrals or computed numerically. Their typical behaviour is illustrated in Figure 8.

The dependence of K_{II} on L is shown in Figures 9–11 for the various strength parameters (cohesion and friction coefficient) at $L_0 = 0.5$.

The nearest root of the equation that comes from the condition $K_{\mathrm{II}} = 0$ should be selected for the determination of the mode II crack length. It is evident from the figure that for $L_0 = 0.5$ the sliding zone length is usually less than one, apart from the case when the shear resistance is absent (solid curve in Figure 9, left) or cohesion is negligible for low friction angles (solid curve in Figure 9, right). In the latter case the length of the zone is greater than $L^* = 1.252$.

The half-length of the sliding zones determined by the condition $K_{\mathrm{II}} = 0$ are shown in Figure 11 for various lengths of the delamination zones, for $k = \tan 30°$.
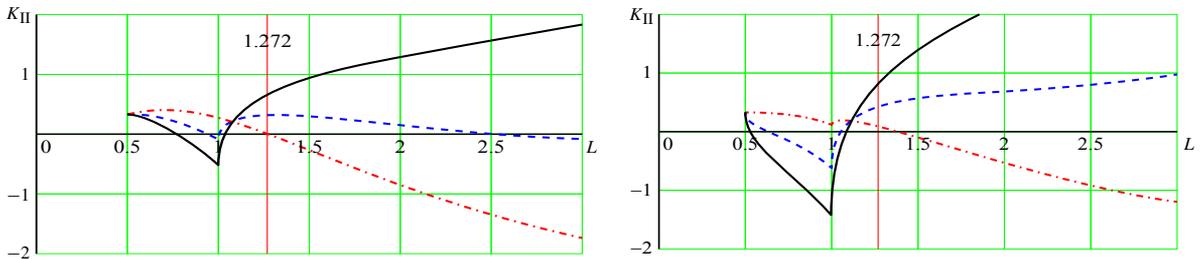
Figure 9. Dependence of dimensionless K_{II} on L for various values of the friction angle (left) and the cohesion (right), for $L_0 = 0.5$ and $C = 0$; dash-dotted line corresponds to $\rho = 0°$, dashed line to $\rho = 15°$, solid line to $\rho = 30°$.
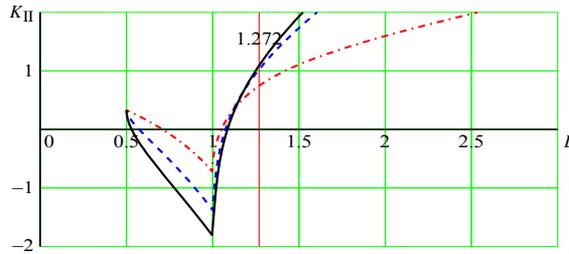
Figure 10. Dependence of dimensionless K_{II} on L for various combinations of the friction angles and cohesion for $L_0 = 0.5$; dash-dotted line corresponds to $\rho = 0°$, dashed line corresponds to $\rho = 15°$, solid line corresponds to $\rho = 30°$.
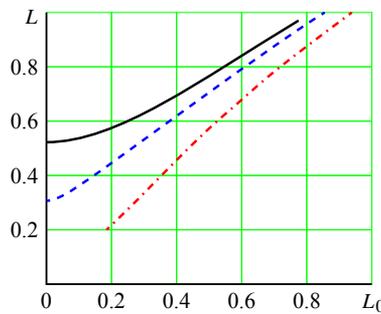
Figure 11. The half-length of the sliding zone L as a function of the half-length of the delamination zone L_0 for various cohesions at $k = \tan 30°$; dash-dotted line corresponds to $C = 0.5$, dashed line corresponds to $C = 0.1$, solid line corresponds to $C = 0.5$.

6. Three sliding zones

In order to find the length of the sliding zones one can employ the solution presented in [Gakhov 1966] for the inversion of the Cauchy integrals on m open contours:

$$\frac{1}{\pi} \int_\Gamma \frac{\varphi(t)}{t - \tau} \, dt = f(\tau). \tag{52}$$

The solution bounded at all ends has the form

$$\varphi(t) = -R(t) \frac{1}{\pi} \int_\Gamma \frac{f(\tau)}{R(\tau)} \frac{d\tau}{\tau - t}. \tag{53}$$

This is possible if the following conditions are satisfied:

$$\int_\Gamma \frac{f(\tau)}{R(\tau)} \tau^{j-1} \, d\tau = 0, \quad j = 1, \dots, m, \tag{54}$$

where $R(z)$ is a complex-valued function defined by

$$R(z) = \prod_{k=1}^m \sqrt{(z - a_k)(z - b_k)}. \tag{55}$$

In the case considered it is possible that three symmetric slip zones can appear on a straight line; therefore formula (55) takes the form

$$R(t) = \sqrt{(t^2 - A^2)(t^2 - B^2)(L^2 - t^2)}, \quad \text{Im}\, t = 0. \tag{56}$$

The right-hand side of (24) should be used as the function $f(t)$ in (54). The conditions in (54) are automatically satisfied for $j = 1, 3$ due to the odd right-hand side in (33). The rest take the form

$$\int_0^L \frac{h(y)}{R(y)} y \, dy + \int_A^B \frac{h(y)}{R(y)} y \, dy = 0, \tag{57}$$

where we denote

$$h(y) = \tfrac{1}{2}(f(y) - f(-y)) = -(L_0^2 + 1)^{3/2} \frac{y(1 - y^2)}{(1 + y^2)^2} + \chi(y)(C - k\sigma_{xx}^{\text{total}}(y)). \tag{58}$$

The conditions for single-valuedness of the tangential displacements should also be satisfied. Since the right-hand side in (24) is odd, the solution of (53) is even, i.e., can be presented in the form

$$\varphi(t) = -R(t)\frac{1}{\pi} \int_\Gamma \frac{h(y)y}{R(y)} \frac{dy}{y^2 - t^2}. \tag{59}$$

Therefore in (27) only two independent conditions remain, namely

$$\int_0^L \varphi(t) \, dt = 0, \quad \int_A^B \varphi(t) \, dt = 0. \tag{60}$$

Substitution of (59) in (60) leads to the following system of equations:

$$\int_0^L R(t) \int_0^L \frac{h(y)y}{R(y)} \frac{dy}{y^2 - t^2} \, dt + \int_0^L R(t) \int_A^B \frac{h(y)y}{R(y)} \frac{dy}{y^2 - t^2} \, dt = 0,$$
$$\int_A^B R(t) \int_0^L \frac{h(y)y}{R(y)} \frac{dy}{y^2 - t^2} \, dt + \int_A^B R(t) \int_A^B \frac{h(y)y}{R(y)} \frac{dy}{y^2 - t^2} \, dt = 0. \tag{61}$$

Therefore one has three nonlinear equations (equations (57) and (61)) for the determination of the three unknowns L, A, B. The solution obviously depends on the parameters L_0, C and $k = \tan \rho$. The form of the right-hand side indicates that some solutions may exist; however, the uniqueness is not obvious. The solution of the system has been obtained numerically. Figure 12 shows the results for $L_0 = 0.8$. In particular, it is seen from Figure 12 that the length of the internal shear zone L is rather weakly influenced by the values of cohesion and friction, while the influence of these parameters on the positions of the tips of the external shear zone is much stronger, especially the influence on the position of the external tip of the zone. It is seen that for given values of L_0 and $k = \tan \rho$ the sizes of the external shear zones decrease with increasing cohesion (which is predictable), and at some critical value of cohesion these zones vanish. However, the numerical procedure became extremely unstable for values approaching these critical points.
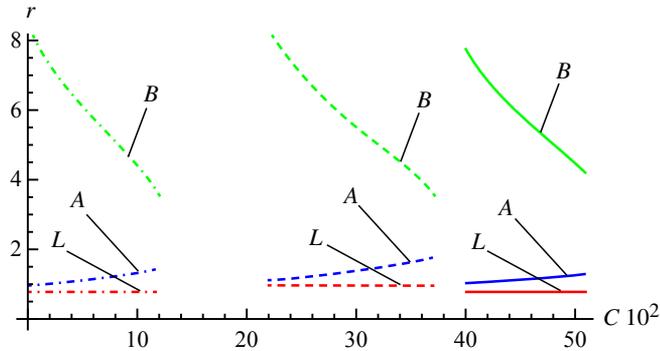
Figure 12. Equilibrium positions of the crack tips depending on relative cohesion C for various k: solid lines correspond to $k = 0$; dashed lines correspond to $k = 0.1$; dash-dotted lines correspond to $k = 0.33$.

7. Conclusion

The problem of wedging of an elastic isotropic homogeneous plane with a weak interface has been solved analytically. The wedge has been modelled by a pair of edge dislocations. The possibility of appearance of either one or three sliding zones (modelled by pure shear cracks) and a delamination zone (combined open-shear crack) along the weak interface has been demonstrated. The positions of the tips of the sliding zones depend on the stresses due to the dislocation, external stress field and the length of the delamination zone, which in turn is determined by the externally applied stress and stresses induced by the dislocation. The positions of the tips of the sliding zones have been computed for a specific configuration.

Acknowledgements

References

[Akulich and Zvyagin 2008] A. V. Akulich and A. V. Zvyagin, "Interaction between hydraulic and natural fractures", *Fluid Dyn.* **43**:3 (2008), 428–435.

[Bui 2006] H. D. Bui, *Fracture mechanics: Inverse problems and solutions*, Springer, 2006.

[Bui and Oueslati 2004] H. D. Bui and A. Oueslati, "Solutions exactes de fissure d'interface sous contact frottant avec un milieu indéformable", *C. R. Mécanique* **332**:9 (2004), 709–716.

[Bui and Oueslati 2005] H. D. Bui and A. Oueslati, "The sliding interface crack with friction between elastic and rigid bodies", *J. Mech. Phys. Solids* **53**:6 (2005), 1397–1421.

[Comninou and Dundurs 1983] M. Comninou and J. Dundurs, "Spreading of slip from a region of low friction", *Acta Mech.* **47**:1–2 (1983), 65–71.

[Cook et al. 1964] J. Cook, J. E. Gordon, C. C. Evans, and D. M. Marsh, "A mechanism for the control of crack propagation in all-brittle systems", *Proc. R. Soc. A* **282**:1391 (1964), 508–520.

[Cooke and Underwood 2001] M. L. Cooke and C. A. Underwood, "Fracture termination and step-over at bedding interfaces due to frictional slip and interface opening", *J. Struct. Geol.* **23**:2–3 (2001), 223–238.

[Dundurs and Comninou 1981] J. Dundurs and M. Comninou, "An educational elasticity problem with friction, I: Loading, and unloading for weak friction", *Trans. ASME Ser. E J. Appl. Mech.* **48**:4 (1981), 841–845.

[Gakhov 1966] F. D. Gakhov, *Boundary value problems*, Pergamon Press, New York, 1966. Reprinted Dover, New York, 1990.

[Galybin 1997] A. N. Galybin, "A model of mining-induced fault sliding", *Int. J. Rock Mech. Min.* **34**:3–4 (1997), 91.e1–91.e13. ISRM International Symposium 36th U.S. Rock Mechanics Symposium.

[Galybin and Mukhamediev 2012] A. N. Galybin and S. A. Mukhamediev, "On modelling of fluid-driven fracture branching in jointed rocks", pp. Paper#557 in *19th European conference on fracture, fracture mechanics for durability reliability and safety, Kazan, Russia 26–31, August*, 2012. Published on CD-ROM.

[Galybin and Mukhamediev 2014] A. N. Galybin and S. A. Mukhamediev, "Fracture development on a weak interface ahead of a fluid-driven crack"", *Eng. Fract. Mech.* **129** (2014), 90–101.

[Goldstein and Osipenko 2012] R. V. Goldstein and N. M. Osipenko, "Fracture initiation at the contact under shear", pp. Paper#399 in *19th European conference on fracture, fracture mechanics for durability reliability and safety, Kazan, Russia 26–31, August*, 2012. Published on CD-ROM.

[Goldstein and Osipenko 2015] R. V. Goldstein and N. M. Osipenko, "Initiation of a secondary crack across a frictional interface", *Eng. Fract. Mech.* **140** (2015), 92–105.

[Gorbatikh et al. 2001] L. Gorbatikh, B. Nuller, and M. Kachanov, "Sliding on cracks with non-uniform frictional characteristics", *Int. J. Solids Struct.* **38**:42–43 (2001), 7501–7524.

[Gudmundsson 2011] A. Gudmundsson, "Deflection of dykes into sills at discontinuities and magma-chamber formation", *Tectonophysics* **500**:1–4 (2011), 50–64. Emplacement of magma pulses and growth of magma bodies.

[Mendelsohn and Whang 1988] D. A. Mendelsohn and K. H. Whang, "Partial release and relocking of a frictionally locked crack due to moving tensile loads", *J. Appl. Mech.* (*ASME*) **55**:2 (06/01 1988), 383–388.

[Muskhelishvili 1977] N. I. Muskhelishvili, *Some basic problems of the mathematical theory of elasticity: fundamental equations, plane theory of elasticity, torsion and bending*, English ed., Noordhoff, Leiden, 1977.

[Zhou et al. 2010] J. Zhou, Y. Jin, and M. Chen, "Experimental investigation of hydraulic fracturing in random naturally fractured blocks", *Int. J. Rock Mech. Min.* **47**:7 (2010), 1193–1199.

ALEXANDER N. GALYBIN: a.n.galybin@gmail.com
The Schmidt Institute of Physics of the Earth, Russian Academy of Sciences, Gruzinskaya str. 10-1, Moscow, 123995, Russia

ROBERT V. GOLDSTEIN: goldst@ipmnet.ru
A. Yu. Ishlinsky Institute for Problems in Mechanics, Russian Academy of Sciences, prosp. Vernadskogo 101-1, Moscow, 119526, Russia

KONSTANTIN B. USTINOV: ustinov@ipmnet.ru
A. Yu. Ishlinsky Institute for Problems in Mechanics, Russian Academy of Sciences, prosp. Vernadskogo 101-1, Moscow, 119526, Russia

msp

EDGE FLUTTER OF LONG BEAMS UNDER FOLLOWER LOADS

EMMANUEL DE LANGRE AND OLIVIER DOARÉ

The linear instability of a beam tensioned by its own weight is considered. It is shown that for long beams, in the sense of an adequate dimensionless parameter, the characteristics of the instability caused by a follower force do not depend on the length. The asymptotic regime significantly differs from that of short beams: flutter prevails for all types of follower loads, and flutter is localised at the edge of the beam. An approximate solution using matched asymptotic expansion is proposed for the case of a semi-infinite beam. Using a local criterion based on the stability of waves, the characteristics of this regime as well as its range of application can be well predicted. These results are finally discussed in relation with cases of flow-induced instabilities of slender structures.

1. Introduction

The linear stability of a beam under the action of a follower force exerted at one of its extremities has been the subject of intensive research, as can be seen from the extensive review in [Langthjem and Sugiyama 2000]. The interest in this problem lies in its potential applications and also in the large variety of fundamental topics of mechanics involved in the solution method. Practical examples of direct application in the field of fluid-structure interactions are numerous: fluid-conveying pipes, plates subjected to axial flow and towed cylindrical bodies are modelled by equations that are similar, though not identical, to those of a beam under a compressive follower force [Païdoussis 1998; 2003]. More generally, follower forces have been extensively discussed in the literature, including in terms of their physical reality; see [Elishakoff 2005] for a full review. The case of a cantilevered beam of finite length under a partial follower force is well documented [Bolotin 1963], with many results on the effect of characteristics of the beam or of the load on the critical load that causes instability, and on the nature of the instability, be it divergence (buckling) or flutter.

We seek here to establish the characteristics of instability of a beam in the case where its length is much larger than the region where an unstable motion will develop. This arises when a constant load, such as gravity acting on a vertically hanging beam, produces a tension that increases along the beam, from zero at the lower free end to a maximum at the upper fixed end. The increasing tension induces a corresponding increasing stiffness. Motion is then confined to the lower end, corresponding to *edge flutter*. This has been studied both experimentally and numerically in three of the problems of flow-induced vibrations mentioned above: hanging fluid-conveying pipes [de Langre et al. 2001; Doaré and de Langre 2002], hanging ribbons under axial flow [Lemaitre et al. 2005] and towed cylinders under axial flow [de Langre et al. 2007; Obligado and Bourgoin 2013]. In all these systems it was observed that there exists a limit state in which the length does not affect the stability. This limit state is found for

length larger than a limit value given by simple considerations on the local stability of bending waves [Doaré and de Langre 2002; de Langre et al. 2007].

The objective of this paper is to establish similar results in the generic case of a beam under a partial follower force (or subtangential force), tensioned by a load such as gravity.

In Section 2 we shall recall the equations of motion and the possible choices of dimensionless variables. The effect of the beam length on stability is analysed in Section 3, using numerical computations of the eigenmodes. In Section 4 we address the particular case of a semi-infinite beam, using various types of modelling. The application of the results given in the paper to problems of flow-induced instabilities is discussed in Section 5.

2. Equations of motion

We consider a vertical beam of length L loaded by its own weight; see Figure 1.
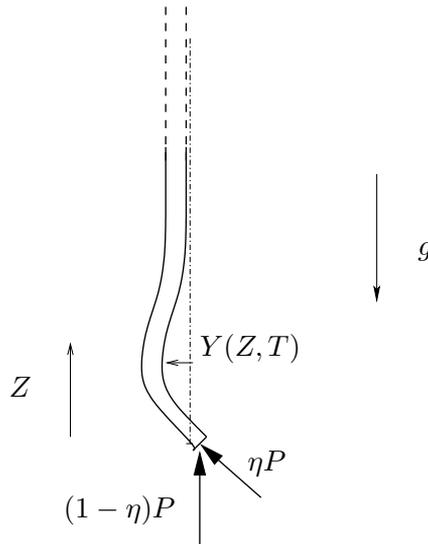
Figure 1. Semi-infinite hanging beam with a partial follower force.

A partial follower force is applied at its lower end [Langthjem and Sugiyama 2000]. The linear equation governing the in-plane lateral deflection $Y(Z, T)$ reads

$$EI\frac{\partial^4 Y}{\partial Z^4} + \frac{\partial}{\partial Z}\left[(P - mgZ)\frac{\partial Y}{\partial Z}\right] + m\frac{\partial^2 Y}{\partial T^2} = 0, \tag{1}$$

where EI is the flexural rigidity, P is the load, g is gravity and m is the mass per unit length. No damping is considered here, though it is known to significantly influence some aspects of the problem; see, for instance, [Detinko 2003]. The boundary conditions at the lower end, $Z = 0$, are

$$EI\frac{\partial^2 Y}{\partial Z^2}(0) = 0, \quad EI\frac{\partial^3 Y}{\partial Z^3}(0) + (1 - \eta)P\frac{\partial Y}{\partial Z}(0) = 0, \tag{2}$$

where η is a coefficient that expresses the part of the loading that follows the beam slope; $\eta = 0$ corresponds to a nonfollower force and $\eta = 1$ to a pure follower force. At the upper end, we assume a clamped condition,

$$Y(L) = 0, \quad \frac{\partial Y}{\partial Z}(L) = 0. \tag{3}$$

Using the length of the beam, L, as a reference, we define the dimensionless variables

$$z = \frac{Z}{L}, \quad y = \frac{Y}{L}, \quad t = \left(\frac{EI}{m}\right)^{1/2} \frac{1}{L^2} T, \quad p = \frac{PL^2}{EI}, \quad \gamma = \frac{mgL^3}{EI}. \tag{4}$$

Then (1) may be rewritten in dimensionless form as

$$\frac{\partial^4 y}{\partial z^4} + \frac{\partial}{\partial z}\left[(p - \gamma z)\frac{\partial y}{\partial z}\right] + \frac{\partial^2 y}{\partial t^2} = 0, \tag{5}$$

with the boundary conditions

$$\frac{\partial^2 y}{\partial z^2}(0) = 0, \quad \frac{\partial^3 y}{\partial z^3}(0) + (1 - \eta)p\frac{\partial y}{\partial z}(0) = 0, \quad y(1) = 0, \quad \frac{\partial y}{\partial z}(1) = 0. \tag{6}$$

This dimensionless set of equations is adequate to analyse the effect of γ on the critical loading, but only if the length L is kept constant. As we need to vary the length L, it is necessary to define a new set of dimensionless parameters. We now use a length scale defined by the ratio of the two stiffnesses of the beam, namely the flexural rigidity and the stiffness related to tension induced by gravity [Doaré and de Langre 2002],

$$L_g = \left(\frac{EI}{mg}\right)^{1/3}, \tag{7}$$

which will be referred to as the gravity length. This length scales like the critical length that causes buckling of the beam under its own weight. Using L_g as the reference length to define dimensionless variables, we have

$$x = \frac{Z}{L_g}, \quad y = \frac{Y}{L_g}, \quad \tau = \left(\frac{EI}{m}\right)^{1/2} \frac{1}{L_g^2} T, \quad q = \frac{PL_g^2}{EI}, \quad \ell = \frac{L}{L_g}, \tag{8}$$

where L_g has been substituted for L. These are related to the previous set of variables by

$$x = z\ell, \quad \tau = t\ell^2, \quad q = \frac{p}{\ell^2}, \quad \ell = \gamma^{1/3}. \tag{9}$$

Equation (1) now becomes

$$\frac{\partial^4 y}{\partial x^4} + \frac{\partial}{\partial x}\left[(q - x)\frac{\partial y}{\partial x}\right] + \frac{\partial^2 y}{\partial \tau^2} = 0, \tag{10}$$

and the corresponding boundary conditions are

$$\frac{\partial^2 y}{\partial x^2}(0) = 0, \quad \frac{\partial^3 y}{\partial x^3}(0) + (1 - \eta)q\frac{\partial y}{\partial x}(0) = 0, \quad y(\ell) = 0, \quad \frac{\partial y}{\partial x}(\ell) = 0. \tag{11}$$
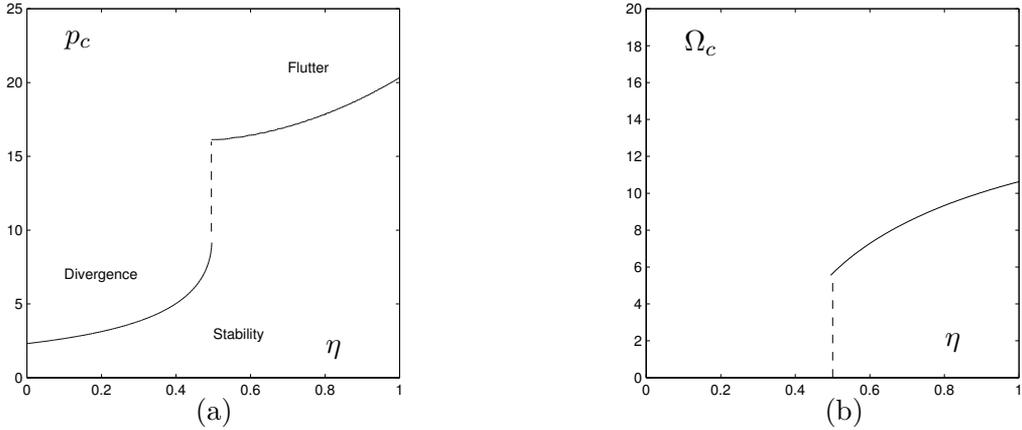
Figure 2. (a) Critical load and (b) frequency at instability, for short beams. Dashed vertical lines are guides for the eyes that do not correspond to calculations.

3. Stability of finite beams

3.1. *Solution for short beams.* For short beams, in the sense that $\ell \ll 1$, the critical load q_c may be derived by considering that $\gamma \ll 1$, so that (5) becomes

$$\frac{\partial^4 y}{\partial z} + p \frac{\partial^2 y}{\partial z^2} + \frac{\partial^2 y}{\partial t^2} = 0. \tag{12}$$

The corresponding stability diagram of p_c versus η is that of the generalised Beck's column [Langthjem and Sugiyama 2000], and is shown in Figure 2(a). For $\eta < 0.5$, instability arises in the form of a divergence, whereas flutter prevails for $\eta > 0.5$. The corresponding frequency at the flutter limit is shown in Figure 2(b). The critical load and frequency at flutter expressed in the dimensionless variables of (8) are

$$q_c(\eta, \ell) = \frac{p_c(\eta)}{\ell^2}, \quad \omega_c(\eta, \ell) = \frac{\Omega_c(\eta)}{\ell^2}. \tag{13}$$

3.2. *Effect of length.* We now investigate the effect of the length ℓ on the stability threshold and the nature of the instability. The numerical method utilised to this end is the finite difference method, as in [Sugiyama and Kawagoe 1975]. It allows us to compute the eigenvalues ω and the eigenvectors φ, such that

$$\varphi^{(4)} + [(q - x)\varphi']' - \omega^2 \varphi = 0 \tag{14}$$

with

$$\varphi''(0) = \varphi^{(3)}(0) + (1 - \eta)q\varphi'(0) = \varphi(\ell) = \varphi'(\ell) = 0. \tag{15}$$

The critical load and the nature of the corresponding instability can be determined from the evolution of the real and imaginary parts of the frequency. The beam is unstable if the frequency ω has a negative imaginary part. If the real part is zero, the instability results in an exponential growth in time of the deformation, without oscillation, and the instability is of the divergence type. If the real part is nonzero, the instability results in an exponential growth of oscillations, and the instability is of the flutter type.

Figure 3 shows the evolution of the critical load with length, for several values of η of particular interest.

For $\eta = 0$, Figure 3(a), which is the case of a nonfollower force, the critical load decreases steeply with length up to about $\ell = 5$, where it reaches a limit value and does not change when the length is increased further. Instability is of the divergence type for all lengths. In the same figure are shown computations from [Naguleswaran 2004; Triantafyllou and Chryssostomidis 1984] for intermediate values of the length. In [Triantafyllou and Chryssostomidis 1984], the static instability of a towed beam is considered, which yields equations similar to those used here. Details of the equivalence are discussed in Section 5, but suffice it to say here that we may use the results in Figure 4 of [Triantafyllou and Chryssostomidis 1984] with the change of variables $\ell = \varepsilon \lambda^{2/3}$ and $q = \lambda^{2/3}$. It is seen that those results and those of this paper are in very good agreement. For $\eta = 0.2$, Figure 3(b), the critical load for divergence also decreases and reaches a limit value, but the flutter threshold becomes lower than that for divergence for beams longer than $\ell = 5$. For $\eta = 0.3$, Figure 3(c), no divergence is found for $\ell > 3$. Instability in that range of ℓ is of the flutter type. For $\eta = 1$, Figure 3(d), the system loses stability by flutter, similarly to Beck's column; the critical load for flutter decreases with ℓ until it reaches a limit value.

From these four cases it can be stated that there exists a limit configuration for all long beams, say $\ell > 10$. For these lengths, the type of instability, flutter or divergence, may differ from that observed for short beams at the same value of η.

This is further confirmed in the evolutions of the stability diagram $q_c(\eta)$ shown in Figure 4. At $\ell = 1$, the diagram is similar, though not identical, to that for short beams; since $\ell = 1$, we have here $q_c = p_c$, and Figures 2 and 4(a) can be directly compared. At $\ell = 100$, Figure 4(b), a limit state is almost reached, where stability is always lost by flutter, for all values of η.

Figure 5 shows the mode shape at the critical load, which may be a divergence or a flutter instability depending on the values of η and ℓ, as shown above. Note that at the instability threshold φ is real, even for flutter instability. In fact, in (14), when ω is real, so is φ. For $\eta = 0$, Figure 5(a), the mode shape, here for divergence, becomes independent of the length when $\ell > 3$. This is consistent with Figure 3(a), where the critical load was found to be stationary in this range. For $\eta = 0.3$ and $\eta = 1$, Figures 5(b) and (c), the mode shapes also converge to a constant shape as the length is increased. There, the displacement is confined to the lower part of the beam. Note that the instability is of the flutter type, except for $\eta = 0.3$ at $\ell = 1$. Yet the limit mode shape closely resembles that of the divergence instability at $\eta = 0$.

4. Stability of a semi-infinite beam

4.1. *Boundary conditions.* We now seek to determine the characteristics of the instability when the beam is assumed to be of infinite length in the X axis. This is expected to be the solution to which the results of the preceding section converge as ℓ is increased. Whereas the boundary condition at the lower end is unchanged, the condition that the beam is clamped at $X = L$ needs to be replaced by the conditions that the displacement remains finite as X goes to infinity and that in this limit, propagating waves only radiate in the direction of increasing X. These conditions, in dimensionless form, read

$$\lim_{x \to \infty} |y| = 0 \quad \lim_{x \to \infty} \frac{\partial y}{\partial x} \frac{\partial y}{\partial t} < 0. \tag{16}$$
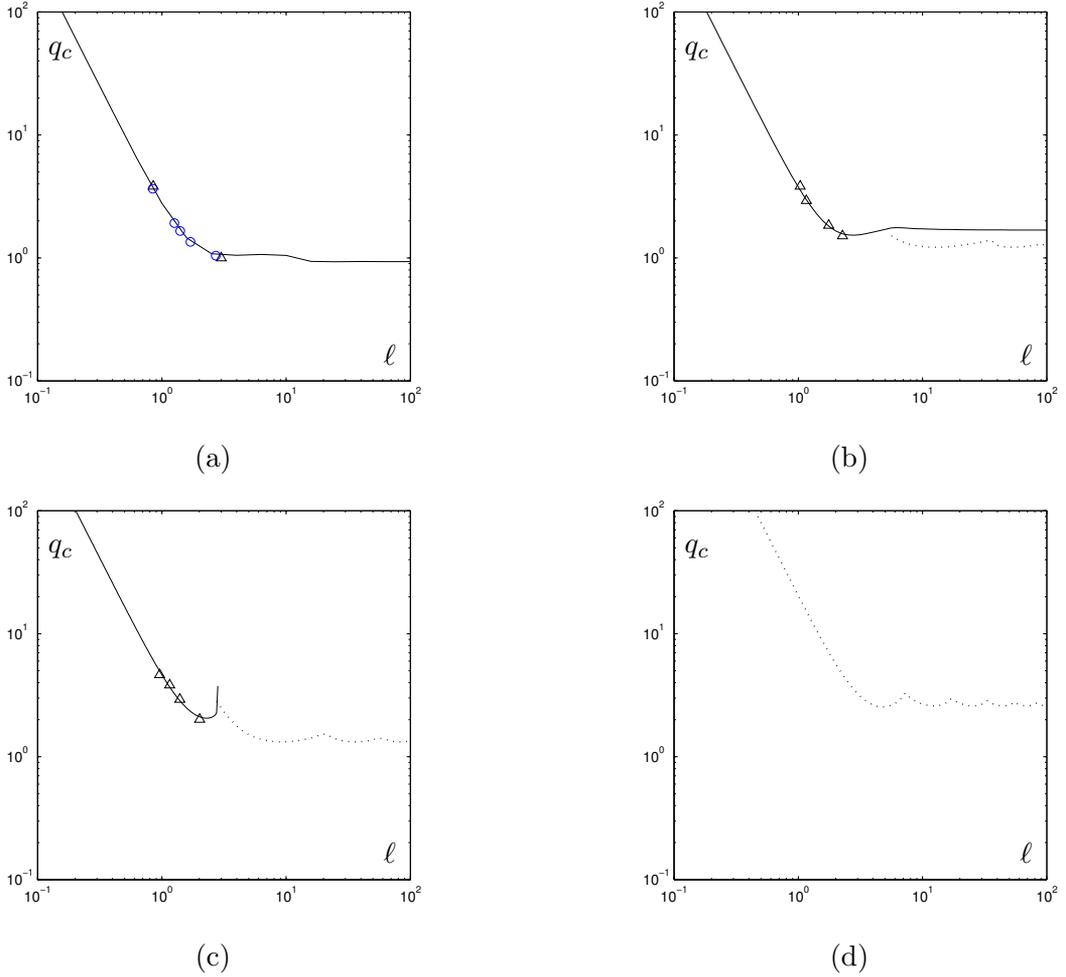
Figure 3. Effect of length on the critical load for divergence and flutter instabilities: (a) $\eta = 0$, (b) $\eta = 0.2$, (c) $\eta = 0.3$, (d) $\eta = 1$. The notation (—) represents results for divergence; $(\cdots)$, results for flutter; $(\circ)$, computations by [Naguleswaran 2004]; (Δ), computations by [Triantafyllou and Chryssostomidis 1984].

4.2. *Divergence instability.* The case of divergence instability may be analysed by neglecting all time derivatives in the equations, so that (10) becomes

$$\frac{\partial^4 y}{\partial x^4} + \frac{\partial}{\partial x}\left[(q-x)\frac{\partial y}{\partial x}\right] = 0 \tag{17}$$

and the boundary conditions are only

$$\frac{\partial^2 y}{\partial x^2}(0) = 0, \quad \frac{\partial^3 y}{\partial x^3}(0) + (1-\eta)q\frac{\partial y}{\partial x}(0) = 0, \quad \lim_{x\to\infty}|y| = 0. \tag{18}$$
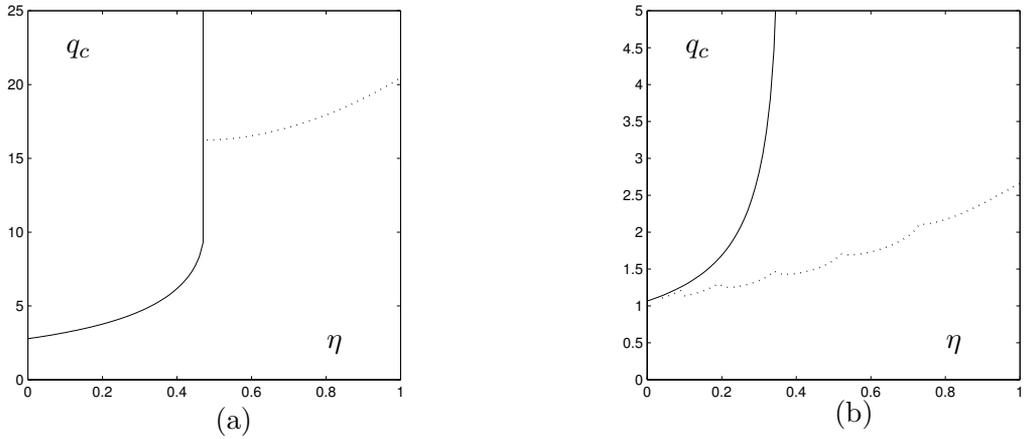
Figure 4. Effect of the ratio η on the critical load for divergence (—) and flutter $(\cdots)$. (a) Short beam, $\ell = 1$, (b) long beam, $\ell = 100$.
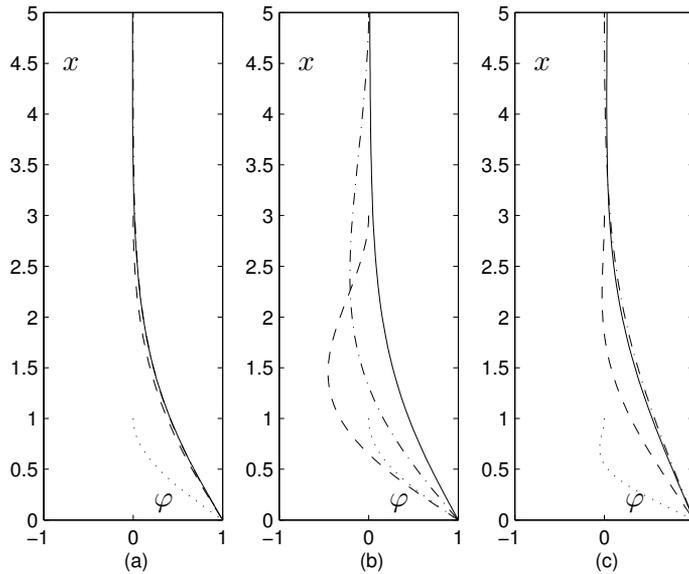
Figure 5. Mode shape at the critical load. (a) $\eta = 0$, (b) $\eta = 0.3$, (c) $\eta = 1$. $(\cdots)$, $\ell = 1$; $(- -)$, $\ell = 3$; $(- \cdot -)$, $\ell = 5$; (—), $\ell = 10$.

By defining $\lambda = q^{3/2}$ and $Z = x - q$, this set of equations is identical to that solved by Triantafyllou and Chryssostomidis [1984] for the case of a towed cylinder. Using their solution with our variables, the critical load for divergence $q_c(\eta)$ is found to satisfy

$$\text{Ai}'(-q_c) - q_c \eta \left[\frac{1}{3} - \int_0^{-q_c} \text{Ai}(s)\, ds \right] = 0, \tag{19}$$

where Ai is the Airy function [Abramowitz and Stegun 1972].

4.3. *Flutter instability.* We give here an approximate solution for the critical load for flutter of a semi-infinite beam, which is an extension of [de Langre et al. 2001] for a purely follower force, $\eta = 1$. The approach used in the matched asymptotic expansions follows that proposed in [Triantafyllou and Triantafyllou 1991] for the dynamics of vibrating strings tensioned by gravity.

We consider (10), with the boundary conditions (11) at the bottom end and (16) for a semi-infinite beam. We seek harmonic solutions of this set of equations, of the form

$$y(x, t) = \text{Real}[\varphi(x)e^{i\omega t}] \tag{20}$$

as a function of the follower force magnitude q. Instability will be associated with $\text{Im}(\omega) < 0$. The variation in space of the solution satisfies

$$\varphi^{(4)} + [(q - x)\varphi']' - \omega^2\varphi = 0, \tag{21}$$

with boundary conditions

$$\varphi^{(2)}(0) = 0, \quad \varphi^{(3)}(0) + (1 - \eta)q\varphi'(0) = 0, \tag{22}$$

where the prime denotes derivation with respect to x. The condition for radiating waves reads

$$\lim_{x \to \infty} \left(\text{Real}[\varphi'(x)e^{i\omega t}] \, \text{Real}[i\omega\varphi(x)e^{i\omega t}]\right) < 0. \tag{23}$$

Let us consider first the lower part of the beam, where x is of the order of q. In this "inner" domain of length q, we may derive an approximate solution $\varphi_i(x)$ by simply lumping all its inertia at the lower end of the beam, so that the boundary conditions at $x = 0$ read now

$$\varphi_i^{(2)}(0) = 0, \quad \varphi_i^{(3)}(0) + (1 - \eta)q\varphi_i'(0) = q\omega^2\varphi_i(0), \tag{24}$$

and (21) reduces to

$$\varphi_i^{(4)} + [(q - x)\varphi_i']' = 0. \tag{25}$$

The corresponding solution reads

$$\varphi_i(x) = a + \int_0^x \left[b\,\text{Ai}(s - q) + c\,\text{Bi}(s - q) + d\,\text{Gi}(s - q)\right]ds, \tag{26}$$

where Ai, Bi and Gi are the Airy functions, a, b, c, d being four coefficients. For the sake of clarity, we now use the notation $\overline{F}(x) = \int_0^x F(s)\,ds$ and F for $F(-q)$ unless otherwise specified, where F could be any of the Airy functions above.

In terms of the coefficients a, b, c, d, the boundary conditions at the lower end are

$$b\,\text{Ai}' + c\,\text{Bi}' + d\,\text{Gi}' = 0, \tag{27}$$

$$b\,\text{Ai}'' + c\,\text{Bi}'' + d\,\text{Gi}'' + (1 - \eta)q(b\,\text{Ai} + c\,\text{Bi} + d\,\text{Gi}) = aq\omega^2. \tag{28}$$

Conversely, in the upper part of the beam, that is, where $x \gg q$, we rescale the equations by using new variables in space and time, namely

$$\chi = x\varepsilon, \quad r = \frac{\omega}{\sqrt{\varepsilon}}, \tag{29}$$

where $\varepsilon = L_g / \Lambda$, the length Λ being an arbitrary large length scale. Using this set of variables, (21) reads

$$\varepsilon^3 \varphi^{(4)} + [(\varepsilon^2 q - \varepsilon \chi) \varphi']' - \varepsilon r^2 \varphi = 0, \tag{30}$$

where the prime now denotes differentiation with respect to χ. This allows us to derive the equation at the leading order in the "outer" domain,

$$(-\chi \varphi_e')' - r^2 \varphi_e = 0, \tag{31}$$

the solution of which, in terms of Bessel functions, is (see also in [Elishakoff and Pellegrini 1987])

$$\varphi_e(\chi) = \alpha J_0(2r\sqrt{\chi}) + \beta Y_0(2r\sqrt{\chi}). \tag{32}$$

The radiation condition, (23), implies that

$$\alpha - i\beta = 0. \tag{33}$$

We may now match the inner and outer solutions by considering their respective limits [Abramowitz and Stegun 1972; Triantafyllou and Triantafyllou 1991]. Equating these two limits yields three conditions for the coefficients defining the inner and outer solutions, namely

$$c = 0, \quad d = \beta, \quad a + b\left[\frac{1}{3} - \overline{\mathrm{Ai}}\right] + d\left[\frac{2\gamma + \ln 3}{3\pi} - \overline{\mathrm{Gi}}\right] = \alpha + \beta \frac{2}{\pi}(\ln \omega + \gamma), \tag{34}$$

where γ is Euler's constant. The set of boundary conditions (27), (28), (33), with the three matching conditions (34), are six linear equations between the six coefficients α, β, a, b, c, d. This defines an implicit relationship between the two parameters ω and q, so that there exists a nontrivial solution

$$-\eta q[\mathrm{Gi}' \, \mathrm{Ai} - \mathrm{Gi} \, \mathrm{Ai}'] - \frac{1}{\pi} \mathrm{Ai}' + q\omega^2 \left[\left(\frac{1}{3} - \overline{\mathrm{Ai}} \right) \mathrm{Gi}' - \left(\frac{\ln 3 - 4\gamma - 3i\pi - 6\ln\omega}{3\pi} - \overline{\mathrm{Gi}} \right) \mathrm{Ai}' \right] = 0. \tag{35}$$

The particular value of the flutter instability threshold q_c may be directly derived by assuming that ω is real in (35). As all functions of q in (35) are real, this implies that

$$\mathrm{Ai}'(-q_c) = 0, \quad q_c \simeq 1.02. \tag{36}$$

The real part of the frequency at the instability threshold is then derived using (35) and (36) as

$$\omega_c^2 = \eta \frac{\mathrm{Ai}(-q_c)}{\frac{1}{3} - \overline{\mathrm{Ai}}(-q_c)}. \tag{37}$$

At $\eta = 0$, the solution of [Triantafyllou and Chryssostomidis 1984] for divergence is recovered, both in terms of critical load and frequency. Using this approximate solution, flutter is found to exist for all values of η, and the corresponding critical load does not vary with η. In Figure 6(a) this is compared with the numerical solution for very long beams, $\ell = 100$. The approximate solution, (36), predicts a lower bound, $q_c = 10.2$, equal to that for $\eta = 0$. The flutter frequency is very well predicted, as may be seen in Figure 6(b). At the instability threshold, the modal shape φ is real and reduces to

$$\varphi(x) = \int_0^x \mathrm{Ai}(s - p) \, ds - \tfrac{1}{3}. \tag{38}$$
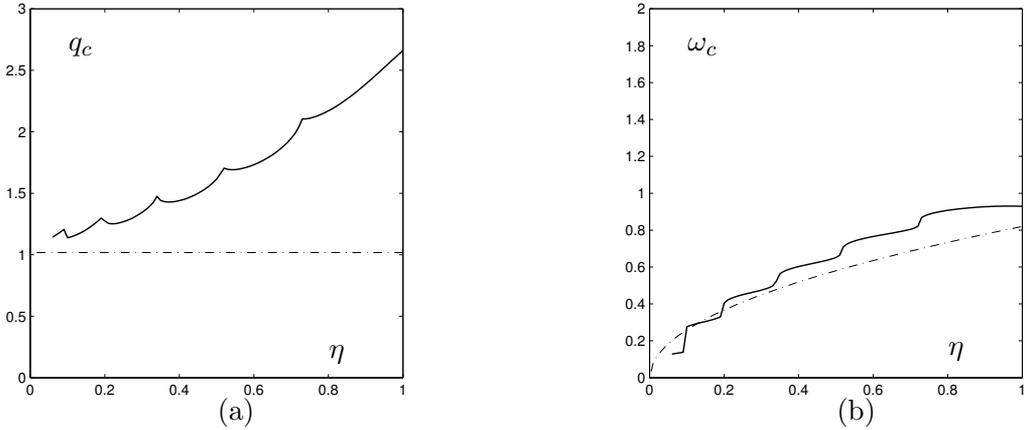
Figure 6. (a) Critical load q_c and (b) frequency ω_c of flutter of a long beam. (—), numerical results for $\ell = 100$; $(-\cdot-)$ solution for the semi-infinite beam using matched asymptotic expansions; see (36) and (37).
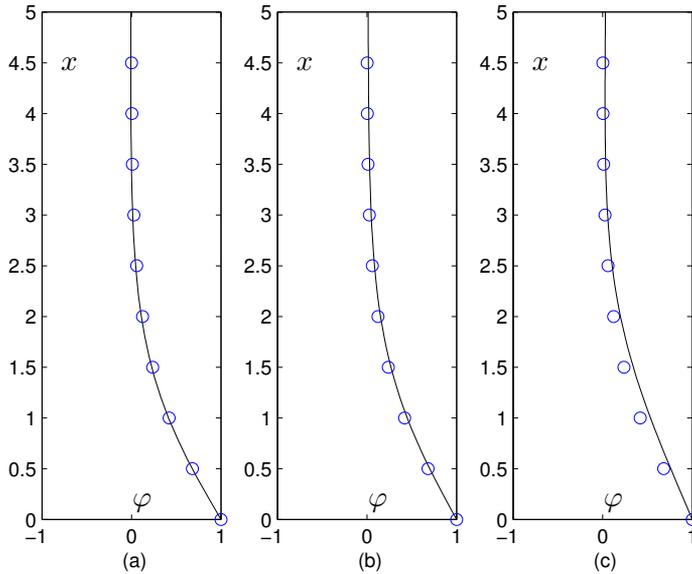
Figure 7. Mode shape at the critical load for a long beam. (a) $\eta = 0$, (b) $\eta = 0.3$, (c) $\eta = 1$. (—), numerical results for $\ell = 10$; (∘), solution for the semi-infinite beam using matched asymptotic expansions; see Equation (38).

This is compared in Figure 7 with the computed mode shapes at $\ell = 10$. For $\eta = 0$, Figure 7(a), (38) is actually the exact solution for a semi-infinite beam, which derives from the results of [Triantafyllou and Chryssostomidis 1984]. For $\eta = 0.3$ and even $\eta = 1$, it is remarkable that (38) stills gives a very good approximation of the mode shape at the flutter threshold; see Figures 7(b) and (c).

4.4. *A model based on local wave stability.* Following [Doaré and de Langre 2002], we consider now a criterion based on the local characteristics of waves, at a given position x. From (10), the dispersion relation is

$$k^4 - (q - x)k^2 - \omega^2 = 0, \tag{39}$$

where k is the wavenumber and ω is the frequency of the wave. All points such that $x < q$ bear unstable waves. Beams of length ℓ larger than q are expected to have a behaviour not affected by length, as waves are damped above $x = q$.

In dimensional variables, this allows us to define the length L_N for neutral stability,

$$L_N = \frac{P}{mg}, \tag{40}$$

above which the medium only bears stable waves. In (1) this is the point where the local tension goes through zero. Considering that the part of the beam above this, $Z > L_N$, plays a negligible role in the instability, we may approximate the critical load for the *semi-infinite* beam by that for a *finite* beam of length L_N: a beam of length L_N, without gravity, has a dimensional critical load

$$P_c = \frac{EI}{L_N^2} p_c, \tag{41}$$

where p_c is the dimensionless critical load for short beams. As the length L_N varies with the load P, this results in

$$P_c^3 = EI (mg)^2 p_c. \tag{42}$$

Using now dimensionless variables pertaining to the case of long beams, this reads

$$q_c = p_c^{1/3}; \tag{43}$$

similarly, we have

$$\omega_c = \frac{\Omega_c}{p_c^{2/3}}. \tag{44}$$

In Figure 8(a), this is plotted for comparison with numerical results for the very long beam. The order of magnitude of the critical load is well recovered. Yet divergence is predicted for $\eta < 0.5$, instead of flutter. Note also that the critical load at $\eta = 1$ is very well predicted. Figure 8(b) summarises this approach: the limit line $\ell = q$ is found to be a good approximation of the transition between the behaviour of short beams, which depends on length, and that of long beams, which does not. For short beams, the approximation (13) applies. For long beams, (43) is a good approximation.

5. Discussion

5.1. *Domains of instability.* In the results presented in this paper, two regions can be identified in a beam tensioned by a load such as gravity. In the part near the free end, $x \ll 1$ in our dimensionless variables, that is, $Z \ll L_g = (EI/Mg)^{1/3}$, the stiffness that opposes lateral displacement is dominantly that of the flexural rigidity. Conversely, for $x \gg 1$, the stiffness is due to the tension that results from gravity.
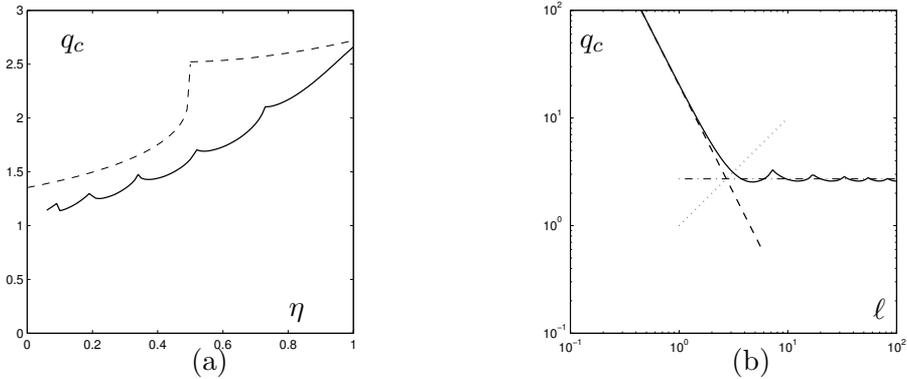
Figure 8. Models for the critical load based on local wave stability. (a) Critical load numerical results (—) for $\ell = 100$; $(- -)$, model based on local wave stability; see (43) and (44). (b) Effect of length $\eta = 1$. (—), computations of Section 3.2; $(- -)$, short beam model; $(\cdots)$, transition line; $(- \cdot -)$, long beam model.

For a given beam, if its length L is much smaller than L_g, or $\ell \ll 1$, gravity effects can be neglected everywhere. In terms of stability the behaviour is that of short beams in our denomination. The upper boundary condition, here clamping, plays a crucial role, and the instability may be divergence or flutter. If the length is much larger than L_g, so that $\ell \gg 1$, gravity effects dominate in all the upper part. This results in a confinement of the instability in the lower part of the beam, which appears in all the mode shapes. The upper boundary condition plays a lesser role. It is remarkable that the characteristics of the instability of these long beams seem to be much simpler than that of short beams: flutter prevails in all cases, and the critical load, the frequency and the mode shape have very simple evolutions.

For long beams flutter is reached when the load q is of order 1. In that range of loading, the neutral point where tension vanishes, at $x = q$, is located near the limit between the two regions, $x = 1$. The critical load is then such that, in dimensionless variables,

$$P \simeq (EI)^{1/3}(mg)^{2/3}, \tag{45}$$

which shows the balance between the loading P and the two stiffnesses of the systems, EI for the flexural rigidity and mg for the tension induced by gravity.

It should be recalled here that damping was not considered in our calculations. Damping may significantly modify the critical value for flutter instability even when small [Langthjem and Sugiyama 2000], and has been found to have both stabilising and destabilising effects. In some cases, such as that of Beck's column, it has been found that addition of damping destabilises the system and changes the instability type from flutter to buckling. In gyroscopic systems such as fluid-conveying pipes or plates in axial flows, damping was found to destabilise neutral waves at zero frequency [Doaré 2010; 2014], which may also cause the instability to change from flutter to buckling in finite length systems. The generalisation to the present case of a semi-infinite system tensioned by gravity needs to be addressed to see how damping could alter the buckling/flutter stability maps, and if it prevents flutter from prevailing for all values of the follower force coefficient η.

5.2. *Relation to flow-induced instabilities.* The equivalence between the loading produced by the flow along a structure and a follower force exerted at its free end is discussed in [Païdoussis 1998; 2003]. Depending on the geometry of the problem, the load may be either a fully follower load (fluid-conveying pipe) or partially a follower load (cylinder with axial flow). In the latter case, the shape of the downstream free end strongly influences the value of η.

For systems mainly tensioned by gravity, such as hanging fluid-conveying pipes or hanging ribbons under axial flow [Doaré and de Langre 2002; Lemaitre et al. 2005], the equations of motion can be put in the common dimensionless form

$$\frac{\partial^4 y}{\partial x^4} + \frac{\partial}{\partial x}\left[(v^2 - x)\frac{\partial y}{\partial x}\right] + 2v\sqrt{\beta}\frac{\partial^2 y}{\partial x \partial \tau} + \frac{\partial^2 y}{\partial \tau^2} = 0, \tag{46}$$

where the dimensionless variables have been defined using the length L_g, as we did in the present paper. Here v is a dimensionless flow velocity and β expresses the proportion of the fluid mass in the total mass. The boundary conditions at the lower end read

$$\frac{\partial^2 y}{\partial x^2}(0) = 0, \quad \frac{\partial^3 y}{\partial x^3}(0) = 0, \tag{47}$$

which expresses the case of a purely follower load. Equation (46) is identical to (10), except for the gyroscopic term which is dependent on β. The stability diagram for the case of a long hanging pipe was analysed in [Doaré and de Langre 2002] and for long hanging ribbons in [Lemaitre et al. 2005]. The critical velocity v_c was found to depend on the length in a manner very similar to that found in this paper. For very long pipes, flutter arises at a critical velocity v_c that depends only on β. Defining $q_c = v^2$, and in the particular limit of $\beta = 0$, the results of [Doaré and de Langre 2002] should converge to those found in this paper for $\eta = 1$. This is not exactly the case when the results of [Doaré and de Langre 2002] are used, as there calculations have been done for small but nonvanishing values of β. It is a well known feature that the case $\beta = 0$ is only found as the limit of very small values (10^{-3}) of β [Païdoussis 1998].

If the tensioning load is not gravity but a flow-induced friction on the slender structure, the form of the problem is changed in several ways [Païdoussis 2003]. First, the tensioning load increases with the flow velocity, which does not allow one to define an equivalent to the length L_g, as for gravity. The reference length that can then be defined scales the flow-induced forces that are proportional to volume (added stiffness forces) and those that are proportional to surface area (friction). Second, the friction load is not constant in direction, as is gravity, but acts tangentially to the instantaneous position of the beam. Third, in the case of axial flow outside of a structure, the flow may also induce forces perpendicular to the instantaneous position of the beam, in the form of a transverse drag. Moreover, the boundary condition at the free end includes other terms that depend on the local geometry of the flow. If all time-dependent terms are neglected, to determine the static stability of the beam under flow, the equation defining the deflection reads [Triantafyllou and Chryssostomidis 1984]

$$\frac{\partial^4 y}{\partial s^4} + v^2\frac{\partial}{\partial s}\left[(1 - s)\frac{\partial y}{\partial s}\right] = 0. \tag{48}$$

Upon defining $x = v^{2/3}s$ and $q = v^{2/3}$, the equation for the static behaviour of the beam, (17), is recovered. If the end condition sustains a force only in the beam axis, as in [Naguleswaran 2004], the results at $\eta = 0$ are recovered. For the analysis of dynamic instability, not only inertial terms need to be considered, as in the case of this paper. A gyroscopic term, as in (46), and a damping term appear, further complicating the behaviour of the system. In the analysis of a long towed cylinder edge flutter was also found [de Langre et al. 2007], confirming the generality of the results presented here in a generic case.

References

[Abramowitz and Stegun 1972] M. Abramowitz and I. A. Stegun (editors), *Handbook of mathematical functions: with formulas, graphs, and mathematical tables*, vol. 55, 10th ed., Wiley, New York, 1972.

[Bolotin 1963] V. V. Bolotin, *Nonconservative problems of the theory of elastic stability*, Macmillan, New York, 1963.

[Detinko 2003] F. M. Detinko, "Lumped damping and stability of Beck column with a tip mass", *Int. J. Solids Struct.* **40**:17 (2003), 4479–4486.

[Doaré 2010] O. Doaré, "Dissipation effect on local and global stability of fluid-conveying pipes", *J. Sound Vib.* **329**:1 (2010), 72–83.

[Doaré 2014] O. Doaré, "Dissipation effect on local and global fluid-elastic instabilities", pp. 67–84 in *Nonlinear physical systems: spectral analysis, stability and bifurcations*, edited by O. N. Kirillov and D. E. Pelinovsky, Wiley, Hoboken, NJ, 2014.

[Doaré and de Langre 2002] O. Doaré and E. de Langre, "Local and global instability of fluid-conveying pipes on elastic foundations", *J. Fluid. Struct.* **16**:1 (2002), 1–14.

[Elishakoff 2005] I. Elishakoff, "Controversy associated with the so-called "follower forces": critical overview", *Appl. Mech. Rev.* (*ASME*) **58**:2 (2005), 117–142.

[Elishakoff and Pellegrini 1987] I. Elishakoff and F. Pellegrini, "Exact and effective approximate solutions of some divergence-type non-conservative problems", *J. Sound Vib.* **114**:1 (1987), 143–147.

[de Langre et al. 2001] E. de Langre, O. Doaré, and F. Pellet, "Force suiveuse critique sur une colonne pesante semi-infinie: modèle et expériences", *Comptes Rendus de l'Académie des Sciences-Series IIB-Mechanics* **329**:3 (2001), 175–178.

[de Langre et al. 2007] E. de Langre, M. P. Païdoussis, O. Doaré, and Y. Modarres-Sadeghi, "Flutter of long flexible cylinders in axial flow", *J. Fluid Mech.* **571** (2007), 371–389.

[Langthjem and Sugiyama 2000] M. A. Langthjem and Y. Sugiyama, "Dynamic stability of columns subjected to follower loads: a survey", *J. Sound Vib.* **238**:5 (2000), 809–851.

[Lemaitre et al. 2005] C. Lemaitre, P. Hémon, and E. de Langre, "Instability of a long ribbon hanging in axial air flow", *J. Fluid. Struct.* **20**:7 (2005), 913–925.

[Naguleswaran 2004] S. Naguleswaran, "Transverse vibration of an uniform Euler–Bernoulli beam under linearly varying axial force", *J. Sound Vib.* **275**:1-2 (2004), 47–57.

[Obligado and Bourgoin 2013] M. Obligado and M. Bourgoin, "An experimental investigation of the equilibrium and stability of long towed cable systems", *New J. Phys.* **15**:4 (2013), 043019.

[Païdoussis 1998] M. P. Païdoussis, *Fluid-structure interactions: slender structures and axial flows, I*, Academic Press, San Diego, CA, 1998.

[Païdoussis 2003] M. P. Païdoussis, *Fluid-structure interactions: slender structures and axial flows, II*, Elsevier, San Diego, CA, 2003.

[Sugiyama and Kawagoe 1975] Y. Sugiyama and H. Kawagoe, "Vibration and stability of elastic columns under the combined action of uniformly distributed vertical and tangential forces", *J. Sound Vib.* **38**:3 (1975), 341–355.

[Triantafyllou and Chryssostomidis 1984] G. S. Triantafyllou and C. Chryssostomidis, "Analytic determination of the buckling speed of towed slender cylindrical beams", *J. Energy Resour. Technol.* (*ASME*) **106**:2 (1984), 246–249.

[Triantafyllou and Triantafyllou 1991] M. S. Triantafyllou and G. S. Triantafyllou, "The paradox of the hanging string: An explanation using singular perturbations", *J. Sound Vib.* **148**:2 (1991), 343–351.

EMMANUEL DE LANGRE: delangre@ladhyx.polytechnique.fr
Département de Mécanique, LadHyX, École Polytechnique, 91128 Palaiseau, France

OLIVIER DOARÉ: olivier.doare@ensta-paristech.fr
Unité de Mécanique, ENSTA-Paristech, 828 Boulevard des Maréchaux, 91120 Palaiseau, France

msp

ON THE STRONG INFLUENCE OF IMPERFECTIONS UPON THE QUICK DEVIATION OF A MODE I+III CRACK FROM COPLANARITY

JEAN-BAPTISTE LEBLOND AND VÉRONIQUE LAZARUS

This work explores the possibility that quick deviations of cracks loaded in mode I+III from coplanarity may be greatly facilitated by inevitable fluctuations of the fracture toughness. The idea is that such fluctuations must induce in-plane undulations of the crack front resulting, because of the presence of the mode III load, in nonzero values of the local stress intensity factor of mode II, implying future local out-of-plane deviations of the crack which might be "unstable" in Cotterell and Rice's sense if the local nonsingular stress parallel to the direction of propagation is positive.

Exploration of this idea implies evaluation of the variations of the local stress intensity factors and nonsingular stresses arising from a slight but otherwise arbitrary in-plane perturbation of a semi-infinite crack. These quantities were calculated in works of Gao and Rice, but the evaluation of the nonsingular stresses was incomplete, and is supplemented here by using the theory of 3D weight functions due to Rice and Bueckner.

Inspection of the results shows that for in-plane sinusoidal undulations of the crack front of sufficient (though still small) amplitude, the conditions of nonzero local stress intensity factor of mode II and positive local nonsingular stress parallel to the direction of propagation are simultaneously met on some parts of the front, implying the possibility of future local deviations of the crack from coplanarity that are "unstable" in Cotterell and Rice's sense, and thus confirming the idea investigated.

1. Introduction

The propagation of cracks loaded in mixed-mode I+III has been investigated in various materials: inorganic glass [Sommer 1969], polymeric glass [Knauss 1970], epoxy resin [Hull 1995], PMMA [Lazarus et al. 2008], Homalite [Lin et al. 2010], alumina [Suresh and Tschegg 1987], steels [Hourlier and Pineau 1979; Yates and Miller 1989; Lazarus 1997; Lazarus et al. 2001b], rocks [Pollard et al. 1982; Pollard and Aydin 1988; Cooke and Pollard 1996], gypsum and cheese [Goldstein and Osipenko 2012], to name just a few experimental papers on the subject. In all cases, it was observed that the crack propagates through formation of small fracture facets which may either abruptly "tilt" or gradually "twist" about the direction of propagation.

It has been remarked by Hourlier and Pineau [1979] that two types of facets are in fact formed: "type A" ones, rotating in such a way that the local stress intensity factor (SIF) of mode I increases with the distance of propagation while that of mode III decreases, and "type B" ones rotating oppositely so that the behavior of the local SIF is the reverse. Hourlier and Pineau also noted that the crack propagates preferentially along type A facets. A rationale for this observation was provided by Lazarus et al. [2001a;

2001b], who showed, using theoretical estimates of the SIF after some short continuous twisting, that for a given facet length, the energy release rate is larger at the center of type A facets than at that of type B facets, implying that propagation of the former facets is more "energetically favored" than that of the latter ones.

Pons and Karma [2010] performed numerical simulations of crack propagation in mode I+III based on a "phase field" model developed by Karma et al. [2001], which included a phenomenological description of failure mechanisms in the process zone around the crack front. These simulations reproduced both the gradual deviation of the crack from its original plane through formation of an array of inclined facets, and the quicker propagation of type A facets as compared to type B ones, in a remarkable way.

Although the theoretical framework employed in [Pons and Karma 2010] differed from standard linear elastic fracture mechanics (LEFM), it has been shown by Hakim and Karma [2009] that in the limit where the system size becomes much larger than the process zone size, Karma et al.'s phase field model [2001] in fact predicts that quasistatic crack propagation in isotropic media is governed by a combination of two classical LEFM criteria: a condition of uniform energy release rate along the front (Griffith's criterion [1921]), and a condition of zero SIF of mode II (Goldstein and Salganik's *principle of local symmetry* [1974]). This was the motivation for Leblond et al.'s theoretical analysis [2011], within the framework of LEFM, of the possible bifurcation from coplanar to noncoplanar propagation of cracks loaded in mode I+III. This analysis combined assumptions of constant value of the local energy release rate and zero value of the local mode II SIF all along the crack front, in line with the findings of Hakim and Karma [2009] and Pons and Karma [2010], with technical results of Gao and Rice [1986] and Movchan et al. [1998] on in-plane and out-of-plane perturbations of a plane crack. A bifurcation from coplanar to noncoplanar propagation was concluded to exist for values of the ratio of the mode III to mode I SIF larger than some threshold depending on Poisson's ratio.

However, the threshold was found to be of the order of 0.5 for standard values of Poisson's ratio. The bifurcation analysis could therefore *not* explain the fact that deviations of the crack from its original plane are currently observed for much smaller values of the ratio of the mode III to mode I SIF — a threshold of the order of 0.05 was mentioned in [Sommer 1969], and Pham and Ravi-Chandar [2014] have even claimed that there is no threshold at all.

The aim of this paper is to propose a possible explanation for this observation. The idea is that even for low values of the ratio of the mode III to mode I SIF, for which no bifurcation is predicted, deviations from coplanarity might occur because of a strong influence of imperfections upon the propagation path — quite in the same way as the influence of imperfections explains, for thin shells, the quick deviations from the fundamental deformed state currently observed for loads much lower than the theoretical buckling load. A typical example of inevitable imperfections consists of random fluctuations of the fracture toughness within the crack plane. Such fluctuations are bound to generate in-plane undulations of the crack front. It is intuitively obvious, and has been proved rigorously by Gao and Rice [1986], that the mode III load must generate nonzero and opposite local mode II SIF on the two sides of a local coplanar protrusion of the front; this implies that the crack will tend to extend out of its original plane in opposite directions on these two sides, thus giving birth to an incipient noncoplanar facet. If, in addition, Cotterell and Rice's well-known "directional stability criterion" [1980] happens to be violated because of a locally positive nonsingular stress in the direction of crack propagation, the deviation of this facet from the original crack plane may quickly increase as the crack propagates, even in the absence of a true bifurcation.
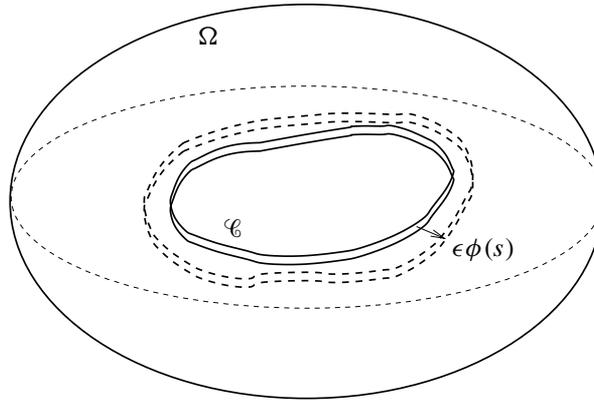
Figure 1. Slight in-plane perturbation of a plane crack in an arbitrary body.

Investigation of this idea, in the typical case of a semi-infinite crack in some infinite body, requires that the local SIF and nonsingular stresses be known for such a crack, endowed with a slightly, coplanarly perturbed front. The calculation of the SIF was carried out in [Rice 1985] and [Gao and Rice 1986], with definitive results. That of the nonsingular stresses was carried out in [Gao 1992], but with restrictive hypotheses and incomplete results, making the completion of the task an indispensable prerequisite.

The paper is organized as follows:

- Section 2 briefly recalls some elements of the theory of 3D weight functions [Rice 1985; Bueckner 1987], which serve as a basis in the analysis to follow.

- From there, Section 3 presents the calculation of the first-order variation of the stresses on the crack plane resulting from some small but otherwise arbitrary in-plane perturbation of the crack front.

- We then derive from there, in Section 4, the first-order variations of the nonsingular stresses under similar conditions.

- Section 5 briefly recalls Leblond's 3D extension [1999] of Cotterell and Rice's original 2D directional stability analysis of a propagating crack [1980], indispensable for the application of the preceding results to crack propagation in mode I+III.

- Finally, Section 6 considers the case of a sinusoidal in-plane perturbation of the crack front, and examines whether Cotterell and Rice's directional stability criterion [1980] (as extended to the 3D case) is met or not, distinguishing between those parts of the undulated front about to give birth to type A and type B facets.

2. Elements of Rice and Bueckner's 3D weight function theory

Consider an arbitrary body Ω made of some linear elastic isotropic material, and containing an arbitrary planar crack (Figure 1). Assume that prescribed displacements are imposed on the portion $\partial\Omega_u$ of the boundary of this body, while prescribed tractions are imposed on the complementary portion $\partial\Omega_T$. This loading generates a distribution of SIF $K_I^0(s)$, $K_{II}^0(s)$, $K_{III}^0(s)$, where s denotes a curvilinear abscissa along the crack front $\mathscr{C}$, on this front.

Now slightly perturb $\mathscr{C}$ within the crack plane, while keeping the loading applied on $\partial\Omega_u$ and $\partial\Omega_T$ unchanged. Let $\epsilon\phi(s)$, where ϵ is a small parameter and $\phi(s)$ a given, fixed function, denote the distance from the original front to the perturbed one, as measured perpendicularly to the former front. The components $\delta u_i(\boldsymbol{r})$, in an arbitrary orthonormal basis $(\boldsymbol{e}_1, \boldsymbol{e}_2, \boldsymbol{e}_3)$, of the resulting variation of displacement $\delta\boldsymbol{u}$ at the point $\boldsymbol{r}$ of the body, are given to first order by Rice's formula [1985]:

$$\delta u_i(\boldsymbol{r}) = \int_{\mathscr{C}} 2\Lambda_{\alpha\beta} h_{i\alpha}(\boldsymbol{r}, s) K_\beta^0(s) \epsilon\phi(s)\, ds. \tag{1}$$

In this expression:

- the indices α and β take the values I, II and III, and Einstein's implicit summation convention is used for them;

- the coefficients $\Lambda_{\alpha\beta}$ are those appearing in the quadratic form of the SIF defining the energy release rate, given by[1]

$$\Lambda_{\text{I,I}} = \Lambda_{\text{II,II}} = \frac{1-\nu^2}{E}, \quad \Lambda_{\text{III,III}} = \frac{1+\nu}{E}, \quad \text{other } \Lambda_{\alpha\beta} = 0, \tag{2}$$

  where E and ν denote Young's modulus and Poisson's ratio;

- finally, the $h_{i\alpha}(\boldsymbol{r}, s)$ are the *3D weight functions* of the cracked geometry considered [Rice 1985; Bueckner 1987]; $h_{i\alpha}(\boldsymbol{r}, s)$ represents the α-th SIF generated at the point s of the crack front by a unit point force applied in the direction $\boldsymbol{e}_i$ at the point $\boldsymbol{r}$ of the body, zero displacements being simultaneously prescribed on $\partial\Omega_u$ and zero tractions on $\partial\Omega_T$.

Now, f being an arbitrary function of position and $\boldsymbol{r}$ an arbitrary point on the crack plane lying inside the crack contour, let

$$\langle f \rangle(\boldsymbol{r}) \equiv \tfrac{1}{2}[f(\boldsymbol{r}^+) + f(\boldsymbol{r}^-)] \tag{3}$$

denote the average of the values of this function at the points $\boldsymbol{r}^+$, $\boldsymbol{r}^-$ of the upper $(+)$ and lower $(-)$ faces of the crack. With this notation, application of (1) on the crack faces yields

$$\langle \delta u_i \rangle(\boldsymbol{r}) = \int_{\mathscr{C}} 2\Lambda_{\alpha\beta} \langle h_{i\alpha} \rangle(\boldsymbol{r}, s) K_\beta^0(s) \epsilon\phi(s)\, ds, \tag{4}$$

where $\langle h_{i\alpha}\rangle(\boldsymbol{r}, s)$, a *crack-face weight function* (CFWF), now represents the α-th SIF generated at the point s of the crack front by two half-unit point forces applied in the direction $\boldsymbol{e}_i$ at the points $\boldsymbol{r}^+$, $\boldsymbol{r}^-$ of the crack faces, zero displacements being simultaneously prescribed on $\partial\Omega_u$ and zero tractions on $\partial\Omega_T$.

3. First-order variation of the stresses on the crack faces

3.1. *Generalities.* Consider now, more specifically, a semi-infinite crack located in some infinite body subjected to prescribed forces only (Figure 2). Following the usual convention, define a Cartesian frame (O, x, y, z) with O on the unperturbed crack front, x in the direction of propagation, y in the direction of the normal to the crack plane, and z in the direction of the crack front. Also, characterize the position of the unperturbed front Oz through its distance a to some fixed "reference line" parallel to it in the crack plane.

---

[1]For the sake of clarity, commas separating the indices are exceptionally introduced into this equation.
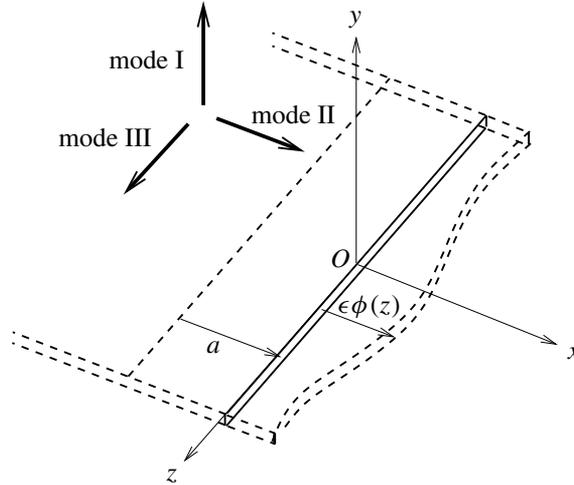
Figure 2. Slight in-plane perturbation of a semi-infinite crack loaded arbitrarily.

Equation (4) then takes the special form, with obvious notations,

$$\langle \delta u_i \rangle(x, z) = \int_{-\infty}^{+\infty} 2\Lambda_{\alpha\beta} \langle h_{i\alpha} \rangle(x, z; z') K_\beta^0(z') \epsilon \phi(z') \, dz'. \tag{5}$$

The aim of this section is to derive from there the expressions of the average variations $\langle \delta\sigma_{xx} \rangle$, $\langle \delta\sigma_{zz} \rangle$ and $\langle \delta\sigma_{xz} \rangle$ of the in-plane stresses on the crack faces. When (5) is used for this sole purpose, some simplifications arise:

- It is enough to know the in-plane components $\langle \delta u_x \rangle$, $\langle \delta u_z \rangle$ of the average variation of displacement $\langle \delta \boldsymbol{u} \rangle$; the out-of-plane component $\langle \delta u_y \rangle$ is not needed.

- The expressions of these in-plane components involve the CFWFs $\langle h_{x\alpha} \rangle$ and $\langle h_{z\alpha} \rangle$, which are nonzero only for $\alpha = \mathrm{I}$, since the loadings implied, consisting of half-unit point forces applied on the crack faces in the directions x and z, are symmetric with respect to the crack plane and therefore do not generate any mode II or III.

The formulae required therefore simply read, by (2),

$$\begin{cases} \langle \delta u_x \rangle(x, z) = 2 \dfrac{1-\nu^2}{E} \displaystyle\int_{-\infty}^{+\infty} \langle h_{xI} \rangle(x, z; z') K_\mathrm{I}^0(z') \epsilon \phi(z') \, dz', \\[2ex] \langle \delta u_z \rangle(x, z) = 2 \dfrac{1-\nu^2}{E} \displaystyle\int_{-\infty}^{+\infty} \langle h_{zI} \rangle(x, z; z') K_\mathrm{I}^0(z') \epsilon \phi(z') \, dz'. \end{cases} \tag{6}$$

3.2. *Variations of the displacement components and their spatial derivatives.* The CFWFs $\langle h_{xI} \rangle$, $\langle h_{zI} \rangle$ for a semi-infinite crack have been calculated in [Bueckner 1987; Kuo 1993; Movchan et al. 1998]. The simplest way of expressing the results is as follows [Kuo 1993]: assume that point forces of intensities F_x and F_z are simultaneously applied in the directions x and z on the points $(x, y = 0^+, z)$ and $(x, y = 0^-, z)$ of the upper and lower crack faces; these forces together generate a mode I SIF k_I at the point z' of the crack front given by

$$k_I(z') \equiv 2F_x \langle h_{xI} \rangle(x, z; z') + 2F_z \langle h_{zI} \rangle(x, z; z') = \frac{1}{4\sqrt{\pi}} \frac{1-2\nu}{1-\nu} \operatorname{Re}\left\{ \frac{F_x + i F_z}{[-x + i(z' - z)]^{3/2}} \right\}, \qquad (7)$$

where the cut of the complex power function is along the half-line of nonpositive reals. Since this compact formula "couples" the CFWFs $\langle h_{xI} \rangle$ and $\langle h_{zI} \rangle$, it seems appropriate, when inserting it into the expressions (6) of $\langle \delta u_x \rangle$ and $\langle \delta u_z \rangle$, to introduce arbitrary real parameters α, β and consider the single quantity $\langle \alpha \delta u_x + \beta \delta u_z \rangle$ rather than $\langle \delta u_x \rangle$ and $\langle \delta u_z \rangle$ individually. One thus gets

$$\langle \alpha \delta u_x + \beta \delta u_z \rangle(x, z) = 2 \frac{1-\nu^2}{E} \int_{-\infty}^{+\infty} \langle \alpha h_{xI} + \beta h_{zI} \rangle(x, z; z') K_I^0(z') \epsilon \phi(z') \, dz'$$

$$= \frac{(1+\nu)(1-2\nu)}{4\sqrt{\pi} E} \operatorname{Re}\left\{ \int_{-\infty}^{+\infty} \frac{\alpha + i\beta}{[-x + i(z' - z)]^{3/2}} K_I^0(z') \epsilon \phi(z') \, dz' \right\},$$

or, equivalently, after integration by parts,

$$\langle \alpha \delta u_x + \beta \delta u_z \rangle(x, z) = \frac{(1+\nu)(1-2\nu)}{2\sqrt{\pi} E} \operatorname{Re}\left\{ \int_{-\infty}^{+\infty} \frac{\beta - i\alpha}{[-x + i(z' - z)]^{1/2}} (K_I^0 \epsilon \phi)'(z') \, dz' \right\}. \qquad (8)$$

Differentiating this equation with respect to x and z, and then ascribing the values $(1, 0)$ and $(0, 1)$ to the pair (α, β), one gets the average spatial derivatives of the components of the variation of displacement:

$$\begin{cases} \left\langle \dfrac{\partial \delta u_x}{\partial x} \right\rangle(x, z) = -\left\langle \dfrac{\partial \delta u_z}{\partial z} \right\rangle(x, z) = \dfrac{(1+\nu)(1-2\nu)}{4\sqrt{\pi} E} \operatorname{Im}\left\{ \displaystyle\int_{-\infty}^{+\infty} \dfrac{(K_I^0 \epsilon \phi)'(z')}{[-x + i(z' - z)]^{3/2}} \, dz' \right\}, \\[4mm] \left\langle \dfrac{\partial \delta u_x}{\partial z} \right\rangle(x, z) = \left\langle \dfrac{\partial \delta u_z}{\partial x} \right\rangle(x, z) \quad = \dfrac{(1+\nu)(1-2\nu)}{4\sqrt{\pi} E} \operatorname{Re}\left\{ \displaystyle\int_{-\infty}^{+\infty} \dfrac{(K_I^0 \epsilon \phi)'(z')}{[-x + i(z' - z)]^{3/2}} \, dz' \right\}. \end{cases} \qquad (9)$$

3.3. *Variations of the stress components.* The stress components σ_{yx}, σ_{yy} and σ_{yz} being zero on the crack faces, the average variations $\langle \delta \sigma_{xx} \rangle$, $\langle \delta \sigma_{zz} \rangle$, $\langle \delta \sigma_{xz} \rangle$ of the in-plane stresses on these faces may be obtained from the expressions (9) through application of the plane stress elastic stiffness tensor:

$$\begin{cases} \langle \delta \sigma_{xx} \rangle(x, z) = -\langle \delta \sigma_{zz} \rangle(x, z) = \dfrac{1-2\nu}{4\sqrt{\pi}} \operatorname{Im}\left\{ \displaystyle\int_{-\infty}^{+\infty} \dfrac{(K_I^0 \epsilon \phi)'(z')}{[-x + i(z' - z)]^{3/2}} \, dz' \right\}, \\[4mm] \langle \delta \sigma_{xz} \rangle(x, z) \qquad\qquad = \dfrac{1-2\nu}{4\sqrt{\pi}} \operatorname{Re}\left\{ \displaystyle\int_{-\infty}^{+\infty} \dfrac{(K_I^0 \epsilon \phi)'(z')}{[-x + i(z' - z)]^{3/2}} \, dz' \right\}. \end{cases} \qquad (10)$$

Equation $(10)_1$ implies in particular that the average variation $\langle \delta \sigma_{xx} + \delta \sigma_{zz} \rangle$ is zero whatever the perturbation of the crack front; this means that *at a given point of the broken region of the crack plane, the average 2D trace of the stress tensor, $\langle \sigma_{xx} + \sigma_{zz} \rangle$, is independent of the position and shape of the crack front*. This remarkable property is noted here in the special case of a semi-infinite crack, but was shown by Gao [1992] to in fact hold for *any* planar crack of arbitrary contour in some infinite body.

The variations of the nonsingular stresses will be deduced from the asymptotic behavior of $\langle \delta \sigma_{xx} \rangle$, $\langle \delta \sigma_{zz} \rangle$, $\langle \delta \sigma_{xz} \rangle$ near the crack front, that is in the limit $x \to 0^-$. This makes it necessary to evaluate the limit

$$\lim_{x \to 0^-} \int_{-\infty}^{+\infty} \frac{(K_I^0 \epsilon \phi)'(z')}{[-x + i(z' - z)]^{3/2}} \, dz'.$$

In order to do so, rewrite the integral as

$$\int_{-\infty}^{+\infty} \frac{(K_I^0 \epsilon \phi)'(z')}{[-x + i(z' - z)]^{3/2}} \, dz'$$

$$= \int_{-\infty}^{+\infty} \frac{(K_I^0 \epsilon \phi)'(z') - (K_I^0 \epsilon \phi)'(z)}{[-x + i(z' - z)]^{3/2}} \, dz' + (K_I^0 \epsilon \phi)'(z) \int_{-\infty}^{+\infty} \frac{dz'}{[-x + i(z' - z)]^{3/2}}.$$

The second integral in the right-hand side is obviously zero, and the first one goes to the limit

$$\int_{-\infty}^{+\infty} \frac{(K_I^0 \epsilon \phi)'(z') - (K_I^0 \epsilon \phi)'(z)}{[i(z' - z)]^{3/2}} \, dz'$$

as $x \to 0^-$. (Note that this integral is convergent at the point $z' = z$ since the integrand behaves like $|z' - z|^{-1/2}$ near it.) Evaluating $[i(z' - z)]^{3/2}$ using the definition of the complex power function and distinguishing between the cases $z' < z$ and $z' > z$, one concludes that

$$\lim_{x \to 0^-} \int_{-\infty}^{+\infty} \frac{(K_I^0 \epsilon \phi)'(z')}{[-x + i(z' - z)]^{3/2}} \, dz' = -\frac{1}{\sqrt{2}} \int_{-\infty}^{+\infty} \frac{(K_I^0 \epsilon \phi)'(z') - (K_I^0 \epsilon \phi)'(z)}{|z' - z|^{3/2}} \, dz'$$

$$-\frac{i}{\sqrt{2}} \int_{-\infty}^{+\infty} \operatorname{sgn}(z' - z) \frac{(K_I^0 \epsilon \phi)'(z') - (K_I^0 \epsilon \phi)'(z)}{|z' - z|^{3/2}} \, dz', \quad (11)$$

where $\operatorname{sgn}(x)$ denotes the sign of x.

Inserting (11) into the expressions (10) of $\langle \delta\sigma_{xx} \rangle$, $\langle \delta\sigma_{zz} \rangle$, $\langle \delta\sigma_{xz} \rangle$, one finally gets the desired limits:

$$\begin{cases} \langle \delta\sigma_{xx} \rangle(0^-, z) = -\langle \delta\sigma_{zz} \rangle(0^-, z) \\ \qquad = -\frac{1-2\nu}{4\sqrt{2\pi}} \int_{-\infty}^{+\infty} \operatorname{sgn}(z' - z) \frac{(K_I^0 \epsilon \phi)'(z') - (K_I^0 \epsilon \phi)'(z)}{|z' - z|^{3/2}} \, dz', \\ \langle \delta\sigma_{xz} \rangle(0^-, z) = -\frac{1-2\nu}{4\sqrt{2\pi}} \int_{-\infty}^{+\infty} \frac{(K_I^0 \epsilon \phi)'(z') - (K_I^0 \epsilon \phi)'(z)}{|z' - z|^{3/2}} \, dz'. \end{cases} \quad (12)$$

4. First-order variations of the nonsingular stresses

4.1. *Special case of an immobile point of the crack front.* In a first step, we wish to derive the variations of the nonsingular stresses for an *immobile* point of the crack front, having $\phi(z) = 0$. In such a case the point of observation of the in-plane stresses to be used to define the nonsingular stresses, located just behind the crack front, does not move when this front is perturbed; hence the local variations of the nonsingular stresses are simply related to the local average variations of the in-plane stresses.

More specifically, define a Cartesian frame $(P, x_1, x_2 \equiv y, x_3)$ "adapted" to the perturbed crack front at the immobile point P considered (Figure 3). To first order in the perturbation, the unit vectors e_1, e_2, e_3 corresponding to the coordinates x_1, x_2, x_3 are related to the vectors e_x, e_y, e_z corresponding to the coordinates x, y, z adapted to the unperturbed front through the relations

$$e_1 = e_x - \epsilon\phi'(z)e_z, \quad e_2 = e_y, \quad e_3 = e_z + \epsilon\phi'(z)e_x. \quad (13)$$

In the local frame, the average in-plane stress components $\langle \sigma_{11} \rangle$, $\langle \sigma_{33} \rangle$, $\langle \sigma_{13} \rangle$

- are zero for the first, singular term of the Williams expansion of the stresses;
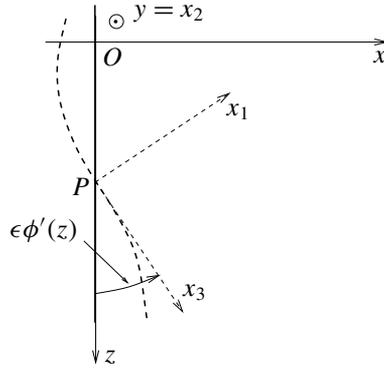
Figure 3. Definition of local axes for the perturbed front.

- are equal to the nonsingular stresses T_{11}, T_{33}, T_{13} for the second term;
- vanish close to the crack front for the next terms.

Hence T_{11}, T_{33}, T_{13} may be identified to the limits of $\langle \sigma_{11} \rangle$, $\langle \sigma_{33} \rangle$, $\langle \sigma_{13} \rangle$ when the point of observation of these quantities gets infinitely close to the crack front. Therefore, unperturbed values and variations of quantities being denoted with symbols ^{0} and δ respectively, the average perturbed stress tensor $\langle \boldsymbol{\sigma}^0 + \delta \boldsymbol{\sigma} \rangle$ on the crack faces close to the front may be expressed as

$$
\begin{aligned}
\langle \boldsymbol{\sigma}^0 + \delta \boldsymbol{\sigma} \rangle (0^-, z) &= [T_{11}^0(z) + \delta T_{11}(z)] \boldsymbol{e}_1 \otimes \boldsymbol{e}_1 + [T_{33}^0(z) + \delta T_{33}(z)] \boldsymbol{e}_3 \otimes \boldsymbol{e}_3 \\
&\quad + [T_{13}^0(z) + \delta T_{13}(z)](\boldsymbol{e}_1 \otimes \boldsymbol{e}_3 + \boldsymbol{e}_3 \otimes \boldsymbol{e}_1) \\
&= [T_{11}^0(z) + \delta T_{11}(z)] \boldsymbol{e}_x \otimes \boldsymbol{e}_x + [T_{33}^0(z) + \delta T_{33}(z)] \boldsymbol{e}_z \otimes \boldsymbol{e}_z \\
&\quad + [T_{13}^0(z) + \delta T_{13}(z)](\boldsymbol{e}_x \otimes \boldsymbol{e}_z + \boldsymbol{e}_z \otimes \boldsymbol{e}_x) \\
&\quad + 2T_{13}^0(z) \epsilon \phi'(z) \boldsymbol{e}_x \otimes \boldsymbol{e}_x - 2T_{13}^0(z) \epsilon \phi'(z) \boldsymbol{e}_z \otimes \boldsymbol{e}_z \\
&\quad + [T_{33}^0(z) - T_{11}^0(z)] \epsilon \phi'(z)(\boldsymbol{e}_x \otimes \boldsymbol{e}_z + \boldsymbol{e}_z \otimes \boldsymbol{e}_x),
\end{aligned}
$$

where (13) has been used.

But, on the other hand, this average perturbed stress tensor may also be expressed as

$$
\langle \boldsymbol{\sigma}^0 + \delta \boldsymbol{\sigma} \rangle (0^-, z) =
$$
$$
\langle \sigma_{xx}^0 + \delta \sigma_{xx} \rangle (0^-, z) \boldsymbol{e}_x \otimes \boldsymbol{e}_x + \langle \sigma_{zz}^0 + \delta \sigma_{zz} \rangle (0^-, z) \boldsymbol{e}_z \otimes \boldsymbol{e}_z + \langle \sigma_{xz}^0 + \delta \sigma_{xz} \rangle (0^-, z)(\boldsymbol{e}_x \otimes \boldsymbol{e}_z + \boldsymbol{e}_z \otimes \boldsymbol{e}_x).
$$

Comparison of these two formulae and identification of the first-order terms yields the following expressions for the variations of the nonsingular stresses:

$$
\begin{cases}
\delta T_{11}(z) = -2T_{13}^0(z) \epsilon \phi'(z) + \langle \delta \sigma_{xx} \rangle (0^-, z), \\
\delta T_{33}(z) = 2T_{13}^0(z) \epsilon \phi'(z) + \langle \delta \sigma_{zz} \rangle (0^-, z), \\
\delta T_{13}(z) = [T_{11}^0(z) - T_{33}^0(z)] \epsilon \phi'(z) + \langle \delta \sigma_{xz} \rangle (0^-, z),
\end{cases}
\tag{14}
$$

where the average variations of the stresses are given by the equations (12).

4.2. *General case.* In order to now evaluate the variations of the nonsingular stresses in the general case where $\phi(z) \neq 0$, we use the same trick as in [Rice 1985; Gao and Rice 1986] on the variations of the SIF: we decompose the perturbation $\epsilon\phi$ in the form

$$\epsilon\phi(z') = \epsilon\phi(z) + \epsilon\bar{\phi}(z'), \quad \text{where } \bar{\phi}(z') \equiv \phi(z') - \phi(z). \tag{15}$$

- The first term of the decomposition represents a translation of the unperturbed crack front by the distance $\epsilon\phi(z)$, which generates a variation of the nonsingular stress T_{ij} equal to $(\partial T_{ij}^0/\partial a)(z)\epsilon\phi(z)$, where $(\partial T_{ij}^0/\partial a)(z)$ is the derivative of the unperturbed nonsingular stress T_{ij}^0 with respect to the position a of the straight crack front; see Figure 2.[2]

- The second term represents a motion in which the point z remains immobile. Therefore, the equations (14) may be used, with $\bar{\phi}(z')$ instead of $\phi(z')$, to evaluate the resulting variations of the nonsingular stresses.

Adding the contributions of the two terms, and using the equations (12) for the average variations of the stresses and the definition (15)$_2$ of the function $\bar{\phi}$, one finally gets the following formulae for the variations of the nonsingular stresses in the general case:

$$\delta T_{11}(z) = \frac{\partial T_{11}^0}{\partial a}(z)\epsilon\phi(z) - 2T_{13}^0(z)\epsilon\phi'(z) - \frac{1-2\nu}{4\sqrt{2\pi}} \int_{-\infty}^{+\infty} \left\{ (K_I^0\epsilon\phi')(z') - (K_I^0\epsilon\phi')(z) \right.$$
$$\left. + (K_I^0)'(z')[\epsilon\phi(z') - \epsilon\phi(z)] \right\} \frac{\text{sgn}(z'-z)}{|z'-z|^{3/2}} \, dz'; \tag{16}$$

$$\delta T_{33}(z) = \frac{\partial T_{33}^0}{\partial a}(z)\epsilon\phi(z) + 2T_{13}^0(z)\epsilon\phi'(z) + \frac{1-2\nu}{4\sqrt{2\pi}} \int_{-\infty}^{+\infty} \left\{ (K_I^0\epsilon\phi')(z') - (K_I^0\epsilon\phi')(z) \right.$$
$$\left. + (K_I^0)'(z')[\epsilon\phi(z') - \epsilon\phi(z)] \right\} \frac{\text{sgn}(z'-z)}{|z'-z|^{3/2}} \, dz'; \tag{17}$$

$$\delta T_{13}(z) = \frac{\partial T_{13}^0}{\partial a}(z)\epsilon\phi(z) + [T_{11}^0(z) - T_{33}^0(z)]\epsilon\phi'(z) - \frac{1-2\nu}{4\sqrt{2\pi}} \int_{-\infty}^{+\infty} \left\{ (K_I^0\epsilon\phi')(z') - (K_I^0\epsilon\phi')(z) \right.$$
$$\left. + (K_I^0)'(z')[\epsilon\phi(z') - \epsilon\phi(z)] \right\} \frac{dz'}{|z'-z|^{3/2}}. \tag{18}$$

It is worth noting that, *unlike the average variation* $\langle \delta\sigma_{xx} + \delta\sigma_{zz} \rangle$, *the variation* $\delta T_{11} + \delta T_{33}$ *is nonzero in general*. The effect arises solely from the terms $(\partial T_{11}^0/\partial a)(z)\epsilon\phi(z)$ and $(\partial T_{33}^0/\partial a)(z)\epsilon\phi(z)$ in the right-hand sides of (16) and (17), the sum of which has no reason to be zero. In physical terms, even though $\langle \sigma_{xx} + \sigma_{zz} \rangle$, *at a given, fixed point* of the broken region of the crack plane, is independent of the position and shape of the crack front, evaluating the variation of $T_{11} + T_{33}$ implies *following the point of observation* of $\langle \sigma_{xx} + \sigma_{zz} \rangle$ as the front moves, which inevitably entails a variation of this quantity.

4.3. *Comparison with the work of Gao.* Gao [1992] did not consider only the case of an initially straight crack front as in the present work, but also that of a circular one. However, he introduced a number of restrictive hypotheses not made here:

---

[2]The additional dependence of this quantity and other ones upon the argument a is omitted to alleviate the notation.

- A pure mode I loading was assumed. However, our general expressions (16), (17) and (18) for δT_{11}, δT_{33} and δT_{13}, respectively, show that considering more general mixed-mode loadings would not in fact have changed anything, since the unperturbed SIFs K_{II}^0, K_{III}^0 of modes II and III do not appear in them.

- The unperturbed SIF K_{I}^0 of mode I was assumed to be independent of the position z along the crack front. The possible variation of K_{I}^0 along this front does modify the expressions (16)–(18) through the term $(K_{\text{I}}^0)'(z')[\epsilon\phi(z') - \epsilon\phi(z)]$ appearing in the integrand in each of them.

- The perturbation of the crack front was assumed to be sinusoidal. This was in fact equivalent to providing the expressions for δT_{11}, δT_{33}, δT_{13} in Fourier space. However, our expressions (16), (17), (18) in the physical space are interesting in themselves, and getting them from those of [Gao 1992] through inverse Fourier transform is not a completely straightforward operation.

With these hypotheses, Gao obtained expressions for δT_{11}, δT_{33}, δT_{13} coinciding exactly with the integral terms in the right-hand sides of our equations (16), (17), (18), as evaluated for a sinusoidal perturbation. However all additional terms proportional to the $\partial T_{ij}^0/\partial a$ and T_{ij}^0 were absent. These terms were apparently really missing in the sense that the hypotheses made did not seem to permit discarding them.

5. Cotterell and Rice's directional stability criterion for 3D cracks

In this section, we briefly recall, as a prerequisite for Section 6, Leblond's 3D extension [1999] of Cotterell and Rice's classical 2D analysis of directional stability of a propagating crack [1980].

We therefore consider, within an arbitrary 3D body, an initially planar crack of arbitrary contour, and denote by s some curvilinear abscissa along this contour. This crack is loaded through some system of prescribed forces and/or displacements generating distributions of SIF $K_{\text{I}}(s)$, $K_{\text{II}}(s)$, $K_{\text{III}}(s)$ and non-singular stresses $T_{11}(s)$, $T_{33}(s)$, $T_{13}(s)$ along its front. These distributions are arbitrary except that the mode II SIF $K_{\text{II}}(s)$ is assumed to be everywhere small.

Because of the presence of mode II, the crack propagates in a slightly noncoplanar way. More specifically, at each point $P(s)$ of the original crack front, propagation of the crack results in the creation of some small, slightly kinked and curved extension; the length of this extension is $\eta\psi(s)$ where η is a small parameter and ψ a given function, and its equation reads, in the local "adapted" frame $(P(s), x_1, x_2, x_3)$ defined as in Figure 3,

$$x_2 = \theta(s)x_1 + a(s)x_1^{3/2} + O(x_1^2), \tag{19}$$

where $\theta(s)$ ($\ll 1$) is the local "kink angle" and $a(s)$ a local "curvature parameter" (Figure 4, where $K_{\text{II}}(s)$ is assumed to be negative in order for $\theta(s)$ to be positive; see (21) below). The peculiar shape of the curve defined by (19), resulting from the term proportional to $x_1^{3/2}$ instead of simply x_1^2, will be seen to be necessary for the propagation criterion to be satisfied.

Leblond [1999] and Leblond et al. [1999] have derived, under such conditions, the expansions of the SIFs $K_{\text{I}}(s; \eta)$, $K_{\text{II}}(s; \eta)$, $K_{\text{III}}(s; \eta)$ along the extended front in powers of η. At order $\eta^{1/2}$, these "extended SIFs" depend upon the geometrical and mechanical parameters only through their *local* values at that point where they are evaluated,[3] and are given by formulae very similar to those of [Cotterell

---

[3]This does not remain true at order $\eta^1 = \eta$: the expressions of the extended SIF at a given point depend at that order upon the whole distribution of geometrical and mechanical parameters on the crack front; see [Leblond et al. 1999].
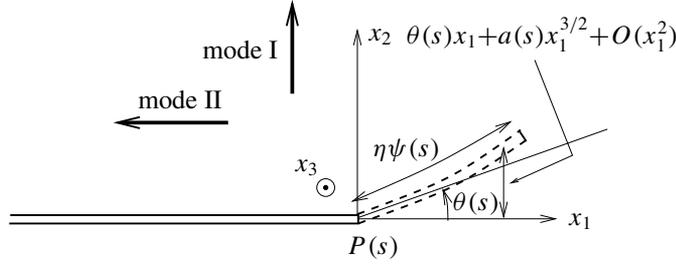
Figure 4. Geometric hypotheses and notations for Cotterell and Rice's directional stability analysis of a propagating crack.

and Rice 1980] for the 2D case, except for the extra dependence of all quantities on s. In particular, the expansion of $K_{II}(s; \eta)$ reads

$$K_{II}(s; \eta) = K_{II}(s) + \tfrac{1}{2}\theta(s)K_I(s) + \left[-2\sqrt{2/\pi}\,\theta(s)T_{11}(s) + \tfrac{3}{4}a(s)K_I(s)\right]\sqrt{\eta\psi(s)} + O(\eta). \quad (20)$$

(Note that $\lim_{\eta\to 0^+} K_{II}(s; \eta)$ differs from $K_{II}(s)$ because of the kink.) This equation may be used to predict the values of the local kink angle $\theta(s)$ and curvature parameter $a(s)$, assuming the shape of the propagating crack to be governed by Goldstein and Salganik's principle of local symmetry [1974], which demands that $K_{II}(s; \eta)$ be constantly zero after the initial kink. This condition yields:

- at order $\eta^0 = 1$,

$$\theta(s) = -2\frac{K_{II}(s)}{K_I(s)}; \quad (21)$$

- at order $\eta^{1/2}$,

$$a(s) = \tfrac{8}{3}\sqrt{2/\pi}\,\frac{T_{11}(s)}{K_I(s)}\theta(s). \quad (22)$$

Equation (22) permits us to discuss the local directional stability of crack propagation. Cotterell and Rice [1980] indeed consider that directional stability prevails if the effect of the curvature parameter $a(s)$ tends to counterbalance that of the kink angle $\theta(s)$ and bring the crack back to its original plane, that is, if these quantities are of opposite signs.[4] This leads to the following criterion (since necessarily $K_I(s) > 0$):

$$\text{directional stability} \iff T_{11}(s) < 0. \quad (23)$$

6. Application to deviation of a mode I+III crack from coplanarity

6.1. *Position of the problem.* We now consider a semi-infinite crack loaded in mode I+III in an infinite body (Figure 5). The unperturbed SIFs K_I^0, K_{III}^0 on the straight configuration of the crack front are assumed to be uniform along this front. Inevitable fluctuations of the fracture toughness within the crack plane are assumed to generate small in-plane undulations of the front depicted by the typically sinusoidal perturbation

$$\epsilon\phi(z) \equiv \epsilon\cos(kz) \quad (k > 0). \quad (24)$$

---

[4]Though reasonable, this condition does not result from some fundamental stability theory, but simply from some *ad hoc* postulate; this is why such prudent expressions as "directional stability in the sense of Cotterell and Rice" and "Cotterell and Rice's directional stability criterion" are used in this paper.
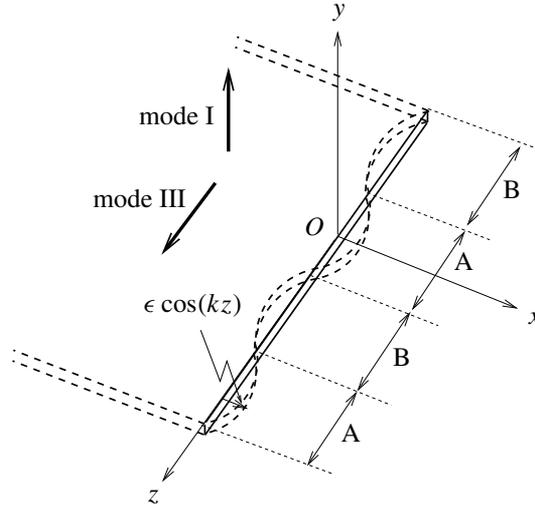
Figure 5. In-plane sinusoidal perturbation of a semi-infinite crack loaded in mode I+III.

In Figure 5, the zones of the perturbed crack front having $\cos(kz) > 0$ and < 0 are indicated with the symbols A and B, respectively, meaning that they are anticipated to generate future noncoplanar facets of these types. Indeed, the former, more advanced zones will generate facets lying ahead of the mean position of the front, which is a typical property of type A ones (see the introduction); conversely, the latter, less advanced zones will generate facets lying behind the same position, which is typical of type B ones.

Making use of the results of the preceding sections, we wish to study the deviation from coplanarity and directional stability of the incipient facets on the two types of zones. This first requires us to determine the distributions of the second SIF K_{II} and first nonsingular stress T_{11} along the coplanarly perturbed crack front.

6.2. *Expression of the perturbed mode II stress intensity factor.* Gao and Rice [1986] have calculated, for the semi-infinite crack considered, the variations of the SIF resulting from some arbitrary coplanar perturbation of the front; their result for the mode II SIF reads

$$\delta K_{\text{II}}(z) = \frac{\partial K_{\text{II}}^0}{\partial a}(z)\epsilon\phi(z) - \frac{2}{2-\nu} K_{\text{III}}^0(z)\epsilon\phi'(z) + \frac{1}{2\pi}\frac{2-3\nu}{2-\nu} \text{PV} \int_{-\infty}^{+\infty} K_{\text{II}}^0(z')\frac{\epsilon\phi(z') - \epsilon\phi(z)}{(z'-z)^2} \, dz', \quad (25)$$

where $(\partial K_{\text{II}}^0/\partial a)(z)$ is the derivative of the unperturbed mode II SIF K_{II}^0 with respect to the position a of the straight crack front (see Figure 2) and the symbol PV $\int$ denotes the Cauchy principal value of an integral. In the special case considered here, where K_{II}^0 and K_{III}^0 are, respectively, zero and uniform along the unperturbed front and the perturbation $\epsilon\phi$ is of the form (24), this yields

$$K_{\text{II}}(z) = \delta K_{\text{II}}(z) = \frac{2}{2-\nu} K_{\text{III}}^0 k\epsilon \sin(kz) \tag{26}$$

for the mode II SIF K_{II} along the perturbed front.

6.3. *Expression of the perturbed first nonsingular stress.* In order to now evaluate the nonsingular stress T_{11} along the coplanarly perturbed crack front, we introduce the following hypotheses:

- The unperturbed SIFs K_I^0 and K_{III}^0 are comparable in magnitude. Also, the unperturbed nonsingular stresses T_{ij}^0 and their derivatives $\partial T_{ij}^0/\partial a$ with respect to the position of the straight crack front are of the order of $K_I^0 L^{-1/2}$ and $K_I^0 L^{-3/2}$, respectively, where L is the characteristic length defined by the loading (in the absence of any characteristic length scale defined by the geometry itself).

- The characteristic length L is much larger than the typical distance of fluctuation of the fracture toughness, and therefore than the wavelength $\lambda \equiv 2\pi/k$ of the perturbation resulting from the nonuniformity of this toughness.

The perturbation $\epsilon\phi$ and its derivative $\epsilon\phi'$ being of the order of ϵ and $k\epsilon$, respectively, it follows from the first hypothesis that the first, second and third terms in the right-hand side of the expression (16) of δT_{11} are of the order of $K_I^0 L^{-3/2}\epsilon$, $K_I^0 L^{-1/2}k\epsilon$ and $K_I^0 k^{3/2}\epsilon$, respectively. Since the second hypothesis implies that $kL \gg 1$, the first and second terms are negligible compared to the third one. It follows that, for the sinusoidal perturbation considered,

$$
\begin{aligned}
\delta T_{11}(z) &\simeq -\frac{1-2\nu}{4\sqrt{2\pi}} \int_{-\infty}^{+\infty} K_I^0 [-k\epsilon \sin(kz') + k\epsilon \sin(kz)] \frac{\operatorname{sgn}(z'-z)}{|z'-z|^{3/2}} \, dz' \\
&= \frac{1-2\nu}{4\sqrt{2\pi}} K_I^0 k\epsilon \operatorname{Im}\left[\int_{-\infty}^{+\infty} (e^{ikz'} - e^{ikz}) \frac{\operatorname{sgn}(z'-z)}{|z'-z|^{3/2}} \, dz' \right] \\
&= \frac{1-2\nu}{4\sqrt{2\pi}} K_I^0 k\epsilon \operatorname{Im}\left[e^{ikz} \int_{-\infty}^{+\infty} (e^{ik\zeta} - 1) \frac{\operatorname{sgn}(\zeta)}{|\zeta|^{3/2}} \, d\zeta \right] \\
&= \frac{1-2\nu}{2\sqrt{2\pi}} K_I^0 k\epsilon \operatorname{Im}\left[i e^{ikz} \int_{0}^{+\infty} \sin(k\zeta) \frac{\operatorname{sgn}(\zeta)}{\zeta^{3/2}} \, d\zeta \right],
\end{aligned}
$$

where use has been made of the change of variable $\zeta \equiv z' - z$ and parity properties. Calculation of the last integral using [Gradshteyn and Ryzhik 1980, formulae (3.7614) and (8.338.3)] then yields

$$
\delta T_{11}(z) \simeq \left(\tfrac{1}{2} - \nu\right) K_I^0 k^{3/2}\epsilon \cos(kz). \tag{27}
$$

This expression happens to exactly coincide with [Gao 1992, formula (44)]. This means that the terms disregarded by Gao without proper justification (see Section 4.3 above) are indeed negligible with the hypotheses introduced above.

Equation (27) confirms that δT_{11} is of order $K_I^0 k^{3/2}\epsilon$, as anticipated, whereas T_{11}^0 is of order $K_I^0 L^{-1/2}$. We therefore introduce the following final hypothesis:

- The characteristic length L defined by the loading, and the fluctuations of toughness generating the in-plane undulations of the crack front, are sufficiently large for the dimensionless quantity $k^{3/2}\epsilon L^{1/2} = k\epsilon\sqrt{kL}$ to be much larger than unity. (Note that this hypothesis does not contradict that of smallness of the perturbation: indeed, one may have $|\epsilon\phi'| \sim k\epsilon \ll 1$ but $k\epsilon\sqrt{kL} \gg 1$, since kL is assumed to be much larger than unity.)

Then the unperturbed nonsingular stress T_{11}^0 is negligible compared to its variation δT_{11}, so that

$$
T_{11}(z) \simeq \delta T_{11}(z) \simeq \left(\tfrac{1}{2} - \nu\right) K_I^0 k^{3/2}\epsilon \cos(kz). \tag{28}
$$

6.4. *Analysis of deviation from coplanarity and directional stability.* As remarked by Gao and Rice [1986], (26) implies that the mode II SIF $K_{\mathrm{II}}(z)$ takes nonzero and opposite values on the two sides of a local bump or hollow of the coplanarly perturbed crack front. It then follows from (21) (with $K_{\mathrm{I}}(z)$, $K_{\mathrm{II}}(z)$ instead of $K_{\mathrm{I}}(s)$, $K_{\mathrm{II}}(s)$) that the subsequent kink angle $\theta(z)$ will also take nonzero and opposite values on these two sides, implying formation of an incipient noncoplanar facet gradually rotating about the direction of propagation of the crack.

To pursue the analysis, assume for instance K_{III}^0 to be positive and consider a zone of the coplanarly perturbed crack front having $\cos(kz) > 0$, thus lying ahead of its mean position. Over such a zone, the function $\sin(kz)$ increases so that, by (21) and (26), the kink angle $\theta(z)$ of the future noncoplanar facet is a decreasing function of z. Looking at Figure 5 and imagining a facet with this property, one easily sees that it tends to rotate in time in the *positive* direction about the axis Ox, and that this rotation tends to gradually enhance the local value of the mode I SIF and lower that of the mode III SIF. Such evolutions of the SIF are, as explained in the introduction, typical of type A facets. This confirms the anticipated property that a facet formed from a locally more advanced zone of the crack front must be of this type.

Conversely, over a zone having $\cos(kz) < 0$, thus lying behind the mean position of the front, $\sin(kz)$ decreases, $\theta(z)$ increases, the facet rotates in the negative direction about the axis Ox, so that the mode I SIF decreases in time, whereas that of mode III increases. Such evolutions are typical of type B facets. This again confirms the anticipated property that facets formed from less advanced zones of the crack front must be of that other type.

The preceding analysis, however, says nothing about the directional stability of the facets. To examine this question, consider the expression (28) for the nonsingular stress $T_{11}(z)$ on the coplanarly perturbed crack front. On a zone having $\cos(kz) > 0$, about to generate a type A facet, this nonsingular stress is positive, so that Cotterell and Rice's directional stability criterion (23) is violated, implying directional instability; conversely, on a zone having $\cos(kz) < 0$, about to generate a type B facet, Cotterell and Rice's criterion is met, implying directional stability. This suggests that, in addition to the tendency of type A facets to propagate ahead of type B ones, *there is a tendency of the former facets to deviate more and more in time from the original crack plane, versus of the latter ones to come back to it*. These elements provide some theoretical ground for the intuitive idea that the crack would ideally like to develop exclusively along noncoplanar facets of type A, type B ones being present only because they are geometrically necessary to join them.

It is important to note that the tendencies just mentioned are completely independent of the value of the ratio $K_{\mathrm{III}}^0/K_{\mathrm{I}}^0$ (as long as K_{III}^0 is nonzero, which is a necessary condition for out-of-plane deviations of the crack to appear). Thus, increasing deviations from coplanarity of type A facets generated by in-plane fluctuations of the fracture toughness are probable because of a Cotterell–Rice-type instability, even for low values of this ratio. *An instability of this type is therefore a good candidate for the explanation of increasing deviations of mode* I+III *cracks from coplanarity observed experimentally for values of $K_{\mathrm{III}}^0/K_{\mathrm{I}}^0$ smaller, or even much smaller than Leblond et al.'s theoretical threshold for occurrence of a bifurcation* [2011].[5]

One may analyze in more detail the importance of the Cotterell–Rice-type instability as a function of

---

[5]It cannot be the sole explanation, however, since such deviations *could* be observed in Pons and Karma's numerical simulations [2010] of crack propagation in mode I+III based on Karma et al.'s phase field model [2001], though they did *not* include fluctuations of the fracture toughness.
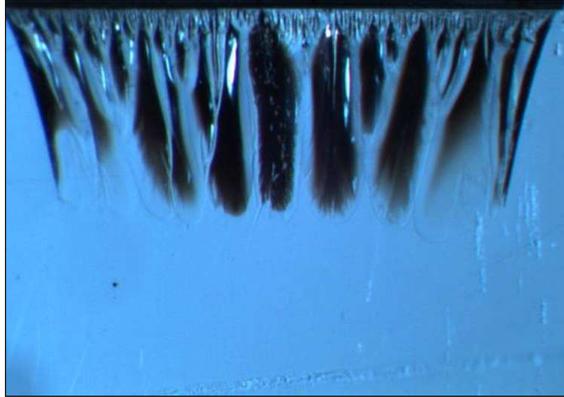
Figure 6. Fracture facets in mode I+III. Experiment by Buchholz, photograph by Lazarus.

the wavelength $\lambda = 2\pi/k$ of the coplanar crack front perturbation. This requires comparing the values of the curvature parameter $a(z)$ of the incipient facets for various initial in-plane sinusoidal perturbations of the crack front, having different wavelengths. Combination of equations (21) and (22) (with $K_I(z)$, $K_{II}(z)$, $T_{11}(z)$ instead of $K_I(s)$, $K_{II}(s)$, $T_{11}(s)$), (26) and (28) yields

$$a(z) = -\frac{16}{3}\sqrt{\frac{2}{\pi}}\frac{1-2\nu}{2-\nu}\frac{K_{III}^0}{K_I^0}k^{5/2}\epsilon^2\sin(kz)\cos(kz). \qquad (29)$$

This expression makes it clear that, when comparing the curvature parameters $a(z)$ of various perturbations, one should fix their amplitude ϵ in some way, otherwise the obvious effect of this amplitude will mask that of the wavenumber k. A logical way of doing so is to consider "homothetic" perturbations identical in shape but not in size, that is, sinusoidal fronts having the same maximal "slope" $k\epsilon$ in the crack plane but different wavenumbers k. Equation (29) shows that $a(z)$ is proportional to $(k\epsilon)^2\sqrt{k}$, that is, to $\sqrt{k}$ or $1/\sqrt{\lambda}$ for a given value of $k\epsilon$. Therefore, the smaller the value of λ, the larger that of $a(z)$ in absolute value; in other words, *the smaller the wavelength of the initial in-plane perturbation, the more directionally unstable the incipient facets it generates, if of type A, and the more directionally stable these facets, if of type B*. This theoretical conclusion finds some experimental support in the fact that incipient facets actually observed are generally of tiny initial wavelength, apparently limited in smallness only by the microstructure of the material. This is illustrated in Figure 6, which shows a photograph taken by Lazarus of a mode I+III fracture surface generated in a glass specimen by Buchholz, where the initial crack is located at the very top and propagates toward the bottom. (The photograph also shows that the wavelength of the facets does *not* remain small when their length increases, due to the gradual "coarsening" resulting from their progressive coalescence; such a phenomenon of course completely eludes the present analysis limited to *incipient* facets.)

7. Conclusion

This paper was devoted to the investigation of the idea that quick deviations of cracks loaded in mode I+III from their original plane might be made much easier by a strong influence of imperfections. Such an influence could stand as a plausible explanation for the fact that, as reported notably by Sommer [1969]

and Pham and Ravi-Chandar [2014], such deviations are frequently observed experimentally for small values of the ratio of the mode III to mode I unperturbed SIFs, lying below or even much below the theoretical threshold for occurrence of a bifurcation calculated by Leblond et al. [2011].

A typical example of inevitable imperfections consists of small fluctuations of the fracture toughness within the initial crack plane, which generate small in-plane undulations of the crack front. Rice [1985] and Gao and Rice [1986] calculated the distributions of the SIFs of the three modes resulting from a slight but otherwise arbitrary in-plane perturbation of the front of a semi-infinite crack loaded arbitrarily; in particular, Gao and Rice showed that the local mode II SIF takes nonzero and opposite values on the two sides of a local protrusion of this front, implying future local deviations of the propagating crack from coplanarity of opposite signs on these two sides, giving birth to an incipient "fracture facet" gradually rotating about the direction of propagation.

Gao and Rice, however, left open the question of the "directional stability" of these facets. It was precisely the main purpose of the present paper to complement their work by analyzing this question, using Cotterell and Rice's well-known "directional stability criterion" [1980] (duly extended to the 3D case by Leblond [1999]).

Since Cotterell and Rice's stability condition is on the sign of the nonsingular stress parallel to the direction of propagation, its application to the analysis of directional stability of the facets requires knowledge of the distributions of the nonsingular stresses for a crack with a slightly, coplanarly perturbed front. The necessary calculations were performed by Gao [1992], but with some restrictive hypotheses and unjustifiably omitting some terms, which made it necessary to revisit the problem. This has been done here by using the theory of 3D weight functions [Rice 1985; Bueckner 1987]. Fully general formulae have been obtained for the variations of the nonsingular stresses resulting from some slight but otherwise arbitrary in-plane perturbation of a semi-infinite crack, confirming and completing the partial results of [Gao 1992].

The formula obtained for the variation of the nonsingular stress parallel to the direction of crack propagation was then applied to a typically sinusoidal coplanar perturbation of the front. A distinction was made between the more advanced zones of the front, about to generate an incipient facet of "type A" rotating about the direction of propagation, so as to raise the local proportion of mode I versus mode III, and the less advanced ones, about to generate a facet of "type B", rotating oppositely so as to lower this proportion.

It has been found that, provided that the length scale defined by the loading and the fluctuations of the fracture toughness are large enough, the nonsingular stress parallel to the direction of propagation is positive on the former zones, implying directional instability, and negative on the latter ones, implying directional stability. This shows that even for low values of the ratio of the mode III to mode I unperturbed SIFs, crack propagation in mode I+III may occur through preferential formation of noncoplanar facets of type A, because of a local Cotterell–Rice-type instability — which confirms the idea investigated.

It has also been found that the smaller the wavelength of the initial in-plane perturbation, the stronger Cotterell and Rice's instability on the resulting incipient facets of type A. This implies preferential development of type A facets of *small* initial wavelength, in agreement with experimental observations.

References

[Bueckner 1987] H. F. Bueckner, "Weight functions and fundamental fields for the penny-shaped and the half-plane crack in three-space", *Int. J. Solids Struct.* **23**:1 (1987), 57–93.

[Cooke and Pollard 1996] M. L. Cooke and D. D. Pollard, "Fracture propagation paths under mixed mode loading within rectangular blocks of polymethyl methacrylate", *J. Geophys. Res.* **101**:B2 (1996), 3387–3400.

[Cotterell and Rice 1980] B. Cotterell and J. R. Rice, "Slightly curved or kinked cracks", *Int. J. Fract.* **16**:2 (1980), 155–169.

[Gao 1992] H. Gao, "Variation of elastic T-stresses along slightly wavy 3D crack fronts", *Int. J. Fract.* **58**:3 (1992), 241–257.

[Gao and Rice 1986] H. Gao and J. R. Rice, "Shear stress intensity factors for a planar crack with slightly curved front", *J. Appl. Mech.* (*ASME*) **53**:4 (1986), 774–778.

[Goldstein and Osipenko 2012] R. V. Goldstein and N. M. Osipenko, "Successive development of the structure of a fracture near the front of a longitudinal shear crack", *Dokl. Phys.* **57**:7 (2012), 281–284.

[Goldstein and Salganik 1974] R. V. Goldstein and R. L. Salganik, "Brittle fracture of solids with arbitrary cracks", *Int. J. Fract.* **10**:4 (1974), 507–523.

[Gradshteyn and Ryzhik 1980] I. S. Gradshteyn and I. M. Ryzhik, *Table of integrals, series, and products*, Academic Press, New York, 1980.

[Griffith 1921] A. A. Griffith, "The phenomena of rupture and flow in solids", *Phil. Trans. R. Soc. A* **221**:587 (1921), 163–198.

[Hakim and Karma 2009] V. Hakim and A. Karma, "Laws of crack motion and phase-field models of fracture", *J. Mech. Phys. Solids* **57**:2 (2009), 342–368.

[Hourlier and Pineau 1979] F. Hourlier and A. Pineau, "Fissuration par fatigue sous sollicitations polymodales (mode I ondulé + mode III permanent) d'un acier pour rotors 26NCDV14", *Mém. Sci. Rev. Métall.* **76** (1979), 175–185.

[Hull 1995] D. Hull, "The effect of mixed mode I/III on crack evolution in brittle solids", *Int. J. Fract.* **70**:1 (1995), 59–79.

[Karma et al. 2001] A. Karma, D. A. Kessler, and H. Levine, "Phase-field model of mode III dynamic fracture", *Phys. Rev. Lett.* **87** (2001), Article ID #045501.

[Knauss 1970] W. G. Knauss, "An observation of crack propagation in anti-plane shear", *Int. J. Fract.* **6**:2 (1970), 183–187.

[Kuo 1993] M. K. Kuo, "Stress intensity factors for a semi-infinite plane crack under a pair of point forces on the faces", *J. Elasticity* **30**:3 (1993), 197–209.

[Lazarus 1997] V. Lazarus, *Quelques problèmes tridimensionnels de mécanique de la rupture fragile*, thesis, Université Pierre et Marie Curie, Paris, 1997, Available at https://tel.archives-ouvertes.fr/tel-00273453.

[Lazarus et al. 2001a] V. Lazarus, J.-B. Leblond, and S.-E. Mouchrif, "Crack front rotation and segmentation in mixed mode I + III or I + II + III. Part I: Calculation of stress intensity factors", *J. Mech. Phys. Solids* **49**:7 (2001), 1399–1420.

[Lazarus et al. 2001b] V. Lazarus, J.-B. Leblond, and S.-E. Mouchrif, "Crack front rotation and segmentation in mixed mode I + III or I + II + III. Part II: Comparison with experiments", *J. Mech. Phys. Solids* **49**:7 (2001), 1421–1443.

[Lazarus et al. 2008] V. Lazarus, F.-G. Buchholz, M. Fulland, and J. Wiebesiek, "Comparison of predictions by mode II or mode III criteria on crack front twisting in three or four point bending experiments", *Int. J. Fract.* **153**:2 (2008), 141–151.

[Leblond 1999] J.-B. Leblond, "Crack paths in three-dimensional elastic solids, I: Two-term expansion of the stress intensity factors—application to crack path stability in hydraulic fracturing", *Int. J. Solids Struct.* **36**:1 (1999), 79–103.

[Leblond et al. 1999] J.-B. Leblond, V. Lazarus, and S.-E. Mouchrif, "Crack paths in three-dimensional elastic solids, II: Three-term expansion of the stress intensity factors—applications and perspectives", *Int. J. Solids Struct.* **36**:1 (1999), 105–142.

[Leblond et al. 2011] J.-B. Leblond, A. Karma, and V. Lazarus, "Theoretical analysis of crack front instability in mode I + III", *J. Mech. Phys. Solids* **59**:9 (2011), 1872–1887.

[Lin et al. 2010] B. Lin, M. E. Mear, and K. Ravi-Chandar, "Criterion for initiation of cracks under mixed-mode I + III loading", *Int. J. Fract.* **165**:2 (2010), 175–188.

[Movchan et al. 1998] A. B. Movchan, H. Gao, and J. R. Willis, "On perturbations of plane cracks", *Int. J. Solids Struct.* **35**:26-27 (1998), 3419–3453.

[Pham and Ravi-Chandar 2014] K. Pham and K. Ravi-Chandar, "Further examination of the criterion for crack initiation under mixed-mode I+III loading", *Int. J. Fract.* **189**:2 (2014), 121–138.

[Pollard and Aydin 1988] D. D. Pollard and A. Aydin, "Progress in understanding jointing over the past century", *Geol. Soc. Am. Bull.* **100**:8 (1988), 1181–1204.

[Pollard et al. 1982] D. D. Pollard, P. Segall, and P. T. Delaney, "Formation and interpretation of dilatant echelon cracks", *Geol. Soc. Am. Bull.* **93**:12 (1982), 1291–1303.

[Pons and Karma 2010] A. J. Pons and A. Karma, "Helical crack-front instability in mixed-mode fracture", *Nature* **464** (2010), 85–89.

[Rice 1985] J. R. Rice, "First-order variation in elastic fields due to variation in location of a planar crack front", *J. Appl. Mech. (ASME)* **52**:3 (1985), 571–579.

[Sommer 1969] E. Sommer, "Formation of fracture 'lances' in glass", *Eng. Fract. Mech.* **1**:3 (1969), 539–546.

[Suresh and Tschegg 1987] S. Suresh and E. K. Tschegg, "Combined mode I–mode III fracture of fatigue-precracked alumina", *J. Am. Ceram. Soc.* **70**:10 (1987), 726–733.

[Yates and Miller 1989] J. R. Yates and K. J. Miller, "Mixed mode (I+III) fatigue thresholds in a forging steel", *Fatigue Fract. Eng. Mater. Struct.* **12**:3 (1989), 259–270.

JEAN-BAPTISTE LEBLOND: jbl@lmm.jussieu.fr
Institut Jean Le Rond d'Alembert, Sorbonne Universités UPMC Université Paris 06, CNRS, UMR 7190, 75005 Paris 06, France

VÉRONIQUE LAZARUS: veronique.lazarus@u-psud.fr
CNRS, Université Paris-Sud 11, Lab FAST, UMR 7608, 91405 Orsay, France

msp

INTERACTION BETWEEN A CIRCULAR INCLUSION AND A CIRCULAR VOID UNDER PLANE STRAIN CONDITIONS

Vlado A. Lubarda

The interaction force between a circular inclusion characterized by uniform eigenstrain and a nearby circular void is determined by evaluating the J-integral around the void. The Kienzler–Zhuping formula was used to determine the hoop stress along the boundary of the void in terms of the infinite-medium solution to the inclusion problem. Specific results are given for the inclusion with dilatational eigenstrain. The M-integrals around the void and inclusion are then evaluated, the former being proportional to the energy release rates associated with a self-similar expansion of the void. The energy rate associated with an isotropic expansion of the inclusion differs from the M-integral around the inclusion. The relationship between the two is derived. It is shown that the greater the distance from the void, the greater the energy associated with the presence of the inclusion and the greater the energy rate associated with its growth, which suggests that the presence of nearby free surfaces facilitates the eigenstrain transformations. The attraction exerted on a circular inclusion with a uniform shear eigenstrain by the free surface of a half-space is also evaluated. Peculiar variation of this configurational force with the distance between the inclusion and the free surface is noted and discussed.

1. Introduction

Kienzler and Zhuping [1987] derived an appealing formula for the hoop stress along the boundary of a circular void of radius a in an infinite medium under plane stress or plane strain conditions, due to remote loading or an internal source of stress, which reads

$$\sigma_\theta(a, \theta) = 2[\sigma_\theta^0(a, \theta) - \sigma_r^0(a, \theta)] + \tfrac{1}{2}[\sigma_\theta^0(0, \theta) + \sigma_r^0(0, \theta)]. \tag{1}$$

The stress field in an infinite medium without a void due to the same source of stress is denoted by the superscript ^{0}, and (r, θ) are the polar coordinates with the origin at the center of the void. This formula received relatively little attention in the literature, although it did stimulate research efforts that led to the formulation of the so-called heterogenization procedure [Honein and Herrmann 1988; 1990], according to which the solution to the problem of two or more inhomogeneities under remote or other types of loading is expressed in terms of the solution to the corresponding homogeneous problem. An important part of the latter analysis is that the elastic field produced by the prescribed tractions or displacements over the boundary of a circular hole in an infinite medium can be expressed in terms of the elastic field produced by the same quantities acting on the boundary of a circular disk, and vice versa. We use the Kienzler–Zhuping formula in this paper to evaluate the J-integral along the boundary of a circular void, or

along the straight edge of a half-space, without using or deriving the solution to the entire boundary value problem at hand. Based on this, we determine the configurational force exerted by the free surface on a nearby source of internal stress. The latter is taken to be a circular inclusion with a uniform dilatational eigenstrain. The M-integrals around the void and the inclusion are evaluated. The M_O-integral around the void is proportional to the energy release rate associated with a self-similar expansion of the void, if the surface of the void is traction-free. The energy rate associated with an isotropic expansion of the inclusion differs from the ratio M_C/b, where the M_C-integral is evaluated around the boundary of the inclusion of radius b. The relationship between the two quantities is derived. The attraction exerted on a circular inclusion with a uniform shear eigenstrain by the free surface of a half-space is also evaluated. Peculiar variation of this configurational force with the distance between the inclusion and the free surface is noted and discussed.

The determination of physical quantities, such as the dislocation interaction force or the stress-intensity factor in various dislocation and fracture mechanics problems, without solving the corresponding boundary value problems, was earlier considered by Eshelby [1975], Freund [1978], Rice [1985], Kienzler and Kordisch [1990], and Lubarda and Markenscoff [2007], among others. More recently, Lubarda [2015] employed the antiplane-strain version of the Kienzler–Zhuping formula, first recognized by Lin et al. [1990], to determine the configurational force between a circular void and inclusion characterized by uniform eigenshear. The study of inclusions and interactions among them plays an important role in materials science problems concerned with displacive transformations and transformation toughening mechanisms in crystalline metallic materials and ceramics. A comprehensive review of recent works on inclusions can be found in [Zhou et al. 2013].

2. Circular inclusion near a circular void

Suppose that a circular cylinder of radius b is taken out from an infinite medium and given a uniform plane eigenstrain $(\epsilon_x^\bullet, \epsilon_y^\bullet, \epsilon_{xy}^\bullet)$. When the cylinder is inserted back into the medium, with their interface perfectly bonded, the stress fields expressed in polar coordinates (ρ, φ) with respect to the center C of the inclusion (Figure 1), are

$$
\begin{aligned}
\sigma_\rho^{0,\text{in}} &= -2k\big[(\epsilon_\rho^\bullet + \epsilon_\varphi^\bullet) + \tfrac{1}{2}(\epsilon_\rho^\bullet - \epsilon_\varphi^\bullet)\big], \\
\sigma_\varphi^{0,\text{in}} &= -2k\big[(\epsilon_\rho^\bullet + \epsilon_\varphi^\bullet) - \tfrac{1}{2}(\epsilon_\rho^\bullet - \epsilon_\varphi^\bullet)\big], \\
\sigma_{\rho\varphi}^{0,\text{in}} &= -2k\epsilon_{\rho\varphi}^\bullet,
\end{aligned}
\tag{2}
$$

where $\epsilon_\rho^\bullet + \epsilon_\varphi^\bullet = \epsilon_x^\bullet + \epsilon_y^\bullet$, $k = \mu/[4(1-\nu)]$, and

$$
\begin{aligned}
\epsilon_\rho^\bullet - \epsilon_\varphi^\bullet &= (\epsilon_x^\bullet - \epsilon_y^\bullet)\cos 2\varphi + 2\epsilon_{xy}^\bullet \sin 2\varphi, \\
2\epsilon_{\rho\varphi}^\bullet &= -(\epsilon_x^\bullet - \epsilon_y^\bullet)\sin 2\varphi + 2\epsilon_{xy}^\bullet \cos 2\varphi.
\end{aligned}
\tag{3}
$$

The expressions (2) are obtained from the results for circular inclusions presented in [Lubarda 1998] and [Lubarda and Markenscoff 1999], which were derived by using the Papkovich–Neuber potentials. They can also be obtained from the general ellipsoidal inclusion analysis in [Eshelby 1957; 1959]. The
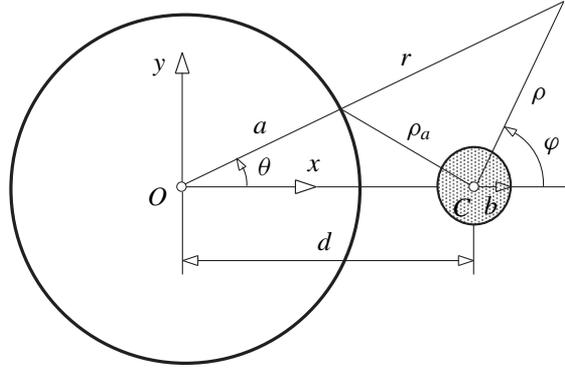
Figure 1. A circular inclusion of radius b in an infinite medium near the void of radius a. The eigenstrain of the inclusion is $(\epsilon_x^{\bullet}, \epsilon_y^{\bullet}, \epsilon_{xy}^{\bullet})$. The centers of the inclusion and void are separated by the distance d. The distance from the center C of the inclusion to an arbitrary point on the boundary of the void is ρ_a. The polar coordinates (ρ, φ) are with respect to the point C, and (r, θ) with respect to the point O.

in-plane stress components outside of the inclusion are

$$
\begin{aligned}
\sigma_\rho^{0,\text{out}} &= -2k\frac{b^2}{\rho^2}\left[(\epsilon_\rho^{\bullet} + \epsilon_\varphi^{\bullet}) + \frac{1}{2}\left(4 - 3\frac{b^2}{\rho^2}\right)(\epsilon_\rho^{\bullet} - \epsilon_\varphi^{\bullet})\right], \\
\sigma_\varphi^{0,\text{out}} &= 2k\frac{b^2}{\rho^2}\left[(\epsilon_\rho^{\bullet} + \epsilon_\varphi^{\bullet}) - \frac{3}{2}\frac{b^2}{\rho^2}(\epsilon_\rho^{\bullet} - \epsilon_\varphi^{\bullet})\right], \\
\sigma_{\rho\varphi}^{0,\text{out}} &= 2k\frac{b^2}{\rho^2}\left(2 - 3\frac{b^2}{\rho^2}\right)\epsilon_{\rho\varphi}^{\bullet}.
\end{aligned}
\tag{4}
$$

When rewritten in terms of the polar coordinates (r, θ) with respect to the point O, the outside stress field (omitting the superscript "out") is

$$
\begin{aligned}
\sigma_r^0 + \sigma_\theta^0 &= \sigma_\rho^0 + \sigma_\varphi^0, \\
\sigma_r^0 - \sigma_\theta^0 &= (\sigma_\rho^0 - \sigma_\varphi^0)\cos 2(\varphi - \theta) - 2\sigma_{\rho\varphi}^0 \sin 2(\varphi - \theta), \\
2\sigma_{r\theta}^0 &= (\sigma_\rho^0 - \sigma_\varphi^0)\sin 2(\varphi - \theta) + 2\sigma_{\rho\varphi}^0 \cos 2(\varphi - \theta).
\end{aligned}
\tag{5}
$$

In these expressions,

$$
\begin{aligned}
\sin\varphi &= \frac{r\sin\theta}{\rho}, \quad \cos\varphi = \frac{r\cos\theta - d}{\rho}, \\
\sin(\varphi - \theta) &= \frac{d\sin\theta}{\rho}, \quad \cos(\varphi - \theta) = \frac{r - d\cos\theta}{\rho}, \\
\rho^2 &= r^2 + d^2 - 2rd\cos\theta.
\end{aligned}
\tag{6}
$$

The total strain energy in the entire medium (inside and outside of the inclusion, per unit thickness) can be determined from the equation [Lubarda and Markenscoff 1999]

$$
E_T^0 = -\frac{1}{2}\int_{A^{\text{in}}} \sigma_{ij}^{0,\text{in}}\epsilon_{ij}^{\bullet}\,dA = -\frac{1}{2}\left(\sigma_\rho^{0,\text{in}}\epsilon_\rho^{\bullet} + \sigma_\varphi^{0,\text{in}}\epsilon_\varphi^{\bullet} + 2\sigma_{\rho\varphi}^{0,\text{in}}\epsilon_{\rho\varphi}^{\bullet}\right)b^2\pi,
\tag{7}
$$

which gives

$$E_T^0 = \pi k b^2 \left\{ (\epsilon_x^\bullet + \epsilon_y^\bullet)^2 + \tfrac{1}{2} \left[(\epsilon_x^\bullet - \epsilon_y^\bullet)^2 + 4\epsilon_{xy}^{\bullet 2} \right] \right\}. \tag{8}$$

The rate of energy change associated with an infinitesimal increase of the inclusion radius δb is

$$\frac{\delta E_T^0}{\delta b} = 2\pi k b \left\{ (\epsilon_x^\bullet + \epsilon_y^\bullet)^2 + \tfrac{1}{2} \left[(\epsilon_x^\bullet - \epsilon_y^\bullet)^2 + 4\epsilon_{xy}^{\bullet 2} \right] \right\}. \tag{9}$$

This can also be deduced from the expression for the specific configurational force (f^0) (per unit length of the circumference of the inclusion, at each point orthogonal to the circumference), defined such that [Gavazza 1977]

$$\delta E_T^0 = -(2\pi b) f^0 \delta b, \quad f^0 = \tfrac{1}{2} (\sigma_{ij}^{0,\text{in}} + \sigma_{ij}^{0,\text{out}})_{\rho=b} \epsilon_{ij}^\bullet. \tag{10}$$

This formula has recently been extended to problems of dynamically expanding inclusions in a comprehensive sequence of papers by Markenscoff and Ni [2010; 2011].

2.1. *Dilatational eigenstrain.* If the inclusion is given a purely dilatational eigenstrain $\epsilon_x^\bullet = \epsilon_y^\bullet = \epsilon^\bullet$ and $\epsilon_{xy}^\bullet = 0$, the outside stress field in polar coordinates (ρ, φ), relative to the center of the inclusion, is

$$\sigma_\varphi^{0,\text{out}} = -\sigma_\rho^{0,\text{out}} = 4k\epsilon^\bullet \frac{b^2}{\rho^2}, \quad \sigma_{\rho\varphi}^{0,\text{out}} = 0. \tag{11}$$

When this is substituted into (5), the outside stress field in polar coordinates (r, θ), relative to the center of the void, becomes

$$\sigma_\theta^0(r, \theta) = -\sigma_r^0(r, \theta) = 4k\epsilon^\bullet \frac{b^2}{\rho^2} \left(1 - \frac{2d^2 \sin^2 \theta}{\rho^2} \right),$$
$$\sigma_{r\theta}^0(r, \theta) = -8k\epsilon^\bullet \frac{b^2 d}{\rho^3} (r - d\cos\theta) \sin\theta. \tag{12}$$

The outside stress field is deviatoric ($\sigma_r^0 + \sigma_\theta^0 = 0$). Thus, from the Kienzler–Zhuping formula (1), it follows that along the boundary of the void $r = a$, the hoop stress due to inserted inclusion is

$$\sigma_\theta(a, \theta) = 2[\sigma_\theta^0(a, \theta) - \sigma_r^0(a, \theta)] = 4\sigma_\theta^0(a, \theta); \tag{13}$$

that is, in view of (12),

$$\sigma_\theta(a, \theta) = \frac{4\mu\epsilon^\bullet}{1 - \nu} \frac{b^2}{\rho_a^2} \left(1 - \frac{2d^2 \sin^2 \theta}{\rho_a^2} \right), \quad \rho_a^2 = a^2 + d^2 - 2ad\cos\theta. \tag{14}$$

The total strain energy (per unit thickness) due to inserted inclusion in an infinite medium, and its rate, are

$$E_T^0 = \frac{\pi\mu b^2 \epsilon^{\bullet 2}}{1 - \nu}, \quad \frac{\delta E_T^0}{\delta b} = \frac{2\pi\mu b \epsilon^{\bullet 2}}{1 - \nu}, \tag{15}$$

which follows from (8) and (9). Thus, from (10), the configurational force per unit length of the circumference of the inclusion is $f^0 = -p^0 \epsilon^\bullet$, and $p^0 = \mu\epsilon^\bullet/(1 - \nu)$ is the interface pressure.
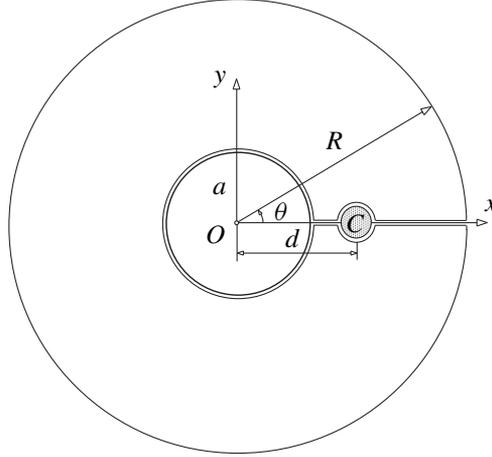
Figure 2. The closed contour around the void of radius a and its center at O, and the inclusion of radius b and its center at C, used to evaluate the J- and M-integrals. The radius R of the remote circle tends to infinity.

3. Configurational force between the inclusion and void

The J_β-integral for the plane strain elasticity problems can be expressed in terms of the Eshelby's energy momentum tensor $P_{\alpha\beta}$ [Eshelby 1956; 1957] as

$$J_\beta = \oint P_{\alpha\beta} n_\alpha \, dl, \quad P_{\alpha\beta} = W \delta_{\alpha\beta} - \sigma_{\alpha\gamma} u_{\gamma,\beta}, \quad (\alpha, \beta = x, y). \tag{16}$$

In particular,

$$J_x = \oint (W n_x - t_x u_{x,x} - t_y u_{y,x}) \, dl, \tag{17}$$

where $t_x = \sigma_x n_x + \sigma_{xy} n_y$ and $t_y = \sigma_{yx} n_x + \sigma_y n_y$ are the traction components over the contour whose outward normal has the components (n_x, n_y). An analysis based on dual conservation integrals, originally introduced by Bui [1973; 1974], could also be used, but is not pursued in this paper; see [Lubarda and Markenscoff 2007] and [Lubarda 2012] for its application to other problems. When evaluated over a closed contour which does not embrace a singularity or a defect, the integral in (17) vanishes. Such a contour, going around the void and the inclusion, along the positive x-axis, and around a remote circle of large radius $R \gg (a, b, d)$, is shown in Figure 2. The contributions to J_x along the lines just above and below the x-axis cancel each other, and the contribution from the remote circle vanishes because the stresses fall off as $1/R^2$ in the limit $R \to \infty$, as in an unvoided infinite medium, because for large R the stress field becomes increasingly unaware of the presence of the void near the inclusion. Thus, $J_x = J_x^{\text{void}} + J_x^{\text{incl}} = 0$; i.e.,

$$J_x^{\text{incl}} = -J_x^{\text{void}}. \tag{18}$$

The J_x-integral along the boundary of the void ($r = a$, $n_x = \cos\theta$, $n_y = \sin\theta$) is

$$J_x^{\text{void}} = a \int_0^{2\pi} W(a, \theta) \cos\theta \, d\theta = \frac{1-\nu}{4\mu} a \int_0^{2\pi} \sigma_\theta^2(a, \theta) \cos\theta \, d\theta, \tag{19}$$

because $\sigma_x n_x + \sigma_{xy} n_y = 0$, $\sigma_{yx} n_x + \sigma_y n_y = 0$, and $W = \sigma_\theta \epsilon_\theta / 2 = (1 - \nu)\sigma_\theta^2/(4\mu)$ along the traction-free boundary of the void. By incorporating the stress expression (14) into (19), it follows that

$$J_x^{\text{void}} = \frac{8\mu a \epsilon^{\bullet 2}}{1 - \nu}\left(\frac{b}{a}\right)^4\left[I_1 - 4\left(\frac{d}{a}\right)^2 I_2 + 4\left(\frac{d}{a}\right)^4 I_3\right], \tag{20}$$

where

$$I_1 = \int_0^\pi \frac{\cos\theta\, d\theta}{\rho_0^4} = \frac{2\pi(d/a)}{[(d/a)^2 - 1]^3},$$

$$I_2 = \int_0^\pi \frac{\sin^2\theta\cos\theta\, d\theta}{\rho_0^6} = \frac{\pi[3(d/a)^2 - 1]}{4(d/a)^3[(d/a)^2 - 1]^3}, \tag{21}$$

$$I_3 = \int_0^\pi \frac{\sin^4\theta\cos\theta\, d\theta}{\rho_0^8} = \frac{\pi[2(d/a)^2 - 1]}{4(d/a)^5[(d/a)^2 - 1]^3},$$

and $\rho_0^2 = 1 - 2(d/a)\cos\theta + (d/a)^2$. These integral expressions were derived by using the general formula [Gradshteyn and Ryzhik 1965]

$$\int_0^\pi \frac{\cos n\theta\, d\theta}{(1 - 2\alpha\cos\theta + \alpha^2)^m} = \frac{\pi}{\alpha^n(\alpha^2 - 1)^{2m-1}}\sum_{k=0}^{m-1}\binom{m+n-1}{k}\binom{2m-k-2}{m-1}(\alpha^2 - 1)^k, \tag{22}$$

valid for $\alpha^2 > 1$, in conjunction with the appropriate integration by parts. The trigonometric identity $8\sin^4\theta = 3 - 4\cos 2\theta + \cos 4\theta$ was also conveniently utilized. The expressions were also verified by the Matlab evaluation of integrals. Consequently, by substituting (21) into (20), the J-integral around the void becomes

$$J_x^{\text{void}} = \bar{J}_x\left(\frac{b}{a}\right)^4 \frac{d/a}{[(d/a)^2 - 1]^3}, \quad \bar{J}_x = \frac{8\pi\mu a\epsilon^{\bullet 2}}{1 - \nu}. \tag{23}$$

This represents the material or configurational force exerted on the void by a nearby inclusion (per unit length in the z-direction). It represents the energy release rate associated with an imagined void translation within the material toward the inclusion (by diffusion or otherwise), keeping the position of the inclusion fixed. The opposite force of the same magnitude is exerted on the inclusion by the surface of the void. The maximum value of the force is reached at the minimum distance between the centers of the inclusion and the void for which the presented analysis applies ($d_{\min} = a + b$), and is equal to

$$J_{x,\max}^{\text{void}} = \bar{J}_x \frac{(b/a)(1 + b/a)}{(2 + b/a)^3}. \tag{24}$$

The variation of J_x^{void} (normalized by $\bar{J}_x$) versus d/a for several values of b/a is shown in Figure 3.

In the limit of infinitely large radius of the void, the inclusion behaves as if it is near the free surface of a half-space. If the distance from the center of the inclusion to that surface is denoted by c, the force on the inclusion is found to be

$$J_x^{\text{incl}} = -\frac{\pi\mu\epsilon^{\bullet 2}}{1 - \nu}\frac{b^4}{c^3}. \tag{25}$$

The force on an ellipsoidal inclusion with uniform dilatational eigenstrain near the free surface of a half-space was evaluated and discussed by Mura [1987]. More recently, Zhou et al. [2013] provided
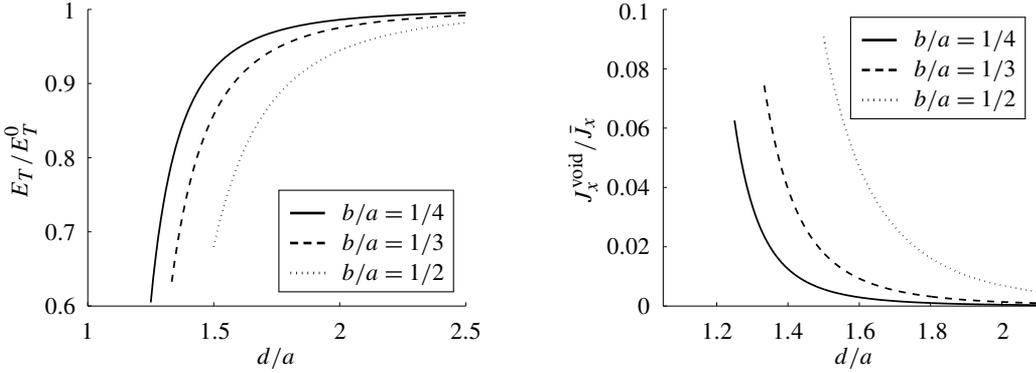
Figure 3. Left: the variation of the strain energy E_T/E_T^0 with d/a, according to (29), for the indicated values of the ratio b/a. Right: the variation of the configurational forces J_x^{void} with d/a, according to (23), for the same values of the ratio b/a. The scaling force parameter is $\bar{J}_x = 8\pi\mu a\epsilon^{\bullet 2}/(1-\nu)$. The left endpoints of the curves (at $d/a = 1 + b/a$, when the inclusion is tangent to the void) specify the minimum strain energy and maximum configurational force corresponding to a selected value of the ratio b/a.

a comprehensive survey of recent works on inclusions and inhomogeneities in an infinite space and a half-space, addressing the problems of a single inclusion, two inclusions, and multiple inclusions, as well as dislocations and cracks.

4. Total strain energy

The total strain energy in the medium with inserted inclusion near a traction-free void is the sum of the strain energy term corresponding to the inclusion inserted in an infinite medium far away from the void, thus given by the first expression in (15), and the term dependent on d which accounts for the interaction between the void and inclusion. The latter includes the strain energy of the auxiliary (image) field and the cross term due to energy of the auxiliary $\hat{\sigma}_{ij}$ field on the infinite-medium strain field, as well as the energy of the infinite-medium stress field on the auxiliary $\hat{\epsilon}_{ij}$ strain field. Thus,

$$E_T = \frac{\pi\mu b^2 \epsilon^{\bullet 2}}{1-\nu} + \hat{E}_T(d, b). \tag{26}$$

The energy $\hat{E}_T$ can be conveniently determined by noting that its negative gradient with respect to the distance between the inclusion and the void must be equal to the configurational force on the void, as given by the expression (23):

$$-\frac{\partial \hat{E}_T}{\partial d} = \frac{8\pi\mu\epsilon^{\bullet 2}}{1-\nu} \frac{adb^4}{(d^2 - a^2)^3}. \tag{27}$$

Upon integration, this gives

$$\hat{E}_T = -\frac{2\pi\mu\epsilon^{\bullet 2}}{1-\nu} \frac{a^2 b^4}{(d^2 - a^2)^2}, \tag{28}$$

up to an immaterial constant term. Consequently, by substituting (28) into (26), the total strain energy becomes

$$E_T = E_T^0\left[1 - \frac{2a^2b^2}{(d^2 - a^2)^2}\right], \quad E_T^0 = \frac{\pi\mu b^2 \epsilon^{\bullet 2}}{1 - \nu}. \tag{29}$$

Therefore, the introduction of the void in an infinite medium with the inserted inclusion decreases the strain energy, the decrease being greater for larger voids that are closer to the inclusion. This is sketched in Figure 3 (left image).

For later use, we also evaluate from (29) the following quantities:

$$-a\frac{\partial E_T}{\partial a} = \frac{4\pi\mu a^2 \epsilon^{\bullet 2}}{1 - \nu}\left(\frac{b}{a}\right)^4 \frac{(d/a)^2 + 1}{[(d/a)^2 - 1]^3}, \tag{30}$$

$$-b\frac{\partial E_T}{\partial b} = \frac{2\pi\mu a^2 \epsilon^{\bullet 2}}{1 - \nu}\left[-\left(\frac{b}{a}\right)^2 + \left(\frac{b}{a}\right)^4 \frac{4}{[(d/a)^2 - 1]^2}\right], \tag{31}$$

which will be discussed in relation to M-integrals in the next two sections.

5. M-integral around the void

The M-integral of the plane strain elasticity with respect to the coordinate origin at the point O can be expressed as [Knowles and Sternberg 1972; Budiansky and Rice 1973]

$$M_O = \oint P_{\alpha\beta}x_\beta n_\alpha \, dl = \oint \left[x(P_{xx}n_x + P_{yx}n_y) + y(P_{xy}n_x + P_{yy}n_y)\right] dl; \tag{32}$$

that is,

$$M_O = \oint \left[W(xn_x + yn_y) - t_x(xu_{x,x} + yu_{x,y}) - t_y(xu_{y,x} + yu_{y,y})\right] dl. \tag{33}$$

By using the same closed contour from Figure 2, as in the evaluation of the J_x-integral, the contribution from the remote circle M_O^R tends to 0 as R tends to ∞, because the stresses decay as $1/R^2$ far away from the inclusion. Thus, $M_O^{\text{void}} + M_O^{\text{incl}} = 0$, where

$$M_O^{\text{void}} = a^2 \int_0^{2\pi} W(a, \theta) \, d\theta = \frac{(1 - \nu)a^2}{4\mu} \int_0^{2\pi} \sigma_\theta^2(a, \theta) \, d\theta. \tag{34}$$

Upon using the circumferential stress expression (14), the integration in (34) gives

$$M_O^{\text{void}} = \frac{8\mu a^2 \epsilon^{\bullet 2}}{1 - \nu}\left(\frac{b}{a}\right)^4\left[K_1 - 4\left(\frac{d}{a}\right)^2 K_2 + 4\left(\frac{d}{a}\right)^4 K_3\right], \tag{35}$$

where

$$K_1 = \int_0^\pi \frac{d\theta}{\rho_0^4} = \frac{\pi[(d/a)^2 + 1]}{[(d/a)^2 - 1]^3},$$

$$K_2 = \int_0^\pi \frac{\sin^2\theta \, d\theta}{\rho_0^6} = \frac{\pi}{2[(d/a)^2 - 1]^3}, \tag{36}$$

$$K_3 = \int_0^\pi \frac{\sin^4\theta \, d\theta}{\rho_0^8} = \frac{\pi[3(d/a)^2 - 1]}{8(d/a)^4[(d/a)^2 - 1]^3}.$$
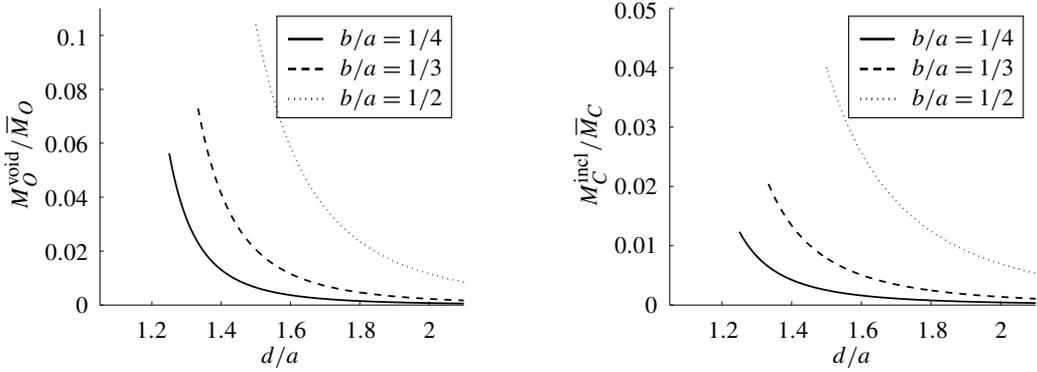
Figure 4. The variation of M_O^{void} (left) and M_C^{void} (right) with d/a for the indicated values of the ratio b/a. The scaling factor for both plots is $\overline{M}_O = \overline{M}_C$, as defined in (37).

The substitution of (36) into (35) yields

$$M_O^{\text{void}} = \overline{M}_O \left(\frac{b}{a}\right)^4 \frac{(d/a)^2 + 1}{[(d/a)^2 - 1]^3}, \quad \overline{M}_0 = \frac{1}{2} \bar{J}_x a = \frac{4\pi\mu a^2 \epsilon^{\bullet 2}}{1 - \nu}. \tag{37}$$

Physically, the ratio M_O^{void}/a represents the energy release rate associated with isotropic void growth (by material absorption over the surface of the void), keeping the position of the inclusion fixed relative to the center of the void. Indeed, the comparison of (37) with (30) shows that $M_O^{\text{void}} = -a(\partial E_T/\partial a)$.

6. M integral around the inclusion

By using the well-known relationship between the M-integrals relative to the coordinate origins at O and C [Rice 1985],

$$M_O^{\text{incl}} = M_C^{\text{incl}} + d \cdot J_x^{\text{incl}}, \tag{38}$$

and in view of the relationship $M_O^{\text{void}} + M_O^{\text{incl}} = 0$, it follows that

$$M_C^{\text{incl}} = -(M_O^{\text{void}} + d \cdot J_x^{\text{incl}}). \tag{39}$$

Consequently, by substituting into (39) the expression for M_O^{void} from (37) and the expression for $J_x^{\text{incl}} = -J_x^{\text{void}}$ from (23), the M_C integral around the inclusion is found to be

$$M_C^{\text{incl}} = \overline{M}_C \left(\frac{b}{a}\right)^4 \frac{1}{[(d/a)^2 - 1]^2}, \quad \overline{M}_C = \overline{M}_O. \tag{40}$$

If $d \gg a$, then M_C^{incl} approaches zero, as if the inclusion was in an infinite medium without the void ($M_C^{\text{incl},\infty} = 0$). The variation of M_O^{void} and M_C^{incl} with d/a for several values of the ratio b/a is shown in Figure 4. In the limit of infinitely large radius of the void, the M-integral around the inclusion is

$$M_C^{\text{incl}} = \frac{\pi\mu\epsilon^{\bullet 2}}{1 - \nu} \frac{b^4}{c^2}, \tag{41}$$

in duality with (25) through the relation $M_C^{\text{incl}} = -c J_x^{\text{incl}}$.
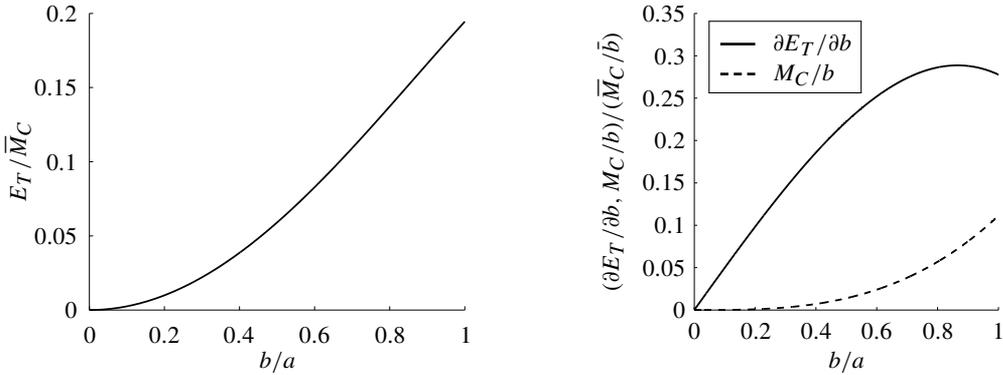
Figure 5. Left: the variation of the strain energy E_T, given by (29) and normalized by $\overline{M}_C$, with b/a in the case $d = 2a$. Right: the corresponding variation of $\delta E_T/\delta b$ and M_C^{incl}/b, given by (42) and normalized by $\overline{M}_C/\bar{b}$, where $\bar{b} = a$.

6.1. *Expansion of the inclusion.* The ratio M_C^{incl}/b does not represent the energy rate associated with the isotropic growth (self-similar expansion) of the inclusion ($\delta E_T/\delta b$), which is given by (31). In fact, the two are related by

$$\frac{\delta E_T}{\delta b} = \frac{2\pi \mu b \epsilon^{\bullet 2}}{1 - \nu} - \frac{2M_C^{\text{incl}}}{b}. \tag{42}$$

Figure 5 (right image) shows the variation of $\delta E_T/\delta b$ and M_C^{incl}/b (both normalized by $\overline{M}_C/b$) with b/a, in the case $d = 2a$. The energy (E_T) plot itself is shown in Figure 5 (left image). The maximum value of the rate $\delta E_T/\delta b$ is $0.2887\,\overline{M}_C/a$, taking place for $b = 0.866a$. The energy rate in the case when the inclusion is tangent to the void ($b = a$) is $0.2778\,\overline{M}_C/a$. Figure 6 shows the variation of the energy E_T and the energy rate $\delta E_T/\delta b$ with the distance d/a in the case of a circular inclusion of radii $b = a$, $b = 3a/4$, and $b = a/2$. In the limit as $d \to \infty$, the energy E_T approaches the value E_T^0 according to (29), while the energy rate $\delta E_T/\delta b$ approaches the value $\frac{1}{2}(b/a)^2$ times $\overline{M}_C/b$, according to (42). Therefore, the greater the distance from the void, the greater the energy E_T associated with the presence of the inclusion, and the greater the rate of energy $\delta E_T/\delta b$ associated with the increase of the inclusion. This suggests that the presence of a nearby free surface facilitates the eigenstrain transformation, which may be of importance for the study of displacive transformations and transformation toughening mechanisms in crystalline metallic materials and ceramics.

If the specific configurational force f is introduced, the rate of total strain energy associated with a uniform expansion of inclusion can be expressed as

$$\frac{\delta E_T}{\delta b} = -\int_0^{2\pi} f(b, \theta) b \, d\theta, \quad f = \left[\tfrac{1}{2}(\sigma_{ij}^{0,\text{in}} + \sigma_{ij}^{0,\text{out}})_{\rho=b} + \hat{\sigma}_{ij}(b, \theta) \right] \epsilon_{ij}^{\bullet}, \tag{43}$$

where $\hat{\sigma}_{ij}(b, \theta)$ are the stress components of the auxiliary problem around the inclusion. This type of expression for f was originally derived by Gavazza [1977]. For the dilatational eigenstrain, (43) reduces to

$$\frac{\delta E_T}{\delta b} = \frac{2\pi \mu b \epsilon^{\bullet 2}}{1 - \nu} - b\epsilon^{\bullet} \int_0^{2\pi} \hat{\sigma}_{kk}(b, \theta) \, d\theta. \tag{44}$$
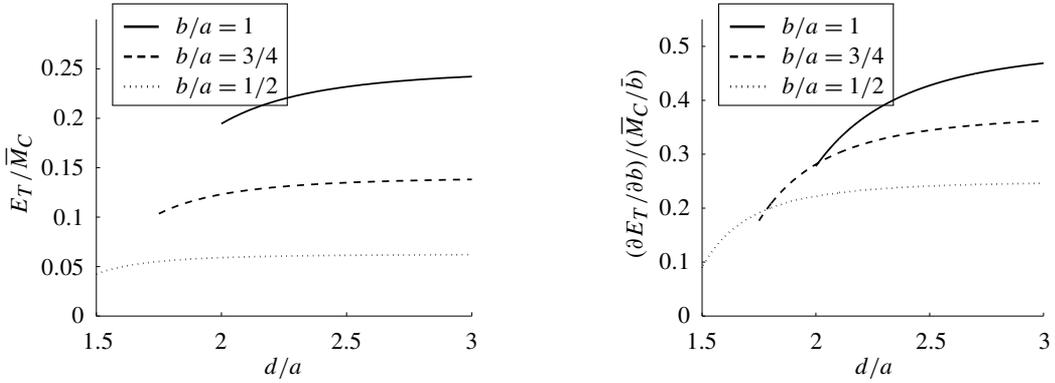
Figure 6. Left: the variation of the strain energy E_T, given by (29) and normalized by $\overline{M}_C$, with the normalized distance d/a, for the three indicated radii of the inclusion. Right: the corresponding variation of $\delta E_T/\delta b$, given by (42) and normalized by $\overline{M}_C/\bar{b}$, where $\bar{b} = a$.

To evaluate $\hat{\sigma}_{kk}(b, \theta)$, one would have to solve the auxiliary boundary-value problem, which was circumvented in the earlier derivation of the rate $\delta E_T/\delta b$. The average normal stress around the inclusion can, however, be determined immediately by comparing (44) with (31):

$$\frac{1}{2\pi} \int_0^{2\pi} \hat{\sigma}_{kk}(b, \theta)\, \mathrm{d}\theta = \frac{4\mu\epsilon^{\bullet 2}}{1 - \nu} \frac{a^2 b^2}{(d^2 - a^2)^2}. \tag{45}$$

7. Circular inclusion in a half-space

Figure 7 (left image) shows a circular inclusion of radius b whose center is at distance c from the free surface ($x = 0$) of a half-space. If the inclusion was given a uniform shear eigenstrain $\epsilon_{xy}^{\bullet}$, the longitudinal stress along the free surface can be calculated from

$$\sigma_y(0, y) = 2[\sigma_y^0(0, y) - \sigma_x^0(0, y)], \tag{46}$$

where the infinite medium stress field outside the inclusion is specified in Section 2. Upon using the stress-transformation formulas between the (ρ, φ) and (x, y) coordinate systems, it follows that

$$\sigma_y(0, y) = -\bar{\sigma}_y c b^2 \left(2 - \frac{3b^2}{c^2 + y^2}\right) \frac{y(c^2 - y^2)}{(c^2 + y^2)^3}, \quad \bar{\sigma}_y = \frac{8\mu\epsilon_{xy}^{\bullet}}{1 - \nu}. \tag{47}$$

The plot of this stress along the y-axis for several values of the ratio c/b is shown in Figure 8.

The configurational force between the inclusion and the free surface of a half-space is determined from

$$J_x^{\text{incl}} = -\int_{-\infty}^{\infty} W(0, y)\, \mathrm{d}y = -\frac{1 - \nu}{4\mu} \int_{-\infty}^{\infty} \sigma_y^2(0, y)\, \mathrm{d}y. \tag{48}$$

Upon the substitution of (47) and integration, (48) becomes

$$J_x^{\text{incl}} = \bar{J}_x \frac{32(c/b)^4 - 72(c/b)^2 + 45}{5(c/b)^7}, \quad \bar{J}_x = -\frac{5\pi\mu}{32(1 - \nu)} b\epsilon_{xy}^{\bullet 2}, \tag{49}$$
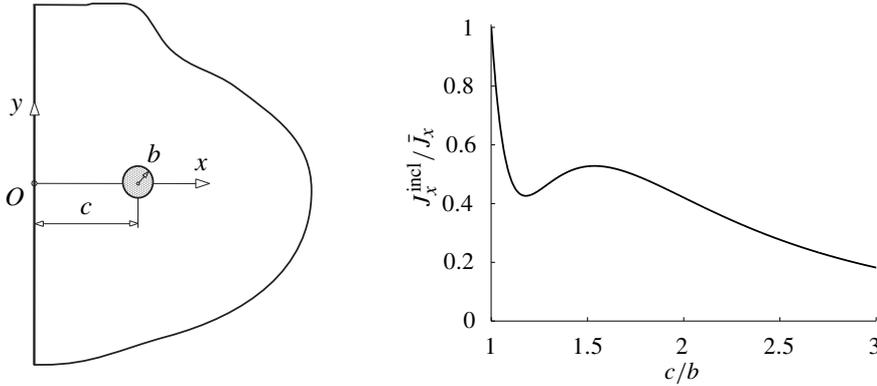
Figure 7. Left: a circular inclusion of radius b with its center at the distance c from the free surface of the half-space. Right: the variation of J_x with c/b. The scaling factor is $\bar{J}_x = -5\pi\mu\epsilon_{xy}^{\bullet}/[32(1-\nu)]$.

where $\bar{J}_x$ is the value of J_x when $c = b$. In the evaluation of integrals, the following recursive relations were used [Gradshteyn and Ryzhik 1965]:

$$\int_0^\infty \frac{y^m\,\mathrm{d}y}{(1+y^2)^n} = \frac{m-1}{2n-m-1}\int_0^\infty \frac{y^{m-2}\,\mathrm{d}y}{(1+y^2)^n}, \quad n > m/2,$$

$$\int_0^\infty \frac{\mathrm{d}y}{(1+y^2)^n} = \frac{2n-3}{2n-2}\int_0^\infty \frac{\mathrm{d}y}{(1+y^2)^{n-1}}, \quad n > 1. \tag{50}$$

The variation of J_x^{incl} with c/b is shown in Figure 7 (right image). For the values of the ratio c/b between 1.1794 and 1.5359 there is a peculiar increase of the force with the increase of c/b, after which the configurational force resumes its expected decay with the increase of c/b. The brief interruption of the force decay in this region with the increase of the ratio c/b is a consequence of the markedly different nature of the stress variation $\sigma_y(0, y)$, corresponding to different values of the ratio c/b, as shown in Figure 8.

8. Conclusion

The J- and M-integrals along the boundary of a circular void, or along the straight edge of a half-space, due to a nearby circular inclusion with uniform dilatational or shear eigenstrain, are evaluated by using the Kienzler–Zhuping formula, without solving the entire boundary value problem at hand. Three types of interactions between inclusion and void are considered. First, the configurational force exerted on the void by the inclusion is determined by means of the J-integral evaluation. This represents the energy release rate associated with an imagined void translation within the material toward the inclusion (by diffusion or otherwise), keeping the position of the inclusion fixed. Second, the energy release rate is evaluated associated with a self-similar expansion of the void (by material absorption over the surface of the void), keeping the position of the inclusion fixed relative to the center of the void. This energy rate is related to the M-integral around the void. Third, the energy rate associated with an isotropic expansion of the inclusion is evaluated and related to the M-integral around the inclusion. The former differs from the
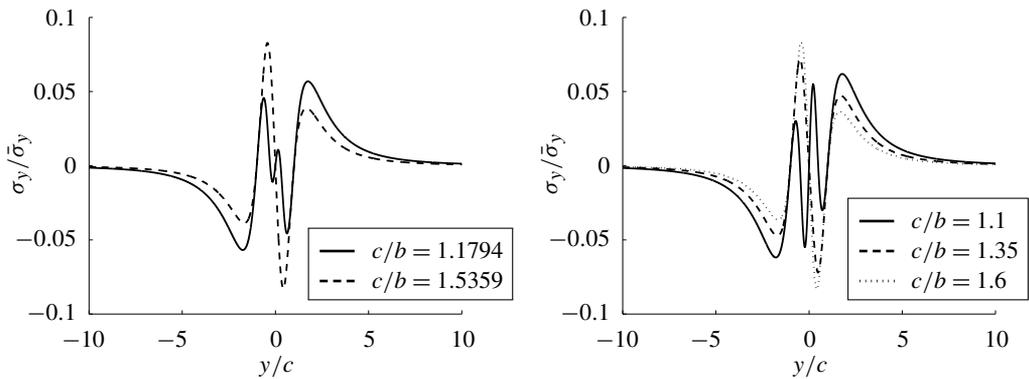
Figure 8. The variation of the stress component $\sigma(0, y)$ along the y-axis for several values of the ratio c/b. The left image is for the values of c/b corresponding to the local minimum and maximum of J_x, and the right image is for three other values of c/b. The utilized scaling factor is $8\mu\epsilon_{xy}^{\bullet}/(1 - \nu)$. The values of the ratio c/b at which the configurational force has a local maximum and minimum are the roots of $(c/b)^2 = (15 \pm \sqrt{15})/8$. The corresponding force values are $0.5280\bar{J}_x$ and $0.4262\bar{J}_x$.

latter. The relationship between the two quantities is derived and discussed. It is shown that the greater the distance from the void, the greater the energy associated with the presence of the inclusion and the energy rate associated with its growth. This suggests that the presence of a nearby free surface facilitates the eigenstrain transformation, which may be of importance for the study of displacive transformations and transformation toughening mechanisms in crystalline metallic materials and ceramics. The attraction exerted on a circular inclusion with a uniform shear eigenstrain by the free surface of a half-space is also evaluated. Peculiar variation of this configurational force with the distance between the inclusion and the free surface is noted and discussed.

Acknowledgements

References

[Budiansky and Rice 1973] B. Budiansky and J. R. Rice, "Conservation laws and energy-release rates", *J. Appl. Mech.* (*ASME*) **40** (1973), 201–203.

[Bui 1973] H. D. Bui, "Dualité entre les intégrales indépendantes du contour dans la théorie des solides fissurés", *C. R. Acad. Sci. Paris A* **276** (1973), 1425–1428.

[Bui 1974] H. D. Bui, "Dual path independent integrals in the boundary-value problems of cracks", *Eng. Fract. Mech.* **6** (1974), 287–296.

[Eshelby 1956] J. D. Eshelby, "The continuum theory of lattice defects", pp. 79–144 in *Solid State Physics* **3**, edited by F. Seitz and D. Turnbull, Academic Press, New York, 1956.

[Eshelby 1957] J. D. Eshelby, "The determination of the elastic field of an ellipsoidal inclusion, and related problems", *Proc. R. Soc. Lond. A* **241** (1957), 376–396.

[Eshelby 1959] J. D. Eshelby, "The elastic field outside an ellipsoidal inclusion", *Proc. R. Soc. Lond. A* **6252** (1959), 561–569.

[Eshelby 1975] J. D. Eshelby, "The calculation of energy release rates", pp. 69–84 in *Prospects of fracture mechanics* (Delft, 1974), edited by G. C. Sih et al., Noordhoff, Leyden, 1975.

[Freund 1978] L. B. Freund, "Stress intensity factor calculations based on a conservation integral", *Int. J. Solids Struct.* **14** (1978), 241–250.

[Gavazza 1977] S. D. Gavazza, "Forces on pure inclusions and Somigliana dislocations", *Scr. Metall.* **11**:11 (1977), 979–981.

[Gradshteyn and Ryzhik 1965] I. S. Gradshteyn and I. M. Ryzhik, *Table of integrals, series, and products*, Academic Press, New York, 1965. 8th ed. edited by D. Zwillinger, Elsevier, Amsterdam, 2014.

[Honein and Herrmann 1988] T. Honein and G. Herrmann, "The involution correspondence in plane elastostatics for regions bounded by a circle", *J. Appl. Mech.* (*ASME*) **55**:3 (1988), 566–573.

[Honein and Herrmann 1990] T. Honein and G. Herrmann, "On bonded inclusions with circular or straight boundaries in plane elastostatics", *J. Appl. Mech.* (*ASME*) **57** (1990), 850–856.

[Kienzler and Kordisch 1990] R. Kienzler and H. Kordisch, "Calculation of J_1 and J_2 using the L and M integrals", *Int. J. Fract.* **43**:3 (1990), 213–225.

[Kienzler and Zhuping 1987] R. Kienzler and D. Zhuping, "On the distribution of hoop stresses around circular holes in elastic sheets", *J. Appl. Mech.* (*ASME*) **54**:1 (1987), 110–114.

[Knowles and Sternberg 1972] J. K. Knowles and E. Sternberg, "On a class of conservation laws in linearized and finite elastostatics", *Arch. Ration. Mech. Anal.* **44**:3 (1972), 187–211.

[Lin et al. 1990] W.-W. Lin, T. Honein, and G. Herrmann, "A novel method of stress analysis of elastic materials with damage zones", pp. 609–615 in *Yielding, damage, and failure of anisotropic solids*, edited by J. P. Boehler, EGF Publications **5**, Mechanical Engineering Publications, London, 1990.

[Lubarda 1998] V. A. Lubarda, "Sliding and bonded circular inclusions in concentric cylinders", *Proc. Monten. Acad. Sci. Arts* **12** (1998), 123–139.

[Lubarda 2012] V. A. Lubarda, "Dual Eshelby stress tensors and related integrals in micropolar elasticity with body forces and couples", *Eur. J. Mech. A Solids* **36** (2012), 9–17.

[Lubarda 2015] V. A. Lubarda, "Circular inclusion near a circular void: determination of elastic antiplane shear fields and configurational forces", *Acta Mech.* **226**:3 (2015), 643–664.

[Lubarda and Markenscoff 1999] V. A. Lubarda and X. Markenscoff, "Energies of circular inclusions: sliding versus bonded interfaces", *Proc. R. Soc. Lond. A* **455**:1983 (1999), 961–974.

[Lubarda and Markenscoff 2007] V. A. Lubarda and X. Markenscoff, "Dual conservation integrals and energy release rates", *Int. J. Solids Struct.* **44** (2007), 4079–4091.

[Markenscoff and Ni 2010] X. Markenscoff and L. Ni, "The energy-release rate and "self-force" of dynamically expanding spherical and plane inclusion boundaries with dilatational eigenstrain", *J. Mech. Phys. Solids* **58**:1 (2010), 1–11.

[Markenscoff and Ni 2011] X. Markenscoff and L. Ni, "'Driving forces' and radiated fields for expanding/shrinking half-space and strip inclusions with general eigenstrain", *Quart. Appl. Math.* **69**:3 (2011), 529–548.

[Mura 1987] T. Mura, *Micromechanics of defects in solids*, 2nd ed., Mechanics of Elastics and Inelastic Solids **3**, Kluwer, Dordrecht, 1987.

[Rice 1985] J. R. Rice, "Conserved integrals and energetic forces", pp. 33–56 in *Fundamentals of deformation and fracture: Eshelby Memorial Symposium* (Sheffield, 1984), edited by B. A. Bilby et al., Cambridge University Press, 1985.

[Zhou et al. 2013] K. Zhou, H. J. Hoh, X. Wang, L. M. Keer, J. H. L. Pang, B. Song, and Q. J. Wang, "A review of recent works on inclusions", *Mech. Mater.* **60** (2013), 144–158.

VLADO A. LUBARDA: vlubarda@ucsd.edu
Departments of NanoEngineering and Mechanical and Aerospace Engineering, University of California, San Diego, 9500 Gilman Drive, La Jolla, CA 92093-0411, United States

msp

DYNAMIC CONSERVATION INTEGRALS AS DISSIPATIVE MECHANISMS IN THE EVOLUTION OF INHOMOGENEITIES

XANTHIPPI MARKENSCOFF AND SHAILENDRA PAL VEER SINGH

By the application of Noether's theorem, conservation laws in linear elastodynamics are derived by invariance of the Lagrangian functional under a class of infinitesimal transformations. The recent work of Gupta and Markenscoff (2012) providing a physical meaning to the dynamic J-integral as the variation of the Hamiltonian of the system due to an infinitesimal translation of the inhomogeneity if linear momentum is conserved in the domain, is extended here to the dynamic M- and L-integrals in terms of the "if" conditions. The variation of the Lagrangian is shown to be equal to the negative of the variation of the Hamiltonian under the above transformations for inhomogeneities, which provides a physical meaning to the dynamic J-, L- and M-integrals as dissipative mechanisms in elastodynamics. We prove that if linear momentum is conserved in the domain, then the total energy loss of the system per unit scaling under the infinitesimal scaling transformation of the inhomogeneity is equal to the dynamic M-integral, and if linear and angular momenta are conserved then the total energy loss of the system per unit rotation under the infinitesimal rotational transformation is equal to the dynamic L-integral.

1. Introduction

Conservation laws can be expressed as dissipative mechanisms related to the variation of the energy of the system due to infinitesimal configurational variations in the inhomogeneities. Eshelby [1951] used the energy momentum tensor to define the *force on an elastic singularity* as a variation of the total energy of the body due to the infinitesimal displacement of the defect. Furthermore, he provided additional insights by extending this idea in a series of papers [Eshelby 1956; 1970; 1975] through his ingenious cutting and rewelding thought experiment. Rice [1968] independently discovered the two-dimensional path-independent J-integral for a crack. Günther [1962] and Knowles and Sternberg [1972] derived two additional nontrivial conservation laws (M- and L-integrals) by applying Noether's theorem [Noether 1918] in linear elastostatics. Rice and Drucker [1967] calculated the energy changes during the growth of voids and cracks. Budiansky and Rice [1973] interpreted these new laws as energy release rates associated with the expansion and the rotation rates of a cavity or a crack. Rice [1985] provided further applications of these integrals to the defects.

Fletcher [1976] extended the application of Noether's theorem to derive the conservation laws in linear elastodynamics, and established the completeness of the corresponding conservation laws under a certain group of the infinitesimal transformations. Hermann [1981; 1982] presented a unified formulation to recover the conservations laws by employing different vector calculus operations on the Lagrangian

density. Eischen and Herrmann [1987] extended this formulation to account for material inhomogeneity temperature gradients, anisotropy, and body forces. Herrmann and Kienzler [1999] represented these balance laws of continuum mechanics by 4×4 tensors.

Markenscoff [2006] expressed the conservation integrals as a variation of the total energy of the system by extending Eshelby's thought experiment to elastodynamics. In elastostatics, Gupta and Markenscoff [2008] showed that the total energy dissipation due to material translation of the inhomogeneity equals the configurational force (J-integral) times the infinitesimal displacement of the inhomogeneity, if and only if equilibrium is preserved in the domain. They extended the proof to elastodynamics [Gupta and Markenscoff 2012], where the variation of the Lagrangian or the Hamiltonian is equal to the dynamic J-integral if and only if the linear momentum is conserved in the domain.

In elastodynamics, Fletcher [1976] proved that the Lagrangian functional was invariant under a certain group of infinitesimal transformations; Kienzler and Herrmann [2000, p. 66] also have a detailed proof for elastostatics, which we extend to elastodynamics. We impose the scaling transformation to derive the M-integral, and for infinitesimal rotational transformation we derive the dynamic L-integral. Furthermore, we also relate the variation of the Lagrangian to the variation of the Hamiltonian for scaling and rotation of the inhomogeneity. This allows us to give an energy dissipative meaning to the above "if" statements and to the dynamic J-, L-, and M-integrals as dissipated energy by mechanisms not considered in elasticity theory [Eshelby 1951, p. 108].

2. Mathematical framework

We briefly present the mathematical framework of the derivation of the conservation integrals from Noether's theorem in linear elastodynamics.

Consider the Lagrangian functional [Gelfand et al. 2000; Fletcher 1976]

$$\Pi^{\mathscr{L}} = \int_R \mathscr{L}(x_\alpha, u_i, u_{i_{x_\alpha}}) \, dx_1 \, dx_2 \, dx_3 \, dx_4, \quad i = 1, 2, 3, \ \alpha = 1, 2, 3, 4, \tag{1}$$

where R is the region of integration. In elastodynamics, the independent variables are the material coordinates x_1, x_2, x_3 and x_4 is the time variable, and the dependent variable u_i is the displacement field. For the infinitesimal transformations on the independent and the dependent variables,

$$x_\alpha^* = x_\alpha + \epsilon \phi_\alpha(x_\beta, u_i, u_{i,\beta}) + O(\epsilon^2), \quad i = 1, 2, 3, \ \alpha, \beta = 1, 2, 3, 4, \tag{2a}$$

$$u_j^* = u_j + \epsilon \psi_j(x_\beta, u_i, u_{i,\beta}) + O(\epsilon^2), \quad i, j = 1, 2, 3, \ \beta = 1, 2, 3, 4, \tag{2b}$$

where ϵ is the infinitesimal transformation parameter. The variation of the functional (1) is written as

$$\delta \Pi^{\mathscr{L}} = \int_{R^*} \mathscr{L}(x_\alpha^*, u_i^*, u_{i_{x_\alpha^*}}^*) \, dx_1^* \, dx_2^* \, dx_3^* \, dx_4^* - \int_R \mathscr{L}(x_\alpha, u_i, u_{i_{x_\alpha}}) \, dx_1 \, dx_2 \, dx_3 \, dx_4, \tag{3}$$

where R^* is a new region of integration. In view of equations (2a)–(2b), Equation (3) can be further written as [Gelfand et al. 2000, p. 176]

$$\delta \Pi^{\mathscr{L}} = \int_R \left\{ \frac{\partial \mathscr{L}}{\partial u_j} - \frac{\partial}{\partial x_\alpha} \frac{\partial \mathscr{L}}{\partial u_{j,\alpha}} \right\} \overline{\delta u_j} \, dx_1 \, dx_2 \, dx_3 \, dx_4 + \int_R \frac{\partial}{\partial x_\alpha} \left\{ \frac{\partial \mathscr{L}}{\partial u_{j,\alpha}} \overline{\delta u_j} + \mathscr{L} \delta x_\alpha \right\} dx_1 \, dx_2 \, dx_3 \, dx_4, \tag{4}$$

where (see also [Gelfand et al. 2000, Figure 10, p. 171])

$$\delta u_j = u_j^*(x_\alpha^*) - u_j(x_\alpha) = \{u_j^*(x_\alpha^*) - u_j^*(x_\alpha)\} + \{u_j^*(x_\alpha) - u_j(x_\alpha)\} \approx \frac{\partial u_j^*}{\partial x_\alpha}\delta x_\alpha + \overline{\delta u_j} \approx \frac{\partial u_j}{\partial x_\alpha}\delta x_\alpha + \overline{\delta u_j} \quad (5)$$

or

$$\overline{\delta u_j} = \delta u_j - u_{j,\alpha}\delta x_\alpha. \tag{6}$$

Furthermore, in terms of the transformations ϕ_α and ψ_j, (4) becomes

$$\delta\Pi^{\mathscr{L}} = \epsilon\int_R\left\{\frac{\partial\mathscr{L}}{\partial u_j} - \frac{\partial}{\partial x_\alpha}\frac{\partial\mathscr{L}}{\partial u_{j,\alpha}}\right\}\overline{\psi}_j\,dx_1\,dx_2\,dx_3\,dx_4 + \epsilon\int_R\frac{\partial}{\partial x_\alpha}\left\{\frac{\partial\mathscr{L}}{\partial u_{j,\alpha}}\overline{\psi}_j + \mathscr{L}\phi_\alpha\right\}dx_1\,dx_2\,dx_3\,dx_4, \tag{7}$$

where, from relation (6),

$$\overline{\psi}_j = \psi_j - u_{j,\alpha}\phi_\alpha. \tag{8}$$

Note that, above and in the sequel, the partial derivatives with respect to x_i and t, for any $A(x_j, u_j, \dot{u}_j, u_{j,k})$, are defined as

$$\frac{\partial(A)}{\partial x_i} = \frac{\partial(A)}{\partial x_i}\bigg|_{\exp} + \frac{\partial(A)}{\partial u_l}u_{l,i} + \frac{\partial(A)}{\partial\dot{u}_l}\dot{u}_{l,i} + \frac{\partial(A)}{\partial u_{l,m}}u_{l,mi} \tag{9a}$$

and

$$\frac{\partial(A)}{\partial t} = \frac{\partial(A)}{\partial t}\bigg|_{\exp} + \frac{\partial(A)}{\partial u_l}\dot{u}_l + \frac{\partial(A)}{\partial\dot{u}_l}\ddot{u}_l + \frac{\partial(A)}{\partial u_{l,m}}\dot{u}_{l,m}. \tag{9b}$$

Under the infinitesimal transformations (2a)–(2b), the functional $\Pi^{\mathscr{L}}$ is said to be invariant at $\boldsymbol{u}$ if

$$\delta\Pi^{\mathscr{L}} = 0. \tag{10}$$

Furthermore, if $\boldsymbol{u}$ satisfies the Euler–Lagrange equations [Gelfand et al. 2000]

$$\frac{\partial\mathscr{L}}{\partial u_j} - \frac{\partial}{\partial x_\alpha}\frac{\partial\mathscr{L}}{\partial u_{j,\alpha}} = 0, \tag{11}$$

then the first term in (7) vanishes, and it yields

$$\int_R\frac{\partial}{\partial x_\alpha}\left\{\frac{\partial\mathscr{L}}{\partial u_{j,\alpha}}\overline{\psi}_j + \mathscr{L}\phi_\alpha\right\}dx_1\,dx_2\,dx_3\,dx_4 = 0. \tag{12}$$

Let Ω be a region in three-dimensional space occupied by a linearly elastic solid, undergoing small deformations and containing an inhomogeneity which is a surface of discontinuity in the strain and velocity. Let $u_j(x_i, t)$ denote the displacement, ε_{ij} the small strains, C_{ijkl} the components of the elasticity tensor, ρ the density — which in linear elasticity is assumed constant, independent of time — and $(\cdot)$ the time derivative, and denote the Cauchy stress by $\sigma_{ij} = C_{ijkl}\varepsilon_{kl}$. The Lagrange density is defined as

$$\mathscr{L} = T - W \tag{13}$$

where the strain energy density is

$$W = \tfrac{1}{2}C_{ijkl}\varepsilon_{ij}\varepsilon_{kl} = \tfrac{1}{2}C_{ijkl}u_{i,j}u_{k,l}, \tag{14}$$

and the specific kinetic energy is

$$T = \tfrac{1}{2}\rho\dot{u}_i\dot{u}_i. \tag{15}$$

We write the total Lagrangian functional for $\Omega \subset \mathbb{R}^3$ and $[0, t] \subset \mathbb{R}$, and assume further $\mathscr{L} \in \mathscr{C}^\infty$, so that $\mathscr{L}$ possesses continuous partial derivatives of all orders with respect to the element of its matrix arguments on its domain of definition:

$$\Pi^{\mathscr{L}}(u_{i,j}, \dot{u}_i) = \int_0^t \int_\Omega \mathscr{L}(u_{i,j}, \dot{u}_i)\, dV\, dt = \int_0^t \int_\Omega \{T(\dot{u}_i) - W(u_{i,j})\}\, dV\, dt. \tag{16}$$

For $\mathscr{L} = T - W$, the Euler–Lagrange equations (11) give

$$\frac{\partial \sigma_{ij}}{\partial x_i} - \frac{\partial(\rho \dot{u}_j)}{\partial t} = 0, \tag{17}$$

which represents the conservation of the linear momentum. If the Euler–Lagrange equations (11) are satisfied, then (12) should be satisfied in order for the Lagrangian functional $\Pi^{\mathscr{L}}$ to be invariant under the transformations (2a)–(2b). This will give the equations to derive the families ϕ_α and ψ_j of infinitesimal transformations.

Equation (12) is expanded in space and time variables as

$$\int_0^t \int_\Omega \left[\frac{\partial}{\partial x_i} \left\{ \frac{\partial \mathscr{L}}{\partial u_{j,i}} \overline{\psi}_j + \mathscr{L}\phi_i \right\} + \frac{\partial}{\partial t} \left\{ \frac{\partial \mathscr{L}}{\partial \dot{u}_j} \overline{\psi}_j + \mathscr{L}\phi_4 \right\} \right] dV\, dt = 0. \tag{18}$$

Using (13), (18) is written

$$\int_0^t \int_\Omega \left[\frac{\partial}{\partial x_i} \{-\sigma_{ij}\overline{\psi}_j + \mathscr{L}\phi_i\} + \frac{\partial}{\partial t}\{\rho \dot{u}_j \overline{\psi}_j + \mathscr{L}\phi_4\} \right] dV\, dt = 0. \tag{19}$$

The above relation applied to infinitesimal transformations given by equations (2a)–(2b) provides the corresponding conservation laws for translation, scaling and rotation of the inhomogeneities (under which the Lagrangian remains invariant), which are additional field equations and are derived in the following section.

3. Family of infinitesimal transformations and dynamic conservation laws

In this section we extend the work of Kienzler and Herrmann [2000, p. 66] to elastodynamics in order to obtain the family of infinite transformations under which the Lagrangian remains invariant. In this section, for the sake of notational simplicity, we define and use

$$\frac{d}{dx_i} \equiv \frac{\partial}{\partial x_i}, \tag{20a}$$

$$\frac{d}{dt} \equiv \frac{\partial}{\partial t}, \tag{20b}$$

where the partial derivatives with respect to x_i and t are taken as in equations (9a)–(9b), respectively.

Equation (19) is true for any arbitrary volume Ω and any arbitrary time interval, so we can write

$$\frac{d}{dx_i}\{-\sigma_{ij}\overline{\psi}_j + \mathscr{L}\phi_i\} + \frac{d}{dt}\{\rho \dot{u}_j \overline{\psi}_j + \mathscr{L}\phi_4\} = 0. \tag{21}$$

Next, using $\overline{\psi}_j$ from (8), expanded in space and time variables $\overline{\psi}_j = \psi_j - u_{j,l}\phi_l - \dot{u}_j\phi_4$, we rewrite (21) as

$$\frac{d}{dx_i}\{-\sigma_{ij}(\psi_j - u_{j,l}\phi_l - \dot{u}_j\phi_4) + \mathcal{L}\phi_i\} + \frac{d}{dt}\{\rho\dot{u}_j(\psi_j - u_{j,l}\phi_l - \dot{u}_j\phi_4) + \mathcal{L}\phi_4\} = 0, \qquad (22)$$

and we employ linear momentum balance to obtain

$$-\sigma_{ij}\frac{d}{dx_i}(\psi_j - u_{j,l}\phi_l - \dot{u}_j\phi_4) + \frac{d}{dx_i}(\mathcal{L}\phi_l)\delta_{il} + \rho\dot{u}_j\frac{d}{dt}(\psi_j - u_{j,l}\phi_l - \dot{u}_j\phi_4) + \frac{d}{dt}(\mathcal{L}\phi_4) = 0. \qquad (23)$$

Differentiating explicitly the terms on the left-hand side of (23) with the derivatives

$$\frac{d\mathcal{L}}{dx_i} = \frac{\partial\mathcal{L}}{\partial x_i} + \frac{\partial\mathcal{L}}{\partial u_{k,j}}\frac{\partial u_{k,j}}{\partial x_i} + \frac{\partial\mathcal{L}}{\partial\dot{u}_k}\frac{\partial\dot{u}_k}{\partial x_i} = -\sigma_{jk}u_{k,ji} + \rho\dot{u}_k\dot{u}_{k,i}, \qquad (24a)$$

$$\frac{d\mathcal{L}}{dt} = \frac{\partial\mathcal{L}}{\partial t} + \frac{\partial\mathcal{L}}{\partial u_{k,j}}\frac{\partial u_{k,j}}{\partial t} + \frac{\partial\mathcal{L}}{\partial\dot{u}_k}\frac{\partial\dot{u}_k}{\partial t} = -\sigma_{jk}\dot{u}_{k,j} + \rho\dot{u}_k\ddot{u}_k, \qquad (24b)$$

$$\frac{d\phi_j}{dx_i} = \frac{\partial\phi_j}{\partial x_i} + \frac{\partial\phi_j}{\partial u_k}u_{k,i}, \qquad \frac{d\phi_4}{dx_i} = \frac{\partial\phi_4}{\partial x_i} + \frac{\partial\phi_4}{\partial u_k}u_{k,i}, \qquad (24c)$$

$$\frac{d\phi_j}{dt} = \frac{\partial\phi_j}{\partial t} + \frac{\partial\phi_j}{\partial u_k}\dot{u}_k, \qquad \frac{d\phi_4}{dt} = \frac{\partial\phi_4}{\partial t} + \frac{\partial\phi_4}{\partial u_k}\dot{u}_k, \qquad (24d)$$

$$\frac{d\psi_j}{dx_i} = \frac{\partial\psi_j}{\partial x_i} + \frac{\partial\psi_j}{\partial u_k}u_{k,i} \qquad \frac{d\psi_j}{dt} = \frac{\partial\psi_j}{\partial t} + \frac{\partial\psi_j}{\partial u_k}\dot{u}_k. \qquad (24e)$$

Therefore, (23) becomes

$$-\sigma_{ij}\left(\frac{\partial\psi_j}{\partial x_i} + \frac{\partial\psi_j}{\partial u_k}u_{k,i}\right) + \sigma_{ij}u_{j,l}\left(\frac{\partial\phi_l}{\partial x_i} + \frac{\partial\phi_l}{\partial u_k}u_{k,i}\right) + \phi_l\sigma_{ij}u_{j,li} + \sigma_{ij}\dot{u}_j\left(\frac{\partial\phi_4}{\partial x_i} + \frac{\partial\phi_4}{\partial u_k}u_{k,i}\right)$$

$$+ \phi_4\sigma_{ij}\dot{u}_{j,i} + \mathcal{L}\left(\frac{\partial\phi_l}{\partial x_i} + \frac{\partial\phi_l}{\partial u_k}u_{k,i}\right)\delta_{il} + \phi_l\delta_{il}(-\sigma_{jk}u_{k,ji} + \rho\dot{u}_k\dot{u}_{k,i}) + \rho\dot{u}_j\left(\frac{\partial\psi_j}{\partial t} + \frac{\partial\psi_j}{\partial u_k}\dot{u}_k\right)$$

$$- \rho\dot{u}_ju_{j,l}\left(\frac{\partial\phi_l}{\partial t} + \frac{\partial\phi_l}{\partial u_k}\dot{u}_k\right) - \phi_l\rho\dot{u}_j\dot{u}_{j,l} - \rho\dot{u}_j\dot{u}_j\left(\frac{\partial\phi_4}{\partial t} + \frac{\partial\phi_4}{\partial u_k}\dot{u}_k\right) - \phi_4\rho\dot{u}_j\ddot{u}_j$$

$$+ \mathcal{L}\left(\frac{\partial\phi_4}{\partial t} + \frac{\partial\phi_4}{\partial u_k}\dot{u}_k\right) + \phi_4(-\sigma_{jk}\dot{u}_{k,j} + \rho\dot{u}_k\ddot{u}_k) = 0. \qquad (25)$$

Rearranging this equation as in [Kienzler and Herrmann 2000, p. 64] leads to

$$0 = \frac{\partial\phi_l}{\partial u_k}[\sigma_{ij}u_{j,l}u_{k,l} - Wu_{k,i}\delta_{il}] \qquad\qquad [\sim u_{i,l}^3] \qquad (26a)$$

$$+ \frac{\partial\phi_l}{\partial u_k}[Tu_{k,i}\delta_{il} - \rho\dot{u}_j\dot{u}_ku_{j,l}] \qquad\qquad [\sim u_{j,l}\dot{u}_k^2] \qquad (26b)$$

$$+ \frac{\partial\phi_4}{\partial u_k}[\sigma_{ij}\dot{u}_ju_{k,l} - W\dot{u}_k] \qquad\qquad [\sim u_{i,j}^2\dot{u}_k] \qquad (26c)$$

$$+ \frac{\partial\phi_4}{\partial u_k}[T\dot{u}_k - \rho\dot{u}_j\dot{u}_j\dot{u}_k] \qquad\qquad [\sim \dot{u}_k^3] \qquad (26d)$$

$$+ \frac{\partial\psi_j}{\partial u_k}[-u_{k,i}\sigma_{ij}] + \frac{\partial\phi_l}{\partial x_i}[\sigma_{ij}u_{j,l} - W\delta_{il}] + \frac{\partial\phi_4}{\partial t}[-W] \qquad [\sim u_{j,k}^2] \qquad (26e)$$

$$+ \frac{\partial \psi_j}{\partial u_k}[\rho \dot{u}_j \dot{u}_k] + \frac{\partial \phi_l}{\partial x_i}[T \delta_{il}] + \frac{\partial \phi_4}{\partial t}[-\rho \dot{u}_j \dot{u}_j + T] \qquad [\sim \dot{u}_k^2] \qquad (26f)$$

$$+ \frac{\partial \phi_l}{\partial t}[-\rho \dot{u}_j u_{j,l}] + \frac{\partial \phi_4}{\partial x_i}[\sigma_{ij} \dot{u}_j] \qquad [\sim u_{j,l} \dot{u}_j] \qquad (26g)$$

$$+ \frac{\partial \psi_j}{\partial x_i}[\sigma_{ij}] \qquad [\sim u_{i,j}] \qquad (26h)$$

$$+ \frac{\partial \psi_j}{\partial t}[-\rho \dot{u}_j]. \qquad [\sim \dot{u}_j] \qquad (26i)$$

Setting all the coefficients equal to zero leads to the requirement that the functions ϕ_l, ϕ_4 and ψ_j satisfy an overdetermined system of linear differential equations.

From (26a) it follows that ϕ_l must not be a function of u_j. Thus,

$$\phi_l = \phi_l(x_k, t); \qquad (27)$$

with this, part (26b) is also satisfied. From (26c) it follows that ϕ_4 must not be a function of u_k. Thus,

$$\phi_4 = \phi_4(x_k, t); \qquad (28)$$

with this, part (26d) is also satisfied. From (26i) it follows that ψ_j must not be a function of t. Thus,

$$\psi_j = \psi_j(x_k, u_l). \qquad (29)$$

Using relations (27)–(29), from (26e) or (26f) it follows that

$$\frac{\partial \psi_j}{\partial u_k} = h_{jk}(x_l), \qquad (30)$$

that is,

$$\psi_j = h_{jk}(x_l)u_k + g_j(x_l). \qquad (31)$$

From (26h) it follows that the functions $h_{jk}(x_l)$ are actually constants, and, due to the symmetry of the stress tensor, the terms $\partial g_j / \partial x_i$ form a skew-symmetric constant matrix. Thus,

$$\psi_j = \alpha_{jk}u_k + \Omega_k \varepsilon_{kil} x_i + r_j. \qquad (32)$$

Because $\partial \psi_j / \partial u_k$ is matrix of constant coefficients, from (26e) or (26f), we further conclude that ϕ_l must not be a function of t as well; thus,

$$\phi_l = \phi_l(x_k); \qquad (33)$$

furthermore, ϕ_4 must not be a function of x_i as well; thus,

$$\phi_4 = \phi_4(t). \qquad (34)$$

With this, (26g) is also satisfied. Therefore, we can write

$$\psi_j = \alpha_{jk}u_k + \Omega_k \varepsilon_{kil} x_i + r_j, \qquad (35a)$$

$$\phi_j = \beta_{jk}x_k + a_j, \qquad (35b)$$

$$\phi_4 = l_0 t + t_0. \qquad (35c)$$

Now we split the constant matrices α_{ij} and β_{ij} into symmetric and antisymmetric parts and, further, the symmetric parts into spherical and deviatoric parts, as follows:

$$\beta_{ji} = l\delta_{ij} + \beta'_{ji} + m_n\varepsilon_{nij}, \tag{36a}$$

$$\alpha_{jk} = l\gamma\delta_{kj} + \alpha'_{jk} + \omega_n\varepsilon_{nkj}, \tag{36b}$$

with l, γ, m_n, ω_n, β'_{ji}, α'_{jk} being constant parameters or matrices of constant coefficients, satisfying

$$\beta'_{ji} = \beta'_{ij}, \quad \alpha'_{jk} = \alpha'_{kj}, \quad \beta'_{jj} = \alpha'_{jj} = 0. \tag{37}$$

With this, using (26e) and (26f) we obtain

$$(l\gamma\delta_{kj} + \alpha'_{jk} + \omega_n\varepsilon_{nkj})[-u_{k,i}\sigma_{ij} + \rho\dot{u}_j\dot{u}_k] + (l\delta_{il} + \beta'_{li} + m_n\varepsilon_{nil})[\sigma_{ij}u_{j,l} + \mathscr{L}\delta_{il}] + l_0[-\rho\dot{u}_j\dot{u}_j + \mathscr{L}] = 0; \tag{38}$$

after rearranging, we can write

$$l(-\gamma\delta_{kj}u_{k,i}\sigma_{ij} + \gamma\delta_{kj}\rho\dot{u}_j\dot{u}_k + \delta_{il}\sigma_{ij}u_{j,l} + \delta_{il}\mathscr{L}\delta_{il}) + l_0(-2T + \mathscr{L}) + \omega_n\varepsilon_{nkj}(-u_{k,i}\sigma_{ij} + \rho\dot{u}_j\dot{u}_k)$$
$$+ m_n\varepsilon_{nil}(\sigma_{ij}u_{j,l} + \mathscr{L}\delta_{il}) + \alpha'_{jk}(-u_{k,i}\sigma_{ij} + \rho\dot{u}_j\dot{u}_k) + \beta'_{il}(\sigma_{ij}u_{j,l} + \mathscr{L}\delta_{il}) = 0, \tag{39}$$

and we further simplify to write

$$l[-\gamma 2W + \gamma 2T + 2W + n(T - W)] + l_0(-2T + \mathscr{L}) \tag{40a}$$

$$+ \varepsilon_{npq}\sigma_{ip}(\omega_n u_{q,i} + m_n u_{i,q}) \tag{40b}$$

$$+ (\beta'_{il}\sigma_{ij}u_{j,l} - \alpha'_{jk}u_{k,i}\sigma_{ij}) + \alpha'_{jk}\rho\dot{u}_j\dot{u}_k = 0, \tag{40c}$$

where $n = \delta_{ii}$ is the number of space dimensions. If $l_0 = l$, then, for the first term (40a) to vanish, we have

$$-2\gamma W + 2\gamma T + 2W + n(T - W) - 2T + T - W = 0 \quad \Longrightarrow \quad \gamma = \tfrac{1}{2}(1 - n), \tag{41}$$

and the second term (40b) vanishes if

$$m_n = \omega_n, \tag{42}$$

provided that the material is isotropic, i.e., $\varepsilon_{npq}\sigma_{ip}[u_{q,i} + u_{i,q}] = 0$ [Eshelby 1975]. The third term (40c) vanishes only if $\alpha'_{jk} = \beta'_{il} = 0$, which means that

$$\beta_{ji} = l\delta_{ij} + \omega_n\varepsilon_{nij}, \quad \alpha_{ji} = \tfrac{1}{2}l(1 - n)\delta_{ij} + \omega_n\varepsilon_{nij} \quad \text{and} \quad \phi_4 = lt + t_0. \tag{43}$$

Hence, we state the suitable infinitesimal transformations

$$\phi_j = \omega_n\varepsilon_{nij}x_i + lx_j + a_j, \tag{44a}$$

$$\phi_4 = lt + t_0, \tag{44b}$$

$$\psi_j = \omega_n\varepsilon_{nij}u_i + \tfrac{1}{2}l(1 - n)u_j + \Omega_n\varepsilon_{nij}x_i + r_j, \tag{44c}$$

or

$$x_j^* = x_j + \epsilon(\omega_n\varepsilon_{nij}x_i + lx_j + a_j), \tag{45a}$$

$$t^* = t + \epsilon(lt + t_0), \tag{45b}$$

$$u_j^* = u_j + \epsilon\left(\omega_n\varepsilon_{nij}u_i + \tfrac{1}{2}l(1 - n)u_j + \Omega_n\varepsilon_{nij}x_i + r_j\right), \tag{45c}$$

where l, t_0 are constant parameters and ω_n, a_j, Ω_n, r_j are vectors with constant components. The vectors r_j and Ω_n describe a rigid-body translation and rotation, respectively, while a_j and ω_n describe material translation (coordinate translation) and material rotation (coordinate rotation), respectively, and the parameter l represents the scaling. The above family of transformations agrees with [Fletcher 1976] in three dimensions ($n = 3$). Applying the transformations indicated by equations (45a)–(45c) for the material translation, scaling and rotation separately to (19), the conservation laws for elastodynamics are derived in the following subsections.

3.1. *Invariance of the Lagrangian under translation.* For the infinitesimal translation of the material, we utilize the transformation [Fletcher 1976] such that the new coordinates are $x_i^* = x_i + \epsilon a_i$ and the new time and displacement field remain invariant ($t^* = t$, $u_i^* = u_i$), where ϵa_i is the infinitesimal translation. After comparing the transformation with equations (45) and (44), we have

$$\phi_i = a_i, \quad \phi_4 = 0, \quad \text{and} \quad \psi_j = 0; \tag{46}$$

therefore, from (8),

$$\overline{\psi}_j = -u_{j,k} a_k. \tag{47}$$

Inserting the above transformation in (19) to obtain the conservation law for translation, we obtain

$$\int_0^t \int_\Omega \left[\frac{\partial}{\partial x_i} \{ (\mathscr{L} \delta_{ik} + \sigma_{ij} u_{j,k}) a_k \} - \frac{\partial}{\partial t} \{ \rho \dot{u}_j u_{j,k} a_k \} \right] dV \, dt = 0. \tag{48}$$

The relation is true for any a_k; therefore, we get

$$\int_0^t \int_\Omega \left[\frac{\partial}{\partial x_i} \{ \mathscr{L} \delta_{ik} + \sigma_{ij} u_{j,k} \} - \frac{\partial}{\partial t} \{ \rho \dot{u}_j u_{j,k} \} \right] dV \, dt = 0. \tag{49}$$

Equation (49) holds true for any arbitrary volume Ω and any arbitrary time interval, so we have

$$\frac{\partial}{\partial x_i} \{ \mathscr{L} \delta_{ik} + \sigma_{ij} u_{j,k} \} - \frac{\partial}{\partial t} \{ \rho \dot{u}_j u_{j,k} \} = 0, \tag{50}$$

which is in agreement with [Fletcher 1976, Equation 3.4]. Equation (50) is an additional field equation valid anywhere in the domain of analyticity. Ni and Markenscoff [2009] have used (50) as a field equation to obtain the logarithmic singularity of the near field of an accelerating (generally moving) dislocation rather than by singular asymptotics of the full solution [Callias and Markenscoff 1988].

Analogously to statics, for linear elastodynamics we define the dynamic J-integral as [Bui 1978; Maugin 1993; Markenscoff 2006]

$$J_k^{\text{dyn}} \equiv - \int_\Omega \left[\frac{\partial}{\partial x_i} \{ \mathscr{L} \delta_{ik} + \sigma_{ij} u_{j,k} \} - \frac{\partial}{\partial t} \{ \rho \dot{u}_j u_{j,k} \} \right] dV. \tag{51}$$

The dynamic J-integral would be zero if the region Ω excludes the inhomogeneity, but it would be nonzero if the volume Ω includes it. The above expression for the dynamic J-integral agrees in the static case with [Eshelby 1959; Günther 1962; Rice 1968; Knowles and Sternberg 1972].

3.1.1. *Relation of J_k^{dyn} with the energy release rate.* If Ω is a region of analyticity excluding the inhomogeneity then, from (50), using relation (13), we can write

$$\int_\Omega \left[\frac{\partial}{\partial x_i} \{(T - W)\delta_{ik} + \sigma_{ij}u_{j,k}\} - \frac{\partial}{\partial t}\{\rho \dot{u}_j u_{j,k}\} \right] dV = 0, \tag{52}$$

which, equivalently, is written as

$$\int_\Omega \left[\frac{\partial}{\partial x_i} \{(W + T)\delta_{ik} - \sigma_{ij}u_{j,k}\} - 2\frac{\partial T}{\partial x_k} + \frac{\partial}{\partial t}\{\rho \dot{u}_j u_{j,k}\} \right] dV = 0. \tag{53}$$

We may write this in a form similar to [Gupta and Markenscoff 2012, Equation 10], as

$$\int_\Omega \frac{\partial}{\partial x_i} \{(W + T)\delta_{ik} - \sigma_{ij}u_{j,k}\} \, dV + \int_\Omega [\rho \ddot{u}_j u_{j,k} - \rho \dot{u}_i \dot{u}_{i,k}] \, dV = 0. \tag{54}$$

By considering the region of analyticity Ω as $\Omega = \Omega_2 - \Omega_1$, i.e., as the difference between two regions Ω_2 and Ω_1 (with $\Omega_1 \subset \Omega_2$) that include the inhomogeneity, and by using the divergence theorem to convert the first volume integral into a surface integral, we have

$$\int_{S_1 + S_2} \{(W + T)n_k - \sigma_{ij}u_{j,k}n_i\} \, dS + \int_{\Omega_2 - \Omega_1} [\rho \ddot{u}_j u_{j,k} - \rho \dot{u}_i \dot{u}_{i,k}] \, dV = 0, \tag{55}$$

where n_i is the outward unit normal vector to the surface $S_1 + S_2$. It follows that

$$\int_{S_1} \{(W + T)n_k - \sigma_{ij}u_{j,k}n_i\} \, dS + \int_{\Omega_1} [\rho \ddot{u}_j u_{j,k} - \rho \dot{u}_i \dot{u}_{i,k}] \, dV$$

$$= \int_{S_2} \{(W + T)n_k - \sigma_{ij}u_{j,k}n_i\} \, dS + \int_{\Omega_2} [\rho \ddot{u}_j u_{j,k} - \rho \dot{u}_i \dot{u}_{i,k}] \, dV = J_k^{\text{dyn}}. \tag{56}$$

We now consider the volume Ω_1 to shrink to zero as the contour S_1 shrinks onto the moving inhomogeneity and moves with it. As the volume Ω_1 shrinks to zero, in view of the fact that "the elastic field in the immediate vicinity of the moving inhomogeneity at any instant is indistinguishable from the local field of an appropriate steady state moving inhomogeneity, for which $\partial/\partial t = -v\partial/\partial x$" [Freund 1972], the volume integral in the region Ω_1 vanishes, so that (55) yields the expression for J_k^{dyn} as

$$J_k^{\text{dyn}} = \lim_{S_1 \to 0} \int_{S_1} \{(W + T)n_k - \sigma_{ij}u_{j,k}n_i\} \, dS, \tag{57}$$

where S_1 is an arbitrary surface surrounding the inhomogeneity, moving with it and shrinking upon it. The above relation of J_k^{dyn} agrees with [Freund 1990, p. 269] and [Markenscoff 2006, Equation 14]. This expression will relate J_k^{dyn} to the energy release rate for the moving inhomogeneity, as treated in Section 5.1 (see (116)).

3.2. *Invariance of the Lagrangian under scaling.* For the self-similar expansion of the material, consider the smooth scaling such that the new coordinates and time are $x_i^* = x_i + \epsilon l x_i$ and $t^* = t + \epsilon l t$, respectively, and the new displacement field is $u_i^* = u_i + \frac{1}{2}(1 - n)\epsilon l u_i$, where l is the scaling parameter and n is the number of space dimensions. After comparing the transformation with equations (45) and (44), we have

$$\phi_i = l x_i, \quad \phi_4 = l t \quad \text{and} \quad \psi_j = \tfrac{1}{2}(1 - n)l u_j; \tag{58}$$

therefore, from (8),

$$\overline{\psi}_j = l\left(\tfrac{1}{2}(1-n)u_j - u_{j,k}x_k - t\dot{u}_j\right). \tag{59}$$

Substituting the above transformation in (19) to obtain the conservation law for scaling, we write

$$\int_0^t \int_\Omega \left[\frac{\partial}{\partial x_i}\left\{-\sigma_{ij}l\left(\tfrac{1}{2}(1-n)u_j - u_{j,k}x_k - t\dot{u}_j\right) + \mathcal{L}lx_i\right\} \right.$$
$$\left. + \frac{\partial}{\partial t}\left\{\rho\dot{u}_jl\left(\tfrac{1}{2}(1-n)u_j - u_{j,k}x_k - t\dot{u}_j\right) + \mathcal{L}lt\right\} \right] dV\, dt = 0. \tag{60}$$

The relation is true for any scaling parameter l, therefore we get

$$\int_0^t \int_\Omega \left[\frac{\partial}{\partial x_i}\left\{\mathcal{L}x_i + \sigma_{ij}\left(\tfrac{1}{2}(n-1)u_j + u_{j,k}x_k + t\dot{u}_j\right)\right\} \right.$$
$$\left. + \frac{\partial}{\partial t}\left\{t\mathcal{L} - \rho\dot{u}_j\left(\tfrac{1}{2}(n-1)u_j + u_{j,k}x_k + t\dot{u}_j\right)\right\} \right] dV\, dt = 0. \tag{61}$$

Equation (61) holds true for any arbitrary volume Ω and any arbitrary time interval, so we have

$$\frac{\partial}{\partial x_i}\left\{\mathcal{L}x_i + \sigma_{ij}\left(\tfrac{1}{2}(n-1)u_j + u_{j,k}x_k + t\dot{u}_j\right)\right\} + \frac{\partial}{\partial t}\left\{t\mathcal{L} - \rho\dot{u}_j\left(\tfrac{1}{2}(n-1)u_j + u_{j,k}x_k + t\dot{u}_j\right)\right\} = 0. \tag{62}$$

Equation (62) is compared to [Fletcher 1976, Equation 3.5] for a three-dimensional case ($n = 3$) and it is an additional field equation valid anywhere in the domain of analyticity.

Analogously to statics, for linear elastodynamics we define the dynamic M-integral as

$$M^{\mathrm{dyn}} \equiv -\int_\Omega \left[\frac{\partial}{\partial x_i}\left\{\mathcal{L}x_i + \sigma_{ij}\left(\tfrac{1}{2}(n-1)u_j + u_{j,k}x_k + t\dot{u}_j\right)\right\} \right.$$
$$\left. + \frac{\partial}{\partial t}\left\{t\mathcal{L} - \rho\dot{u}_j\left(\tfrac{1}{2}(n-1)u_j + u_{j,k}x_k + t\dot{u}_j\right)\right\} \right] dV. \tag{63}$$

The dynamic M-integral would be zero if the region Ω excludes the inhomogeneity, but it would be nonzero if the volume Ω includes the inhomogeneity. The above expression for the dynamic M-integral agrees in the static case with [Günther 1962; Knowles and Sternberg 1972]. After further rearrangements, we may write the M-integral as

$$M^{\mathrm{dyn}} = -\int_\Omega x_\alpha \left[\frac{\partial}{\partial x_i}\{\mathcal{L}\delta_{i\alpha} + \sigma_{ij}u_{j,\alpha}\} - \frac{\partial}{\partial t}\{\rho\dot{u}_j u_{j,\alpha}\} \right] dV, \tag{64}$$

where the x_i are the material coordinates for $i = 1, 2, 3$, and $x_4 = t$ (time variable).

3.3. *Invariance of the Lagrangian under rotation.*
From the family of transformations we have two types of rotation: one is rigid-body rotation (Ω_n) and the other is material rotation (ω_n). By choosing nonzero physical rotation in equations (45) and (44) we obtain the angular momentum balance law, and by choosing nonzero material rotation we obtain the expression for the dynamic L-integral.

3.3.1. *Rigid-body rotation*: $\Omega_n \neq 0$, $\omega_n = 0$. In the case of a rigid-body rotation of the material, consider the smooth transformation in x_i and u_i such that the coordinates and the time variable remain unchanged ($x_i^* = x_i$, $t^* = t$), and the new displacement field is $u_i^* = u_i + \varepsilon_{ilm}\epsilon\Omega_m x_l$, where $\epsilon\Omega_m$ is the infinitesimal physical rotation. After comparing the transformation with equations (45) and (44), we have

$$\phi_i = 0, \quad \phi_4 = 0 \quad \text{and} \quad \psi_j = \varepsilon_{jlm}\Omega_m x_l; \tag{65}$$

therefore, from (8),

$$\overline{\psi}_j = \Omega_m \varepsilon_{jlm} x_l. \tag{66}$$

Inserting the above transformation in (19) to obtain the conservation law for rotation, we obtain

$$\int_0^t \int_\Omega \left[\frac{\partial}{\partial t} \{\rho \dot{u}_j \Omega_m \varepsilon_{jlm} x_l\} + \frac{\partial}{\partial x_i} \{-\sigma_{ij} \Omega_m \varepsilon_{jlm} x_l\} \right] dV \, dt = 0. \tag{67}$$

The relation is true for any Ω_m; therefore, the expression for the conservation of angular momentum is

$$\varepsilon_{jlm} \int_0^t \int_\Omega \left[\frac{\partial}{\partial t} (\rho \dot{u}_j x_l) - \frac{\partial}{\partial x_i} (\sigma_{ij} x_l) \right] dV \, dt = 0. \tag{68}$$

The above equation holds true for any arbitrary volume Ω and arbitrary time interval, so we have

$$\frac{\partial}{\partial t} (\varepsilon_{jlm} \rho \dot{u}_j x_l) - \frac{\partial}{\partial x_i} (\varepsilon_{jlm} \sigma_{ij} x_l) = 0, \tag{69}$$

which is the field equation for the angular momentum balance.

3.3.2. *Material or coordinate rotation*: $\Omega_n = 0$, $\omega_n \neq 0$. In case of the material or coordinate rotation of an *isotropic* material, consider the smooth transformation in x_i and u_i such that the new coordinates are $x_i^* = x_i + \varepsilon_{ilm} \epsilon \omega_m x_l$, new time remains unchanged ($t^* = t$), and the new displacement field is $u_i^* = u_i + \varepsilon_{ilm} \epsilon \omega_m u_l$, where $\epsilon \omega_m$ is the infinitesimal material rotation. After comparing the transformation with equations (45) and (44), we have

$$\phi_i = \varepsilon_{ilm} \omega_m x_l, \quad \phi_4 = 0 \quad \text{and} \quad \psi_j = \varepsilon_{jlm} \omega_m u_l; \tag{70}$$

therefore, from (8),

$$\overline{\psi}_j = \omega_m (\varepsilon_{jlm} u_l - \varepsilon_{klm} u_{j,k} x_l). \tag{71}$$

Inserting the above transformation in (19) to obtain the conservation law for rotation, we obtain

$$\int_0^t \int_\Omega \left[\frac{\partial}{\partial t} \{\rho \dot{u}_j \omega_m (\varepsilon_{jlm} u_l - \varepsilon_{klm} u_{j,k} x_l)\} \right.$$
$$\left. + \frac{\partial}{\partial x_i} \{-\sigma_{ij} \omega_m (\varepsilon_{jlm} u_l - \varepsilon_{klm} u_{j,k} x_l) + \mathcal{L} \varepsilon_{ilm} \omega_m x_l\} \right] dV \, dt = 0. \tag{72}$$

The relation is true for any ω_m; therefore we get

$$\int_0^t \int_\Omega \left[\frac{\partial}{\partial x_i} (\varepsilon_{mlj} u_l \sigma_{ij} + \varepsilon_{mkl} x_l u_{j,k} \sigma_{ij} - \varepsilon_{mli} x_l \mathcal{L}) + \frac{\partial}{\partial t} (\rho \varepsilon_{mjl} u_l \dot{u}_j + \rho \varepsilon_{mlk} x_l \dot{u}_j u_{j,k}) \right] dV \, dt = 0. \tag{73}$$

Equation (73) holds true for any arbitrary volume Ω and any arbitrary time interval, so we have

$$\frac{\partial}{\partial x_i} (\varepsilon_{mlj} u_l \sigma_{ij} + \varepsilon_{mkl} x_l u_{j,k} \sigma_{ij} - \varepsilon_{mli} x_l \mathcal{L}) + \frac{\partial}{\partial t} (\rho \varepsilon_{mjl} u_l \dot{u}_j + \rho \varepsilon_{mlk} x_l \dot{u}_j u_{j,k}) = 0. \tag{74}$$

Equation (74) is compared to [Fletcher 1976, Equation 3.6]; however, Fletcher's expression has a negative sign in front of the second term of the first integrand on the left-hand side. In addition to equations (50) and (62), (74) is an additional field equation of elastodynamics valid anywhere in the domain of analyticity.

Analogously to statics, for linear elastodynamics we define the dynamic L-integral as

$$L_m^{\text{dyn}} \equiv - \int_\Omega \left[\frac{\partial}{\partial x_i} \left(\varepsilon_{mlj} u_l \sigma_{ij} + \varepsilon_{mkl} x_l u_{j,k} \sigma_{ij} - \varepsilon_{mli} x_l \mathscr{L} \right) + \frac{\partial}{\partial t} \left(\rho \varepsilon_{mjl} u_l \dot{u}_j + \rho \varepsilon_{mlk} x_l \dot{u}_j u_{j,k} \right) \right] dV. \quad (75)$$

The dynamic L-integral would be zero if the region Ω excludes the inhomogeneity, but it would be nonzero if the volume Ω includes the inhomogeneity. The above expression for the dynamic L-integral agrees in the static case with [Günther 1962; Knowles and Sternberg 1972]. After further rearrangements, for an isotropic material, we may write the L-integral as

$$L_m^{\text{dyn}} = - \int_\Omega \varepsilon_{mkl} x_l \left[\frac{\partial}{\partial x_i} \{ \mathscr{L} \delta_{ik} + \sigma_{ij} u_{j,k} \} - \frac{\partial}{\partial t} \{ \rho \dot{u}_j u_{j,k} \} \right] dV. \quad (76)$$

In the next section, we present these conservation laws as dissipative mechanisms for the corresponding infinitesimal transformations of translation, scaling and rotation of the inhomogeneities.

4. Conservation integrals as dissipative mechanisms

With the objective of relating the conservation integrals J, M and L to the corresponding energy loss of the system, in this section we express the variation of the Lagrangian in terms of balance laws of linear and angular momenta and the "conserved" integrals. Subsequently, the variation of the Lagrangian will be related to the variation of the Hamiltonian, which, in term, will be related to the total energy loss of the system.

Equation (7) is written, after expanding in space and time variables,

$$\delta \Pi^{\mathscr{L}} = \epsilon \int_0^t \int_\Omega \left\{ \frac{\partial \mathscr{L}}{\partial u_j} - \frac{\partial}{\partial x_i} \frac{\partial \mathscr{L}}{\partial u_{j,i}} - \frac{\partial}{\partial t} \frac{\partial \mathscr{L}}{\partial \dot{u}_j} \right\} \overline{\psi}_j \, dV \, dt$$
$$+ \epsilon \int_0^t \int_\Omega \left[\frac{\partial}{\partial x_i} \left\{ \frac{\partial \mathscr{L}}{\partial u_{j,i}} \overline{\psi}_j + \mathscr{L} \phi_i \right\} + \frac{\partial}{\partial t} \left\{ \frac{\partial \mathscr{L}}{\partial \dot{u}_j} \overline{\psi}_j + \mathscr{L} \phi_4 \right\} \right] dV \, dt, \quad (77)$$

In view of equations (13)–(15), the term $\partial \mathscr{L}/\partial u_j$ vanishes, $\partial \mathscr{L}/\partial u_{j,i} = -\sigma_{ij}$, and $\partial \mathscr{L}/\partial \dot{u}_j = \rho \dot{u}_j$; therefore, (77) can be written as

$$\delta \Pi^{\mathscr{L}} = \epsilon \int_0^t \int_\Omega \left\{ \frac{\partial \sigma_{ij}}{\partial x_i} - \frac{\partial (\rho \dot{u}_j)}{\partial t} \right\} \overline{\psi}_j \, dV \, dt$$
$$+ \epsilon \int_0^t \int_\Omega \left[\frac{\partial}{\partial x_i} \{ -\sigma_{ij} \overline{\psi}_j + \mathscr{L} \phi_i \} + \frac{\partial}{\partial t} \{ \rho \dot{u}_j \overline{\psi}_j + \mathscr{L} \phi_4 \} \right] dV \, dt. \quad (78)$$

Next, (78) is applied to the infinitesimal transformations $\boldsymbol{\phi}$ and $\boldsymbol{\psi}$ corresponding to translation, scaling and rotation of the inhomogeneities.

4.1. Translation of the inhomogeneity. For translation of the inhomogeneity, we utilize the transformation [Fletcher 1976] such that the new coordinates are $x_i^* = x_i + \epsilon a_i$ and the new time and displacement field remain invariant ($u_i^* = u_i$), where ϵa_i is the infinitesimal translation of the inhomogeneity. After comparing the transformation with equations (45) and (44), we have

$$\phi_i = a_i, \quad \phi_4 = 0 \quad \text{and} \quad \psi_j = 0; \quad (79)$$

therefore, from (8),

$$\overline{\psi}_j = \psi_j - u_{j,\alpha}\phi_\alpha = -u_{j,k}a_k. \tag{80}$$

Substituting the above transformation in (78) gives [Gupta and Markenscoff 2012]

$$\delta\Pi^{\mathscr{L}} = \epsilon \int_0^t \int_\Omega \left\{ \frac{\partial \sigma_{ij}}{\partial x_i} - \frac{\partial(\rho\dot{u}_j)}{\partial t} \right\} (-u_{j,k}a_k)\, dV\, dt$$
$$+ \epsilon \int_0^t \int_\Omega \left[\frac{\partial}{\partial x_i}\{(\mathscr{L}\delta_{ik} + \sigma_{ij}u_{j,k})a_k\} + \frac{\partial}{\partial t}\{-\rho\dot{u}_j u_{j,k}a_k\} \right] dV\, dt. \tag{81}$$

Taking the translation vector a_k out of the second integral of the right-hand side, we write

$$\delta\Pi^{\mathscr{L}} = -\epsilon \int_0^t \int_\Omega \left\{ \frac{\partial \sigma_{ij}}{\partial x_i} - \frac{\partial(\rho\dot{u}_j)}{\partial t} \right\} u_{j,k}a_k\, dV\, dt$$
$$+ \epsilon a_k \int_0^t \int_\Omega \left[\frac{\partial}{\partial x_i}\{\mathscr{L}\delta_{ik} + \sigma_{ij}u_{j,k}\} - \frac{\partial}{\partial t}\{\rho\dot{u}_j u_{j,k}\} \right] dV\, dt. \tag{82}$$

Taking the time derivative of the above equation, we obtain

$$\delta\dot{\Pi}^{\mathscr{L}} = -\epsilon \int_\Omega \left\{ \frac{\partial \sigma_{ij}}{\partial x_i} - \frac{\partial(\rho\dot{u}_j)}{\partial t} \right\} u_{j,k}a_k\, dV + \epsilon a_k \int_\Omega \left[\frac{\partial}{\partial x_i}\{\mathscr{L}\delta_{ik} + \sigma_{ij}u_{j,k}\} - \frac{\partial}{\partial t}\{\rho\dot{u}_j u_{j,k}\} \right] dV. \tag{83}$$

From (51), the integral in the second term of the right-hand side of (83) is $-J_k^{\text{dyn}}$, so we can rewrite (83) as

$$\delta\dot{\Pi}^{\mathscr{L}} = -\int_\Omega \left\{ \frac{\partial \sigma_{ij}}{\partial x_i} - \frac{\partial(\rho\dot{u}_j)}{\partial t} \right\} u_{j,k}a_k\, dV - \epsilon a_k J_k^{\text{dyn}}. \tag{84}$$

In (84), the term in the curly brackets in the integrand is the linear momentum balance expression (Equation (17)), which vanishes by the Euler–Lagrange equations applied to the Lagrangian.

4.2. *Scaling of the inhomogeneity.* For the self-similar expansion, consider the smooth scaling such that the new coordinates and time are $x_i^* = x_i + \epsilon l x_i$ and $t^* = t + \epsilon l t$, respectively, and the new displacement field is $u_i^* = u_i + \frac{1}{2}(1-n)\epsilon l u_i$, where l is the scaling parameter and n is the number of space dimensions. After comparing the transformation with equations (45) and (44), we have

$$\phi_i = l x_i, \quad \phi_4 = l t \quad \text{and} \quad \psi_j = \tfrac{1}{2}(1-n)l u_j; \tag{85}$$

therefore, from (8), we have

$$\overline{\psi}_j = \psi_j - u_{j,\alpha}\phi_\alpha = l\left(\tfrac{1}{2}(1-n)u_j - u_{j,k}x_k - t\dot{u}_j\right). \tag{86}$$

Substituting the above transformation in (78) to obtain the variation of the Lagrangian for scaling of the inhomogeneity, we write

$$\delta\Pi^{\mathscr{L}} = \epsilon \int_0^t \int_\Omega \left\{ \frac{\partial \sigma_{ij}}{\partial x_i} - \frac{\partial(\rho\dot{u}_j)}{\partial t} \right\} \overline{\psi}_j\, dV\, dt + \epsilon \int_0^t \int_\Omega \left[\frac{\partial}{\partial x_i}\{-\sigma_{ij}l\left(\tfrac{1}{2}(1-n)u_j - u_{j,k}x_k - t\dot{u}_j\right) + \mathscr{L}l x_i\} \right.$$
$$\left. + \frac{\partial}{\partial t}\{\rho\dot{u}_j l\left(\tfrac{1}{2}(1-n)u_j - u_{j,k}x_k - t\dot{u}_j\right) + \mathscr{L}l t\} \right] dV\, dt. \tag{87}$$

Taking the scaling parameter l out of the second integral on the right-hand side, we write

$$\delta\Pi^{\mathscr{L}} = \epsilon \int_0^t \int_\Omega \left\{ \frac{\partial\sigma_{ij}}{\partial x_i} - \frac{\partial(\rho\dot{u}_j)}{\partial t} \right\} \overline{\psi}_j \, dV \, dt + \epsilon l \int_0^t \int_\Omega \left[\frac{\partial}{\partial x_i} \left\{ \mathscr{L}x_i + \sigma_{ij}\left(\tfrac{1}{2}(n-1)u_j + u_{j,k}x_k + t\dot{u}_j\right) \right\} \right.$$
$$\left. + \frac{\partial}{\partial t} \left\{ t\mathscr{L} - \rho\dot{u}_j\left(\tfrac{1}{2}(n-1)u_j + u_{j,k}x_k + t\dot{u}_j\right) \right\} \right] dV \, dt. \quad (88)$$

Taking the time derivative of the above equation, we write

$$\delta\dot{\Pi}^{\mathscr{L}} = \epsilon \int_\Omega \left\{ \frac{\partial\sigma_{ij}}{\partial x_i} - \frac{\partial(\rho\dot{u}_j)}{\partial t} \right\} \overline{\psi}_j \, dV + \epsilon l \int_\Omega \left[\frac{\partial}{\partial x_i} \left\{ \mathscr{L}x_i + \sigma_{ij}\left(\tfrac{1}{2}(n-1)u_j + u_{j,k}x_k + t\dot{u}_j\right) \right\} \right.$$
$$\left. + \frac{\partial}{\partial t} \left\{ t\mathscr{L} - \rho\dot{u}_j\left(\tfrac{1}{2}(n-1)u_j + u_{j,k}x_k + t\dot{u}_j\right) \right\} \right] dV. \quad (89)$$

From (63), the integral in the second term of the right-hand side of (89) is $-M^{\mathrm{dyn}}$, so we can rewrite (89) as

$$\delta\dot{\Pi}^{\mathscr{L}} = \int_\Omega \left\{ \frac{\partial\sigma_{ij}}{\partial x_i} - \frac{\partial(\rho\dot{u}_j)}{\partial t} \right\} \overline{\psi}_j \, dV - \epsilon l M^{\mathrm{dyn}}. \quad (90)$$

In (90), the term in the curly brackets in the integrand is the linear momentum balance expression (Equation (17)), which vanishes by the Euler–Lagrange equations applied to the Lagrangian.

4.3. *Rotation of the inhomogeneity.* Following the *lever arm* $(u_l + x_l)$ described by Eshelby [1956, p. 106], and taking $\Omega_n = \omega_n$ in (45) for the rotation of the inhomogeneity in an *isotropic* material, we consider the smooth transformation in x_i and u_i such that the new coordinates are $x_i^* = x_i + \varepsilon_{ilm}\epsilon\omega_m x_l$, new time remains unchanged ($t^* = t$), and the new displacement field is $u_i^* = u_i + \varepsilon_{ilm}\epsilon\omega_m(u_l + x_l)$, where ω_m is the rotation vector. After comparing the transformation with equations (45) and (44), we have

$$\phi_i = \varepsilon_{ilm}\omega_m x_l, \quad \phi_4 = 0 \quad \text{and} \quad \psi_j = \varepsilon_{jlm}\omega_m(u_l + x_l); \quad (91)$$

therefore, from (8), we have

$$\overline{\psi}_j = \psi_j - u_{j,k}\phi_k = \omega_m\left(\varepsilon_{jlm}(u_l + x_l) - \varepsilon_{klm}u_{j,k}x_l\right). \quad (92)$$

Substituting the above transformation into (78) to obtain the variation of the Lagrangian for rotation of the inhomogeneity, we write

$$\delta\Pi^{\mathscr{L}} = \epsilon \int_0^t \int_\Omega \left\{ \frac{\partial\sigma_{ij}}{\partial x_i} - \frac{\partial(\rho\dot{u}_j)}{\partial t} \right\} \overline{\psi}_j \, dV \, dt + \epsilon \int_0^t \int_\Omega \left[\frac{\partial}{\partial t} \left\{ \rho\dot{u}_j\omega_m(\varepsilon_{jlm}(u_l + x_l) - \varepsilon_{klm}u_{j,k}x_l) \right\} \right.$$
$$\left. + \frac{\partial}{\partial x_i} \left\{ -\sigma_{ij}\omega_m(\varepsilon_{jlm}(u_l + x_l) - \varepsilon_{klm}u_{j,k}x_l) + \mathscr{L}\varepsilon_{ilm}\omega_m x_l \right\} \right] dV \, dt, \quad (93)$$

after collecting the angular momentum balance terms, we write

$$\delta\Pi^{\mathscr{L}} = \epsilon \int_0^t \int_\Omega \left\{ \frac{\partial\sigma_{ij}}{\partial x_i} - \frac{\partial(\rho\dot{u}_j)}{\partial t} \right\} \overline{\psi}_j \, dV \, dt - \epsilon\omega_m \int_0^t \int_\Omega \left[\frac{\partial}{\partial x_i}(\varepsilon_{jlm}x_l\sigma_{ij}) - \frac{\partial}{\partial t}(\rho\varepsilon_{jlm}x_l\dot{u}_j) \right] dV \, dt$$
$$+ \epsilon\omega_m \int_0^t \int_\Omega \left[\frac{\partial}{\partial x_i}(-\varepsilon_{jlm}u_l\sigma_{ij} + \varepsilon_{klm}x_l u_{j,k}\sigma_{ij} + \varepsilon_{ilm}x_l\mathscr{L}) + \frac{\partial}{\partial t}(\rho\varepsilon_{jlm}u_l\dot{u}_j - \rho\varepsilon_{klm}x_l\dot{u}_j u_{j,k}) \right] dV \, dt, \quad (94)$$

after further rearrangements we obtain

$$\delta \Pi^{\mathscr{L}} = \epsilon \int_0^t \int_\Omega \left\{ \frac{\partial \sigma_{ij}}{\partial x_i} - \frac{\partial(\rho \dot{u}_j)}{\partial t} \right\} \overline{\psi}_j \, dV \, dt - \epsilon \omega_m \int_0^t \int_\Omega \left[\frac{\partial}{\partial t} (\rho \varepsilon_{mlj} x_l \dot{u}_j) - \frac{\partial}{\partial x_i} (\varepsilon_{mlj} x_l \sigma_{ij}) \right] dV \, dt$$

$$+ \epsilon \omega_m \int_0^t \int_\Omega \left[\frac{\partial}{\partial x_i} (\varepsilon_{mlj} u_l \sigma_{ij} + \varepsilon_{mkl} x_l u_{j,k} \sigma_{ij} - \varepsilon_{mli} x_l \mathscr{L}) + \frac{\partial}{\partial t} (\rho \varepsilon_{mjl} u_l \dot{u}_j + \rho \varepsilon_{mlk} x_l \dot{u}_j u_{j,k}) \right] dV \, dt. \quad (95)$$

Taking the time derivative of the above equation, we write

$$\delta \dot{\Pi}^{\mathscr{L}} = \epsilon \int_\Omega \left\{ \frac{\partial \sigma_{ij}}{\partial x_i} - \frac{\partial(\rho \dot{u}_j)}{\partial t} \right\} \overline{\psi}_j \, dV - \epsilon \omega_m \int_\Omega \left[\frac{\partial}{\partial t} (\rho \varepsilon_{mlj} x_l \dot{u}_j) - \frac{\partial}{\partial x_i} (\varepsilon_{mlj} x_l \sigma_{ij}) \right] dV$$

$$+ \epsilon \omega_m \int_\Omega \left[\frac{\partial}{\partial x_i} (\varepsilon_{mlj} u_l \sigma_{ij} + \varepsilon_{mkl} x_l u_{j,k} \sigma_{ij} - \varepsilon_{mli} x_l \mathscr{L}) + \frac{\partial}{\partial t} (\rho \varepsilon_{mjl} u_l \dot{u}_j + \rho \varepsilon_{mlk} x_l \dot{u}_j u_{j,k}) \right] dV. \quad (96)$$

From (75), the integral in the third term of the right-hand side of (96) is $-L_m^{\mathrm{dyn}}$, so we can rewrite (96) as

$$\delta \dot{\Pi}^{\mathscr{L}} = \epsilon \int_\Omega \left\{ \frac{\partial \sigma_{ij}}{\partial x_i} - \frac{\partial(\rho \dot{u}_j)}{\partial t} \right\} \overline{\psi}_j \, dV - \epsilon \omega_m \int_\Omega \left[\frac{\partial}{\partial t} (\rho \varepsilon_{mlj} x_l \dot{u}_j) - \frac{\partial}{\partial x_i} (\varepsilon_{mlj} x_l \sigma_{ij}) \right] dV - \epsilon \omega_m L_m^{\mathrm{dyn}}. \quad (97)$$

In (97), the term in the curly brackets in the first integrand is the linear momentum balance expression (Equation (17)) and the second integrand on the right-hand side is the angular momentum expression (Equation (69)).

It may be noted that we obtain both the expression for the angular moment balance and the dynamic L-integral from the variation of the Lagrangian functional because the rigid-body rotation (Equation (65)) and the material rotation (Equation (70)) are both considered. The transformation of rigid-body rotation (Section 3.3.1) by itself leads to the expression for the angular momentum balance [Fletcher 1976, Equation 3.3], and the transformation of material rotation (Section 3.3.2) leads to the expression for the dynamic L-integral [Fletcher 1976, Equation 3.6]. By using both together we are able to obtain the dissipative statement (97), as further discussed in the following sections.

5. Relation of the variations of the Lagrangian and Hamiltonian under the transformations of translation, scaling and rotation of inhomogeneities

In the previous sections, Noether's theorem was applied to the Lagrangian functional of the system from which the conservation of linear momentum is derived as the Euler–Lagrange equations (11). In this section, we relate the variation of the Lagrangian to the variation of the Hamiltonian under translation, scaling and rotation of the inhomogeneities so that we can explicitly relate the conservation integrals with energy release rates ([Gupta and Markenscoff 2012]; and private communication with Gupta).

The Hamiltonian density is defined as

$$\mathscr{H} = T + W, \quad (98)$$

where the strain energy density is $W = \frac{1}{2} C_{ijkl} \varepsilon_{ij} \varepsilon_{kl} = \frac{1}{2} C_{ijkl} u_{i,j} u_{k,l}$ and the specific kinetic energy is $T = \frac{1}{2} \rho \dot{u}_i \dot{u}_i$. We consider the total Hamiltonian functional for $\Omega \subset \mathbb{R}^3$ and $[0, t] \subset \mathbb{R}$:

$$\Pi^{\mathscr{H}}(u_{i,j}, \dot{u}_i) = \int_0^t \int_\Omega \mathscr{H}(u_{i,j}, \dot{u}_i) \, dV \, dt = \int_0^t \int_\Omega \{ T(\dot{u}_i) + W(u_{i,j}) \} \, dV \, dt. \quad (99)$$

The functional (99) represents the total mechanical energy stored in an arbitrary part Ω of the body during the time interval $[0, t]$. Applying (7) to the Hamiltonian (98) and expanding in space and time variables, we write (similarly to (77) for the Lagrangian $\mathscr{L} = T - W$) the variation of the Hamiltonian functional (99) under the infinitesimal transformation (2a)–(2b) as

$$\delta\Pi^{\mathscr{H}} = \epsilon \int_0^t \int_\Omega \left\{ \frac{\partial\mathscr{H}}{\partial u_j} - \frac{\partial}{\partial x_i}\frac{\partial\mathscr{H}}{\partial u_{j,i}} - \frac{\partial}{\partial t}\frac{\partial\mathscr{H}}{\partial\dot{u}_j} \right\} \overline{\psi}_j \, dV \, dt + \epsilon \int_0^t \int_\Omega \frac{\partial}{\partial x_i}\left\{ \frac{\partial\mathscr{H}}{\partial u_{j,i}}\overline{\psi}_j + \mathscr{H}\phi_i \right\} dV \, dt$$
$$+ \epsilon \int_0^t \int_\Omega \frac{\partial}{\partial t}\left\{ \frac{\partial\mathscr{H}}{\partial\dot{u}_j}\overline{\psi}_j + \mathscr{H}\phi_4 \right\} dV \, dt. \quad (100)$$

In view of equations (98), (14) and (15), the term $\partial\mathscr{H}/\partial u_j$ vanishes and $\partial\mathscr{H}/\partial u_{j,i} = \sigma_{ij}$, and $\partial\mathscr{H}/\partial\dot{u}_j = \rho\dot{u}_j$; therefore, the above equation can be written as

$$\delta\Pi^{\mathscr{H}} = \epsilon \int_0^t \int_\Omega \left\{ -\frac{\partial\sigma_{ij}}{\partial x_i} - \frac{\partial(\rho\dot{u}_j)}{\partial t} \right\} \overline{\psi}_j \, dV \, dt + \epsilon \int_0^t \int_\Omega \frac{\partial}{\partial x_i}\{\sigma_{ij}\overline{\psi}_j + (W+T)\phi_i\} \, dV \, dt$$
$$+ \epsilon \int_0^t \int_\Omega \frac{\partial}{\partial t}\{\rho\dot{u}_j\overline{\psi}_j + (W+T)\phi_4\} \, dV \, dt. \quad (101)$$

Note that the first term on the right-hand side of the above equation is not the same as the first term of the variation of the Lagrangian (Equation (78)), which is the linear momentum balance term. Next, we rearrange the terms so as to produce the linear momentum balance expression in the first integrand and make a connection to the variation of the Lagrangian:

$$\delta\Pi^{\mathscr{H}} = \epsilon \int_0^t \int_\Omega \left\{ -\frac{\partial\sigma_{ij}}{\partial x_i} + \frac{\partial(\rho\dot{u}_j)}{\partial t} \right\} \overline{\psi}_j \, dV \, dt + \epsilon \int_0^t \int_\Omega \frac{\partial}{\partial x_i}\{\sigma_{ij}\overline{\psi}_j + (W+T)\phi_i\} \, dV \, dt$$
$$+ \epsilon \int_0^t \int_\Omega \left\{ -\overline{\psi}_j\frac{\partial}{\partial t}(\rho\dot{u}_j) + \rho\dot{u}_j\frac{\partial}{\partial t}\overline{\psi}_j + \frac{\partial}{\partial t}[(W+T)\phi_4] \right\} dV \, dt. \quad (102)$$

We further rearrange as to produce terms with $(W - T)$ in the remaining terms on the right-hand side:

$$\delta\Pi^{\mathscr{H}} = \epsilon \int_0^t \int_\Omega \left\{ -\frac{\partial\sigma_{ij}}{\partial x_i} + \frac{\partial(\rho\dot{u}_j)}{\partial t} \right\} \overline{\psi}_j \, dV \, dt + \epsilon \int_0^t \int_\Omega \frac{\partial}{\partial x_i}\{\sigma_{ij}\overline{\psi}_j + (W-T)\phi_i\} \, dV \, dt$$
$$+ \epsilon \int_0^t \int_\Omega \left\{ -\overline{\psi}_j\frac{\partial}{\partial t}(\rho\dot{u}_j) - \rho\dot{u}_j\frac{\partial}{\partial t}\overline{\psi}_j + \frac{\partial}{\partial t}[(W-T)\phi_4] \right\} dV \, dt$$
$$+ 2\epsilon \int_0^t \int_\Omega \left\{ \frac{\partial}{\partial x_i}(T\phi_i) + \frac{\partial}{\partial t}(T\phi_4) + \rho\dot{u}_j\frac{\partial}{\partial t}\overline{\psi}_j \right\} dV \, dt. \quad (103)$$

We further rewrite this expression using (13), so that the expression in the variation of the Hamiltonian involves the Lagrangian:

$$\delta\Pi^{\mathscr{H}} = \epsilon \int_0^t \int_\Omega \left\{ -\frac{\partial\sigma_{ij}}{\partial x_i} + \frac{\partial(\rho\dot{u}_j)}{\partial\partial t} \right\} \overline{\psi}_j \, dV \, dt + \epsilon \int_0^t \int_\Omega \frac{\partial}{\partial x_i}\{\sigma_{ij}\overline{\psi}_j - \mathscr{L}\phi_i\} \, dV \, dt$$
$$+ \epsilon \int_0^t \int_\Omega \frac{d}{dt}\{-\rho\dot{u}_j\overline{\psi}_j - \mathscr{L}\phi_4\} \, dV \, dt + 2\epsilon \int_0^t \int_\Omega \left\{ \frac{\partial}{\partial x_i}(T\phi_i) + \frac{\partial}{\partial t}(T\phi_4) + \rho\dot{u}_j\frac{\partial}{\partial t}\overline{\psi}_j \right\} dV \, dt. \quad (104)$$

Using (78), which is the expression for the variation of the Lagrangian, we have

$$\delta\Pi^{\mathcal{H}} = -\delta\Pi^{\mathcal{L}} + 2\epsilon \int_0^t \int_\Omega \left\{ \frac{\partial}{\partial x_i}(T\phi_i) + \frac{\partial}{\partial t}(T\phi_4) + \rho\dot{u}_j \frac{\partial}{\partial t}\overline{\psi}_j \right\} dV\,dt, \tag{105}$$

which can be written, using (8), as

$$\delta\Pi^{\mathcal{H}} = -\delta\Pi^{\mathcal{L}} + 2\epsilon \int_0^t \int_\Omega \left\{ \frac{\partial}{\partial x_i}(T\phi_i) + \frac{\partial}{\partial t}(T\phi_4) + \rho\dot{u}_j \frac{\partial}{\partial t}(\psi_j - u_{j,i}\phi_i - \dot{u}_j\phi_4) \right\} dV\,dt, \tag{106}$$

Now we employ the relation (106) of the variations of the Lagrangian and Hamiltonian to the corresponding infinitesimal transformations of translation, rotation, and scaling of the inhomogeneity.

5.1. *Translation of the inhomogeneity.* In this case we use the transformation such that $\phi_i = a_i$, $\phi_4 = 0$ and $\psi_j = 0$, i.e., translation of the inhomogeneity. Inserting it in (106) gives

$$\begin{aligned}
\delta\Pi^{\mathcal{H}} &= -\delta\Pi^{\mathcal{L}} + 2\epsilon \int_0^t \int_\Omega \left\{ \frac{\partial}{\partial x_i}(Ta_i) + \rho\dot{u}_j \frac{\partial}{\partial t}(-u_{j,i}a_i) \right\} dV\,dt \\
&= -\delta\Pi^{\mathcal{L}} + 2\epsilon \int_0^t \int_\Omega \left\{ \rho\dot{u}_k\dot{u}_{k,i}a_i - \rho\dot{u}_j\dot{u}_{j,i}a_i \right\} dV\,dt \\
&= -\delta\Pi^{\mathcal{L}}.
\end{aligned} \tag{107}$$

Thus, under an infinitesimal translation of the inhomogeneity, the variation of the Lagrangian is equal to the negative variation of the Hamiltonian, which was already shown by Gupta and Markenscoff [2012]. Taking the time derivative of (107), we can write

$$\delta\dot{\Pi}^{\mathcal{H}} = -\delta\dot{\Pi}^{\mathcal{L}}, \tag{108}$$

which, using (84), can be written as

$$\delta\dot{\Pi}^{\mathcal{H}} = -\delta\dot{\Pi}^{\mathcal{L}} = \epsilon \int_\Omega \left\{ \frac{\partial\sigma_{ij}}{\partial x_i} - \frac{\partial(\rho\dot{u}_j)}{\partial t} \right\} u_{j,k}a_k\,dV + \epsilon a_k J_k^{\text{dyn}}, \tag{109}$$

where J_k^{dyn} is defined by (51). Considering the definition of the Hamiltonian $\Pi^{\mathcal{H}}(u_{i,j}, \dot{u}_i)$ according to (99), we define $\delta\mathcal{E}^{\text{tot}}$ as

$$\delta\mathcal{E}^{\text{tot}} \equiv \delta\dot{\Pi}^{\mathcal{H}}, \tag{110}$$

where $\delta\mathcal{E}^{\text{tot}}$ is the change of the total energy in the volume Ω under the infinitesimal transformations of (45), evaluated at time t. The external forces are assumed to be absent. Now, from equations (110) and (109) we can write

$$\delta\mathcal{E}^{\text{tot}} = \epsilon \int_\Omega \left\{ \frac{\partial\sigma_{ij}}{\partial x_i} - \frac{\partial(\rho\dot{u}_j)}{\partial t} \right\} u_{j,k}a_k\,dV + \epsilon a_k J_k^{\text{dyn}}. \tag{111}$$

In (111), the term in the curly brackets in the integrand is the linear momentum balance expression (Equation (17)), which will vanish due to conservation of linear momentum. So, if linear momentum is conserved in the whole domain, then (111) can be written as

$$\delta\mathcal{E}^{\text{tot}} = \epsilon a_k J_k^{\text{dyn}}. \tag{112}$$

Moreover, as shown in [Gupta and Markenscoff 2012], if $\delta\mathscr{E}^{\text{tot}} = \epsilon a_k J_k^{\text{dyn}}$ then the first term on the right-hand side of (111) will vanish, and, if $u_{j,k}$ is invertible, then the term in the curly brackets (linear momentum balance expression) will vanish since the integral is valid for any arbitrary volume Ω. Therefore, (111) can be stated as the proposition that, under an infinitesimal translation of the inhomogeneity (transformation (79)), the change of the total energy of the system per unit infinitesimal translation of the inhomogeneity is equal to the dynamic J-integral *if and only if* linear momentum is conserved in the whole domain [Gupta and Markenscoff 2012], provided that $u_{j,k}$ is invertible.

If the inhomogeneity is moving with the velocity $\epsilon\dot{a}_k \equiv v_k$, then we can write the rate of the total energy change $\delta\dot{\mathscr{E}}^{\text{tot}}$ as

$$\delta\dot{\mathscr{E}}^{\text{tot}} = v_k J_k^{\text{dyn}}. \tag{113}$$

The above equation agrees in the static case with [Budiansky and Rice 1973; Lubarda and Markenscoff 2007]. With the expression for J_k^{dyn} given in (57), Equation (113) yields

$$\delta\dot{\mathscr{E}}^{\text{tot}} = \lim_{S_d \to 0} \int_{S_d} \left\{ (W+T)n_k v_k - \sigma_{ij} u_{j,k} n_i v_k \right\} dS, \tag{114}$$

where S_d is an arbitrary surface surrounds the inhomogeneity, moving with it and shrinking on it, and the n_k are the components of the unit outward normal $\boldsymbol{n}$ to the surface S_d. Furthermore, near the core of the moving inhomogeneity, leading-order terms of the fields satisfy the relation $\partial/\partial t = -v_k \partial/\partial x_k$ [Freund 1972], so we can write $u_{j,k} v_k = -\dot{u}_j$ in (114) to obtain

$$\delta\dot{\mathscr{E}}^{\text{tot}} = \lim_{S_d \to 0} \int_{S_d} \left\{ (W+T)v_n + \sigma_{ij}\dot{u}_j n_i \right\} dS, \tag{115}$$

where v_n is the component of the velocity of the inhomogeneity in the direction of the outward normal $\boldsymbol{n}$ to the surface S_d. In agreement with the expression for the energy release rate into the core of the moving inhomogeneity as given by Eshelby [1970, Equation 78] we define the energy release rate $\mathscr{G}$ by

$$v\mathscr{G} \equiv \delta\dot{\mathscr{E}}^{\text{tot}} = \lim_{S_d \to 0} \int_{S_d} \left\{ (W+T)v_n + \sigma_{ij}\dot{u}_j n_i \right\} dS, \tag{116}$$

which represents rate of energy loss of the system flowing into the inhomogeneity under translation. Equation (116) is in agreement with the energy release for a moving crack by [Atkinson and Eshelby 1968, Equation 9; Freund 1972, Equation 13; Freund 1990, p. 262], for dislocations [Clifton and Markenscoff 1981] and moving phase boundaries [Markenscoff and Ni 2010; Ni and Markenscoff 2015]. As proven in [Freund 1972], the above expression is path-independent for a crack, and will also be now for an inhomogeneity, since it is a weaker singularity.

5.2. *Scaling of the inhomogeneity.* In this case we use the transformation such that $\phi_i = lx_i$, $\phi_4 = lt$ and $\psi_j = \frac{1}{2}(1-n)lu_j$, i.e., scaling of the inhomogeneity. Inserting it in (106) gives

$$
\begin{aligned}
\delta\Pi^{\mathcal{H}} &= -\delta\Pi^{\mathcal{L}} + 2\epsilon \int_0^t \int_\Omega \left\{ \frac{\partial}{\partial x_i}(Tlx_i) + \frac{\partial}{\partial t}(Tlt) + \rho\dot{u}_j\frac{\partial}{\partial t}\left(\tfrac{1}{2}(1-n)lu_j - u_{j,i}lx_i - \dot{u}_j lt\right) \right\} dV\, dt \\
&= -\delta\Pi^{\mathcal{L}} + 2\epsilon \int_0^t \int_\Omega \Big\{ lx_i\rho\dot{u}_k\dot{u}_{k,i} + nlT + lt\rho\dot{u}_k\ddot{u}_k + Tl + \tfrac{1}{2}(1-n)l\rho\dot{u}_j\dot{u}_j - lx_i\rho\dot{u}_j\dot{u}_{j,i} \\
&\hspace{8cm} - lt\rho\dot{u}_j\ddot{u}_j - l\rho\dot{u}_j\dot{u}_j \Big\}\, dV\, dt \\
&= -\delta\Pi^{\mathcal{L}} + 2\epsilon \int_0^t \int_\Omega \left\{ nTl + Tl + (1-n)Tl - 2Tl \right\} dV\, dt \\
&= -\delta\Pi^{\mathcal{L}},
\end{aligned}
\tag{117}
$$

where n is equal to number of spatial dimensions.

Thus, under an infinitesimal scaling of the inhomogeneity, the variation of the Lagrangian is equal to the negative variation of the Hamiltonian. Taking the time derivative of (117), we can write

$$
\delta\dot{\Pi}^{\mathcal{H}} = -\delta\dot{\Pi}^{\mathcal{L}},
\tag{118}
$$

which, using (90), can be written as

$$
\delta\dot{\Pi}^{\mathcal{H}} = -\delta\dot{\Pi}^{\mathcal{L}} = -\epsilon \int_\Omega \left\{ \frac{\partial\sigma_{ij}}{\partial x_i} - \frac{\partial(\rho\dot{u}_j)}{\partial t} \right\} \overline{\psi}_j\, dV + \epsilon l M^{\mathrm{dyn}},
\tag{119}
$$

where M^{dyn} is defined by (63). Now, from (99) and (119), we can define

$$
\delta\dot{\mathcal{E}}^{\mathrm{tot}} \equiv \delta\dot{\Pi}^{\mathcal{H}} = -\epsilon \int_\Omega \left\{ \frac{\partial\sigma_{ij}}{\partial x_i} - \frac{\partial(\rho\dot{u}_j)}{\partial t} \right\} \overline{\psi}_j\, dV + \epsilon l M^{\mathrm{dyn}},
\tag{120}
$$

where $\delta\dot{\mathcal{E}}^{\mathrm{tot}}$ is the change of the total energy in the volume Ω due to the scaling of the inhomogeneity evaluated at time t. In (120), the term in the curly brackets in the integrand is the linear momentum balance expression (Equation (17)). Therefore, (120) can be stated as the proposition that if linear momentum is conserved in the whole domain, then the change of the total energy of the system per unit infinitesimal scaling ϵl, under the scaling transformation (85), is equal to the dynamic M-integral.

5.3. *Rotation of the inhomogeneity.* In this case we use the transformation such that $\phi_i = \varepsilon_{ilm}\omega_m x_l$, $\phi_4 = 0$ and $\psi_j = \varepsilon_{jlm}\omega_m(u_l + x_l)$, i.e., rotation of the inhomogeneity. Inserting it in (106) gives

$$
\begin{aligned}
\delta\Pi^{\mathcal{H}} &= -\delta\Pi^{\mathcal{L}} + 2\epsilon \int_0^t \int_\Omega \left\{ \frac{\partial}{\partial x_i}(T\varepsilon_{ilm}\omega_m x_l) + \rho\dot{u}_j\frac{\partial}{\partial t}(\varepsilon_{jlm}\omega_m(u_l + x_l) - u_{j,i}\varepsilon_{ilm}\omega_m x_l) \right\} dV\, dt \\
&= -\delta\Pi^{\mathcal{L}} + 2\epsilon \int_0^t \int_\Omega \Big\{ \varepsilon_{ilm}\omega_m x_l\rho\dot{u}_k\dot{u}_{k,i} + T\varepsilon_{ilm}\omega_m\delta_{il} \\
&\hspace{6cm} + \rho\dot{u}_j\varepsilon_{jlm}\omega_m\dot{u}_l - \rho\dot{u}_j\dot{u}_{j,i}\varepsilon_{ilm}\omega_m x_l \Big\}\, dV\, dt.
\end{aligned}
\tag{121}
$$

The first term of the integrand on the right-hand side cancels with the fourth term, the second term is zero because δ_{il} is symmetric in i and l but ε_{ilm} is skew-symmetric in i and l, and similarly the third

term is also zero because $\dot{u}_j \dot{u}_l$ is symmetric in j and l but ε_{jlm} is skew-symmetric in j and l. Hence, we obtain

$$\delta \Pi^{\mathcal{H}} = -\delta \Pi^{\mathcal{L}}. \tag{122}$$

Thus, under an infinitesimal rotation of the inhomogeneity, for an isotropic material the variation of the Lagrangian is equal to the negative variation of the Hamiltonian. Taking the time derivative of (122), we can write

$$\delta \dot{\Pi}^{\mathcal{H}} = -\delta \dot{\Pi}^{\mathcal{L}}, \tag{123}$$

which, using (97), can be written as

$$\delta \dot{\Pi}^{\mathcal{H}} = -\delta \dot{\Pi}^{\mathcal{L}} = -\epsilon \int_{\Omega} \left\{ \frac{\partial \sigma_{ij}}{\partial x_i} - \frac{\partial (\rho \dot{u}_j)}{\partial t} \right\} \overline{\psi}_j \, dV$$
$$+ \epsilon \omega_m \int_{\Omega} \left[\frac{\partial}{\partial t} (\rho \varepsilon_{mlj} x_l \dot{u}_j) - \frac{\partial}{\partial x_i} (\varepsilon_{mlj} x_l \sigma_{ij}) \right] dV + \epsilon \omega_m L_m^{\text{dyn}}, \tag{124}$$

where L_m^{dyn} is defined by (75). Now, from (99) and (124), we can define

$$\delta \mathcal{E}^{\text{tot}} \equiv \delta \dot{\Pi}^{\mathcal{H}} = -\epsilon \int_{\Omega} \left\{ \frac{\partial \sigma_{ij}}{\partial x_i} - \frac{\partial (\rho \dot{u}_j)}{\partial t} \right\} \overline{\psi}_j \, dV$$
$$+ \epsilon \omega_m \int_{\Omega} \left[\frac{\partial}{\partial t} (\rho \varepsilon_{mlj} x_l \dot{u}_j) - \frac{\partial}{\partial x_i} (\varepsilon_{mlj} x_l \sigma_{ij}) \right] dV + \epsilon \omega_m L_m^{\text{dyn}}, \tag{125}$$

where $\delta \mathcal{E}^{\text{tot}}$ is the change of the total energy in the volume Ω due to the rotation of the inhomogeneity evaluated at time t. In (125), the term in the curly brackets in the first integrand is the linear momentum balance expression (Equation (17)) and the second integrand on the right hand side is the angular momentum expression (Equation (69)). Therefore, (125) can be stated as the proposition that, for an isotropic material, if linear and angular momenta are conserved in the whole domain, then the change of the total energy of the system per unit infinitesimal rotation $\epsilon \omega_m$, under the rotation transformation (91) with "*lever arm $x_i + u_i$*" is equal to the dynamic L-integral.

6. Dissipative propositions

6.1. *Translation of the inhomogeneity.* From relation (111), we state the following proposition:

Proposition 1 [Gupta and Markenscoff 2012]. *Under the translation transformation of Equation (79), the total energy loss of the system per unit infinitesimal translation is equal to the dynamic J-integral if and only if linear momentum is conserved in the domain, provided that $u_{i,j}$ is invertible.*

This proposition extends to elastodynamics the earlier proposition for the static J-integral [Gupta and Markenscoff 2008].

6.2. *Scaling of the inhomogeneity.* From relation (120), we state the following proposition:

Proposition 2. *If linear momentum is conserved in the domain, under the scaling transformation of Equation (85) the total energy loss of the system per unit infinitesimal scaling parameter is equal to the dynamic M-integral.*

This proposition is immediately extended to elastostatics for the static M-integral.

6.3. *Rotation of the inhomogeneity.* From relation (125), we state the following proposition:

Proposition 3. *If linear and angular momenta are conserved in the domain, for an isotropic material under the rotation transformation of Equation (91) the total energy loss of the system per unit infinitesimal rotation is equal to the dynamic L-integral.*

This proposition is immediately extended to elastostatics for the static *L*-integral.

These propositions express the fact that, when analyticity is lost due to the inhomogeneity (inhomogeneities create discontinuities in the stress), the classical energy conservation of elasticity theory is not valid any longer. Extending his famous result (force on an elastic singularity) to the other transformations, we quote here Eshelby [1951, p. 108]: "When all sources of internal stress and inhomogeneity within Σ are given a small displacement $\delta\xi_l$, the energy $F_l\delta\xi_l$ is available for conversion into kinetic energy or dissipation by some process not considered in the elastic theory."

7. Conclusions

By applying Noether's theorem, we derived the group of infinitesimal transformations of translation, scaling and rotation in elastodynamics under which the Lagrangian functional remains invariant and obtained the corresponding conservation laws. For inhomogeneities, we demonstrated that, under these transformations, the variation of the Lagrangian is equal to the negative of the variation of the Hamiltonian, and this provide the relations between the conservation integrals and the total energy loss of the system due to these transformations. This leads to the propositions that, under scaling of the inhomogeneity, if linear momentum is conserved in the domain, then the total energy loss of the system per unit infinitesimal scaling is equal to the dynamic *M*-integral, and under rotation, if linear and angular momenta are conserved in the domain, then the total energy loss of the system per unit infinitesimal rotation is equal to the dynamic *L*-integral. Thus, the propositions are physically interpreted as dissipative mechanisms for the loss of the Hamiltonian energy due to translation, scaling or rotation of the inhomogeneity; these propositions extend the static counterparts [Budiansky and Rice 1973] to elastodynamics.

References

[Atkinson and Eshelby 1968] C. Atkinson and J. D. Eshelby, "The flow of energy into the tip of a moving crack", *Int. J. Fract. Mech.* **4**:1 (1968), 3–8.

[Budiansky and Rice 1973] B. Budiansky and J. R. Rice, "Conservation laws and energy-release rates", *J. Appl. Mech.* (*ASME*) **40**:1 (1973), 201–203.

[Bui 1978] H. D. Bui, "Stress and crack-displacement intensity factors in elastodynamics", pp. 91–96 in *Advances in research on the strength and fracture of materials, 3A: Analysis and mechanics* (Waterloo, ON, 1977), edited by D. M. R. Taplin, Pergamon, Elmsford, NY, 1978.

[Callias and Markenscoff 1988] C. Callias and X. Markenscoff, "Singular asymptotics of integrals and the near-field radiated from nonuniformly moving dislocations", *Arch. Ration. Mech. Anal.* **102**:3 (1988), 273–285.

[Clifton and Markenscoff 1981] R. J. Clifton and X. Markenscoff, "Elastic precursor decay and radiation from nonuniformly moving dislocations", *J. Mech. Phys. Solids* **29**:3 (1981), 227–251.

[Eischen and Herrmann 1987] J. W. Eischen and G. Herrmann, "Energy release rates and related balance laws in linear elastic defect mechanics", *J. Appl. Mech.* (*ASME*) **54**:2 (1987), 388–392.

[Eshelby 1951] J. D. Eshelby, "The force on an elastic singularity", *Phil. Trans. R. Soc. A* **244**:877 (1951), 87–112.

[Eshelby 1956] J. D. Eshelby, "The continuum theory of lattice defects", *Solid State Phys.* **3** (1956), 79–144.

[Eshelby 1959] J. D. Eshelby, "Scope and limitations of the continuum approach", pp. 41–58 in *Internal stresses and fatigue in metals*, edited by G. N. Rassweiler and W. I. Grube, Elsevier, Amsterdam, 1959. Reprinted as pp. 269–286 in *Collected works of J. D. Eshelby: the mechanics of defects and inhomogeneities*, edited by X. Markenscoff and A. Gupta, Solid Mechanics and its Applications **133**, Springer, Dordrecht, 2006.

[Eshelby 1970] J. D. Eshelby, "Energy relations and the energy-momentum tensor in continuum mechanics", pp. 77–155 in *Inelastic behavior of solids*, edited by M. Kanninen et al., McGraw-Hill, New York, 1970. Reprinted as pp. 82–119 in *Fundamental contributions to the continuum theory of evolving phase interfaces in solids*, edited by J. M. Ball et al., Springer, Berlin, 1999.

[Eshelby 1975] J. D. Eshelby, "The elastic energy-momentum tensor", *J. Elasticity* **5**:3-4 (1975), 321–335.

[Fletcher 1976] D. C. Fletcher, "Conservation laws in linear elastodynamics", *Arch. Ration. Mech. Anal.* **60**:4 (1976), 329–353.

[Freund 1972] L. B. Freund, "Energy flux into the tip of an extending crack in an elastic solid", *J. Elasticity* **2**:4 (1972), 341–349.

[Freund 1990] L. B. Freund, *Dynamic fracture mechanics*, Cambridge University Press, 1990.

[Gelfand et al. 2000] I. M. Gelfand, S. V. Fomin, and R. A. Silverman, *Calculus of variations*, Dover, Mineola, NY, 2000.

[Günther 1962] W. Günther, "Über einige randintegrale der elastomechanik", *Abh. Brauchschw. Wiss. Ges.* **14** (1962), 53–72.

[Gupta and Markenscoff 2008] A. Gupta and X. Markenscoff, "Configurational forces as dissipative mechanisms: a revisit", *C. R. Mécanique* **336**:1 (2008), 126–131.

[Gupta and Markenscoff 2012] A. Gupta and X. Markenscoff, "A new interpretation of configurational forces", *J. Elasticity* **108**:2 (2012), 225–228.

[Herrmann 1981] A. G. Herrmann, "On conservation laws of continuum mechanics", *Int. J. Solids Struct.* **17**:1 (1981), 1–9.

[Herrmann 1982] A. G. Herrmann, "Material momentum tensor and path-independent integrals of fracture mechanics", *Int. J. Solids Struct.* **18**:4 (1982), 319–326.

[Herrmann and Kienzler 1999] G. Herrmann and R. Kienzler, "On the representation of basic laws of continuum mechanics by 4×4 tensors", *Mech. Res. Commun.* **26**:2 (1999), 145–150.

[Kienzler and Herrmann 2000] R. Kienzler and G. Herrmann, *Mechanics in material space: with applications to defect and fracture mechanics*, Springer, Berlin, 2000.

[Knowles and Sternberg 1972] J. K. Knowles and E. Sternberg, "On a class of conservation laws in linearized and finite elastostatics", *Arch. Ration. Mech. Anal.* **44**:3 (1972), 187–211.

[Lubarda and Markenscoff 2007] V. A. Lubarda and X. Markenscoff, "Dual conservation integrals and energy release rates", *Int. J. Solids Struct.* **44**:11 (2007), 4079–4091.

[Markenscoff 2006] X. Markenscoff, "Eshelby generalization for the dynamic J, L, M integrals", *C. R. Mécanique* **334**:12 (2006), 701–706.

[Markenscoff and Ni 2010] X. Markenscoff and L. Ni, "The energy-release rate and 'self-force' of dynamically expanding spherical and plane inclusion boundaries with dilatational eigenstrain", *J. Mech. Phys. Solids* **58**:1 (2010), 1–11.

[Maugin 1993] G. A. Maugin, *Material inhomogeneities in elasticity*, Applied Mathematics and Mathematical Computation **3**, Chapman and Hall, London, 1993.

[Ni and Markenscoff 2009] L. Ni and X. Markenscoff, "The logarithmic singularity of a generally accelerating dislocation from the dynamic energy-momentum tensor", *Math. Mech. Solids* **14**:1-2 (2009), 38–51.

[Ni and Markenscoff 2015] L. Ni and X. Markenscoff, "On self-similarly expanding Eshelby inclusions: spherical inclusion with dilatational eigenstrain", *Mech. Mater.* (online publication February 2015).

[Noether 1918] E. Noether, "Invariante variationsprobleme", *Nachr. Akad. Wiss. Göttingen Math.-Phys. Kl.* **1918** (1918), 235–257.

[Rice 1968] J. R. Rice, "A path independent integral and the approximate analysis of strain concentration by notches and cracks", *J. Appl. Mech.* (*ASME*) **35**:2 (1968), 379–386.

[Rice 1985] J. R. Rice, "Conserved integrals and energetic forces", pp. 33–56 in *Fundamentals of deformation and fracture*, edited by B. A. Bilby et al., Cambridge University Press, 1985.

[Rice and Drucker 1967] J. R. Rice and D. C. Drucker, "Energy changes in stressed bodies due to void and crack growth", *Int. J. Fract. Mech.* **3**:1 (1967), 19–27.

XANTHIPPI MARKENSCOFF: xmarkens@ucsd.edu
Department of Mechanical and Aerospace Engineering, University of California, San Diego, 9500 Gilman Drive, La Jolla, CA 92093-0411, United States

SHAILENDRA PAL VEER SINGH: spsingh@ucsd.edu
Department of Mechanical and Aerospace Engineering, University of California, San Diego, La Jolla, CA 92093-0411, United States

msp

INTEGRAL EQUATIONS FOR 2D AND 3D PROBLEMS OF THE SLIDING INTERFACE CRACK BETWEEN ELASTIC AND RIGID BODIES

ABDELBACET OUESLATI

This paper revisits the sliding interface crack problem between elastic and rigid half-planes studied by Bui and Oueslati and provides an alternative method of derivation of the solution, which will then be extended to three-dimensional (3D) crack problems. Based upon the displacement continuation technique of complex potentials, an appropriate Green function for the isolated edge dislocation dipole at the interface is given. Then by considering the sliding condition along the interface crack, the field equations can be obtained for the two-dimensional (2D) problem. Furthermore, it is shown that the edge dislocation dipole in 2D appears to be a particular form of the fundamental Kupradze–Basheleishvili tensor in 3D, which provides a method for deriving the coupled nonlinear integral equations for the same frictional interface plane crack of an arbitrary shape. The present work describes how the 3D sliding interface crack is related to the same problem in 2D.

1. Introduction

Cracks lying along the bonds between dissimilar materials or between elastic and rigid bodies are called interface cracks. They are encountered in delamination of composites, film-substrate combinations, fiber-reinforced materials, etc. Consequently, they are of great practical and theoretical importance and have been widely investigated in the literature.

It is well known that, in opening mode under tensile remote stress, there are overlaps of the interface crack faces due to the oscillatory behavior for the stress ahead of the crack tips [Williams 1959; England 1965; Rice 1988; Willis 1971]. To overcome this physical inconsistency, Comninou [1977; Comninou and Dundurs 1980] introduced a contact region behind the crack tip. If the compressive normal load is high enough, then the contact zone is the entire crack faces. Thus, the closed interface crack model combined with unilateral contact with friction must be considered. In the literature, many works are devoted to asymptotic solutions, including the effect of Coulomb's law of dry friction [Deng 1994; Audoly 2000; Bui and Oueslati 2005; Bui 1975; Bui and Oueslati 2004]. It is worth noting that analysis of frictional cracks is rather complex because firstly the problem is nonlinear and secondly the solution is not generally unique when no information is available on the crack history.

Crack problems have been often analyzed on the basis of Green's function or distribution of dislocations [Weertman 1996; Hills et al. 1996]. For interface cracks in bimaterials, the Green function is based on the solution of an edge dislocation at the interface, provided by [Nakahara et al. 1972]. Interface edge dislocation between two elastic layers was also studied by Suo and Hutchinson [1990]. In these solutions, the singularities of displacement and stresses are merely of the same nature as in the homogeneous case

with a little change in some coefficients: with displacement $\boldsymbol{u} \cong O(\log r)$ and u_1 discontinuous (term in $\operatorname{atan}(x_2/x_1)$) and with stress $\boldsymbol{\sigma} \cong O(1/r)$.

When the crack problems become 3D, the conventional methods such as Muskhelishvili's complex potentials can no longer be applied and appropriate methods have been developed. Without being exhaustive, it can be mentioned that the Neuber–Papkovich representation has been used [Kassir and Sih 1973]. An elegant and powerful tool is provided by the potential theory introduced by Kupradze [1963]. This method was used by Bui [1975] and Kossecka [1971] for deriving the integral equation for the crack opening displacement. Later Bui [1977] and Weaver [1977] proposed an integral equations method for the plane crack problem with an arbitrary shape. Furthermore, the weight functions for cracked bodies, introduced by Bueckner [1973], are often used for obtaining the stress intensity factors (SIFs) for 3D cracks. Fukuama and Madariaga [1995] derived a boundary integral equation for plane cracks in the static and dynamic cases. It is worth noting that few 3D crack problems have been solved analytically and the trend is to use numerical computations.

In the present work, we revisit the problem of the interface crack between an elastic half-plane and a rigid one in the presence of Coulomb's law of dry friction. The study is limited to the sliding branch of the friction law. In [Bui and Oueslati 2005], the solutions in complex form for nonhomogeneous loading at infinity were worked out. Here we derive this solution in a different manner by considering distribution of edge dislocation dipoles that correspond to the 2D expression of the fundamental Kupradze–Basheleishvili tensor in 3D. This remark allows us to extend the approach of solution to the 3D interface crack. A set of coupled integral equations for the crack displacement discontinuities is obtained.

2. Basic equations for the 2D sliding interface crack

Consider an elastic solid, with Lamé coefficient μ and λ, occupying the upper half-space Ω^+ and bonded to the lower rigid half-plane Ω^- along the x_1 axis, except on the crack $[b, a]$. We do not know the location of the crack tips b and a, which have to be determined by the solution of the equations.

Following [Bui and Oueslati 2005], let the uncracked system be subjected to some remote, not necessarily homogeneous, stress fields $\sigma_{ij}^\infty(x)$. Let the resulting stress field near the interface, prior to delamination, such that $u_1 = u_2 = 0$ at the interface be noted $\sigma_{ij}^0(\boldsymbol{x})$. We consider that $\sigma_{ij}^0(\boldsymbol{x})$ is prescribed load at the interface level, prior to delamination.

Localized shear stress and normal stress at the interface will likely cause delamination if the magnitude of the shear stress is high enough. It should be noted that the inhomogeneous applied stress field has been considered by Simonov [1990] for a frictionless interface crack. Note that, prior to delamination, no slip occurs if the excess stress $Q := f\sigma_{22}^0(x_1, 0) - \sigma_{12}^0(x_1, 0)$ is negative. This is the no-slip condition.

Consider the equations in quasistatic plane strain elasticity with the complex variable $z = x_1 + ix_2$. Displacements and stresses are expressed in terms of analytical functions $\phi(z)$ and $\psi(z)$ in Ω^+ with possible poles at infinity and singularities at the crack tips [Muskhelishvili 1977]:

$$2\mu(u_1 - iu_2) = \{\kappa\overline{\phi(z)} - \bar{z}\phi'(z) - \psi(z)\}, \tag{1}$$

$$(\sigma_{11} + \sigma_{22}) = 4\operatorname{Re}\{\phi'(z)\}, \tag{2}$$

$$(\sigma_{22} + i\sigma_{12}) = \overline{\phi'(z)} + \phi'(z) + \bar{z}\phi''(z) + \psi'(z). \tag{3}$$

The boundary conditions are

$$u_1 = u_2 = 0 \qquad \text{on the bonded zone,} \tag{4}$$

$$u_2 = 0, \quad |\sigma_{12}| = -f\sigma_{22} \quad (\sigma_{22} \le 0) \quad \text{on the sliding crack} \tag{5}$$

with the following conditions at infinity:

$$\sigma(\boldsymbol{x}) \to \sigma^\infty(\boldsymbol{x}) \quad \text{for } |\boldsymbol{x}| \to \infty \text{ in } \Omega^+, \tag{6}$$

$$\phi'(z \to \infty) = \tfrac{1}{4}(\sigma_{11}^\infty + \sigma_{22}^\infty) - \frac{i}{1+\kappa}\sigma_{12}^\infty, \tag{7}$$

$$\psi'(z \to \infty) = \tfrac{1}{2}(\sigma_{22}^\infty - \sigma_{11}^\infty) + i\sigma_{12}^\infty, \tag{8}$$

where $\kappa = 3 - 4\nu$ in plane strain (ν is the Poisson ratio) and f is the friction coefficient. In (5), the inequality $\sigma_{22} \le 0$ is not prescribed but has to be checked a posteriori. The crack is defined by the cut along $[b, a]$. Particles of Ω^+ along the cut can move horizontally.

Equations (1)–(8) are strictly defined in the upper plane. However, we assume that $\phi(z)$ and $\psi(z)$ can be extended to the whole plane with a cut along the crack by analytical continuations across the bonded zones. Of course, expressions in the right-hand sides of (1)–(3) have no physical meaning in the lower half-plane for the problem considered. They are introduced for mathematical purposes in the derivation of the solution. Nevertheless, we shall see that the formal solution obtained in the lower half-plane corresponds to a similar problem of the elastic half-plane Ω^- adhering on the rigid upper body Ω^+. These solutions for the displacement fields in both problems are linked together by antisymmetry.

From condition (4) on the bonded zone, we obtain

$$2\mu(u_1 - iu_2) = \{\kappa\overline{\Phi(z)} - \bar{z}\phi'(z) - \psi(z)\}$$
$$= \{\kappa\bar{\Phi}(z) - z\phi'(z) - \psi(z)\} = 0 \quad \text{(on the unbroken zone).}$$

This equation suggests the following definition for the function $\psi(z)$ not only in Ω^+ but also in Ω^-:

$$\psi(z) := \kappa\bar\phi(z) - z\phi'(z). \tag{9}$$

The continuation used in (9) is normally referred to as a displacement continuation (rather than the more common stress continuation). Using (9) for (3) and (1), we find on the real axis $z = \bar{z}$

$$\sigma_{22} - i\sigma_{12} = \phi'(z) + \kappa\phi'(\bar{z}), \tag{10}$$

$$2\mu(u_1 - iu_2) = \{\kappa\overline{\phi(z)} - \bar{z}\phi'(z) - \psi(z)\} = \kappa\{\overline{\phi(z)} - \bar\phi(z)\}, \tag{11}$$

$$2\mu(u_1 + iu_2) = \{\kappa\phi(z) - z\overline{\phi'(z)} - \overline{\psi(z)}\} = \kappa\{\phi(z) - \phi(\bar{z})\}. \tag{12}$$

We recover the adherence condition $u_1 - iu_2 = 0$ on the bonded zone where the function $\phi(z)$ is continuous $\phi(z) = \phi(\bar{z})$. The condition that $u_2 = 0$, on the cut, corresponds to the imaginary part of the right-hand side of (12) being zero on the cut.

We introduce the auxiliary stress field $\theta_{ij}(\boldsymbol{x})$, the corresponding auxiliary displacement field $\boldsymbol{q}(\boldsymbol{x})$, and the associate auxiliary complex functions $\Theta(z)$ and $\Xi(z)$ by putting

$$\boldsymbol{\theta} = \boldsymbol{\sigma} - \boldsymbol{\sigma}^0. \tag{13}$$
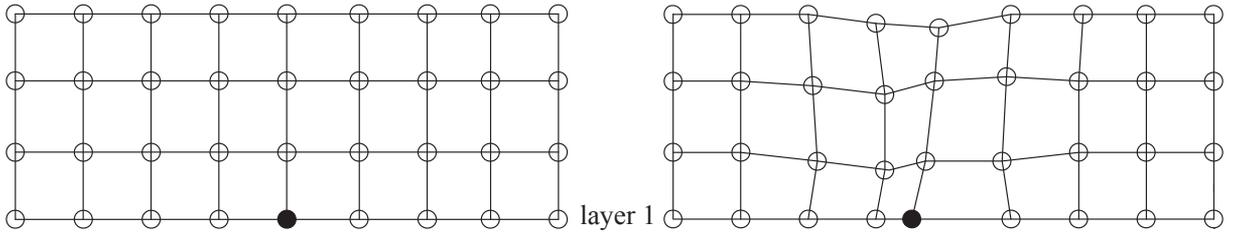
Figure 1. Atoms of layer 1 stuck on the rigid interface, except the black atom.

On the crack, since the displacement components associated to $\boldsymbol{\sigma}^0(\boldsymbol{x})$ vanish, the auxiliary displacement fields $q_1(x_1, 0)$ and $q_2(x_1, 0)$ coincide with the current displacement fields $u_1(x_1, 0)$ and $u_2(x_1, 0)$. At infinity, the stress field $\theta_{ij}(\boldsymbol{x})$ vanishes; hence, the function $\Theta'(z)$ vanishes at infinity:

$$\Theta'(z) \cong O(1/z) \quad \text{at infinity.} \tag{14}$$

Moreover, the continuity condition (or the compatibility condition) on the displacement (12) holds for the auxiliary fields $\boldsymbol{q}$ and gives

$$2\mu(q_1 + iq_2) = \kappa\{\Theta(z) - \Theta(\bar{z})\} \quad \text{for } z = \bar{z}. \tag{15}$$

3. The isolated edge dislocation dipole

Let us consider an atomic model of defect at the interface between an elastic medium and a rigid body shown in Figure 1. Suppose that all atoms of layer 1 are fixed, being stuck on the rigid interface, except the black atom, which is debonded from the substratum and can glide to the left.

When we move around the black atom along the lattice, from one atom of layer 1 to another one in the same layer 1, we recover the same unchanged positions of atoms. It is expected that displacement and stress fields in the upper half-plane are more singular than in the case of edge dislocation in homogeneous medium. To investigate the mathematical nature of such an isolated "defect" at the origin of the real axis as shown in Figure 1, where $q_2 = 0$ on the real axis, $q_1 = 0$ for $(x_1 \neq 0, x_2 = 0)$, and $q_1 \neq 0$ at $(x_1 = 0, x_2 = 0)$, we consider the displacement on the real axis from the Ω^+ side, given as

$$2\mu(q_1 + iq_2) = k\{\Theta(z) - \Theta(\bar{z})\} \quad (z = \bar{z}). \tag{16}$$

In the continuation of functions in Ω^- through the bonded zone, we may consider the lower half-plane as an elastic medium stuck on the rigid upper half-plane, except along the crack; in Ω^-, the displacement field is antisymmetric. Therefore, the defect shown in Figure 1 corresponds to the solution in Ω^+ of an edge dislocation dipole in shear mode as in Figure 2 (left). The edge dislocation dipole in the opening mode is depicted in Figure 2 (right).

Consider the function defined in the whole space (upper and lower complex plane Ω^+ and Ω^-) as

$$\Theta^{(h)}(z) = \chi \frac{1}{2ih\pi}\{\log(z + h) - \log(z)\} \tag{17}$$

with complex $\chi = c_1 + ic_2$, $c_1 > 0$ and $c_2 < 0$, and the cut along $(-h, 0)$.
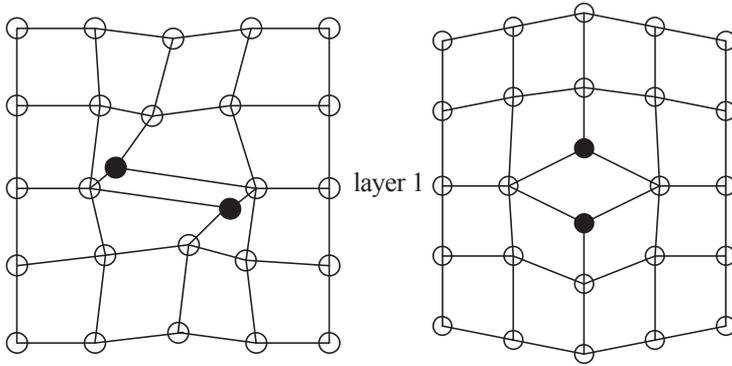
Figure 2. Edge dislocation dipoles in shear mode (left) and opening mode (right). Atoms of layer 1 are fixed, except the (double) black atoms moving in opposite directions in Ω^+ and Ω^-.

Outside the cut, $\Theta^{(h)}(z)$ is continuous so that $q_1^{(h)} + iq_2^{(h)} = 0$ on the part of the real axis where $x_2 = 0$, $x_1 < -h$, and $x_1 > 0$.

On the upper face of the cut, we find

$$2\mu(q_1^{(h)} + iq_2^{(h)}) = k(\Theta^{(h)}(z^+) - \Theta^{(h)}(z^-)) = -\frac{k}{h}(c_1 + ic_2). \tag{18}$$

Now taking the limit of (17) as $h \to 0$, we obtain firstly the derivative of the logarithm function:

$$\Theta^{(0)}(z) = \chi \frac{1}{2i\pi} \frac{1}{z}. \tag{19}$$

Secondly, the limit of the constant function (18) over the interval $[-h, 0]$ of vanishing length $h \to 0$, which is nothing but the Dirac delta function:

$$2\mu(q_1^{(0)} + iq_2^{(0)}) = -k(c_1 + ic_2)\delta(x_1). \tag{20}$$

The displacement singularity given in Ω^+ by the function (19) is higher than that of an isolated edge dislocation in homogeneous medium. At the defect itself, the displacement (20) can be considered as the Green function. Note that, for an edge dislocation in a bimaterial, the Dirac delta function appears in the stresses at the interface: $\sigma_{22} + i\sigma_{12} = 2\bar{B}(1/x_1 + \pi i\beta'\mu\delta(x_1))$ (for $x_2 = 0$), where B and β' are some bimaterial constants [Suo and Hutchinson 1990]. Here the Dirac delta function is found in the displacement at the interface. The components of the displacement at x in the upper half-plane, $x_2 > 0$, due to an isolated edge dislocation dipole at the origin $y = 0$, in the pure shear mode $\chi = c_1$ ($c_2 = 0$), are given as (with $\Theta(z) = \Theta^0(z) = c_1/2i\pi z$ and $\bar{\Theta}'(\bar{z}) = -c_1/2i\pi\bar{z}^2$)

$$2\mu(q_1 + iq_2) = k\{\Theta(z) - \Theta(\bar{z})\} + (\bar{z} - z)\bar{\Theta}'(\bar{z}) \quad \text{for } x_2 > 0, \tag{21}$$

$$2\mu q_1(x_1 + i0) = -kc_1\delta(x_1) \quad \text{and} \quad 2\mu q_2 = 0 \qquad \text{for } x_2 = 0^+. \tag{22}$$

Thus, we obtain for $x_2 > 0$

$$2\mu(q_1 + iq_2) = -c_1\frac{k}{\pi}\frac{x_2}{x_1^2 + x_2^2} - c_1\frac{x_2(x_1^2 - x_2^2)}{\pi(x_1^2 + x_2^2)^2} - 2ic_1\frac{x_1x_2^2}{\pi(x_1^2 + x_2^2)^2}. \tag{23}$$
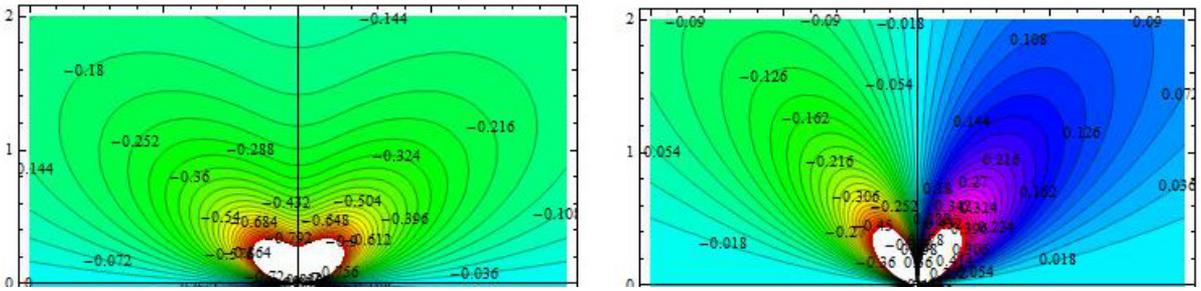
Figure 3. Contours of the displacement field given by (23) ($c_1 = 1$): on the left $2\mu q_1$ and on the right $2\mu q_2$.

The contours of the displacement field in the upper half-plane due to an isolated dipole dislocation given by (23) are depicted in Figure 3.

The displacement at $x = (x_1, x_2)$ in the entire plane due to an edge dislocation dipole at $y = (y_1, 0)$ on the real axis (of normal e^2), not necessarily at the origin, satisfies the elastic equilibrium equation and the following boundary condition on the real axis ($x^\pm = (x_1, \pm 0)$):

$$-\frac{2\mu}{kc_1} q^{(0)}(x^\pm, y, e^2) = \pm\delta(x - y)e^1 \quad (x_2 = y_2 = 0). \tag{24}$$

We recover in (20), (21), (22), and (24) the particular 2D form of the Kupradze–Basheleishvili fundamental tensor $B(x, y, n_P)$ given for 3D solids [Kupradze 1963] with components (see Appendix A)

$$B_i^j(x, y, n(y)) = \frac{1}{2\pi(\lambda + 3\mu)}\{2\mu\delta_{ij} + 3(\lambda + \mu)(x_i - y_i)(x_j - y_j)\rho^{-2}\}\frac{\partial}{\partial n_y}\frac{1}{\rho}, \tag{25}$$

where $\rho = \sqrt{(x_i - y_i)(x_i - y_i)}$. The elastic displacement vector $B^j(x, y, n_P)$ at point x is discontinuous at $x = y$ on the plane P of normal n_P. The discontinuity along the unit vector e^j is given by

$$B^j(x^\pm, y, n_P) = \pm\delta_P(x - y)e^j, \tag{26}$$

where $\delta_P(x - y)$ is the Dirac delta function on the plane P. Therefore, the vector $q^{(0)}(x^\pm, y, e^2)$ is the particular form in 2D of the vector $B^1(x^\pm, y, e^2)$ in 3D with $x^\pm = (x_1, x_2, \pm 0)$.

By integrating (25) with respect to y_3, $-\infty < y_3 < \infty$, we obtain the 2D singular defect $q^{(0)}(x^\pm, y, e^2)$ for P normal to e^2. Point defects with properties (24) or (26) are purely mathematical. They are boundary Green functions for determining the displacement field in 2D and 3D.

4. Solution of the Dirichlet boundary value problem and the singular integral equation for the 2D sliding crack

Consider the following boundary value problem of the elastic half-plane $x_2 > 0$, where both components of displacement $q_1(t)$ and $q_2(t) = 0$ are prescribed on the interface ($x_2 = 0$) with $q_1(\pm\infty) = 0$. Find the stresses on $x_2 = 0$.

Using results of the previous section, in the pure shear mode and from (19) and (20), the solution is

$$\Theta(z) = \frac{1}{2i\pi} \int_{-\infty}^{+\infty} \frac{-2\mu q_1(t)}{\kappa} \frac{dt}{z-t}.$$

(27)

Remark. It is possible to derive the potential $\Theta(z)$ given by (27) by another method. To this end, we search for a solution of (15) using the Cauchy integral kernel $1/(z-t)$ and by considering $\chi(t)$ as unknown density:

$$\Theta(z) = \frac{1}{2i\pi} \int_{-\infty}^{+\infty} \chi(t) \frac{dt}{z-t} = -\frac{1}{2i\pi} \int_{-\infty}^{+\infty} \chi(t) \frac{dt}{t-z}.$$

(28)

Thus, using $2\mu(q_1 + iq_2) = \kappa\{\Theta(z) - \Theta(\bar{z})\}$ $(z = \bar{z})$, we obtain the density as $\chi(t) = -2\mu q_1(t)/\kappa$.

The stress in $x_2 > 0$ is then given by (10) as

$$\theta_{22}(x_1) - i\theta_{12}(x_1) = \Theta'(z) + \kappa\Theta'(\bar{z})$$

$$= -\frac{1}{2i\pi} \int_{-\infty}^{+\infty} \chi'(t) \frac{dt}{t-z} - \frac{\kappa}{2i\pi} \int_{-\infty}^{+\infty} \chi'(t) \frac{dt}{t-\bar{z}}$$

$$= \frac{2\mu}{\kappa} \left\{ \frac{1}{2i\pi} \int_{-\infty}^{+\infty} q_1'(t) \frac{dt}{t-z} + \kappa \frac{1}{2i\pi} \int_{-\infty}^{+\infty} q_1'(t) \frac{dt}{t-\bar{z}} \right\}.$$

Using Plemelj formulas ($z = x_1 + i0$ and $\bar{z} = x_1 - i0$), we then obtain the solution (pv = principal value) for the stress at the interface as

$$\theta_{12}(x_1) = \frac{\mu}{\kappa\pi}(1+\kappa)(\text{pv}) \int_{-\infty}^{+\infty} q_1'(t) \frac{dt}{t-x_1},$$

(29)

$$\theta_{22}(x_1) = \frac{\mu}{\kappa}(1-\kappa)q_1'(x_1).$$

(30)

Equations (29) and (30) are particular forms (for $q_2(t) = 0$) of the general solution derived in [Bui 1968], where general boundary conditions $q_1(t) \neq 0$ and $q_2(t) \neq 0$ are considered and where the Kupradze–Basheleishvili tensor $B(x, y, n)$ has been used.

Equations (5), (29), and (30) allow us to establish the integral equation for the unknown $q_1'(x_1)$ in the frictional sliding interface crack problem considered in this paper with data σ_{12}^0 and σ_{22}^0. To this end, we have to express the friction condition on the current stresses $\sigma_{12} = f\sigma_{22}$, with $\sigma = \sigma^0 + \theta$, as

$$\theta_{12} - f\theta_{22} = f\sigma_{22}^0 - \sigma_{12}^0$$

and then obtain the integral equation

$$-f\frac{\mu}{\kappa}(1-\kappa)q_1'(x_1) + \frac{\mu}{\kappa\pi}(1+\kappa)(\text{pv}) \int_b^a q_1'(t) \frac{dt}{t-x_1} = f\sigma_{22}^0(x_1) - \sigma_{12}^0(x_1).$$

(31)

It is a Carleman integral equation with the unknown $q_1'(x)$, the gradient of the horizontal displacement on the sliding crack lip. The general theory of such integral equations is provided in [Muskhelishvili 1977; Tricomi 1985] for example.

Let us introduce the coefficients $A = -f(\mu/\kappa)(1-\kappa)$ and $B = i(\mu/\kappa)(1+\kappa)$. The index of this integral equation is $\tau = (1/2i\pi) \log G$, where $G = (A-B)/(A+B) = -((\kappa+1)+if(\kappa-1))/((\kappa+1)-if(\kappa-1))$.

According to [Muskhelishvili 1977], the solution of the integral equation (31) vanishing at infinity is

$$q'_1(x_1) = \frac{X^+(x_1) + X^-(x_1)}{2(A+B)X^+(x_1)} (f\sigma_{22}^0(x_1) - \sigma_{12}^0(x_1))$$
$$+ \frac{X^+(x_1) - X^-(x_1)}{2i\pi} (\text{pv}) \int_b^a \frac{f\sigma_{22}^0(t) - \sigma_{12}^0(t)}{(A+B)X^+(t)} \frac{dt}{(t-x_1)}, \quad (32)$$

where $X(z) = (z-b)^{n/2-\tau}(z-a)^{m/2+\tau}$ is the fundamental solution of the homogenous Riemann–Hilbert problem $X^+(z) = GX^-(z)$.

The closed-form expression of (32) gives

$$q'_1(x_1) = \frac{f\kappa(\kappa-1)}{\mu((\kappa+1)^2 + f^2(\kappa-1)^2)} (f\sigma_{22}^0(x_1) - \sigma_{12}^0(x_1))$$
$$- \frac{\kappa(\kappa-1)X^+(x_1)}{\mu\pi((\kappa+1)^2 + f^2(\kappa-1)^2)} (\text{pv}) \int_b^a \frac{f\sigma_{22}^0(t) - \sigma_{12}^0(t)}{X^+(t)} \frac{dt}{(t-x_1)}. \quad (33)$$

Some noticeable features are that G is equal to g, the coefficient of the Hilbert problem established in [Bui and Oueslati 2005, (22)], the index τ coincides with the coefficient α, and

$$\frac{f\sigma_{22}^0(x_1) - \sigma_{12}^0(x_1)}{A+B} = \frac{k}{\mu} E_0(x),$$

where $E_0(x)$ is the second member of the Hilbert problem derived in [Bui and Oueslati 2005].

The closed form and physical solution (square-integrable solution) of the integral equation (33) for a polynomial remote loading $(\sigma_{22}^0, \sigma_{12}^0)$ for example can be found in [Bui and Oueslati 2005].

5. Integral equations for the sliding planar crack of an arbitrary shape

Analysis of the 3D problem of sliding delamination between an elastic half-space Ω^+ ($x_3 > 0$) and a rigid body under Coulomb's friction is very difficult. We do not attempt to solve this problem and restrict ourselves simply to the following one: given the auxiliary shear stresses $\theta_{31}(x_1, x_2, 0)$ and $\theta_{32}(x_1, x_2, 0)$ and normal stress $\theta_{33}(x_1, x_2, 0)$ on the interface plane P ($x_3 = 0$), prior to delamination, find the integral equations for tangential auxiliary displacements $\varphi_1(x_1, x_2) := q_1(x_1, x_2, 0)$ and $\varphi_2(x_1, x_2) := q_2(x_1, x_2, 0)$ in the planar crack S.

First of all, we generalize (29) and (30) to 3D problems. Let $\boldsymbol{x} = (x_1, x_2, x_3)$, $\boldsymbol{y} = (y_1, y_2, 0)$, and $\boldsymbol{z} = (z_1, z_2, 0)$. The fundamental Kupradze–Basheleishvili tensor (25) gives the displacement field in Ω^+:

$$q_i(\boldsymbol{x}) = \int_S B_i^j(\boldsymbol{x}, \boldsymbol{y}, \boldsymbol{e}^3)\varphi_j(\boldsymbol{y}) \, dS_y. \quad (34)$$

To verify that, we take the limit $\boldsymbol{x} \to \boldsymbol{y}^+ = (y_1, y_2, 0^+)$ and using (26) obtain $q_j(\boldsymbol{y}^+) = \varphi_j(\boldsymbol{y})$. Note that the displacement of points in P lying outside S vanishes. This means that (34) corresponds exactly to the displacement field of the elastic body Ω^+ stuck on the rigid surface P, except on the crack S.

The density $\varphi_j(\boldsymbol{y})$ of the double layer potential (34) (see Appendix C) is exactly the displacement in S. For convenience, the displacement representation in terms of the single layer potential is outlined in Appendix B.

From (34), we can calculate the stress field in Ω^+ and also on P. Such a calculation is somewhat delicate because of strongly singular kernels. However, explicit formulas for the stresses on P have been given in [Bui 1968; 1977]:

- tangential stresses

$$\theta_{3\alpha}(\boldsymbol{y}) = \frac{\mu}{2\pi}(\text{pv}) \int_S \frac{\partial \varphi_\alpha}{\partial z_\beta} \frac{\partial}{\partial y_\beta} \frac{1}{\rho(\boldsymbol{y}, \boldsymbol{z})} \, dS_z + \frac{\mu(\lambda + \mu)}{2\pi(\lambda + 3\mu)}(\text{pv}) \int_S \left(\frac{\partial \varphi_1}{\partial z_1} + \frac{\partial \varphi_2}{\partial z_2} \right) \frac{\partial}{\partial y_\alpha} \frac{1}{\rho(\boldsymbol{y}, \boldsymbol{z})} \, dS_z, \quad (35)$$

- normal stress

$$\theta_{33}(\boldsymbol{y}) = \frac{2\mu^2}{\lambda + 3\mu} \left(\frac{\partial \varphi_1}{\partial y_1} + \frac{\partial \varphi_2}{\partial y_2} \right). \tag{36}$$

We are now in a position to derive the integral equations for the frictional interface crack S with prescribed stresses $(\sigma_{31}^0, \sigma_{32}^0, \sigma_{33}^0)$ on the plane P. Assume that $\sigma_{31}^0 < 0$, $\sigma_{32}^0 < 0$, and $\sigma_{33}^0 < 0$. Such an assumption can only be verified a posteriori so that the friction law can be written as $\sigma_{31} - f\sigma_{33}\cos(\psi) = 0$ and $\sigma_{32} - f\sigma_{33}\sin(\psi) = 0$, where $\psi = \text{atan}(\varphi_2/\varphi_1)$. We then obtain the coupled *nonlinear* integral equations for φ_α, which are the generalizations of (31) to 3D problems:

$$\frac{\mu}{2\pi}(\text{pv}) \int_S \frac{\partial \varphi_1}{\partial z_\beta} \frac{\partial}{\partial y_\beta} \frac{1}{\rho(\boldsymbol{y}, \boldsymbol{z})} \, dS_z + \frac{\mu(\lambda + \mu)}{2\pi(\lambda + 3\mu)}(\text{pv}) \int_S \left(\frac{\partial \varphi_1}{\partial z_1} + \frac{\partial \varphi_2}{\partial z_2} \right) + \frac{\partial}{\partial y_1} \frac{1}{\rho(\boldsymbol{y}, \boldsymbol{z})} \, dS_z$$

$$- f \frac{\varphi_1}{\sqrt{\varphi_1^2 + \varphi_2^2}} \frac{2\mu^2}{(\lambda + 3\mu)} \left(\frac{\partial \varphi_1}{\partial y_1} + \frac{\partial \varphi_2}{\partial y_2} \right) = f\sigma_{33}^0(\boldsymbol{y}) - \sigma_{31}^0(\boldsymbol{y}) \quad (37)$$

and

$$\frac{\mu}{2\pi}(\text{pv}) \int_S \frac{\partial \varphi_2}{\partial z_\beta} \frac{\partial}{\partial y_\beta} \frac{1}{\rho(\boldsymbol{y}, \boldsymbol{z})} \, dS_z + \frac{\mu(\lambda + \mu)}{2\pi(\lambda + 3\mu)}(\text{pv}) \int_S \left(\frac{\partial \varphi_1}{\partial z_1} + \frac{\partial \varphi_2}{\partial z_2} \right) \frac{\partial}{\partial y_2} \frac{1}{\rho(\boldsymbol{y}, \boldsymbol{z})} \, dS_z$$

$$- f \frac{\varphi_2}{\sqrt{\varphi_1^2 + \varphi_2^2}} \frac{2\mu^2}{(\lambda + 3\mu)} \left(\frac{\partial \varphi_1}{\partial y_1} + \frac{\partial \varphi_2}{\partial y_2} \right) = f\sigma_{33}^0(\boldsymbol{y}) - \sigma_{32}^0(\boldsymbol{y}). \quad (38)$$

It is out of the scope of this paper to derive the solution to (37)–(38), even by a numerical method. However, it is worth noting that these integral equations extend over the crack surface only, which has many advantages for numerical analysis.

Finally, if we interpret the SIFs K_I and K_II along the crack front, as factors of the tangential displacement discontinuity [Bui 2006], then the two sliding modes are nonlinearly coupled in the frictional 3D crack problems.

6. Conclusion

In this paper, the problem of the frictional sliding interface crack between an elastic half-plane and a rigid one has been analyzed by considering distribution of edge dislocation dipoles along the crack faces. We recover the field equations obtained in [Bui and Oueslati 2005] by means of complex potential representation. Then this approach has been extended to the planar interface crack with an arbitrary shape thanks to the fundamental Kupradze–Basheleishvili tensor. A couple of nonlinear integral equations for the crack

displacement discontinuities have been derived. It is worth noting that these integrals are taken only over the crack face, which will be interesting in numerical computations. This is a topic for future work.

Appendix A: The Kupradze–Basheleishvili tensor

Let Ω be an elastic solid in 3D space $\mathbb{R}^3$ with a piecewise smooth boundary $\partial\Omega$ and $\boldsymbol{x}$ be the Cartesian coordinates. The elastic operator L is defined such that the Lamé–Navier equation reads

$$L\boldsymbol{u} := \mu\Delta\boldsymbol{u} + (\lambda + \mu)\nabla\nabla\cdot\boldsymbol{u} + \boldsymbol{f} = 0 \quad \text{in } \Omega,$$

where $\boldsymbol{u}$ is the displacement field in the solid Ω and $\boldsymbol{f}$ denotes for the body force.

The corresponding traction acting on the boundary of $\partial\Omega$ with the outward unit normal $\boldsymbol{n}$ is obtained from the displacement $\boldsymbol{u}$ by applying the traction operator

$$T^n := 2\mu\frac{\partial}{\partial n} + \lambda\boldsymbol{n}\,\mathrm{div} + \mu\boldsymbol{n}\wedge\mathrm{rot}.$$

The fundamental Kupradze–Basheleishvili operator associated to a plane P_y, with normal $\boldsymbol{n}_y$ at the point $\boldsymbol{y}$, is defined by the tensor $\boldsymbol{B}$ satisfying

$$L\boldsymbol{B}^k(\boldsymbol{x}, \boldsymbol{y}; \boldsymbol{n}_y) = 0, \quad k \in \{1, 2, 3\}, \ \boldsymbol{x} \notin P_y \text{ for fixed } \boldsymbol{y} \in P_y,$$

and the boundary conditions

$$\boldsymbol{B}^k(\boldsymbol{x}, \boldsymbol{y}; \boldsymbol{n}_y) = \boldsymbol{0}, \quad \boldsymbol{x}, \boldsymbol{y} \in P_y \text{ and } \boldsymbol{x} \neq \boldsymbol{y}.$$

The components of $\boldsymbol{B}^k(\boldsymbol{x}, \boldsymbol{y}; \boldsymbol{n}_y)$ read

$$B_i^k(\boldsymbol{x}, \boldsymbol{y}, \boldsymbol{n}_y) = \frac{1}{2\pi(\lambda + 3\mu)}\{2\mu\delta_{ik} + 3(\lambda + \mu)(x_i - y_i)(x_k - y_k)\rho^{-2}\}\frac{\partial}{\partial n_y}\frac{1}{\rho},$$

where $\rho = \sqrt{(x_i - y_i)(x_i - y_i)}$ is the Euclidean distance between $\boldsymbol{x}$ and $\boldsymbol{y}$. It should be noted that $\boldsymbol{B}^k(\boldsymbol{x}, \boldsymbol{y}; \boldsymbol{n}_y) = -\boldsymbol{B}^k(\boldsymbol{y}, \boldsymbol{x}; \boldsymbol{n}_y)$.

Following [Bui 2006], it can be shown, for a point $\boldsymbol{x}$ on the plane P_y, that the vectors defined by

$$\boldsymbol{B}^k(\boldsymbol{x}^\pm, \boldsymbol{y}; \boldsymbol{n}_y) = \pm\boldsymbol{e}^k\delta_{P_y}(\boldsymbol{y} - \boldsymbol{x})$$

are opposite Dirac delta distributions. Physically, the k-component of the Kupradze–Basheleishvili tensor is a dislocation dipole in the $\boldsymbol{e}^k$ direction. The previous relation is often used to describe the displacement jump on the crack faces.

Appendix B: Single layer potential

The displacement field solution of the elastic problem in the absence of body force can be obtained in terms of an integral surface $S_i(\boldsymbol{x})$ with a continuous density ψ_i and a kernel $V_i^k(\boldsymbol{x}, \boldsymbol{z})$:

$$S_i(\boldsymbol{x}) = 2\int_{\partial\Omega} V_i^k(\boldsymbol{x}, \boldsymbol{z})\psi_k(\boldsymbol{z})\,dS_z.$$

By analogy with Newton's potential, this integral is called the single layer potential. It is continuous across the surface $\partial\Omega$, but the corresponding stresses with a component along the normal should be discontinuous.

According to [Kupradze 1963], the stress vector exerted on the boundary $\partial\Omega$ is obtained by using the traction operator T^n to both sides of the previous equation:

$$T^n S(y^{\pm}) = \pm \psi(y) + 2(\text{pv}) \int_{\partial\Omega} V_i^k(x, z) \psi_k(z) \, dS_z.$$

Appendix C: Double layer potential

The displacement field solution of the elastic problem in the absence of body force can be represented by an elastic potential $D_i(x)$ with a continuous density ϕ_i:

$$D_i(x) = \int_{\partial\Omega} B_i^k(x, z; n_z) \phi_k(z) \, dS_z.$$

It can be established that $D(x)$ is discontinuous across the surface $\partial\Omega$ [Kupradze 1963]:

$$D(x^+) - D(x^-) = 2\phi(x).$$

The limit of $D(x)$ when x tends to x^- belonging to the surface $\partial\Omega$ gives

$$D_i(x^-) = \phi_i(x^-) + \int_{\partial\Omega} B_i^k(x, z; n_z) \phi_k(z) \, dS_z.$$

References

[Audoly 2000] B. Audoly, "Asymptotic study of the interfacial crack with friction", *J. Mech. Phys. Solids* **48**:9 (2000), 1851–1864.

[Bueckner 1973] H. F. Bueckner, "Field singularities and related integral representations", pp. 239–314 in *Methods of analysis and solutions of crack problems*, edited by G. C. Sih, Mechanics of Fracture **1**, Springer, Dordrecht, 1973.

[Bui 1968] H. D. Bui, "Transformation des données aux limites relatives au demi-plan élastique homogène et isotrope", *Int. J. Solids Struct.* **4**:10 (1968), 1025–1030.

[Bui 1975] H. D. Bui, "Application des potentiels élastiques à l'étude des fissures planes de forme arbitraire en milieu tridi-mensionnel", *C. R. Acad. Sci. Paris A* **280** (1975), 1157–1160.

[Bui 1977] H. D. Bui, "An integral equations method for solving the problem of a plane crack of arbitrary shape", *J. Mech. Phys. Solids* **25**:1 (1977), 29–39.

[Bui 2006] H. D. Bui, *Fracture mechanics: inverse problems and solutions*, Solid Mechanics and its Applications **139**, Springer, Dordrecht, 2006.

[Bui and Oueslati 2004] H. D. Bui and A. Oueslati, "Solutions exactes de fissure d'interface sous contact frottant avec un milieu indéformable", *C. R. Mécanique* **332**:9 (2004), 709–716.

[Bui and Oueslati 2005] H. D. Bui and A. Oueslati, "The sliding interface crack with friction between elastic and rigid bodies", *J. Mech. Phys. Solids* **53**:6 (2005), 1397–1421.

[Comninou 1977] M. Comninou, "Interface crack with friction in the contact zone", *J. Appl. Mech.* **44**:4 (1977), 780–781.

[Comninou and Dundurs 1980] M. Comninou and J. Dundurs, "Effect of friction on the interface crack loaded in shear", *J. Elasticity* **10**:2 (1980), 203–212.

[Deng 1994] X. Deng, "An asymptotic analysis of stationary and moving cracks with frictional contact along bimaterial and in homogeneous solids", *Int. J. Solids Struct.* **31**:17 (1994), 2407–2429.

[England 1965] A. H. England, "A crack between dissimilar media", *J. Appl. Mech.* **32**:2 (1965), 400–402.

[Fukuama and Madariaga 1995] E. Fukuama and R. Madariaga, "Integral equation method for plane crack with an arbitrary shape in 3D elastic medium", *Bull. Seismol. Soc. Am.* **85**:2 (1995), 614–628.

[Hills et al. 1996] D. A. Hills, P. A. Kelly, D. N. Dai, and A. M. Korsunsky, *Solution of crack problems: the distributed dislocation technique*, Solid Mechanics and its Applications **44**, Springer, Dordrecht, 1996.

[Kassir and Sih 1973] M. K. Kassir and G. C. Sih, "Application of Papkovich–Neuber potentials to a crack problem", *Int. J. Solids Struct.* **9**:5 (1973), 643–654.

[Kossecka 1971] E. Kossecka, "Defects as surface distributions of double forces", *Arch. Mech. Stos.* **23** (1971), 481–494.

[Kupradze 1963] V. D. Kupradze, *Progress in solid mechanics, III: Dynamical properties in elasticity*, North Holland, Amsterdam, 1963.

[Muskhelishvili 1977] N. I. Muskhelishvili, *Some basic problems of the mathematical theory of elasticity: fundamental equations, plane theory of elasticity, torsion and bending*, 2nd ed., Springer, Dordrecht, 1977.

[Nakahara et al. 1972] S. Nakahara, J. B. C. Wu, and J. C. M. Li, "Dislocations in a welded interface between two isotropic media", *Mater. Sci. Eng.* **10** (1972), 291–296.

[Rice 1988] J. R. Rice, "Elastic fracture mechanics concepts for interfacial cracks", *J. Appl. Mech.* **55**:1 (1988), 98–103.

[Simonov 1990] L. V. Simonov, "An interface crack in an inhomogeneous stress field", *Int. J. Fract.* **46**:3 (1990), 223–235.

[Suo and Hutchinson 1990] Z. Suo and J. W. Hutchinson, "Interface crack between two elastic layers", *Int. J. Fract.* **43**:1 (1990), 1–18.

[Tricomi 1985] F. G. Tricomi, *Integral equations*, Dover, New York, 1985.

[Weaver 1977] J. Weaver, "Three-dimensional crack analysis", *Int. J. Solids Struct.* **13**:4 (1977), 321–330.

[Weertman 1996] J. Weertman, *Dislocation based fracture mechanics*, World Scientific, Singapore, 1996.

[Williams 1959] M. L. Williams, "The stresses around a fault or crack in dissimilar media", *Bull. Seismol. Soc. Am.* **49**:2 (1959), 199–204.

[Willis 1971] J. R. Willis, "Fracture mechanics of interfacial cracks", *J. Mech. Phys. Solids* **19**:6 (1971), 353–368.

ABDELBACET OUESLATI: abdelbacet.oueslati@univ-lille1.fr
Laboratoire de Mécanique de Lille, CNRS UMR 8107, Université de Lille 1, 59655 Villeneuve d'Ascq, France

msp

ASYMPTOTIC STRESS FIELD IN THE VICINITY OF
A MIXED-MODE CRACK UNDER PLANE STRESS CONDITIONS
FOR A POWER-LAW HARDENING MATERIAL

LARISA V. STEPANOVA AND EKATERINA M. YAKOVLEVA

The stress-strain state analysis near the crack tip in a power-law material under mixed-mode loading conditions is investigated. By the use of the eigenfunction expansion method the stress-strain state near the mixed-mode crack tip under plane stress conditions is found. The type of the mixed-mode loading is specified by the mixity parameter, which varies from 0 to 1. The value of the mixity parameter corresponding to a mode II crack loading is equal to 0, whereas the value corresponding to a mode I crack loading is equal to 1. It is shown that the eigenfunction expansion method results in a nonlinear eigenvalue problem. The numerical solutions of the nonlinear eigenvalue problems for all values of the mixity parameter and for all practically important values of the strain hardening (or creep) exponent are obtained. It is found that mixed-mode loading of the cracked plate gives rise to a change in the stress singularity in the vicinity of the crack tip. Mixed-mode loading of the cracked plate results in new asymptotics of the stress field, which is different from the classical Hutchinson–Rice–Rosengren (HRR) stress field. The approximate solution of the nonlinear eigenvalue problem is obtained by a perturbation theory technique (artificial small parameter method). In the framework of the perturbation theory approach, a small parameter representing the difference between the eigenvalue of the nonlinear problem and the undisturbed linear problem is introduced. The asymptotic analysis carried out shows clearly that the stress singularity in the vicinity of the crack tip changes under mixed-mode loading in the case of plane stress conditions. The angular distributions of the stress and strain components (eigenfunctions) in the full range of values of the mixity parameter are given.

1. Introduction. Mixed-mode loading of cracked structures
and near crack-tip fields under mixed-mode loading.

Knowledge of stress, strain and displacement fields in the vicinity of the crack tip under mixed-mode loading conditions is important for the justification of fracture mechanics criteria and has attracted considerable attention [Berto and Lazzarin 2014; Bui 2011; Kuna 2013; Pestrikov and Morozov 2012; Vildeman et al. 2012; Wei 2010]. So far, mainly crack problems for pure opening mode I at symmetrical loading have been thoroughly treated [Bui 2006; Wei 2010; Pestrikov and Morozov 2012]. The corresponding fracture criteria have been obtained on the assumption that the crack continues to extend along its original line (two-dimensional case) or plane (three-dimensional case) in a straightforward manner on the ligament. If mode I loading is superimposed with mode II and/or III loading, the symmetry is violated and the situation is called mixed-mode loading. Stress fields around a mixed-mode crack tip in

different materials have been investigated by many researchers [Dong and Pan 1990; Smith et al. 2001; Shlyannikov 2003; Pan and Lin 2006; Shlyannikov and Kislova 2009; Rahman and Hancock 2006; Berto and Lazzarin 2013; Berto and Lazzarin 2014; Leblond and Frelat 2014; Akbardoost and Ayatollahi 2014]. The study of mixed-mode loads is of particular importance: mixed-mode loading of cracked specimens is of profound importance from theoretical [Bui 2011; Pestrikov and Morozov 2012; Wei 2010], computational [Kuna 2013] and experimental [Decreuse et al. 2012; Ondraček and Materna 2014; Vildeman et al. 2012; Wei et al. 2011] points of view. Currently, mixed-mode crack problems in materials with nonlinear constitutive relations (power law constitutive equations of deformation plasticity theory, steady state creep Norton's law) have aroused considerable interest in many areas of fracture mechanics [Berto and Lazzarin 2013; Botvina et al. 2013; Hello et al. 2012; Richard et al. 2014; Shlyannikov and Kislova 2009; Shlyannikov 2012; 2013; Shlyannikov and Zakharov 2014; Shlyannikov et al. 2014]. Obviously, the principle of superposition of the solutions for mode I and mode II loadings cannot be applied for nonlinear materials. For the case of nonlinear material behavior it is necessary to propose new methods and approaches for the analysis of the near crack tip stress-strain state under mixed-mode loads. In the present paper, the approximate analysis and numerical analysis of the stress and strain fields ahead of the crack tip under mixed-mode loading in the case of plane stress conditions are developed. It should be noted that the angular distributions and the stress singularity in the neighborhood of the crack tip under mixed-mode loading in the case of plane strain conditions are carefully studied [Loghin and Joseph 2001; 2003; Richard et al. 2014; Shlyannikov and Kislova 2009; Shlyannikov 2012].

Loghin and Joseph [2001] were the first to propose a displacement-based finite element formulation to determine the leading two terms in the expansions of stresses and strains around singular points in power law hardening materials. The authors used the approach to study the effects of mixed-mode loading on the structure. The asymptotic solution for mixed-mode loading of the cracked structure in plane strain conditions was obtained, but the asymptotic form of the mode I dominant plane stress could not be determined.

Shlyannikov and Kislova [2009] proposed a method for calculating the elastic-plastic stress intensity factors for the full range of mixed-mode loading from tensile to shear cracks. The state of an arbitrary oriented slit-like straight crack in the form of a mathematical notch under biaxial loading was considered. The solution is based on a combination of both the compatibility strain equation and the Airy stress potential with its derivatives. The elastic-plastic material behavior is represented by the Ramberg–Osgood model. On the basis of the results obtained, the influence of both mode-mixity and material plastic properties on the elastic-plastic stress intensity factors is analyzed. In [Richard et al. 2014], an overview of theories, experiments and simulations of cracks and crack growth under mixed-mode loading is given. First some concepts and basic theories are described for two-dimensional and three-dimensional crack mixed-mode loading situations. Furthermore, several mixed-mode fracture specimens and loading devices are presented. The theoretical and experimental results are compared with respect to practical use of the described concepts and theories. Finally, the paper [Richard et al. 2014] presents crack growth simulations. Shlyannikov [2012] derived equations for ultimate failure strain under complex static and low-cyclic loading and gave experimental verification for different types of biaxial loads. Experimental and calculation data obtained on the basis of a generalized equivalence condition to solve problems of crack mechanics for complex stress states are presented [loc. cit.]. Models and methods for determining the crack direction, path, velocity and time of crack growth under biaxial loading are

considered. Botvina et al. [2013] presented the results of studying the development of plastic flow zones and damage of steel 20 in conditions of shear, separation, mixed-mode loading and eccentric cyclic loading. The influence of the shear component on the evolution of plastic strain zones, mechanical and acoustic properties (parameters of acoustic emission, the velocity and attenuation of ultrasonic waves) is elucidated. It is shown that an increase in the shear component of the load changes the shape of the zone of plastic deformation, initiates formation of additional microcracks, increases the total fracture energy, reduces the slope indices of cumulative distributions of the amplitude of acoustic signals and microcracks, and also induces an increase in the ultrasonic attenuation coefficient and heat capacity of the samples. Analysis of changes in the studied parameters of damage and fracture mechanics provided identification of the main stages of damage accumulation under tensile load. The main aim of the study [Berto and Lazzarin 2013] is to present a set of equations for accurately describing the crack tip stress components, particularly for those cases where the modes I and II stress intensity factors, used in combination with the T-stress component, are unable to capture with satisfying precision the complete stress field ahead the crack tip. The case of a plate with a central crack under mixed-mode (I+II) loading is discussed to show the different contributions of the higher-order terms in the overall stress field. In [Berto and Lazzarin 2014], an extensive review of local approaches applicable near stress raisers, both sharp and blunt, for mode I, mode II and mode III loading conditions in brittle and quasibrittle failure assessment is presented. The authors develop a new approach based on the volume strain energy density and show many applications for assessment of the brittle fracture of a large number of materials and specimens under mixed-mode loading conditions. In [Hello et al. 2012] there are closed-form expressions for the whole sequences of coefficients related to the problem of a finite crack in an infinite plane medium with mode I and mode II remote load.

Fatigue crack paths for inclined cracks are studied in [Shlyannikov 2013] through experiments and computations under different mixed-mode loading conditions where the elaborated theoretical model is applied for modeling crack growth trajectories in common experimental fracture mechanics specimen geometries. For the particular specimen geometries considered, the T-stress distributions are calculated along the curved crack path. It is shown that there is a greater variation of T-stress along the crack trajectories under mixed-mode fracture for specimens with different geometries. The experimental results for mixed-mode fracture trajectories during crack growth are compared with theoretical predictions. Discrepancies in fatigue crack path have been observed in various specimen configurations. The results presented in this study for fracture specimens seem to indicate the relevance of the crack tip constraint parameter, the T-stress, to fatigue crack path behavior that traditional linear fracture mechanics fails to explain. In [Shlyannikov and Zakharov 2014], fatigue crack growth rate is analyzed through experimental study and numerical computations under different biaxial and mixed-mode loading conditions. Cruciform specimens under biaxial loading and compact tension-shear specimens are considered. The different degrees of mode mixity, from pure mode I to pure mode II, are given by combinations of the far-field stress level, load biaxiality and inclined crack angle. For the particular specimen geometries considered, the T-stress and the numerical constant of the plastic stress field distributions are obtained as a function of the dimensionless crack length, load biaxiality and mode mixity. The method is also suggested for calculating the plastic stress intensity factor for any mixed-mode I/II loading based on the T-stress and power law solutions. It is either demonstrated that the plastic stress intensity factor accounting for the in-plane and out-of-plane constraint effect can be used to characterize the multiaxial crack growth

rate for a variety of specimen geometries. Cruciform specimens of two configurations with an inclined crack subject to a system of biaxial loads are proposed [Shlyannikov et al. 2014] to study cracks under mixed-mode loading conditions. A method for infiltrating the mixed-mode displacement of cracks in the deformed state is suggested. For the particular specimen geometries considered, the T-stress and the geometry-dependent correction factors, as well as the numerical constant of the plastic stress distributions, are obtained as a function of the dimensionless crack length, load biaxiality and mode mixity.

Asymptotic representations of the stress, strain rate and continuity fields in the vicinity of the mixed-mode crack under plane strain conditions are obtained in [Stepanova and Adylina 2014]. On the basis of the similarity form of the solution and the hypothesis of the completely damaged zone in the crack tip region, the stress and continuity fields under a complete range of mixed-mode I/II states of loading (from pure tension to pure shear) are given. Higher-order term asymptotic expansions of the stress components and the continuity parameter are derived. A new numerical method to tackle nonlinear eigenvalue problems allowing one to find the whole spectrum of eigenvalues is proposed. However, several difficulties emerge in analyzing the nonlinear eigenvalue problem arising from the mixed-mode crack problem under plane stress conditions. The aim of the present study is to give an accurate solution of the nonlinear eigenvalue problem following from the stress-strain state analysis in the vicinity of the mixed-mode crack under plane stress conditions. It should be noted that plane stress state problems for notched bodies and cracked specimens are still not clearly understood. The angular distributions of the stress components in the vicinity of the mixed-mode crack tip under plane stress conditions have not been discussed in detail, but clearly this must be done to have an accurate description of the stress and strain fields in the vicinity of the crack tip. Recently there have been proposed solutions for the plane stress problems [Lomakin and Melnikov 2009; 2011; Vildeman et al. 2014]. The objective of this paper is to study the stress singularities in the vicinity of the mixed-mode crack tip under plane stress conditions. The governing equations for the power law constitutive relations are transformed to nonlinear eigenvalue problems of ordinary differential equations (ODEs) based on the assumption that the stress fields are asymptotic near the mixed-mode crack tip. The asymptotic and numerical methods are further developed in the present work to analyze eigenvalue problems of ODEs.

2. Governing equations and asymptotic analysis. Mixity parameter.

Consider a stationary crack in a power-law material under plane stress conditions. Applied loading is accounted as mixed-mode I/II loading. Polar coordinates are introduced and centered at the crack tip. With reference to the polar coordinates, the equilibrium equations can be written as

$$r\sigma_{rr,r} + \sigma_{r\theta,\theta} + \sigma_{rr} - \sigma_{\theta\theta} = 0, \quad r\sigma_{r\theta,r} + \sigma_{\theta\theta,\theta} + 2\sigma_{r\theta} = 0. \tag{2-1}$$

The compatibility condition has the form

$$2(r\varepsilon_{r\theta,\theta})_{,r} = \varepsilon_{rr,\theta\theta} - r\varepsilon_{rr,r} + r(r\varepsilon_{\theta\theta})_{,rr}. \tag{2-2}$$

For a material subjected to a power-law hardening, the constitutive equations for plane stress conditions can be written as

$$\varepsilon_{rr} = \tfrac{1}{2}B\sigma_e^{n-1}(2\sigma_{rr} - \sigma_{\theta\theta}), \quad \varepsilon_{\theta\theta} = \tfrac{1}{2}B\sigma_e^{n-1}(2\sigma_{\theta\theta} - \sigma_{rr}), \quad \varepsilon_{r\theta} = \tfrac{3}{2}B\sigma_e^{n-1}\sigma_{r\theta}, \tag{2-3}$$

where $\sigma_e = \sqrt{\sigma_{rr}^2 + \sigma_{\theta\theta}^2 - \sigma_{rr}\sigma_{\theta\theta} + 3\sigma_{r\theta}^2}$ is the von Mises equivalent stress, and B, n are the material constants.

It should be noted that in the case considered the analogy between nonlinear elastic behavior and creep holds. That implies that all relations and solutions obtained for a nonlinear elastic (plastic) material with the constitutive equations (2-3) can be transferred to creep processes with the constitutive relations of Norton's creep law simply by replacing the strains by strain rates. The solution of equations (2-1)–(2-3) should satisfy the traditional traction-free boundary conditions on the crack surfaces $\sigma_{r\theta}(r, \theta = \pm\pi) = 0$, $\sigma_{\theta\theta}(r, \theta = \pm\pi) = 0$. The mixed-mode loading can be characterized in terms of the mixity parameter M^p, which is defined as [Shih 1973; 1974]

$$M^p = (2/\pi) \arctan \left| \lim_{r \to 0} \frac{\sigma_{\theta\theta}(r, \theta = 0)}{\sigma_{r\theta}(r, \theta = 0)} \right|. \tag{2-4}$$

The mixity parameter M^p equals 0 for pure mode II, 1 for pure mode I, and $0 < M^p < 1$ for different mixities of modes I and II. Thus, for combined-mode fracture, the mixity parameter M^p completely specifies the near-crack-tip fields for a given value of the hardening exponent n. By postulating the Airy stress function $\chi(r, \theta)$ expressed in the polar coordinate system, the stress components in the plane strain and the plane stress states are expressed as

$$\sigma_{\theta\theta} = \chi_{,rr}, \quad \sigma_{rr} = \chi_{,r}/r - \chi_{,\theta\theta}/r^2, \quad \sigma_{r\theta} = -(\chi_{,\theta})_{,r}.$$

As for the asymptotic stress field at the crack tip $r \to 0$, one can postulate the Airy stress function

$$\chi(r, \theta) = Kr^{\lambda+1} f(\theta), \tag{2-5}$$

where K is an indeterminate coefficient, λ is an indeterminate exponent and $f(\theta)$ is an indeterminate function of the polar angle. In view of the asymptotic presentation (2-5), the asymptotic stress field at the crack tip is found to be $\sigma_{ij}(r, \theta) = Kr^{\lambda-1}\tilde{\sigma}_{ij}(\theta)$, or

$$\sigma_{rr}(r, \theta) = Kr^{\lambda-1}[(\lambda+1)f(\theta) + f''(\theta)],$$
$$\sigma_{\theta\theta}(r, \theta) = Kr^{\lambda-1}(\lambda+1)\lambda f(\theta), \tag{2-6}$$
$$\sigma_{r\theta}(r, \theta) = -Kr^{\lambda-1}\lambda f'(\theta),$$

where $\lambda - 1$ denotes the exponent representing the singularity of the stress field, and will be called the stress singularity exponent hereafter. According to (2-3), the asymptotic strain field as r tends to 0 takes the form $\varepsilon_{ij}(r, \theta) = K^n r^{(\lambda-1)n}\tilde{\varepsilon}_{ij}(\theta)$, or, in expanded form,

$$\varepsilon_{rr}(r, \theta) = \tfrac{1}{2}BK^n r^{(\lambda-1)n} f_e^{n-1}[(\lambda+1)(2-\lambda)f(\theta) + 2f''(\theta)],$$
$$\varepsilon_{\theta\theta}(r, \theta) = \tfrac{1}{2}BK^n r^{(\lambda-1)n} f_e^{n-1}[(\lambda+1)(2\lambda-1)f(\theta) - f''(\theta)],$$
$$\varepsilon_{r\theta}(r, \theta) = -\tfrac{3}{2}BK^n r^{(\lambda-1)n} f_e^{n-1}\lambda f'(\theta).$$

The compatibility condition (2-2) results in the following nonlinear fourth-order ODE for $f(\theta)$:

$$0 = f^{\text{IV}} f_e^2 \{(n-1)[(\lambda+1)(2-\lambda)f + 2f'']^2 + 2f_e^2\}$$

$$+ 6[(\lambda)n + 1]\lambda[(n-1)f_e^2 hf' + f_e^4 f''] + (n-1)(n-3)h^2[(\lambda+1)(2-\lambda)f + 2f'']$$

$$+ (n-1)f_e^2[(\lambda+1)(2-\lambda)f + 2f'']$$

$$\times \Big\{[(\lambda+1)f' + f''']^2 + [(\lambda+1)f + f''](\lambda+1)f'' + (\lambda+1)^2\lambda^2(f'^2 + ff'')$$

$$- \tfrac{1}{2}(\lambda+1)^2\lambda ff'' - [(\lambda+1)f' + f'''](\lambda+1)\lambda f'$$

$$- \tfrac{1}{2}[(\lambda+1)f + f''](\lambda+1)\lambda f'' + 3\lambda^2(f''^2 + f'f''')\Big\}$$

$$+ f_e^4(\lambda+1)(2-\lambda)f'' - (\lambda-1)nf_e^4[(\lambda+1)(2-\lambda)f + 2f'']$$

$$+ [(\lambda-1)n + 1](\lambda-1)nf_e^4[(\lambda+1)(2\lambda-1)f - f''] + 2(n-1)f_e^2 h[(\lambda+1)(2-\lambda)f' + 2f''], \quad (2\text{-}7)$$

where we have adopted the notation

$$f_e = \sqrt{[(\lambda+1)f + f'']^2 + (\lambda+1)^2\lambda^2 f^2 - [(\lambda+1)f + f''](\lambda+1)\lambda f + 3\lambda^2 f'^2},$$

$$h = [(\lambda+1)f + f''][(\lambda+1)f' + f'''] + (\lambda+1)^2\lambda^2 ff' - \tfrac{1}{2}[(\lambda+1)f' + f'''](\lambda+1)\lambda f$$

$$- \tfrac{1}{2}[(\lambda+1)f + f''](\lambda+1)\lambda f' + 3\lambda^2 f'f''.$$

The boundary conditions imposed on the function $f(\theta)$ follow from the traction-free boundary conditions on the crack surfaces:

$$f(\theta = \pm\pi) = 0, \quad f'(\theta = \pm\pi) = 0. \quad (2\text{-}8)$$

Thus, the eigenfunction expansion method results in a nonlinear eigenvalue problem: it is necessary to find eigenvalues λ leading to nontrivial solutions of (2-7) satisfying the boundary conditions (2-8). Therefore, the order of the stress singularity is the eigenvalue and the angular variations of the field quantities correspond to the eigenfunctions. When we consider mode I loading or mode II loading conditions, the symmetry or antisymmetry requirements of the problem with respect to the crack plane at $\theta = 0$ are utilized. Due to the symmetry (or antisymmetry), the solution is sought for one of the half-planes, for instance, $0 \le \theta \le \pi$. In analyzing the crack problem under mixed-mode loading conditions, the symmetry or antisymmetry arguments cannot be used, and it is necessary to seek the solution in the whole plane $-\pi \le \theta \le \pi$. To find the numerical solution, one has to take into account the value of the mixity parameter M^p characterizing the mixities of mode I and mode II loadings. For this purpose, in the framework of the proposed technique, (2-7) is numerically solved on the interval $[0, \pi]$, and the two-point boundary value problem is reduced to the initial value problem with the initial conditions reflecting the value of the mixity parameter:

$$f(\theta = 0) = 1, \quad f'(\theta = 0) = (\lambda+1)/\tan\left(\tfrac{1}{2}M^p\pi\right), \quad f(\theta = \pi) = 0, \quad f'(\theta = \pi) = 0. \quad (2\text{-}9)$$

The first initial condition is the normalization condition. The second condition follows from (2-4) specifying the value of the mixity parameter. At the next stage, the numerical solution of (2-7) is found on the interval $[-\pi, 0]$, with the following boundary conditions which have to be satisfied:

$$f(\theta = -\pi) = 0, \quad f'(\theta = -\pi) = 0, \quad f(\theta = 0) = 1, \quad f'(\theta = 0) = (\lambda+1)/\tan\left(\tfrac{1}{2}M^p\pi\right). \quad (2\text{-}10)$$

An analogous approach was adopted in [Stepanova and Adylina 2014], where the near mixed-mode crack-tip stress field under plane strain conditions was analyzed. It is assumed that the eigenvalue of the problem considered equals the eigenvalue of the classical HRR problem, $\lambda = n/(n+1)$; see [Hutchinson 1968b; 1968a; Rice and Rosengren 1968] for pure mode I and pure mode II conditions; [Rice 1967; 1968] for pure mode III conditions. However, it turns out that when we construct the numerical solution for the mixed-mode crack problem under plane stress conditions the radial stress component $\sigma_{rr}(r, \theta)$ at $\theta = 0$ has a discontinuity, whereas for the cases of pure mode I and pure mode II loadings, when $M^p = 1$ and $M^p = 0$ are valid, the radial stress component is continuous at $\theta = 0$. Numerical analysis carried out previously for mixed-mode crack problem under plane strain conditions leads to the continuous angular distributions of the radial stress component $\sigma_{rr}(r, \theta)$ at $\theta = 0$ [Shlyannikov and Kislova 2009; Shlyannikov 2012]. In order to obtain the asymptotic solution of the mixed-mode I/II crack problem under plane stress conditions and to analyze the behavior of the radial stress components, one can use the artificial small parameter method often used for the solution of nonlinear eigenvalue problems [Andrianov and Awrejcewicz 2013; Andrianov et al. 2014; Nayfeh 2000; 2011].

3. Nonlinear eigenvalue problem. Perturbation theory method.

One of the effective methods for the solution of nonlinear eigenvalue problems is the perturbation theory technique based on an artificially introduced small parameter [Andrianov and Awrejcewicz 2013; Andrianov et al. 2014; Nayfeh 2000; 2011; Sliva et al. 2010]. An analytical expression for the eigenvalues of the nonlinear eigenvalue problem (2-7)–(2-8) can be derived by applying the perturbation theory method. For this purpose, the eigenvalue λ is split up into $\varepsilon = \lambda - \lambda_0$, where λ_0 refers to the "undisturbed" linear problem and ε is the deviation on account of the nonlinearity. Furthermore, the hardening exponent n and the stress function $f(\theta)$ are represented as power series:

$$\lambda = \lambda_0 + \varepsilon, \quad f(\theta) = f_0(\theta) + \varepsilon f_1(\theta) + \varepsilon^2 f_2(\theta) + \dots, \quad n = 1 + \varepsilon n_1 + \varepsilon^2 n_2 + \dots, \quad (3\text{-}1)$$

where $f_0(\theta)$ refers to the solution of the linear problem. Introducing (3-1) into (2-7), grouping together the terms with the same powers of ε and equating to zero, the set of the boundary value problems for $f_k(\theta)$ is obtained.

By equating the coefficients of ε^0, we obtain

$$f_0^{\text{IV}} + 2(\lambda_0^2 + 1) f_0'' + (\lambda_0^2 - 1)^2 f_0 = 0,$$

$$f_0(\theta = 0) = 1, \quad f_0'(\theta = 0) = (\lambda_0 + 1)/\tan\left(\tfrac{1}{2} M^p \pi\right), \quad f_0(\theta = \pi), \quad f_0'(\theta = \pi), \quad (3\text{-}2)$$

$$f_0(\theta = -\pi), \quad f_0'(\theta = -\pi), \quad f_0(\theta = 0) = 1, \quad f_0'(\theta = 0) = (\lambda_0 + 1)/\tan\left(\tfrac{1}{2} M^p \pi\right);$$

by equating the coefficients of ε^1, we obtain

$$f_1^{\text{IV}} + 2(\lambda_0^2 + 1) f_1'' + (\lambda_0^2 - 1)^2 f_1 = -n_1 \big[x_0 (f_0^{\text{IV}} x_0/2 + w_0)/(2g_0) + h_0 (x_0' g_0 - x_0 h_0 + 3\lambda_0^2 g_0 f_0')/g_0^2 \big]$$

$$- \tfrac{1}{2} f_0'' \big[(\lambda_0 - 1)(4\lambda_0 - 1) n_1 + 8\lambda_0 \big] - \tfrac{1}{2} f_0 (\lambda_0^2 - 1) \big[(\lambda_0 - 1)(4\lambda_0 + 1) n_1 + 8\lambda_0 \big],$$

$$f_1(\theta = 0) = 0, \quad f_1'(\theta = 0) = 1/\tan\left(\tfrac{1}{2} M^p \pi\right), \quad f_1(\theta = \pi), \quad f_1'(\theta = \pi), \quad (3\text{-}3)$$

$$f_1(\theta = -\pi), \quad f_1'(\theta = -\pi), \quad f_1(\theta = 0) = 0, \quad f_1'(\theta = 0) = 1/\tan\left(\tfrac{1}{2} M^p \pi\right);$$

by equating the coefficients of ε^2, we obtain

$$
\begin{aligned}
f_2^{\mathrm{IV}} &+ 2(\lambda_0^2 + 1)f_2'' + (\lambda_0^2 - 1)^2 f_2 = -2g_1\big[f_1^{\mathrm{IV}} + 2(\lambda_0^2 + 1)f_1'' + (\lambda_0^2 - 1)^2 f_1\big]/g_0 \\
&- 3\lambda_0[2 + n_1(\lambda_0 - 1)]f_1'' - \tfrac{1}{2}(1 - 2\lambda_0)\big[f_1'' + (\lambda_0 - 1)f_1\big] + \tfrac{1}{2}[1 + n_1(\lambda_0 - 1)]x_1 \\
&- \tfrac{1}{2}\lambda_0(\lambda_0 - 1)(4\lambda_0 + 1)f_1 + \tfrac{1}{2}(1 - 2\lambda_0)[1 + n_1(\lambda_0 - 1)]y_1 \\
&- 3\lambda_0[n_1 + n_2(\lambda_0 - 1)]f_1'' - 3[1 + n_1(\lambda_0 - 1)]f_0'' + \tfrac{1}{2}f_0'' - \tfrac{1}{2}(\lambda_0 - 1)f_0 \\
&+ \tfrac{1}{2}[1 + n_1(\lambda_0 - 1)](1 - 2\lambda_0)\big[f_0 + (4\lambda_0 + 1)f_0\big] - \lambda_0(\lambda_0 - 1)f_0 \\
&- \tfrac{1}{2}(2\lambda_0 - 1)[n_1 + n_2(\lambda_0 - 1)]y_0 - \tfrac{1}{2}[1 + n_1(\lambda_0 - 1)]^2 y_0 + \tfrac{1}{2}[n_1 + n_2(\lambda_0 - 1)]x_0 \\
&- g_1\big\{6\lambda_0[2 + n_1(\lambda_0 - 1)]f_0'' + (1 - 2\lambda_0)\big[f_0'' - (\lambda_0 - 1)f_0\big] - [1 + n_1(\lambda_0 - 1)]x_0\big\}/g_0 \\
&- g_1\big\{\lambda_0(\lambda_0 - 1)(4\lambda_0 + 1)f_0 + (2\lambda_0 - 1)[1 + n_1(\lambda_0 - 1)]y_0\big\}/g_0 \\
&- n_2\big\{x_0\big(f_0^{\mathrm{IV}}x_0/2 + w_0\big)/(2g_0) + h_0\big(g_0 x_0' - x_0 h_0 + 3\lambda_0^2 g_0 f_0'\big)/g_0^2\big\} \\
&- n_1\big[x_0 g_0(f_1^{\mathrm{IV}}x_0/2 + w_1) + x_0 g_1(f_0^{\mathrm{IV}}x_0/2 + w_0) + g_0 x_1(f_0^{\mathrm{IV}}x_0 + w_0)\big]/(2g_0^2) \\
&- n_1\big\{h_0[x_1'g_0 - x_1 h_0 + 3\lambda_0^2 g_0 f_1'] + h_0[x_0'g_1 - x_0 h_1 + 3\lambda_0^2 g_1 f_0']\big\}/g_0^2 \\
&- n_1\big\{6\lambda_0[2 + n_1(\lambda_0 - 1)]g_0 h_0 f_0' - (1 - 2\lambda_0)\big[2h_0^2 f_0 - 2g_0 h_0 f_0'\big] + n_1 h_0^2 x_0\big\}/(2g_0^2) \\
&- n_1(1 - 2\lambda_0)f_0(f_0^{\mathrm{IV}}x_0 + w_0)/(2g_0) - n_1 h_1\big(x_0'g_0 - x_0 h_0 + 3\lambda_0^2 g_0 f_0'\big)/g_0^2;
\end{aligned}
\tag{3-4}
$$

$$
f_2(\theta = 0) = 0, \quad f_2'(\theta = 0) = 1/\tan\!\big(\tfrac{1}{2}M^p\pi\big), \quad f_2(\theta = \pi), \quad f_2'(\theta = \pi),
$$
$$
f_2(\theta = -\pi), \quad f_2'(\theta = -\pi), \quad f_2(\theta = 0) = 0, \quad f_2'(\theta = 0) = 1/\tan\!\big(\tfrac{1}{2}M^p\pi\big),
$$

where we have adopted the notation

$$
\begin{aligned}
x_k &= (\lambda_0 + 1)(2 - \lambda_0)f_k + 2f_k'', \quad y_k = (\lambda_0 + 1)(2\lambda_0 - 1)f_k - f_k'', \quad u_k = (\lambda_0 + 1)f_k + f_k'', \\
v_k &= (\lambda_0 + 1)\lambda_0 f_k, \quad g_0 = u_0^2 + v_0^2 - u_0 v_0 + 3\lambda_0^2 f_0'^2, \\
h_0 &= u_0 u_0' + v_0 v_0' - \tfrac{1}{2}u_0' v_0 - \tfrac{1}{2}u_0 v_0' + 3\lambda_0^2 f_0' f_0'', \\
w_0 &= u_0'^2 + (\lambda_0 + 1)u_0 f_0'' + v_0'^2 + v_0 v_0'' - \tfrac{1}{2}(\lambda_0 + 1)v_0 f_0'' - u_0 v_0' - \tfrac{1}{2}u_0 v_0'' + 3\lambda_0^2(f_0''^2 + f_0' f_0'''), \\
g_1 &= 2u_0(u_1 + f_0) + 2v_0\big[v_1 + (2\lambda + 1)f_0\big] - u_0\big[v_1 + (2\lambda + 1)f_0\big] - v_0(u_1 + f_0) \\
&\quad + 6\lambda_0 f_0'(\lambda_0 f_1' + f_0'), \\
h_1 &= u_0(u_1' + f_0') + u_0'(u_1 + f_0) + v_0\big[v_1' + (2\lambda_0 + 1)f_0'\big] + v_0'\big[v_1 + (2\lambda_0 + 1)f_0\big] \\
&\quad - \tfrac{1}{2}u_0'\big[v_1 + (2\lambda_0 + 1)f_0\big] - \tfrac{1}{2}u_0\big[v_1' + (2\lambda_0 + 1)f_0'\big] - \tfrac{1}{2}v_0(u_1' + f_0') - \tfrac{1}{2}v_0'(u_1 + f_0) \\
&\quad + 3\lambda_0 f_0'(\lambda_0 f_1'' + f_0'') + 3\lambda_0 f_0''(\lambda_0 f_1' + f_0'), \\
w_1 &= 2u_0'(u_1' + f_0') + u_0\big[(\lambda_0 + 1)f_1'' + f_0''\big] + (\lambda_0 + 1)f_0''(u_1 + f_0) + 2v_0'\big[v_1' + (2\lambda_0 + 1)f_0'\big] \\
&\quad + v_0'\big[v_1'' + (2\lambda_0 + 1)f_0''\big] + v_0''\big[v_1 + (2\lambda_0 + 1)f_0\big] - \tfrac{1}{2}(\lambda_0 + 1)f_0''\big[v_1 + (2\lambda_0 + 1)f_0\big] \\
&\quad - \tfrac{1}{2}v_0\big[(\lambda_0 + 1)f_1'' + f_0''\big] - v_0'(u_1' + f_0') - u_0'\big[v_1' + (2\lambda_0 + 1)f_0'\big] - \tfrac{1}{2}v_0''(u_1 + f_0) \\
&\quad - \tfrac{1}{2}u_0\big[v_1'' + (2\lambda_0 + 1)f_0''\big] + 6\lambda_0 f_0''(\lambda_0 f_1' + f_0') + 3\lambda_0 f_0'''(\lambda_0 f_1' + f_0') + 3\lambda_0 f_0'(\lambda_0 f_1''' + f_0''').
\end{aligned}
$$

The solution of the linear ordinary differential equation (3-2) for the function $f_0(\theta)$ satisfying the traction-free boundary conditions has the form

$$f_0^{\mathrm{I}} = \beta \cos(\alpha\theta) - \alpha \cos(\beta\theta), \quad \alpha = \lambda_0 - 1, \quad \beta = \lambda_0 + 1,$$

for the crack opening mode I (for symmetric stress fields), and it has the form

$$f_0^{\mathrm{II}} = \sin(\alpha\theta) - \sin(\beta\theta)$$

for the shear crack mode II (the skew-symmetric stress fields), where the spectrum of the eigenvalues is determined by the characteristic equation $\sin 2\pi\lambda_0 = 0$, whence one can easily find $\lambda_0 = \frac{1}{2}m$, where m is an integer. Thus it is shown that an infinite number of eigenvalues exists. In view of the linearity of (3-2) for the mixed-mode crack problem, the solution is the superposition of the symmetric and antisymmetric parts of the stress field with respect to the crack plane:

$$f_0(\theta) = C_1[\beta \cos(\alpha\theta) - \alpha \cos(\beta\theta)] + C_2[\sin(\alpha\theta) - \sin(\beta\theta)], \tag{3-5}$$

where C_1 and C_2 are unknown coefficients which have to be determined from the boundary conditions of the actual crack problem and represent the modes I and II, respectively. In view of (2-4), the unknown constants C_1 and C_2 are related to the mixity parameter $M^p = 2\arctan[(\lambda_0 + 1)C_1/C_2]/\pi$. The zeroth-order problem (3-2) has the nontrivial solution (3-5), hence the inhomogeneous problems (3-3), (3-4) for the functions $f_1(\theta)$ and $f_2(\theta)$ will not have solutions unless a solvability condition is satisfied [Nayfeh 2000; 2011]. Therefore, if λ_0 is not an eigenvalue of the homogeneous problem (i.e., the homogeneous problem has only the trivial solution), the inhomogeneous problem has a unique solution for every continuous right-hand side $G_k(\theta)$ of the differential equation for $f_k(\theta)$, $k > 0$. On the other hand, if λ_0 is an eigenvalue of the homogeneous problem (i.e., the homogeneous problem has a nontrivial solution), the inhomogeneous problem does not have a solution unless [Nayfeh 2000; 2011]

$$\int_{-\pi}^{\pi} G_k(\theta) u(\theta) \, d\theta = 0. \tag{3-6}$$

That is, $G_k(\theta)$ is orthogonal to the eigenfunction $u(\theta)$, corresponding to the eigenvalue λ_0. These results constitute the so-called Fredholm alternative theorem: for a given value λ_0, either the inhomogeneous problem has a unique solution for each continuous right-hand side of the equation, or else the homogeneous problem has a nontrivial solution [Nayfeh 2000; 2011]. To determine the solvability condition (3-6) we use the concept of adjoint problems [Stepanova 2008a; 2008b; 2009a; Stepanova and Igonin 2014]. The boundary value problem (3-3) is self-adjoint since the differential equation and the boundary conditions of the adjoint problem coincide with the differential equation and boundary conditions of the homogeneous problem (3-2). Therefore, $u(\theta) = f_0(\theta)$, where the function $f_0(\theta)$ is determined by (3-5). According to (3-6), the compatibility condition of the boundary value problem (3-3) has the form $\int_{-\pi}^{\pi} G_1(\theta) f_0(\theta) \, d\theta = 0$, or, in expanded form,

$$\int_{-\pi}^{\pi} \left\{ -n_1[x_0(\tfrac{1}{2} f_0^{\mathrm{IV}} x_0 + w_0)/(2g_0) + h_0(g_0 x_0' - x_0 h_0 + 3\lambda_0^2 g_0 f_0')/g_0^2] \right.$$
$$\left. - \tfrac{1}{2} f_0''[(\lambda_0 - 1)(4\lambda_0 - 1)n_1 + 8\lambda_0] - \tfrac{1}{2} f_0(\lambda_0^2 - 1)[(\lambda_0 - 1)(4\lambda_0 + 1)n_1 + 8\lambda_0] \right\} f_0(\theta) \, d\theta = 0. \tag{3-7}$$

M^p	n_1	n_2	M^p	n_1	n_2	M^p	n_1	n_2
0	4.000000	8.000000	0.3	4.065772	7.941876	0.8	4.224060	7.926086
0.05	4.001766	7.999995	0.4	4.118594	7.804045	0.9	4.084774	7.958755
0.1	4.007088	7.999954	0.5	4.184135	7.749316	0.95	4.023759	7.999543
0.2	4.028722	7.978646	0.6	4.249098	7.600224	1	4.000000	8.000000
			0.7	4.279336	7.577773			

Table 1. Coefficients of the asymptotic expansion of the hardening exponent n.

The compatibility condition of the boundary value problem for the function $f_1(\theta)$ (3-7) allows us to find the coefficient n_1. The values of n_1 for different values of the mixity parameter are shown in Table 1. Having obtained the function $f_1(\theta)$, one can determine the unknown function $f_2(\theta)$. Using the analogous reasoning, one can formulate the compatibility condition for the solution of the boundary value problem for $f_2(\theta)$ and calculate numerically the values of the coefficient n_2 of the asymptotic expansion of the hardening exponent n for different values of the mixity parameter. Table 1 summarizes the results of computations and gives the coefficients n_1 and n_2 for different values of the mixity parameter.

From the results obtained one can see that the mixed-mode loading leads to change of the stress singularity in the vicinity of the crack tip under plane stress conditions. Previously, it was found [Stepanova 2008a; 2009a] that for mode I and mode II crack problems the perturbation theory technique results in the equation $n_k = (-1)^{k+1}/(\lambda_0 - 1)^{k+1}$ (where, for the HRR problem, $\lambda_0 = \frac{1}{2}$), and the third asymptotic expansion in (3-1) yields $n = \lambda/(1-\lambda)$, or $\lambda = n/(n+1)$. This eigenvalue corresponds to the classical HRR stress field. The results obtained and given in Table 1 clearly show that the mixed-mode loading leads to a change in the stress singularity exponent in the vicinity of the crack tip. Otherwise, the values of the coefficients n_1 and n_2 were 4 and 8, respectively, as they were in the case of plane strain conditions. In other words, if the coefficients n_1 and n_2 were equal to 4 and 8, respectively, then we would have $n_k = (-1)^{k+1}/(\lambda_0 - 1)^{k+1}$, [Stepanova 2008a; 2009a] and we would sum the binomial series for n and obtain the classical HRR stress field. However, as is indicated by Table 1, the values of n_1 and n_2 deviate from 4 and 8, respectively. Thus, mixed-mode loading causes a change in the stress singularity in the neighborhood of the crack tip. When we analyze the stress-strain state in the vicinity of the crack tip under mixed-mode loading, it is assumed that the stress singularity does not change and the eigenvalue corresponds to the HRR problem, $\lambda = n/(n+1)$ (i.e., it is assumed a priori that the eigenvalue equals $\lambda = n/(n+1)$ and the hypothesis is confirmed by the solution [Shlyannikov and Kislova 2009]). However, in the case of plane stress conditions, as the artificial small parameter method shows, the hypothesis cannot be accepted and it is necessary to find the eigenvalues of the problem as a part of the solution. In the next part of the paper, the numerical solution of the nonlinear eigenvalue problem will be considered.

4. Numerical solution of the nonlinear eigenvalue problem. Computational scheme. Eigenvalues and eigenfunctions.

As mentioned earlier, traditionally, it is assumed that the eigenvalue of the nonlinear eigenvalue problem equals the eigenvalue of the HRR problem: $\lambda = n/(n+1)$. However, the assumption results in the discontinuity of the radial stress component on the line extending the crack. The asymptotic analysis

based on the artificial small parameter method and described above has shown additionally that the eigenvalue corresponding to the HRR stress field cannot be the eigenvalue of the mixed-mode crack problem under plane stress conditions. In view of the above arguments, the eigenvalue of the problem considered will be determined from the requirement of the continuity of the radial stress component at $\theta = 0$. The analogous approach for solving the nonlinear eigenvalue problems has been applied in [Stepanova and Adylina 2014], where the approach allowed the determination of the whole spectrum of the eigenvalues, resulting in the contours of the completely damaged zone converging to the limit contour. The procedure of the numerical solution of the nonlinear eigenvalue problem is based on the following assumptions. In the case of the mixed-mode crack problem the symmetry and antisymmetry arguments cannot be used, and it is necessary to find the solution on the interval $[-\pi, \pi]$. In conducting the numerical solution, the interval $[-\pi, \pi]$ can be divided into two intervals: $[0, \pi]$ and $[-\pi, 0]$. First, (2-7) is numerically solved in the interval $[0, \pi]$, and the two-point boundary value problem (2-7), (2-9) is reduced to the initial problem with the initial conditions

$$f(\theta = 0) = 1, \quad f'(\theta = 0) = (\lambda + 1)/\tan\left(\tfrac{1}{2}M^p\pi\right), \quad f''(\theta = 0) = A_2, \quad f'''(\theta = 0) = A_3. \quad (4\text{-}1)$$

The unknown constants A_2 and A_3 are determined such that the boundary conditions on the upper crack surface are satisfied:

$$f(\theta = \pi) = 0, \quad f'(\theta = \pi) = 0. \quad (4\text{-}2)$$

The constants A_2 and A_3 having been obtained, (2-7) is numerically solved on the interval $[-\pi, 0]$. For this purpose, the two-point boundary value problem is reduced to the initial problem with the initial conditions

$$f(\theta = -\pi) = 0, \quad f'(\theta = -\pi) = 0, \quad f''(\theta = -\pi) = B_2, \quad f'''(\theta = -\pi) = B_3. \quad (4\text{-}3)$$

The unknown constants B_2 and B_3 are chosen in such a way that the equilibrium equations of the element belonging to the line $\theta = 0$ are satisfied. The equilibrium equations require the continuity of the shear and circumferential stress components $\sigma_{r\theta}(r, \theta)$ and $\sigma_{\theta\theta}(r, \theta)$ at $\theta = 0$, which implies the continuity of the functions $f(\theta)$ and $f'(\theta)$ at $\theta = 0$ (and, therefore, the boundary conditions (2-10), and hence discontinuities of the radial stress components are allowed). Thus, the two unknown constants B_2 and B_3 are determined in such a way that the solution on the interval $[-\pi, 0]$ satisfies the boundary conditions at $\theta = 0$. When this algorithm is realized, it is usually supposed that the eigenvalue equals the eigenvalue of the HRR stress field. If it is necessary to find eigenvalues different from $\lambda = n/(n + 1)$, and, as a whole, the spectrum of the eigenvalues, then the question arises: which additional physical and (or) mathematical reasons need to be invoked for finding the eigenspectrum? If λ is a required value, then under integration of (2-7) in the interval $[0, \pi]$ one has the three unknown parameters λ, A_2 and A_3, and only the two boundary conditions (4-2) from which the unknowns can be obtained. Obviously, it is necessary to have an additional condition. For the purpose of determination of the eigenvalue λ one can analyze the behavior of the radial stress component in the case of plane strain conditions [Shlyannikov and Kislova 2009; Stepanova and Adylina 2014]. One can see that the radial stress component is continuous as a function of the polar angle at $\theta = 0$ for the values of the mixity parameter and the hardening exponent. It should be noted that the continuity of the radial stress component is not a priori required (i.e., the eigenvalue corresponding to the HRR field $\lambda = n/(n + 1)$ has been chosen and the radial stress

M^p	λ	$f''(\theta = 0)$	$f'''(\theta = 0)$	$f''(\theta = -\pi)$	$f'''(\theta = -\pi)$
0.1	0.749848	−1.013963	−17.857405	−11.119908	0.112696
0.2	0.749363	−1.009899	−8.639267	−5.450935	0.210905
0.3	0.748445	−1.002588	−5.438885	−3.518917	0.244099
0.4	0.746893	−0.991172	−3.732943	−2.521575	0.262339
0.5	0.744332	−0.974435	−2.613062	−1.898950	0.276300
0.6	0.740101	−0.951096	−1.774144	−1.465507	0.290927
0.7	0.733089	−0.921053	−1.087827	−1.143866	0.311439
0.8	0.721666	−0.889149	−0.501650	−0.898579	0.348145
0.9	0.710960	−0.878015	−0.059127	−0.724120	0.428064

Table 2. New eigenvalues λ for $n = 3$ for different values of the mixity parameter.

component $\sigma_{rr}(r, \theta)$ turned out to be continuous for all the values of the mixity parameter and for all the values of the hardening exponent). Therefore, the eigenvalue is sought from the requirement of the continuity of the radial stress component $\sigma_{rr}(r, \theta)$ at $\theta = 0$. Thus, the spectrum of the eigenvalues is numerically obtained.

The numerical integration of differential equation (2-7) to obtain $f(\theta)$ for $[0, \pi]$ is performed by the fourth-order Runge–Kutta method, using symbolic computation in Mathematica as a powerful, convenient and versatile tool widely used in solid mechanics [Constantinescu and Korsunsky 2007], while the solution of the simultaneous nonlinear equations

$$f(\pi) = F_1(A_2, A_3) = 0, \quad f'(\pi) = F_2(A_2, A_3) = 0$$

for A_2, A_3 for a prescribed value of λ is obtained by the Gauss–Newton least-square method so that they satisfy the condition $(f(\pi))^2 + (f'(\pi))^2 < 10^{-7}$. Next the solution is sought for the interval $[-\pi, 0]$ and the numerical integration of (2-7) is performed by the fourth-order Runge–Kutta method whereas the solution of simultaneous nonlinear equations

$$f(-\pi) = F_3(B_2, B_3) = 0, \quad f'(-\pi) = F_4(B_2, B_3) = 0$$

for B_2, B_3 for the same prescribed value of λ is obtained by Gauss–Newton least-square method so that they satisfy the condition $(f(-\pi))^2 + (f'(-\pi))^2 < 10^{-7}$. Then one can compare the values of the radial stress component at $\theta = 0$: $\tilde{\sigma}_{rr}(\theta = 0^-)$ and $\tilde{\sigma}_{rr}(\theta = 0^+)$. The eigenvalue λ is said to be found if the inequality $|\tilde{\sigma}_{rr}(\theta = 0^+) - \tilde{\sigma}_{rr}(\theta = 0^-)| < 10^{-7}$ is valid.

Results of computations are shown in Tables 2–7, where the new eigenvalues λ and the values of the functions $f''(\theta = 0)$, $f'''(\theta = 0)$, $f''(\theta = -\pi)$ and $f'''(\theta = -\pi)$ for the different values of the mixity parameter M^p and the hardening exponent n are given.

Circumferential variations of the stress and strain components obtained are shown in Figures 1–8. The contours of the equal equivalent stress are shown in Figure 9. It is shown that the angular stress distributions are fully continuous and do not contain the discontinuities.

In [Ondraček and Materna 2014], FEM evaluation of the dissipated energy in front of a crack tip under 2D mixed-mode loading conditions was performed. Two different meshes were created to simulate mode I and mode II fatigue crack growth. In both cases, the plane stress and strain calculations were

M^p	λ	$f''(\theta = 0)$	$f'''(\theta = 0)$	$f''(\theta = -\pi)$	$f'''(\theta = -\pi)$
0.1	0.833249	−1.059014	−17.175345	−12.817403	0.217377
0.2	0.832975	−1.054353	−8.270256	−6.295063	0.214040
0.3	0.832434	−1.045751	−5.310084	−4.075287	0.211815
0.4	0.831456	−1.031834	−3.692485	−2.931140	0.210848
0.5	0.829711	−1.010626	−2.474608	−2.217574	0.211543
0.6	0.826595	−0.980308	−1.877300	−1.720923	0.214889
0.7	0.821183	−0.942182	−0.945119	−1.353750	0.223389
0.8	0.813522	−0.910480	−0.379570	−1.085758	0.244019
0.9	0.813057	−0.918935	−0.078809	−0.934756	0.294866

Table 3. New eigenvalues λ for $n = 5$ for different values of the mixity parameter.

M^p	λ	$f''(\theta = 0)$	$f'''(\theta = 0)$	$f''(\theta = -\pi)$	$f'''(\theta = -\pi)$
0.1	0.874951	−1.068014	−16.399514	−14.051259	0.275592
0.2	0.874787	−1.063523	−8.019713	−6.907737	0.218081
0.3	0.874448	−1.054980	−5.004927	−4.477821	0.197231
0.4	0.873779	−1.040530	−3.427356	−3.225923	0.186395
0.5	0.872529	−1.017364	−2.369760	−2.444916	0.180489
0.6	0.870107	−0.983152	−1.789715	−1.900363	0.178418
0.7	0.865837	−0.941813	−0.850487	−1.498387	0.181311
0.8	0.863118	−0.931654	−0.409135	−1.230020	0.194901
0.9	0.863005	−0.939455	−0.117494	−1.070440	0.230710

Table 4. New eigenvalues λ for $n = 7$ for different values of the mixity parameter.

M^p	λ	$f''(\theta = 0)$	$f'''(\theta = 0)$	$f''(\theta = -\pi)$	$f'''(\theta = -\pi)$
0.1	0.899969	−1.067810	−15.870539	−14.973046	0.300772
0.2	0.899986	−1.063699	−7.757085	−7.364961	0.214921
0.3	0.899637	−1.055617	−4.929978	−4.777032	0.184458
0.4	0.899167	−1.041283	−3.428549	−3.445052	0.168585
0.5	0.898187	−1.017020	−2.446724	−2.613278	0.159358
0.6	0.896185	−0.979984	−1.473179	−2.032212	0.154562
0.7	0.892756	−0.938703	−0.786691	−1.605170	0.154589
0.8	0.892187	−0.945074	−0.441700	−1.335332	0.164138
0.9	0.892132	−0.951743	−0.148784	−1.166821	0.191437

Table 5. New eigenvalues λ for $n = 9$ for different values of the mixity parameter.

performed. The crack zones under conditions of plane stress are rather oval shaped. The shape of the equal equivalent stress contours shown in the first three rows of Figure 9 is similar to results of [Ondraček and Materna 2014].

M^p	λ	$f''(\theta = 0)$	$f'''(\theta = 0)$	$f''(\theta = -\pi)$	$f'''(\theta = -\pi)$
0.1	0.916646	-1.064886	-15.509504	-15.687120	0.308561
0.2	0.916575	-1.061186	-7.505140	-7.718823	0.207926
0.3	0.916414	-1.053681	-4.740118	-5.009507	0.172524
0.4	0.916060	-1.039712	-3.250966	-3.614202	0.154108
0.5	0.915260	-1.014674	-2.235656	-2.742892	0.143208
0.6	0.913531	-0.975351	-1.415360	-2.133091	0.137003
0.7	0.911361	-0.945900	-0.796175	-1.696655	0.135580
0.8	0.911145	-0.954022	-0.468121	-1.415250	0.142450
0.9	0.911123	-0.959920	-0.172574	-1.239380	0.164364

Table 6. New eigenvalues λ for $n = 11$ for different values of the mixity parameter.

M^p	λ	$f''(\theta = 0)$	$f'''(\theta = 0)$	$f''(\theta = -\pi)$	$f'''(\theta = -\pi)$
0.1	0.928557	-1.061240	-15.147594	-16.257399	0.307317
0.2	0.928507	-1.057923	-7.398140	-8.001191	0.199333
0.3	0.928389	-1.051006	-4.705468	-5.194292	0.161542
0.4	0.928110	-1.037485	-3.273920	-3.748906	0.141919
0.5	0.927433	-1.011819	-2.331595	-2.845877	0.130222
0.6	0.925895	-0.970589	-1.366626	-2.212890	0.123306
0.7	0.924700	-0.958252	-0.8289902	-1.777736	0.121104
0.75	0.924300	-0.965607	-0.634815	-1.606930	0.122390
0.8	0.924467	-0.960475	-0.489375	-1.478170	0.126133
0.9	0.924460	-0.965742	-0.190855	-1.295977	0.144355
0.95	0.924459	-0.967010	-0.044076	-1.245296	0.162210

Table 7. New eigenvalues λ for $n = 13$ for different values of the mixity parameter.
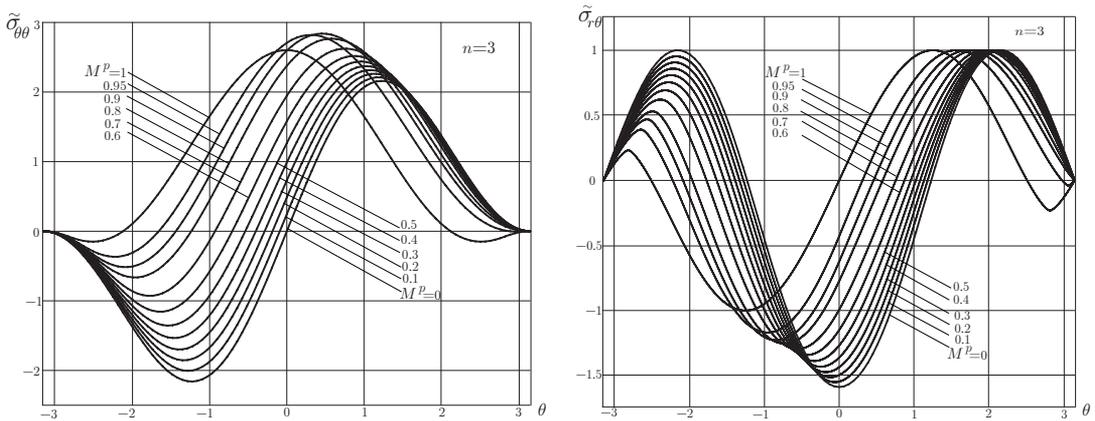
Figure 1. Circumferential variations of the stress components $\tilde{\sigma}_{\theta\theta}$ and $\tilde{\sigma}_{r\theta}$ for different values of the mixity parameter. Strain hardening exponent $n = 3$.
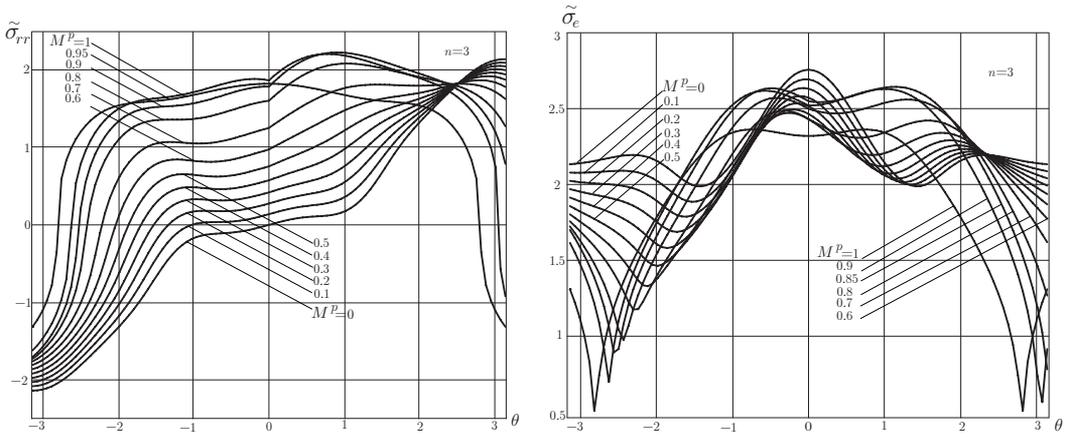
Figure 2. Circumferential variations of the stress component $\tilde{\sigma}_{rr}$ and the equivalent stress $\tilde{\sigma}_e$ for different values of the mixity parameter. Strain hardening exponent $n = 3$.
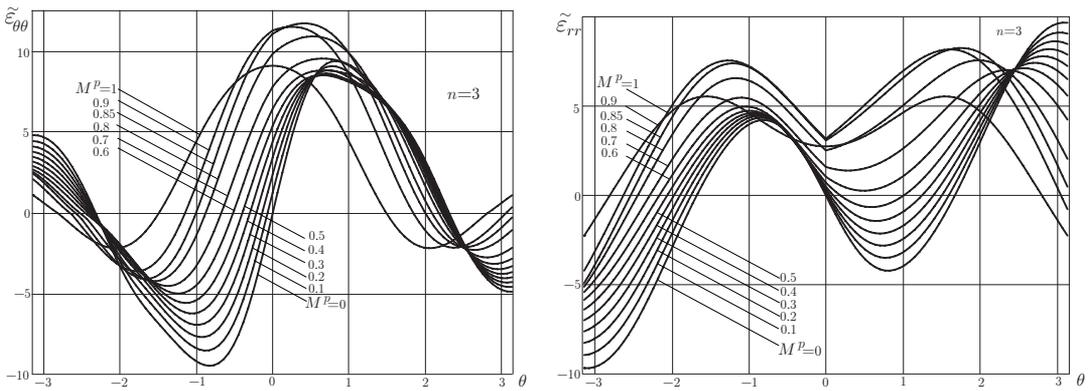
Figure 3. Circumferential variations of the strain components $\tilde{\varepsilon}_{\theta\theta}$ and $\tilde{\varepsilon}_{rr}$ for different values of the mixity parameter. Strain hardening exponent $n = 3$.
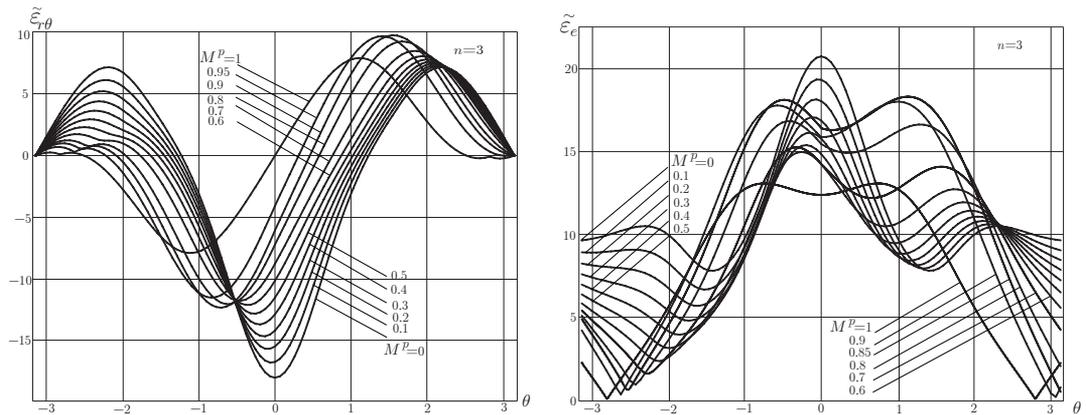
Figure 4. Circumferential variations of the strain component $\tilde{\varepsilon}_{r\theta}$ and the equivalent strain $\tilde{\varepsilon}_e$ for different values of the mixity parameter. Strain hardening exponent $n = 3$.
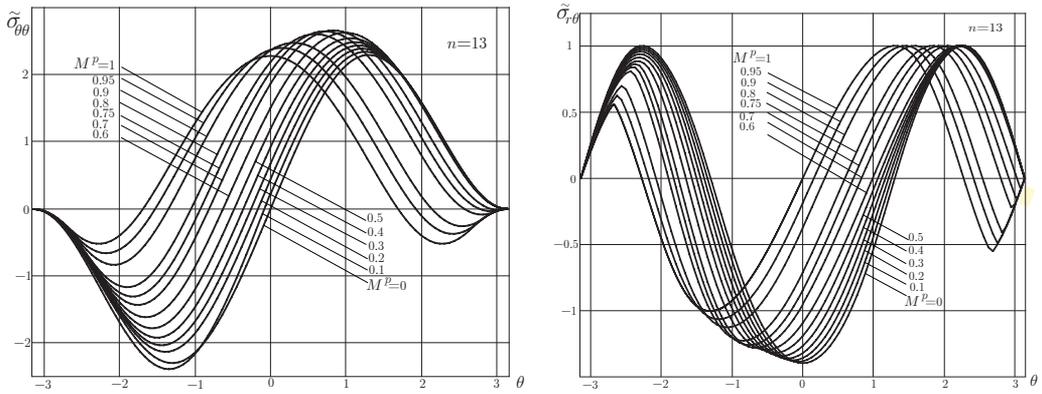
Figure 5. Circumferential variations of the stress components $\tilde{\sigma}_{\theta\theta}$ and $\tilde{\sigma}_{r\theta}$ for different values of the mixity parameter. Strain hardening exponent $n = 13$.
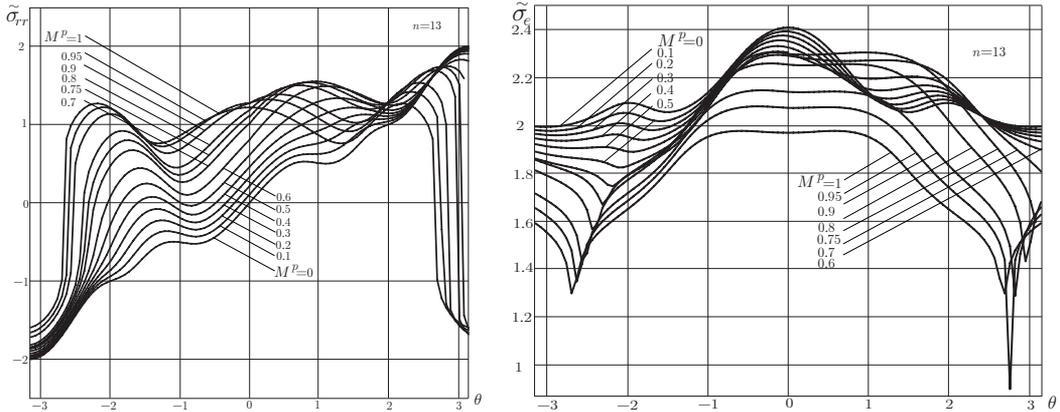
Figure 6. Circumferential variations of the stress component $\tilde{\sigma}_{rr}$ and the equivalent stress $\tilde{\sigma}_e$ for different values of the mixity parameter. Strain hardening exponent $n = 13$.

$M^p = 0.3$		$M^p = 0.5$		$M^p = 0.7$		$M^p = 0.8$	
n	$\delta, \%$	n	$\delta, \%$	n	$\delta, \%$	n	$\delta, \%$
3	0.207	3	0.75	3	2.25	3	3.77
5	0.107	5	0.43	5	1.45	5	2.37
7	0.063	7	0.28	7	1.04	7	1.35
9	0.040	9	0.20	9	0.80	9	0.86
11	0.027	11	0.15	11	0.57	11	0.60
13	0.019	13	0.12	13	0.41	13	0.44

Table 8. The difference between λ and λ_{HRR} for $M^p = 0.3, 0.5, 0.7, 0.8$.

One can evaluate the deviation of the new eigenvalue λ from the eigenvalue corresponding to the classical HRR stress field λ_{HRR}. The discrepancy $\delta = (\lambda_{\text{HRR}} - \lambda) * 100\% / \lambda_{\text{HRR}}$ for different values of the hardening exponent n and for different values of the mixity parameter M^p is given by Table 8.
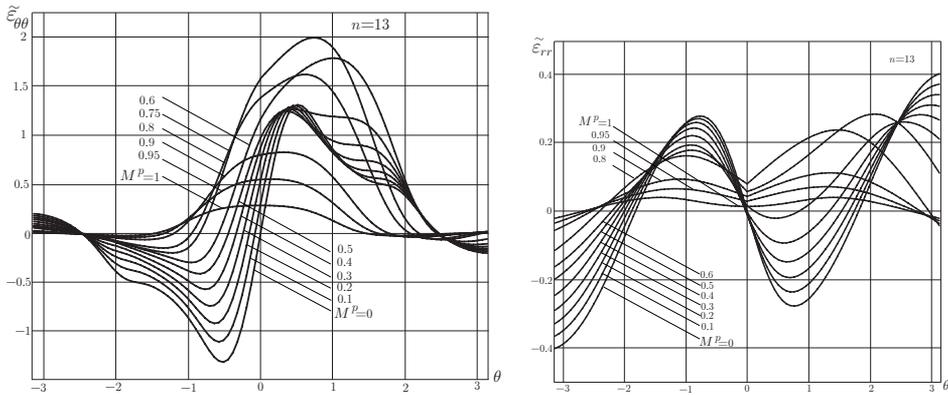
Figure 7. Circumferential variations of the strain components $\tilde{\varepsilon}_{\theta\theta}$ and $\tilde{\varepsilon}_{rr}$ for different values of the mixity parameter. Strain hardening exponent $n = 13$.
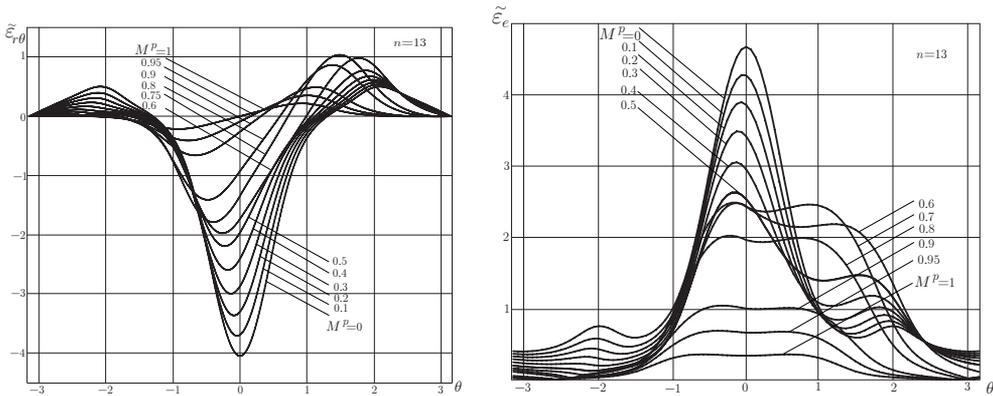
Figure 8. Circumferential variations of the strain component $\tilde{\varepsilon}_{r\theta}$ and the equivalent strain $\tilde{\varepsilon}_e$ for different values of the mixity parameter. Strain hardening exponent $n = 13$.

One can see from Table 8 that the difference tends to zero as the hardening exponent n increases, for all values of the mixity parameter. Thus, in the limiting case of perfect plasticity one can obtain the classical strain singularity r^{-1} and the vanishing singularity of the stress field in the vicinity of the crack tip. In the limiting case of perfect plasticity, the stresses should be bounded as $r \to 0$, and one can obtain the analytical solution of the problem in the asymptotic form

$$\sigma_{ij}(r,\theta) = \sigma_{ij}^{(0)}(\theta) + r^{\alpha}\sigma_{ij}^{(1)}(\theta) + \cdots, \quad \sigma_e(r,\theta) = 1 - r^{\alpha}\sigma^{(1)}(\theta) + \cdots, \quad \alpha > 0, \ r \to 0, \quad (4\text{-}4)$$

where the stresses are normalized by the yield stress. The governing system of equations following from the equilibrium equations and the Huber–Mises yield criterion can be found for functions $\sigma_{ij}^{(0)}(\theta)$:

$$\sigma_{r\theta,\theta}^{(0)} + \sigma_{rr}^{(0)} - \sigma_{\theta\theta}^{(0)} = 0, \quad \sigma_{\theta\theta,\theta}^{(0)} + 2\sigma_{r\theta}^{(0)} = 0, \quad (\sigma_{rr}^{(0)})^2 + (\sigma_{\theta\theta}^{(0)})^2 - \sigma_{rr}^{(0)}\sigma_{\theta\theta}^{(0)} + 3(\sigma_{r\theta}^{(0)})^2 = 1. \quad (4\text{-}5)$$
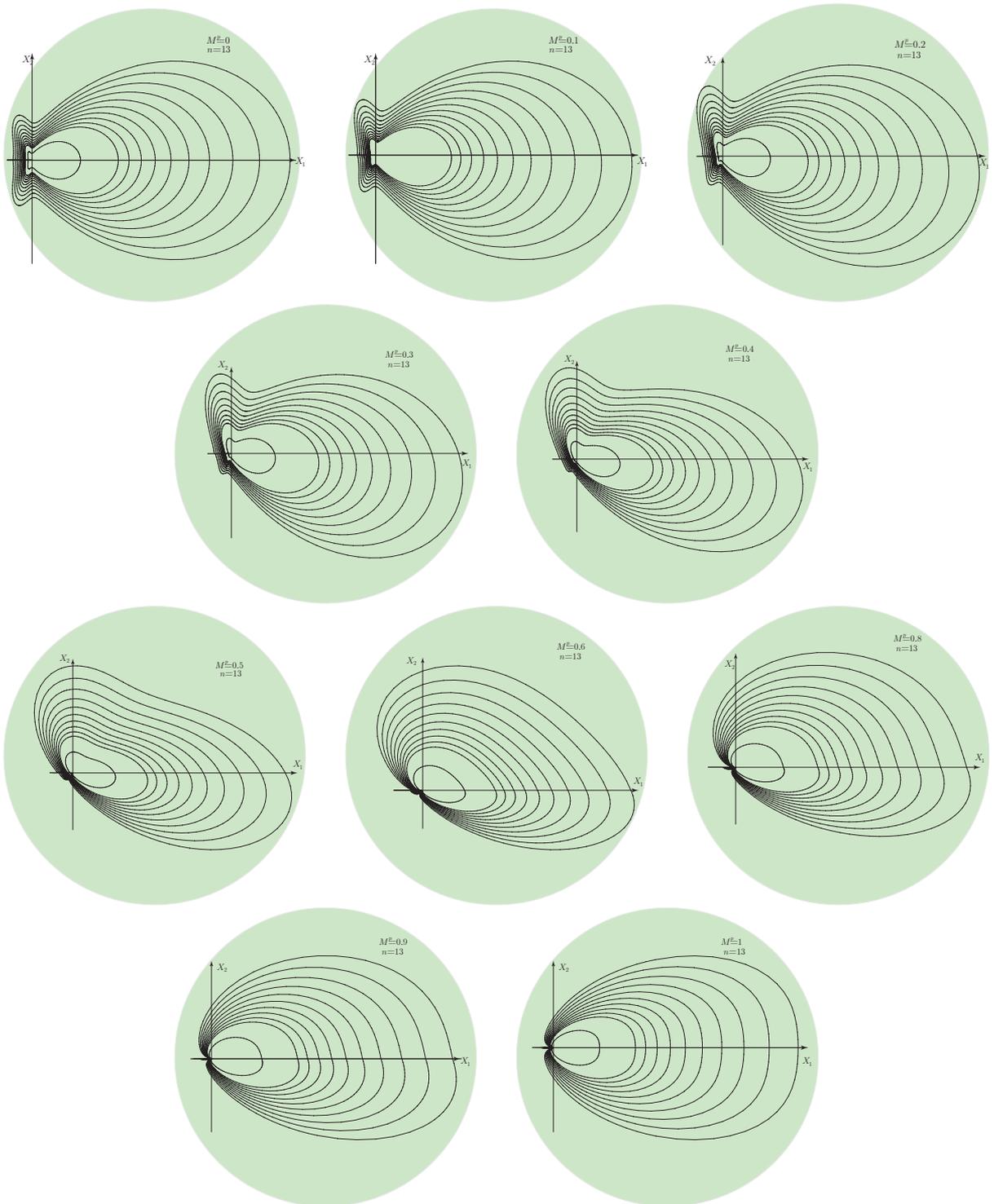
Figure 9. The contours of the equal equivalent stress $\sigma_e(r, \theta)$ in the vicinity of the crack tip.

The analytical expressions for the angular distributions $\sigma_{ij}^{(0)}(\theta)$ of the stress components for $M^p = 0.25$ are given as follows:

- For $-\pi \leq \theta \leq \theta_\alpha$, $\theta_\alpha = -2.186257912 = -125.26°$, we have

$$\sigma_{rr}^{(0)} = \tfrac{1}{2}(1 + \cos 2\theta), \quad \sigma_{\theta\theta}^{(0)} = \tfrac{1}{2}(1 - \cos 2\theta), \quad \sigma_{r\theta}^{(0)} = -\tfrac{1}{2}\sin 2\theta,$$

- For $\theta_\alpha \leq \theta \leq \theta_\beta$, $\theta_\beta = -1.686144171 = -96.60°$, we have

$$\sigma_{rr}^{(0)} = \tfrac{1}{\sqrt{3}}\cos(\theta + c_3), \quad \sigma_{\theta\theta}^{(0)} = \tfrac{2}{\sqrt{3}}\cos(\theta + c_3), \quad \sigma_{r\theta}^{(0)} = \tfrac{1}{\sqrt{3}}\sin(\theta + c_3),$$

  where $c_3 = 1.230959418 = 70.53°$.

- For $\theta_\beta \leq \theta \leq \theta_\gamma$, $\theta_\gamma = -0.9114267175 = -52.22°$, $\vartheta_1 = \theta_\beta + c_3$, we have

$$\sigma_{rr}^{(0)} = \tfrac{\sqrt{3}}{2}\cos\vartheta_1 - \tfrac{1}{2\sqrt{3}}\cos\vartheta_1\cos 2(\theta - \theta_\beta) + \tfrac{1}{\sqrt{3}}\sin\vartheta_1\sin 2(\theta - \theta_\beta),$$

$$\sigma_{\theta\theta}^{(0)} = \tfrac{\sqrt{3}}{2}\cos\vartheta_1 + \tfrac{1}{2\sqrt{3}}\cos\vartheta_1\cos 2(\theta - \theta_\beta) - \tfrac{1}{\sqrt{3}}\sin\vartheta_1\sin 2(\theta - \theta_\beta),$$

$$\sigma_{r\theta}^{(0)} = \tfrac{1}{2\sqrt{3}}\cos\vartheta_1\sin 2(\theta - \theta_\beta) + \tfrac{1}{\sqrt{3}}\sin\vartheta_1\cos 2(\theta - \theta_\beta).$$

- For $\theta_\gamma \leq \theta \leq \theta_\delta$, $\theta_\delta = 0.924219118 = 52.95°$, we have

$$\sigma_{rr}^{(0)} = \tfrac{1}{\sqrt{3}}\cos(\theta + c_1), \quad \sigma_{\theta\theta}^{(0)} = \tfrac{2}{\sqrt{3}}\cos(\theta + c_1), \quad \sigma_{r\theta}^{(0)} = \tfrac{1}{\sqrt{3}}\sin(\theta + c_1),$$

  where $c_1 = 1.366576756 = 78.30°$.

- For $\theta_\delta \leq \theta \leq \theta_\varepsilon$, $\theta_\varepsilon = 2.081741596 = 119.27°$, $\vartheta_2 = \theta_\varepsilon + c_2$, $c_2 = 1.910633236 = 109.47°$, we have

$$\sigma_{rr}^{(0)} = \tfrac{\sqrt{3}}{2}\cos\vartheta_2 - \tfrac{1}{2\sqrt{3}}\cos\vartheta_2\cos 2(\theta - \theta_\beta) + \tfrac{1}{\sqrt{3}}\sin\vartheta_2\sin 2(\theta - \theta_\beta),$$

$$\sigma_{\theta\theta}^{(0)} = \tfrac{\sqrt{3}}{2}\cos\vartheta_2 + \tfrac{1}{2\sqrt{3}}\cos\vartheta_2\cos 2(\theta - \theta_\beta) - \tfrac{1}{\sqrt{3}}\sin\vartheta_2\sin 2(\theta - \theta_\beta),$$

$$\sigma_{r\theta}^{(0)} = \tfrac{1}{2\sqrt{3}}\cos\vartheta_2\sin 2(\theta - \theta_\beta) + \tfrac{1}{\sqrt{3}}\sin\vartheta_2\cos 2(\theta - \theta_\beta).$$

- For $\theta_\varepsilon \leq \theta \leq \theta_\zeta$, $\theta_\zeta = 2.186257912 = 125.26°$, we have

$$\sigma_{rr}^{(0)} = \tfrac{1}{\sqrt{3}}\cos(\theta + c_2), \quad \sigma_{\theta\theta}^{(0)} = \tfrac{2}{\sqrt{3}}\cos(\theta + c_2), \quad \sigma_{r\theta}^{(0)} = \tfrac{1}{\sqrt{3}}\sin(\theta + c_2).$$

- For $\theta_\zeta \leq \theta \leq \pi$, we have

$$\sigma_{rr}^{(0)} = -\tfrac{1}{2}(1 + \cos 2\theta), \quad \sigma_{\theta\theta}^{(0)} = -\tfrac{1}{2}(1 - \cos 2\theta), \quad \sigma_{r\theta}^{(0)} = \tfrac{1}{2}\sin 2\theta.$$

Here the approach developed in [Dong and Pan 1990; Rahman and Hancock 2006; Stepanova 2009b] has been applied. The circumferential distributions of the stress tensor components $\sigma_{ij}^{(0)}(\theta)$ in the neighborhood of the crack tip for $M^p = 0.5$ are given as follows:

- For $-\pi \leq \theta \leq \theta_\alpha$, $\theta_\alpha = -3.082081755 = -176.60°$, we have

$$\sigma_{rr}^{(0)} = -\tfrac{1}{2}(1 + \cos 2\theta), \quad \sigma_{\theta\theta}^{(0)} = -\tfrac{1}{2}(1 - \cos 2\theta), \quad \sigma_{r\theta}^{(0)} = \tfrac{1}{2}\sin 2\theta.$$

- For $\theta_\alpha \leq \theta \leq \theta_\beta$, $\theta_\beta = -2.069949494 = -118.60°$, we have

$$\sigma_{rr}^{(0)} = \frac{\sqrt{3}}{2} \cos \vartheta_1 - \frac{1}{2\sqrt{3}} \cos \vartheta_1 \cos 2(\theta - \theta_\beta) + \frac{1}{\sqrt{3}} \sin \vartheta_1 \sin 2(\theta - \theta_\beta),$$
$$\sigma_{\theta\theta}^{(0)} = \frac{\sqrt{3}}{2} \cos \vartheta_1 + \frac{1}{2\sqrt{3}} \cos \vartheta_1 \cos 2(\theta - \theta_\beta) - \frac{1}{\sqrt{3}} \sin \vartheta_1 \sin 2(\theta - \theta_\beta),$$
$$\sigma_{r\theta}^{(0)} = \frac{1}{2\sqrt{3}} \cos \vartheta_1 \sin 2(\theta - \theta_\beta) + \frac{1}{\sqrt{3}} \sin \vartheta_1 \cos,$$

where $\vartheta_1 = \theta_\beta + c_1$, $c_1 = 1.107148718 = 63.43°$.

- For $\theta_\beta \leq \theta \leq \theta_\gamma$, $\theta_\gamma = 0.988154515 = 56.62°$, we have

$$\sigma_{rr}^{(0)} = \frac{1}{\sqrt{3}} \cos(\theta + c_1), \quad \sigma_{\theta\theta}^{(0)} = \frac{2}{\sqrt{3}} \cos(\theta + c_1), \quad \sigma_{r\theta}^{(0)} = \frac{1}{\sqrt{3}} \sin(\theta + c_1).$$

- For $\theta_\gamma \leq \theta \leq \theta_\delta$, $\theta_\delta = 2.232478539 = 127.91°$, we have

$$\sigma_{rr}^{(0)} = a + \frac{1}{4}(1 + \cos 2\theta_\delta) \cos 2(\theta - \theta_\delta) + \frac{1}{2} \sin 2\theta_\delta \sin 2(\theta - \theta_\delta),$$
$$\sigma_{\theta\theta}^{(0)} = a - \frac{1}{4}(1 + \cos 2\theta_\delta) \cos 2(\theta - \theta_\delta) - \frac{1}{2} \sin 2\theta_\delta \sin 2(\theta - \theta_\delta),$$
$$\sigma_{r\theta}^{(0)} = -\frac{1}{4}(1 + \cos 2\theta_\delta) \sin 2(\theta - \theta_\delta) + \frac{1}{2} \sin 2\theta_\delta \cos 2(\theta - \theta_\delta),$$

where $a = \frac{1}{4}(-1 + 3 \cos 2\theta_\delta)$.

- For $\theta_\delta \leq \theta \leq \pi$, we have

$$\sigma_{rr}^{(0)} = -\frac{1}{2}(1 + \cos 2\theta), \quad \sigma_{\theta\theta}^{(0)} = -\frac{1}{2}(1 - \cos 2\theta), \quad \sigma_{r\theta}^{(0)} = \frac{1}{2} \sin 2\theta.$$

The circumferential distributions of the stress components $\sigma_{ij}^{(0)}(\theta)$ in the vicinity of the crack tip for $M^p = 0.75$ are given as follows:

- For $-\pi \leq \theta \leq \theta_\alpha$, $\theta_\alpha = -2.904522467 = -166.42°$, we have

$$\sigma_{rr}^{(0)} = -\frac{1}{2}(1 + \cos 2\theta), \quad \sigma_{\theta\theta}^{(0)} = -\frac{1}{2}(1 - \cos 2\theta), \quad \sigma_{r\theta}^{(0)} = \frac{1}{2} \sin 2\theta.$$

- For $\theta_\alpha \leq \theta \leq \theta_\beta$, $\theta_\beta = -1.759907174 = -100.84°$, we have

$$\sigma_{rr}^{(0)} = \frac{\sqrt{3}}{2} \cos \vartheta_1 - \frac{1}{2\sqrt{3}} \cos \vartheta_1 \cos 2(\theta - \theta_\beta) + \frac{1}{\sqrt{3}} \sin \vartheta_1 \sin 2(\theta - \theta_\beta),$$
$$\sigma_{\theta\theta}^{(0)} = \frac{\sqrt{3}}{2} \cos \vartheta_1 + \frac{1}{2\sqrt{3}} \cos \vartheta_1 \cos 2(\theta - \theta_\beta) - \frac{1}{\sqrt{3}} \sin \vartheta_1 \sin 2(\theta - \theta_\beta),$$
$$\sigma_{r\theta}^{(0)} = \frac{1}{2\sqrt{3}} \cos \vartheta_1 \sin 2(\theta - \theta_\beta) + \frac{1}{\sqrt{3}} \sin \vartheta_1 \cos 2(\theta - \theta_\beta),$$

where $\vartheta_1 = \theta_\beta + c_1$, $c_1 = 0.6918358137 = 39.64°$.

- For $\theta_\beta \leq \theta \leq \theta_\gamma$, $\theta_\gamma = 1.119349842 = 64.13°$, we have

$$\sigma_{rr}^{(0)} = \frac{1}{\sqrt{3}} \cos(\theta + c_1), \quad \sigma_{\theta\theta}^{(0)} = \frac{2}{\sqrt{3}} \cos(\theta + c_1), \quad \sigma_{r\theta}^{(0)} = \frac{1}{\sqrt{3}} \sin(\theta + c_1).$$
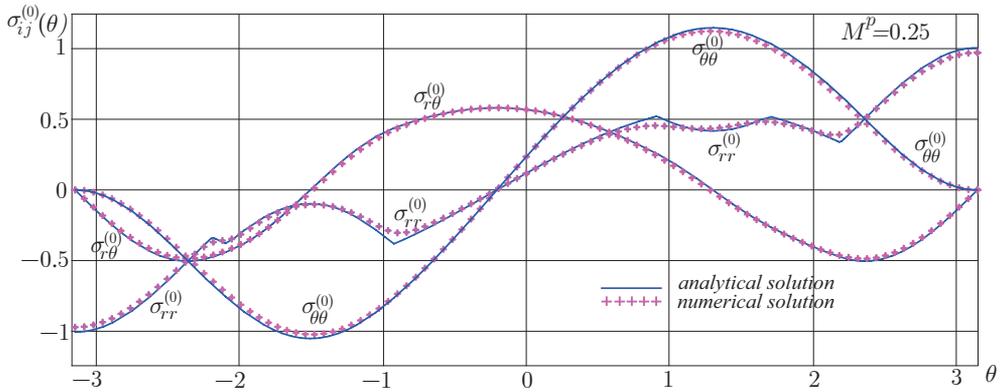
Figure 10. The angular distributions of the stress tensor components in the vicinity of the crack tip for $M^p = 0.25$
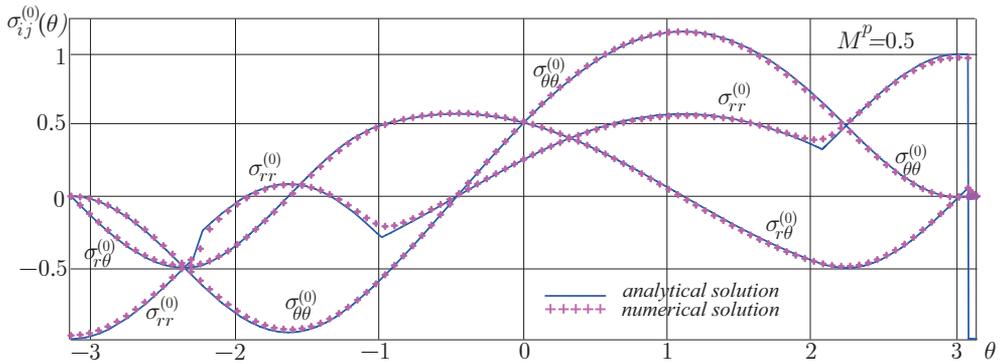
Figure 11. The angular distributions of the stress tensor components in the vicinity of the crack tip for $M^p = 0.5$

- For $\theta_\gamma \leq \theta \leq \theta_\delta$, $\theta_\delta = 2.385429690 = 136.68°$, we have

$$\sigma_{rr}^{(0)} = a + \tfrac{1}{4}(1 + \cos 2\theta_\delta) \cos 2(\theta - \theta_\delta) + \tfrac{1}{2} \sin 2\theta_\delta \sin 2(\theta - \theta_\delta),$$
$$\sigma_{\theta\theta}^{(0)} = a - \tfrac{1}{4}(1 + \cos 2\theta_\delta) \cos 2(\theta - \theta_\delta) - \tfrac{1}{2} \sin 2\theta_\delta \sin 2(\theta - \theta_\delta)$$
$$\sigma_{r\theta}^{(0)} = -\tfrac{1}{4}(1 + \cos 2\theta_\delta) \sin 2(\theta - \theta_\delta) + \tfrac{1}{2} \sin 2\theta_\delta \cos 2(\theta - \theta_\delta),$$

where $a = \tfrac{1}{4}(-1 + 3 \cos 2\theta_\delta)$.

- For $\theta_\delta \leq \theta \leq \pi$, we have

$$\sigma_{rr}^{(0)} = -\tfrac{1}{2}(1 + \cos 2\theta), \quad \sigma_{\theta\theta}^{(0)} = -\tfrac{1}{2}(1 - \cos 2\theta), \quad \sigma_{r\theta}^{(0)} = \tfrac{1}{2} \sin 2\theta.$$

The angular distributions of the stress tensor components obtained are shown in Figures 10–12. The data points are numerical results, while the solid lines represent the analytical solution.

One can see from Figures 10–12 that the radial stress $\tilde{\sigma}_{rr}(\theta)$ is continuous at $\theta = 0$. Continuity of the radial stress $\tilde{\sigma}_{rr}(\theta)$ in the limiting case of perfect plasticity confirms the previously accepted assumption.
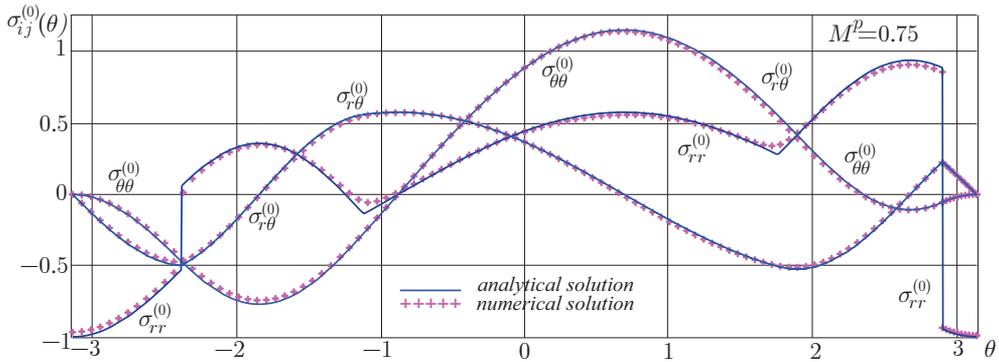
Figure 12. The angular distributions of the stress tensor components in the vicinity of the crack tip for $M^p = 0.75$.

5. Conclusions and discussion of results

In the study the asymptotic analysis and numerical solutions of the nonlinear eigenvalue problems arising from the mixed-mode crack problem in a power law material under plane stress conditions are presented. The method proposed allows us to find the whole spectrum of eigenvalues for a complete range of mixed-mode I/II states of loading from tensile to shear crack problems. The solution is based on the eigenfunction expansion method in the vicinity of the crack tip. The asymptotic presentation of the Airy stress potential reduces the mixed-mode crack problem considered to a nonlinear eigenvalue problem. One eigenvalue corresponding to the pure tensile (mode I) and pure shear (mode II) crack problems is well known and corresponds to the HRR stress field: $\lambda = n/(n+1)$. Following a common practice [Shlyannikov and Kislova 2009; Shlyannikov 2012], it is conventionally assumed that for combined mode I–mode II fracture the eigenvalue corresponding to the HRR problem is the eigenvalue of the nonlinear eigenvalue problem arising from the mixed-mode crack problem. For the case of plane strain conditions, the assumption is valid. The assumption is confirmed by the asymptotic solutions obtained [Shlyannikov and Kislova 2009; Shlyannikov 2012]. However, for the case of plane stress conditions, this hypothesis entails discontinuous radial stress components ahead of the crack tip. All the solutions to the mode I crack and mode II crack problems for plane stress conditions, as well as the solutions for mixed-mode loading [Rahman and Hancock 2006; Shlyannikov and Kislova 2009; Shlyannikov 2012; Stepanova and Adylina 2014], show a continuous radial stress component at $\theta = 0$. In the present paper, it is shown that the mixed-mode loading of the cracked plate results in a new stress singularity around the crack tip. The asymptotic analysis and the numerical calculations performed lead to the new stress field asymptotics in the vicinity of the mixed-mode crack under plane stress conditions. The asymptotic analysis based on the artificial small parameter method of the perturbation theory provided a possibility to reveal the new stress singularity in the vicinity of the crack tip. Next, a technique for numerical determination of the eigenvalues of the nonlinear eigenvalue problem is proposed. Using this technique, the new eigenvalues resulting in continuous radial stress components at $\theta = 0$ are found. It is shown that the method proposed gives the eigenvalues corresponding to the HRR problem in particular cases of mode I and mode II crack problems. The theoretical significance of the present paper is that, from the method described here, one

can clearly know all the mathematically possible distributions of stress singularities at the crack tip under mixed-mode loading.

It is important to develop asymptotic analysis methods and their applications for nonlinear eigenvalue problems in solid mechanics [Andrianov and Awrejcewicz 2013] and, in particular, in nonlinear fracture mechanics and continuum damage mechanics [Barenblatt 2014; Murakami 2012; Voyiadjis 2014], in order to find new and better methods to reliably determine fatigue and fracture behavior. In nonlinear fracture mechanics, the eigenfunction expansion method is one of the most commonly encountered approaches [Murakami 2012; Stepanova 2008a; 2008b; 2009a; Stepanova and Fedina 2008; Stepanova and Igonin 2014]. The method leads to nonlinear eigenvalue problems which stipulate the possible distributions of stress singularities at the crack tip, and the determination of the whole eigenspectrum requires invoking developed asymptotic and computational techniques and their combinations. For instance, it is shown [Stepanova 2008a; 2008b; Stepanova and Igonin 2014] that damage accumulation around the crack tip alters the stress-strain state and results in decreasing the stress singularity in the vicinity of the crack tip. The asymptotic fields in and around the damage zone are quite different from those under K (or J or C^*) dominance in both singularity and distributions. The stress singularity exponent is determined from the nonlinear eigenvalue problem, which needs to be thoroughly solved. The solution of the nonlinear eigenvalue problems provides the solution of the crack problem as a whole. The approach proposed and solutions obtained here can be useful either to find the similarity solutions of the second kind (incomplete similarity) [Barenblatt 2013; 2014; Ritchie 2005] and the solutions of nonlinear eigenvalue problems related to them [Barenblatt 2014; Sih and Tang 2006; Stepanova 2008a; 2008b; Stepanova and Adylina 2014]. It is shown that the meso-mechanical effect of damage accumulation near the crack tip results in new intermediate stress field asymptotic behavior and requires the solution of nonlinear eigenvalue problems. The new eigenvalues can be used for analyzing the near crack tip fields in damaged materials in coupled formulation [Stepanova and Adylina 2014]

In view of the recent research emphases on multiscaling [Tang and Sih 2005; Sih and Tang 2005; 2006; Sih 2008; Stepanova and Igonin 2014], the multiple singularity solution at a point seems to signify the inherent characteristics of micro- and meso-defects. Determination of multiple singularity solutions requires solutions of nonlinear eigenvalue problems. For instance, the model based on the Kachanov–Rabotnov damage evolution law and the power-law of steady-state creep is an example of a problem with the inherent property of incomplete similarity [Stepanova and Adylina 2014]. The method proposed in this paper can be used for the determination of the intermediate asymptotic stress behavior in coupled creep-damage crack problems under mixed-mode loading conditions, since the equations of the problem must have similarity form of the solution and we can derive the solution of the crack problem if the ansatz for the solution of nonlinear eigenvalue problems is obtained. It should be noted also that the class of nonlinear eigenvalue problems arising in nonlinear fracture mechanics is essential in connection with creating multiscale models of fracture [Barenblatt 2013; 2014; Stepanova and Adylina 2014] with multisingularities with different orders at the crack point. A singularity representation scheme has to be considered where the local damage at the different scales will be modeled by different orders of the stress singularities. Different stress singularities can be related to different loading type and severity of material damage.

In [Tang and Sih 2005; Sih and Tang 2005; 2006; Sih 2008], it is elucidated that microscopic effects can have a significant influence on the macroscopic behavior of material. A new approach is needed to

describe the multiscale character of the material microstructure. In [Tang and Sih 2005], a singularity representation scheme where scale effects are modeled by different orders of the stress singularities is proposed. The degree of damage in the vicinity of the crack tip is reflected by the orders of the stress singularities.

In accordance with these models, it is necessary to introduce the hierarchy of the zones in the vicinity of the crack tip with dominating role of different stress asymptotic behavior and to realize the matching procedures between different stress asymptotic solutions. The accurate construction of all the intermediate zones with one or other stress asymptotics requires the knowledge of the whole spectrum of eigenvalues, and these problems are still open.

References

[Akbardoost and Ayatollahi 2014] J. Akbardoost and M. R. Ayatollahi, "Experimental analysis of mixed mode crack propagation in brittle rocks: the effect of non-singular terms", *Eng. Fract. Mech.* **129** (2014), 77–89.

[Andrianov and Awrejcewicz 2013] I. V. Andrianov and J. Awrejcewicz, *Методы асимптотического анализа и синтеза в нелинейной динамике и механике деформируемого твердого тела*, Institute of Computer Investigations, Izhevsk, 2013.

[Andrianov et al. 2014] I. V. Andrianov, J. Awrejcewicz, V. V. Danishevs'kyy, and A. O. Ivankov, *Asymptotic methods in the theory of plates with mixed boundary conditions*, Wiley, Chichester, 2014.

[Barenblatt 2013] G. I. Barenblatt, *Similarity, self-similarity and intermediate asymptotics*, Springer, Berlin, 2013.

[Barenblatt 2014] G. I. Barenblatt, *Flow, deformation and fracture: lectures on fluid mechanics and the mechanics of deformable solids for mathematicians and physicists*, Cambridge Texts in Applied Mathematics **49**, Cambridge University Press, 2014.

[Berto and Lazzarin 2013] F. Berto and P. Lazzarin, "Multiparametric full-field representations of the in-plane stress fields ahead of cracked components under mixed mode loading", *Int. J. Fatigue* **46** (2013), 16–26.

[Berto and Lazzarin 2014] F. Berto and P. Lazzarin, "Recent developments in brittle and quasi-brittle assessment of engineering materials by means of local approaches", *Mater. Sci. Eng. R* **75** (2014), 1–48.

[Botvina et al. 2013] L. R. Botvina, N. A. Chzarkova, M. R. Tutin, A. P. Soldatenkov, Y. A. Demina, and V. P. Levin, "Развитие пластических зон и поврежденности при различных видах нагружения", *Zavod. Lab. Diagn. Mater.* **79**:5 (2013), 46–55. Translated title: "Development of plastic flow zones and damage under various types of loading".

[Bui 2006] H. D. Bui, *Fracture mechanics: inverse problems and solutions*, Springer, Dordrecht, 2006.

[Bui 2011] A. Erlacher and H. Markenscoff (editors), *On duality, symmetry and symmetry lost in solid mechanics: selected works of H. D. Bui*, Presses Ponts et Chaussées, Paris, 2011.

[Constantinescu and Korsunsky 2007] A. Constantinescu and A. Korsunsky, *Elasticity with Mathematica: an introduction to continuum mechanics and linear elasticity*, Cambridge University Press, 2007.

[Decreuse et al. 2012] P. Y. Decreuse, S. Pommier, M. Poncelet, and B. Raka, "A novel approach to model mixed mode plasticity at the crack tip and crack growth. Experimental validations using velocity fields from digital image correlation", *Int. J. Fatigue* **42** (2012), 271–283.

[Dong and Pan 1990] P. Dong and J. Pan, "Asymptotic crack-tip fields for perfectly plastic solids under plane-stress and mixed-mode loading conditions", *J. Appl. Mech.* (*ASME*) **57**:3 (1990), 635–638.

[Hello et al. 2012] G. Hello, M. Ben Tahar, and J.-M. Roelandt, "Analytical determination of coefficients in crack-tip stress expansions for a finite crack in an infinite plane medium", *Int. J. Solids Struct.* **49**:3–4 (2012), 556–566.

[Hutchinson 1968a] J. W. Hutchinson, "Plastic stress and strain fields at a crack tip", *J. Mech. Phys. Solids* **16**:5 (1968), 337–347.

[Hutchinson 1968b] J. W. Hutchinson, "Singular behaviour at the end of tensile crack in a hardening material", *J. Mech. Phys. Solids* **16**:1 (1968), 13–31.

[Kuna 2013] M. Kuna, *Finite elements in fracture mechanics: theory—numerics—applications*, Solid Mechanics and its Applications **201**, Springer, Dordrecht, 2013.

[Leblond and Frelat 2014] J.-B. Leblond and J. Frelat, "Development of fracture facets from a crack loaded in mode I+III: solution and application of a model 2D problem", *J. Mech. Phys. Solids* **64** (2014), 133–153.

[Loghin and Joseph 2001] A. Loghin and P. F. Joseph, "Asymptotic solutions for mixed mode loading of cracks and wedges in power law hardening materials", *Eng. Fract. Mech.* **68**:14 (2001), 1511–1534.

[Loghin and Joseph 2003] A. Loghin and P. F. Joseph, "Mixed mode fracture in power law hardening materials near mode I", *Int. J. Fract.* **123** (2003), 81–106.

[Lomakin and Melnikov 2009] E. V. Lomakin and A. M. Melnikov, "Пластическое плоское напряженное состояние тел, свойства которых зависят от вида напряженного состояния", *Vychisl. Mekh. Splosh. Sred.* **2**:2 (2009), 48–64. English abstract available; translated title: "Plane stress state of media with plastic properties sensitive to the type of stress".

[Lomakin and Melnikov 2011] E. V. Lomakin and A. M. Melnikov, "Задачи плоского напряженного состояния тел с вырезами, пластические свойства которых зависят от вида напряженного состояния", *Izv. Akad. Nauk SSSR Mekh. Tverd. Tela* **46**:1 (2011), 77–89. Translated as "Plane stress state problems for notched bodies whose plastic properties depend on the form of the stress state" in *Mech. Solids* **46**:1 (2011), 62–69.

[Murakami 2012] S. Murakami, *Continuum damage mechanics: a continuum mechanics approach to the analysis of damage and fracture*, Solid Mechanics and its Applications **185**, Springer, Dordrecht, 2012.

[Nayfeh 2000] A. H. Nayfeh, *Perturbation methods*, Wiley, New York, 2000.

[Nayfeh 2011] A. H. Nayfeh, *The method of normal forms*, 2nd ed., Wiley, Weinheim, 2011.

[Ondráček and Materna 2014] J. Ondráček and A. Materna, "FEM evaluation of the dissipated energy in front of a crack tip under 2D mixed mode loading condition", *Procedia Mater. Sci.* **3** (2014), 673–678.

[Pan and Lin 2006] J. Pan and P.-C. Lin, "Analytical solutions for crack-tip sectors in perfectly plastic Mises materials under mixed in-plane and out-of-plane shear loading conditions", *Eng. Fract. Mech.* **73**:13 (2006), 1797–1813.

[Pestrikov and Morozov 2012] V. M. Pestrikov and E. M. Morozov, *Механика разрушения: курс лекций*, EPC Professiya, St. Petersburg, 2012.

[Rahman and Hancock 2006] M. Rahman and J. W. Hancock, "Elastic perfectly-plastic asymptotic mixed mode crack tip fields in plane stress", *Int. J. Solids Struct.* **43**:13 (2006), 3692–3704.

[Rice 1967] J. R. Rice, "Stresses due to a sharp notch in a work hardening elastic-plastic material loaded by longitudinal shear", *J. Appl. Mech.* (*ASME*) **34**:2 (1967), 287–298.

[Rice 1968] J. R. Rice, "Mathematical analysis in the mechanics of fracture", Chapter 3, pp. 191–311 in *Fracture: an advanced treatise*, vol. 2, edited by H. Liebowitz, Academic Press, New York, 1968.

[Rice and Rosengren 1968] J. R. Rice and G. F. Rosengren, "Plane strain deformation near a crack tip in a power-law hardening material", *J. Mech. Phys. Solids* **16**:1 (1968), 1–12.

[Richard et al. 2014] H. A. Richard, B. Schramm, and N.-H. Schirmeisen, "Cracks on mixed mode loading: theories, experiments, simulations", *Int. J. Fatigue* **62** (2014), 93–103.

[Ritchie 2005] R. O. Ritchie, "Incomplete self-similarity and fatigue-crack growth", *Int. J. Fract.* **132**:3 (2005), 197–203.

[Shih 1973] C. F. Shih, *Elastic-plastic analysis of combined mode crack problems*, thesis, Harvard University, Cambridge, MA, 1973.

[Shih 1974] C. F. Shih, "Small scale yielding analysis of mixed mode plane-strain crack problems", pp. 187–210 in *Fracture analysis* (College Park, MD, 1973), vol. 2, ASTM Special Technical Publication **560**, American Society for Testing and Materials, Philadelphia, 1974.

[Shlyannikov 2003] V. N. Shlyannikov, *Elastic-plastic mixed-mode fracture criteria and parameters*, Lecture Notes in Applied Mechanics **7**, Springer, Berlin, 2003.

[Shlyannikov 2012] V. N. Shlyannikov, "Решение задач нелинейного деформирования и разрушения материалов при сложном напряженном состоянии", *Fiz. Mezomekh.* **15**:1 (2012), 57–67. Translated as "Solution of nonlinear strain and fracture problems for materials in complex stress states" in *Phys. Mesomech.* **15**:3–4 (2012), 176–184.

[Shlyannikov 2013] V. N. Shlyannikov, "T-stress for crack paths in test specimens subject to mixed mode loading", *Eng. Fract. Mech.* **108** (2013), 3–18.

[Shlyannikov and Kislova 2009] V. N. Shlyannikov and S. Y. Kislova, "Параметры смешанных форм деформирования для трещины в виде математического разреза", *Izv. Saratov Univ. Mat. Mekh. Inform.* **9**:1 (2009), 77–84. English abstract avaiable; translated title: "Mode mixity parameters for mathematical crack type".

[Shlyannikov and Zakharov 2014] V. N. Shlyannikov and A. P. Zakharov, "Multiaxial crack growth rate under variable T-stress", *Eng. Fract. Mech.* **123** (2014), 86–99.

[Shlyannikov et al. 2014] V. N. Shlyannikov, A. V. Tumanov, and A. P. Zakharov, "The mixed mode crack growth rate in cruiciform specimens subject to biaxial loading", *Theor. Appl. Fract. Mech.* **73** (2014), 68–81.

[Sih 2008] G. C. Sih, "Мезомеханика, понятие сегментации и мультискейлинговый подход: нано-микро-макро", *Fiz. Mezomekh.* **11**:3 (2008), 5–18. Translated as "Birth of mesomechanics arising from segmentation and multiscaling: nano-micro-macro" in *Phys. Mesomech.* **11**:3–4 (2008), 124–136.

[Sih and Tang 2005] G. C. Sih and X. S. Tang, "Scaling of volume energy density function reflecting damage by singularities at macro-, meso- and microscopic level", *Theor. Appl. Fract. Mech.* **43**:2 (2005), 211–231.

[Sih and Tang 2006] G. C. Sih and X. S. Tang, "Simultaneous occurence of double micro/macro stress singularities for multiscale crack model", *Theor. Appl. Fract. Mech.* **46**:2 (2006), 87–104.

[Sliva et al. 2010] G. Sliva, A. Brezillon, J. M. Cadou, and L. Duigou, "A study of the eigenvalue sensitivity by homotopy and perturbation methods", *J. Comput. Appl. Math.* **234**:7 (2010), 2297–2302.

[Smith et al. 2001] D. J. Smith, M. R. Ayatollahi, and M. J. Pavier, "The role of T-stress in brittle fracture for linear elastic materials under mixed-mode loading", *Fatigue Fract. Eng. Mater. Struct.* **24**:2 (2001), 137–150.

[Stepanova 2008a] L. V. Stepanova, "Eigenspectra and orders of stress singularity at a mode I crack tip for a power-law medium", *C. R. Mécanique* **336**:1-2 (2008), 232–237.

[Stepanova 2008b] L. V. Stepanova, "О собственных значениях в задаче о трещине антиплоского сдвига в материале со степенными определяющими уравнениями", *Prikl. Mekh. Tekh. Fiz.* **49**:1 (2008), 173–180. Translated as "Eigenvalues of the antiplane-shear crack problem for a power-law material" in *J. Appl. Mech. Tech. Phys.* **49**:1 (2008), 142–147.

[Stepanova 2009a] L. V. Stepanova, "Анализ собственных значений в задаче о трещине в материале со степенным определяющим законом", *Zh. Vychisl. Mat. Mat. Fiz.* **49**:8 (2009), 1399–1415. Translated as "Eigenvalue analysis for a crack in a power-law material" in *Comput. Math. Math. Phys.* **49**:8 (2009), 1332–1347.

[Stepanova 2009b] L. V. Stepanova, "Асимптотика напряжений и скоростей деформаций вблизи вершины трещины поперечного сдвига в материале, поведение которого описывается дробно-линейным законом", *Prikl. Mekh. Tekh. Fiz.* **50**:1 (2009), 165–176. Translated as "Asymptotics of stresses and strain rates near the tip of a transverse shear crack in a material whose behavior is described by a fractional-linear law" in *J. Appl. Mech. Tech. Phys.* **50**:1 (2009), 137–146.

[Stepanova and Adylina 2014] L. V. Stepanova and E. M. Adylina, "Напряженно-деформированное состояние в окрестности вершины трещины в условиях смешанного нагружения", *Prikl. Mekh. Tekh. Fiz.* **55**:5 (2014), 181–194. Translated as "Stress-strain state in the vicinity of a crack tip under mixed loading" in *J. Appl. Mech. Tech. Phys.* **55**:5 (2014), 885–895.

[Stepanova and Fedina 2008] L. V. Stepanova and M. E. Fedina, "Автомодельное решение задачи о трещине отрыва в связанной постановке", *Prikl. Mat. Mekh.* **72**:3 (2008), 516–527. Translated as "Self-similar solution of a tensile crack problem in a coupled formulation" in *J. Appl. Math. Mech.* **72**:3 (2008), 360–368.

[Stepanova and Igonin 2014] L. V. Stepanova and S. A. Igonin, "Perturbation method for solving the nonlinear eigenvalue problem arising from fatigue crack growth problem in a damaged medium", *Appl. Math. Model.* **38**:14 (2014), 3436–3455.

[Tang and Sih 2005] X. S. Tang and G. C. Sih, "Weak and strong singularities reflecting multiscale damage: micro-boundary conditions for free-free, fixed-fixed and free-fixed constraints", *Theor. Appl. Fract. Mech.* **43**:1 (2005), 5–62.

[Vildeman et al. 2012] V. E. Vildeman, M. P. Tretyakov, T. V. Tretyakova, R. V. Bulbovich, S. V. Babyshkin, A. V. Il'inych, D. S. Lobanov, and A. V. Ipatova, *Экспериментальные исследования свойств материалов при сложных термомеханических воздействиях*, Fizmatlit, Moscow, 2012.

[Vildeman et al. 2014] V. E. Vildeman, E. V. Lomakin, and M. P. Tretyakov, "Закритическое деформирование сталей при плоском напряженном состоянии", *Izv. Akad. Nauk SSSR Mekh. Tverd. Tela* **49**:1 (2014), 26–36. Translated as "Postcritical deformation of steels in plane stress state" in *Mech. Solids* **49**:1 (2014), 18–26.

[Voyiadjis 2014] G. Z. Voyiadjis, *Handbook of damage mechanics: nano to macro scale for materials and structures*, Springer, Berlin, 2014.

[Wei 2010] R. P. Wei, *Fracture mechanics: integration of mechanics, materials science and chemistry*, Cambridge University Press, 2010.

[Wei et al. 2011] Z. Wei, X. Deng, M. A. Sutton, J. Yan, C.-S. Cheng, and P. Zavattieri, "Modeling of mixed-mode crack growth in ductile thin sheets under combined in-plane and out-of-plane loading", *Eng. Fract. Mech.* **78**:17 (2011), 3082–3101.

LARISA V. STEPANOVA: stepanovalv@samsu.ru
Department of Mathematical Modelling in Mechanics, Samara State University, 1 Akad. Pavlov, Samara, 443011, Russia

EKATERINA M. YAKOVLEVA: adulinaem@samsu.ru
Department of Mathematical Modelling in Mechanics, Samara State University, 1 Akad. Pavlov, Samara, 443011, Russia

msp

msp

ANTIPLANE SHEAR FIELD
FOR A CLASS OF HYPERELASTIC INCOMPRESSIBLE BRITTLE MATERIAL:
ANALYTICAL AND NUMERICAL APPROACHES

CLAUDE STOLZ AND ANDRES PARRILLA GOMEZ

This paper reconsiders the problem of determining the elastostatics fields near the tip of a crack in a body deformed by an antiplane shear for a class of incompressible, homogeneous, isotropic materials. The study is generalized to the formation of a quasicrack under the same conditions of loading for brittle material that cannot support any further loading when a critical strength is reached. The crack is then replaced by a totally damaged zone where the stress is identically zero. The shape of the boundary between the damaged and undamaged body is found analytically. A numerical approach is proposed to address the problem for more general constitutive law. The analytical solution is recovered by a process of shape optimization.

1. Introduction

In classical fracture mechanics, the solution of equilibrium for linearized elastostatics proposes an outer expansion of the displacement with respect to the distance from the crack tip. Some studies have taken into account the nonlinear effects on the inner expansion of the displacement in finite elastostatics or in elastoplasticity. The finite antiplane shear near the tip of a crack in an incompressible nonlinear elastic solid has been studied [Knowles and Sternberg 1980; 1981]. The displacement field possesses singularities or discontinuities in its gradient depending on the shape of the stress-strain curve. For these studies, the stress is defined for any amount of shear that is not bounded.

For hyperelastic material such as elastomers, rupture may occur when a maximal stretch is reached. When this critical value is reached, the material is broken and cannot support further tension: then a damaged zone develops inside the body. The purpose of this paper is to determine the shape of the damaged zone under antiplane shear conditions.

Neuber [1968] investigated the mechanism of nonlinear stress-concentration near a notch and crack propagation. The solution is obtained for any nonlinear stress-strain laws monotonically increasing and all loading intensities. The boundary of the notch consists of two parallel straight lines and a cycloid along which the amount of shear is uniform. Bui and Ehrlacher [1980] solved the same problem for a linear elastic-brittle material; the thickness of the damaged zone is determined as a function of the stress intensity factor of the equivalent crack. A similar solution has been obtained for elastoplasticity [Bui 1980].

More recently, brittle hyperelastic material solution for constitutive laws that permit loss of ellipticity has been considered. Under antiplane shear, the boundary governed by the critical value of shear is a cycloid [Stolz 2010] using the hodograph scheme as proposed in [Knowles and Sternberg 1980].

Under the antiplane condition, during the propagation, the cracks tend to deviate from their plane. The purpose of this paper is not to study the propagation of the crack in a three-dimensional space. The antiplane problem is considered here to provide an analytical solution to evaluate the ability of the proposed numerical scheme to determine a stress-free boundary independently of the mesh of a body.

2. Preliminaries and finite antiplane shear

Consider an isotropic homogeneous incompressible elastic body. Suppose that the body occupies an open region Ω in a nondeformed configuration, and let us consider a deformation defined by the plane displacement $w(\boldsymbol{x})$,

$$\boldsymbol{y}(\boldsymbol{x}) = \boldsymbol{x} + w(x_1, x_2)\boldsymbol{e}_3, \tag{2-1}$$

that maps the domain Ω onto its deformation image ω. We assume that the mapping is regular and invertible. Let

$$\boldsymbol{F} = \boldsymbol{I} + w_{,i}\boldsymbol{e}_3 \otimes \boldsymbol{e}_i, \qquad \boldsymbol{F}^{-1} = \boldsymbol{I} - w_{,i}\boldsymbol{e}_3 \otimes \boldsymbol{e}_i, \tag{2-2}$$

the deformation gradient and its inverse. For an incompressible medium, the volume must be locally preserved and thus

$$J = \det \boldsymbol{F} = 1. \tag{2-3}$$

The left Cauchy–Green deformation tensor

$$\boldsymbol{B} = \boldsymbol{I} + w_{,i}(\boldsymbol{e}_3 \otimes \boldsymbol{e}_i + \boldsymbol{e}_i \otimes \boldsymbol{e}_3) + (w_{,x_1}^2 + w_{,x_2}^2)\boldsymbol{e}_3 \otimes \boldsymbol{e}_3 \tag{2-4}$$

has the fundamental scalar invariants

$$I_1 = \operatorname{Tr} \boldsymbol{B}, \qquad I_2 = \tfrac{1}{2}(I_1^2 - \operatorname{Tr}(\boldsymbol{B}^2)), \qquad I_3 = J^2 = 1. \tag{2-5}$$

The invariants I_1 and I_2 are equal:

$$I_1 = I_2 = 3 + R^2, \tag{2-6}$$

where R is the norm of ∇w.

For hyperelastic isotropic incompressible material, the free energy is a function E of these invariants; in the case of antiplane shear, this energy is reduced to a function Ψ:

$$\Psi(I_1) = E(I_1, I_2). \tag{2-7}$$

For the energy Ψ, the constitutive behavior is written as

$$\boldsymbol{\Theta} = 2\Psi'(I_1)\boldsymbol{F}^T + \eta \boldsymbol{F}^{-1}, \qquad \boldsymbol{\sigma} = 2\Psi'(I_1)\boldsymbol{B} + \eta \boldsymbol{I}, \tag{2-8}$$

where $\boldsymbol{\Theta}$ is the first Piola–Kirchhof stress tensor and $\boldsymbol{\sigma}$ the (actual) Cauchy stress tensor and where the Lagrange multiplier η is associated with the constraint (2-3).

The balance of linear momentum in the absence of body forces leads to the equilibrium equation

$$\operatorname{Div} \boldsymbol{\Theta}^T = 2(\Psi'(I_1)w_{,\beta})_{,\beta} = 0, \tag{2-9}$$

where $\beta = 1, 2$ and the summation is implied. This equation is that obtained in small perturbation for nonlinear elastic material with modulus $\mu = \Psi'(I_1)$.

As $\boldsymbol{\sigma} \cdot \boldsymbol{e}_3 = 0$, the associated Piola stress tensor $\boldsymbol{\Theta}$ is then reduced to

$$\boldsymbol{\Theta} = 2\Psi'(\boldsymbol{F}^T - \boldsymbol{F}^{-1}), \tag{2-10}$$

and the balance of linear momentum leads to an elliptic differential equation under the condition

$$2\Psi' + 4R^2\Psi'' \geq 0, \tag{2-11}$$

which corresponds to the fact that the local stress-strain curve $\tau(R) = 2R\Psi'(R) = R\mu(R)$ is an increasing function of R.

2A. *Power law for $\alpha \leq 1$.* Assume now that the local stress-strain relations are given by

$$\begin{cases} R \leq R_o, & \tau = \mu_o R, \\ R_o \leq R \leq R_m, & \tau = \mu_o R_o (R/R_o)^\alpha = \hat{\mu} R^\alpha, \\ R_m \leq R, & \tau = 0. \end{cases} \tag{2-12}$$

Then for $R \leq R_o$, the differential equation is elliptic. For $R_m \geq R \geq R_o$, ellipticity is ensured if $\alpha \geq 0$; otherwise, the differential equation becomes hyperbolic.

2B. *Neo-Hookean material.* For $\alpha = 1$ and $R_m = \infty$, the material is neo-Hookean. For this case, the differential equation reduces to Laplace's equation and for a straight crack ($-\infty \leq X_1 \leq 0$ and $X_2 = 0$) the solution of equilibrium is identical to the solution of Irwin obtained for linearized elastostatic. In the radial coordinates around the crack tip, the displacement is obtained as

$$w \to \frac{2K}{\mu_o}\sqrt{\frac{r}{2\pi}}\sin\frac{\theta}{2}, \quad r \to \infty. \tag{2-13}$$

3. The small-scale nonlinear quasicrack problem and hodograph transformation

To determine the mechanical fields over the domain Ω, the hodograph transformation is useful as pointed out by [Knowles and Sternberg 1980; 1981]. Other techniques can be used [Neuber 1968]. In the hodograph transformation, the components of the gradient ∇w become the new independent variables:

$$(x_1, x_2) \to (\xi_1, \xi_2), \quad \xi_\alpha = w_{,\alpha}(x_1, x_2). \tag{3-1}$$

The displacement appears as a potential ($dw = \xi_\alpha \, dx_\alpha$). The mapping is invertible provided the Jacobian $H = w_{,11}w_{,22} - (w_{,12})^2$ does not vanish. Denote by U the Legendre transformation of w with respect to ξ_α:

$$U(\xi_1, \xi_2) = x_\alpha w_{,\alpha}(x_1, x_2) - w(x_1, x_2). \tag{3-2}$$

By differentiating U with respect to ξ, the conjugate equations are obtained:

$$x_\alpha = \frac{\partial U}{\partial \xi_\alpha}, \quad w = \xi \cdot \nabla U - U. \tag{3-3}$$

In the hodograph plane, the polar coordinates are used ($\xi_1 = R\cos\Theta$ and $\xi_2 = R\sin\Theta$); then this inverse of the mapping is given by

$$x_1 = \cos\Theta\frac{\partial U}{\partial R} - \frac{\sin\Theta}{R}\frac{\partial U}{\partial\Theta}, \quad x_2 = \sin\Theta\frac{\partial U}{\partial R} + \frac{\cos\Theta}{R}\frac{\partial U}{\partial\Theta}. \tag{3-4}$$

The stress field satisfies

$$\tau_1 = \sigma_{13} = \mu(R)R\cos\Theta, \qquad \tau_2 = \sigma_{23} = \mu(R)R\sin\Theta. \tag{3-5}$$

The equation of motion (2-9) is rewritten in the hodograph plane (R, Θ) using the mapping (3-4). The notation $(\cdot)'$ indicates a differentiation with respect to R. The differential equation obtained in statics takes the expression

$$\frac{\partial}{\partial R}\left(\mu(R)R\frac{\partial U}{\partial R}\right) + \frac{(\mu(R)R)'}{R}\frac{\partial^2 U}{\partial \Theta^2} = 0. \tag{3-6}$$

This equation is homogeneous of degree 1 in U. Using (3-2), the displacement w is

$$w = R^2 \frac{\partial}{\partial R}\frac{U}{R}. \tag{3-7}$$

3A. *Crack in a neo-Hookean material.* A solution of (3-6) for a given modulus $\mu(R)$ is

$$U(R, \Theta) = A_o R I_o(R)\cos\Theta, \quad R \geq 0, \ 0 \leq \Theta \leq \pi, \tag{3-8}$$

where the function $I_o(R)$ is

$$I_o(R) = \int_R^\infty \frac{dt}{\mu(t)t^3}. \tag{3-9}$$

For neo-Hookean materials, the modulus $\mu(t)$ is a constant μ_o and the solution is then

$$U(R, \Theta) = \frac{A_o}{2\mu_o R}\cos\Theta, \qquad w = -\frac{A_o}{\mu_o R}\cos\Theta. \tag{3-10}$$

The images of the crack lips $(\theta = \pm\pi)$ are the two ξ_1 axes $\Theta = 0$ and $\Theta = \pi$. The boundary conditions on the crack lips are

$$\frac{\partial U}{\partial \Theta} = 0 \quad \text{for all } R, \ \Theta = 0, \text{ and } \Theta = \pi. \tag{3-11}$$

Taking into account the hodograph transformation (3-4) and Irwin's solution (2-13), we obtain the identification

$$\Theta = \tfrac{1}{2}(\pi + \theta), \qquad A_o = \frac{K^2}{\pi\mu_o}. \tag{3-12}$$

3B. *On the solution for power law for $R_m \to \infty$.* It is easy to verify that the potential U_α given by

$$U_\alpha(R, \Theta) = A_\alpha R\cos\Theta \int_R^{R_o} \frac{dt}{\hat{\mu}_o t^{\alpha+2}} = A_\alpha R I_\alpha(R)\cos\Theta \tag{3-13}$$

satisfies the conservation (2-9) of linear momentum for $\alpha \neq -1$.

For the proposed strain-stress law with $R_m \to \infty$, the solution U is obtained:

- on domain $R \leq R_o$, $\alpha = 1$ and $U = A_1 R I_1(R)\cos\Theta$ and
- on domain $R \geq R_o$, $U = A_\alpha R I_\alpha(R)\cos\Theta$.

The constant A_1 is determined by the condition of the loading at infinity (4-5). The potential at shear amount $R = R_o$ is continuous.

For $\alpha \geq 0$, the differential equation is elliptic for all amounts of shear, and the continuity of the displacement for $R = R_o$ for all Θ gives the constant A_α. On this curve, the stress is also continuous.

For $\alpha < 0$ and $R \geq R_o$, the differential equation is hyperbolic. In this case, the elliptic and hyperbolic domains are not disjoint. The potential is continuous for $R = R_o$ but not the displacement. The solution in the elliptic domain must be equal to the solution in the hyperbolic domain: $w_e(R_e, \Theta_e) = w_h(R_h, \Theta_h)$ at the common point ($x_1^e(R_e, \Theta_e) = x_1^h(R_h, \Theta_h)$, $x_2^e(R_e, \Theta_e) = x_2^h(R_h, \Theta_h)$). These equations determine a curve where the gradient of the displacement is discontinuous [Knowles and Sternberg 1981] and the stress vector is continuous. The continuity of the stress vector implies that $A_\alpha = A_o$. The resulting potential is that of Knowles and Sternberg [1981].

3C. *On the quasicrack geometry.* To obtain the geometry of the quasicrack, other solutions of (2-9) must be added. Peculiar functions of the differential equation are

$$R\left(\frac{2\alpha}{\alpha+1} \log R \cos \Theta - \Theta \sin \Theta\right), \qquad R \cos \Theta, \qquad R \sin \Theta. \qquad (3\text{-}14)$$

The first one corresponds to a shift along x_2 when Θ goes from 0 to π, the second permits an x_1 shift of a unit value, and the last one corresponds to a shift along e_2 of a unit value.

4. The quasicrack solution

For the considered example, the geometry of the crack is the straight line $-\infty \leq x_1 \leq 0$. The direction of the line is e_1. The applied loading is that of a crack obtained in classical linearized elasticity or embedded in neo-Hookean material as presented in Section 1. For an inner point of view, the local behavior is nonlinear and the amount of shear is limited by a critical value R_m as described by the proposed constitutive law.

For the considered constitutive law, the solution in the hodograph plane is built by the combination of the solution for the linear part of the constitutive law and the solution for the nonlinear part with the help of peculiar solutions.

Using the above results, the potential U is searched by

$$\begin{cases} 0 \leq R \leq R_o, \quad U = U_o(R, \Theta), \\ \qquad U_o = A_o R \cos \Theta \int_R^{R_o} \frac{dt}{\mu_o t^3} - B_o R(\log R \cos \Theta - \Theta \sin \Theta) + C_o R \cos \Theta, \\ R_o \leq R \leq R_m, \quad U_1 = \widehat{U}(R, \Theta), \\ \qquad U_1 = A_1 R \cos \Theta \int_R^{R_o} \frac{dt}{\hat{\mu}_o t^{\alpha+2}} - B_1 R\left(\frac{2\alpha}{\alpha+1} \log R \cos \Theta - \Theta \sin \Theta\right) + C_1 R \cos \Theta. \end{cases} \qquad (4\text{-}1)$$

The constants $(A_o, A_1, B_o, B_1, C_o, C_1)$ are determined by

(a) continuity conditions of the potential in $R = R_o$,

(b) continuity of the displacement w everywhere,

(c) asymptotic behavior when $R \to 0$, and

(d) traction-free boundary conditions along the boundary of the damaged zone.

4A. *Determination of the constants.*

(a) The continuity of the potential implies that $B_o = B_1 = B$ and the relation

$$B\frac{2\alpha}{\alpha+1}R_o \log R_o + C_1 R_o = B R_o \log R_o + C_o R_o. \tag{4-2}$$

Then the displacement is given by

$$\begin{cases} 0 \le R \le R_o, & w = w_o(R, \Theta) = -\left(\frac{A_o}{\mu_o R} + B R\right)\cos\Theta, \\[2mm] R_o \le R \le R_m, & w = \hat{w}(R, \Theta) = -\left(\frac{A_1}{\hat{\mu}_o R^\alpha} + \frac{2B\alpha}{\alpha+1}R\right)\cos\Theta. \end{cases} \tag{4-3}$$

(b) The displacement is continuous on $R = R_o$:

$$A_1 + \mu_o R_o^2 B\frac{\alpha-1}{\alpha+1} = A_o. \tag{4-4}$$

(c) The displacement satisfies the matching condition at ∞, so we obtain

$$A_o = \frac{K^2}{\pi\mu_o}. \tag{4-5}$$

(d) The boundary along the damaged zone is traction-free.

To simplify the expression, we adopt an dimensionless formulation. Let us define new parameters (a, a_1, b)

$$\frac{A_o}{\mu_o R_o^2} = \frac{K^2}{\pi\tau_o^2} = a, \qquad \frac{A_1}{\mu_o R_o^2} = aa_1, \qquad B = ba. \tag{4-6}$$

We adopt $C_o = 2 - B + B \log R_o$ in order to determine the position of the quasicrack along $x_2 = 0$, and we consider the notation $X_i = x_i/a$ and $\rho = R/R_o$. Then $\rho_o = 1$ and $\rho_m = R_m/R_o$.

The condition (4-5) is then rewritten as

$$a_1 + b\frac{\alpha-1}{\alpha+1} = 1. \tag{4-7}$$

With this notation, the traction-free boundary condition (d) is now explained.

For that, the image of the hodograph plane is determined:

• $0 \le \rho \le 1$,

$$X_1 = -\frac{1}{2} - \frac{1}{2\rho^2}\cos 2\Theta - b\log\rho,$$

$$X_2 = -\frac{1}{2\rho^2}\sin 2\Theta + b\left(\Theta - \frac{\pi}{2}\right),$$

$$W = -\left(\frac{1}{\rho} + b\rho\right)\cos\Theta,$$

- $1 \le \rho \le \rho_m$,

$$X_1 = -\left(\frac{a_1}{\rho^{\alpha+1}} + b\frac{\alpha-1}{\alpha+1}\right)\frac{\cos 2\Theta}{2} - \left(\frac{a_1}{\rho^{\alpha+1}} + b\right)\frac{\alpha-1}{2(\alpha+1)} - \frac{2b\alpha}{\alpha+1}\log\rho - \frac{a_1}{\alpha+1},$$

$$X_2 = -\left(\frac{a_1}{\rho^{\alpha+1}} + b\frac{\alpha-1}{\alpha+1}\right)\frac{\sin 2\Theta}{2} + b\left(\Theta - \frac{\pi}{2}\right),$$

$$W = -\left(\frac{a_1}{\rho^{\alpha}} + \frac{2\alpha}{\alpha+1}b\rho\right)\cos\Theta.$$

We have moved the frame along e_2 with a shift of $-b\pi/2$ to emphasize the symmetry of the geometry with respect to e_1. For $\rho = \rho_a$, the curve $(X_1(\rho_a, \Theta), X_2(\rho_a, \Theta))$ is a cycloid. With this geometry, the traction-free boundary condition is given by

$$\tau_1 \, dX_2 - \tau_2 \, dX_1 = 0. \tag{4-8}$$

The boundary is decomposed into three parts: the two horizontal lines $\Theta = \pi/2 \pm \pi/2$ and the cycloid where $\rho = \rho_m$. The traction-free boundary condition is satisfied for $\Theta = \pi/2 \pm \pi/2$ for all ρ and implies along the cycloid where $\rho = \rho_m$

$$\left(\frac{2b}{\alpha+1} - \frac{a_1}{\rho_m^{\alpha+1}}\right)\cos\Theta = 0. \tag{4-9}$$

This relation can be combined with (4-5); then

$$1 = \frac{2b}{\alpha+1}\left(\rho_m^{\alpha+1} + \frac{\alpha-1}{2}\right). \tag{4-10}$$

It can be noticed that the thickness H of the damaged zone is $H = ba\pi$.

For $\rho_m \to \infty$, the quantity b vanishes, the quasicrack tends to the classical crack, and the thickness H vanishes.

4B. *Connection with release rate of energy.* The strain energy for the critical shear R_m is given by

$$E(R_m) = \int_o^{R_m} \tau(t)\,dt = \frac{1}{\mu_o}\frac{\tau_o^2}{\alpha+1}\left(\rho_m^{\alpha+1} + \frac{\alpha-1}{2}\right). \tag{4-11}$$

As a is a function of the equivalent loading K, the relation (4-10) determines the thickness of the damaged zone

$$\tfrac{1}{2}a\pi = \frac{H}{\alpha+1}\left(\rho_m^{\alpha+1} + \frac{\alpha-1}{2}\right) = \frac{1}{2}\frac{K^2}{\tau_o^2}. \tag{4-12}$$

The flux of the energy along the cycloid is given by

$$D_d = HE(R_m) = \pi a\frac{\tau_o^2}{2\mu_o} = \frac{K^2}{2\mu_o}. \tag{4-13}$$

This flux is exactly the energy release rate for the equivalent crack given by the condition of loading at infinity

$$\mathcal{G} = J = HE. \tag{4-14}$$

This emphasizes the fact that, in the presence of discontinuities of the displacement gradient along a curve Σ, the equivalent J-integral is obtained by the limit

$$\mathcal{G} = \lim_{\Gamma \to \Sigma} \int (E n_1 - \boldsymbol{N}\boldsymbol{\Theta} \cdot \boldsymbol{F} \cdot \boldsymbol{e}_1) \, ds = \int_C (E n_1 - \boldsymbol{N}\boldsymbol{\Theta} \cdot \boldsymbol{F} \cdot \boldsymbol{e}_1) \, ds \tag{4-15}$$

for all curve C containing the cycloid. The invariance of the integral can be proved as proposed in [Knowles and Sternberg 1972].

4C. _Property of the solution for $\alpha \geq 0$._ The balance equations for linear momentum are elliptic. If $\rho_o \geq \rho_1$, the volume bounded by the cycloid $(X(\rho_o, \Theta), Y(\rho_o, \Theta))$ contains the volume bounded by the cycloid $(X(\rho_1, \Theta), Y(\rho_1, \Theta))$. This is the case described by Neuber [1968].

In our approach, we have an additional equation that determines the thickness of the damaged zone with respect to the external loading. The equations of equilibrium are elliptic, and there are no discontinuities of the displacement gradient.

It can be noticed that we can use Rice's J-integral to evaluate the stress intensity factor K, taking into account the invariance of the J-type integral in hyperelasticity [Knowles and Sternberg 1972].

For $\rho_m = 1$, the results obtained by Bui and Ehrlacher are recovered, $b = 1$, and the solution is

$$X_1 = -\frac{1}{2} - \frac{1}{2\rho^2} \cos 2\Theta - \log \rho,$$

$$X_2 = -\frac{1}{2\rho^2} \sin 2\Theta + \left(\Theta - \frac{\pi}{2}\right),$$

$$W = -\left(\frac{1}{\rho} + \rho\right) \cos \Theta,$$

and the thickness of the damaged zone satisfies the relation

$$H = \pi a = \frac{K^2}{\tau_o^2}. \tag{4-16}$$

An estimation of the thickness for steel gives H of the order of $100 \, \mu$m.

For $\alpha = 0$ and $\rho_m > 1$, the solution obtained by Bui [1980] is recovered.

It can be noticed that here the solution is obtained for nonlinear elastic behavior. This shows that Bui's solution is only a static solution. If we consider a propagation with constant velocity, the equation must be completely reformulated because in this case the inertia terms are not negligible with respect to the tangent modulus of the behavior.

Then the given relations are generalizations of these previous results to the case of hyperelastic brittle material.

4D. _Property of the solution for $\alpha < 0$._ In this case, the differential equation becomes hyperbolic for $\rho \geq 1$. The proposed potential U is the sum of two contributions: one independent of b and another one depending linearly on b. The first one corresponds exactly to the solution of Knowles and Sternberg for a classical crack in nonlinear elasticity.

But when ρ_m is finite, the main difficulty is to ensure the continuity of the displacement along the common boundary between the domains of ellipticity and hyperbolicity. It can be noticed that the limit
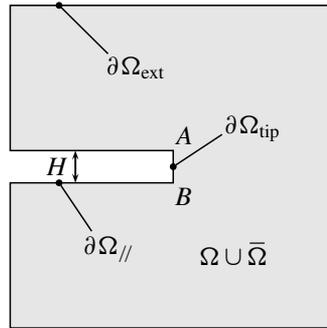
Figure 1. Meshed domain and boundary notations.

of the given potential when ρ_m tends to infinity is exactly the potential of Knowles and Sternberg because at the limit $b = 0$.

Another interesting limit is obtained for fixed value ρ_m and $\alpha \to -\infty$: the potential U tends toward the potential of the elastic brittle material, and the solution is the solution of Bui and Ehrlacher.

The general case will be discussed in a further paper; some new requirements about regularity are necessary to obtain a valuable solution.

5. Numerical approach

The problem of a quasicrack is now considered from a numerical point of view. The main difficulty is to determine the shape of the quasicrack with an optimization algorithm using a nonlinear solver. The goal of the numerical analysis is to determine numerically the traction-free boundary shape of the quasicrack and to exhibit the relationship between the thickness H, the material properties, and the stress intensity factor K of the equivalent crack.

To evaluate the ability of the proposed algorithm, we consider the constitutive law (2-12) with no loss of local ellipticity ($0 \leq \alpha \leq 1$).

Two main issues in the calculation have to be investigated: how to allow the free boundary to move and then how to adapt the stress intensity factor K during the calculation.

The meshed domain is a square with a quasicrack of a given thickness H as shown in Figure 1. The side of the square is ten times bigger than the quasicrack thickness. The boundary of the domain is decomposed into four parts: the outer boundary $\partial\Omega_{\text{ext}}$, the two crack lips $\partial\Omega_{//}$, and the nonmaterial boundary $\partial\Omega_{\text{tip}}$.

- The boundary $\partial\Omega_{\text{ext}}$ is supposed to be far enough from the equivalent crack tip to legitimately impose the loading determined in (4-5) and (2-13). At this stage, the stress intensity factor remains unknown.

- The boundary $\partial\Omega_{//}$ is a stress-free boundary; then $\boldsymbol{\sigma} \cdot n = 0$, where n is a normal vector to the material domain.

- The boundary $\partial\Omega_{\text{tip}}$ is used to close the meshed domain but has no physical meaning. The meshed domain is quite different than the material domain. The material boundary is represented by a curve Γ. In order to determine its position, a level set is used.
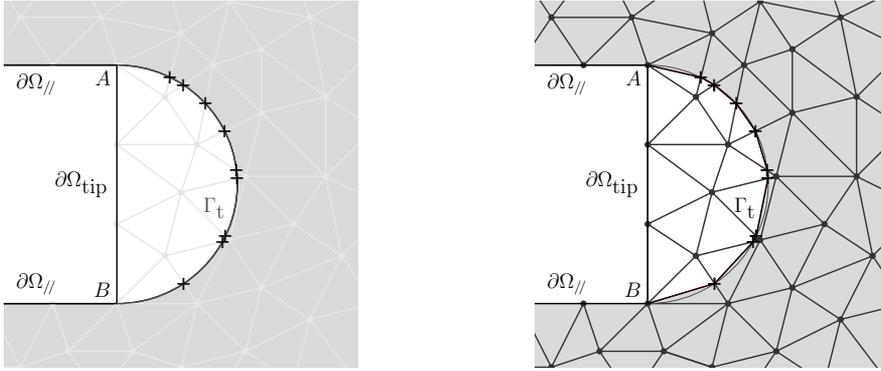
Figure 2. Material domain (gray) and damaged zone (white) are separated by the iso-zero of a level set Γ that is discretized as Γ_t. A coarse mesh is used here for a better understanding.

The level set Φ is chosen as the signed distance to Γ: Φ is positive in the material domain and negative outside. The level-set iso-zero ($\Phi(x, t) = 0$) is the equation of Γ. Numerically, the level-set iso-zero matches Γ on the edges of the elements and approximates Γ inside the elements (see Figure 2) by Γ_t. Some elements are then cut by the material boundary, and the method "XFEM" is used to integrate only on the material domain [Moës et al. 1999; Daux et al. 2000].

It is important to note that the material domain will never contain $\partial\Omega_{\text{tip}}$. The level-set iso-zero is forced to contain the points A and B, so the material boundary Γ is the continuation of $\partial\Omega_{//}$ even if the curves are not forced to be tangent to A or B.

Global rigid solid motion is avoided by fixing a Dirichlet null condition on an arbitrary point of the material domain. The numerical solution is obtained by two complementary iterative processes: one to determine the equilibrium and another one to optimize the position of Γ.

During the computation of the equilibrium with a given position Γ_t, the amount of shear can exceed the critical value $R > R_m$. In that case, the same power law (2-12) is used for $R > R_m$. Knowing this state, an optimization process is then proposed to update the position of Γ_t with respect to the critical value R_m.

The shape optimization algorithm works as presented in Algorithm 1. To solve the mechanical non-linear problem, for a given Γ_t, an iterative algorithm is used (see Algorithm 2).

Shape optimization, convergence criterion, geometry evolution, and stress intensity factor updates are described in next subsections.

Initial shape Γ_o, solve
while traction-free boundary is not admissible with R_m **do**
    Compute hyperelasticity problem
    Update the level set
    Update the material domain and Γ_t
end while

Algorithm 1. Coarse description of shape optimization algorithm.

Resolution of a nonlinear elasticity problem
Determination of initial loading K and initial displacement w_o
while criterion$(\Delta K, \Delta w) >$ TOL **do**
   Compute w_n, Iter $=$ Iter $+1$,
if Iter $>$ ITERMAX **then**
      Update K
      Compute a new correction w_{n+1}, Iter $= 0$
   end if
end while

Algorithm 2. Stress intensity factor update.

5A. *Resolution of the hyperelastic boundary value problem.* Applying a classical Newton–Raphson method to the hyperelasticity problem leads to instabilities for some values of α. The tangent operator associated with the constitutive law has the form

$$\begin{cases} \tau'(R) = \mu_0 & \text{for } R < R_o, \\ \tau'(R) = \mu_0\alpha(R/R_o)^{\alpha-1} & \text{for } R > R_o. \end{cases} \tag{5-1}$$

This operator is discontinuous at $R = R_o$. For $R \geq R_o$, the value of the tangent operator can be so small that the stability of the algorithm is not ensured; the method is then relaxed by $u_{k+1} = u_k + \lambda\delta u_k$ with $\lambda \in [0, 1]$, and the tangent operator is replaced by a proportional value of it. So a line search method is used and defined as

$$\begin{cases} \tilde{\tau}'(R) = \mu_0 & \text{for } R < R_o, \\ \tilde{\tau}'(R) = \mu_0(R/R_o)^{\alpha-1} & \text{for } R > R_o. \end{cases} \tag{5-2}$$

5B. *Shape optimization.* Once the hyperelasticity problem has been solved, the boundary Γ_t must be updated according to the condition $R = R_m$.

The evolution of Γ_t corresponds to updating the level-set iso-zero. The equation $\Phi(\boldsymbol{x}, t) = 0$ is the equation of a moving surface whose evolution is governed by its normal velocity a. The normal vector to Γ_t is given by $\nabla\Phi/\|\nabla\Phi\|$.

The velocity a is determined with respect to the condition $R = R_m$.

Firstly, strain field R is smoothed by solving a minimization problem whose variational formulation is,

$$\text{for all } \tilde{R}^*, \quad \int_\Omega \tilde{R}\tilde{R}^* \, d\Omega = \int_\Omega R(w)\tilde{R}^* \, d\Omega, \tag{5-3}$$

where $\tilde{R}$ and $\tilde{R}^*$ are continuous and w is the displacement field solution of the hyperelasticity problem.

Then the normal velocity $a = -k(\tilde{R} - R_{\text{ref}})/R_m$ is computed, $k > 0$. This velocity is smoothed over Γ_t by solving a diffusion problem in order to avoid instabilities in its evolution:

$$\text{for all } a^*, \quad \int_{\Gamma_t} \tilde{a}a^* \, d\Gamma + \nu \int_{\Gamma_t} \nabla\tilde{a}\nabla a^* \, d\Gamma = \int_{\Gamma_t} aa^* \, d\Gamma, \tag{5-4}$$

where $\tilde{a}$ is the smoothed velocity field.

Shape optimization will be stopped when $\|a\|_\infty < a_{\text{tol}}$, where a_{tol} is about $\frac{1}{1000}$ of the geometry characteristic length.

5C. *Geometry evolution and the updating of the level set.* As Γ_t is updated by the normal velocity a determined previously, the level set has to be updated over the whole meshed domain. Two conditions must be satisfied. The updated level set must still be a signed distance function, and its iso-zero has to be located at a distance $\tilde{a}(s)$ of Γ_t, where s is a curvilinear abscissa of Γ_t. According to the definition of the normal velocity, the new position of Γ is then $\Gamma_{t+dt} = \Gamma_t + \tilde{a}(s)\boldsymbol{n}\,dt$ with $\boldsymbol{n}$ the normal vector to Γ_t.

Let Φ be the level set and φ the shift for which we are looking. The solution must satisfy

$$\begin{cases} \|\nabla\Phi + \nabla\varphi\| = 1 & \text{in } \Omega, \\ \varphi = \tilde{a} & \text{on } \Gamma. \end{cases} \tag{5-5}$$

Moreover, Φ verifies $\|\nabla\Phi\| = 1$ and the system is equivalent to

$$\begin{cases} \Phi \cdot \varphi = 0 & \text{in } \Omega, \\ \varphi = \tilde{a} & \text{on } \Gamma_t. \end{cases} \tag{5-6}$$

This problem can be solved as an anisotropic diffusion problem:

$$\text{for all } \varphi^*, \quad \int_{\Gamma_t} \widetilde{\varphi}\varphi^*\,d\Gamma + \mu\int_{\Omega\cup\overline{\Omega}}(\nabla\varphi\nabla\Phi)(\nabla\varphi^*\nabla\Phi)\,d\Omega = \int_{\Gamma_t}\tilde{a}\varphi^*\,d\Gamma, \tag{5-7}$$

where $\overline{\Omega}$ is the whole domain that contains the nonmaterial domain.

When φ is known, the level set Φ can be updated.

5D. *The stress intensity factor update.* The thickness H is fixed; to satisfy the condition $R = R_m$ over Γ_t, the stress intensity factor K must be updated during the iterative process of the hyperelastic problem resolution.

To have a good approximation of the stress intensity factor, three methods have been considered here. The most expensive one is to smooth the strain field over the whole material domain Ω as in (5-3) and to take its value at the points $\Gamma_t \cup \partial\Omega_{/\!/}$. It is assumed that, at these points, R must be equal to R_m. The other methods consist of smoothing the strain field only over the free boundary Γ by solving a diffusion equation,

$$\text{for all } \tilde{R}^*, \quad \int_{\Gamma}(\tilde{R}\tilde{R}^* + L^2\nabla\tilde{R}\nabla\tilde{R}^*)\,d\Gamma = \int_{\Gamma}R(w)\tilde{R}^*\,d\Gamma, \tag{5-8}$$

where L^2 is the virtual diffusion coefficient. Then the mean value or the maximum one of the smoothed field is taken as a reference. The last option has been used to obtain the results presented here.

Stress intensity factor updates are expensive. They are not performed at each iteration of the nonlinear solver. However, a double convergence criterion is used: both displacement field and stress intensity factor tolerances have to be respected.

6. Some numerical results

Some tests are presented in order to estimate the performance of the method. The analytical solution of Section 4 is used to estimate the numerical accuracy of the algorithm.
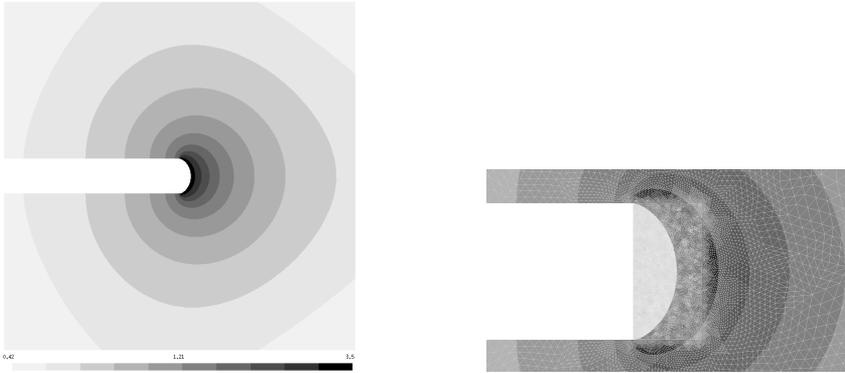
Figure 3. Smoothed strain $\tilde{R}$ (see (5-3)) at convergence: whole domain and detail over the quasicrack tip.

The algorithm has been applied to study the iso-R shapes and stress intensity factor values K for different values of ρ_m and α in the case of the power law (2-12). Finally, a bilinear brittle material is also studied.

6A. *Power law behavior with $\alpha > 0$.*

The shape of the traction-free boundary Γ_t. The criterion used to characterize the solution quality is the root mean square of the distance of each node of the boundary mesh to the analytical solution. This quantity is a length and represents the gap between the approximated and the analytical solutions. This value is compared to a characteristic length of the problem: the quasicrack thickness H.

Assume that the initial chosen shape is a semicircle. The initial gap is then 25% of characteristic length. At convergence, obtained after 88 iterations, the gap is reduced to 0.098%.

It is important to note that a precision of 0.002% is obtained at the first iteration when the computation is initialized with the analytical geometry.

Stress intensity factor. Analytical and numerical stress intensity factors K/R_o have been compared for different (R_m, α); the discrepancy is less than 1.2%. This shows that the thickness is very well evaluated.

The iso-R shape. The iso-R_o and iso-R_m are plotted at convergence in Figure 6. The relative gap is 0.005% for the curve R_m and 0.27% for the curve R_o.

The shape of the cycloids is well recovered.
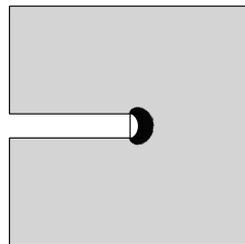
Figure 4. Elastic domain (gray) and hyperelastic one (black).
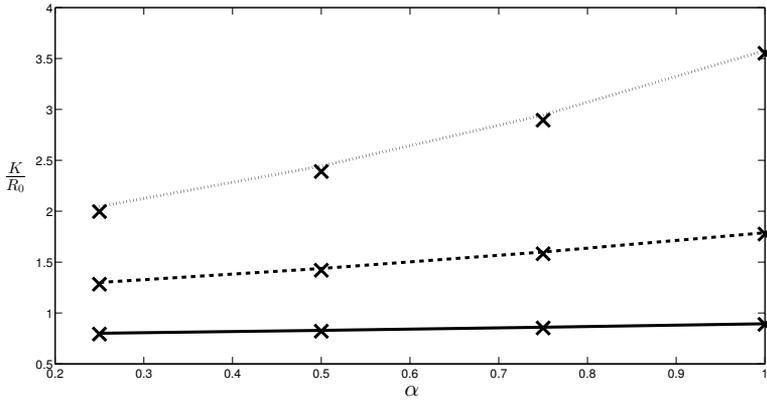
Figure 5. K/R_0 results for analytical and numerical calculations ($\times$) for the power law.

6B. *The bilinear constitutive law.* We consider now a bilinear constitutive law:

$$\begin{cases} R \leq R_o, & \tau = \mu_o R, \\ R_o \leq R \leq R_m, & \tau = \tau_o + ((\tau_m - \tau_o)/(R_m - R_o))(R - R_o), \\ R_m \leq R, & \tau = 0. \end{cases} \tag{6-1}$$

We note $\alpha = \tau_m/\tau_o$.

In Figure 7, the stress intensity factor K/R_o is plotted analytically using the equation connecting the J-integral and the thickness of the damaged zone:

$$J = \frac{K^2}{2\mu_o} = HE(R_m),$$

$$E(R_m) = \tfrac{1}{2}\tau_o R_o + \tau_o(R_m - R_o) + \tfrac{1}{2}(\tau_m - \tau_o)(R_m - R_o).$$

The numerical results are close to the analytical ones.

7. Conclusion

We have determined the shape of the damaged zone under antiplane shear conditions for hyperelastic brittle material. The analytical results are a generalization of preceding results obtained by Bui for brittle material. The thickness of the damaged zone is determined by the critical strain energy at rupture and the loading.

	$\rho_m = 2$		$\rho_m = 4$		$\rho_m = 8$	
α	analytical	numerical	analytical	numerical	analytical	numerical
0.25	0.8007	0.7931	1.3001	1.2825	2.0458	1.9964
0.50	0.8292	0.8216	1.4376	1.4199	2.4428	2.3896
0.75	0.8604	0.8528	1.5992	1.5821	2.9444	2.8941
1.00	0.8944	0.8878	1.7889	1.7756	3.5777	3.5513

Table 1. Analytical and numerical results, power law behavior.
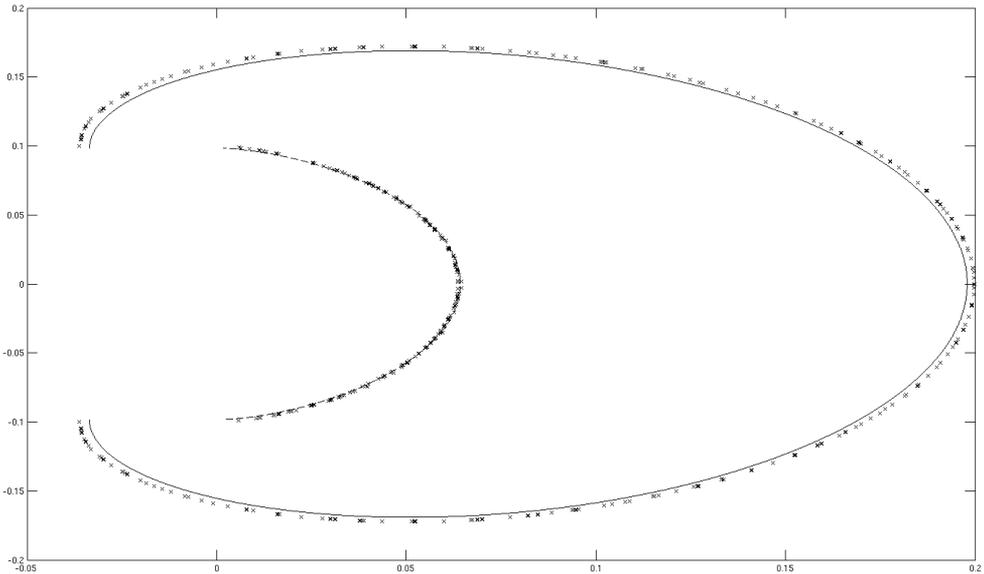
Figure 6. Comparison of the analytical (dashed line for R_o and solid for R_m) and numerical shapes ($\times$).

The case of power law stress-strain curve is discussed; it is used to evaluate the ability of a numerical optimization process applied to determine the damaged zone. An iterative scheme is proposed first to determine an equilibrium state and secondly to optimize the position of the boundary of the damage zone. The numerical results are close to the analytical results. The same algorithm is used for other constitutive laws.

The approach must be extended to other cases of loading especially mode I and more general local behavior.
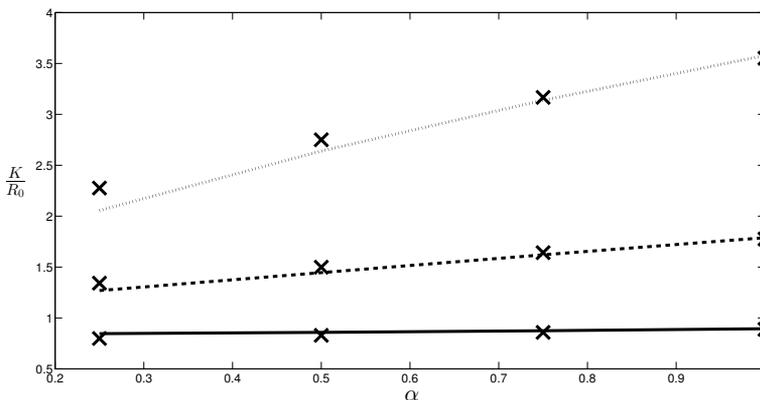
Figure 7. K/R_0 results for analytical and numerical calculations for bilinear behavior.

α	$\rho_m = 2$		$\rho_m = 4$		$\rho_m = 8$	
	analytical	numerical	analytical	numerical	analytical	numerical
0.25	0.8462	0.7986	1.2692	1.3420	2.0556	2.2759
0.50	0.8585	0.8291	1.4454	1.4986	2.6398	2.7504
0.75	0.8747	0.8584	1.6202	1.6413	3.1381	3.1667
1.00	0.8944	0.8878	1.7889	1.7756	3.5777	3.5513

Table 2. Analytical and numerical comparison, bilinear material.

The proposed method based on level-set and XFEM modelization should be extended also to the damage transition to rupture modeled by thick level set [Moës et al. 2011], where the damage d evolves from 0 to 1 in a layer of finite thickness l_c. Two particular level-set values must be introduced: one $\Phi(\mathbf{x}, t) = 0$ to described the boundary where $d = 0^+$, the other $\Phi(\mathbf{x}, t) = l_c$ where $d = 1$. The case presented here is $l_c = 0$. For $l_c \neq 0$, this type of approach addresses the existence or not of a quasicrack for constitutive behavior with smooth transition between damage to rupture.

References

[Bui 1980] H. D. Bui, "Solution explicite d'un problème de frontière libre en élastoplasticité avec endommagement", *C. R. Acad. Sci. Paris B Sci. Phys.* **290** (1980), 345–348.

[Bui and Ehrlacher 1980] H. D. Bui and A. Ehrlacher, "Propagation dynamique d'une zone endommagée dans un solide élastique-fragile en mode III et en régime permanent", *C. R. Acad. Sci. Paris B Sci. Phys.* **290** (1980), 273–276.

[Daux et al. 2000] C. Daux, N. Moës, J. Dolbow, N. Sukumar, and T. Belytschko, "Arbitrary branched and intersecting cracks with the extended finite element method", *Int. J. Numer. Methods Eng.* **48**:12 (2000), 1741–1760.

[Knowles and Sternberg 1972] J. K. Knowles and E. Sternberg, "On a class of conservation laws in linearized and finite elastostatics", *Arch. Ration. Mech. Anal.* **44**:3 (1972), 187–211.

[Knowles and Sternberg 1980] J. K. Knowles and E. Sternberg, "Discontinuous deformation gradients near the tip of a crack in finite anti-plane shear: an example", *J. Elasticity* **10**:1 (1980), 81–110.

[Knowles and Sternberg 1981] J. K. Knowles and E. Sternberg, "Antiplane shear fields with discontinuous deformation gradients near the tip of a crack in finite elastostatics", *J. Elasticity* **11**:2 (1981), 129–164.

[Moës et al. 1999] N. Moës, J. Dolbow, and T. Belytschko, "A finite element method for crack growth without remeshing", *Int. J. Numer. Methods Eng.* **46**:1 (1999), 131–150.

[Moës et al. 2011] N. Moës, C. Stolz, P.-E. Bernard, and N. Chevaugeon, "A level set based model for damage growth: the thick level set approach", *Int. J. Numer. Methods Eng.* **86**:3 (2011), 358–380.

[Neuber 1968] H. Neuber, "A physically nonlinear notch and crack model", *J. Mech. Phys. Solids* **16**:4 (1968), 289–294.

[Stolz 2010] C. Stolz, "Closed form solution for the finite anti-plane shear field for a class of incompressible brittle solids", *C. R. Mécanique* **338**:12 (2010), 663–669.

CLAUDE STOLZ: claude.stolz@ec-nantes.fr
Génie civil et Mécanique, UMR CNRS 6183, 1 rue de la Noë, 44321 Nantes, France

and

IMSIA EDF UMR CNRS 9219, 1 avenue Charles de Gaulle, 92141 Clamart, France

ANDRES PARRILLA GOMEZ: andres.parrilla-gomez@ec-nantes.fr
Génie civil et Mécanique, UMR CNRS 6183, 1 rue de la Noë, 44321 Nantes, France

msp

SOME APPLICATIONS OF OPTIMAL CONTROL
TO INVERSE PROBLEMS IN ELASTOPLASTICITY

CLAUDE STOLZ

The aim of this paper is to present the applications of the optimal control theory to solve several inverse problems for elastoplastic materials and structures. The optimal control theory permits to determine the internal state of a body from the knowledge both of the initial and the final, residual, geometry resulting from an unknown loading history.

1. Introduction

This article presents the applications of the optimal control theory to solve several inverse problems in non-linear mechanics, more precisely elastoplastic materials. Two decades ago Prof. H. D. Bui presented, in his book on inverse problems, some solution examples for the Cauchy problem based on control theory. This work is an extension of the ideas presented in that work [Bui 1993] for the case of structures with an elastoviscoplastic material behavior.

We shall start with the assumption of known constitutive equations and will only address the question of the determination of the internal state of the body resulting from an unknown loading history. In order to complement the missing loading data, we shall further suppose that both the initial and the final shape of the body are known. This problem setting has several applications ranging from the identification of causes of accidents to optimization of industrial processes and different solution methods have been proposed; see for example [Ballard and Constantinescu 1994; Constantinescu and Tardieu 2001; Gao and Mura 1989]. The solution proposed next is based on the optimal control theory, through the minimization of a suitably chosen functional cost among a class of admissible loading histories, as briefly discussed in [Stolz 2008]. It presents the additional advantage of proposing simultaneously an internal state and a possible loading history.

The paper starts with the introduction of the solution method based on optimal control theory to inverse problems in linear elasticity. Next a generalisation is presented for elastoplasticty and viscoplasticity. The final complexity is reached for elastoplastic problems under cyclic loading, where the optimal control method proved to be a powerfull tool to determine the limit cycle in elastoplasticity [Peigney and Stolz 2001; 2003] or the wear and the consequent the loss of material [Peigney 2004]. The approach is illustrated by a series of solutions of example problems.

2. Inverse problems in linear elasticity

2A. *Setting of the problem.* Let us consider a material body occupying in the reference configuration the volume Ω. The boundary of the body, denoted by $\partial\Omega$, is partitioned in two complementary parts Γ_o

Keywords: elastoplasticity, inverse problem, adjoint problem, optimal control.
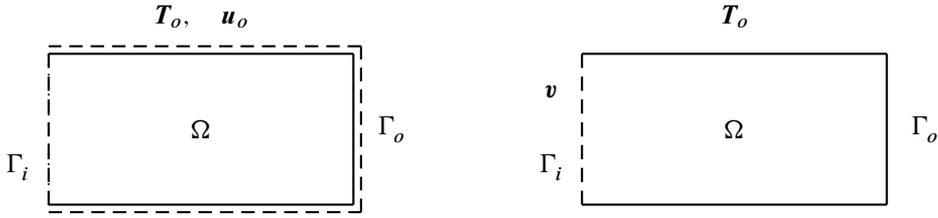
Figure 1. Left: a non-well posed problem: T_o and u_o are applied on Γ_o. Right: the well-posed problem: v on Γ_i (dashed) and T_o on Γ_o are prescribed.

and Γ_i, (see Figure 1). On the Γ_o part, both the displacement field u_o and the surface traction field T_o are known.

The inverse problem, considered next is the determination of both the displacement on the boundary part Γ_i and the complete displacement field u over Ω.

The unknown complete displacement field u should satisfy the following systems of partial differential equations and boundary conditions:

$$
\begin{array}{lll}
\textit{Compatibility}: & \boldsymbol{\varepsilon}(\boldsymbol{u}) = \tfrac{1}{2}(\nabla \boldsymbol{u} + \nabla^t \boldsymbol{u}), & \text{over } \Omega, \\
\textit{Constitutive law}: & \boldsymbol{\sigma} = \mathbb{C} : \boldsymbol{\varepsilon}(\boldsymbol{u}), & \text{over } \Omega, \\
\textit{Equilibrium}: & \operatorname{div} \boldsymbol{\sigma} = 0, & \text{over } \Omega, \\
\textit{Boundary conditions } \mathrm{BCu}: & \boldsymbol{u} = \boldsymbol{u}_o, & \text{on } \Gamma_o, \\
\textit{Boundary conditions } \mathrm{BCT}: & \boldsymbol{n}.\boldsymbol{\sigma} = \boldsymbol{T}_o, & \text{on } \Gamma_o.
\end{array}
$$

This problem is not well posed in the Hadamard sense [Lions 1968], in the sense that existence and uniqueness of the solution is generally not insured and that small errors in the input data will conducts to large errors in the output data, the displacement field u. Several solution methods have been dedicated to this problem setting: direct integration of Cauchy problem [Bui 1993; Bourgeois 1998], the quasi-reversibility method [Lions 1968; Bourgeois 1998], etc.

The solution proposed here is focused on the application of optimal control theory. An example of application is the steady-state heat conduction problem, where optimal control theory has been used to determine the history of heat sources [Delattre et al. 2002].

2B. *A well posed problem.* The ill posed character of the initial problem setting can be corrected, by relaxing the overdetermined data on Γ_o boundary and proposing data for Γ_i. For the overall probelm setting, this means changing the boundary conditions (BCu) with the conditions (BCi) applied on the complementary boundary Γ_i:

$$\mathrm{BCi}: \quad \boldsymbol{u} = \boldsymbol{v}, \quad \text{on } \Gamma_i. \tag{2-1}$$

As a consequence, boundary condition are complete, defined on complementary parts and the corrected problem is know well posed. One can recognize, the form of a classical problem in small strain linear elasticity.

For the optimal control problem setting we shall denote this problem as the primal problem. Moreover, its solution $\boldsymbol{u}_{\mathrm{sol}}(\boldsymbol{v}, \boldsymbol{T}_o)$ is then a linear function of the prescribed values on the surface tractions and displacements boundaries: $\boldsymbol{T}_o$ on Γ_o and $\boldsymbol{v}$ on Γ_i.

2C. *The idea of control.* The prescribed displacement $\boldsymbol{v}$ on the complementary boundary Γ_i, introduced before (2-1), will now play the role of a control variable which is optimized in order to satisfy the following condition: the solution of the primal problem $\boldsymbol{u}_{\text{sol}}(\boldsymbol{v}, \boldsymbol{T}_o)$ must match to the displacement field $\boldsymbol{u}_o$ on the boundary Γ_o. From a mathematical point of view, the optimal displacement $\boldsymbol{v}$ realizes the minimum of the functional J defined as

$$J(\boldsymbol{v}) = \int_{\Gamma_o} \tfrac{1}{2} \|\boldsymbol{u}(\boldsymbol{v}, \boldsymbol{T}_o) - \boldsymbol{u}_o\|^2 \, \mathrm{d}s + r \int_{\Gamma_i} \tfrac{1}{2} \|\boldsymbol{v}\|^2 \, \mathrm{d}s. \tag{2-2}$$

2D. *The optimization method.* A series of operations, adding the variational form of the primal problem to the functional J and using the boundary conditions, transforms the problem in a new optimization problem. The solution $\boldsymbol{u}$ of the inverse problem realizes an optimal point for the functional $\mathcal{J}$:

$$\mathcal{J}(\boldsymbol{u}, \boldsymbol{u}^*) = - \int_{\Omega} \boldsymbol{\varepsilon}(\boldsymbol{u}) : \mathbb{C} : \boldsymbol{\varepsilon}(\boldsymbol{u}^*) \, \mathrm{d}\Omega + \int_{\Gamma_o} \boldsymbol{u}^*.\boldsymbol{T}_o \, \mathrm{d}s + h \int_{\Gamma_o} \tfrac{1}{2} \|\boldsymbol{u} - \boldsymbol{u}_o\|^2 \, \mathrm{d}s + r \int_{\Gamma_i} \tfrac{1}{2} \|\boldsymbol{u}\|^2 \, \mathrm{d}s,$$

among the set of kinematically admissible fields $\boldsymbol{u}^*$ such that $\boldsymbol{u}^* = 0$ over Γ_i.

Outline of proof. The optimal point of the functional is characterized by the canceling of its first order variations. The variations of $\mathcal{J}$ are defined by

$$\delta\mathcal{J} = - \int_{\Omega} \Big(\boldsymbol{\sigma} : \boldsymbol{\varepsilon}(\delta\boldsymbol{u}^*) + \boldsymbol{\sigma}^* : \boldsymbol{\varepsilon}(\delta\boldsymbol{u})\Big) \, \mathrm{d}\Omega + \int_{\Gamma_o} \delta\boldsymbol{u}^*.\boldsymbol{T}_o \, \mathrm{d}s$$

$$+ h \int_{\Gamma_o} (\boldsymbol{u} - \boldsymbol{u}_o).\delta\boldsymbol{u} \, \mathrm{d}s + r \int_{\Gamma_i} \boldsymbol{u}.\delta\boldsymbol{u} \, \mathrm{d}s = \frac{\partial\mathcal{J}}{\partial\boldsymbol{u}^*}.\delta\boldsymbol{u}^* + \frac{\partial\mathcal{J}}{\partial\boldsymbol{u}}.\delta\boldsymbol{u}.$$

where we have set $\boldsymbol{\sigma} = \mathbb{C} : \boldsymbol{\varepsilon}(\boldsymbol{u})$ and $\boldsymbol{\sigma}^* = \mathbb{C} : \boldsymbol{\varepsilon}(\boldsymbol{u}^*)$, and $\delta\boldsymbol{u}$ and $\delta\boldsymbol{u}^*$ are free kinematically admissible with 0 virtual displacements field.

The optimization of the functional $\mathcal{J}$ leads to two sets of equations, representing respectively the primal and the adjoint problem.

The condition $\partial\mathcal{J}/\partial\boldsymbol{u}^* = 0$ corresponds to the equations of the already defined primal problem:

$$\operatorname{div}\boldsymbol{\sigma} = 0, \qquad \boldsymbol{\sigma} = \mathbb{C} : \boldsymbol{\varepsilon}(\boldsymbol{u}) \quad \text{over } \Omega, \qquad \boldsymbol{\sigma}.\boldsymbol{n} = \boldsymbol{T}_o \quad \text{on } \Gamma_o. \tag{2-3}$$

The variations $\partial\mathcal{J}/\partial\boldsymbol{u} = 0$ corresponds to the equations of the so-called adjoint problem (2-4). This set is satisfied by the adjoint displacement field $\boldsymbol{u}^*$ and the condition of optimality (2-5):

$$0 = \operatorname{div}\boldsymbol{\sigma}^* \quad \text{over } \Omega, \qquad \boldsymbol{\sigma}^*.\boldsymbol{n} = h(\boldsymbol{u} - \boldsymbol{u}_0) \quad \text{on } \Gamma_o, \qquad \boldsymbol{u}^* = 0 \quad \text{on } \Gamma_i, \tag{2-4}$$

$$r\boldsymbol{u} = \boldsymbol{n}.\boldsymbol{\sigma}^* \quad \text{on } \Gamma_i. \tag{2-5}$$

One can further remark that the adjoint problem has the same structure as the primal problem, i.e. linear elasticity and small strain. However, the physical dimensions of the fields depend on the choice of the cost functional. This is a direct mathematical consequence of the fact that linearized elasticity is a self-adjoint problem.

In the next section, we now extend this method for solving inverse problems in the case of viscoplastic and elastoplastic materials.

3. Examples of inverse problem in elastoplasticity

Consider a body Ω with a known local material behaviour. Starting from the initial known shape of the body and an unknown loading history, the body occupies a different residual shape. The inverse problem studied next should estimate both the internal state governed by the plastic strain and a loading history compatible with the measured residual geometry.

The solution method of this inverse problem in elastoplasticity rests on several general assumptions:

- The loading history is given by the surface tractions: $\boldsymbol{T}(x, t_f) = \boldsymbol{T}_o, t \in (0, t_f)$ on Γ_o belonging to a class of possible loading histories.
- The elastoplastic evolution problem is solved and consequently the plastic strain $\boldsymbol{\varepsilon}_p(x, t)$ is an direct output of this evolution problem.
- The optimal loading history $\boldsymbol{T}^{\mathrm{op}}$ is chosen among the given class of admissible loading histories, such that the final shape, defined by the displacement field corresponding to the final time step, i.e. $\boldsymbol{u}(x, t_f)$ matches the measured residual displacement $\boldsymbol{u}_o$. This condition is expressed by the minimum of the cost functional J defined by

$$J(\boldsymbol{T}, \boldsymbol{\varepsilon}_p, t_f) = \int_{\Gamma_o} \frac{r}{2} \|\boldsymbol{u}(t_f) - \boldsymbol{u}_o\|^2 \, \mathrm{ds}, \tag{3-1}$$

which measures the mismatch between the two displacement fields.

These assumptions will permit to estimate the loading history and the internal state from the given data $\boldsymbol{u}_o, \boldsymbol{T}_o$. The natural control variables introduced in this problem are the histories of the surface traction $\boldsymbol{T}(x, t)$ and the plastic strain field $\boldsymbol{\varepsilon}_p(x, t)$.

To illustrate the solution of the elastoplastic inverse problem using the proposed method, let us consider the following examples: (i) a three-bar lattice under traction, (ii) the bending of a beam in plane strain and (iii) a hollow sphere under pressure.

In a first step, on these examples a particular solution of the direct problem is obtained in order to define a final residual shape. In the second step, starting from this final shape as given data, the optimal control theory provides the solution of the inverse elastoplastic problem.

3A. *A three-bar lattice under traction.* Let us consider the problem of an elastoplastic lattice, consisting of three bars of lengths $L_1 = L$, $L_2 = L_3 = L\sqrt{2}$, as depicted in Figure 2. The displacement of the point O is denoted by $\boldsymbol{u} = v\boldsymbol{e}_1 + h\boldsymbol{e}_2$.
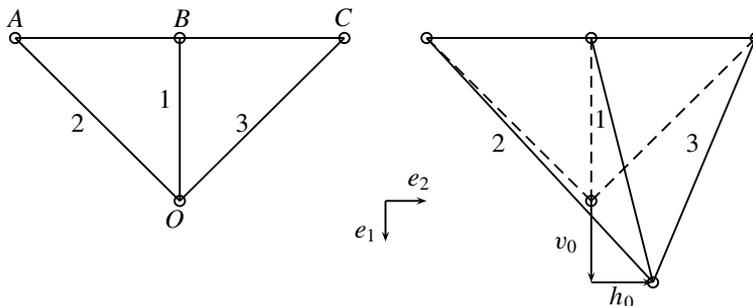
Figure 2. Three elastoplastic bars: initial (left) and residual configuration (right).
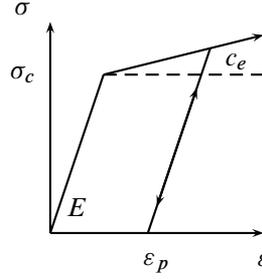
Figure 3. The constitutive law.

In the initial state the bars are stress free. After an unknown loading and unloading history, the lattice is in a final configuration, exhibiting a residual global displacement $\boldsymbol{u}_o = (v_o, h_o)$. This final shape is depending on the internal plastic strains δ_p^i.

Let us assume that the material behaves as an elastoplastic medium with linear hardening law as depicted in Figure 3. The material parameters of the model are: E is the Young's modulus, S is the section of the bar the hardening modulus c_o. One defines $c_e = E c_o/(E + c_o)$.

Under an external loading, characterized by the force (V, H) applied in O with an increasing and decreasing amplitude the bars recover the static equilibrium in the absence of external forces and the final position of the point O is now (v_o, h_o). Let us assume that the distribution of plastic stretches is $(\delta_i^p, \ i = 1, 3)$ in the bars.

The equilibrium state of the system in terms of displacement, stretches and normal tractions must satisfy the set of equations:

- *Compatibility:*

$$\delta_1 = v, \quad \delta_2 = \frac{v + h}{\sqrt{2}}, \quad \delta_3 = \frac{v - h}{\sqrt{2}}. \tag{3-2}$$

- *Constitutive behaviour:*

$$\delta_1 = K N_1 + \delta_1^p, \quad \delta_2 = K \sqrt{2} N_2 + \delta_2^p, \quad \delta_3 = K \sqrt{2} N_3 + \delta_3^p. \tag{3-3}$$

- *Equilibrium:*

$$V = N_1 + \frac{N_2 + N_3}{\sqrt{2}}, \quad H = \frac{N_2 - N_3}{\sqrt{2}}. \tag{3-4}$$

- *Domain of reversibility:*

$$|N_i - c_i \delta_i^p| \le N_c. \tag{3-5}$$

Here $c_1 = S \dfrac{c_o}{L} = c$, $c_2 = c_3 = \dfrac{c}{\sqrt{2}}$ and $K = \dfrac{L}{ES}$, $N_i = S\sigma_i$, $\varepsilon_i L_i = \delta_i$, $\varepsilon_i^p L_i = \delta_i^p$.

3A1. *The direct problem.* For a given loading history $(V(t), H(t), t \in [0, t_f])$, one can compute the evolution of the system taking into account the elastoplastic constitutive law. The stresses N_i, $i = 1, 3$, lie in the convex set of reversibility, (3-5). The evolution of the plastic stretches is governed by the normality rule described as

$$|N_i - c_i \delta_i^p| \le N_c, \quad \lambda_i \ge 0, \quad \dot{\delta}_i^p = \lambda_i \frac{N_i - c_i \delta_i^p}{N_c} = \lambda_i n_i, \quad \lambda_i(|N_i - c_i \delta_i^p| - N_c) = 0. \tag{3-6}$$

In the initial configuration there is no external loads and no prestresses, therefore the lattice is considered stress free. As a consequence, the plastic stretches are identically to zero until one of the normal traction N_i reaches the critical yield value $\pm N_c$. The initial domain of reversibility, corresponding to the initial elastic domain of the lattice, in terms of external loads (V, H) is obtained by solving the system consisting of (3-2), (3-3), (3-4) with vanishing plastic stretches $\delta_i^p = 0$ and the imposing the inequations $|N_i| - N_c \leq 0$:

$$|N_1| = \left| \frac{2V}{2 + \sqrt{2}} \right| \leq N_c, \quad |N_2| = \left| \frac{V}{2 + \sqrt{2}} + \frac{H}{\sqrt{2}} \right| \leq N_c, \quad |N_3| = \left| \frac{V}{2 + \sqrt{2}} - \frac{H}{\sqrt{2}} \right| \leq N_c.$$

If the applied load (V, H) leaves the reversibility domain, plasticity occurs. In this case, after a loading-unloading cycle a distribution of plastic stretches δ_i^p is obtained in the bars of the lattice. Therefore, when the applied stresses (V, H) return to $(0, 0)$, the lattice will not be stress free and will exhibit a residual shape (v^p, h^p). Let us denote, the residual stresses, i.e. tractions in the bars, N_i^r.

For the application of an external load, starting from this state, a new equilibrium of tractions in each bar N_i is obtained satisfying the equalities

$$N_1 = \frac{2V}{2 + \sqrt{2}} + N_1^r, \quad N_2 = \frac{V}{2 + \sqrt{2}} + \frac{H}{\sqrt{2}} + N_2^r, \quad N_3 = \frac{V}{2 + \sqrt{2}} - \frac{H}{\sqrt{2}} + N_3^r. \tag{3-7}$$

Again this state has to be compatible with the actual domain of reversibility, which takes into account the existence of residual stresses: $|N_i - c_i \delta_i^p| - N_c \leq 0$.

At the final unloaded state, when the external loads are $(H, V) = (0, 0)$, the global displacement is (v^p, h^p) and the local stretches $\delta_i = \delta_i^{ir}$ of the final residual configuration satisfy the equations (3-2), (3-3), (3-4). Let us now remark, that the internal residual stresses N_i^r depend only of the incompatibility of the plastic stretches $\delta_{\text{in}} = \sqrt{2}\delta_1^p - \delta_2^p - \delta_3^p$ and

$$N_1^r = -\frac{\delta_{\text{in}}}{K(2 + \sqrt{2})}, \quad N_2^r \sqrt{2} = N_3^r \sqrt{2} = \frac{\delta_{\text{in}}}{K(2 + \sqrt{2})}. \tag{3-8}$$

Moreover, the residual shape satisfies

$$v^p = \frac{2}{2 + \sqrt{2}}(\delta_1^p + \tfrac{1}{2}(\delta_2^p + \delta_3^p)), \quad h^p \sqrt{2} = \delta_2^p - \delta_3^p. \tag{3-9}$$

3A2. *The solution for a loading history with $H = 0$.* Consider a loading-unloading process with $H = 0$. In this case, $N_2 = N_3$ and $h = 0$. The phase of increasing V will be decomposed in three steps as a function of the maximum value of V_m.

- *Elastic step.* For increasing V, the first part of the loading corresponds to a linear elastic response of the lattice

$$v = K N_1 = 2K N_2, \quad N_1 + \sqrt{2}N_2 = V. \tag{3-10}$$

This occurs under the condition $V_m \leq V_1$:

$$v = \frac{K\sqrt{2}}{1 + \sqrt{2}}V, \quad V \leq V_1 \frac{1 + \sqrt{2}}{\sqrt{2}}N_c. \tag{3-11}$$

- *Plasticity of bar 1.* In the case when $V_m \geq V_1$, bar 1 is deformed plastically, starting with the assumption $\delta_2^p = \delta_3^p = 0$, one obtains

$$N_1 = N_c + c\delta_1^p, \quad KN_1 = v - \delta_1^p, \tag{3-12}$$

then

$$\delta_1^p = \frac{v - KN_c}{1 + Kc}, \quad V = \frac{N_c}{1 + Kc} + \left(\frac{c}{1 + Kc} + \frac{1}{K\sqrt{2}}\right)v. \tag{3-13}$$

Let us consider a state δ_1^p, and a variation of the external loading $\dot{V} > 0$, then $\dot{\delta}_1^p \geq 0$ and the solution satisfies the normality rule. This solution is valid if and only if $|N_2| - N_c \leq 0$. The inequality implies that $V_m \leq V_2$ where V_2 is given by

$$V_2 = (1 + \sqrt{2})N_c + \frac{Kc}{1 + Kc}N_c. \tag{3-14}$$

- *Plasticity of the whole system.* When $V_m > V_2$ the three bars are deformed plastically. The system consisting of (3-2), (3-4), (3-3) is rewritten with $h = 0$, $\delta_2^p = \delta_3^p$, and the condition of plasticity:

$$N_1 = N_c + c\delta_1^p, \quad N_2 = N_c + \frac{c}{\sqrt{2}}\delta_2^p. \tag{3-15}$$

Using (3-3) and (3-4), we have

$$v = KN_c + (1 + Kc)\delta_1^p = 2KN_c + \sqrt{2}(1 + Kc)\delta_2^p, \tag{3-16}$$

$$V = N_c(1 + \sqrt{2}) + \frac{cK}{1 + Kc}N_c + \frac{c}{1 + Kc}\frac{1 + \sqrt{2}}{\sqrt{2}}(v - 2KN_c). \tag{3-17}$$

The residual displacement is obtained as

$$\frac{1 + \sqrt{2}}{\sqrt{2}}v^p = \delta_1^p + \delta_2^p. \tag{3-18}$$

3A3. *Inverse problems.* Let us assume that the residual shape is given by the displacement $\boldsymbol{u}_o = (v_o, u_o)$. We shall determine the best history of loading $(H(t), V(t), t \in [0, t_f])$ given by the problem of optimization based on the functional

$$J = \tfrac{1}{2}(v(t_f) - v_o)^2 + \tfrac{1}{2}(h(t_f) - h_o)^2 = \tfrac{1}{2}\left\|\boldsymbol{u}(\delta_p^i)(t_f) - \boldsymbol{u}_o\right\|^2, \tag{3-19}$$

According to this mathematical definition, the solution $(v(t_f), h(t_f))$ of the direct problem obtained from the optimal history is close to the measured displacement (v_o, h_o). Generally, the solution of this problem is not unique, there are several local minima and some restrictions on the history and on the plastic strain must be added to obtain a unique solution.

There are two classes of inverse problems which can be illustrated by the simple example. Class 1 consists in estimating the internal state without determining a loading history, taking as control variables the plastic stretches. Class 2 addresses the determination of a complete history of the loading and of the internal state.

<u>Class 1</u>: *Estimation of the plastic strain.* In this case, the plastic stretches are the control variables and we consider only the residual state. We seek to optimize the internal state such that the functional $J_o(\delta_i^p)$ is minimum, where J_o is

$$J_o = \tfrac{1}{2}r(v - v_o)^2 + \tfrac{1}{2}r(h - h_o)^2 = \frac{r}{2}\left\|\boldsymbol{u}(\delta_p^i) - \boldsymbol{u}_o\right\|^2. \tag{3-20}$$

In this functional, we must solve the system satisfied by the residual state only. Eliminating the equations of compatibility, we can introduce an adjoint state (h^*, v^*) to take the equilibrium into account simultaneously with the local constitutive law. Introducing the rigidities $C_1 = \dfrac{1}{K}$, $C_2 = C_3 = \dfrac{1}{K\sqrt{2}}$ of each bar and the functional $\mathcal{L}$, given by

$$\mathcal{L}(\boldsymbol{u}^*, \boldsymbol{u}, \delta_i^p) = -v^* C_1(v - \delta_1^p) - \frac{v^* + h^*}{\sqrt{2}} C_2\left(\frac{v + h}{\sqrt{2}} - \delta_2^p\right) - \frac{v^* - h^*}{\sqrt{2}} C_3\left(\frac{v - h}{\sqrt{2}} - \delta_3^p\right), \tag{3-21}$$

the equilibrium satisfies the variational formulation

$$\frac{\partial \mathcal{L}}{\partial \boldsymbol{u}^*} = 0, \quad \forall \boldsymbol{u}^* = (h^*, v^*). \tag{3-22}$$

Now the inverse problem is solved by minimization of the functional

$$\hat{J}(\boldsymbol{u}, \boldsymbol{u}^*, \delta_i^p) = J_o + \mathcal{L}. \tag{3-23}$$

In general the functional $\hat{J}$ posseses many minima and the addition of constraints is then necessary to ensure uniqueness.

For example we can minimize simultaneously a norm of the plastic stretches $D = N_c \sum_i \tfrac{1}{2} L_i(\delta_p^i)^2$, and the functional takes the form:

$$J(\delta_p^i) = \frac{r}{2}\left\|\boldsymbol{u}(\delta_p^i) - \boldsymbol{u}_r\right\|^2 - \mathcal{L} + q N_c \sum_i \tfrac{1}{2} L_i(\delta_p^i)^2.$$

Outline of proof. The variations with respect to $\boldsymbol{u}^*$ ensure the equilibrium equations

$$N_1 + \frac{1}{\sqrt{2}}(N_2 + N_3) = 0, \quad \frac{1}{\sqrt{2}}(N_2 - N_3) = 0, \tag{3-24}$$

and the constitutive law

$$N_1 = C_1(v - \delta_1^p), \quad N_2 = C_2\left(\frac{v + h}{\sqrt{2}} - \delta_2^p\right), \quad N_3 = C_3\left(\frac{v - h}{\sqrt{2}} - \delta_2^p\right). \tag{3-25}$$

Denoting the adjoint stresses by

$$N_1^* = C_1 v^*, \quad N_2^* = C_2 \frac{v^* + h^*}{\sqrt{2}}, \quad N_3^* = C_3 \frac{v^* - h^*}{\sqrt{2}}. \tag{3-26}$$

From the variations with respect to $\boldsymbol{u} = (h, v)$, we obtain the equations of the adjoint state:

$$N_1^* + \frac{1}{\sqrt{2}}(N_2^* + N_3^*) = r(v - v_o), \quad \frac{1}{\sqrt{2}}(N_2^* - N_3^*) = r(h - h_o). \tag{3-27}$$

Finally the variations with respect to δ_i^p give the conditions of optimality

$$N_i^* + q N_c L_i \delta_i^p = 0. \tag{3-28}$$

The system is complete and has a unique solution depending on the choice of r, q.

However, if the norm D is changed into the internal stored energy W in the residual tension N_i^r,

$$W = \tfrac{1}{2} L\big((N_1^r)^2 + \sqrt{2}(N_2^r)^2 + \sqrt{2}(N_3^r)^2\big), \tag{3-29}$$

this energy is convex in δ_{in} but not in δ_i^p, the resulting functional is not convex in δ_p^i and the uniqueness is not guaranteed.

Class 2: *Estimation of the loading history.*

In order to obtain information about the history of loading the direct problem of evolution must be solved for a class of loading.

For example, consider the family of radial loading given by $(H, V) = \mu(t)(H_o, V_o)$, if we assume that during the unloading step no plasticity occurs, then the loading is characterized by the maximum of μ and the direction (H_o, V_o).

From the given residual shape (v_o, h_o), we apply a loading (V, H) and assuming that the answer is purely elastic, we can define (v_m, h_m) by

$$v_m = v_o + \frac{K\sqrt{2}}{1 + \sqrt{2}} V, \quad h_m = h_o + K\sqrt{2}H. \tag{3-30}$$

For an estimation δ_i^p of the plastic stretches, the domain of reversibility is known and (V, H) must be inside this domain. We propose to find δ_i^p and (V, H) such that the displacement (v, h), satisfying the problem of equilibrium and the domain of reversibility, is close to the displacement (v_m, h_m). For that purpose we introduce the functional

$$\mathcal{J}(u, u^*, \delta_i^p, V, H) = \frac{r}{2} \|u - u_m\|^2 + \mathcal{L} + \sum_i \frac{\alpha_i L_i}{2} (|N_i - c_i \delta_i^p| - N_c)^2. \tag{3-31}$$

In this expression, the tractions N_i satisfy the constitutive law (3-3). The three constants α_i are chosen as $\alpha_i = \alpha > 0$ or $\alpha_i = 0$ depending or whether the bar i has been deformed plastically or not.

Denoting the adjoint traction by N_i^* as in (3-26), it is easy to prove that the optimality conditions on $\mathcal{J}$ with respect to u^*, that is $\dfrac{\partial \mathcal{J}}{\partial u^*} = 0$ give exactly the equations (3-4), (3-3). The conditions with respect to u: $\dfrac{\partial \mathcal{J}}{\partial u} = 0$ are equivalent to the adjoint problem (n_i being defined as in (3-6)):

$$r(v - v_m) = -\sum_{i=1}^{3} n_i \alpha_i L_i C_i (|N_i - c_i \delta_i^p| - N_c) + N_1^* + \frac{N_2^* + N_3^*}{\sqrt{2}}, \tag{3-32}$$

$$r(h - h_m) = -\sum_{i=2}^{3} n_i \alpha_i L_i C_i (|N_i - c_i \delta_i^p| - N_c) + \frac{N_2^* - N_3^*}{\sqrt{2}}. \tag{3-33}$$

The optimization with respect to δ_i^p gives

$$N_i^* - \alpha_i n_i (|N_i - c_i \delta_i^p| - N_c) \frac{1 + Kc}{K} = 0, \tag{3-34}$$

and finally the optimization with respect to the loading (V, H) defines the adjoint displacement

$$v^* = r(v - v_m) \frac{K\sqrt{2}}{1 + \sqrt{2}}, \qquad u^* = r(h - h_m)K\sqrt{2}. \tag{3-35}$$

The system is complete. For a given residual shape, we must choose the α_i a priori. For a solution of the optimization, we must verify that the inequalities (3-5) are satisfied.

3A4. *Inverse problem when $h_o = 0$.* In this case, it is natural to consider that $\delta_2^{ir} = \delta_3^{ir}$ and then $H = 0$, $N_2 = N_3$ and $\delta_2 = \delta_3$.

We consider $V \geq 0$, then $n_i = 1$. For $v_o \neq 0$, we consider first that the plasticity occured only in bar 1, then $\alpha_2 = \alpha_3 = 0$ and $\delta_2^p = \delta_3^p = 0$. Then, $N_2^* = N_3^* = 0$, this implies that $v^* = 0$ and $|N_1 - c\delta_1^p| - N_c = 0$ simultaneously with $v = v_m$. We deduce immediatly that

$$v = \frac{2K}{2 + \sqrt{2}} V + \frac{2}{2 + \sqrt{2}} \delta_1^p, \qquad \delta_1^p = \frac{2}{2 + \sqrt{2}} v_o, \tag{3-36}$$

$$V = (1 + \sqrt{2})N_c + \frac{c}{1 + Kc}(v - KN_c) + \frac{K}{\sqrt{2}} v. \tag{3-37}$$

This is the solution if the traction in the bars (2 and 3) are in the domain of reversibility ($N_2 \leq N_c$). This condition implies $v = 2KN_2 < 2KN_c$ that is equivalent to $V \leq V_2$. If this condition is not fulfilled, we consider that $\alpha_2 = \alpha_3 = \alpha$ and $u^* = 0$. The equilibrium implies that

$$V = \frac{v}{K} \frac{1 + \sqrt{2}}{\sqrt{2}} - \frac{\delta_1^p + \delta_2^p}{K}, \qquad v^p = \frac{\sqrt{2}}{1 + \sqrt{2}} (\delta_1^p + \delta_2^p). \tag{3-38}$$

Using the definition of the adjoint stresses (3-26), the optimisation with respect to δ_i^p two relations and the optimisation with respect to v we obtain

$$v^* = \alpha(N_1 - c\delta_1^p - N_c)(1 + Kc), \tag{3-39}$$

$$v^* = 2\alpha\left(N_2 - \frac{c}{\sqrt{2}} \delta_2^p - N_c\right)(1 + Kc), \tag{3-40}$$

$$r(v^p - v_o) = -\frac{1 + \sqrt{2}}{K\sqrt{2}} v^* + \frac{1 + 2\sqrt{2}}{K(1 + Kc)} v^*. \tag{3-41}$$

The optimality condition (3-35), after the elimination of v, implies that $v^* = 0$ and $v^p = v_o$. The value of V is recovered.

For the given residual state obtained from a radial loading-unloading history, we recover the maximum loading and the internal state using the optimal control theory.

3B. *Study of an elastoplastic beam in plane motion.* The beam is initially rectilinear. After an unknown vertical distribution of loading, the beam takes a residual shape due to plastic strain.
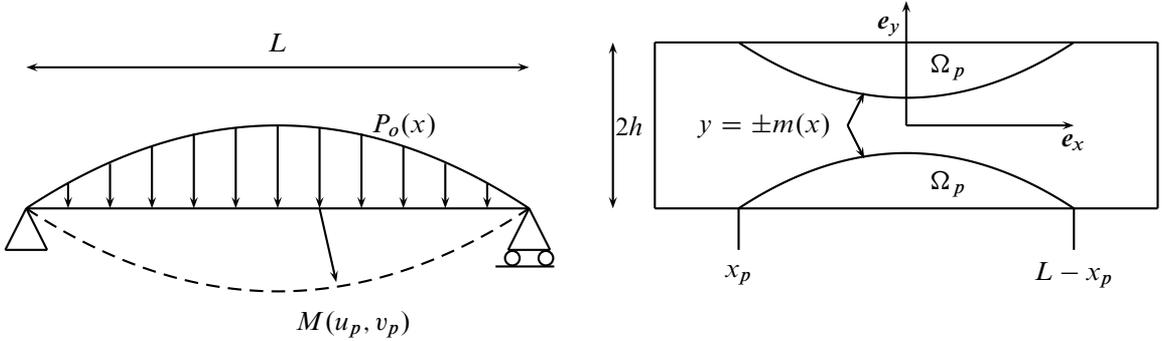
Figure 4. The initial state and final state (- -) of the beam. The geometry and the plastic zone Ω_p.

The goal of the inverse problem is to estimate a plastic strain distribution with an associated loading which is compatible with this residual shape.

The plane motion of the beam is characterized by the displacement u along e_x and a vertical displacement v in direction e_y. We consider that $u(0, t) = v(0, t) = v(L, t) = 0$. We assume that the stress and the total strain are uniaxial:

$$\boldsymbol{\sigma} = \sigma \boldsymbol{e}_x \otimes \boldsymbol{e}_x, \quad \boldsymbol{\varepsilon} = (u' + yv'')\boldsymbol{e}_x \otimes \boldsymbol{e}_x, \tag{3-42}$$

and the plastic strain is described by the function $\alpha(x, y)$:

$$\boldsymbol{\varepsilon}_p = \alpha(x, y)\boldsymbol{e}_x \otimes \boldsymbol{e}_x. \tag{3-43}$$

Then the free energy is given by

$$w(u, v, \alpha) = \tfrac{1}{2}E(u' + yv'' - \alpha)^2 + \tfrac{1}{2}H\alpha^2. \tag{3-44}$$

The thermodynamical force A associated to the plastic strain must be within the domain of reversibility

$$A = \sigma - H\alpha, \quad f(A) = \|A\| - k \le 0, \tag{3-45}$$

and the evolution of the plastic strain inside the beam is given by the normality rule.

$$\dot{\alpha} = \lambda A / \|A\|, \quad \lambda f = 0, \quad \lambda \ge 0, \quad f \le 0. \tag{3-46}$$

For a given distribution of α and a given pressure on the beam, the displacement (u, v) minimizes the potential energy of the beam

$$E(u, v, \alpha) = \int_0^L \int_{-h}^h w \, dy \, dx + \int_0^L p(x)v(x) \, dx. \tag{3-47}$$

The traction N and the moment M are defined as

$$N = ES(u' - <\alpha>), \quad M = EIv'' - ES\langle y\alpha \rangle, \tag{3-48}$$

where $S = 2h$, $I = \frac{2}{3}h^3$, $\langle f \rangle = \dfrac{1}{2h}\displaystyle\int_{-h}^{h} f\, dy$. With these notations, the equilibrium of the beam satisfies

$$N_{,x} = 0, \quad M_{,xx} + p = 0, \quad N(L) = 0, \quad M(0) = M(L) = 0. \tag{3-49}$$

Then the thermodynamical force A is

$$A = \frac{N}{S} + E\langle \alpha \rangle + y\left(\frac{M}{I} + \frac{ES}{I}\langle y\alpha \rangle\right) - (E + H)\alpha. \tag{3-50}$$

The norm of A does not exceed k.

3B1. *The direct problem for a loading-unloading process.* For a distribution of pressure $p(x) = \mu(t)P_o(x)$ with $\mu(t) = qt$ for $t \in [0, t_m]$ and $\mu(t) = q(t_m - t)$ for $t \in [t_m, 2t_m]$, we solve the direct problem.

We consider that the plastic zone Ω_p is symmetric with respect to e_x, then $\alpha(x, y, t) = \alpha(x, -y, t)$. The value of the thermodynamical force A determines the form of $\alpha(x, y)$:

$$\alpha(x, y, t) = \alpha_o(x, t) + y\alpha_1(x, t). \tag{3-51}$$

The evolution of the beam follows three phases: a response purely elastic, an evolution with plasticity, and a purely elastic unloading.

- *Elastic phase:* For the proposed loading, the response of the beam is linear elastic when $f(A) \le 0$, $\forall(x, y)$ and

$$\alpha(x, y) = 0 \quad \text{for } t < t_c.$$

At $t = t_c$ some points of the beam are such that $f(A) = 0$. After this critical time $(t > t_c)$, the plasticity develops inside the beam, the boundary of the plastic zone Ω_p is the plane curve $y = \pm m(x, t)$.

- *Phase of loading in plasticity:* In the plastic zone Ω_p

$$\Omega_p = \{(x, y) \in \Omega / y \le -m(x, t), \ y \ge m(x, t), \ x \in]x_p(t), L - x_p(t)[\}, \tag{3-52}$$

the thermodynamical force $A(x, y)$ satisfies $A = k$, this implies that

$$\alpha_o = -\frac{k}{E + H}, \quad \langle y\alpha \rangle = \frac{1}{2h}\int_{-h}^{m} y\alpha \, dy. \tag{3-53}$$

And we obtain

$$\frac{M}{I} + \frac{kE}{I(E + H)}(h^2 - m^2) - \frac{2E}{3I}m^3\alpha_1 - H\alpha_1 = 0. \tag{3-54}$$

The plastic strain is then determined if we know the equation of the curve $y = \pm m(x, t)$.

In the complementary domain, namely, $-m(x, t) \ge y \ge m(x, t)$ for $x \in [x_p(t), L - x_p(t)]$, the local response is purely elastic:

$$A = \frac{My}{I} + \frac{2Ey}{I}\frac{k}{2(E + H)}(h^2 - m^2) + \frac{2Ey}{3I}\alpha_1(h^3 - m^3). \tag{3-55}$$

On the boundary of this domain, the continuity of A determines the equation of the boundary $y = -m(x, t)$:

$$-k = \frac{Mm}{I} + \frac{2Em}{I}\frac{k}{2(E + H)}(h^2 - m^2) + \frac{2Em}{3I}\alpha_1(h^3 - m^3). \tag{3-56}$$

In the complementary domain, namely for $x \in]0, x_p[\cup]x_p, L[$, we have

$$A = \frac{My}{I}. \tag{3-57}$$

For the sake of simplificity, we consider now the case of perfect plasticity, $H = 0$, for which an explicit equation for the boundary is obtained:

$$m(x, t) = \sqrt{3\left(h^2 + \frac{M(x, t)}{k}\right)}. \tag{3-58}$$

The local fields satisfy the equations

$$u(x, t) = 0, \tag{3-59}$$

$$v''(x, t) = \frac{k}{Em} \quad \text{if } x \in [x_p(t), L - x_p(t)], \tag{3-60}$$

$$v''(x, t) = -\frac{M}{EI} \quad \text{otherwise}, \tag{3-61}$$

and the plastic strain is

$$\alpha(x, y) = \frac{k}{E}\left(\text{sign}(y) - \frac{y}{m}\right). \tag{3-62}$$

These equations are true for $t \in [0, t_m]$. At $t = t_m$ the moment M is maximum M_m.

• *Phase of unloading:* From $t \geq t_m$ the loading decreases. Let us assume that the loading rests within the domain of reversibility, then $\lambda(x, y) = 0$ and the unloading is purely elastic and that we obtain the value $M(x, 2t_m) = M_m(x)$ at $t = 2t_m$ then the solution satisfies:

• In the plastic zone, namely for $x \in [x_p(t_m), L - x_p(t_m)]$,

$$v_f''(x) = v''(x, 2t_m) = \frac{k}{E\sqrt{3\left(h^2 + \frac{M_m(x)}{k}\right)}} + \frac{M_m(x)}{EI} = \psi(M_m). \tag{3-63}$$

• In the complementary part,

$$v_f''(x) = 0 = \psi(M_m). \tag{3-64}$$

This solution determines the residual shape if the condition of elastic unloading is satisfied that is $M(x, t) \leq -\frac{2}{3}kh^2$.

The distribution of the moment M_m depends only on $P_o(x)$ and then the residual shape is governed by the equations

$$M_m'' = P_o, \quad v'' = \psi(M_m), \quad M_m(0) = M_m(L) = 0, \quad v(0) = v(L) = 0. \tag{3-65}$$

3B2. *The inverse problem.* We assume that the residual displacement v_o is given, and we try to determine the best process p of loading-unloading which gives a displacement $v(p)$ as close as possible to v_o by solving the direct problem. The loading p is controlled such that the functional

$$J(p) = \frac{1}{2}\int_0^L (v(p) - v_o)^2 \, dx + \frac{1}{2}r\int_0^L p^2 \, dx. \tag{3-66}$$

For a given family $p(x, t)$ we can solve the direct problem, and then optimize J. The equations of the direct problem are equivalent to the variational form by introducing the functional $\mathcal{L}$, which depends on adjoint fields:

$$\mathcal{L} = \int_0^L \left(M^*(p - M'') + v^*(\psi(M) - v'') \right) dx. \tag{3-67}$$

The solution of the inverse problem is obtained as optimization of $\mathcal{J} = J + \mathcal{L}$, the variations for the adjoint fields give rise to the equations of the direct problem, and the condition of optimality is obtained as a boundary condition:

$$0 = \int_0^L (M^* + rp)\, p^*\, dx. \tag{3-68}$$

Assume that $v_o(x)$ is the solution of the elastoplastic problem with $P_o(x) = p_o$. The goal of the inverse problem is to find the best $p(x, t)$ for which the displacement $v(p)$ is close to v_o.

The analysis with uniform $p(x, t)$ gives the exact solution. It is obvious because the solution of the direct problem with uniform p satisfies the equations of the inverse problem and the condition of optimality determines the value of p.

Other profiles for $P(x)$ can be used. For example, the choice of a triangular shape or a sinus shape for $P_o(x)$ gives a very close plastic zone. This can be shown numerically. The error on the shape does not exceed 1%.

4. Estimation of the internal state in elastoplasticity.

Consider now a body Ω. The body is submitted to an increasing loading, but the history of the loading is not known. Only the final shape $\boldsymbol{u}_o$ and the final loading $\boldsymbol{T}_o$ on the boundary Γ_o are known.

For an elastoplastic material, the stress satisfies the constitutive law

$$\boldsymbol{\sigma} = \mathbb{C} : (\boldsymbol{\varepsilon}(u) - \boldsymbol{\varepsilon}_p), \quad f(\boldsymbol{\sigma}, \boldsymbol{\varepsilon}_p) \le 0, \tag{4-1}$$

where the domain of reversibility $f(\boldsymbol{\sigma}, \boldsymbol{\varepsilon}_p) \le 0$, is defined by the convex function f.

These stresses are in equilibrium with given boundary conditions ($\boldsymbol{T}_o$ on Γ_o) and are divergence free if there is no body force:

$$\mathrm{div}\,\boldsymbol{\sigma} = 0 \quad \text{over } \Omega, \qquad \boldsymbol{n}.\boldsymbol{\sigma} = \boldsymbol{T}_o \quad \text{over } \Gamma_o. \tag{4-2}$$

The plastic strain is isochoric:

$$\mathrm{Tr}\,\boldsymbol{\varepsilon}_p = 0. \tag{4-3}$$

To estimate the internal state, from the known residual shape, we can solve a problem of linear elasticity controlled by $\boldsymbol{\varepsilon}_p$: find the displacement $\boldsymbol{v}$ satisfying the following conditions:

- *Compatibility*: $2\boldsymbol{\varepsilon}(u) = \nabla\boldsymbol{u} + \nabla^t\boldsymbol{u}$,
- *Constitutive law*: $\boldsymbol{\sigma} = \mathbb{C} : (\boldsymbol{\varepsilon} - \boldsymbol{\varepsilon}_p)$,
- *Boundary condition*: $\boldsymbol{n}.\boldsymbol{\sigma} = \boldsymbol{T}_o$ over Γ_o, $\boldsymbol{u} = 0$ over Γ_i.

The best estimation of $\boldsymbol{\varepsilon}_p$ must be such that on Γ_o the displacement solution of the direct problem $\boldsymbol{v}_{\mathrm{sol}}(\boldsymbol{\varepsilon}_p)$ is close to $\boldsymbol{u}_o$ on Γ_o.

Previously, we proposed to solve the problem of evolution for an elastoplastic material for a given class of loading history, but this is a tedious task, because we must solve the direct problem many times to determine the optimal state. We propose to consider another way to estimate the elastoplastic state.

To obtain a solution of the optimization close to a problem of elastoplasticity, we decompose the body Ω into two domains, one where $\boldsymbol{\varepsilon}_p = 0$ and a plastic zone Ω_p where the stresses are close to the domain of reversibility.

These constraints are prescribed during the optimization process by introducing new terms in the functional to minimize:

$$J(\boldsymbol{u}, \boldsymbol{\varepsilon}_p, \Omega_p) = \frac{1}{2} \int_{\Gamma_o} h \|\boldsymbol{u} - \boldsymbol{u}_o\|^2 \, d\Omega + \frac{\beta}{2} \int_{\Omega_p} \left(f(\boldsymbol{\sigma}(\boldsymbol{u}, \boldsymbol{\varepsilon}_p), \boldsymbol{\varepsilon}_p) \right)^2 \, d\Omega. \tag{4-4}$$

The yielding function $f(\boldsymbol{\sigma}, \boldsymbol{\varepsilon}_p)$ is rewritten in terms of the local behaviour:

$$f(\boldsymbol{\sigma}(\boldsymbol{u}, \boldsymbol{\varepsilon}_p), \boldsymbol{\varepsilon}_p) = Y(\boldsymbol{\varepsilon}(\boldsymbol{u}), \boldsymbol{\varepsilon}_p). \tag{4-5}$$

To satisfy the problem of equilibrium, we introduce an adjoint state such that

$$\int_\Omega \nabla \boldsymbol{u}^* : \mathbb{C} : (\nabla \boldsymbol{u} - \boldsymbol{\varepsilon}_p) \, d\Omega - \int_{\Gamma_o} \boldsymbol{u}^* . \boldsymbol{T}_o \, ds = 0 \quad \text{for all } \boldsymbol{u}^* \text{ satisfying } \boldsymbol{u}^* = 0 \text{ over } \Gamma_i, \tag{4-6}$$

where the constitutive law has been taken into account. The displacement $\boldsymbol{u}$ and the adjoint displacement $\boldsymbol{u}^*$ are continuous along the boundary of the plastic zone.

Then, the functional to be optimized is reduced to

$$\mathcal{J}(\overset{\star}{\boldsymbol{u}}, \boldsymbol{u}, \boldsymbol{\varepsilon}_p, \Omega_p) = \frac{1}{2} \int_{\Gamma_o} h \|\boldsymbol{u} - \boldsymbol{u}_o\|^2 \, d\Omega + \frac{\beta}{2} \int_{\Omega_p} (Y(\boldsymbol{\varepsilon}(\boldsymbol{u}), \boldsymbol{\varepsilon}_p))^2 \, d\Omega,$$
$$- \int_\Omega \nabla \overset{\star}{\boldsymbol{u}} : \mathbb{C} : (\nabla \boldsymbol{u} - \boldsymbol{\varepsilon}_p) \, d\Omega + \int_{\Gamma_o} \overset{\star}{\boldsymbol{u}} . \boldsymbol{T}_o \, ds.$$

4A. Elements of proof. The displacements $\boldsymbol{u}$ and $\overset{\star}{\boldsymbol{u}}$ are continuous on the boundary of the plastic zone Γ_p, therefore their variations satisfy Hadamard conditions of continuity along Γ_p. When the position of Γ_p is moved by its normal velocity $\delta\phi$, the variations of the displacement satisfy

$$|[\delta\boldsymbol{u}]| + \delta\phi |[\nabla\boldsymbol{u}]| . \boldsymbol{n} = 0, \quad |[\delta\overset{\star}{\boldsymbol{u}}]| + \delta\phi |[\nabla\overset{\star}{\boldsymbol{u}}]| . \boldsymbol{n} = 0. \tag{4-7}$$

- *Variations with respect to $\overset{\star}{\boldsymbol{u}}$ ($\partial\mathcal{J}/\partial\overset{\star}{\boldsymbol{u}} = 0$) are equivalent to the equations of the direct problem for a given distribution of $\boldsymbol{\varepsilon}_p$*

$$\boldsymbol{\sigma} = \mathbb{C} : (\boldsymbol{\varepsilon}(\boldsymbol{u}) - \boldsymbol{\varepsilon}_p), \quad \text{div } \boldsymbol{\sigma} = 0, \quad \boldsymbol{\sigma}\boldsymbol{n} = \boldsymbol{T}_o \quad \text{over } \Gamma_o, \quad |[\boldsymbol{\sigma}]| . \boldsymbol{n} = 0 \quad \text{over } \Gamma_p. \tag{4-8}$$

- *The variations with respect to $\boldsymbol{u}$ ($\partial\mathcal{J}/\partial\boldsymbol{u} = 0$) determine the adjoint state:*

$$\overset{\star}{\boldsymbol{\sigma}} = \mathbb{C} : \boldsymbol{\varepsilon}(\overset{\star}{\boldsymbol{u}}) - \beta Y \frac{\partial Y}{\partial \boldsymbol{\varepsilon}} \quad \text{over } \Omega_p,$$

$$\overset{\star}{\boldsymbol{\sigma}} = \mathbb{C} : \boldsymbol{\varepsilon}(\overset{\star}{\boldsymbol{u}}) \quad \text{over } \Omega/\Omega_p,$$

$$\text{div } \overset{\star}{\boldsymbol{\sigma}} = 0,$$

$$\overset{\star}{\boldsymbol{\sigma}} . \boldsymbol{n} = h(\boldsymbol{u} - \boldsymbol{u}_o) \quad \text{over } \Gamma_o,$$

$$|[\overset{\star}{\boldsymbol{\sigma}}]|.\boldsymbol{n} = \beta Y \frac{\partial Y}{\partial \boldsymbol{\varepsilon}}.\boldsymbol{n} \qquad\qquad \text{over } \Gamma_p.$$

- *The condition of optimality* with respect to $\boldsymbol{\varepsilon}_p$ determines the plastic strain

$$\text{dev}(\mathbb{C} : \nabla \overset{\star}{\boldsymbol{u}}) + \beta Y \frac{\partial Y}{\partial \boldsymbol{\varepsilon}_p} = 0, \tag{4-9}$$

where $\text{dev}(\boldsymbol{a}) = \boldsymbol{a} - \text{tr}(\boldsymbol{a})\boldsymbol{I}/3$.

- *Variation with respect to the domain* Ω_p. Finally, the condition of optimality on the plastic zone gives an equation of continuity of the energy

$$-\left|[\boldsymbol{\varepsilon}(\overset{\star}{\boldsymbol{u}}) : \mathbb{C} : (\boldsymbol{\varepsilon}(\boldsymbol{u}) - \boldsymbol{\varepsilon}_p)]\right| + \boldsymbol{\sigma} : \left|[\nabla \overset{\star}{\boldsymbol{u}}]\right| + \overset{\star}{\boldsymbol{\sigma}}_- : \left|[\nabla \boldsymbol{u}]\right| + \tfrac{1}{2}\beta Y^2 = 0. \tag{4-10}$$

This optimization permits the determination of a plastic zone with an evaluation of the plastic strain.

The quality of the solution depends on the choice of the coefficients α, β, k. That can be investigated through analytical solutions for elastoplastic materials on simple geometries such as cylinders or spheres.

Consider the solution of a direct problem of an increasing loading process. The final state is a distribution of $\boldsymbol{\varepsilon}_p$, such that along the boundary of the plastic zone, the plastic strain is $\boldsymbol{\varepsilon}_p = 0$, and $f = 0$. Then it is obvious that the solution of the evolution problem satisfies the minimum of the proposed functional. It can be noticed that the condition of optimality (4-10) is verified, because the plastic strain vanishes on Γ_p and $Y = 0$, the other contributions are identically zero because the elastic moduli are continuous, the displacements $\boldsymbol{u}$, the traction $\boldsymbol{\sigma}.\boldsymbol{n}$ are continuous and $\overset{\star}{\boldsymbol{\sigma}} = 0$, $\overset{\star}{\boldsymbol{u}} = 0$.

4B. *Case of a hollow sphere.* The solution of a hollow sphere under radial tension is well known for an elasto perfectly-plastic material. The external radius of the sphere is R_e, the radius of the void is R_i and the porosity is $c = R_i^3/R_e^3$ (see Figure 5). For an increasing loading the internal state is determined and is used for the boundary conditions applied to R_e for the inverse problem.

4B1. *Solution of the direct problem.* The plastic zone Ω_p is the spherical domain $r \in [R_i, R_p]$, where $p = R_p^3/R_e^3$. The solution is purely radial: $\boldsymbol{u} = u(r)\boldsymbol{e}_r$. The Cauchy stress is given by

$$\boldsymbol{\sigma} = \sigma_{rr}(r)\boldsymbol{e}_r \otimes \boldsymbol{e}_r + \sigma_{tt}(r)(\boldsymbol{e}_\theta \otimes \boldsymbol{e}_\theta + \boldsymbol{e}_\phi \otimes \boldsymbol{e}_\phi), \tag{4-11}$$
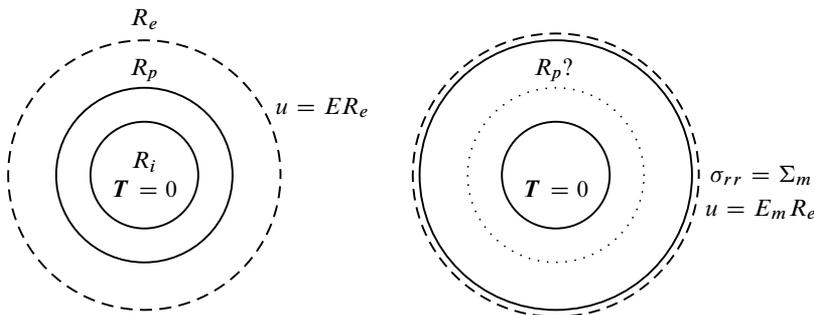
Figure 5. The hollow sphere. Left: the direct problem. Right; the inverse problem under given boundary conditions on R_e. On the dashed circle the displacement is prescribed, on the solid-line circle the traction is given.

and the domain of reversibility is determined by $Y = \sigma_{tt} - \sigma_{rr} - \sigma_o \leq 0$ where σ_o is a constant. The plastic strain has the form

$$\boldsymbol{\varepsilon}_p = \varepsilon_p(2\boldsymbol{e}_r \otimes \boldsymbol{e}_r - \boldsymbol{e}_\theta \otimes \boldsymbol{e}_\theta - \boldsymbol{e}_\phi \otimes \boldsymbol{e}_\phi), \quad \varepsilon_p = \frac{3\kappa + 4\mu}{18\kappa\mu}\sigma_o\left(1 - \frac{R_p^3}{r^3}\right). \tag{4-12}$$

For an increasing imposed E the global response of the sphere is

$$\Sigma = 3K(c)(E - E_p) = \sigma_{rr}(R_e), \quad K(c) = (1 - c)\frac{4\kappa\mu}{3\kappa c + 4\mu}, \tag{4-13}$$

$$E = \frac{u}{r}(R_e), \qquad E_p = \frac{3\kappa + 4\mu}{18\mu\kappa}\frac{\sigma_o}{1-c}\left(p - c - c\ln\frac{p}{c}\right). \tag{4-14}$$

During the loading process,

$$E = \frac{2\sigma_o}{3}\left(\frac{p}{4\mu} + \frac{1}{3\kappa}\left(1 + \ln\frac{p}{c}\right)\right), \quad \Sigma = \frac{2}{3}\sigma_o\left(1 - p + \ln\frac{p}{c}\right), \quad \sigma_{rr} = 2\sigma_o\ln\frac{r}{R_i} \text{ over } \Omega_p.$$

We remark that the radius R_p of the plastic zone is a increasing function with E.

4B2. *The inverse problem.* We assume that the measurement on the external boundary of the sphere is the strain E_m and the tension Σ_m. We consider that the fields depend only upon r and $\boldsymbol{\varepsilon}_p$ is isochoric, then the function $\mathcal{J}$ is

$$\mathcal{J}(\boldsymbol{u}, \overset{\star}{\boldsymbol{u}}, \varepsilon_p, R_p) = \frac{1}{2}hR_e^2\left(\frac{u(R_e)}{R_e} - E_m\right)^2$$

$$+ \frac{\beta}{2}\int_{R_i}^{R_p} Y^2 r^2\,dr - \int_{R_i}^{R_e} \nabla\overset{\star}{\boldsymbol{u}} : \mathbb{C} : (\nabla\boldsymbol{u} - \boldsymbol{\varepsilon}_p)\,r^2\,dr + R_e^2\,\Sigma_m\,u^*(R_e), \tag{4-15}$$

where Y is evaluated in terms of $u(r)$ and ε_p:

$$Y = 2\mu\left(\frac{u}{r} - \frac{du}{dr}\right) + 6\mu\varepsilon_p - \sigma_o.$$

The plastic domain is controlled by R_p. The plastic zone must be optimized. The variations with respect to ε_p give

$$4\mu\left(\frac{du^*}{dr} - \frac{u^*}{r}\right) - 6\beta\mu Y = 0. \tag{4-16}$$

The variations with respect to $u(r)$ furnish the equations of the adjoint state:

$$0 = \frac{d\sigma_{rr}^*}{dr} + \frac{2}{r}(\sigma_{rr}^* - \sigma_{tt}^*) \qquad\qquad \text{if } r \geq R_p, \tag{4-17}$$

$$0 = \frac{d\sigma_{rr}^*}{dr} + \frac{2}{r}(\sigma_{rr}^* - \sigma_{tt}^*) - 2\mu\beta\left(\frac{dY}{dr} + \frac{3}{r}Y\right) \quad \text{if } r \leq R_p, \tag{4-18}$$

where the local constitutive law $\overset{\star}{\boldsymbol{\sigma}} = \mathbb{C} : \boldsymbol{\varepsilon}(\overset{\star}{\boldsymbol{u}})$ has been taken into account. Then the adjoint displacement

$\overset{\star}{u}$ satisfies

$$u^* = \begin{cases} a_e r + B_e/r^2 & \text{if } r \geq R_p, \\ u^* = a_p r + B_p/r^2 & \text{if } r \leq R_p, \end{cases} \qquad (4\text{-}19)$$

and the local function Y is then deduced:

$$Y = -\frac{2}{3\alpha} r \frac{d}{dr}\left(\frac{u^*}{r}\right) = \frac{2B_p}{\beta r^3}. \qquad (4\text{-}20)$$

Having determined Y, the stresses in Ω_p are obtained by integration of local equations of equilibrium resulting from the variations of $\mathscr{J}$ with respect to $\overset{\star}{u}$:

$$\sigma_{rr} = 2\sigma_o \ln\frac{r}{R_i} + \frac{4B_p}{3\beta}\left(\frac{1}{r^3} - \frac{1}{R_i^3}\right). \qquad (4\text{-}21)$$

We also know σ_{tt} from Y and $3\text{Tr}(\boldsymbol{\varepsilon}) = \sigma_{rr} + 2\sigma_{tt}$ gives the displacement in Ω_p:

$$3\kappa(r^2 u - R_i^2 u_i) = 2\sigma_o r^3 \log\frac{r}{R_i} + \frac{4B_p}{3R_i^3\beta}(r^3 - R_i^3). \qquad (4\text{-}22)$$

Along $r = R_p$ we obtain

$$3\kappa\left(p\frac{u_p}{R_p} - c\frac{u_i}{R_i}\right) = \frac{2\sigma_o}{3} p \log\frac{p}{c} + (p-c)\frac{4B_p}{3\beta R_i^3}. \qquad (4\text{-}23)$$

Finally the problem of optimization is reduced to the system $(B_p = b_p R_p^3, \ B_e = b_e R_p^3)$

$$\Sigma_m = 3\kappa a - 4\mu b\, p,$$

$$\sigma_{rr}^*(R_e) = 3\kappa a_e - 4\mu b_e p = hR_e(a + bp - E_m),$$

$$a_e + b_e = a_p + b_p,$$

$$3\kappa a_p - 4\mu b_p p/c = 2\mu\alpha f(R_i) = -\frac{4\mu p}{c} b_p,$$

$$3\kappa(a_e - a_p) - 4\mu(b_e - b_p) = 4\mu b_p,$$

$$3\kappa a - 4\mu b = 2\sigma_o \ln\frac{p}{c} + \frac{4}{3\beta} b_p\left(1 - \frac{p}{c}\right).$$

It is obvious that $a_p = 0$. For a given R_p this system has an unique solution.

To this system, we must add the condition (4-10), corresponding to the variation of the functional with respect to R_p.

Assuming that (E_m, Σ_m) is a solution of the direct problem (E, Σ), the solution of inverse problem is obtained taking $b_p = 0$ and the adjoint field $\overset{\star}{u} = 0$. Along $r = R_p$, we have $Y = 0$. As a consequence, we can now recover the solution of the direct problem.

However for boundary conditions, $\Sigma_m = \Sigma + \Delta\Sigma$ and $E_m = E + \Delta E$, where the Σ_m, E_m is not a solution of a direct problem under radial loading, the solution of the inverse problem is the sum of the solution of the direct problem and of that of the gap between it and the solution at R_p. It is easy to show that the solution is unique, especially the radius R_p is close to the radius obtained by the direct problem if the measured strain E_m is close to E.

This analysis can be extended to the case of elastoplasticity with linear hardening, and the final conclusions of such an extension are quite similar to the present case. The problem for elastoplastic material is not always regular, and the proposed variational approach is not general.

Next, the case of viscoplasticity is investigated as a regularisation of the elastoplastic problem.

5. Boundary control and extension in viscoplasticity

Let Ω be a domain with external boundary $\partial\Omega$. The body has an elastoviscoplastic behaviour. The state of the body is defined by the value of the strain $\boldsymbol{\varepsilon}$ and internal parameters α. The local behaviour is defined by a free energy $w(\boldsymbol{\varepsilon}, \alpha)$ and we assume that the internal state has an evolution satisfying the normality rule defined by a potential of dissipation Φ. The free energy is defined classically as a reversible part due to elasticity and energy embedded in the residual stresses and hardening

$$w(\boldsymbol{\varepsilon}, \alpha) = \tfrac{1}{2}(\boldsymbol{\varepsilon} - \alpha) : \mathbb{C} : (\boldsymbol{\varepsilon} - \alpha) + W(\alpha). \tag{5-1}$$

The state equations are given by

$$\boldsymbol{\sigma} = \frac{\partial w}{\partial \boldsymbol{\varepsilon}} = \mathbb{C} : (\boldsymbol{\varepsilon} - \alpha), \quad A = -\frac{\partial w}{\partial \alpha}, \tag{5-2}$$

and the evolution of the internal state satisfies

$$\dot{\alpha} = \frac{\partial \Phi}{\partial A}. \tag{5-3}$$

We seek an estimation of the loading history along a part Γ_T knowing both the initial state of the body and the final position at final time t_f of Γ_T.

In linearized elasticity, the problem is easy to solve. Assuming that we know the displacement of the boundary, it is easy to determine the resulting traction on the boundary. Here the problem is more difficult because the final state depends in a fundamental the history of the loading, and this loading path is unknown.

The optimal control theory is used to give some possible answers to the problem of estimating the internal state, while simultaneously providing an optimal loading history compatible with the given residual shape.

Consider that the initial state is naturally $\boldsymbol{u}(x, t_o) = 0, \alpha(x, t_o) = 0, \forall x \in \Omega$. On Γ_u the displacement is prescribed $\boldsymbol{u}(x, t) = 0$. The final state $\boldsymbol{u}(x, t_f) = \boldsymbol{u}_o(x)$ is known along the complementary part Γ_T of the boundary. We seek the best history of the loading $\boldsymbol{T}_o(x, t)$ applied on Γ_T and the internal state $\alpha(x, t)$ such that the resulting displacement along Γ_T is close to the measured displacement $\boldsymbol{u}_o$ at time t_f.

For a given history $\boldsymbol{T}_o(x, t)$ imposed on Γ_T we determine the solution $\boldsymbol{u}(x, t), \alpha(x, t)$ satisfying the primal problem of evolution corresponding to the set of equations

- *Compatibility*: $2\boldsymbol{\varepsilon}(\boldsymbol{u}) = \nabla\boldsymbol{u} + \nabla^t\boldsymbol{u}$ over Ω, $\boldsymbol{u} = 0$ along Γ_u.

- *Equilibrium*: $\operatorname{div}\boldsymbol{\sigma} = 0$ ove rΩ, $\boldsymbol{n}.\boldsymbol{\sigma} = \boldsymbol{T}_o$ along Γ_T.

- *Constitutive law*: $\boldsymbol{\sigma} = \dfrac{\partial w}{\partial \boldsymbol{\varepsilon}} = \mathbb{C} : (\boldsymbol{\varepsilon} - \alpha), \quad A = -\dfrac{\partial w}{\partial \alpha}, \quad \dot{\alpha} = \dfrac{\partial \Phi}{\partial A}.$

For this behaviour, the displacement $\boldsymbol{u}$, the local state $\boldsymbol{\varepsilon}, \alpha$ and the stresses $\boldsymbol{\sigma}$ are functions of position and time.

In particular, the solution of the problem of evolution at t_f defines the displacement $\boldsymbol{u}(x, t_f)$ along Γ_T. The best history $\boldsymbol{T}_o(x, t)$ is determined by an optimality condition. The function to optimize is chosen as

$$J(\boldsymbol{u}, \boldsymbol{T}_o) = \int_{\Gamma_T} \tfrac{1}{2}k\|\boldsymbol{u}(x, t_f) - \boldsymbol{u}_o(x)\|^2 \, \mathrm{ds} + \int_0^{t_f} \int_{\Gamma_T} \tfrac{1}{2}\dot{\boldsymbol{T}}_o.H.\dot{\boldsymbol{T}}_o \, \mathrm{ds\,dt}. \tag{5-4}$$

To solve the problem, we adopt a variational form of the primal problem of evolution by introducing the functional $\mathcal{L}$:

$$\mathcal{L} = -\int_0^{t_f} \int_\Omega (\dot{\boldsymbol{\varepsilon}}, \dot{\alpha})^t.\mathcal{W}.(\boldsymbol{\varepsilon}^*, \alpha^*) \, \mathrm{d\Omega\,dt} + \int_0^{t_f} \int_{\Gamma_T} \dot{\boldsymbol{T}}_o.\boldsymbol{u}^* \, \mathrm{ds\,dt} + \int_0^{t_f} \int_\Omega \left(A^*.\left(-\dot{\alpha} + \frac{\partial \Phi}{\partial A}\right) - \alpha^*.\dot{A}\right) \mathrm{d\Omega\,dt}.$$

where $\mathcal{W}$ is related to the second derivative of the free energy

$$\begin{bmatrix} \dot{\boldsymbol{\sigma}} \\ -\dot{A} \end{bmatrix} = \begin{bmatrix} \dfrac{\partial^2 w}{\partial \boldsymbol{\varepsilon}\, \partial \boldsymbol{\varepsilon}} & \dfrac{\partial^2 w}{\partial \boldsymbol{\varepsilon}\, \partial \alpha} \\[2mm] \dfrac{\partial^2 w}{\partial \alpha\, \partial \boldsymbol{\varepsilon}} & \dfrac{\partial^2 w}{\partial \alpha\, \partial \alpha} \end{bmatrix}.\begin{bmatrix} \dot{\boldsymbol{\varepsilon}} \\ \dot{\alpha} \end{bmatrix} = \mathcal{W}(\boldsymbol{\varepsilon}, \alpha).\begin{bmatrix} \dot{\boldsymbol{\varepsilon}} \\ \dot{\alpha} \end{bmatrix}. \tag{5-5}$$

Let us introduce the notation

$$\begin{bmatrix} \dot{\boldsymbol{\sigma}} \\ \dot{B} \end{bmatrix} = \mathcal{W}(\boldsymbol{\varepsilon}, \alpha).\begin{bmatrix} \dot{\boldsymbol{\varepsilon}} \\ \dot{\alpha} \end{bmatrix}, \quad \begin{bmatrix} \boldsymbol{\sigma}^* \\ B^* \end{bmatrix} = \mathcal{W}(\boldsymbol{\varepsilon}, \alpha).\begin{bmatrix} \boldsymbol{\varepsilon}^* \\ \alpha^* \end{bmatrix}. \tag{5-6}$$

The variations of $\mathcal{L}$ are

$$\delta\mathcal{L} = -\int_0^{t_f} \int_\Omega \left(\delta\dot{\boldsymbol{\varepsilon}} : \boldsymbol{\sigma}^* + \delta\dot{\alpha} B^* + \delta\boldsymbol{\varepsilon}^* \dot{\boldsymbol{\sigma}} + \delta\alpha^* \dot{B}\right) \mathrm{d\Omega\,dt} + \int_0^{t_f} \int_{\Gamma_T} (\delta\dot{\boldsymbol{T}}_o.\boldsymbol{u}^* + \dot{\boldsymbol{T}}_o.\delta\boldsymbol{u}^*) \, \mathrm{ds\,dt}$$

$$+ \int_0^{t_f} \int_\Omega \left(\delta A^*.\left(-\dot{\alpha} + \frac{\partial \Phi}{\partial A}\right) + A^*\left(-\delta\dot{\alpha} + \frac{\partial^2 \Phi}{\partial A\, \partial A}\delta A\right) - \delta\alpha^* \dot{A} - \alpha^* \delta\dot{A}\right) \mathrm{d\Omega\,dt}.$$

Due to the integration over the history $t \in [0, t_f]$, the variations of the functional give the rate equations of the quantities and conditions at final time t_f. It is obvious that the variation with respect to $\boldsymbol{u}^*$ gives directly that $\dot{\boldsymbol{\sigma}}$ is statically admissible with the prescribed history loading on Γ_T:

$$\operatorname{div} \dot{\boldsymbol{\sigma}} = 0, \quad \boldsymbol{n}.\dot{\boldsymbol{\sigma}} = \dot{\boldsymbol{T}}_o. \tag{5-7}$$

The variation with respect to A^* implies the evolution of the internal state α, and the variation with respect to α^* implies the constitutive law: $\dot{A} + \dot{B} = 0$. Conversely the variations with respect to $\boldsymbol{u}, \alpha$ lead to the adjoint problem:

- *Equilibrium*:

$$\operatorname{div} \dot{\boldsymbol{\sigma}}^* = 0, \quad \boldsymbol{n}.\dot{\boldsymbol{\sigma}}^* = 0 \quad \text{on } \Gamma_T.$$

- *Boundary condition*:

$$\dot{\boldsymbol{u}}^*(x, t) = 0, \quad \boldsymbol{u}^*(x, t_f) = 0 \quad \text{along } \Gamma_u.$$

- *Constitutive law*:

$$A^* + B^* = 0, \quad \dot{\alpha}^* = -\frac{\partial^2 \Phi}{\partial A \, \partial A} A^*, \quad \alpha^*(t_f) = 0,$$

$$\boldsymbol{\sigma}^*(x, t_f) = \mathbb{C} : \boldsymbol{\varepsilon}^*(x, t_f) \quad \text{over } \Omega.$$

To ensure the existence of a solution, the two potentials w, Φ must have regular second derivative.

To obtain an estimation of the loading history and of the internal state compatible with the measured displacement $\boldsymbol{u}_o$ over Γ_T at time t_f the functional to optimize is $\mathcal{J} = J + \mathcal{L}$ and the conditions of optimality are then

$$0 = \boldsymbol{u}^* + H.\dot{\boldsymbol{T}}_o \qquad \text{on } \Gamma_T, \tag{5-8}$$

$$0 = \boldsymbol{n}.\boldsymbol{\sigma}^*(t_f) + k(\boldsymbol{u}(t_f) - \boldsymbol{u}_o) \quad \text{on } \Gamma_T, \tag{5-9}$$

where the first condition gives the boundary condition on Γ_T for the adjoint displacement and the second one is imposed by the variation with respect to $\boldsymbol{u}(t_f)$.

It can be noticed that the adjoint problem is a viscoelastic problem, whose modulus of viscosity depends on the primal solution. The viscoplastic potential of dissipation must be regular. Due to the dependance of time in viscoplasticity, the inverse problem must be solved numerically. The solution depends on the duration and the solution is obtained by a optimization with respect to t_f.

5A. *Cyclic loading.* The extension of the presented solution method for cyclic loading has been performed to determine the cyclic asymptotic answer of viscoplastic structures with applications to fatigue. In this case the functional $\mathcal{L}$ is not changed, and the cost function J is chosen as a measure of the gap on periodicity on the generalized stress space $\mathcal{A} = (\boldsymbol{\sigma}, A)$. Such a cost functional is, for example,

$$J(\mathcal{A}) = \int_{\Omega} \tfrac{1}{2}(\mathcal{A}(T) - \mathcal{A}(0)).\mathbb{H}.(\mathcal{A}(T) - \mathcal{A}(0)) \, d\Omega. \tag{5-10}$$

The solution is obtained by a resolution of a problem of minimization, the uniqueness is proved in [Peigney and Stolz 2003].

6. Conclusion

This article proposed a general method for resolution of inverse problems in elastoplasticity. The formulation is based on the definition of the control variables: the plastic strain and the history of loading. For each class of inverse problems, an appropriate functional is chosen. The solution stems from the introduction of an adjoint state solution of the adjoint problem. In elasticity, the adjoint problem has the same form than the primal problem. Applications on bars and on a beam have been presented with analytical resolutions. They give the main ideas developed in this article and are illustrations of the method based on optimal control. In elastoplasticity, for the estimation of the plastic strain and the plastic zone, the solution of the inverse problem for the given examples is the sum of the solution of the primal one and of an elastic one given by the adjoint state which measures the discrepancy with respect to the exact solution.

A general formulation is obtained in elastoviscoplasticity. In this case the solution is given by the introduction of an adjoint state, which is the solution of a viscoelastic problem whose characteristics are

given by the primal solution. In this general case, the problem to solve is dependent upon the history of the local fields. Other applications and examples can be found in [Bourgeois 1998].

References

[Ballard and Constantinescu 1994] P. Ballard and A. Constantinescu, "On the inversion of subsurface residual stresses from surface stress measurements", *J. Mech. Phys. Solids* **42**:11 (1994), 1767–1787.

[Bourgeois 1998] L. Bourgeois, *Contrôle optimal et problèmes inverses en plasticité*, thesis, École Polytechnique, Palaiseau, 1998.

[Bui 1993] H. D. Bui, *Introduction aux problèmes inverses en mécanique des matériaux*, Eyrolles, Paris, 1993.

[Constantinescu and Tardieu 2001] A. Constantinescu and N. Tardieu, "On the identification of elastoviscoplastic constitutive laws from indentation tests", *Inverse Probl. Eng.* **9**:1 (2001), 19–44.

[Delattre et al. 2002] B. Delattre, D. Ivaldi, and C. Stolz, "Application du contrôle optimal à l'identification d'un chargement thermique", *Rev. Eur. Élém. Finis* **11**:2–4 (2002), 393–404.

[Gao and Mura 1989] Z. Gao and T. Mura, "On the inversion of residual stresses from surface displacements", *J. Appl. Mech. (ASME)* **56**:3 (1989), 508–513.

[Lions 1968] J.-L. Lions, *Contrôle optimal de systèmes gouvernés par des équations aux dérivées partielles*, Gauthier-Villars/ Dunod, Paris, 1968.

[Peigney 2004] M. Peigney, "Simulating wear under cyclic loading by a minimization approach", *Int. J. Solids Struct.* **41**:24–25 (2004), 6783–6799.

[Peigney and Stolz 2001] M. Peigney and C. Stolz, "Approche par contrôle optimal des structures élastoviscoplastiques sous chargement cyclique", *C. R. Mécanique* **329**:9 (2001), 643–648.

[Peigney and Stolz 2003] M. Peigney and C. Stolz, "An optimal control approach to the analysis of inelastic structures under cyclic loading", *J. Mech. Phys. Solids* **51**:4 (2003), 575–605.

[Stolz 2008] C. Stolz, "Optimal control approach in nonlinear mechanics", *C. R. Mécanique* **336** (2008), 238–244.

CLAUDE STOLZ: claude.stolz@ec-nantes.fr
GeM UMR CNRS 6183, 1, rue de la Noë, 44321 Nantes, France

and

IMSIA UMR-CNRS 9219, EdF, 1, Av. General Leclerc, 92141 Clamart, France

msp

HARMONIC SHAPES IN ISOTROPIC LAMINATED PLATES

Xu Wang and Peter Schiavone

Harmonic shapes are known to minimize stress disturbance when introduced into an elastic body as either holes or inclusions. This paper is concerned with the design of harmonic shapes in an isotropic laminated plate. Specifically, we require that the harmonic shape does not disturb the sum of the two normal membrane stress resultants and that of the two normal bending moments when inserted into a uniformly loaded laminated plate. Using complex variable methods, we demonstrate how a single harmonic shape (hole or rigid inclusion) and two interacting harmonic shapes can be successfully designed to meet our requirements. In our discussion, the two interacting harmonic shapes include (i) two interacting harmonic holes, (ii) two interacting harmonic rigid inclusions, and (iii) one harmonic hole interacting with another harmonic rigid inclusion.

1. Introduction

The minimization of stress concentrations in composite materials remains a priority among researchers and practitioners alike. To date, various criteria have been proposed and successfully applied to the design of the shape of holes or inclusions which produce minimum stress concentrations when inserted into an elastic body (see for example [Mansfield 1953; Cherepanov 1974; Bjorkman and Richards 1976]). The design of such optimal structural shapes inevitably leads to the solution of an inverse problem in elasticity [Bui 1993; Bonnet and Constantinescu 2005]. The "neutral condition" proposed by Mansfield [1953] and further developed by Ru [1998] and Milton and Serkov [2001] is the most stringent yet most difficult to realize since it requires that the introduction of the corresponding neutral hole or inclusion leaves the stress distribution in the original uncut body completely undisturbed. The "equal strength condition" introduced by Cherepanov [1974] requires that the hoop stress be constant along the boundary of the hole or inclusion. The "harmonic field condition" advanced by Bjorkman and Richards [1976; 1979a] and further developed by Ru [1999a; 1999b] and Wang et al. [2005] requires that the introduction of the harmonic hole or inclusion does not alter the first invariant of the stress field anywhere in the surrounding elastic body. This design condition has many implications: (i) the Laplacian component of the stress field remains unchanged; (ii) there is no change in volume energy; (iii) there is no elastic rotation; (iv) harmonic holes or rigid inclusions produce minimum stress concentrations in constant fields. Interestingly, Bjorkman and Richards [1976; 1979b] observed that, under constant applied fields, the harmonic field condition and the equal strength condition are essentially equivalent in that they produce the same result.

Even though the analysis of bending and stretching deformations of thin plates in the presence of various defects such as dislocations, holes, cracks, anti-cracks and inhomogeneities has received considerable attention (see, for example, [Sih and Rice 1964; Zakharov and Becker 2000; Hasebe and Wang

Keywords: harmonic shape, stress concentration, inverse problem, isotropic laminated plate, conformal mapping.

2000; 2002; Wang and Hasebe 2000a; 2000b; 2001; Cheng and Reddy 2002, 2003; 2004b; 2004a; Yin 2005a; 2005b; Wang and Schiavone 2013; Wang and Zhou 2013], the design of optimal hole shapes to minimize stress concentrations in laminated plates has, in contrast, been investigated by only a few researchers (see, for example, [Vellaichamy et al. 1990; Budiansky et al. 1993; Senocak and Waas 1995]. In this paper, we continue the work in this area by extending Bjorkman and Richards' harmonic field condition for linear plane elasticity to isotropic laminated plates. To achieve our design objective, we make use of the complex variable formulation proposed by Beom and Earmme [1998] and developed recently by Wang and Zhou [2014] for the analysis of isotropic laminated plates.

2. Formulation

Consider an undeformed plate of uniform thickness h in a Cartesian coordinate system $\{x_i\}$ ($i = 1, 2, 3$) in which $x_3 = 0$ is on the main plane. The plate is composed of an isotropic, linearly elastic material that can be inhomogeneous and/or laminated in the thickness direction. Repeated Greek indices imply summation over the range of the index from 1 to 2.

The displacement field in the Kirchhoff plate theory takes the form

$$\tilde{u}_\alpha = u_\alpha + x_3 \vartheta_\alpha, \quad \tilde{u}_3 = w, \tag{1}$$

where the in-plane displacements u_α, deflection w, and the slopes $\vartheta_\alpha = -w_{,\alpha}$ on the main plane are all independent of x_3.

An integral operator is first introduced as follows: $Q(\cdot) = \int_{-h_0}^{h-h_0} (\cdot)\, dx_3$, with h_0 being the distance between the main plane and the lower surface of the plate. Then the constitutive equations of the laminated isotropic plate are [Beom and Earmme 1998]

$$\begin{aligned}
N_{\alpha\beta} &= A_{\alpha\beta\omega\rho}\varepsilon_{\omega\rho} + B_{\alpha\beta\omega\rho}\kappa_{\omega\rho}, \\
M_{\alpha\beta} &= B_{\alpha\beta\omega\rho}\varepsilon_{\omega\rho} + D_{\alpha\beta\omega\rho}\kappa_{\omega\rho},
\end{aligned} \tag{2}$$

where $N_{\alpha\beta}$ and $M_{\alpha\beta}$ are, respectively, the membrane stress resultants and bending moments defined by $N_{\alpha\beta} = Q\sigma_{\alpha\beta}$ and $M_{\alpha\beta} = Qx_3\sigma_{\alpha\beta}$, with $\sigma_{\alpha\beta}$ being the stresses; $\varepsilon_{\alpha\beta}$ and $\kappa_{\alpha\beta}$ are the main plane strains and curvatures, defined as $\varepsilon_{\alpha\beta} = \frac{1}{2}(u_{\alpha,\beta} + u_{\beta,\alpha})$ and $\kappa_{\alpha\beta} = -w_{,\alpha\beta}$; $A_{\alpha\beta\omega\rho}$, $B_{\alpha\beta\omega\rho}$ and $D_{\alpha\beta\omega\rho}$ are the extensional, coupling and bending stiffness tensors, given by

$$\begin{aligned}
A_{\alpha\beta\omega\rho} &= A_{12}\delta_{\alpha\beta}\delta_{\omega\rho} + \tfrac{1}{2}(A_{11} - A_{12})(\delta_{\alpha\omega}\delta_{\beta\rho} + \delta_{\alpha\rho}\delta_{\beta\omega}), \\
B_{\alpha\beta\omega\rho} &= B_{12}\delta_{\alpha\beta}\delta_{\omega\rho} - \tfrac{1}{2}B_{12}(\delta_{\alpha\omega}\delta_{\beta\rho} + \delta_{\alpha\rho}\delta_{\beta\omega}), \\
D_{\alpha\beta\omega\rho} &= D_{12}\delta_{\alpha\beta}\delta_{\omega\rho} + \tfrac{1}{2}(D_{11} - D_{12})(\delta_{\alpha\omega}\delta_{\beta\rho} + \delta_{\alpha\rho}\delta_{\beta\omega}),
\end{aligned} \tag{3}$$

with $\delta_{\alpha\beta}$ being the Kronecker delta, $A_{ij} = QC_{ij}$, $B_{ij} = Qx_3C_{ij}$, and $D_{ij} = Qx_3^2C_{ij}$ ($ij = 11, 12$). In addition, C_{11} and C_{12} can be expressed in terms of the Young's modulus $E = E(x_3)$ and Poisson's ratio $\nu = \nu(x_3)$ of the plate as $C_{11} = E/(1 - \nu^2)$ and $C_{12} = \nu E/(1 - \nu^2)$. Expression (3) implies that the main plane is chosen such that $B_{11} = 0$. Consequently, it is found that

$$h_0 = \frac{\int_0^h X_3 C_{11}\, dX_3}{\int_0^h C_{11}\, dX_3},$$

with $X_3 = x_3 + h_0$ being the vertical coordinate of the given point from the lowest surface of the plate.

In the absence of external loads on the top and bottom surfaces of the plate, the equilibrium equations are given by

$$N_{\alpha\beta,\beta} = 0, \quad R_{\beta,\beta} = 0, \tag{4}$$

where $R_\beta = M_{\alpha\beta,\alpha}$ are the transverse shearing forces.

Substitution of (2) into (4) yields the decoupled equations

$$(A_{11} + A_{12})u_{\beta,\beta\alpha} + (A_{11} - A_{12})u_{\alpha,\beta\beta} = 0, \quad w_{,\alpha\alpha\beta\beta} = 0. \tag{5}$$

By considering (5), the membrane stress resultants, bending moments, transverse shearing forces, in-plane displacements, deflection and slopes on the main plane of the plate, and the four stress functions φ_α and η_α can be expressed in terms of four analytic functions $\phi(z)$, $\psi(z)$, $\Phi(z)$ and $\Psi(z)$ of the complex variable $z = x_1 + \mathrm{i}x_2$ as [Beom and Earmme 1998; Cheng and Reddy 2002; Wang and Zhou 2014]

$$\begin{aligned}
N_{11} + N_{22} &= 4\,\mathrm{Re}\{\phi'(z) + B\Phi'(z)\}, \\
N_{22} - N_{11} + 2\mathrm{i}N_{12} &= 2\big(\bar{z}\phi''(z) + \psi'(z) + B\bar{z}\Phi''(z) + B\Psi'(z)\big),
\end{aligned} \tag{6}$$

$$\begin{aligned}
M_{11} + M_{22} &= 4D(1 + v^D)\,\mathrm{Re}\{\Phi'(z)\} + \frac{B(\kappa^A - 1)}{\mu}\,\mathrm{Re}\{\phi'(z)\}, \\
M_{22} - M_{11} + 2\mathrm{i}M_{12} &= -2D(1 - v^D)\big(\bar{z}\Phi''(z) + \Psi'(z)\big) - \frac{B}{\mu}\big(\bar{z}\phi''(z) + \psi'(z)\big), \tag{7} \\
R_1 - \mathrm{i}R_2 &= 4D\Phi''(z) + \frac{B(\kappa^A + 1)}{2\mu}\phi''(z),
\end{aligned}$$

$$\begin{aligned}
2\mu(u_1 + \mathrm{i}u_2) &= \kappa^A\phi(z) - z\overline{\phi'(z)} - \overline{\psi(z)}, \\
\vartheta_1 + \mathrm{i}\vartheta_2 &= \Phi(z) + z\overline{\Phi'(z)} + \overline{\Psi(z)}, \quad w = -\,\mathrm{Re}\{\bar{z}\Phi(z) + \chi(z)\}, \\
\varphi_1 + \mathrm{i}\varphi_2 &= \mathrm{i}\big(\phi(z) + z\overline{\phi'(z)} + \overline{\psi(z)}\big) + \mathrm{i}B\big(\Phi(z) + z\overline{\Phi'(z)} + \overline{\Psi(z)}\big), \tag{8} \\
\eta_1 + \mathrm{i}\eta_2 &= \mathrm{i}D(1 - v^D)\big(\kappa^D\Phi(z) - z\overline{\Phi'(z)} - \overline{\Psi(z)}\big) + \mathrm{i}\frac{B}{2\mu}\big(\kappa^A\phi(z) - z\overline{\phi'(z)} - \overline{\psi(z)}\big),
\end{aligned}$$

where $\Psi(z) = \chi'(z)$, and

$$\mu = \tfrac{1}{2}(A_{11} - A_{12}), \quad B = B_{12}, \quad D = D_{11}, \quad v^A = \frac{A_{12}}{A_{11}}, \quad v^D = \frac{D_{12}}{D_{11}},$$

$$\kappa^A = \frac{3A_{11} - A_{12}}{A_{11} + A_{12}} = \frac{3 - v^A}{1 + v^A}, \quad \kappa^D = \frac{3D_{11} + D_{12}}{D_{11} - D_{12}} = \frac{3 + v^D}{1 - v^D}. \tag{9}$$

Moreover, the membrane stress resultants, bending moments, transverse shearing forces, and modified Kirchhoff transverse shearing forces $V_1 = R_1 + M_{12,2}$ and $V_2 = R_2 + M_{21,1}$ can be expressed in terms of the four stress functions φ_α and η_α as [Cheng and Reddy 2002]

$$N_{\alpha\beta} = -\epsilon_{\beta\omega}\varphi_{\alpha,\omega}, \quad M_{\alpha\beta} = -\epsilon_{\beta\omega}\eta_{\alpha,\omega} - \tfrac{1}{2}\epsilon_{\alpha\beta}\eta_{\omega,\omega}, \quad R_\alpha = -\tfrac{1}{2}\epsilon_{\alpha\beta}\eta_{\omega,\omega\beta}, \quad V_\alpha = -\epsilon_{\alpha\omega}\eta_{\omega,\omega\omega}, \tag{10}$$

where $\epsilon_{\alpha\beta}$ are the components of the two-dimensional permutation tensor.

Now we consider a laminated plate subjected to remote uniform membrane stress resultants $N_{\alpha\beta}^\infty$ and bending moments $M_{\alpha\beta}^\infty$. The asymptotic behaviors of $\phi(z)$, $\psi(z)$, $\Phi(z)$ and $\Psi(z)$ at infinity can then be

simply derived as

$$\phi(z) \cong \delta_1 z + O(1), \quad \psi(z) \cong \delta_2 z + O(1), \quad \Phi(z) \cong \gamma_1 z + O(1), \quad \Psi(z) \cong \gamma_2 z + O(1), \tag{11}$$

where the two real constants δ_1, γ_1 and the two complex constants δ_2, γ_2 are related to the remote uniform loading through

$$
\begin{aligned}
\delta_1 &= \frac{\mu D(1+\nu^D)(N_{11}^\infty + N_{22}^\infty) - B\mu(M_{11}^\infty + M_{22}^\infty)}{4\mu D(1+\nu^D) - B^2(\kappa^A - 1)}, \\
\gamma_1 &= \frac{4\mu(M_{11}^\infty + M_{22}^\infty) - B(\kappa^A - 1)(N_{11}^\infty + N_{22}^\infty)}{16\mu D(1+\nu^D) - 4B^2(\kappa^A - 1)}, \\
\delta_2 &= \frac{\mu D(1-\nu^D)(N_{22}^\infty - N_{11}^\infty + 2iN_{12}^\infty) + B\mu(M_{22}^\infty - M_{11}^\infty + 2iM_{12}^\infty)}{2\mu D(1-\nu^D) - B^2}, \\
\gamma_2 &= \frac{-2\mu(M_{22}^\infty - M_{11}^\infty + 2iM_{12}^\infty) - B(N_{22}^\infty - N_{11}^\infty + 2iN_{12}^\infty)}{4\mu D(1-\nu^D) - 2B^2}.
\end{aligned}
\tag{12}
$$

In the context of an isotropic laminated plate, Bjorkman and Richards' harmonic field conditions now become that the two sums $N_{11} + N_{22}$ and $M_{11} + M_{22}$ remain unchanged everywhere in the surrounding laminated plate after the introduction of the harmonic hole or inclusion. It is further deduced from $(6)_1$ and $(7)_1$ that $\phi(z)$ and $\Phi(z)$ must take the following form in order to ensure that the shape is harmonic:

$$\phi(z) = \delta_1 z, \quad \Phi(z) = \gamma_1 z. \tag{13}$$

In the next two sections we will address in detail a single harmonic hole or rigid inclusion and two interacting harmonic shapes.

3. A single harmonic hole or rigid inclusion

The single harmonic hole or rigid inclusion forms a simply connected bounded domain with Lipschitz boundary. As such, we consider the conformal mapping function [Kantorovich and Krylov 1950]

$$z = \omega(\xi) = R\Big(\xi + \frac{a_1}{\xi} + \frac{a_2}{\xi^2} + \cdots\Big), \quad \xi(z) = \omega^{-1}(z), \quad |\xi| \ge 1, \tag{14}$$

where R is a real scaling constant and a_i ($i = 1, 2, \dots$) are complex constants. This function conformally maps the exterior of the hole or the rigid inclusion in the z-plane onto the exterior of the unit circle $|\xi| = 1$ in the ξ-plane. For convenience, we write $\psi(z) = \psi(\omega(\xi)) = \psi(\xi)$ and $\Psi(z) = \Psi(\omega(\xi)) = \Psi(\xi)$.

3.1. *A single harmonic hole.* In this case, $\varphi_1 = \varphi_2 = \eta_1 = \eta_2 = 0$ along the edge of the hole. By enforcing this free edge boundary condition on $|\xi| = 1$, we arrive at these expressions for $\psi(\xi)$ and $\Psi(\xi)$:

$$
\begin{aligned}
\psi(\xi) &= \frac{-\big(4\mu D(1-\nu^D) + B^2(\kappa^A - 1)\big)\delta_1 - 8B\mu D\gamma_1}{2\mu D(1-\nu^D) - B^2} R\Big(\frac{1}{\xi} + \bar{a}_1\xi + \bar{a}_2\xi^2 + \cdots\Big), \\
\Psi(\xi) &= \frac{B(\kappa^A + 1)\delta_1 + \big(4\mu D(1+\nu^D) + 2B^2\big)\gamma_1}{2\mu D(1-\nu^D) - B^2} R\Big(\frac{1}{\xi} + \bar{a}_1\xi + \bar{a}_2\xi^2 + \cdots\Big).
\end{aligned}
\tag{15}
$$

By satisfying the asymptotic conditions for $\psi(z)$ and $\Psi(z)$ in the second and fourth expressions of (11), we obtain

$$a_2 = a_3 = \cdots = 0, \tag{16}$$

which implies that the harmonic hole must be of elliptical shape, and

$$
\begin{aligned}
\delta_2 &= \frac{-\left(4\mu D(1-v^D)+B^2(\kappa^A-1)\right)\delta_1 - 8B\mu D\gamma_1}{2\mu D(1-v^D)-B^2}\bar{a}_1, \\
\gamma_2 &= \frac{B(\kappa^A+1)\delta_1 + \left(4\mu D(1+v^D)+2B^2\right)\gamma_1}{2\mu D(1-v^D)-B^2}\bar{a}_1.
\end{aligned}
\tag{17}
$$

Consequently, the remote uniform loading should satisfy the restrictions

$$\frac{N_{11}^\infty - N_{22}^\infty - 2iN_{12}^\infty}{N_{11}^\infty + N_{22}^\infty} = \frac{M_{11}^\infty - M_{22}^\infty - 2iM_{12}^\infty}{M_{11}^\infty + M_{22}^\infty} = \bar{a}_1. \tag{18}$$

The hoop membrane stress resultant $N_{\theta\theta}$ and hoop bending moment $M_{\theta\theta}$ are both constant along the boundary of the elliptic hole:

$$N_{\theta\theta} = N_{11}^\infty + N_{22}^\infty, \quad M_{\theta\theta} = M_{11}^\infty + M_{22}^\infty. \tag{19}$$

Similar to the argument by Bjorkman and Richards [1976], the harmonic hole simultaneously produces minimum values of $N_{\theta\theta}$ and $M_{\theta\theta}$, and thus is optimal. We note that (18) and (19) are in agreement with the corresponding results in [ibid.] for a harmonic hole in an isotropic and homogeneous plate subjected to in-plane loading.

3.2. *A single harmonic rigid inclusion.* In this case, $u_1 = u_2 = \vartheta_1 = \vartheta_2 = 0$ along the edge of the rigid inclusion. By enforcing this boundary condition for a rigidly clamped edge on $|\xi| = 1$, we arrive at these expressions for $\psi(\xi)$ and $\Psi(\xi)$:

$$
\begin{aligned}
\psi(\xi) &= (\kappa^A-1)\delta_1 R\left(\frac{1}{\xi} + \bar{a}_1\xi + \bar{a}_2\xi^2 + \cdots\right), \\
\Psi(\xi) &= -2\gamma_1 R\left(\frac{1}{\xi} + \bar{a}_1\xi + \bar{a}_2\xi^2 + \cdots\right).
\end{aligned}
\tag{20}
$$

By satisfying the asymptotic conditions on $\psi(z)$ and $\Psi(z)$ in the second and fourth expressions of (11), we obtain

$$a_2 = a_3 = \cdots = 0, \tag{21}$$

which implies that the harmonic rigid inclusion must be elliptical and

$$\delta_2 = (\kappa^A-1)\delta_1\bar{a}_1, \quad \gamma_2 = -2\gamma_1\bar{a}_1. \tag{22}$$

Thus, the remote uniform loading should satisfy the restrictions

$$
\begin{aligned}
&\frac{\left(4\mu D(1+v^D)-B^2(\kappa^A-1)\right)(N_{22}^\infty - N_{11}^\infty + 2iN_{12}^\infty)}{\left(2\mu D(1+v^D)+B^2\right)(\kappa^A-1)(N_{11}^\infty + N_{22}^\infty) - 2B\mu(\kappa^A+1)(M_{11}^\infty + M_{22}^\infty)} \\
&= \frac{\left(4\mu D(1+v^D)-B^2(\kappa^A-1)\right)(M_{22}^\infty - M_{11}^\infty + 2iM_{12}^\infty)}{\left(4\mu D(1-v^D)+B^2(\kappa^A-1)\right)(M_{11}^\infty + M_{22}^\infty) - 2BD(\kappa^A-1)(N_{11}^\infty + N_{22}^\infty)} = \bar{a}_1.
\end{aligned}
\tag{23}
$$

The interfacial normal membrane stress resultant $N_{\rho\rho}$ and interfacial normal bending moment $M_{\rho\rho}$ are uniformly distributed along the inclusion/matrix interface as

$$N_{\rho\rho} = (\kappa^A + 1)\delta_1, \quad M_{\rho\rho} = 4D\gamma_1, \tag{24}$$

where δ_1, γ_1 are as in (12).

The hoop membrane stress resultant and hoop bending moment are both constant along the inclusion/matrix interface on the matrix side and are given by

$$
\begin{aligned}
N_{\theta\theta} &= \frac{\left(\mu D(1+\nu^D)(3-\kappa^A) - B^2(\kappa^A-1)\right)(N_{11}^\infty + N_{22}^\infty) + B\mu(\kappa^A+1)(M_{11}^\infty + M_{22}^\infty)}{4\mu D(1+\nu^D) - B^2(\kappa^A-1)}, \\
M_{\theta\theta} &= \frac{\left(4\mu D\nu^D - B^2(\kappa^A-1)\right)(M_{11}^\infty + M_{22}^\infty) + BD(\kappa^A-1)(N_{11}^\infty + N_{22}^\infty)}{4\mu D(1+\nu^D) - B^2(\kappa^A-1)}.
\end{aligned}
\tag{25}
$$

When $B = 0$, (23)–(25) reduce to

$$\frac{2(N_{22}^\infty - N_{11}^\infty + 2iN_{12}^\infty)}{(\kappa^A-1)(N_{11}^\infty + N_{22}^\infty)} = \bar{a}_1, \quad N_{\rho\rho} = \frac{\kappa^A+1}{4}(N_{11}^\infty + N_{22}^\infty), \quad N_{\theta\theta} = \frac{3-\kappa^A}{4}(N_{11}^\infty + N_{22}^\infty), \tag{26}$$

$$\frac{(1+\nu^D)(M_{22}^\infty - M_{11}^\infty + 2iM_{12}^\infty)}{(1-\nu^D)(M_{11}^\infty + M_{22}^\infty)} = \bar{a}_1, \quad M_{\rho\rho} = \frac{M_{11}^\infty + M_{22}^\infty}{1+\nu^D}, \quad M_{\theta\theta} = \frac{\nu^D(M_{11}^\infty + M_{22}^\infty)}{1+\nu^D}. \tag{27}$$

The results in (26) agree with those in [Bjorkman and Richards 1979b] for a harmonic rigid inclusion in an isotropic and homogeneous plate under in-plane loads.

4. Two interacting harmonic shapes

In order to obtain two interacting harmonic shapes (which include three typical cases: (i) two interacting harmonic holes, (ii) two interacting harmonic rigid inclusions, and (iii) one harmonic hole interacting with another harmonic rigid inclusion), we first introduce the conformal mapping function [Wang 2012]

$$z = \omega(\xi) = R\left(\frac{1}{\xi-\lambda} + \frac{a}{\xi-\lambda^{-1}} + \frac{\Lambda^{-1}a}{\rho\xi-\lambda^{-1}} + \sum_{n=1}^\infty (a_n\xi^n + a_{-n}\xi^{-n})\right),$$

$$\xi(z) = \omega^{-1}(z), \quad 1 \le |\xi| \le \rho^{-1/2}, \tag{28}$$

where R is a real scaling constant, λ is a real constant with $1 < |\lambda| < \rho^{-1/2}$, a and Λ are complex constants, and a_n, a_{-n} are complex constants to be determined. In (28), the first-order pole at $\xi = \lambda$ is located within the annulus $1 \le |\xi| \le \rho^{-1/2}$, whereas the two first-order poles at $\xi = \lambda^{-1}$ and $\xi = (\rho\lambda)^{-1}$ are both located outside the annulus. The function (28) will conformally map the matrix region (excluding the two harmonic shapes) in the z-plane onto an annulus $1 \le |\xi| \le \rho^{-1/2}$ in the ξ-plane, and the left and right interfaces L_1 and L_2 formed between the two harmonic shapes and the matrix are mapped onto two coaxial circles with radii 1 and $\rho^{-1/2}$, respectively, in the ξ-plane. It is also apparent that each of the two interacting shapes will be nonelliptical [Wang 2012].

4.1. *Two interacting harmonic holes.* By enforcing the free edge boundary condition on the inner circle $|\xi| = 1$, we obtain these expressions for $\psi(\xi)$ and $\Psi(\xi)$:

$$\psi(\xi) = \frac{-\big(4\mu D(1 - \nu^D) + B^2(\kappa^A - 1)\big)\delta_1 - 8B\mu D\gamma_1}{2\mu D(1 - \nu^D) - B^2}$$
$$\times R\bigg(\frac{1}{\xi^{-1} - \lambda} - \frac{\bar{a}\lambda^2}{\xi - \lambda} + \frac{\bar{\Lambda}^{-1}\bar{a}}{\rho\xi^{-1} - \lambda^{-1}} + \sum_{n=1}^{\infty}(\bar{a}_n\xi^{-n} + \bar{a}_{-n}\xi^n)\bigg),$$

$$\Psi(\xi) = \frac{B(\kappa^A + 1)\delta_1 + \big(4\mu D(1 + \nu^D) + 2B^2\big)\gamma_1}{2\mu D(1 - \nu^D) - B^2}$$
$$\times R\bigg(\frac{1}{\xi^{-1} - \lambda} - \frac{\bar{a}\lambda^2}{\xi - \lambda} + \frac{\bar{\Lambda}^{-1}\bar{a}}{\rho\xi^{-1} - \lambda^{-1}} + \sum_{n=1}^{\infty}(\bar{a}_n\xi^{-n} + \bar{a}_{-n}\xi^n)\bigg). \tag{29}$$

Similarly, by enforcing the free-edge boundary condition on the outer circle $|\xi| = \rho^{-1/2}$, we obtain another set of expressions for $\psi(\xi)$ and $\Psi(\xi)$:

$$\psi(\xi) = \frac{-\big(4\mu D(1 - \nu^D) + B^2(\kappa^A - 1)\big)\delta_1 - 8B\mu D\gamma_1}{2\mu D(1 - \nu^D) - B^2}$$
$$\times R\bigg(\frac{\lambda^{-1}}{1 - \rho\lambda\xi} + \frac{\bar{a}}{\rho^{-1}\xi^{-1} - \lambda^{-1}} - \frac{\bar{\Lambda}^{-1}\bar{a}\lambda^2}{\xi - \lambda} + \sum_{n=1}^{\infty}(\bar{a}_n\rho^{-n}\xi^{-n} + \bar{a}_{-n}\rho^n\xi^n)\bigg),$$

$$\Psi(\xi) = \frac{B(\kappa^A + 1)\delta_1 + \big(4\mu D(1 + \nu^D) + 2B^2\big)\gamma_1}{2\mu D(1 - \nu^D) - B^2}$$
$$\times R\bigg(\frac{\lambda^{-1}}{1 - \rho\lambda\xi} + \frac{\bar{a}}{\rho^{-1}\xi^{-1} - \lambda^{-1}} - \frac{\bar{\Lambda}^{-1}\bar{a}\lambda^2}{\xi - \lambda} + \sum_{n=1}^{\infty}(\bar{a}_n\rho^{-n}\xi^{-n} + \bar{a}_{-n}\rho^n\xi^n)\bigg). \tag{30}$$

The two expressions for $\psi(\xi)$ and $\Psi(\xi)$ obtained in (29) and (30) must coincide. As a result, the unknown parameters in (28) are given by

$$\Lambda = \bar{\Lambda} = 1, \quad a_n = \frac{\lambda^{-n-1} + a\rho^n\lambda^{n+1}}{1 - \rho^{-n}}, \quad a_{-n} = \frac{\lambda^{n-1} + a\lambda^{-n+1}}{\rho^{-n} - 1}, \quad n = 1, 2, \ldots. \tag{31}$$

Remark. The interacting harmonic shapes can now be uniquely determined using (28) for given real numbers Λ, ρ, λ and a given complex number a.

In addition, the satisfaction of the remote boundary conditions on $\psi(z)$ and $\Psi(z)$ in the second and fourth expressions of (11) will yield

$$\delta_2 = -\frac{-\big(4\mu D(1 - \nu^D) + B^2(\kappa^A - 1)\big)\delta_1 - 8B\mu D\gamma_1}{2\mu D(1 - \nu^D) - B^2}\bar{a}\lambda^2,$$
$$\gamma_2 = -\frac{B(\kappa^A + 1)\delta_1 + \big(4\mu D(1 + \nu^D) + 2B^2\big)\gamma_1}{2\mu D(1 - \nu^D) - B^2}\bar{a}\lambda^2. \tag{32}$$

Thus, the remote uniform loading should satisfy the restrictions

$$\frac{N_{11}^\infty - N_{22}^\infty - 2iN_{12}^\infty}{N_{11}^\infty + N_{22}^\infty} = \frac{M_{11}^\infty - M_{22}^\infty - 2iM_{12}^\infty}{M_{11}^\infty + M_{22}^\infty} = -\bar{a}\lambda^2. \tag{33}$$

The hoop membrane stress resultant and hoop bending moment are both uniformly distributed along the boundary of the two harmonic holes as

$$N_{\theta\theta} = N_{11}^\infty + N_{22}^\infty, \quad M_{\theta\theta} = M_{11}^\infty + M_{22}^\infty, \quad z \in L_1 \cup L_2. \tag{34}$$

4.2. *Two interacting harmonic rigid inclusions.* By enforcing the boundary condition for a rigidly clamped edge on the inner circle $|\xi| = 1$, we obtain these expressions for $\psi(\xi)$ and $\Psi(\xi)$:

$$\psi(\xi) = (\kappa^A - 1)\delta_1 R\left(\frac{1}{\xi^{-1} - \lambda} - \frac{\bar{a}\lambda^2}{\xi - \lambda} + \frac{\bar{\Lambda}^{-1}\bar{a}}{\rho\xi^{-1} - \lambda^{-1}} + \sum_{n=1}^\infty (\bar{a}_n\xi^{-n} + \bar{a}_{-n}\xi^n)\right),$$

$$\Psi(\xi) = -2\gamma_1 R\left(\frac{1}{\xi^{-1} - \lambda} - \frac{\bar{a}\lambda^2}{\xi - \lambda} + \frac{\bar{\Lambda}^{-1}\bar{a}}{\rho\xi^{-1} - \lambda^{-1}} + \sum_{n=1}^\infty (\bar{a}_n\xi^{-n} + \bar{a}_{-n}\xi^n)\right). \tag{35}$$

Similarly, by enforcing the boundary condition for a rigidly clamped edge on the outer circle $|\xi| = \rho^{-1/2}$, we again obtain a second set of expressions for $\psi(\xi)$ and $\Psi(\xi)$:

$$\psi(\xi) = (\kappa^A - 1)\delta_1 R\left(\frac{\lambda^{-1}}{1 - \rho\lambda\xi} + \frac{\bar{a}}{\rho^{-1}\xi^{-1} - \lambda^{-1}} - \frac{\bar{\Lambda}^{-1}\bar{a}\lambda^2}{\xi - \lambda} + \sum_{n=1}^\infty (\bar{a}_n\rho^{-n}\xi^{-n} + \bar{a}_{-n}\rho^n\xi^n)\right),$$

$$\Psi(\xi) = -2\gamma_1 R\left(\frac{\lambda^{-1}}{1 - \rho\lambda\xi} + \frac{\bar{a}}{\rho^{-1}\xi^{-1} - \lambda^{-1}} - \frac{\bar{\Lambda}^{-1}\bar{a}\lambda^2}{\xi - \lambda} + \sum_{n=1}^\infty (\bar{a}_n\rho^{-n}\xi^{-n} + \bar{a}_{-n}\rho^n\xi^n)\right). \tag{36}$$

Equating the two expression for $\psi(\xi)$ and $\Psi(\xi)$, we obtain $\Lambda = 1$; a_n and a_{-n} in (28) can also be determined from (31).

In addition, the satisfaction of the remote boundary conditions on $\psi(z)$ and $\Psi(z)$ in the second and fourth expressions of (11) yields

$$\delta_2 = -(\kappa^A - 1)\delta_1\bar{a}\lambda^2, \quad \gamma_2 = 2\gamma_1\bar{a}\lambda^2. \tag{37}$$

Thus, the remote uniform loading is constrained by the equations

$$\frac{\left(4\mu D(1 + v^D) - B^2(\kappa^A - 1)\right)(N_{22}^\infty - N_{11}^\infty + 2iN_{12}^\infty)}{\left(2\mu D(1 + v^D) + B^2\right)(\kappa^A - 1)(N_{11}^\infty + N_{22}^\infty) - 2B\mu(\kappa^A + 1)(M_{11}^\infty + M_{22}^\infty)}$$

$$= \frac{\left(4\mu D(1 + v^D) - B^2(\kappa^A - 1)\right)(M_{22}^\infty - M_{11}^\infty + 2iM_{12}^\infty)}{\left(4\mu D(1 - v^D) + B^2(\kappa^A - 1)\right)(M_{11}^\infty + M_{22}^\infty) - 2BD(\kappa^A - 1)(N_{11}^\infty + N_{22}^\infty)} = -\bar{a}\lambda^2. \tag{38}$$

The interfacial normal membrane stress resultant and interfacial normal bending moment are uniformly distributed along the two inclusion/matrix interfaces as

$$N_{\rho\rho} = (\kappa^A + 1)\delta_1, \quad M_{\rho\rho} = 4D\gamma_1, \quad z \in L_1 \cup L_2. \tag{39}$$

The hoop membrane stress resultant and hoop bending moment are both constant along the two inclusion/matrix interfaces on the matrix side and are given by

$$N_{\theta\theta} = \frac{\left(\mu D(1+\nu^D)(3-\kappa^A) - B^2(\kappa^A-1)\right)(N_{11}^\infty + N_{22}^\infty) + B\mu(\kappa^A+1)(M_{11}^\infty + M_{22}^\infty)}{4\mu D(1+\nu^D) - B^2(\kappa^A-1)},$$

$$M_{\theta\theta} = \frac{\left(4\mu D\nu^D - B^2(\kappa^A-1)\right)(M_{11}^\infty + M_{22}^\infty) + BD(\kappa^A-1)(N_{11}^\infty + N_{22}^\infty)}{4\mu D(1+\nu^D) - B^2(\kappa^A-1)}, \quad z \in L_1 \cup L_2. \tag{40}$$

4.3. *A harmonic hole interacting with a harmonic rigid inclusion.* Without loss of generality, we assume that the left-hand shape is a hole, whilst the right-hand shape is a rigid inclusion. By enforcing the free edge boundary condition on the inner circle $|\xi| = 1$, we obtain these expressions for $\psi(\xi)$ and $\Psi(\xi)$:

$$\psi(\xi) = \frac{-\left(4\mu D(1-\nu^D) + B^2(\kappa^A-1)\right)\delta_1 - 8B\mu D\gamma_1}{2\mu D(1-\nu^D) - B^2}$$

$$\times R\left(\frac{1}{\xi^{-1} - \lambda} - \frac{\bar{a}\lambda^2}{\xi - \lambda} + \frac{\bar{\Lambda}^{-1}\bar{a}}{\rho\xi^{-1} - \lambda^{-1}} + \sum_{n=1}^\infty (\bar{a}_n\xi^{-n} + \bar{a}_{-n}\xi^n)\right),$$

$$\Psi(\xi) = \frac{B(\kappa^A+1)\delta_1 + \left(4\mu D(1+\nu^D) + 2B^2\right)\gamma_1}{2\mu D(1-\nu^D) - B^2}$$

$$\times R\left(\frac{1}{\xi^{-1} - \lambda} - \frac{\bar{a}\lambda^2}{\xi - \lambda} + \frac{\bar{\Lambda}^{-1}\bar{a}}{\rho\xi^{-1} - \lambda^{-1}} + \sum_{n=1}^\infty (\bar{a}_n\xi^{-n} + \bar{a}_{-n}\xi^n)\right). \tag{41}$$

By enforcing the boundary condition for a rigidly clamped edge on the outer circle $|\xi| = \rho^{-1/2}$, we obtain a second set of expressions for $\psi(\xi)$ and $\Psi(\xi)$:

$$\psi(\xi) = (\kappa^A-1)\delta_1 R\left(\frac{\lambda^{-1}}{1-\rho\lambda\xi} + \frac{\bar{a}}{\rho^{-1}\xi^{-1} - \lambda^{-1}} - \frac{\bar{\Lambda}^{-1}\bar{a}\lambda^2}{\xi - \lambda} + \sum_{n=1}^\infty (\bar{a}_n\rho^{-n}\xi^{-n} + \bar{a}_{-n}\rho^n\xi^n)\right),$$

$$\Psi(\xi) = -2\gamma_1 R\left(\frac{\lambda^{-1}}{1-\rho\lambda\xi} + \frac{\bar{a}}{\rho^{-1}\xi^{-1} - \lambda^{-1}} - \frac{\bar{\Lambda}^{-1}\bar{a}\lambda^2}{\xi - \lambda} + \sum_{n=1}^\infty (\bar{a}_n\rho^{-n}\xi^{-n} + \bar{a}_{-n}\rho^n\xi^n)\right). \tag{42}$$

Equating the two expressions for each of $\psi(\xi)$ and $\Psi(\xi)$, we obtain the expressions

$$\Lambda = \bar{\Lambda} = -\frac{(\kappa^A-1)\left(2\mu D(1-\nu^D) - B^2\right)\delta_1}{\left(4\mu D(1-\nu^D) + B^2(\kappa^A-1)\right)\delta_1 + 8B\mu D\gamma_1}$$

$$= -\frac{2\left(2\mu D(1-\nu^D) - B^2\right)\gamma_1}{B(\kappa^A+1)\delta_1 + \left(4\mu D(1+\nu^D) + 2B^2\right)\gamma_1} \tag{43}$$

for the unknown parameters in (28), and

$$a_n = \frac{\lambda^{-n-1} + a\Lambda^{-1}\rho^n\lambda^{n+1}}{1 - \Lambda\rho^{-n}}, \quad a_{-n} = \frac{\lambda^{n-1} + a\lambda^{-n+1}}{\Lambda^{-1}\rho^{-n} - 1}, \quad n = 1, 2, \ldots. \tag{44}$$

It can be further deduced from (43) that the two sums $N_{11}^\infty + N_{22}^\infty$ and $M_{11}^\infty + M_{22}^\infty$ cannot be set arbitrarily, and should satisfy the restriction

$$\frac{B(N_{11}^\infty + N_{22}^\infty)}{\mu(M_{11}^\infty + M_{22}^\infty)} = \alpha, \tag{45}$$

where

$$\alpha = \frac{\nu^A - \nu^D \pm \sqrt{(\nu^A - \nu^D)^2 + 2\beta(1 - \nu^A)}}{1 - \nu^A}, \quad \beta = \frac{B^2}{\mu D} > 0. \tag{46}$$

As a result, the parameter Λ in (43) can be more explicitly determined as

$$\Lambda = -\frac{(\kappa^A - 1)\big(2(1 - \nu^D) - \beta\big)\big(2 + \nu^A + \nu^D - \sqrt{(\nu^A - \nu^D)^2 + 2\beta(1 - \nu^A)}\big)}{\big(4(1 + \nu^D) - \beta(\kappa^A - 1)\big)\big(2 - \nu^A - \nu^D + \sqrt{(\nu^A - \nu^D)^2 + 2\beta(1 - \nu^A)}\big)} \tag{47}$$

if the plus sign is chosen in (46), and

$$\Lambda = -\frac{(\kappa^A - 1)\big(2(1 - \nu^D) - \beta\big)\big(2 + \nu^A + \nu^D + \sqrt{(\nu^A - \nu^D)^2 + 2\beta(1 - \nu^A)}\big)}{\big(4(1 + \nu^D) - \beta(\kappa^A - 1)\big)\big(2 - \nu^A - \nu^D - \sqrt{(\nu^A - \nu^D)^2 + 2\beta(1 - \nu^A)}\big)} \tag{48}$$

if the minus sign is chosen in (46). Equations (47) and (48) suggest that there are two distinct values of Λ for given material parameters ν^A, ν^D and β.

For example, if we set $\nu^A = \frac{1}{4}$, $\nu^D = 0.3$, $\beta = 0.2$, then $\alpha = 0.6667$ and $\Lambda = -0.2903$, or $\alpha = -0.8$ and $\Lambda = -1$.

In addition, the satisfaction of the remote boundary conditions for $\psi(z)$ and $\Psi(z)$ in the second and fourth expressions of (11) yields

$$\delta_2 = -\frac{-\big(4\mu D(1 - \nu^D) + B^2(\kappa^A - 1)\big)\delta_1 - 8B\mu D\gamma_1}{2\mu D(1 - \nu^D) - B^2}\bar{a}\lambda^2,$$

$$\gamma_2 = -\frac{B(\kappa^A + 1)\delta_1 + \big(4\mu D(1 + \nu^D) + 2B^2\big)\gamma_1}{2\mu D(1 - \nu^D) - B^2}\bar{a}\lambda^2. \tag{49}$$

Thus, in addition to condition (45), the remote uniform loading should also satisfy the restrictions

$$\frac{N_{11}^\infty - N_{22}^\infty - 2iN_{12}^\infty}{N_{11}^\infty + N_{22}^\infty} = \frac{M_{11}^\infty - M_{22}^\infty - 2iM_{12}^\infty}{M_{11}^\infty + M_{22}^\infty} = -\bar{a}\lambda^2. \tag{50}$$

The hoop membrane stress resultant and hoop bending moment are both uniformly distributed along the boundary of the left harmonic hole as

$$N_{\theta\theta} = N_{11}^\infty + N_{22}^\infty, \quad M_{\theta\theta} = M_{11}^\infty + M_{22}^\infty, \quad z \in L_1. \tag{51}$$

Meanwhile, the interfacial normal membrane stress resultant and interfacial normal bending moment are uniformly distributed along the right inclusion/matrix interface as

$$N_{\rho\rho} = \frac{(\kappa^A + 1)(1 + \nu^D - \frac{\beta}{\alpha})}{4(1 + \nu^D) - \beta(\kappa^A - 1)}(N_{11}^\infty + N_{22}^\infty),$$

$$M_{\rho\rho} = \frac{4 - \alpha(\kappa^A - 1)}{4(1 + \nu^D) - \beta(\kappa^A - 1)}(M_{11}^\infty + M_{22}^\infty), \quad z \in L_2. \tag{52}$$

The hoop membrane stress resultant and hoop bending moment are both constant along the right inclusion/matrix interface on the matrix side, and are given by

$$N_{\theta\theta} = \frac{(1 + \nu^D)(3 - \kappa^A) + \frac{\beta}{\alpha}(\kappa^A + 1) - \beta(\kappa^A - 1)}{4(1 + \nu^D) - \beta(\kappa^A - 1)}(N_{11}^\infty + N_{22}^\infty),$$

$$M_{\theta\theta} = \frac{4\nu^D + (\alpha - \beta)(\kappa^A - 1)}{4(1 + \nu^D) - \beta(\kappa^A - 1)}(M_{11}^\infty + M_{22}^\infty), \quad z \in L_2.$$

(53)

5. Conclusions

We have proposed a new harmonic condition in the context of isotropic laminated plates. By imposing this condition and by using the complex variable formulation for a laminated plate [Beom and Earmme 1998; Wang and Zhou 2014], we have successfully obtained (i) a single harmonic hole, (ii) a single harmonic rigid inclusion, (iii) two interacting harmonic holes, (iv) two interacting harmonic rigid inclusions, and (v) a harmonic hole interacting with another harmonic rigid inclusion when the laminated plate is subjected to remote uniform membrane stress resultants and bending moments. It is shown that a single harmonic hole or rigid inclusion must be elliptical in shape and that the remote uniform loading should satisfy (18) for a harmonic hole, or (23) for a harmonic rigid inclusion. Our results in Section 4 show that it is permissible to obtain two interacting nonelliptical harmonic shapes composed of (i) two holes, (ii) two rigid inclusions, or (iii) one hole near another rigid inclusion. For the case of two interacting harmonic holes or two interacting harmonic rigid inclusions, $\Lambda \equiv 1$ in (28); for the case of one harmonic hole interacting with another harmonic rigid inclusion, Λ is determined by Equations (47) and (48). The remote loading condition (33) for two interacting harmonic holes is identical in form to (18) for a single harmonic hole, the remote loading condition (38) for two interacting harmonic rigid inclusions is identical in form to (23) for a single harmonic rigid inclusion, whereas the remote loading conditions (45) and (50) for a harmonic hole interacting with another harmonic rigid inclusion are more stringent. It is observed that for all the cases discussed, the hoop membrane stress resultant and hoop bending moments are always constant along any existing boundary and interface (see (19), (25), (34), (40), (51) and (53)). Thus, the obtained harmonic shapes also satisfy the equal strength condition.

Acknowledgements

References

[Beom and Earmme 1998] H. G. Beom and Y. Y. Earmme, "Complex variable method for problems of a laminate composed of multiple isotropic layers", *Int. J. Fract.* **92**:4 (1998), 305–324.

[Bjorkman and Richards 1976] G. S. Bjorkman, Jr. and R. Richards, Jr., "Harmonic holes: an inverse problem in elasticity", *J. Appl. Mech.* (*ASME*) **43** (1976), 414–418.

[Bjorkman and Richards 1979a] G. S. Bjorkman, Jr. and R. Richards, Jr., "Harmonic holes for nonconstant fields", *J. Appl. Mech.* (*ASME*) **46**:3 (1979), 573–576.

[Bjorkman and Richards 1979b] G. S. Bjorkman, Jr. and R. Richards, Jr., "The rigid harmonic inclusion", pp. 781–784 in *Proceedings of the Third Engineering Mechanics Division Specialty Conference* (Austin, TX, 1979), edited by C. P. Johnson, ASCE, New York, 1979.

[Bonnet and Constantinescu 2005] M. Bonnet and A. Constantinescu, "Inverse problems in elasticity", *Inverse Probl.* **21**:2 (2005), R1–R50.

[Budiansky et al. 1993] B. Budiansky, J. W. Hutchinson, and A. G. Evans, "On neutral holes in tailored, layered sheets", *J. Appl. Mech.* (*ASME*) **60**:4 (1993), 1056–1058.

[Bui 1993] H. D. Bui, *Introduction aux problèmes inverses en mécanique des máteriaux*, Eyrolles, Paris, 1993. Translated as *Inverse problems in the mechanics of materials: an introduction*, CRC Press, Boca Raton, FL, 1994.

[Cheng and Reddy 2002] Z.-Q. Cheng and J. N. Reddy, "Octet formalism for Kirchhoff anisotropic plates", *Phil. Trans. R. Soc. A* **458**:2022 (2002), 1499–1517.

[Cheng and Reddy 2003] Z.-Q. Cheng and J. N. Reddy, "Green's functions for infinite and semi-infinite anisotropic thin plates", *J. Appl. Mech.* (*ASME*) **70**:2 (2003), 260–267.

[Cheng and Reddy 2004a] Z.-Q. Cheng and J. N. Reddy, "Green's functions for an anisotropic thin plate with a crack or an anticrack", *Int. J. Eng. Sci.* **42**:3–4 (2004), 271–289.

[Cheng and Reddy 2004b] Z.-Q. Cheng and J. N. Reddy, "Laminated anisotropic thin plate with an elliptic inhomogeneity", *Mech. Mater.* **36**:7 (2004), 647–657.

[Cherepanov 1974] G. P. Cherepanov, "Обратные задачи теории упругости", *Prikl. Mat. Mekh.* **38**:6 (1974), 963–979. Translated as "Inverse problems of the plane theory of elasticity"*J. Appl. Math. Mech.* **38**:6 (1974), 915–931.

[Hasebe and Wang 2000] N. Hasebe and X.-F. Wang, "Green's functions of thin plate bending problem under fixed boundary", *J. Eng. Mech.* (*ASCE*) **126**:2 (2000), 206–213.

[Hasebe and Wang 2002] N. Hasebe and X.-F. Wang, "Green's functions for the bending of thin plates under various boundary conditions and applications: a review", *Thin-Walled Struct.* **40**:7–8 (2002), 611–624.

[Kantorovich and Krylov 1950] L. V. Kantorovich and V. I. Krylov, Приближенные методы высшего анализа, 3rd ed., State Publishing House of Technical Literature, Moscow, 1950. Translated as *Approximate methods of higher analysis*, Wiley, New York, 1958.

[Mansfield 1953] E. H. Mansfield, "Neutral holes in plane sheet: reinforced holes which are elastically equivalent to the uncut sheet", *Quart. J. Mech. Appl. Math.* **6** (1953), 370–378.

[Milton and Serkov 2001] G. W. Milton and S. K. Serkov, "Neutral coated inclusions in conductivity and anti-plane elasticity", *Phil. Trans. R. Soc. A* **457**:2012 (2001), 1973–1997.

[Ru 1998] C.-Q. Ru, "Interface design of neutral elastic inclusions", *Int. J. Solids Struct.* **35**:7–8 (1998), 559–572.

[Ru 1999a] C.-Q. Ru, "Three-phase elliptical inclusions with internal uniform hydrostatic stresses", *J. Mech. Phys. Solids* **47**:2 (1999), 259–273.

[Ru 1999b] C.-Q. Ru, "A new method for an inhomogeneity with stepwise graded interphase under thermomechanical loadings", *J. Elasticity* **56**:2 (1999), 107–127.

[Senocak and Waas 1995] E. Senocak and A. M. Waas, "Neutral cutouts in laminated plates", *Mech. Compos. Mater. Struct.* **2**:1 (1995), 71–89.

[Sih and Rice 1964] G. C. Sih and J. R. Rice, "The bending of plates of dissimilar materials with cracks", *J. Appl. Mech.* (*ASME*) **31**:3 (1964), 477–482.

[Vellaichamy et al. 1990] S. Vellaichamy, B. G. Prakash, and S. Brun, "Optimum design of cutouts in laminated composite structures", *Comput. Struct.* **37**:3 (1990), 241–246.

[Wang 2012] X. Wang, "Uniform fields inside two non-elliptical inclusions", *Math. Mech. Solids* **17**:7 (2012), 736–761.

[Wang and Hasebe 2000a] X.-F. Wang and N. Hasebe, "Green's function for mixed boundary value problem of thin plate", *J. Eng. Mech.* (*ASCE*) **126**:8 (2000), 787–794.

[Wang and Hasebe 2000b] X.-F. Wang and N. Hasebe, "Bending of a thin plate containing a rigid inclusion and a crack", *Eng. Anal. Bound. Elem.* **24**:2 (2000), 145–153.

[Wang and Hasebe 2001] X.-F. Wang and N. Hasebe, "Green's function of a point dislocation for the bending of a composite infinite plate with an elliptical hole at interface", *Arch. Appl. Mech.* **71**:4-5 (2001), 233–248.

[Wang and Schiavone 2013] X. Wang and P. Schiavone, "Interface cracks in Kirchhoff anisotropic thin plates of dissimilar materials", *J. Appl. Mech.* (*ASME*) **80**:4 (2013), Article ID #041025.

[Wang and Zhou 2013] X. Wang and K. Zhou, "Twelve-dimensional Stroh-like formalism for Kirchhoff anisotropic piezoelectric thin plates", *Int. J. Eng. Sci.* **71** (2013), 111–136.

[Wang and Zhou 2014] X. Wang and K. Zhou, "An inclusion of arbitrary shape in an infinite or semi-infinite isotropic multilayered plate", *Int. J. Appl. Mech.* **06**:01 (2014), Article ID #1450001.

[Wang et al. 2005] G. F. Wang, P. Schiavone, and C.-Q. Ru, "Harmonic shapes in finite elasticity under nonuniform loading", *J. Appl. Mech.* (*ASME*) **72**:5 (2005), 691–694.

[Yin 2005a] W.-L. Yin, "Green's function of anisotropic plates with unrestricted coupling and degeneracy, part 1: The infinite plate", *Compos. Struct.* **69**:3 (2005), 360–375.

[Yin 2005b] W.-L. Yin, "Green's function of anisotropic plates with unrestricted coupling and degeneracy, part 2: Other domains and special laminates", *Compos. Struct.* **69**:3 (2005), 376–386.

[Zakharov and Becker 2000] D. D. Zakharov and W. Becker, "Unsymmetric composite laminate with a discontinuity of the in-plane displacement or of the slope", *Acta Mech.* **144**:3-4 (2000), 127–135.

XU WANG: xuwang_sun@hotmail.com
School of Mechanical and Power Engineering, East China University of Science and Technology, 130 Meilong Road, Shanghai, 200237, China

PETER SCHIAVONE: p.schiavone@ualberta.ca
Department of Mechanical Engineering, University of Alberta, 4-9 Mechanical Engineering Building, Edmonton, AB T6G 2G8, Canada

SUBMISSION GUIDELINES

ORIGINALITY

Authors may submit manuscripts in PDF format online at the Submissions page. Submission of a manuscript acknowledges that the manuscript is original and has neither previously, nor simultaneously, in whole or in part, been submitted elsewhere. Information regarding the preparation of manuscripts is provided below. Correspondence by email is requested for convenience and speed. For further information, write to contact@msp.org.

LANGUAGE

Manuscripts must be in English. A brief abstract of about 150 words or less must be included. The abstract should be self-contained and not make any reference to the bibliography. Also required are keywords and subject classification for the article, and, for each author, postal address, affiliation (if appropriate), and email address if available. A home-page URL is optional.

FORMAT

Authors can use their preferred manuscript-preparation software, including for example Microsoft Word or any variant of TeX. The journal itself is produced in LaTeX, so accepted articles prepared using other software will be converted to LaTeX at production time. Authors wishing to prepare their document in LaTeX can follow the example file at www.jomms.net (but the use of other class files is acceptable). At submission time only a PDF file is required. After acceptance, authors must submit all source material (see especially Figures below).

REFERENCES

Bibliographical references should be complete, including article titles and page ranges. All references in the bibliography should be cited in the text. The use of BibTeX is preferred but not required. Tags will be converted to the house format (see a current issue for examples); however, for submission you may use the format of your choice. Links will be provided to all literature with known web locations; authors can supply their own links in addition to those provided by the editorial process.

FIGURES

Figures must be of publication quality. After acceptance, you will need to submit the original source files in vector format for all diagrams and graphs in your manuscript: vector EPS or vector PDF files are the most useful. (EPS stands for Encapsulated PostScript.)

Most drawing and graphing packages—Mathematica, Adobe Illustrator, Corel Draw, MATLAB, etc.—allow the user to save files in one of these formats. Make sure that what you're saving is vector graphics and not a bitmap. If you need help, please write to graphics@msp.org with as many details as you can about how your graphics were generated.

Please also include the original data for any plots. This is particularly important if you are unable to save Excel-generated plots in vector format. Saving them as bitmaps is not useful; please send the Excel (.xls) spreadsheets instead. Bundle your figure files into a single archive (using zip, tar, rar or other format of your choice) and upload on the link you been given at acceptance time.

Each figure should be captioned and numbered so that it can float. Small figures occupying no more than three lines of vertical space can be kept in the text ("the curve looks like this:"). It is acceptable to submit a manuscript with all figures at the end, if their placement is specified in the text by means of comments such as "Place Figure 1 here". The same considerations apply to tables.

WHITE SPACE

Forced line breaks or page breaks should not be inserted in the document. There is no point in your trying to optimize line and page breaks in the original manuscript. The manuscript will be reformatted to use the journal's preferred fonts and layout.

PROOFS

Page proofs will be made available to authors (or to the designated corresponding author) at a Web site in PDF format. Failure to acknowledge the receipt of proofs or to return corrections within the requested deadline may cause publication to be postponed.

Journal of Mechanics of Materials and Structures

Volume 10, No. 3   May 2015

Special issue
In Memoriam: Huy Duong Bui